Department of Defense
Legacy Resource Management Program

PROJECT NUMBER (05-170)

Long-Term Management Strategies for USS ARIZONA, A Submerged Cultural Resource in Pearl Harbor

NATIONAL PARK SERVICE
SUMBERGED RESOURCES CENTER

SEPTEMBER 2008
THIS REPORT IS APPROVED FOR PUBLIC RELEASE

National Park Service
U.S. Department of the Interior

Submerged Resources Center
Santa Fe, New Mexico

Long-Term Management Strategies for USS Arizona, *A Submerged Cultural Resource in Pearl Harbor*

Department of Defense
Legacy Resources Management Program

Legacy Resources Management Project #02-170, #03-170, #04-170, #05-170

Long-Term Management Strategies for USS Arizona, A Submerged Cultural Resource in Pearl Harbor

Department of Defense
Legacy Resources Management Program

Project #02-170, #03-170, #04-170, #05-170

a product of
NATIONAL PARK SERVICE
SUBMERGED RESOURCES CENTER

Long-Term Management Strategies for USS *Arizona*, A Submerged Cultural Resource in Pearl Harbor

Larry E. Murphy and Matthew A. Russell (Editors)
Submerged Resources Center

Brad Carkin
U.S. Geological Survey

James D. Carr
University of Nebraska-Lincoln

Robert De Angelis
Eglin Air Force Base

Michael E. Field
U.S. Geological Survey

Timothy J. Foecke
National Institute of Standards and Technology

Amanda M. Graham
Medical University of South Carolina

Donald L. Johnson
University of Nebraska-Lincoln

Robert E. Kayen
U.S. Geological Survey

Homa J. Lee
U.S. Geological Survey

Kristen Bearce Lee
Harvard University

Li Ma
National Institute of Standards and Technology

John D. Makinson
Rail Sciences, Inc.

Christopher J. McNamara
Harvard University

Ralph Mitchell
Harvard University

M. Katherine Presto
U.S. Geological Survey

Curt D. Storlazzi
U.S. Geological Survey

William N. Weins
University of Nebraska-Lincoln

Brent M. Wilson
University of Nebraska-Lincoln

Submerged Resources Center
Intermountain Region
National Park Service
US Department of the Interior

TABLE OF CONTENTS

ix

LIST OF FIGURES

LIST OF TABLES

ACKNOWLEDGEMENTS

PREFACE

This report represents the final product in partial fulfillment of Department of Defense Legacy Resources Management Fund Projects Nos. 02-170, 03-170, 04-170, and 05-170, which were funded in Fiscal Years 2002–2005. Requested funding was provided in 2002, while only part of requested funding was provided in the other years. Because of incomplete funding, some tasks were reduced or eliminated. This report fulfills the Legacy Project report requirements. Legacy funding was augmented with funding from other sources, principal among these are the National Park Service (NPS) Systemwide Archeological Inventory Program, USS *Arizona* Memorial, *Arizona* Memorial Museum Association, the NPS Submerged Resources Center, and significant in-kind support from the federal agencies and academic institutions that have contributed to this report. Although this is the final report for the Legacy Project, it constitutes an interim synthesis report for the USS *Arizona* Preservation Project, which remains ongoing.

The project's primary focus was to acquire requisite data for understanding and characterizing the complex corrosion and deterioration processes affecting *Arizona*'s hull, both internally and externally, and to model and predict the nature and rate of structural changes resulting from corrosion. The interdisciplinary research approach to characterizing and understanding USS *Arizona* deterioration and integration into a predictive model reported here was designed to produce cumulative data whose synthesis will inform management actions regarding long-term stewardship of this National Historic Landmark site. Beyond informing management decisions about *Arizona*, we believe this research approach has produced results that contribute to each of the disciplines involved, and which are directly applicable to the thousands of steel legacy vessels submerged worldwide. This report represents what we have learned so far about USS *Arizona* and other submerged steel hull's deterioration. Because *Arizona* research is not complete, and data derived from the monitoring program have not been generated and incorporated, report conclusions will be refined and may change as data-gaps are filled and new information is added. Data presented here represents the most informed view of the ship based on scientific observations, investigations and experimentation by outstanding experts in numerous fields, but it is necessarily incomplete because not all research domains have been completed. We have learned a great deal that will allow NPS and U.S. Navy

managers to make correct decisions about immediate needs within a stewardship framework, although lack of complete funding has resulted in gaps in our knowledge about critical aspects of *Arizona*'s deterioration. In that regard, the work reported here is an important step toward refining questions that guide future research directed toward a full understanding of *Arizona*'s deterioration.

CHAPTER 1

Introduction

Larry E. Murphy and Matthew A. Russell

SIGNIFICANCE

USS *Arizona*, a National Historic Landmark—the highest level of national historic significance in the United States—is a U.S. Navy object administered cooperatively by the National Park Service (NPS) and U.S. Navy, and among the most recognized and visited war memorials in the United States (Figure 1.1). A million and a half visitors annually make the short trip across Pearl Harbor to the USS *Arizona* Memorial, which spans the sunken hull. The Memorial is located off the northwest corner of Ford Island in the East Loch of Pearl Harbor, South-central Oahu, Hawaii (Figure 1.2).

The *Pennsylvania*-class battleship USS *Arizona* was completed in 1916 (Figure 1.3) and was sunk in Pearl Harbor, Hawaii on December 7, 1941 during the Japanese attack on the U.S. Navy's Pacific Fleet. In the first 15 minutes of the attack, Japanese aircraft struck *Arizona* with several bombs, strafed the ship, and then at about 0810 delivered the battleship a mortal blow. A Japanese Nakajima B5N2 "Kate" horizontal bomber dropped a single 1,760-pound projectile constructed from a 16-inch armor piercing shell that struck near Turret No. 2 and penetrated deep into the battleship's interior before exploding and sympathetically detonating the black powder magazine, which ignited the forward magazines containing smokeless powder for the forward

turrets (Figure 1.4). When the forward magazine exploded, it destroyed most of the battleship's forward half below the upper deck, presumably including the forward oil bunkers aft to approximately frame 78. The two forward turrets and the conning tower dropped about 20 feet, their foundations destroyed by the blast. The ship sank in minutes, and the explosion ignited fires that raged for two-and-a-half days (Figure 1.5). The explosion and subsequent conflagration killed 1,177 sailors and marines aboard USS *Arizona*—the event remains the largest single-ship loss of life in U.S. naval history. More than 900 men remain entombed within the ship and are considered buried at sea with the battleship as their final resting place. Millions of visitors, many international, consider the vessel a national icon. This naval memorial remains deeply ingrained in American consciousness, and still commands an honor guard from the many capital ships that ply Pearl Harbor today (Figure 1.6).

USS *ARIZONA* PRESERVATION PROJECT

Beginning in 1998, the NPS Submerged Resources Center (SRC) and USS *Arizona* Memorial (USAR), along with many partners, conducted a comprehensive research program

Figure 1.1. The USS *Arizona* Memorial (NPS Photo by Brett Seymour).

directed at understanding the nature and rate of a range of natural processes affecting USS *Arizona*'s deterioration. The USS *Arizona* Preservation Project is a multi-year, interdisciplinary and cumulative effort, with each element of the project contributing to basic research required to make informed management decisions for *Arizona*'s long-term preservation and to minimize environmental hazard from a potential fuel oil release of the estimated 500,000 gallons still onboard the battleship (Russell, et al. 2004). Developing reasonable and effective management alternatives and determining the most desirable actions, particularly those regarding intervention or rehabilitation, cannot be done without a sound, scientifically-based research program conducted within a management framework aimed at collecting data necessary to make informed management decisions. Because of the particular national importance of *Arizona,* any research, as well as any solution to the oil issue, must incorporate a minimum-impact approach, consistent
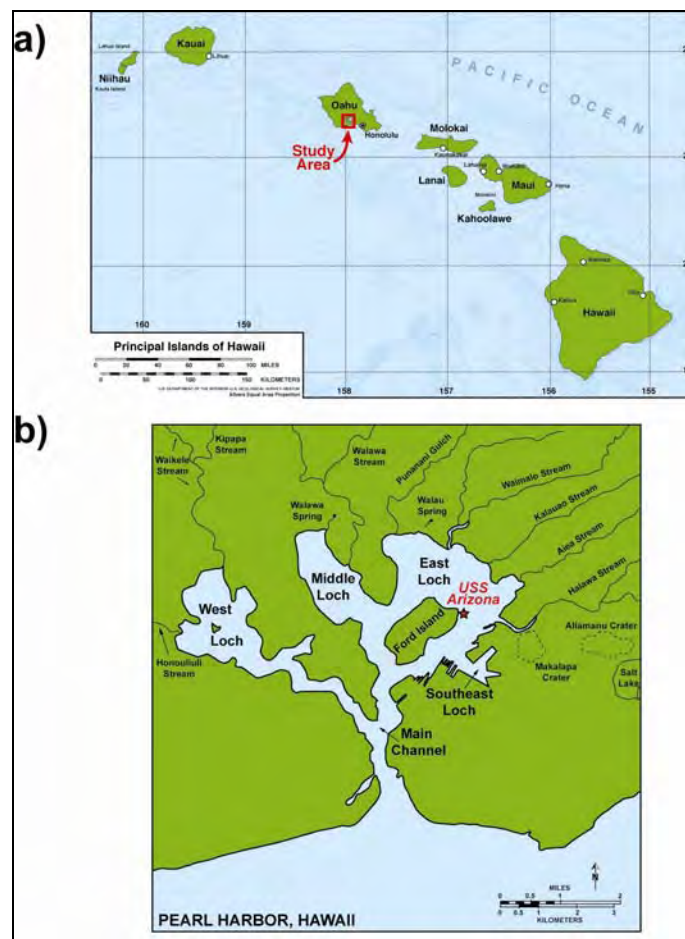
Figure 1.2. Map of the study area. a) Location of Pearl Harbor in relation to the main Hawaiian Island chain; b) Location of the USS *Arizona* Memorial in Pearl Harbor relative to Ford Island (Graphic courtesy of U.S. Geological Survey).

3

Figure 1.3. The USS *Arizona* in the East River in New York City after launching in 1916 (USS *Arizona* Memorial Photo Archives).

Figure 1.4. USS *Arizona* exploding on December 7, 1941 (USS *Arizona* Memorial Photo Archives).
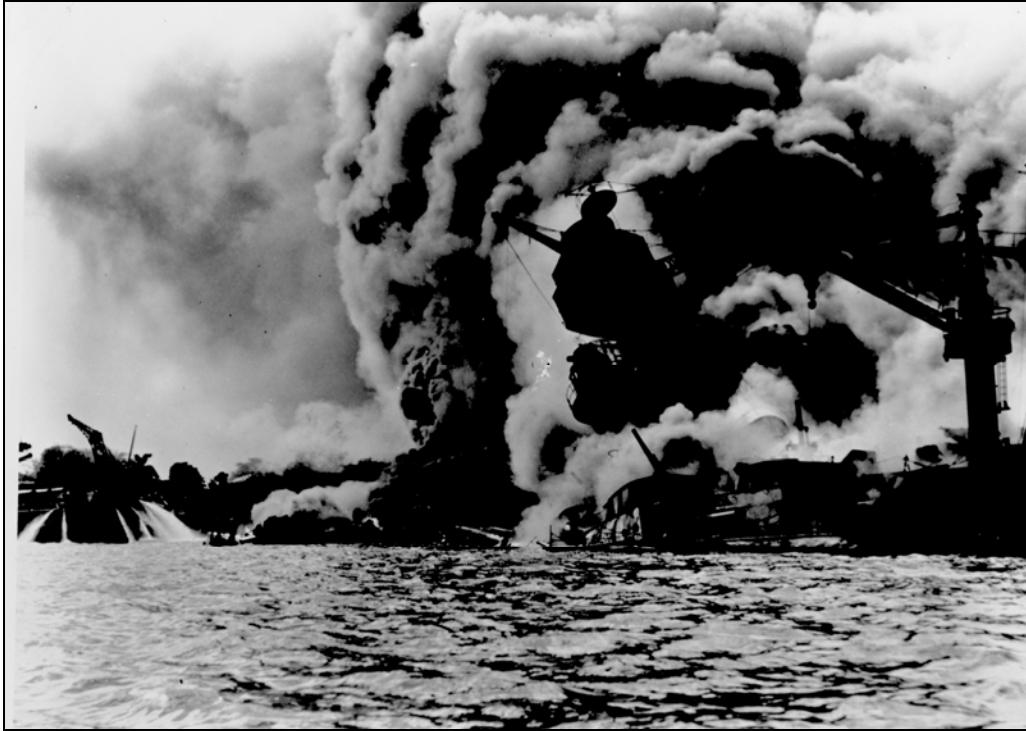
Figure 1.5. USS *Arizona* burning after the Pearl Harbor attack (USS *Arizona* Memorial Photo Archives).

Figure 1.6. USS *Abraham Lincoln*'s officers and crew honoring USS *Arizona*, 2004 (USS *Arizona* Memorial).

with standard NPS policy (Russell and Murphy 1997), but with added respect due the ship as a tomb, or long-term preservation of the ship may be compromised. Unnecessary disturbance to *Arizona*'s hull is likely to be seen by many as more problematic than the limited oil release now occurring, although managers will ultimately have to face the possibility of a large release Bunker C fuel oil. Addressing the oil release problem within a site-preservation framework incorporated in this project provides the best balance of competing social values, and it has the highest probability of success for arriving at the best and most defensible solution for both issues while providing maximum preservation and protection.

In addition to the particular issues surrounding the battleship itself, project principals designed the USS *Arizona* Preservation Project to serve as a model for intervention actions directed at other historic vessels leaking contaminants into the environment, and to produce results directly applicable to preservation and management of historical iron and steel vessels worldwide (Jeffery 2004). Although the project focused on management concerns and collecting physical data necessary to make informed management decisions regarding USS *Arizona*, we planned and conducted the research project within an archeological framework and in the broader context of the archaeology of the Pearl Harbor attack (Delgado 1992; Gould 2000; Lenihan 1989b; Rodgers, et al. 1998).

This chapter highlights previous research conducted on the site and outlines the origin of the current management-based research program on USS *Arizona*. It begins by reviewing the rationale that led to the genesis of the USS *Arizona* Documentation Project in the early 1980s, and then traces the changing management needs to the present day and addresses the question of oil removal. The chapter next details the interdisciplinary nature of the current project and the complex interactions of federal, state, and private partners involved. Finally, it discusses the organization of the rest of this volume.

<div align="center">PROJECT BACKGROUND AND RATIONALE</div>

Previous Research

NPS preservation efforts on USS *Arizona* began when the first superintendent of the USS *Arizona* Memorial asked SRC to document the ship. This request resulted in a five-year project

from 1983–1988 designed to address specific concerns from NPS managers responsible for the historic battleship and memorial (Lenihan 1989b). In late 1980, the U.S. Congress created the USS *Arizona* Memorial as a unit of the National Park system and charged the new superintendent with two fundamental concerns: interpretation and management (Cummins and Dickinson 1989:158). When the NPS took over the Memorial's operation from the Navy, the agency found it faced a nearly insatiable public curiosity about the Pearl Harbor attack overall, and USS *Arizona* specifically, and found it lacked answers to some very basic questions. Because tantalizingly little of *Arizona* is visible above the waterline, and all depictions of the ship were either of it on the surface or during the attack, the most often-asked question was some variation of "what does the ship look like now?" In addition, although official Navy records attribute the damage and eventual sinking of the battleship to aerial bombs, there were eyewitnesses who insist they saw *Arizona* struck by at least one torpedo and saw a bomb penetrate the ship's smoke stack. Varying historical accounts about the events of December 7, 1941 and the aftermath contributed to a general confusion about what really happened. More than 40 years after *Arizona*'s sinking, fundamental questions lingered—questions that could potentially be answered by archeological investigation of the material remains *in situ* on the harbor bottom (Lenihan 1989a).

In addition to public interpretation, the NPS's other priority is resource management and historic preservation. Before the NPS began managing *Arizona* there was little concern for the vessel's preservation by the Navy, although memorialization efforts began soon after the war and led to construction of the present memorial in 1962. With the Navy retaining ownership and NPS mandated to actively manage the site beginning in 1981, however, such basic questions as "what condition is the wreck in?" and "how quickly is it deteriorating?" needed to be addressed before the agency could make effective management decisions about how to treat the vessel's remains. Because *Arizona* is the final resting place for more than 900 sailors and marines, a significant management question becomes whether the site should be left alone to deteriorate naturally or whether the agency intervene to preserve the integrity of the tomb (Cummins and Dickinson 1989:163-164). Although at the time the NPS, nor anyone else, had experience actively managing sunken steel vessels, it did have considerable experience with standing remains on archaeological sites and with historic structures. With this background, from the beginning of its management tenure, the NPS treated *Arizona* as a structural archaeological site

and used archaeological methodology to provide answers to the agency's questions, regarding both site interpretation and management. In response to the practical needs of site managers, the two basic questions NPS archaeologists were asked by the Memorial superintendents during the 1983–1988 project became "what's there?" and, then, "what's happening to what's there?" (Lenihan 1989a).

NPS researchers effectively answered the first question in 1984 by documenting the hull and producing of a series of detailed drawings, basically an archeological site map, based upon thousands of direct measurements (Lenihan and Murphy 1989:83-86)(Figure 1.7). Not only are these images a powerful tool for public interpretation and understanding, they are also the foundation for all additional work on the ship. From these archaeological drawings and additional detail, a scale model was created for the Memorial visitor center to allow visitors to visualize that once on the Memorial, they were standing directly over the remains of the battleship—it connected the few features visible above the water to the ship below (Figure 1.8). The drawings and model directly contribute to an interpretive scheme that highlights the reverential aspects of the site and presents enough information to visitors to allow them understand the site and "to construct their own meaning of the site while partaking in the general atmosphere of subdued restraint and poignancy" (Kelly 1996:56).

The second question, "what's happening to what's there," is essentially directed at determining the nature and rate of corrosion affecting *Arizona*'s steel hull, and is an extremely complex and multifaceted question that could not be easily answered. Researchers in the 1980s addressed *in situ* corrosion of a submerged iron or steel shipwreck by collecting baseline data, including corrosion potential (E_{corr}) of the steel hull using a bathycorrometer, essentially a sea water equivalent silver/silver chloride (Ag/AgCl) reference electrode—a critical data set for evaluating corrosion rate and by examining the concretion and biological organisms attached to the exterior hull (Henderson 1989, see also Chapter 5). At the same time, the first two Memorial superintendents laid out a series of future research objectives based on serious management concerns—objectives that would guide the next phase of research that began in 1998 and that is reported on in this volume (Cummins and Dickinson 1989:167-168). Cummins's and Dickinson's research questions provided the management framework for the USS *Arizona* Preservation Project.
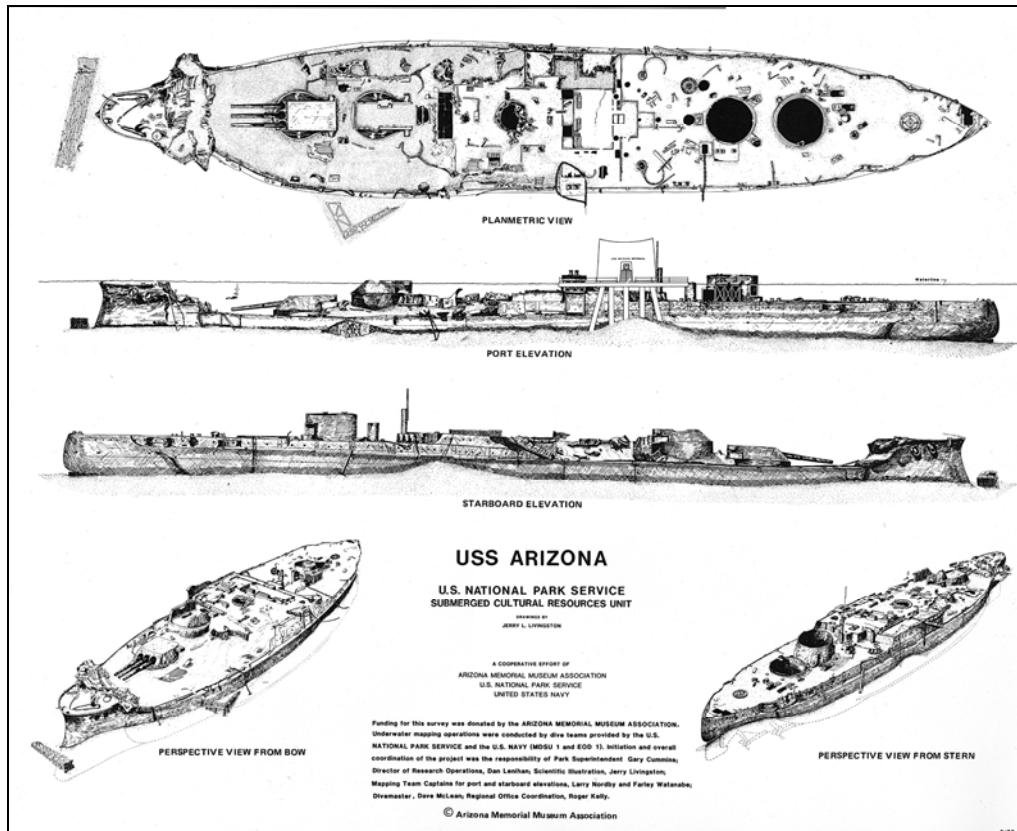
Figure 1.7. Scale drawings of USS *Arizona* (Drawing by NPS-SRC, 1984).
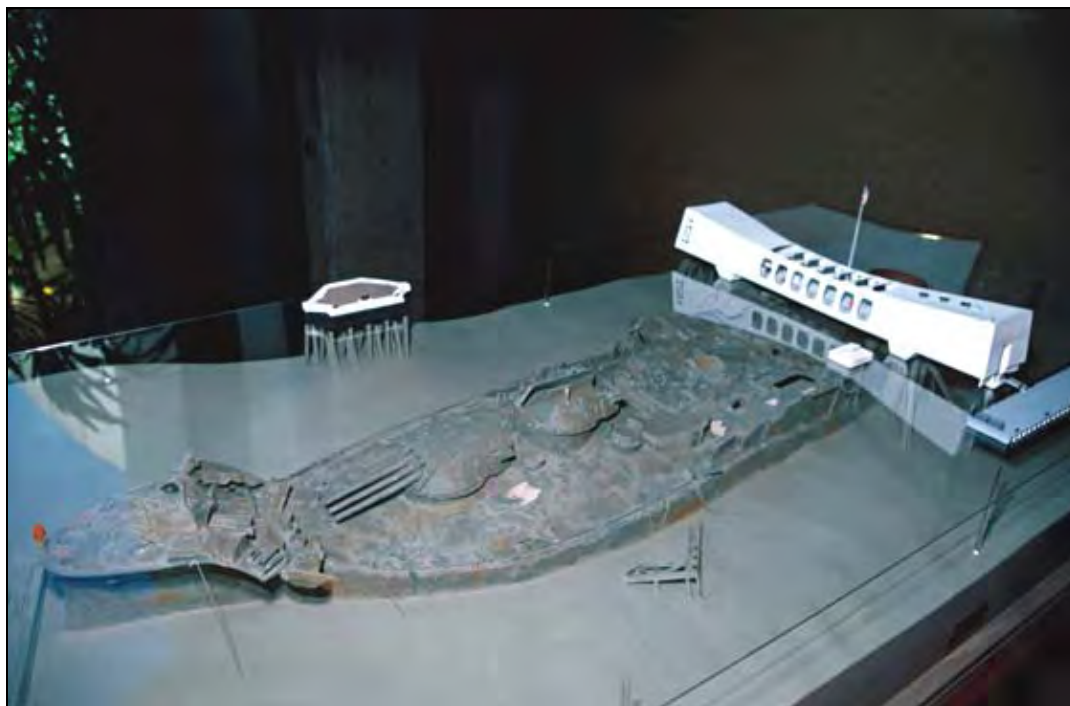
**Figure 1.8. Scale model of USS *Arizona* produced from archeological scale drawings
(NPS Photo by Brett Seymour)**

Current Project Genesis

Corrosion data collected in the 1980s and management needs for effective NPS stewardship suggested that future research should focus on four key areas. First, conduct direct analysis of steel hull samples to determine corrosion rate variability across *Arizona*'s hull fabric. Second, determine the nature and exact mechanism of electrochemical corrosion in order to predict corrosion rates in areas not directly sampled or inaccessible to researchers, and develop a non-destructive methodology to test the predictive corrosion model. Third, using original engineering plans and corrosion data, create a computer-based model to predict the hull's current lifespan if there is no intervention. And fourth, create a long-term management plan including environmental and structural monitoring of *Arizona*'s hull (Cummins and Dickinson 1989:167-168). Although these goals were outlined in 1989, change in management at the USS *Arizona* Memorial resulted in change in management priorities, and no systematic research was conducted nor any attempt to implement the 1989 research recommendations were undertaken until the late 1990s. Kathy Billings became superintendent of the USS *Arizona* Memorial in 1996 and immediately re-focused attention on earlier management goals and objectives, and in 1998, SRC was tasked with implementing the 1989 research strategy. SRC researchers quickly partnered with a variety of outside collaborators to leverage the limited available funding, but also realized a more secure funding base would be necessary to fully implement the comprehensive research program necessary to address management questions.

Often overshadowing larger preservation issues is concern about the estimated 500,000 gallons of oil still contained within *Arizona*'s bunkers. The oil currently bubbles out of the ship one small drop at a time, each shaped like a marble-sized black pearl, totaling about 9–10 quarts a day. Although *Arizona* has been leaking oil steadily since 1941, intense media attention surrounding the Pearl Harbor attack's 60th anniversary in 2001, including three major television documentaries by National Geographic, Discovery Channel and History Channel, an article in National Geographic magazine (Vesilind 2001), and Disney's epic World War II blockbuster *Pearl Harbor* focused public attention on the half-million gallons of oil remaining in *Arizona*'s corroding hull, which was unanimously described as a pending environmental calamity. Based on media characterizations, the U.S. Navy began putting out feelers about the possibility of oil removal. During preliminary discussions with U.S. Navy personnel in Pearl Harbor, NPS

representatives suggested that before hasty, and possibly destructive, measures were taken to mitigate the potential environmental hazard, a comprehensive assessment of *Arizona*'s hull should be undertaken to determine a curve of deterioration and pinpoint exactly where the battleship currently falls on the curve (essentially, following the NPS manager's 1989 objectives). This evaluation would allow NPS and Navy managers to make decisions about the ship based on sound scientific fact, not speculation and media dramatization. The discussions and the concern of Deputy Under Secretary of Defense (Installations and Environment) Raymond F. Dubois, Jr. ultimately lead to project funding from the Department of Defense Legacy Resource Management Fund, which the NPS received from 2002–2005, to plan and execute a multi-year, interdisciplinary project to assess *Arizona*'s corrosion rate and evaluation the nature of the environmental hazard posed by the oil (Russell and Murphy 2003, 2004; Russell, et al. 2004). This funding, which was about half that requested, was leveraged with funding sources from NPS-SRC, the NPS Systemwide Archeological Inventory Program, *Arizona* Memorial Museum Association, several academic institutions and corporate partners, to conduct the research presented in this report.

Although the oil issue was the major impetus for project funding, primary research focus has always been to develop an overall, long-term preservation plan for *Arizona*, which would include investigating the hull's corrosion rate to determine the possible timing of a major oil release. The first step in the research process was to determine the corrosion rate of *Arizona*'s steel hull—how quickly the ship is deteriorating—and therefore, how long before the oil's release becomes imminent. To fully understand corrosion rate, it is necessary to know the precise mechanism of corrosion and the variables involved. Understanding the corrosion mechanism and variables is necessary to extend measured corrosion rates to parts of the ship that are not directly accessible to researchers, such as the interior and areas of the hull below the harbor bottom. Predicting corrosion rate in all parts of the hull, including those where it cannot be directly measured, is necessary for designing and constructing an accurate predictive model of hull deterioration. Ultimately, this predictive model is the USS *Arizona* Preservation Project's main product and project outcome (see Chapter 6).

Oil Removal versus Site Preservation

Inevitably, however, we end up back at the question of oil removal: should preservation of a historically and internationally-significant war grave take precedence over a potentially invasive environmental remediation? USS *Arizona*'s significance is not merely historical, but is also symbolic. As Edward T. Linenthal notes in his book *Sacred Ground: Americans and Their Battlefields*, battlefields, including Pearl Harbor, are "prime examples of sacred patriotic space where memories of the transformative power of war and the sacrificial heroism of the warrior are preserved….The urge to preserve and restore these holy places of the nation comes from an intuitive sense that the essence of America can be found in our sacred environments…[and]…these battlefields provide a conduit through which citizens are able to participate in the power of a heroic past – a past that continues to demand allegiance to its cherished principles" (Linenthal 1991:3-4). Furthermore, Delgado (1989:169) notes, "Pearl Harbor, particularly the USS *Arizona*, has become a national shrine. Pearl Harbor and every trace of the American forces that defended it are now imbued with an almost religious significance." More than 1.5 million people each year visit the Memorial, but "perhaps more important than the modern memorial that straddles *Arizona* is the battleship itself, which is the ultimate shrine. Resting in the silt of Pearl Harbor, the USS *Arizona* is a naval memorial and a war grave. It was the scene of tragedy, triumph and heroism….The wreck now serves as a 'temporal touchstone,' drawing visitors who reflect on the tragedy of the Pearl Harbor attack…" (Delgado 1989:173). In this regard, the site is an important part of the national consciousness.

As we like to characterize the situation, if *Arizona* were any other ship in any other harbor, the oil may have already have been removed. The U.S. Navy and several commercial firms have the technical capability to empty sunken ships of environmentally harmful fluids. In 2002, the U.S. Coast Guard and Titan Maritime, Inc. removed approximately 100,000 gallons of heavy fuel oil from SS *Jacob Luckenbach*, a cargo ship sunk in a collision off San Francisco in 1953, although approximately 29,000 gallons remain (Luckenbach Trustee Council 2006). The following year, the U.S. Navy Naval Sea Systems Command (NAVSEA) removed nearly 2 million gallons of oil from USS *Mississinewa* (AO-59) a US Navy oiler, sunk on November 20, 1944 in Ulithi Lagoon, Micronesia by a *Kaiten* (an Imperial Japanese Navy manned suicide torpedo with a 3,418-lb. warhead)(US Navy 2003). These two vessels represent the range of

difficulty of oil removal, with *Luckenbach* the more difficult. Both vessels are more than 100 feet deep, and both had direct access to oil containment. The *Mississinewa* removal was completely successful; the *Luckenbach* effort was not, although costing nearly $20 million. Oil removal on USS *Arizona* would set the range of difficulty beyond that of *Luckenbach*, and oil removal without sacrificing the structure may not be possible. The fact remains, however, that USS *Arizona* is not just any ship in any harbor, and other factors besides straightforward oil removal need to be considered.

Although oil removal may be potentially possible, it would be an extremely invasive procedure. *Arizona*'s fuel oil bunkers are spread across three deck levels as well as the double bottom, and arranged from bow to stern. The bunkers are highly compartmentalized and individually piped, designed that way so as to prevent catastrophic fuel loss should one part of the battleship sustain a crippling blow. There is no single fuel compartment or storage area, such as on the examples given above, so it is no simple job to "hot tap" the hull to remove the oil. Further complicating matters, all the fuel oil storage bunkers are beneath the present harbor bottom—the ship is sunk into the sediment of Pearl Harbor to its original waterline, making direct access to the bunkers impossible, and the vessel may be full of sediment in the lower areas. Given that oil removal would likely be highly damaging and destructive course of action, the question remains, is this invasive and potentially damaging procedure appropriate or acceptable on a site of USS *Arizona*'s significance? Would it be acceptable even if easier and less invasive? Most, including the NPS, think not, at least not without considerably more information about the impact to the ship as a whole and the remains of its crew specifically. Given the national importance and symbolic significance of *Arizona*'s remains, at this point the balance is decidedly tipped in favor of historic preservation over correction of a minor environmental impact and an as yet unknown environmental hazard of catastrophic oil release. Determining the true nature of the hazard based on scientific investigation provided a major impetus for the project reported here.

Besides the question of oil removal, the other looming management question will be whether intervening in *Arizona*'s natural process of deterioration is warranted, feasible, or desirable. Before weighing the benefits of a potentially very costly and unproven intervention, more information is necessary about various cathodic protection systems and their potential feasibility and effectiveness, as well as how they would affect interior spaces of the ship that

cannot be directly protected. Oil remediation other than removal must be considered for the long term. The decision as to whether it is in society's interest to allow the ship to follow a natural course of deterioration, or to intervene in an attempt to prolong *Arizona*'s existence as a structure, remains to be made.

PROJECT DESIGN AND PARTNERS

The primary project focus was to acquire requisite data from the site and its environs to understand and characterize the complex corrosion and deterioration processes affecting *Arizona*'s hull, both internally and externally, and to model and predict the nature and rate of structural changes resulting from corrosion. The research program, which is outlined in more detail in the next chapter, was designed to be a cumulative progression of multi-disciplinary investigative steps orchestrated by the NPS and incorporating a long-term management perspective. Multiple lines of evidence were pursued simultaneously, some concurrently, some consecutively, each directly or indirectly linked to the others and to the overall project objectives. Operationally, we followed a two-fold strategy of research combined with long-term monitoring. Primary research was directed towards characterizing the overall corrosion processes and determining internal and external corrosion rates. These data were required to develop a predictive model of how *Arizona* is deteriorating, when corrosion will reach the point where structural changes indicate imminent collapse and how that collapse will take place to provide predictability through monitoring. Monitoring activities, which are ongoing, were initially aimed at collecting baseline data for inclusion in corrosion analysis, and are now being used to assess changing conditions over the long-term and to serve as a test for the validity of the mathematical model.

The SRC provided project principals who had been involved in *Arizona* research from the early 1980s (see Lenihan 1989b). We also partnered with other NPS programs (particularly the NPS Resources Inventory and Monitoring Division and NPS GPS Coordinator), military units (U.S. Navy, Mobile Salvage Diving Unit One, Naval Facilities Engineering Service Center, Navy Region Hawaii, Naval Station Pearl Harbor; U.S. Army, 29th Engineer Battalion Survey Platoon; and U.S. Air Force, Eglin Air Force Base), academic institutions and researchers (University of Nebraska, Lincoln; Medical University of South Carolina; Harvard University;

University of Michigan; and University of New Mexico), commercial companies (Discovery Channel; History Channel; HydroFlex; Inspection Technologies, Inc.; National Geographic Magazine and Television; Ocean Technology Systems; Titan Maritime, LLC; Trimble Navigation (+ surveying company), TruVue Imaging; USIA Drysuits, and VideoRay, Inc.), non-profit organizations (Coastal Maritime Archaeology Resources and *Arizona* Memorial Museum Association), and other federal agencies (National Institute of Standards and Technology; National Oceanic and Atmospheric Administration; U.S. Geological Survey, Marine Facility; U.S. Geological Survey, Pacific Science Center; and Naval Historical Center) in addressing the multifaceted questions confronting managers responsible for both USS *Arizona*'s preservation and associated environmental risk. This research partnership is an example of public and private institutions working together effectively for public benefit, and it serves as a model for combining resources to cost-efficiently address issues important to the American people.

ORGANIZATION OF THE VOLUME

Conceptually, this report is divided into four sections. Part I includes chapters that present background information necessary for understanding the development of the USS *Arizona* Preservation Project and for interpreting project results within their broader context. In addition to this introductory chapter, Chapter 2 outlines a detailed research design, explaining each element of the research program in detail and discussing how each element contributes to the larger project goals. This chapter is important for understanding why we chose the specific research directions that we did for the project. The final chapter of Part I is a historical background chapter highlighting cultural site formation processes, which is vital for understanding how the site came to be in the physical condition it is today. This chapter discusses battle damage, US Navy salvage from 1941 to 1943, early memorials and other structures erected on the hull, superstructure removal during the early 1960s in preparation for building the current memorial, and detailed analysis of final vessel configuration and post-depositional salvage and how that has affected its present site condition and state.

The second part of the report consists of individual chapters focused on each of the primary research components. Each chapter is authored by investigators from respective agencies and institutions who had primary research responsibility for each particular segment of

research. The first chapter in Part II (Chapter 4), by researchers from the U.S. Geological

Survey, outlines the environmental baseline for the site based on long-term deployment of

oceanographic and environmental instruments that collected various parameters for more than a

year. Long-term data collected from outside the hull is combined with internal data collected

with instruments mounted on a small, remotely operated vehicle (ROV) to give an overall

environmental characterization of the site. These data are critical for assessing the corrosion rate

of the steel hull.

The next chapter (Chapter 5), authored by researchers from the University of Nebraska,

Lincoln, outlines the results of nearly a decade of corrosion research on *Arizona*'s hull. It

discusses the full array of theoretical, experimental, and practical applications of corrosion

science deployed to understand the specific corrosion processes affecting the battleship, as well

as our best determination of corrosion rate for different parts of the hull.

Chapter 6 focuses on the Finite Element Analysis of *Arizona*'s hull conducted by

scientists from the National Institute of Standards and Technology (NIST). This analysis is the

primary product of the USS *Arizona* Preservation Project, and represents the first time that such a

detailed, computer-based finite element model (FEM) has been used in maritime archaeological

research. The chapter discusses the creation of the *Arizona* FEM by NIST, including

assumptions and model parameters incorporated within the model, scenarios that were run, and

implications for projections of long-range deterioration of the vessel.

Chapter 7, contributed by Harvard University microbiologists, outlines the results of

preliminary experimental research (not completed as yet because of partial funding) identifying

the role of microbial induced corrosion in *Arizona*'s deterioration, particularly in oil-containing

spaces deep inside the lower spaces of the ship. This research offers a critical glimpse of the

ship's interior spaces that are completely inaccessible to researchers, and that were instead

recreated in the laboratory to predict current conditions.

The final chapter of Part II (Chapter 8) outlines a research program directed at

characterizing *Arizona*'s oil, including identifying specific biomarker fingerprints to identify oil

from *Arizona*, as well as an evaluation of oil leaking for various locations around the ship. This

chapter also examines and identifies a microbial film that covers oil trapped in compartment

overheads, as well as stepping back to characterize the broader distribution of oil from *Arizona*

around Pearl Harbor.

The report's third section (Part III) describes aspects of the on-going monitoring program on USS *Arizona*, primarily structural monitoring using high-resolution Global Positioning System (GPS) receivers capable of sub-centimeter accuracy, oil release measurements and artifact tracking. This monitoring program, initiated in 2001 by SRC, will determine if *Arizona*'s remains are stable or if there is active movement, settling or shifting of the hull. Subsequent occupations of our GPS monitoring network in 2003 and 2006 revealed no discernible movement. The monitoring program is described in detail in Chapter 9. In addition, as a control for geological factors that might be the cause of any future observed movement, Chapter 10 discusses the research to establish a geological baseline through subsurface geophysical survey and through geotechnical analysis of both physical cores from around the battleship, and using advanced geophysical techniques to determine whether *Arizona* is supported by stable sediments. Full characterization of sediments immediately around and beneath *Arizona* serves as a critical control for evaluating any future structural movements that may be observed.

Finally, Part IV consists of summary, conclusions, and recommendations that have resulted from the overall research program to date. Chapter 11 summarizes and evaluates the data within a site preservation framework, brings our multiple lines of evidence together in a comprehensive way to address our simple question, "what's happening to what's there?" and outlines a series of site preservation recommendations based on cumulative research results.

REFERENCES

Cummins, G. and B. Dickinson
    1989 The Management Experience. In *Submerged Cultural Resources Study: USS Arizona Memorial and Pearl Harbor National Historic Landmark*, edited by D. J. Lenihan, pp. 157-168. Submerged Resources Center Professional Papers No. 9. National Park Service, Santa Fe.

Delgado, J. P.
    1989 Memorials, Myths and Symbols. In *Submerged Cultural Resources Study: USS Arizona Memorial and Pearl Harbor National Historic Landmark*, edited by D. J. Lenihan, pp. 169-183. Submerged Resources Center Professional Papers No. 9. National Park Service, Santa Fe.

    1992 Recovering the Past of USS Arizona: Symbolism, Myth, and Reality. *Historical Archaeology* 26(4):69-80.

Gould, R. A.
    2000 *Archaeology and the Social History of Ships*. Cambridge University Press, Cambridge.

Henderson, S.
    1989 Biofouling and Corrosion Study. In *Submerged Cultural Resources Study: USS Arizona Memorial and Pearl Harbor National Historic Landmark*, edited by D. J. Lenihan, pp. 117-156. Submerged Resources Center Professional Papers No. 9. National Park Service, Santa Fe.

Jeffery, B.
    2004 World War II Underwater Cultural Heritage Sites in Truk Lagoon: Considering a Case for World Heritage Listing. *International Journal of Nautical Archaeology* 33(1):106-121.

Kelly, M.
    1996 Enshrining History: The Visitor Experience at Pearl Harbor's USS Arizona Memorial. *Museum Anthropology* 20(3):45-57.

Lenihan, D. J.
    1989a Introduction. In *Submerged Cultural Resources Study: USS Arizona Memorial and Pearl Harbor National Historic Landmark*, edited by D. J. Lenihan, pp. 1-12. Submerged Resources Center Professional Papers No. 9. National Park Service, Santa Fe.

    1989b *Submerged Cultural Resources Study: USS Arizona Memorial and Pearl Harbor National Historic Landmark*. Submerged Resources Center Professional Papers No. 9. National Park Service, Santa Fe.

Lenihan, D. J. and L. E. Murphy
    1989 Archeological Record. In *Submerged Cultural Resources Study: USS Arizona Memorial and Pearl Harbor National Historic Landmark*, edited by D. J. Lenihan. Submerged Resources Center Professional Reports No. 9. National Park Service, Santa Fe.

Linenthal, E. T.
    1991 *Sacred Ground: Americans and Their Battlefields*. University of Illinois Press, Chicago.

Luckenbach Trustee Council
    2006 *S.S. Jacob Luckenbach and Associated Mystery Oil Spills Final Damage Assessment and Restoration Plan/Environmental Assessment.* Prepared by California Department of Fish and Game, National Oceanic and Atmospheric Administration, United States Fish and Wildlife Service, National Park Service.

Rodgers, B. A., W. M. Coble and H. K. Van Tilburg
    1998 The Lost Flying Boat of Kaneohe Bay: Archaeology of the First US Casualties of Pearl Harbor. *Historical Archaeology* 32(4):8-18.

Russell, M. A. and L. E. Murphy
    1997 Minimum Impact Archaeology. In *Encyclopaedia of Underwater and Maritime Archaeology*, edited by J. P. Delgado, pp. 278-279. British Museum Press, London.

    2003 *"Long-Term Management Strategies for the USS Arizona: A Submerged Cultural Resource in Pearl Harbor, Hawaii." Legacy Resources Management Fund Project No. 02-170: 2002 Annual Report*. Submerged Resources Center Technical Report No. 14. National Park Service, Santa Fe.

    2004 *"Long-Term Management Strategies for the USS Arizona: A Submerged Cultural Resource in Pearl Harbor, Hawaii." Legacy Resources Management Fund Project No. 03-170: 2003 Annual Report*. Submerged Resources Center Technical Report No. 15. National Park Service, Santa Fe.

Russell, M. A., L. E. Murphy, D. L. Johnson, T. J. Foecke, P. J. Morris and R. Mitchell
    2004 Science for Stewardship: Multidisciplinary Research on USS Arizona. *Marine Technology Society Journal* 38(3):54-63.

U.S. Navy
    2003 Overview of Survey/Salvage Operation: USS Mississnewa, www.supsalv.org/00c2_posseA0_59.asp?destPage=00c2.

Vesilind, P. J.
    2001 Oil and Honor at Pearl Harbor. *National Geographic Magazine* 199(6):84-99.

CHAPTER 2

Research Design

Matthew A. Russell and Larry E. Murphy

INTRODUCTION

Researchers from the National Park Service's (NPS) Submerged Resources Center (SRC) designed the USS *Arizona* Preservation Project from the outset to be multi-year, interdisciplinary and cumulative, with each element contributing to provide the basic research required to make informed management decisions for long-term preservation and to minimize environmental hazard from fuel oil release. In addition, we designed the project to serve as a model for interdisciplinary, management-based science that has direct application to preservation and management of historical iron and steel vessels worldwide, particularly serving as a guide for intervention actions directed at other historic vessels leaking contaminants into the environment.

We viewed this research design not only as an overall guide for fieldwork and analyses, but also as a "living document" that continued to change and evolve as the research progressed, as analyses resolved some issues and as questions became more focused. Even beyond this project, the NPS will continue to revise the research and monitoring on USS *Arizona* to incorporate evolving research approaches, results and questions. This research design has had significant peer review in both academic publications and professional meetings: portions of this research design have been previously published in Russell and Murphy (2003; 2004) and Russell

et al. (2004); it has been presented and discussed twice at the National Academy of Science, Ocean Studies Board subcommittee (Murphy 2002 and 2003); presented to the Society for Historical Archaeology (Murphy and Russell 2006); the George Wright Society (Murphy 2003); and it has been presented to many public and interested veteran groups, for example, the 60th Commemoration of the Pearl Harbor Conference in 2001 (Murphy 2001). In addition, individual scientists involved in the USS *Arizona* Preservation Project developed research approaches and have presented findings and results to peer organizations and published in academic journals. These are discussed in appropriate chapters and a compilation of research results, presentations and publications is presented in the final chapter of the report.

GOALS AND OBJECTIVES

The USS *Arizona* Preservation Project builds upon pioneering site documentation and research led by the National Park Service's Submerged Cultural Resources Unit (later renamed SRC) in the 1980s. The early SRC investigations initiated *in situ* documentation and study of large, submerged steel warships both in the U.S. and internationally (Lenihan 1989). The current project, building upon work done in the 1980's, was designed to provide a broad-based foundation for long-term preservation, management and monitoring of USS *Arizona*.

The primary project focus was to acquire requisite data for understanding and characterizing the complex corrosion and deterioration processes affecting *Arizona*'s hull, both internally and externally, and to model and predict the nature and rate of structural changes resulting from corrosion. Developing reasonable and effective management alternatives and deciding the most desirable actions, particularly those regarding intervention or rehabilitation, could not be effectively done without this information. The current research program was viewed as a critical step in obtaining necessary scientific information upon which to make sound management decisions. A central goal of this research was to develop and recommend short-term and long-term management plans for site preservation based on the results of the research program.

The USS *Arizona* Preservation Project addresses another important issue besides preservation of an internationally important site. USS *Arizona* contains several hundred thousand gallons of fuel oil that has been slowly escaping since its loss in 1941. This oil, a

potentially serious environmental hazard, is contained within the corroding hull. *Catastrophic oil release, although by all indications not imminent, is ultimately inevitable.* Understanding the complex hull corrosion processes, structural changes and oil release patterns offers the most effective and efficient method of mitigating this potential hazard. One of the goals of this project, therefore, was to develop a research strategy for environmental impact risk assessment and abatement to address the oil issue.

Because of the particular national importance of *Arizona,* any solution to the oil issue must incorporate a minimum-impact approach so that long-term site preservation will not be compromised. We conducted all research and monitoring operations with the respect due an American war grave and with minimum impact to the site consistent with NPS principles of stewardship and preservation; no diver entered the vessel. Addressing the oil release problem within a site-preservation framework provides the best balance between the competing social values of preservation and ecology, and it has the highest probability of arriving at the optimal solution for both issues.

Unnecessary disturbance to *Arizona*'s hull is likely to be seen by many as more problematic than the limited oil release now occurring, although managers will ultimately have to face the possibility of a larger release. This has in effect already been done. Because of the nature of Pearl Harbor, there is extensive oil recovery capability staged at Pearl Harbor, and a contingent of practiced professionals stand ready as a response team for oil spills.

PRINCIPAL RESEARCH DOMAINS AND METHODOLOGY

The SRC provided project principals who have been involved in *Arizona* research from the early 1980s (see Lenihan 1989). We also partnered with military units, researchers, academic institutions, commercial companies, research laboratories, professional societies and other federal agencies to address the multifaceted questions confronting managers responsible for both USS *Arizona*'s preservation and any associated environmental risk. This research program was designed to be a cumulative progression of multi-disciplinary investigative steps. Multiple lines of evidence were pursued simultaneously, each directly or indirectly linked to the others and to the overall project objectives. Operationally, the NPS followed a general strategy

of intensive research to develop a predictive model of hull deterioration that could be tested and revised and through long-term monitoring of critical variables.

Primary research was directed towards characterizing overall corrosion processes and determining internal and external corrosion rates. These data were required to develop the predictive model of how *Arizona* is deteriorating and when corrosion will reach the point where structural changes indicate imminent collapse and potential release of oil. The study of iron and steel corrosion of historic material in marine environments began in the mid-1970s. Archeologists and conservation specialists in Australia conducted pioneering research on iron artifacts and later on iron and steel shipwreck deterioration and determined that the major factors affecting shipwreck corrosion are metal composition and metallurgical structure, marine growth, water composition, temperature, extent of water movement, seabed composition and depth of burial beneath the seabed (North and MacLeod 1987:68). Collecting data necessary to characterize critical corrosion processes, building on our prior work on USS *Arizona* (Lenihan 1989) and on the Australian experience, involved evaluating each of these factors, as well as identifying additional unrecognized complex and interrelated processes that affect corrosion in many different ways. When attempting to determine the corrosion history of an object, it must be considered individually—there are very few oceanographic and environmental parameters that are uniform between sites. However, during the course of this research we sought general principles and methods that could be applied from what was learned on *Arizona* to other legacy vessels containing contaminants, which is a global problem. In addition to corrosion research, related research focused on the oil that remains trapped within *Arizona*'s hull and on the geological substrate supporting the ship.

Data collection activities were aimed at not only characterizing the active processes, but also collecting baseline data for inclusion in corrosion analysis that could be used to assess changing conditions and rates over time. These data were used to quantify various on-site conditions such as physical movement of the ship and oil release amounts. Research and monitoring activities are broken down into individual research domains discussed below. Each research domain either directly contributes to primary research goals or plays a key supporting role in project objectives. All are interconnected on some level.

FINITE ELEMENT ANALYSIS

     Principal Questions: How can the cumulative results of *Arizona* research be used for modeling and predicting long-term changes in the hull, and how and when will those changes occur? Can a predictive model be developed that will allow incorporation of new data and information? How do we validate such a model?

     Finite Element Analysis (FEA) was the principal research method used to produce the primary predictive tool that forms the centerpiece of USS *Arizona* research. A Finite Element Model (FEM) is a computer-manipulated mathematical model that calculates theoretical stresses and shape changes in a structure under load using experimental variables based on observationally-derived data. The FEM divides a complex solid into many small components called *elements*, each of which can be one of numerous simple shapes. Properties for the material of each element are input into the software to describe the element's behavior between its end (or finite) points (for example, mechanical properties, heat flow, density, etc.). The end points of each "finite" element are called *nodes*. Conditions are set regarding how nodes connect to one another and loads (known as boundary conditions) are added to the model. As each individual element changes under different boundary conditions, it transmits a slightly changed boundary condition to neighboring elements, which then repeat the process. The result are plots of displacements of nodes and calculated stresses in the structure at all points—taken in the aggregate, the displaced nodes and stresses of all the elements in the FEM offers a predictive model of stress and change under different conditions for an entire structure.

     For historical shipwrecks such as USS *Arizona,* an FEM allows manipulation of multiple variables, such as corrosion rate and hull thickness, to analyze loads and stresses on hull structure for predicting structural change, probable collapse rate, its nature, sequence and consequent impact on structures containing fuel oil. In addition, the FEM provides a fundamental tool to evaluate consequences of proposed management alternatives involving structural intervention or preservation strategies. There are particular difficulties in applying FEMs to shipwrecks, however. Geometry is constantly changing due to ongoing corrosion, loads can be very complex, and load and corrosion interact in such a way as to increase the complexity of the model (for example, stress corrosion cracking). There are ways to overcome these difficulties, but accurate data based on direct measurements and observations are of primary

importance. For the model to be representative of actual conditions, input data such as structural dimensions and connections, corrosion rates and loads must be as precise as possible.

Baseline FEM development was conducted by the National Institute of Standards and Technology (NIST) and focused on modeling the *Arizona* hull structure in its as-built original state for an 80-ft. cross-section, amidships from frame 70 to 90. The 80-ft hull length selected for initial modeling represents the sternmost area affected by the blast that sank the vessel and the ensuing fire. The reason for this selection is that it was believed to be conservative; that is, corrosion in this area would likely be highest, which would incorporate a conservative element into the model when applied to the remainder of the stern, which is in better shape. For maximum precision, the entirety of the stern must be subjected to FEA based on direct corrosion rates. Because this was pioneering research in the sense that FEA has not been applied to corrosion and deterioration of a historical shipwreck before, this preliminary model was a necessary step to refine and test methodologies for developing the overall model required for predicting present and projected future structural strength. It is important to note that the great majority of the work in creating a FEM of a structure is in the generation of the model and mesh in the computer. Remediation scenarios can then be tested and further stability studies can be made by simply changing the inputs and accounting for new measurements, ideas or to test other scenarios.

The next development stage of the FEM was to incorporate structural effects of the blast and fire that sank the vessel. Modeling the structural changes to *Arizona* resulting from the explosion and subsequent fire that sank the ship was the logical starting point for understanding the vessel's present condition and projecting its future condition and rate of deterioration. (Unfortunately, this portion of the research remains unfunded.)

The final stage of FEM development incorporated external and internal corrosion and thickness measurements to complete the model of *Arizona*'s present condition and to allow researchers to extend the model into the future. Predictions about current status and future collapse vary in accuracy depending on the detail of the input data, crafting the correct boundary conditions, and by minimizing simplifying assumptions. For the first issue, the greatest deficiency in data in this case was knowledge of the actual thickness and conditions of hull features both internally and below the present harbor bottom. All other assumptions and simplifications have a much smaller effect on the results than these data. The boundary

conditions were similarly difficult, as the hull is being supported by a water saturated semi-solid that moves relative to the hull.

As the primary "product" of the current research program, much of the data collected during field work and as a result of the ongoing monitoring was designed to be fed directly into revising and refining the FEM to make it as accurate as possible. When combined with corrosion rates and other variables, the model provides predictability required for evaluating timing, necessity and long-range consequences of management actions.

If monitoring change in *Arizona*'s structure over time conforms well with changes predicted by the FEM, researchers will have confidence in extending the model's predictions to areas of the ship (such as the lower decks) that are difficult to access directly for monitoring purposes. If monitoring changes does not accord well with the predictions of the FEM, the disjunction between real and predicted behavior will alert researchers to modify the FEM, gather new data that may have been overlooked in the initial model, or both. Beyond the course of this investigation, we anticipate a dynamic give and take between the FEM and ongoing research.

CORROSION ANALYSIS

Principal Questions: What is the nature and rate of corrosion taking place on *Arizona*? How does concretion formation affect corrosion rate? Is there a difference in corrosion rate among the 1916 steel, the 1930 refit materials, and structure affected by the blast and fires?

Corrosion research on USS *Arizona* focused on understanding and characterizing the specific nature of corrosion occurring on the vessel and determining the corrosion rate for different structural elements of the ship. The goal was to establish a curve of deterioration and "plot" where *Arizona* currently falls on that curve. The rate of corrosion is a crucial parameter necessary for making long-term predictions about *Arizona*'s structural integrity using the FEM. Because the battleship is a large, complex three-dimensional structure, and it is impossible to directly measure corrosion rates for all critical elements, (currently, there are more than 52,000 elements in the FEM) there was necessarily some generalizing and use of inferential data to derive deterioration rates, particularly for inaccessible internal structures. In addition, a comprehensive understanding of all relevant parameters, such as hull steel chemistry and

microstructure, constituent analysis of concretion covering the ship and seawater chemistry, was necessary for making indirect estimates of overall corrosion rates.

The most accurate measure of corrosion rate at our disposal was to compare current structural steel thickness with original thickness found on ship's plans, determine how much metal has been lost over a specific period of time and use the calculated corrosion rate in a linear extrapolation to determine overall corrosion rate for that particular location. Cumulative corrosion analyses ultimately may provide a more accurate variable rate. Present indications are that corrosion rates are initially high soon after submergence, and then they decrease significantly.

Although it was possible to remove some small (10 cm, 4-in. diameter) hull samples (coupons) for direct comparison, in most cases it was not feasible to take direct measurements of steel hull thickness because of the destructive nature of the process and inaccessibility of interior features. Because research on *Arizona* must be carried out in the most non-invasive manner possible, other less-destructive methods for calculating corrosion rate, including ultrasonic thickness measurements, had to be devised, some of which will rely on inferences made from the few direct measurements we had and by comparing other variables critical to the corrosion process. Because the physical environment plays such a large role in how corrosion takes place, baseline environmental data are important in general (see below), but specifically the environment at the hull/concretion interface had to be characterized since that is where corrosion occurs (Johnson et al., this volume).

Exterior Corrosion Analysis

Metallurgical and Metallographic Analysis

Metallurgical and metallographic analyses were designed to establish basic chemical, structural and strength characteristics of steel used in *Arizona*'s original 1914–1915 construction and later 1929–1931 reconstruction. Investigation of steel hull samples was a necessary step towards determining corrosion nature and rate. Analysis originally focused on steel collected from superstructure elements stored on land at Waipio Point, Hawaii that were removed from *Arizona* before construction of the Memorial began in 1960. Samples from both the 1914–1915

and 1929–1931 construction periods were analyzed by scientists from University of Nebraska, Lincoln (UNL). Tests performed include chemical constituent analysis, microstructural examination and Charpy impact testing to determine basic strength characteristics (Johnson, et al. 2000).

Additional metallurgical and metallographic analyses were performed on hull coupons collected *in situ* from *Arizona*'s hull. Four-inch (10 cm) diameter hull samples, including intact exterior and interior concretion, were removed using a purpose-built hydraulic-powered hole saw. A total of eight coupons were removed from external, vertical hull locations on both port and starboard sides. On each side, one sample was taken at the Upper Deck level, near the water line; from the Second Deck level, above the torpedo blister; from the Third Deck level, in the torpedo blister; and from the First Platform level, in the torpedo blister and below the mud line. After removal, each location was plugged using a standard plumber's plastic pipe plug and sealed with marine epoxy to prevent formation of a localized corrosion cell. UNL researchers used standard metallographic methods to examine the hull coupons to measure metal thickness at Rail Sciences Laboratories in Omaha, Nebraska (Johnson et al., this volume). Additional metallurgical and metallographic analyses on the same samples were performed by researchers from NIST.

Concretion Analysis

Fundamental research into the composition and characteristics of the concretion covering *Arizona*'s outer hull was conducted to aid in understanding the kinetics of the corrosion process on the ship and to determine how concretion chemistry correlates with hull metal loss. The hard layer of concretion that forms on iron and steel objects in seawater is a combination of iron corrosion products and marine organisms. Initial organisms are pioneering coralline algae that leave layers of calcium carbonate when they die. The calcium carbonate residue is overlaid by subsequent layers of coralline algae, and the increasing calcium carbonate layers forms a suitable substrate for secondary growth, such as soft corals and mollusks (Henderson 1989; North 1976:254). Outwardly diffusing iron ions replace some of the calcium resulting in a mix of iron corrosion products, calcium carbonate and living marine organisms covering the iron or steel object. The concretion forms a semi-permeable barrier between the bare metal and seawater and

has a significant influence on corrosion by reducing the amount of dissolved oxygen available for the corrosion reaction, increasing acidity at the metal-concretion interface and increasing the chloride ion concentration (North 1976:253).

Concretion investigation on USS *Arizona* focused on x-ray diffraction to isolate compounds that make up the concretion and environmental scanning electron microscopy (ESEM) to determine relative percentages of each element. X-ray diffraction was conducted by the Air Force Research Laboratory, Eglin Air Force Base, while ESEM analysis was completed by the Composite Materials and Structures Center at Michigan State University. Preliminary results of *Arizona*'s concretion analysis are consistent with North's (1976) findings that concretion formed on wrought and cast iron structures contains the mineral siderite, which is formed by the exchange of iron ions for calcium ions. UNL scientists researched how density and electrical resistivity of *Arizona*'s outer hull concretion could be used to characterize the corrosion process and how concretion analysis could be used to indirectly infer corrosion rates, a technique applicable to other sites.

In Situ Hull Corrosion Measurements

When iron or steel is placed in seawater, corrosion begins as a reaction in which the oxidation of metal forms the anodic portion of a corrosion cell, and the consumption of oxygen forms the reduction, or cathodic, part of the reaction. When oxidation and reduction rates are equal, there will be a voltage that characterizes the specific reaction rate (or corrosion rate)—that characteristic voltage is known as the corrosion potential (E_{corr}). In general, a more negative E_{corr} value indicates a lower corrosion rate while a more positive E_{corr} indicates a higher corrosion rate (MacLeod 1987:49-50).

In situ E_{corr} was measured on *Arizona*'s hull using a silver-silver chloride (Ag/AgCl) reference electrode giving a voltage measurement in millvolts (mV). In addition to E_{corr}, pH is another critical parameter giving an indication of corrosion, and the combined data can be directly related to appropriate Pourbaix Diagrams. The Pourbaix Diagram, a two dimensional map of E_{corr} vs. pH, shows regions of stability for corrosion products as a function of E_{corr} and pH and identifies limits for corrosion, immunity from corrosion or limits for formation of protective layers on the metal surface. Diagrams for iron/water and iron/water/CO_2 are

especially useful in characterizing corrosion processes at the steel/concretion interface and into the concretion itself (Johnson et al., this volume). In normal seawater, pH ranges from 7.5 to 8.2, but levels below 6.5 and as low as 4.8 are found under concretion covering actively corroding metal. Lower pH levels (more acidic) typically characterize increased corrosion levels (North and MacLeod 1987:74).

$\qquad$*In situ* corrosion measurements taken systematically along *Arizona*'s hull included pH and E_{corr}. At selected stations on the vessel, pH and E_{corr} was measured at various concretion-depths using pH and Ag/AgCl reference electrodes inserted into holes drilled into the concretion. Hole depths were controlled by several depth jigs to provide uniform data through levels of concretion to the metal surface. Multiple samples were drilled in a vertical transect at each station at varying water depths to characterize how the corrosion process changes with water depth and concretion thickness. In addition, these data were compared over multiple field seasons. Correlation of E_{corr} with corrosion rate was also examined (Johnson et al., this volume).

$\qquad$Another critical *in situ* measurement of USS *Arizona*'s hull included ultrasonic thickness measurements. The eight hull coupons collected in two vertical transects on *Arizona*'s hull provided an empirical measure of corrosion rate at each of these locations when compared to as-built hull thicknesses. Because of the invasive nature of collecting hull coupons, however, it was necessary to develop a more non-invasive technique to expand hull thickness data. Because the specific metal thickness was precisely measured at the eight coupons locations, they provided an excellent control for testing ultrasonic thickness techniques and instruments. Corrosion pits on the interior and exterior of *Arizona*'s steel plates made ultrasonic measurements of plate thickness impractical with current technology, and ultimately, other methods, including corrosion rate based on concretion parameters, proved more reliable.

Interior Corrosion Analysis

$\qquad$Analysis of the nature and rate of interior corrosion on USS *Arizona* was limited to indirect measurements of environmental parameters and E_{corr}, subjective observation of interior conditions based on images taken by a VideoRay remote operated vehicle (ROV), and experimental evaluation of ultrasonic thickness techniques using the ROV as an instrument platform. With no diver access to the inside of *Arizona*'s hull, interior data could only be

collected remotely. The VideoRay ROV was the primary tool used for collecting internal data.
It was used as an instrument platform to carry a YSI 600XLM Multiparameter Sonde to measure
pH, temperature, salinity, dissolved oxygen, oxygen reduction potential and conductivity—the
same parameters being recorded externally (see below). The ROV also carried a GMC
STAPERM silver-silver chloride reference electrode to measure interior E_{corr}. An evaluation was
made for use of an ROV-mounted Cygnus Ultrasonic Thickness Gauge to measure interior
bulkhead thicknesses, but this technology did not prove suitable for this application.

OIL ANALYSES

Principal Questions: What is the nature of *Arizona*'s oil? How and at what rate does it
degrade? What is its impact on the immediate environment of the ship? Is there a "fingerprint"
that distinguishes *Arizona* oil from others? How do we measure oil leak volume?

Analysis of oil leaking from *Arizona*'s hull and trapped in accessible overhead spaces
was designed to collect baseline data about the approximately 500,000 gallons of Bunker C fuel
oil still remaining within the battleship. It was also used indirectly to investigate the condition of
interior oil bunkers. Collaborative research focused on using oil characterization to measure
environmental degradation of oil trapped within different areas of *Arizona*'s hull. Oil constituent
degradation, laboratory determined, proved a useful chronometric tool. The degradation of oil
was used to determine residence time of each oil cache by determining the length of time each
oil release has been in contact with seawater. Medical University of South Carolina (MUSC)
researchers analyzed oil samples using gas chromatography coupled to mass spectrometry in
order to assess the environmental weathering of the oil and to obtain a "fingerprint" of the oil
leaking from the ship by examining the biomarker profile. While Bunker C is susceptible to
biotic and abiotic weathering processes in the environment, it tends to be persistent due to the
increased concentration of high molecular weight hydrocarbons. Using gas chromatography-
flame ionization detection (GC-FID) and gas chromatography-mass spectrometry (GC-MS) to
chemically characterize oil leaking from different regions of the ship, researchers determined
that oil leaking near Barbette No. 4 showed almost no detectable signs of weathering, while oil
trapped in Second Deck overheads and leaking from other locations were depleted of *n*-alkanes
and low molecular weight polycyclic aromatic hydrocarbons. Results of analyses could

differentiate individual oil bunkers, as well as differentiate age of oil (relative to sea water exposure) in cabin overheads and being released from various locations around the battleship. These data have important implications for structural analysis and inferring structural change in the inaccessible interior. This approach provided indicators about the state of deterioration and structural changes of oil bunkers that are inaccessible in the battleship's lower deck areas.

In addition to baseline oil analysis, on-going monitoring is being conducted to measure the amount of oil escaping from the ship at several locations. Using a custom-built oil collection device, researchers periodically capture all oil escaping from each location around *Arizona*'s hull during a 24-hour collection period. This quantifies the leakage rate for long-term monitoring to see whether oil leakage from specific locations is stable or increasing. Currently, we are collaborating on development of a remote oil monitoring system that can quantify the total amount of oil being released in real-time, as well as variations in oil release rates that may correlate with changing environmental conditions, changing hull structure or both.

MICROBIOLOGY

Principal Questions: What microbially induced corrosion is taking place in *Arizona*'s interior and exterior areas, and what is the impact on structural deterioration? Can laboratory experimentation model microbially induced corrosion on the oil/bunker interface?

Microbiological analyses were pursued for several purposes. One of the main applications was to examine the role of microbially induced corrosion (MIC) in the degradation of *Arizona*'s oil bunkers. Biofilms are communities of microorganisms attached to an interface and embedded in a polysaccharide matrix produced by the microorganisms. They are ubiquitous in nature and are a common cause of corrosion. The depletion of oxygen from microhabitats within biofilms has important consequences for the corrosion of metals. Anaerobic conditions can result in the growth of sulfate-reducing bacteria (SRB), a frequent cause of MIC. Metal corrosion is driven by the hydrogenase activity of the SRB. Harvard University researchers experimentally determined the ability of hydrocarbon degrading microorganisms isolated from USS *Arizona* to degrade steel. The objective was to determine the rate of corrosion in the oil-containing bunkers in USS *Arizona*.

In addition to research into MIC, other microbiological investigations were carried out on USS *Arizona*. MUSC scientists developed innovative research to examine the role of microorganisms in fuel oil degradation and the aerobic biodegradation potential of microorganisms associated with the battleship's hull (Figure 2.5). They used denaturing gradient gel electrophoresis (DGGE) analysis to examine the microbial community structure of oil-degrading microorganisms from sediments adjacent to the USS *Arizona* that use oil leaking from the ship as their sole source of carbon. The biodegradation potential of these microbial communities was demonstrated by the extensive degradation of polycyclic aromatic hydrocarbons from Bunker C crude and produced a novel pattern of biomarker degradation.

GEOLOGICAL ANALYSES

Principal Question: How stable are the sediments upon which *Arizona* rests?

The U.S. Geological Survey (USGS) conducted an analysis of the geological substrate surrounding and beneath USS *Arizona* to determine its nature and characteristics. The basic question investigated was how stable are supporting sediments beneath the battleship, and is it possible *Arizona* is experiencing movement due to shifting or compressing sediments? *Arizona*'s overall stability within its supporting matrix is important because it can potentially affect GPS structural monitoring and the FEM. To be accurate, interpretation of GPS monitoring-point movement and predictions regarding structural stability, such as those produced from an FEM, must control for geological support variables. If movement is observed in GPS monitoring, it would be necessary to isolate potential internal changes (shifting, settling and collapsing decks and internal bulkheads) from external movement (the entire ship settling into surrounding sediments). In addition, the FEM had to take into account sediment characteristics surrounding and supporting *Arizona*'s hull, including potential differential support, to give an accurate indication of the vessel's overall structural integrity.

To conduct a comprehensive analysis of the geological substrate around USS *Arizona*, researchers used a combination of geophysical remote sensing and geotechnical analysis of recovered 15-m (50-ft) cores. Stratigraphic description and geotechnical analysis of cores recovered from around *Arizona* provided data about sediment consolidation, compression properties and triaxial shear strength of distinct strata beneath the seabed. Chirp seismic

reflection data collected in a wide area surrounding *Arizona*, combined with precise correlation of sub-bottom records to geological core analysis, extend these geotechnical properties to the subsurface geological strata of Pearl Harbor surrounding the battleship. The combination of these data gave an overall indication of how stable *Arizona* is within its supporting geological matrix.

ENVIRONMENTAL PARAMETERS

Principal Questions: What is the nature of the interior and exterior environment of *Arizona*? How is *Arizona*'s environment changing? How does it affect *Arizona*'s deterioration?

A variety of factors have been identified that directly influence metal corrosion on shipwrecks, including water composition (dissolved oxygen, pH, salinity and conductivity), temperature and extent of water movement (North and MacLeod 1987:68).

Oxygen reduction is typically the main cathodic reaction occurring in steel exposed to seawater, so dissolved oxygen availability at the cathodic site controls the corrosion rate, with higher dissolved oxygen content resulting in higher corrosion. Water at the ocean's surface is generally oxygen-saturated, so overall dissolved oxygen content depends on the amount of mixing that occurs with surface water—increased water movement and mixing results in elevated dissolved oxygen levels. In addition, temperature and dissolved oxygen are inversely proportional, so lower temperature results in increased dissolved oxygen. The pH level is indicative of overall corrosion activity. In normal seawater, pH ranges from 7.5 to 8.2, but levels below 6.5 are found under concretion covering actively corroding metal. Lower pH levels (more acidic) typically characterize active or increased corrosion levels. Salinity is closely related to the corrosion rate of steel in water, so increased salinity usually results in higher corrosion rates. This is evident when comparing metal preservation in freshwater compared to seawater environments—freshwater lakes invariably lead to better preservation of iron and steel. There are several ways that higher salinity affects corrosion, including dramatically increasing conductivity (which facilitates movement of ion between anodic and cathodic areas), increasing dissolved oxygen and supplying ions that can catalyze corrosion reactions, among others (North and MacLeod 1987:74). Higher conductivity can increase corrosion by increasing the movement of ions during the corrosion process.

In general, corrosion increases as temperature increases. Under controlled laboratory conditions, corrosion rate doubles for every 10°C rise in temperature. This relationship is complicated, however, by the effect of temperature on both dissolved oxygen and biological growth. Warmer water supports increased marine growth, which contributes to concretion formation on steel in seawater and that, in turn, generally reduces corrosion rates. In addition, as discussed above, lower temperature results in higher dissolved oxygen content, which consequently means increased corrosion (North and MacLeod 1987:74).

Water movement from waves and currents on a site affects corrosion in several ways, but generally high-energy environmental conditions results in higher corrosion rates. Active water movement can contribute to mechanical erosion of metal surfaces and can also impede development of protective concretion layers by removing accumulating ions before they can precipitate and begin the concretion formation process. Waves and currents also contribute to water mixing and aeration that result in increased dissolved oxygen levels (North and MacLeod 1987:74).

Factors that affect corrosion on metal shipwrecks are complicated and interrelated. Reducing one key factor can increase another, and the results are often unpredictable. It is clear, however, that in order to understand the corrosion history of an object, even a complex object like a World War II battleship, and to begin to define the nature and rate of deterioration affecting the object, an understanding of the various environmental factors at play is necessary. An important aspect of the current research program was long-term monitoring of oceanographic and environmental parameters on USS *Arizona*. This was accomplished with *in situ* multiparameter instruments placed on the hull and on the seabed to the side of the vessel.

Exterior Environment

The USGS analyzed data from oceanographic and water-quality monitoring instruments placed on and near *Arizona* to determine long-term, seasonal variability in key parameters that affect corrosion. Researchers calibrated and deployed a SonTek Triton wave-height and current meter and a YSI 6600 Multiparameter Sonde on *Arizona* in November 2002. These instruments have internal memory and batteries and can be left *in situ* for up to 60 days, recording data multiple times an hour. The instruments were retrieved and downloaded, then recalibrated and

deployed every 60 days by USAR staff. The data were sent to the SRC in Santa Fe, New Mexico, and the USGS in Santa Cruz, California, for compilation and analysis. The instruments collected baseline data including wave height and direction and current velocity and direction around the vessel, and basic environmental parameters including pH, temperature, salinity, dissolved oxygen, oxygen reduction potential and conductivity. The goal was to collect at least a two-year database to discern seasonal variation and patterns of environmental parameters within Pearl Harbor. In addition, USGS researchers deployed two RD instruments 600 kHz Acoustic Doppler Current profilers (ADCP), which collected three-dimensional vertical profile measurements of current speed and direction, single-point measurements of water temperature, and water level data, for a 30 day period in 2005. As discussed above, each of these parameters can affect corrosion rates on the ship.

Interior Environment

Environmental monitoring was also conducted within *Arizona*'s interior cabins to determine internal environmental conditions. Internal conditions were compared to external conditions in an attempt to infer interior corrosion nature and rate. These data were critical to developing a viable FEM that takes into account both interior and exterior hull corrosion. SRC used a VideoRay ROV equipped with a YSI 600XLM Multiparameter Sonde to measure pH, temperature, salinity, dissolved oxygen, oxygen reduction potential and conductivity—the same parameters recorded externally. Initial investigations focused on second deck cabins accessible via open portholes, as well as inside Barbette No. 3. Subsequent investigations recorded environmental parameters in Third Deck spaces—although very few of these areas were accessible to the ROV. Data from both external and internal environmental monitoring was assessed, and the results were factored in developing the *Arizona* FEM.

<div align="center">STRUCTURAL STABILITY DETERMINATION</div>

Principal Questions: How stable is *Arizona*'s hull? How can we measure structural changes?

Monitoring observable changes to USS *Arizona*'s accessible external areas was designed to allow researchers and managers to quantify physical changes to *Arizona*'s fabric. As internal and external structures corrode and weaken, various parts of *Arizona*'s hull may experience shifting, settling or collapse. Since a regular NPS presence on *Arizona* began in 1982, a qualitative assessment by researchers indicated that Upper Deck areas in and around the ship's galley show signs of change—widening cracks and some deck collapse is occurring. At present, measurable change has only occurred to non-structural portions of the vessel—"non-structural" in the sense that Upper Deck areas do not contribute to the battleship's overall structural integrity, especially oil-containing structures. Most Upper Deck structures were removed from *Arizona* before construction of the Memorial, which spans the ship just aft of the galley area. Regardless, active monitoring of the entire ship, including these Upper Deck areas, is ongoing still to watch for evidence of significant structural changes.

External Stability

The primary method used to monitor physical changes to USS *Arizona*'s hull is a series of discrete real-world positions on the ship whose coordinates are derived using very high-resolution Global Positioning System (GPS) instruments. Using dual-frequency GPS receivers, researchers have set a series of monitoring points across *Arizona*'s exposed decks. Initially using stainless steel studs, later changed to PVC disks, in selected locations, NPS surveyors leveled a large, purpose-built underwater tripod over each point (Figure 2.6). Extension poles set on top of the tripod extending above the water's surface allowed the GPS antenna to be placed precisely over the desired point. Using advanced survey techniques, each point was collected with sub-centimeter accuracy in three dimensions. These points were, and continue to be, re-surveyed every two years to determine if, and how, the ship is moving, shifting, or settling. Although the accuracy of each point was mathematically calculated to about 0.5 cm (Circle of Error Probable), it will be necessary to apply a more conservative threshold of change to future monitoring re-occupations. Because of environmental conditions and differences in equipment and stadia variations, a more realistic threshold is 10 cm. Instrument error, set-up error, or most likely, nearly imperceptible antenna movement caused by water movement can create cumulative errors of up to 10 cm. Consequently, we cannot reliably attribute any observed change that is less than

10 cm to vessel movement; however, corroborative evidence would be sought for any level of change. Because the GPS points exist as a network of positions, aggregate changes in the positions of more than one point, even if less than 10 cm, could potentially indicate net movement of hull structure.

In addition to GPS, structural changes were also monitored using a series of crack monitors normally employed to measure how cracks are widening on historic building walls. These plastic monitors were affixed over numerous cracks in the Upper Deck galley where *Arizona*'s deck collapse was qualitatively observed. The crack monitors were checked periodically to see if the cracks were widening or shifting.

Internal Stability

Internal structural monitoring of USS *Arizona* was a qualitative process using the VideoRay ROV to visually examine interior areas and note observable changes over time. Interior investigation took place over multiple years in all accessible areas for measuring and monitoring interior environmental factors and corrosion parameters. During this process, overall internal structural condition was observed and noted.

CONCLUSION

This research approach for USS *Arizona* and USS *Utah* was designed to produce cumulative data whose synthesis will inform management actions to preserve the vessel for future generations. We believe this experimental approach has produced results that will contribute to the disciplines involved and be applicable to numerous iron and steel legacy vessels submerged worldwide. This research partnership for the Pearl Harbor vessels is an example of government agencies, academic institutions, military commands and private institutions working together effectively for public benefit. This collaboration is a model for combining public and private resources to cost-efficiently address issues important to the American people.

REFERENCES

Henderson, S.
    1989 Biofouling and Corrosion Study. In *Submerged Cultural Resources Study: USS Arizona Memorial and Pearl Harbor National Historic Landmark*, edited by D. J. Lenihan, pp. 117-156. Submerged Resources Center Professional Papers No. 9. National Park Service, Santa Fe.

Johnson, D. L., W. N. Weins and J. D. Makinson
    2000 Metallographic Studies of the U.S.S. Arizona. In *Microstructural Science Vol. 27: Understanding Processing, Structure, Property, and Behavior Correlations*, edited by W. N. Weins, pp. 85-91. ASM International, New York.

Lenihan, D. J. (editor)
    1989 *Submerged Cultural Resources Study: USS Arizona Memorial and Pearl Harbor National Historic Landmark*. Submerged Resources Center Professional Papers No. 9. National Park Service, Santa Fe.

MacLeod, I. D.
    1987 Conservation of Corroded Iron Artifacts – New Methods for On-Site Preservation and Cryogenic Deconcreting. *International Journal of Nautical Archaeology and Underwater Exploration* 16(1):49-56.

North, N. A.
    1976 Formation of Coral Concretions on Marine Iron. *International Journal of Nautical Archaeology and Underwater Exploration* 5(3):253-258.

North, N. A. and I. D. MacLeod
    1987 Corrosion of Metals. In *Conservation of Marine Archaeological Objects*, edited by C. Pearson, pp. 68-98. Butterworth & Co., London.

Russell, M. A. and L. E. Murphy
    2003 *"Long-Term Management Strategies for the USS Arizona: A Submerged Cultural Resource in Pearl Harbor, Hawaii." Legacy Resources Management Fund Project No. 02-170: 2002 Annual Report*. Submerged Resources Center Technical Report No. 14. National Park Service, Santa Fe.

    2004 *"Long-Term Management Strategies for the USS Arizona: A Submerged Cultural Resource in Pearl Harbor, Hawaii." Legacy Resources Management Fund Project No. 03-170: 2003 Annual Report*. Submerged Resources Center Technical Report No. 15. National Park Service, Santa Fe.

Russell, M. A., L. E. Murphy, D. L. Johnson, T. J. Foecke, P. J. Morris and R. Mitchell
    2004 Science for Stewardship: Multidisciplinary Research on USS Arizona. *Marine Technology Society Journal* 38(3):54-63.

CHAPTER 3

Historical Record: USS *Arizona* Battle Damage and Salvage

Larry E. Murphy and Matthew A. Russell

INTRODUCTION

Examination of primary documents about USS *Arizona*, particularly post-sinking salvage, was planned as part of the initial research design of the USS *Arizona* Preservation Project for a number of reasons. Several aspects of the ship's history have direct impact on a number of research domains, especially those regarding metallurgical analyses and corrosion characterization. The ship, launched June 19, 1915, underwent a major refit in 1929–1931 (Lott 1978:21-37) (Figure 3.1). The ship suffered high explosive blast effects on December 7, 1941, and it burned intensely for two days before oil and explosives fires could be extinguished. It is important to the research questions to distinguish locations of blast and fire impact on the physical structure. This impact must also be incorporated into the primary product of the USS *Arizona* Preservation Project, which is the Finite Element Model (FEM, see Chapter 6) being developed to provide the predictability requisite for management decisions about the ship. To develop both an accurate and conservative predictive model of *Arizona*'s deterioration, we had to be certain about which metallurgical samples to collect and analyze and where to take corrosion readings and understand their implications for inclusion in the FEM. Because it was impractical to initially model the entire remainder of the hull, a portion of the hull was selected to develop

the FEM to test the process and to establish a likely curve of deterioration of the remaining intact hull. In the long-term, an FEM will be required for the entire ship that incorporates cumulative corrosion and experimental data relevant to hull deterioration. Analysis of historical documents describing *Arizona*'s hull damage soon after the attack and what salvage activities were conducted is discussed in this chapter. These historically based factors have been incorporated into both the sample design and in the FEM. They will also be important to developing the future complete-hull FEM.

ARIZONA'S CONDITION BEFORE AND DURING THE ATTACK

It is critical to know what *Arizona*'s condition was at the time of the attack on December 7, 1941. Two aspects are of primary interest: the amount of fuel aboard and the status of hatches and passageways in the hull.   The former is necessary to develop an estimate as to the amount of oil that may remain on the site, and the latter addresses ease of access of interior spaces for measurement, monitoring or physical intervention within the hull. As a matter of National Park Service (NPS) policy, because of the status of *Arizona* as a war grave and National Historic Landmark, and also as a matter of safety, no divers entered the hull during this research project. All interior examination and data acquisition was by a VideoRay Remotely Operated Vehicle (ROV).   The nature of the blast in the forward portion of the ship is also discussed here.
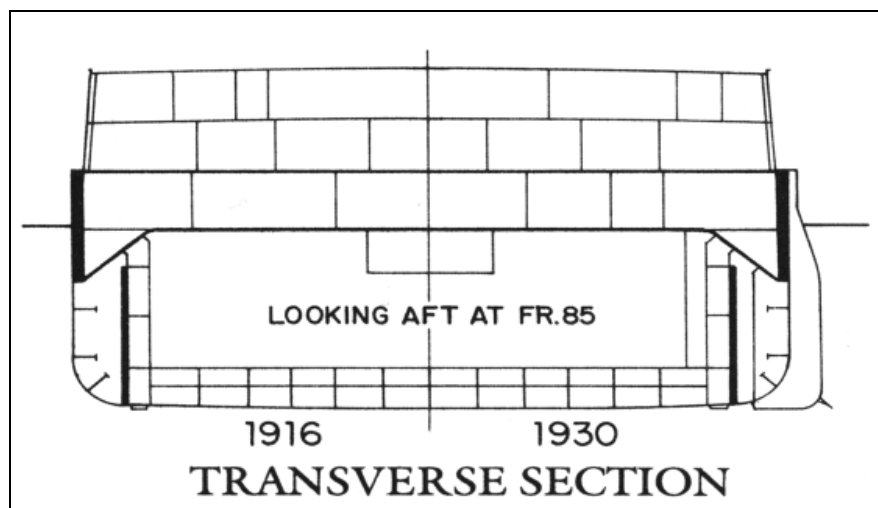
Figure 3.1. Transverse sections showing some of the structural changes to *Arizona*'s hull during 1929-1931 refit (USS *Arizona* Memorial Archives).

ESTIMATE OF OIL CONTAINED IN *ARIZONA*'S HULL

We have not located documents that indicate the amount of fuel Arizona had on board at the time of the attack. The statement by Commander Homann (1942a:2) "The outboard fuel oil tanks were filled to ninety-five percent capacity in the area of the possible torpedo hit" indicates the vessel may have been near emergency capacity.

Before the attack, *Arizona*'s draft forward was 32 ft. 6 in., while aft it was 33 ft. (Homann 1942a:1: Geiselman 1941:1). Draft measurements obtained just prior to the attack inform about the status of fuel that was aboard *Arizona* at the time of the attack.

The specific gravity of Bunker C No. 6 Fuel Oil is approximately 0.95, the higher end of the range for petroleum products. The common conversion factor for petroleum hydrocarbons of 294 gallons per ton is derived from an average specific gravity of 0.83. (National Research Council 2003:189-190). However, using the actual specific gravity for Bunker C of 0.95, Bunker C weighs about 7.6 lbs. per gal., and there would be only 263 gal. per ton. The latter figure is used here for *Arizona* oil calculations. The full load draft for the ship was 30 ft. 1¾ in. with a 4,630-ton normal load of fuel oil; emergency load draft was 33 ft. 3 in. with emergency load of fuel of 6,180 tons (Lott 1978:50). According to the battle reports, *Arizona*'s draft was about 33 ft. (Homann 1942a:1: Geiselman 1941b:1), which indicates nearly a full emergency load of fuel. An estimate of 6,000 tons of fuel aboard *Arizona* equals approximately 1,578,000 gal. An early estimate of *Arizona* hull damage after the attack indicated about 40% of the aft portion of the hull was intact (Commander Base Force to Commander in Chief, Pacific Fleet December 28 1941:6), which would extend damage aft to about frame 85 (which correlates well with other estimates, for example Geiselman 1941:1, who estimated the ship was destroyed forward of frame 88). This is somewhat less than divers' reports of the ship being intact aft of frame 70 (but that the main deck was buckled forward of frame 88). Assuming, however, the 40% estimate correct, it would be reasonable to estimate perhaps 40% of the original oil bunkers would remain undamaged to a point sufficient to contain oil. This means a reasonable estimate of the maximum oil remaining aboard *Arizona* is about 630,000 gal., or about 2,400 tons, less what has leaked since the vessel sank.

There is no direct mention of fuel oil fuel removal operations on *Arizona* in the original salvage documents reviewed so far. However, Commander Homer N. Wallin, who relieved

James M. Steele's command of the Pearl Harbor salvage operations January 9, 1942 and held that position until salvage operations were complete, reported in a summary of the salvage operations (1946:29) that "Fuel oil also was a most valuable commodity and a source scarce article in the spring of 1942. Accordingly, a large amount of oil was pumped from the intact oil tanks of these vessels [*Arizona* and *Utah*], and about a million gallons was recovered from the *Oklahoma*." Certainly, not all, if any, fuel oil was removed; both *Arizona* and *Utah* continue to leak as they have since the attack. In his later volume, Wallin (1968:268) does not mention oil removal from *Arizona*'s intact tanks, only that "the oil which fouled the harbor was gradually removed as it was released from the ship's opened tanks." Further historical research is required to verify oil removal from these vessels and the quantity recovered during salvage operations.

<div align="center">*ARIZONA*'S HULL CONDITION AT THE TIME OF ATTACK</div>

   Arizona's acting commanding officer A.J. Homann responded to queries from the Chief of Naval Operations regarding the condition on *Arizona* during and after the attack (Homann 1942b). The following discussion is from that document. Homann's response to Chief, Naval Operations was generated from interviews with survivors. At the time of his statement, January 28, 1942, divers had only investigated the main and second deck, so survivors' accounts were used to augment direct diver observations. At the time of the attack, all "X" (or "X-ray") doors and fittings were closed, due to the previous night's establishment of Material Condition X-Ray. Many of the engineering spaces, those not actually being used, were in Condition "Z" (or "Zed") and locked. This included the shaft alleys, engine rooms, firerooms, but not the dynamo, evaporators, and ice machines. The attack was so sudden, with the explosion of the forward magazine occurring so soon after the attack began, that little time was available for securing Condition Zed in those areas not already secured.

   Material Condition X-Ray was the damage control condition in peacetime, when steaming in time of war when attack was improbable or unlikely, or when in port where danger from torpedoes, bombs and mines existed. Condition Zed was to be immediately deployed upon sounding of "general quarters" (Madsen 2003:69). Condition X is the minimum safety condition, while Condition Z is the battle closure condition, and Condition Y is between the two (Wallin1968:125).

In a separate correspondence to the Chief, Bureau of Ships, Homann (1942a:2) states: "The ship, at the start of the attack, was in material condition X-ray with usual water-tight doors closed below the third deck, except air ports above the water-line were open. Material Condition Zed had been partially set during the action before the ship was destroyed."

Turrets 3 and 4 were mostly secured in Condition Zed. Because there were no survivors from turrets 1 and 2, there is reason to believe they were in the same condition. Ensign Flannigan (1941:1) reported that the lower room of turret 3 was in Condition Zed. Geiselman (1941:2), *Arizona*'s first acting captain after the attack, reported that the after magazines were voluntarily flooded during the attack.

The boiler division and "B" part of the ship below the third deck was probably in Condition Zed shortly after the attack began. From survivor accounts, "it is fairly certain that Condition Zed was not completely set on the third deck and probably most of the armored hatches were still open" (Homann 1942b:1-2). Homann also states: "an early bomb hit down the stack disrupted the fire main and bilge pumps and there was no water with which to fight the fires." He also noted that survivors' statements indicated that the flooding was general after the magazine explosion, and the water filled Turret 4 at a very rapid rate, which would not occur had Condition Zed been fully secured; all watertight doors would have been sealed.

FORWARD MAGAZINE EXPLOSION

Arizona Acting Commander E.H. Geiselman reported that: "Apparently one large, possibly 2,000-lb, armor-piercing bomb hit forecastle by No. 2 turret, which it is believed penetrated to the black powder magazines, setting off the smokeless powder magazines adjacent and causing the explosion which destroyed the ship forward" (Geiselman 1941) In a later assessment after extensive diving operation on the ship, including an attempt to investigate the path of entry of this bomb, the Commandant of the Pearl Harbor Navy Yard stated that the bomb was reported to have struck the ship near turret No. 2. However, his speculation based on the greater structural damage forward of turret No1, particularly on the port side, was that the bomb may have penetrated on the port side (Paine 1943:2).

In order to model the detonation of the forward magazines and its impact on the hull, an estimate of the munitions contained in the forward portion of the hull is necessary. In the 1913

specifications for No. 39, later BB 39, USS *Arizona*, ammunition stowage requirements (Navy Department 1913:210-212) listed 1,300 14-in. amour piercing projectiles, at 1,410 lbs. apiece. The stowage required for the 14-in. powder charges, smokeless powder packed in 500-lb. powder tanks, was for 1,300 powder charges, or 250 lbs. of powder for each projectile. There is no listing for 14-in. explosive charges to initiate the smokeless powder, although they would be required. The 1913 specifications call for stowage for 5,000 40-lb. tanks of 5-in. powder for 5,000 5-in. projectiles and for 3,400 lbs. of saluting powder, assumed to be black powder, packed in 17 200-lb. powder tanks. In 1916, *Arizona* carried 22 5-in. guns, in 1941, 18 were carried (Lott 1978:51).

In analyzing the forward magazine explosion, Lott (1978:43) quotes from an October 1943 letter that *Arizona* had on board its full complement of smokeless powder in six magazines between frames 31 and 48 on the first platform (Figures 3.2 and 3.3). There was also 1,075 lbs. of black powder in the black powder magazine, which was also stowed on the first platform, centerline between frames 37–39 (Figure 3.2) between the six smokeless powder magazines. Close to the black powder magazine is the small arms locker (Figure 3.2).

The only document located that discusses the amount of powder in the forward magazines was by R. W. Paine, Commandant of the Pearl Harbor Navy Yard (Paine 1943:2-3) His account was developed from conversations with personnel attached to the ship at the time of the attack:

> (1) 308 – 14" shells in each turret, Nos. 1 and 2, on turret shell decks and in handling rooms, 1st platform.
>
> (2) 616 cans of smokeless powder for each turret, Nos. 1 and 2, distributed in six accommodating magazines, A-424-M, A-420-M, A-414-M, A-13-M, A-421-M and A-423-M 1st platform.
>
> (3) 25 – 25# cans and 150 – 3# charges of black powder between Nos. 1 and 2 turrets in the black powder magazine A-415-Mm 1st platform.
>
> (4) 3,400 cans of 5" – 51 caliber smokeless powder in the 5" magazines forward. Powder about equally distributed between magazines on 1st and 2nd platforms, A-432-M, A-431-M and A-324-M.
>
> (5) Approximately 300,000 rounds 50 caliber AA ammunition in forward 50
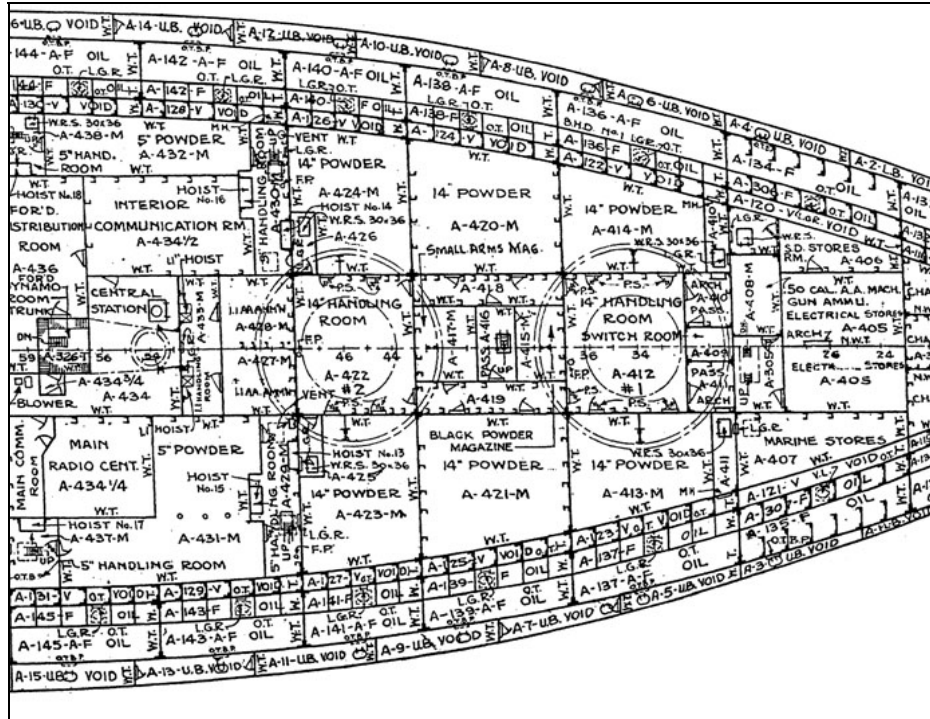
Figure 3.2. *Arizona* blueprint of forward magazines on first platform deck (USS *Arizona* Memorial Archives).
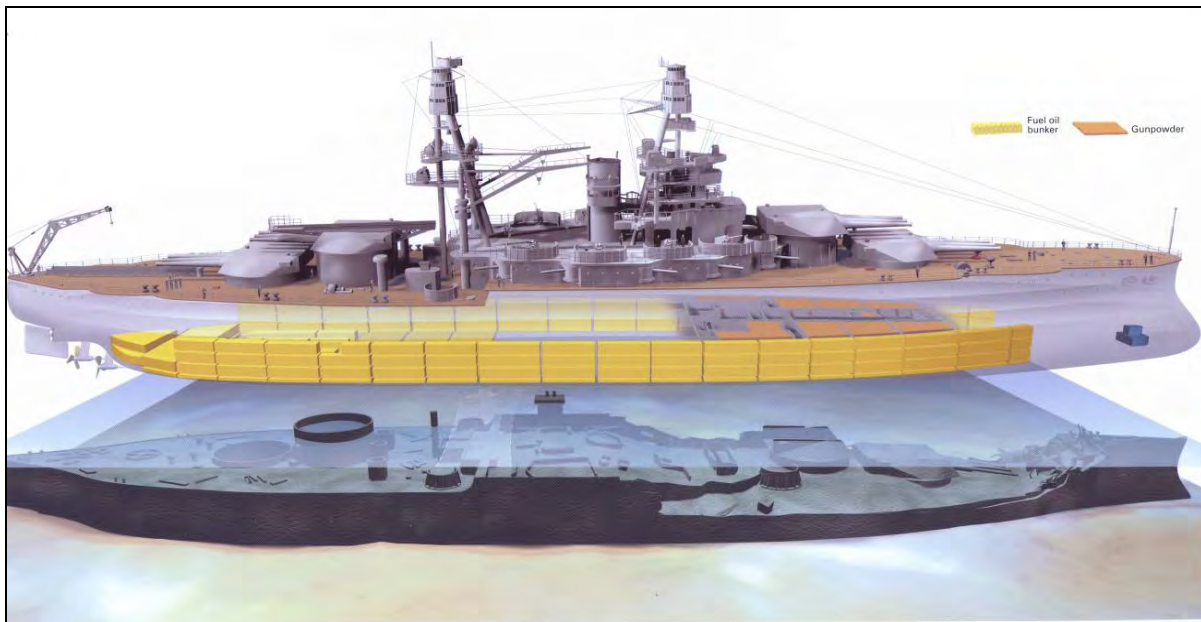
Figure 3.3. Graphic of *Arizona* showing oil bunker and forward magazine locations in relation to hull damage mapped by SRC in the 1980s (Graphic by National Geographic Society).

caliber magazine, A-408-M.

(6) Approximately 3,500 – 5" 51 caliber projectiles in ammunition passages amidships, B-504-m and B-505-M, 3rd deck.

(7) Small arms ammunition, approximately 100,000 rounds of 30 caliber, 5,000 rounds of 45 caliber, and 1,000 service primers, in A-417-m, 1st platform.

(8) 75 – 14" Primers in each turret, Nos. 1 and 2, gun chamber

(9) 50 electrical detonators in trunk A-511-2-T, third deck.

In the *Arizona* ballistic data supplied by Lott (1978:51), 14-in. firing charges for 1941 were 420 lbs., each requiring a 31.5-lb. explosive charge and primer. *Arizona* was carrying 616 shells and "616 cans of smokeless powder." The weight of 14-in. powder cans is not given by Paine, but they must have minimally been 420 lbs. for a total of 258,720 lbs. or 129.4 tons of smokeless powder in the forward magazines and 19,404 lbs. or 9.7 tons of explosive charge and an unknown number of primers for a total of 139.1 tons of 14-in. powder in the forward magazines. Paine (1943) reported 1,075 lbs. of black powder in 25 25-lb. cans and 150 3-lb. cans.

Originally, *Arizona* mounted 22 5-in./51 caliber guns, and specified 5,000 rounds. In 1941, these guns were reduced to 10 with 8 5-in./25 caliber dual purpose guns added (Lott 1978:30), giving a total of 18 5-in. guns. Each 5-in. round required about 25 lbs. of powder and a 2-lb. explosive charge (Lott 1978:51). Paine does not give the weight of the 1941 5-in. powder cans, but in the 1913 *Arizona* stowage weight specifications (Navy Department 1913:211) it lists these cans as 40 lbs. Lott (1978) indicates 5-in./51 caliber guns required a 24.5-lb. firing charge and a 2.04-lb. explosive charge per shot. Assuming the 3,500 5-in. powder cans were 40 lbs., there would have been 140,000 lbs. of 5-in. powder, or 70 tons. This is sufficient for 5,714 5-in. rounds, which would require 11,657 2.04-lb. explosive charges. Paine (1943) does not mention these charges in his listing, but there would have been sufficient explosive charges to fire each round, which adds another 23,780 lbs. or 11.9 tons of powder for an estimated total of 81.9 tons of 5-in. explosives stored in the three forward 5-in. magazines.

In addition to the large gun munitions, there were 100,000 50-caliber rounds and 6,000 rounds of small arms ammunition located in the small arms magazine forward on the first platform. A .50 caliber powder charge is about 230 grains or about one-half ounce of powder,

for a total powder weight for the .50 caliber ammunition of 3,125 lbs. or 1.6 tons of powder. Cumulatively, we estimate there was minimally about 222.6 tons of powder involved in the detonation of the forward magazines, primarily 14-in. and 5-in. smokeless powder and primary explosive.

There is no question that the smokeless powder in the forward six magazines were sympathetically detonated, either by the armor piercing 700 kg bomb's 70-lb. bursting charge or by a topside fire setting off the black powder magazine, which in turn detonated the smokeless powder. The actual detonation chain will likely never be known, and there are several theories, some still actively debated, about what occurred (for example, see Stillwell 1991:274-278). In any case, the detonation of the forward munitions, however devastating, was incomplete. Five-in./51 caliber powder cans were found on Ford Island 350–400 ft. off *Arizona*'s starboard side (Lott 1978:43); unburned 14-in powder grains were found on the quarterdeck of the USS *Tennessee* moored forward of *Arizona*, a distance of 400 ft. and 500 ft. from shore on Ford Island, a distance of 900 ft.; exploded 5-in. powder cans were found along the beach on Ford Island a distance of 350-400 ft., (Paine 1943:4); and 50-caliber rounds remain in the forward bow area.

Paine (1943:3) described the forward magazine explosion:

It appears the explosion in the forward magazines was vented through the sides of the ship from about Fr. 10 to about FR. 70 and upward through the decks forward of turret #1. Due to the general extent of interior damage between Frs. 10 and 70, it is difficult to determine the exact magazines in which high order detonation took place, although the more severe damage is between about Frs. 10 and 33.

USS *ARIZONA* BATTLE DAMAGE

By the afternoon of December 7, USS *Arizona* was determined to be a total loss. The Navy Yard's Planning Section was informed that *Arizona* was: "broken in half and burning. Completely submerged except for the two aft turrets and tripod mast. No job orders issued" (Summary of Damage Reported to Planning Section, Dec. 7, 941), which indicated nothing could be done for the ship. In a memorandum from USS *Pennsylvania*, the flagship, sent by Cmdr,

Homer N. Wallin, Battle Force Material Officer, at 1345 December 7, he states: "The *Arizona* is a total wreck, she is resting on the bottom without much list, and is still burning forward. The foremast has fallen forward about 45°" (Wallin 1941:1)(Figures 3.4 and 3.5). *Arizona*'s hull was reported to have settled for days (Madsen 2003:81), releasing air bubbles from the interior. In Memorandum No. 7, December 9, 1941, from the United States Pacific Fleet Battle Force, USS *California*, Flagship, *Arizona* and *West Virginia* were declared "total wrecks" (p.3).

By December 28, 1942, in a memo from Commander Base Force to Commander in Chief, Pacific Fleet (Commander Base Force to Commander in Chief, Pacific Fleet December 28, 1941:6-7), the assessment of *Arizona* was:

Figure 3.4. *Arizona* burning, forward mast toppled, December 8, 1941 (USS *Arizona* Memorial Photo Archives).

Figure 3.5. *Arizona* damage soon after fires were extinguished December 10, 1941 (USS *Arizona* Memorial Photo Archives).

This ship is damaged by enemy action, internal explosions and fire to such and extent as to be valueless except as to the material in the after 40% of length not damaged by immersion in sea water, and as an expensive source of steel scrap. Subject to further diving surveys, it is recommended that work on this ship be limited to removing No. 3 and 4 turrets as practicable with local weight handling equipment and removing other useable material under other Bureaus and to cutting off, as opportunity affords, of the damaged structure above water.

COMPILATION OF *ARIZONA* BATTLE DAMAGE BY FRAME

Frames 10-70: Most forward interior damage between these frames (Paine 1943:3).

Frames 10-33: the more severe damage is between these frames (Paine 1943:3).

Frame 30: Investigations by salvage divers revealed that the hull bottom had a major crack about 120 ft. from the bow [frame 30]. Divers used water jets and pumps to tunnel beneath the hull to ascertain damage from bow back to frame 78. There was no other damage observed (Raymer 1996:86-91).

Frame 35: Torpedo hit reported by eyewitnesses. This will be discussed below with the "bomb down the stack" observation that was reported at the time.

Bomb Down Stack: Reported by eyewitnesses and in various reports, and discussed below in more detail below.

Bomb that sympathetically detonated forward magazine: Apparently, one large, possibly 2,000-lb., armor-piercing bomb hit the forecastle near No. 2 turret, which it is believed penetrated to the black powder magazines, setting off the smokeless powder magazines adjacent and causing the explosion which destroyed this ship forward (Geiselman 1941:2; Homann 1942a:2). Although divers attempted to investigate the path of entry of this bomb through the ship, extensive damage made it impracticable. "It appears probable, due to the greater structural damage forward of turret #1, especially on the port side, that the bomb may have penetrated on the port side of turret #1" (Paine 1943:2).

Frame 66: "One bomb hit, size of bomb not known, on boat deck at frame 66, port side, by No.4 antiaircraft gun ammunition hoist, extent of damage done by this bomb is not known" (Geiselman 1941:2; Homann 1942a:2).

Frame 67: "One bomb approximately 1000-lb., hit on boat deck just forward of stack, at

frame 67. Width of hole on boat deck is approximately four feet, depth of penetration is not known" (Homann 1942a;1; Geiselman 1941:). This is also listed by McClung (McClung n.d.:1).

Frame 70: The decks have collapsed and slope downward from about frame 70 to about frame 34. Between frames 45 and 34, the upper deck is about 3 ft. the top of the armor on the starboard and at the top of the armor belt on the port side (Paine 1943:5).

Frame 73: "One heavy bomb hit, estimated over 1,000-lb., port side of boat deck just forward of the incinerator, by No. 6 antiaircraft gun. The extent of damage done by this bomb is not known" (Geiselman 1941:2; Homann 1942a:2). This is also listed by McClung (McClung n.d.:1).

Frame 76: Interior damage prevented divers from penetrating further than frame 76 on the main and second decks and not forward of bulkhead 78 below the third deck. However, on the third deck in ammunition passageways A-504-M and A-505-M access was possible as far forward as frame 66. In these spaces the second deck sloped down forward and the third deck was split and blown upward. No access could be gained to the firemen's passage C-501 on the third deck (Paine 1943:5).

Frame 78: "The whole ship forward of frame 78 (after fire room bulkhead) is badly damaged." … "It is not possible for divers to operate inside of the vessel forward of frame 78 due to the very extensive wreckage up to and including the main deck." … "It is believed that all of the vessel aft of frame 78 is floatable, or could be made floatable." … "Construction of a sheet pile cofferdam is not practicable on account of the porosity of the coral" … " the after portion of the vessel could probably be floated satisfactorily" (Furlong July 24, 1942:2). See also Paine October 7 1943 memo, which also discusses damage forward of frame 78.

Frame 78-90: A bomb hole was discovered on the second deck between frames 78 and 90 on the port side. A diver traced its path down two decks to where it was located in the walk-in meat freezer (Raymer 1996:76). This bomb hole is depicted in Figure 3.6.

Frame 85: One 500-lb. bomb hit the port gallery deck. The width of the hole in the deck is approximately 24-in. in diameter, with the depth of penetration unknown (Geiselman 1941:1; Homann 1942a:1). This is also listed by McClung (n.d.:1).

Frame 96: One 500 or 1000-lb. bomb hit the port side of the quarterdeck in M.B. Stowage, with a 24-in. hole in the deck and penetration unknown (Geiselman 1941:1; Davison 1941; Homann 1942a:1). This is also listed by McClung (McClung n.d.:1).

Frame 120: Some bomb damage and fire, starboard side (Commandant, Navy Yard, PH to Chief of Bureau of Ships, March 15, 1942).

Frame 123: 500-lb. bomb hit the face of turret No. 4 on the starboard side, glanced off and passed through the deck at frame 123, starboard side of the quarterdeck, between the captain's hatch and No. 4 turret and exploded in the captain's pantry, destroying both the captain's and admiral's pantry (Geiselman 1941:1; Fuqua 1941; Davison 1941; Miller 1941; Homann 1942:1). McClung (n.d.:1) notes it went "Through the quarterdeck at frame #123 to starboard of No. 4 turret. This bomb exploded in the Captain's pantry" (McClung n.d.:1).

Figure 3.6. Bomb hole, forward of the galley, port side, near frame 78 (NPS Photo by Patrick Smith).

Torpedo: "From the report of the commanding officer of the U.S.S. *Vestal*, which was moored alongside of the *Arizona* to port, bow to stern, the USS *Arizona* apparently sustained a torpedo hit about frame 35, port side. Damage caused by this torpedo hit cannot be determined, as the ship in this area has been completely destroyed. The outboard fuel oil tanks were filled to ninety-five percent capacity in the area of the possible torpedo hit" (Homann 1942a:2). Indications are that this statement originated from the interview that Homann conducted with Lt. CMDR S.G. Fuqua in December 1941 (Fuqua 1941:2).

During hull damage surveys, divers could find no evidence of torpedo damage above the mudline (McClung n.d.:1). Paine (1943:3), after extensive investigation of *Arizona*'s hull noted that "no evidence of torpedo hits has been found, although the condition of the flat bottom forward inboard … is not known. The bottom structure in the forward part of the ship is not accessible from inside and is embedded in the mud outside." The ship had not sunk to stable sediments at that time, so likely there was more hull exposed "above the mudline" when initially inspected than when the ship later reached stability. In the 1980s, NPS divers and U.S. Navy Mobile Diving and Salvage Unit One divers conducted an extensive survey of the portside above and below the mudline with water jet probes to locate possible torpedo damage. Probing along the hull in this area produced negative results. To conclusively determine whether a torpedo hit in this area would require extensive excavation below the mudline.

Bomb Down the Stack: Some eyewitness report a bomb going down the stack. Lt. A. J. Homann, who later became acting *Arizona* commander, personally interviewed and certified several *Arizona* survivors within a couple weeks of the attack. William W. Parker, *Arizona* survivor, reported,

> One bomb hit in front of the forward turret. We think it went down the magazine, for the whole forward part of the ship blew up and caught fire. Myself, and one of the other men must have gotten blowed over the side of the galley deck. About that time, a bomb went down the stack (Parker 1941).

Apparently, Acting *Arizona* Commander E. H. Geiselman (1942:2) made the first official recording of a bomb going down the stack in his December 17, 1941 damage report. He reported

a heavy bomb, 1,000 or 2,000 lbs. had gone down the stack.

Acting *Arizona* Commander Homann (1942a:2, 1942b:2) who relied on survivors' interviews states in correspondence to the Chief, Naval Operations that "an early bomb hit down the stack and disrupted the fire main and bilge pumps." This is also listed by McClung in a report to the Salvage Engineer (McClung n.d.:1). One of the survivors was Lt CMDR S.G. Fuqua, who reported a bomb had gone down the stack, and that it was not known "whether a torpedo hit the face plate of No. 4 turret indirectly" (Fuqua 1941:2). Divers investigating the uptake armor grating in the main deck as far as the wreckage would permit, and the grating was believed to be intact (Paine 1943:5), indicating no bomb went down the stack. Again, like the search for torpedo damage, no damage has been observed by NPS or Navy divers in the deck area around the stack. Based on material evidence, a bomb did not go down the stack and the fire pumps were disabled by the magazine explosion (Figure 3.7).
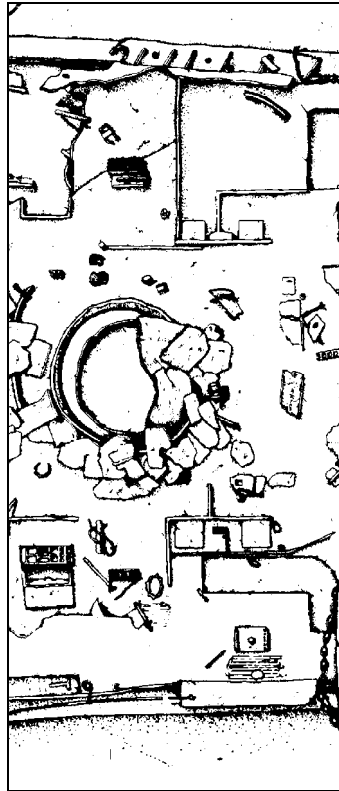
Figure 3.7. Detail of archeological map of *Arizona* depicting the stack area, with bow to the left (Drawing by NPS-SRC).

RESULTS OF COMPREHENSIVE HULL DAMAGE SURVEY

Lt. M. L. McClung (n.d.:2-4), serving as Assistant Salvage Engineer, provided an extensive damage report to the Salvage Engineer. This report, based on diver hull surveys, provides a complete picture of *Arizona*'s condition soon after the attack:

6. A survey of the port side of the ship indicates that aft of frame #70 the hull is intact. Forward of frame #70 the plating on the topside of the blister is pulled away from the ship practically all of the distance to frame #18. The hull above the blister is damaged by explosion from frame #67 forward to a crack from the gunwale to the blister at frame #22. This area above the blister is bulged and blown out so that divers cannot walk on the flat top of the blister. From frame #22 forward the damages lessens until the bow and bow and stem are in fair condition forward of frame #12.

7. The starboard side of the ship shows a condition very similar to the port side. Aft of frame #76 the hull is reported by the divers as intact with no apparent damage. Forward of frame #76 and reaching to frame #72 the rivets in the hull are loose. At frame #72 the blister is cracked from the top down to and below the mud line as far as divers could reach without extensive excavation. The blister is pulled away from the hull. The hull is blown out and torn in a manner similar to that on the port side. This damage reaches to frame #22, then diminishes leaving the bow intact [Figure 3.8 and Figure 3.9].

8. The top hamper of the vessel is burned and buckled to render it useless as anything except scrap.

9. The upper deck forward of No. 2 turret is blown out. The deck has been folded outward and forward so that divers descend thirty feet before striking wreckage which is in such a condition as to prevent inspection.

10. The main deck aft of the break to the upper deck at frame #88 is in good condition with exception of one large hole, 4' by 6' athwart-ship made by the bomb which glanced from the starboard side of No. 4 turret and ten small holes ranging from 5 to 12 inches in diameter within fifteen feet of the
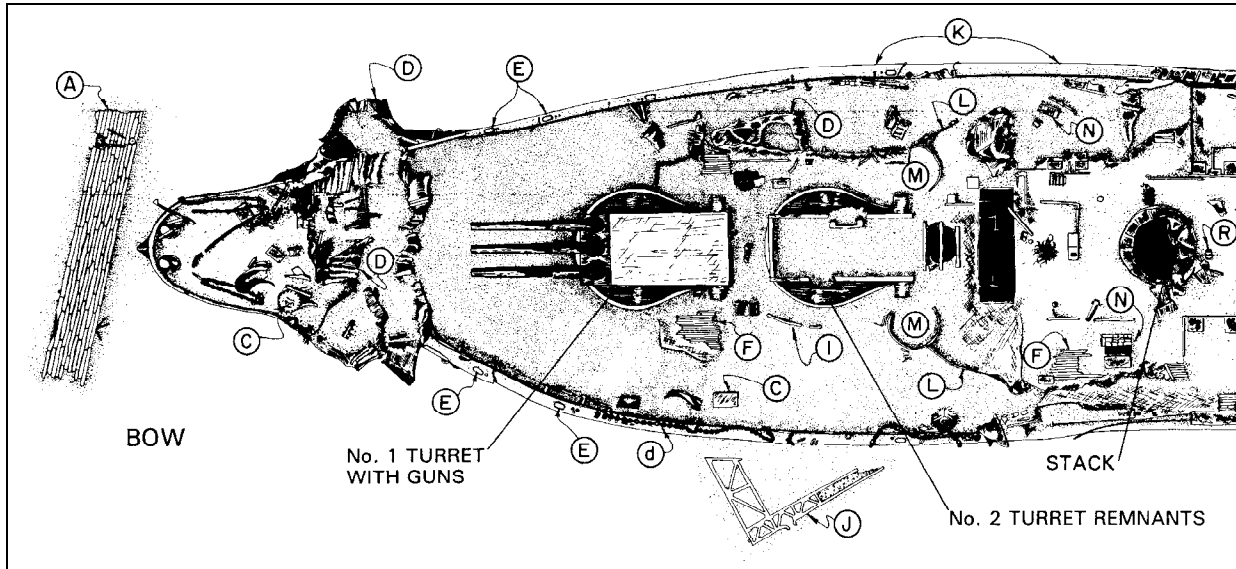
Figure 3.8. Planimetric view of *Arizona* bow damage (Drawing by NPS-SRC).
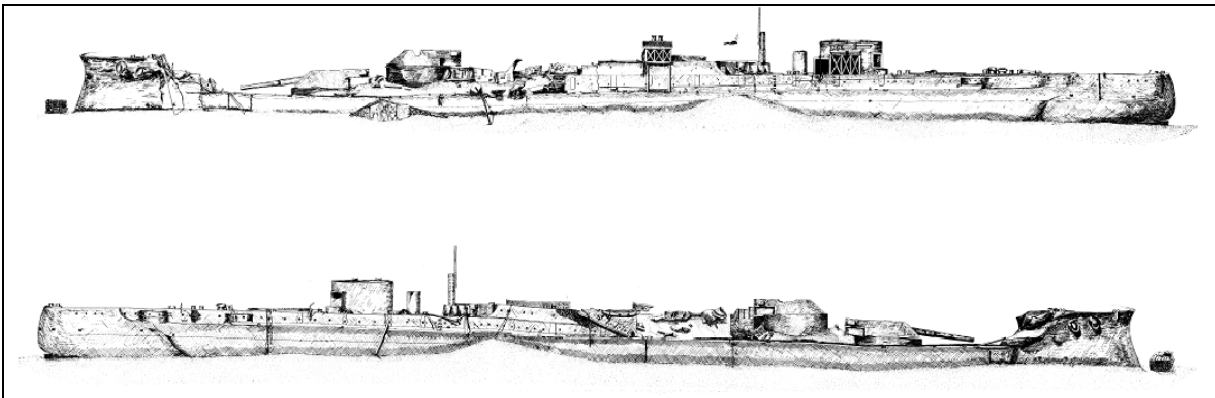
Figure 3.9. *Arizona* profile views port and starboard depicting current condition (Drawing by NPS-SRC).

large hole. Forward of frame #88 the main deck is buckled and twisted as are all bulkheads and partitions, as previously mentioned. The 5 in. batteries on each side of the deck are burned so as to render the guns useless. The ship's divers have tried to explore this part of the ship but have been unable to do so on account of the twisted and broken condition.

11. The ship's divers have removed valuables from the upper and lower Ward-room country. This part of the ship is in good condition with exception of the area damaged by fire and by the bombs which struck near No.4 turret. Between frames #76 and #90 the rooms on the starboard side consisting of the Captain's office, Engineer's office and Disbursing office have been explored and the valuables removed. The center of the ship in this area is a twisted mass of wreckage. The area astern of frame #90 on the starboard side consisting of Junior Officer's staterooms was damaged considerably by fire. The Warrant Officers staterooms on the port side were damaged also by fire. The Captain's cabin, Captain's pantry and wardroom and Officer's stateroom were damaged considerably by the bomb.

12. On the splinter deck the only part explored is the lower wardroom and Officer's quarters. This part of the ship is reported as in good condition.

13. A summary of the condition of the ship is as follows: the top hamper with the exception of the main mast and boat cranes forward of frame #88, is burned and blown to a degree, which renders it useless, the upper, main and splinter decks forward of frame #88 are burned and twisted so that they are not safe for exploration by divers. The forecastle is gone and from all divers' reports the part of the ship below the forecastle is blown and twisted similar to that part which is visible. The portion of the ship aft of frame #88 is in fair condition with exception of the portion damaged by bomb hits and fire.

The hull of the ship is apparently in good condition aft of the forward engine room bulkhead and the sides are reported as good aft of frame #76 on the starboard side and frame #67 on the port side. The condition of the interior of the ship aft of the points mentioned is not known. The guns in No. 3 and No. 4 turrets have been removed. The condition of the guns in No.1 and No.2

turrets is not known as these are under water.

14. The soundings taken before and after Dec. 7, 1941, indicate that mud has been deposited on both sides of the ship abeam of turrets No.1 and No. 2. A reasonable opinion of the cause of this deposit based on experience in submarine rock excavation is that this deposit came from under the ship or the water displaced by the explosion brought the mud when it returned.

PEARL HARBOR SALVAGE

SALVAGE ORGANIZATION AND OPERATIONS

The U.S. Navy formed the Base Force Salvage Organization in the week following the December 7, 1941 attack. Commander James M. Steele, commanding officer of *Utah*, was its first commanding officer. Its goal was a simple one: "to deliver ships and equipment to the Navy Yard for disposition. This was a major undertaking; Pearl Harbor was a ship repair facility, not a salvage unit" (Madsen 2003:36).

Navy salvage beginnings can be traced to 1939 with the hastily organized group at the San Diego Navy Salvage Base (Bartholomew 1990:53). The first trained salvage personnel arrived in Pearl Harbor in early January 1941. A group of six officers and 62 enlisted men who were members of the Navy's first formal salvage school arrived at Pearl Harbor. The school had not been held and these personnel had not yet been trained; instead the class would receive on the job training at Pearl Harbor (Madsen 2003:115; Bartholomew 1990:83).

Several conditions led to the rapid salvage and recovery of stricken vessels in Pearl Harbor. The first is that the damage inflicted, although severe, was not as bad as it could have been. The attack had been directed toward capital ships. Of the 86 ships in Pearl Harbor December 7, 1941, 10 were damaged and 9 sunk (Wallin 1946:1). The Navy Yard and personnel were intact, and there was local industrial support available on Oahu. In addition, there were two contractors, one of which was already involved with Navy operations: Pacific Bridge Company in Hawaii working with underwater concrete, and Merritt-Chapman and Scott, which went under contract with the Navy December 11, 1941 to provide services, material and logistical support for salvage operations (Bartholomew 1990:57-59, 69). In addition, divers were immediately

available at Pearl Harbor from the Navy Yard, Pacific Bridge Company and the two submarine rescue vessels Widgeon and Ortolan (Raymer 1996:29), the Destroyer Repair Units and the submarine base. In all, about a hundred divers were available (Wallin 1946:30). During the Pearl Harbor salvage operation, nearly 20,000 diving hours were conducted by Navy and contract divers with no Navy casualties and only one contractor casualty (Bartholomew 1990:68). Although Wallin's estimate of the diving hours is somewhat less; he reported 3,000 dives and 9,000 diving hours, mostly on *Oglala*, *West Virginia*, *Nevada*, *California* and *Oklahoma* (Wallin 1946:30). It is likely that the estimate of 20,000 hours is more accurate. Lt. Commander H.E. "Pappy" Haynes, who served as dive officer during the salvage operations, reported 2,299 dives with a total dive time of 7,893 hours for *Arizona* work.

Initial salvage operations were directed to putting out the raging fires, followed by actions to keep vessels afloat and prevent capsizing. Immediately following were evaluation dives to ascertain hull damage sustained during the attack. The final task was to patch and refloat the vessels so they could be transported for more complete repair and restored to service. In the case of *Arizona*, there was never serious consideration of raising the severely damaged hull; salvage work was directed to recovery of useful materials, weapons and munitions. During the remarkable salvage operation at Pearl Harbor, all but three of the damaged and sunk vessels were returned to wartime service.

USS *ARIZONA* SALVAGE OPERATIONS

Initial salvage diving on *Arizona* began December 8, 1941, while the ship was still burning. The first dives were conducted by *Arizona* personnel, and their diving continued through April 1942. These dives were made to recover government funds, confidential publications, official records, personal effects, and ordnance equipment (Haynes 1943: 3).

One of the first salvage dives into USS *Arizona*'s interior took place January 12, 1942 by Cmdr. Edward Raymer, who had served aboard *Vestal*. (Raymer 1996:1-6). The diver entered the trunk hatch near the stern and proceeded to the general workshop (machine shop) on the third deck to investigate a hole beneath the mudline on the port stern discovered during the earlier external hull survey. Originally believed to have been made by a torpedo that had not exploded, Raymer discovered it was a bomb constructed from a large caliber artillery shell to which fins

had been welded.

As mentioned, there was no plan to salvage *Arizona* and return it to the fleet. "Salvage" in the case of *Arizona* meant stripping useable materials from the ship. Weapons and ammunition were the top priority. There was no salvage work on *Arizona* from December 30 to January 6, when ammunition removal began (Madsen 2003:113). By January 25, 1942, considerable material had been removed from *Arizona* (Figures 3.10 and 3.11).

Salvage work started on removal of the aft turrets (Progress of Salvage Work, January 25, 1942). A memorandum to file by the Commander Battle Force US Pacific Fleet, January 29, 1942 reporting attack damage stated of *Arizona*, "the ship is considered to be a total wreck except for the material which can be salvaged and reassigned. A considerable amount of ordnance material has already been removed, and work is underway in removing the 12-in. [sic] guns from turrets three and four" (Commander Battle Force January 29, 1942).

The right gun of turret 3 was lifted clear on February 10, 1942. Both turret 3 and 4 were turned 90° to face Ford Island so work could be done (Madsen 2003:139). At that time, the quaterdeck was submerged beneath 10 ft. of water, so a cofferdam was constructed. All three

**Figure 3.10. Diver emerging from after magazine through turret No. 3
(USS *Arizona* Memorial Archive Photo).**

Photo # NH 64303   Divers emerging from the wreck of USS Arizona, 25 May 1943

Figure 3.11. Diver on *Arizona* deck, 1943. Note shallow water diving equipment made from gas mask (USS *Arizona* Memorial Archive Photo).

guns were removed in a week. Removal of the 14-in. shells was going on concurrently through February and into March. The broadside guns had been removed and part of the boat deck was cut away for access to guns 5 and 6 (Madsen 2003:173). The foremast was cut away and removed May 6, 1942, the main mast August 23. The guns from turret 3 and 4 were transferred to the Army for use as shore batteries. Guns of turret 2 were removed in September. Boat cranes and kingposts were removed at this time and much of the wrecked superstructure was removed to Waipio Point (Madsen 2003:218). The final work on *Arizona* was completed October 13, 1943. The entry in the *Salvage Diary* for that date stated, "Continued removal of machinery and equipment incident to discontinuance of salvage operations" (*Salvage Diary, Pearl Harbor*, October 12, 1943).

A bomb hole was discovered on the main deck between frames 78 and 90, and a diver

traced its path for two decks. The bomb was located in the walk-in meat freezer. The bomb was recovered and it was identified as a U.S. 15-in. coastal artillery shell still containing the U.S. imprint on the shell's base. Apparently, the U.S. had sold the obsolete shell to the Japanese as scrap metal. They had made a bomb out of the shell, and like the one located in the machine shop, had welded metal fins to it. This shell was transported to the Bureau of Ordnance in Washington D.C. for examination (Raymer 1996:76).

 Arizona salvage plans were being revised in February 1942, and its salvage remained a low priority. Consideration was being given to removal of the stricken hull. "It is possible that the after part of the ship can be floated, and raised, but this no doubt involves cutting off of the forward by dynamite. The study of the Arizona project will be undertaken when more urgent work is out of the way (Wallin, February 8, 1942:3).

 A month later, Commandant of the Navy Yard, William Furlong reported to the Chief, Bureau of Ships that:

> The *Arizona* is resting on a comparatively solid bottom in berth F-7 with the water
> level about ten feet above the quarter-deck. The after half of the vessel is fairly
> intact except internally in way of some bomb damage and fire in the
> neighborhood of frame 120 on the starboard side [Furlong March 15 1942:1-3].

In this same report (Furlong March 15, 1942), torpedo damage is reported and alternative salvage plans are offered, including mention of a cofferdam:

> 4. Based on damage reports and inspection of the hull below water, it appears that
> the vessel was struck by one torpedo on the port side at about frame 35 and by
> seven bombs in various locations. Due to a magazine explosion forward, the
> whole area forward of the smoke stack is badly wrecked and burned and the hull
> appears to be generally opened up below the present water line. In view of the
> great extent of serious damage in the forward part of the ship, it appears
> impracticable to float the vessel, although floatability could possibly be obtained
> if a cellular sheet piling cofferdam were driven around the ship….Sufficient sheet
> piling and equipment for diving are here for this cofferdam. An alternative would

be to cut up by acetylene burning the whole forward part of the vessel within the
cofferdam and to float the after part of the vessel to shallow water for scraping.
This amount of work would cost perhaps a half million dollars, [about $6.6
million in 2008 dollars], but would provide a large amount of needed scrap
material.

5. As an alternative to proceeding as above to remove the Arizona from her berth,
it is suggested that she be left in her present location but that all visible wreckage
be removed and cut up for scrap. All the structure of the ship above the boat deck
can be removed and reduced to scrap at a moderate cost without adverse effect to
other work….Considerable material and ordnance have already been salvaged.
This plan includes the construction of a battleship berth alongside and outboard of
the Arizona. It would be possible in time to fit turret No. 3 as a fixed battery in
connection with her remaining at her present berth.

BODY RECOVERY

Mounting pressure from Congress for recovery of the remains of *Arizona* casualties led to
body recovery operations a few months after the attack. Many bodies had been reported afloat in
the machine shop area. Salvage divers recovered approximately 45 bodies from the third deck
workshop via the trunk. The advanced state of decomposition precluded intact recovery and
identification; the recovery operation was soon halted (Raymer 1996:84, Madsen 2003:173).
Additional bodies and skeletal remains were encountered during the salvage operations. These
were removed to the hospital, and apparently no further identifications were made. William
H.Furlong, Commandant of the Pearl Harbor Navy Yard, in a memo to the Vice Chief of Naval
Operations (Furlong july 24 1942:4) estimated there were 900 bodies remaining aboard *Arizona*.
It is likely that USS *Shaw* was the first ship to honor *Arizona* with a standing honor
guard. As it passed the sunken hull, it mounted an honor guard at the rail as it passed Arizona on
its way to Mare Island February 8, 1942 (Raymer 1996:85, Madsen 2003: 129-130). Capital
ships have carried the tradition of honoring *Arizona* as they pass by to this day.

USS *ARIZONA* SALVAGE ACTIVITIES: *SALVAGE DIARY, PEARL HARBOR*, 1943

This compilation of selections from the Pearl Harbor Salvage Diary (*Salvage Diary*, *Pearl Harbor* 1943) was chosen because each offers something relevant about *Arizona*'s salvage. As discussed above, very soon after the attack, the decision was clear: there would be no attempt to refloat *Arizona*; only usable materials and scrap, mostly superstructure, were to be recovered—anything useful was to be reconditioned and returned to fleet operations. Salvage operations focused on turrets 2, 3 and 4, the 5-in. broadside battery and anti-aircraft guns and ammunition.

During salvage, the ship was explored and some observations regarding the condition of the ship's interior were made and recorded in this diary. There are several items recorded in the *Salvage Diary* that are important to the USS *Arizona* Preservation Project. Some examples are: the overhanging sides above the armor belt were burned off; most of the superstructure removal took place forward of Frame 78; during gun removal, turrets 2, 3 and 4 were sealed and dewatered; however, magazine hatches between turret 3 and 4 were removed to allow removal of munitions—these spaces should be accessible for corrosion analysis measurements with the VideoRay ROV. Any salvage diver observations regarding interior spaces are retained below. Many of these observations were considered in planning which section of the hull would be modeled and were utilized during interior explorations with the ROV.

March 27, 1942: Removed deck above broadside gun No.6.

March 30, 1942: Continuing underwater cutting on broadside stand 7.

May 1, 1942 : Continuing to cut away wreckage and foremast. Making detailed study of damage to determine whether vessel can be floated. Some evidence of ship's back being broken amidships, this is being checked.

May 18, 1942: Continued with underwater survey and the removal of topside wreckage. It was found that bulkhead 78 is structurally sound from the hold to the third decks.

June 3, 1942: Continued with underwater survey and removal of topside wreckage. Preliminary inspection of port engine room showed no extensive damage. Preparations are being made for the location of an inspection tunnel

under the forward portion of the ship.

June 4, 1942: Continued with underwater survey and removal of topside wreckage. Approximately 100 tons of wreckage have been removed from the starboard side forward.

June 5, 1942: Continued with underwater survey and removal of topside wreckage. A small derrick sooty is being rigged to handle mud siphon for inspection tunnel under forward hull.

June 8, 1942: Continued with underwater survey and removal of topside wreckage. Inspection to date has revealed that center engine room has little or no damage. Continue: preparations for the removal of ammunition from Turret III.

July 3, 1942: Continued with the removal of topside wreckage. Continued with the removal of 14" powder tanks and also work on 5" A.A. guns. The deck in D-410-M seemed to be buckling as the tanks were removed and 4 x 4" shoring is being put in as necessary.

July 5, 1941: Continued with removal of topside wreckage. Work is also proceeding on the tunneling under the forward part of the ship. Completed shoring up in D-410-M (deck has L buckled nine inches due to pressure from below). Removal of ammunition and work on 5" A.A. guns was also continued.

July 9, 1942: Continued with the removal of topside wreckage. Removal of ammunition and work on 5" A.A.guns was continued. Eighty 14" powder tanks were removed from D-410-M.

July 11, 1942: Continued removing ammunition from D409-M and sent 78 - 14" powder tanks to West Loch. Continued with removal of topside wreckage and on 5" A.A guns.

July 19, 1942: Removal of topside structure and wreckage continued. Handling room of Turret III flooded yesterday afternoon and divers were sent down to investigate. Inspection showed that outboard bulkhead seams of D-405-M opened up. The after-magazine door showed signs of inward pressure.

July 25, 1942: Divers cutting holding down bolts and wreckage to clear 5" guns. Also excavating to continue survey of Arizona bottom below blister, port side. Survey on starboard side completed, found extensive wrinkling of hull plating at

turn and just under turn-of-bilge between frames 17 and 19. Continued removal of 14" projectiles from D-407. Sent 40 -14" projectiles to ammunition depot.

July 28, 1942: Continued caulking around water shed of Turret I. Stopped pumps and flooded to close passage way doors.

August 24, 1942: Yard machinist continued working on pump in Turret IV. The pump should be back in commission some time today. Divers continued cutting on starboard 5"/25 gun. Tripod mainmast removed. Ship's bell will be turned over to Public Works for possible use as a PIS alarm.

August 29, 1942: Completed removing 14" powder tanks from D-413-M and D-412-M to shell deck of Turret IV. Removed one body from Turret IV and turned over to medical authorities.

August 30, 1942: Shored up deck in #4 handling room. Making preparations to cut through bulkhead into B-416-M to remove small arms ammunition.

September 4, 1942: Diver completed cutting bulkhead into D-416-M. Diver could not enter magazine due to ammunition boxes.

September 5, 1942: Divers closed armored hatch to D-414. Started pumping magazine area.

September 10, 1942: Continued removing small arms ammunition from D-416- M. Diver continued cutting decks above port broadside gun.

September 12, 1942: Diver closed vents in D-422 1/2-A and D-420-M. Drilled two vent holes in bulkhead between D-416-M and D-422 1/2-M.

September 13, 1942: Diver removed hatch in D-415 to allow room for deep well pump. Flooded magazine area so diver can burn bulkhead between D-416-M, and D-422 1/2-M.

September 16, 1942: Completed removing ammunition from D-422 1/2 - M
All ammunition has been removed from the let platform. Diver started checking vents and doors on 2nd platform.

September 20, 1942: Diver finished cutting drain hole in bulkhead. Diver replaced hatch on first platform which was removed to burn a hole in it for the pump pipe. Set up motor unit and frame for deep well pump.

September 22, 1942: Divers continued closing vents on second platform.

Checking all material, machines, etc. in preparation for removing 5" ammunition from second platform.

September 23, 1942: Divers continued closing vents and other openings on 2nd platform. Awaiting crane service to install deep well pump.

September 23, 1942: Divers continued checking vents, doors and other closures. The door leading to D-304-M is sprung and difficult to make tight.

September 30, 1942: Diver burned one drain hole between D-302-M and D-302 1/2-M. Started pumping second platform area [Figure 3.12]. Recovered remains of 8 bodies and sent to area hospital.

October 3, 1942: Continued pumping operations to keep 2nd platform magazines unwatered. Continued removal of debris from 2nd platform magazines. Started making preparations to rig lights. Diver continued working on 5" gun on port side.

October 9, 1942: Continued pumping operations. Started removing catapult charges from D-306 1/2 M. Removed shell carrier and piston from Turret III so as to enlarge mess hole.

October 12, 1942: Continued pumping operations. Continued removing catapult ammunition. Closed 5"1/25 cal. ammunition hoist on 3rd deck to stop leakage from trunk into magazines, and opened door to D-404-M and D-409-M.

October 14, 1942: Started removing 5"/25 cal. ammunition from D-304-M. Continued pumping operations.

October 15, 1942: Continued pumping operations. Continued removing 5"/25 cal. ammunition from D-304 1/2-M.

October 19 1942: Continued pumping operations. Made preparations to start removing 5"/25 cal. Ammunition from D-306-M. Repairing gear, checking lighter, etc. Yard diver continued underwater cutting to remove structural wreckage forward. Recovered one paravane.

November 2, 1942: Continued pumping turret #3. Continued removal of holding down clips, and machinery in turret #3. Yard divers continued cutting scrap steel in forward section of ship. Divers made inspection and took measurements for cofferdam to be installed on main deck at stern for unwatering airplane crane machinery compartments and removal of kingpost and machinery.

Figure 3.12. Pump and platform used to unwater second platform magazines, Space D-307, Frame 119-120, October 5, 1942 (USS *Arizona* Memorial Photo Archive).

November 6, 1942: Continued pumping operations. Completed removal of holding down clips, Turret 3. Continued removal of motors and disassembling train, worm and pinion. Began preparations for removal of top plates, turret #2 and top plates of conning tower. Continued diving operations on aviation crane. Continued cutting of interior wreckage forward for recovery of scrap steel.

November 25, 1942: (1) Continue pumping operations in turrets #3 and #4. Continued removing chains in powder hoists in turret #4. (2) Divers continued cutting underwater scrap forward of frame #78. No scrap metal removed due to lack of crane service. (3) Continued removal of bolts holding roof plates of turret #2. Completed cutting connections of roof plate of conning tower to interior bulkheads. (4) Continued work toward removal of stern airplane crane machinery.

December 4, 1942: (1) Continued pumping operations in turrets #3 and #4, Removed small battery compartment exhaust blower and motor from shell deck, (2) Divers made exploratory dive, attempting to reach handling roan underneath #1 turret. Unable to reach handling room because of wrecked hatch. (3) Continued removal of bolts in roof of conning tower. Continued

removing wiring and structure inside of conning tower (4) Divers cutting
underwater scrap steel forward of frame #78. None removed.

December 5, 1942: (1) Continued pumping operations in turrets #3 and #4.
(2) Divers continued attempts to reach handling room, turret #2 to determine
possibility of unwatering turret. They were unable to find a passage
to handling room because of wreckage. Continued cutting bulkheads in turret #2.
Continued preparing section of key roof plate for removal. (3) Continued
preparing roof of conning tower for removal. Drilling out brass holding down
bolts. (4) Continued cutting underwater scrap metal for of frame #78. None
removed from ship.

December 8, 1942: (1) Continued pumping operations in turrets #3 and #4. (2)
Divers continued cutting wing in bulkheads of gun chamber, turret 2. This is
moose [loose?] to gain free access to angle joining top and side armor plates.
Continued jacking up section of key plate of roof to prepare for lifting. (3) Divers
continued cutting underwater scrap metal forward of frame 08. None removed
from ship. (4) On stern airplane crane, removed socket bearings of kingpost and
pinion Lear on 2nd deck. Started cutting access hole to 3rd deck.

December 9, 1942: (1) Continued pumping operations in Turrets 3 and 4.   (2)
Divers continued cutting gun chamber bulkheads in Turret 2. Continued removal
of section of center plate in roof of Turret 2. (3) Divers continued
cutting underwater scrap forward of frame n. No scrap steel removed from ship
today. (4) Cutting access hole in 2nd deck aft into D-512-E for removal from 3rd
deck of hoisting machinery of stern airplane crane.

January 16, 1943: (1) Continued diving operations on conning tower
central tube. Discontinued removal of keys in armor. Expect to lift top half of tube
without disassembly (Weight about 100 tons.). Resumed closing bottom of tube
for unwatering. Removing hatch at bottom of tube to repair gasket. (2) Continued
cutting underwater scrap metal forward of frame #78. Removed some lockers and
wreckage. (3) Divers searched for anchors and towing bridle. Towing bridle was
previously removed from ship. Anchors were apparently blown clear of ship, and
have not been located. (Note: Letter from BuShips has requested information as to

possibility of recovering the above items.)

January 21, 1943: (1) Divers removed port shell dumping cradle in gun chamber, turret #2. Began cutting of bulkheads abreast powder hoists to gain access for installation of powder hoist covers. (2) Installed stage in conning tower armored central tube. Removed one 1 1/2"x9" bolt of about 50 bolts joining upper and middle section of tube. (3) Divers continued cutting underwater scrap metal forward of frame #78. None removed from ship. (4) Removed about 900 ft. of 2" wire rope towing cable from reel in D-504. Completed removing 8" manila mooring line from reel at frame #104, starboard side, 2nd deck. Removed considerable amount of 2 1/2" manila line from another reel at same location.

February 1, 1943: (1) Continued operations in turret #2. Divers closing off powder hoists and fitting covers on blower openings in gun pit. (2) Diver continued cutting away structure outside conning tower central tube. (3) Divers continued cutting underwater scrap metal forward of frame #76. None removed from ship.

February 13, 1943: (1) Divers continued installing and making tight covers on gunports, turret #2. Diver worked under wreckage of drip pan overhang of turret and ventilators so that openings in overhang may be closed. (2) Continued pumping in turrets #3 and #4. Expect 150 ton crane to be available to remove turret #3 side armor plates today, after which temporary ventilation will be reinstalled and work started toward removal of at turret. (3) Divers continued cutting underwater scrap metal forward of frame #78. Removed 6 tons of scrap steel and about 30 feet of anchor chain.

 February 22, 1943: (1) Continued pumping turret #2. Diver completed plugging ventilation holes in overhang. Manufactured discharge rope and flange for electric deep well pump. Lashed deep well pump together with 10" and 6" gasoline pumps in turret #2. Lowered water level, sufficiently to determine location of several leaks. Divers changed shoring of power hoist covers. (2) Continued pumping turrets #3 and #4. Shipfitters continued clearing area for laying out cut at point where turret #3 is to be separated for lifting, and fitting metal parts to wooden lifting guides. Shipwrights making up and fitting lifting guides. (3) Divers jetted

mud from damaged area forward of frame 22, cut underwater wreckage at bulkhead #20, completed freeing center wildcat for removal; continued cutting for removal of conning tower foundation, and continued cutting for removal of wreckage projecting beyond side of ship at frame 66.

February 23, 1943: (1) Divers worked in turret #2 stopping leaks disclosed by lowering of water level by pumping. (2) Shipwrights continued making up and fitting wooden guides to be installed in shell deck, turret #3. Shipfitters and drillers continued fitting metal face pieces on guides. Installed muffler on Diesel engine of pump in turret #4, and continued pumping turrets #3 and #4. (3) Divers recovered center wildcat and about six tons of scrap steel at fr.20.

Continued underwater cutting as follows: damaged bulkheads on 3rd deck at fr. 24, port; bounding angle around conning tower tube; upper deck projecting over side at fr. 66, port; and superstructure deck aft of conning tower, port side.

February 26, 1943: (1) Diver continued closing leaks in turret #2 gun chamber. Water level lowered to approximately 4 ft. from top of side armor. (2) Continued pumping turrets #3 and #4. Installed a 44' electric deep well pump in turret #3. Continued making up lifting guides for turret #3. Clearing space at circle deck for placing shoring to support lower section of turret. Clearing area for laying out cut at point where turret is to be separated. (3) Divers recovered 69 gas masks, Mark III, from compartment d-311. Masks delivered to berth 5 for disposal. (4) Divers jetted mud and silt from wreckage at frame 20, port; cut on wreckage in same area; attempted to lift large section of steel outside ship at fr. 30, starboard ; and cut on wreckage aft of conning tower. About 6 tons of scrap metal removed from ship.

February 28, 1943: (1) Lifted armor plate #T-2 from roof of turret #2. (2) Continued pumping turrets #3 and #4 and installing lifting guides on shell deck. Made preparations for placing shoring on circle deck. Laid out line for cut to separate upper and lower sections of turret. (3) Divers resurveyed section of forecastle deck over starboard bow; cutting on bulkheads on forecastle deck fr.21 port; cutting structure around conning tower central tube and boat deck aft of #2 turret to clear way for later removal of guns from #2 turret; and completed cutting

overhanging wreckage at fr.66, port. No scrap removed from ship.

March 1, 1943: (1) Divers continued closing leaks in turret #2. Water level has now been lowered to about 6 ft. by pumping. (2) Continued pumping turrets #3 and #4. Continued installing, lifting guides and placing shoring to support lower section, turret #3. Expect to finish shoring today and begin cutting tomorrow. (3) Divers cutting wreckage in side of ship about fr.20 and aft of conning tower tube about fr.55. Removed and placed on forward quay a piece of scrap weighing about 15 tons with deck winch attached. This piece was over side of ship at fr.30, starboard.

March 2, 1943: (1) Continued pumping in turret #2. Began cutting overhead beams holding forward roof plate. (2) Continued pumping turrets #3 and #4. Continued installation of guides and shoring in turret #3. (3) Diver cutting damaged bulkhead at fr. 20 and cutting wreckage aft of conning tower to fr.62 to clear area for removal of 14" guns in turret #2. (4) Lifted out section of boat deck at fr. 56 port, and placed on forward quay to be cut up for handling with truck.

March 4, 1943: (1) After rearranging 10" hose, resumed pumping turret #2 and burning over head beams holding forward roof plate. (2) Removed upper section of conning tower central tube. (Wt. about 100 tons). (3)Continued installation of guides and shoring in turrets #3 and clearing out handling room for placing shores to circle deck. Continued pumping turrets #3 and #4. (4) Diver Cutting wreckage forward of #1 turret and aft of conning tower to frame #62. Cutting up scrap on forward quay for removal. None removed.

March 10, 1943: (1) Divers opened W.T.D.s from engine room C-1 into shaft alley D-3 and from shaft alley D-1 into shaft alley D-5; opened W.T.D. from engine room C-1 into shaft alley D-1. Divers also checked, from outside of the ship, all the airports on the starboard side of the second deck from frame 70 to frame 106 and found them securely closed. (2) Divers continued installation of airlock extension at frame 105 starboard side for #7 access hole. (3) Cut an access hole into blister C-87-2-V between frame 86 and frame 87 on the starboard side. (4) Continued skimming fuel oil from the various access holes, and also pumped fuel oil from C- 87-F into the Intrepid. (5) Continued pumping gaseous water

from #3 and #6 access holes.

March 13, 1943: (1) Diver worked under overhang of turret #2 closing openings which had been overlooked. This work is difficult due to very limited working space. (2) Continued pumping turrets #3 and #4. Began placing shores in handling room and timber guides on shell deck, turret #4. (3) Divers cutting wreckage at fr.20, 3rd deck; aft of turret #2 to fr. 62; and at r.70, starboard; and removing pyrotechnics in C.T. foundation. No scrap removed from ship.

March 14, 1943: (1) Closed openings in overhang of turret #2. Reduced water level to a point below shell table. It is now possible to remove after roof plate, rangefinder, and then remove shell table to clear way for removing 14" guns. Began cutting loose after roof plate. (2) Continued installation of shores and guides in turret #4 and clearing area for cut to separate turret for lifting. Continued pumping turrets #3 and #4. (3) Recovered and delivered to Yard one ship's anchor with about 12 feet of chain. Placed about 30 feet of anchor chain on forward quay. Recovered about tons of scrap steel and placed on forward quay to be cut up for truck handling. None removed from ship. (4) Diver cutting wreckage projecting from side at fr. 24, port.

March 17, 1943: (1) Pumping turret #2. Cutting loose after roof plate. (2) Continued bracing shores in handling room, turret #4. Laid out horizontal cut for separation of turret. Lifting pads for upper sections of turrets #3 and #4 have been delivered to the ship. The 3" diameter bolt holes in the pads are smaller than holes in bulkheads to which pads are to be bolted. Holes must be reamed and bolts fitted. Continued pumping turrets #3 and #4. (3) Divers cutting underwater wreckage at fr. 20 and aft of turret #2. Removed about 8 tons of scrap from ship. Diver caulking around range finder ports, turret #2. (4) Divers continued recovering gas masks from D-311. Delivered 6 dry cans and 3 leaky cans of masks to berth #5.

March 24, 1943: (1) Pumping turret #2 gun chamber. Continued jacking up roof plates and removing shell loading table. (2) Continued pumping turrets #3 and #4. Continued fitting lifting pads and reaming out holes in lifting pads and in bulkheads, and taking measurements for machining of fitted bolts. (3) Continued

alteration of supports for deep well pump abreast turret #4. Employed diver for this work. (4) Divers commenced removal of port deck winch abreast turret #3. Divers cutting underwater wreckage at fr. 20, main and 2nd decks, and aft of turret #2. No scrap metal removed from ship.

April 2, 1943: (1) Completed repairs to 10" pump on turret #2 and began installing an additional 10" gasoline pump. (2) Continued pumping turrets #3 and #4. Received and installed five bolts for lifting pads in turrets #4. (3) Divers continued removal of port deck winch, aft. Divers cutting underwater wreckage at fr.17-20, main and 2nd deck and aft of turret#2 to fr.60. No scrap removed from ship. (4) Connecting airlines for divers to compressors on boat deck and installing new volume tank.

April 4, 1943: (1) Completed installation of additional ten-inch pump (gasoline) on turret # 2. Pumped water down to within about four feet of deck in gun pit. Continued removing project loading cable. (2) Continued pumping turrets #3 and #4. Began removing part of temporary mooring abreast turret #3, port side. (3) Removed from ship and delivered to berth #5, one electric motor from port deck winch, aft at six shell transportation slings (14"). Removed one ton scrap. (4) Installed additional electrical power cable from ship overhead line on Ford Island. (Three conductor, #? cable.) (5): Divers cutting underwater wreckage at frame 24-26, second deck and on wreckage aft of turret #4 to frame #66.

April 7, 1943: (1) Pumping turret #2. Began removing shell rammers and rammer motors. (2) Continued pumping operations in turrets #3 and #4 (3) Continued removal of outboard and of temporary quay abreast of #3 turret. (4) Divers burning section of skin of ship projecting outward above armor at fr.19-21. Cutting wreckage amidship at frame16. Cutting wreckage aft at turret #2 and assisting in removal of quay. (5) Divers removing starboard deck winch aft. No scrap metal removed from ship.

April 10, 1943: (1) Pumping turret #2. Began removal of electric winch motor and rammer motors. (2) Continued pumping turrets #3 and #4. Began installation of lifting pads for second lift in turret #3. (3) Continued removal of dolphins abreast turret #3. (4) Divers cutting underwater wreckage projecting from side at fr.19-21,

port, and wreckage aft of turret #2. Recovered approximately 30 feet of anchor chain from mud outside port bow. Diver assisted in removal of dolphins. No scrap removed from ship.

April 17, 1943: (1) Allowed turret #2 to remain flooded. Waiting for concrete in port shell hoist tube to set before pumping down. (2) Completed holding down clips for cofferdam around turret #4 barbette. Began moving equipment from turret #3 in preparation for lifting. (3) Divers jetting mud from wreckage inside bow at frame 20. Cutting wreckage aft or turret #2 down to and including upper deck. No scrap removed from ship.

April 19, 1943: (1) Pumped turret #2. Began removing part of port shell hoist tube and made preparations for pouring concrete in starboard tube. (2) Removed discharge pipe from deep well pump in turret #3. Cast loose pump for removal. The 150 ton crane was not available due to wind above 12 knots. (3) Delivered port deck winch, aft to berth #5 for overhaul. (4) Divers cutting on wreckage aft of turret #2 to upper deck level. No scrap removed from ship.

April 27, 1943: (1) Pumping turret #2. Removed welded covers from side armor bolt heads on starboard side. (2) Continued pumping in turrets #3 and #4. Removed deep well pump from turret #4. (3) Diver continued closing area around fr. #2. inside bow for cutting. Cutting wreckage aft of turret #2 to frame 64 down to and including upper deck. Divers examined sides of ship forward and found projections at frames 10-20, port and starboard.

April 28, 1943: Pumping turret #2 gun chamber. Removed one electric auxiliary projectile hoist motor and one gear box. (2) Diver cutting water shed of turret #4 to free side armor for lifting. (3) Divers cleaning mud and silt from area around frames 20 in side bow. Lifted several sections of wreckage from area at frame 60, upper deck, including one bake oven, unfit for salvage. (4) Removed approximately 6 1/2 tons of scrap from ship.

April 29, 1943: (1) Pumping turret #2. Cleaned out scrap metal from gun chamber. Making preparations for removing counter-balance mechanisms from guns. (2) Diver continued to cut on watershed of turret #4 to prepare side armor for lifting. Diver continued jetting mud from wreckage inside bow at frame 20.

Continued removing scrap from area aft of conning tower. (4) Making up air ejector pipe for tunneling under bow to determine condition of bottom in area of magazine explosion. (5) No scrap metal removed from ship.

May 1, 1943: (1) Pumping turret #2. Removed counter balance mechanism from loft gun. Began to remove same center gun. (2) Diver completed cutting watershed of turret #4. Began clearing barbette of obstructions to allow fitting of cofferdam. Diver continued clearing mud from wreckage around frame 20 inside bow. Cutting section of skin of ship projecting outboard at frame 21, above armor belt. Cutting wreckage aft of turret #2 on upper deck, frame 64. No scrap removed from ship. (3) Continued fabrication of air ejector pipe.

May 3, 1943: (1) Pumping turret #2. Completed removal of counterbalance mechanisms from guns. (2) Removed the 4 side armor plates from turret #4. (3) Diver cutting obstructions from barbette of turret #4 to allow fitting of cofferdam, after removal of upper section of turret. (4) Cutting underwater wreckage aft of #2 turret to fr. 64. on upper deck. No scrap removed from ship.

May 12, 1943: (1) Pumping turrets #3 and #4. Continued cutting to free foundation of turret #4 for removal. (2) Set 10" gasoline pump in turret #2. Shifted 10" gas pump from wood quay to top of turret #2. (3) Began removal of temporary wood quay, F-7-S. (4) Divers cutting wreckage aft of turret #2 on main deck in order to lift upper deck to frame 64. No scrap removed from ship.

May 19, 1943: (1) Continued removal of forward wood quay and pilings. (2) Continued installation of lifting pads in turret #4 on foundation. (3) Made arrangements for installing an additional electric deep well pump in turret #3 in order to further unwater turrets #3 and #4 for removal of eight magazine doors and door frames. (4) Divers continued cutting aft of turret #2 on conning tower structure; continued cutting holes in turret #4 to drain water from area to be cut for lifting foundation.

May 21, 1943: (1) Continued pumping turrets #3 and #4. Completed installation of lifting pads on foundation, turret#4. Continued cutting to free foundation for lifting. (2) Removed four doors from hinges, two at each end of passageways between turrets #3 and #4 on 1st platform. (3) Divers continued cutting on

conning tower foundation structure.

May 28, 1943: (1) Removed recoil and counter-recoil nuts from 14" guns in turret #2. (2) Flooded turrets #3 and #4. Opened four magazine doors in #4 handling room and blanked off air vent in D-413-M. Will unwater turret today in order to remove required magazine doors and frames. (1) Pumped to lower water level in turret #2 sufficiently for removal of the differential cylinders from counter-recoil mechanisms on guns. (2) Diver began cutting out magazine door frames in passageways between #3 and #4 turrets, end doors to D-413-M and D-412-M. (3) Divers continued cutting on conning tower foundation.

May 29, 1943: (1) Diver inspected elevating drive shafts in turret #2 to locate point of separation from Waterbury speed gear. (2) Removed 2 magazine doors with powder scuttles and door frames. Delivered to berth #5. (3) Diver removing doors from hinges in #4 handling room, and continued cutting on conning tower foundation. (4) Continued repairs to deep well pump motor in turret #3.

June 3, 1943: (1) Diver continued cutting to free rear plate, turret #2, for removal. (2) Diver continued cutting out magazine door frames, turret #4. Removed from ship three doors with powder passing scuttles and one door frame. (3) Continued cutting scrap steel to be removed from ship.

July 14, 1943: (1) Diver clearing area aft of turret #2 to frame 60 for removal of guns. (2) Diver cleared debris from hatch in bottom of conning tower central tube. The area below this hatch was found to be so chocked with wreckage that the diver could not gain access. Diver began diving on main deck, abreast turret #2, port side, in an attempt to gain access to 1st and 2nd platforms to inspect structural damage.

July 17, 1943: (1) Diver could not find access to 1st platform in forward part of ship due to wreckage. Attempts were made at frames 34, 28 and at frame 6. (2) Continued clearing wreckage aft at turret #2. Completed removal of castings from front plate of turret #2.

July 17, 1943: (1) Discontinued inspection of structural damage in forward part of ship for BuShips. Diver reported that it is impossible to reach magazine area on first and second platforms without extensive underwater cutting. (2) Divers

continued clearing area aft of turret #2 and recovered one stamp-canceling machine from Post Office. Used two divers.

July 26, 1943: (1) Removed two magazine doors and frames from turret #3, making a total of eight doors and eight door frames removed from magazines turrets #3 and #4. (2) Suspended operations on this ship pending the availability of the 150-ton floating crane.

August 1, 1943: (1) Resumed operations, since 150 ton crane is expected to be available on 1 August. (2) Began measuring depth of water to top of blister from frame 70 forward. Measurements are taken at 15 foot intervals and will be made on both sides of ship. This is being done to check previous measurements in damage survey.

August 2, 1943: (1) Attempted to lift foundation of turret #4 from underwater, but foundation could not be moved. Plan to reinstall pumps and underwater turrets #3 and #4 to investigate and free foundation for lifting.(2) Completed soundings to top of blister from frame 75 forward.

August 4, 1943: (1) Divers removed cover from hatch at frames 119-120 in 1st platform and replaced after pump access hole in hatch had been closed by a welded patch. (2) Manufactured cover plate for ventilation opening in compartment D-142-M, in preparation for unwatering turrets #3 and #4. (3) Diver took soundings port and starboard, to the top of the blower at the after end.

August 5, 1943: (1) Removed center 14" gun of turret #2. MkVIII, Mod.4, #18L3 from under water. Gun was placed on deck of 150 ton crane, breech opened by hand and entire gun sprayed with Tectyl. The powder chamber contained a fourteen inch drill projectile and a brass backing out slug. Used two divers to assist riggers.

August 6, 1943: (1) Diver completed securing W. T. hatch leading to D-307 and installed cover plates on exhaust vents in D-412-M and D-413-M. This work is in preparation for unwatering turret #4.

August 21, 1943: (1) Began installation of pumps on turret #2. (2) Divers commenced taking soundings of various points on ship for use in completing

sketch plan of condition of the ship.

August 24, 1943: (1) Continued the installation of pumps for the unwatering of the gun chamber of #2 turret. Utilized the services of divers as necessary. (2) Took elevation of various parts of the ship in order to determine its present position.

October 11, 1943: (1) Diver continued cutting off deck lug holding down bolts in turret #2, starboard. This work is difficult and slow due to poor access and the recessing of bolt heads in the casting. (2) In view of the time that would be required and since all material from the gun chamber and pit has been recovered, except the deck lug castings, which it is understood are not desired by BuOrd [Bureau of Ordnance], salvage work on turret #2 and thus on the ship as a whole will be stopped as of this date.

CONCLUSIONS

This chapter is incomplete; there is much more work needed regarding two critical elements: modeling overall ship damage including the forward magazine explosion and its impact on the hull and archival research to locate divers' and engineers' sketches and drawings and additional documentation to incorporate into the FEM. Originally, we intended to contract this research out during the course of research between 1999–2007. Unfortunately, funding was inadequate to complete these tasks.

However, review of salvage records as reported in this chapter was sufficient to aid in selection of which portion of the hull to focus corrosion analysis upon and determine which portion of the ship should be modeled for the FEM. Understanding the extent of interior damage at the aft end of the explosion and where the fires occurred informed the selection of frames 70–90 for the FEM. Early damage reports indicated that the ship was intact aft of the area of frame 70 to 76, although fires had reached to frame 88 (Homann 1941a:1), and the main deck in that area was reported "buckled and twisted as are all bulkheads and partitions" (McClung n.d.) and sloping toward the bow (Paine 1943). These reports contradict somewhat *Arizona*'s first Acting Commander Geiselman's early report of December 17, 1941 where he states that the attack had "…completely destroyed the ship forward of frame 88 by fire and explosion of forward

magazines. The fires being finally extinguished after burning two days. It is believed that considerable equipment aft of frame 90 can eventually be salvaged." There were no structural alterations other than removal of superstructure, turrets and crane aft of frame 66. Frame 70 would be the furthest forward the hull would remain sound, although the upper deck area forward of the galley has begun to sag (see Chapter 9).

The reason for selecting frames 70–90 for the focus of research is that corrosion measurements based on hull structure that had been subjected to blast and fire (the forward portion of Frames 70–90) would provide a conservative estimate for the aft hull portions and for the hull areas containing oil bunkers that were not subjected to either flames nor blast. Indications are that mild steel subjected to heat from fire and explosion may corrode underwater at a faster rate than mild steel that has not been heat damaged (see Chapter 5). Corrosion measurements for the forward portion of the modeled hull, if based upon heat-damaged steels in the frame 70–90 area, would most likely be higher than on areas aft of frame 90. Consequently, using corrosion rates based on damaged mild steel for the FEM would be conservative, that is, the model would incorporate the fastest corrosion rates likely to be encountered anywhere on the aft portion of the hull or within the interior. Prediction of structural change and eventual collapse would be conservative in that the projection would indicate the closest date for expected structural change.

REFERENCES

Bartholomew, C.A. Capt.
    1990 *Mud, Muscle, and Miracles: Marine Salvage in the United States Navy*.
    Department of the Navy, Washington, D.C.

Commander Battle Force, US Pacific Fleet
    January 29, 1942 Memorandum for File: Damages Sustained by the Ships of the Battle
    Force, Pacific Fleet as a result of the Japanese Air Raid on December 7, 1941. Wallin
    Papers, Box 2, 50 Salvage Reports, Naval History Center, Washington, D.C.

Commander Base Force to Commander in Chief, Pacific Fleet
    December 28, 1941 Damaged Ships – Preliminary Estimates of Problems of Salvage.
    7pp. Wallin Papers, Box 1,50 Salvage Reports, Naval History Center, Washington, D.C.

Davison, H.D.
    1941 Statement of Ensign H. D. Davison, US Navy, USS *Arizona*. Wallin Papers, Box 2,
    50 Salvage Reports, Naval History Center, Washington, D.C.

Flannigan, G. S. Ensign
    1941 Statement of G.S. Flannigan, Ensign, D-V (a), USS *Arizona*. Wallin Papers, Box 2,
    50 Salvage Reports, Naval History Center, Washington, D.C.

Fuqua, S.G. CDR
    December 15, 1941 USS *Arizona* BB-39, Pearl Harbor Attack: Report of Salvage
    Operations Following Preliminary Dives to Inspect Hull Damage and to Determine what
    Sections of the Vessel Could be Entered. Memo From Commanding Officer, USS
    Arizona to Commander Battleships, Battle Force. Wallin Papers, Box 2, 50 Salvage
    Reports, Naval History Center, Washington, D.C.

    1941 Statement, USN of the attack on the USS Arizona, 7 December 1941. Wallin
    Papers, Box 2, 50 Salvage Reports, Naval History Center, Washington, D.C.

Furlong, W.R.
    March 15, 1942 Salvage operations on USS *Arizona*, USS *Oklahoma*, and USS *Utah* –
    Decision as to Extent of. Wallin Papers, Box 1,50 Salvage Reports, Naval History Center,
    Washington, D.C.

    July 24, 1942 Memo from Commandant, Navy Yard, Pearl Harbor to the Vice Chief of
    Naval Operations. On file, USS *Arizona* Memorial Archives, Honolulu.

Geiselman, E.H.
    December 17 1941 From Commanding Officer, USS Arizona to Commander
    Battleships, Battle Force. Material Damages sustained in attack on December 7, 1941. 3
    pp. Wallin Papers, Box 2, 50 Salvage Reports, Naval History Center, Washington, D.C.

Haynes, H.E. Lt. CDR
    November 14, 1943 Memo from Diving Supervisor to Salvage Superintendent re; Diving Operations in Connection with the Salvage of the USS *Arizona*. On file, USS *Arizona* Memorial Archives, Honolulu.

Homann, A. J. Cmdr.
    January 28, 1942 (a) Material Damage Sustained in Attack on December 7. 1941. Memo from USS *Arizona* Commanding Officer to the Chief, Bureau of Ships. Wallin Papers, Box 2, 50 Salvage Reports, Naval History Center, Washington, D.C.

    1942 (b) Information on Damage Control, ref. Pacific Fleet Conf. Lrt. No2Cl-42 of January 6, 1942. Memo from USS Arizona Commanding Officer to Chief, Naval Operations. Wallin Papers, Box 2, 50 Salvage Reports, Naval History Center, Washington, D.C.

Lott, A.S. General Editor
    1978 *USS* Arizona *Ship's Data: A Photographic History*. Fleet Reserve Association, Honolulu.

Madsen, D.
    2003 *Resurrection: Salvaging the Battle Fleet at Pearl Harbor.* Naval Institute Press, Annapolis.

McClung, M. L. Lt.
    n.d. Survey of Damage on U.S.S. *Arizona*. Reference; Verbal Orders to Conduct a Survey of the Hull of U. S. S. *Arizona*. Correspondence from the Assistant Salvage Engineer to The Salvage Engineer. Wallin Papers, Box 2, 50 Salvage Reports, Naval History Center, Washington, D.C.

Miller J. D.
    1941 Bombing of USS *Arizona*, Report of Ensign Jim D. Miller. Wallin Papers, Box 2, 50 Salvage Reports, Naval History Center, Washington, D.C.

National Research Council of the National Academies
    2003 *Oil in the Sea III: Inputs, Fates, and Effects.* The National Academies Press, Washington, D.C.

Navy Department, Bureau of Construction and Repair
    1913 *Detail Specifications for Building Battleship No. 39 for the United States Navy*. Government Printing Office, Washington D.C. On file, USS *Arizona* Memorial Archives, Honolulu.

Paine R.W.
    October 7, 1943 Memo from Commandant Navy Yard , Pearl Harbor to Chief, Bureau of Ships. Subject: U.S.S. *Arizona* (BB-39) War Damage Report. On file, USS *Arizona* Memorial Archives, Honolulu.

Parker W.W.
    1941 Statement of William W. Parker, SEA1c, USN. Wallin Papers, Box 2, 50 Salvage
    Reports, Naval History Center, Washington, D.C.

Raymer, Commander E. C.
    1996 *Descent into Darkness Pearl Harbor, 1941: A Navy Diver's Memoir*. Presidio
    Press, Novato.

Salvage Diary, Pearl Harbor
    1943 1 March – 1942 through 15 November, 1943. Industrial Department War Diary
    Collection, Naval Historical Center, Washington D.C.

Stillwell, Paul
    1991 *Battleship* Arizona: *An Illustrated History.* Naval Institute Press, Annapolis.

Summary of Damage Reported to the Planning Section,
    December 7, 1941.Wallin Papers, Naval Historical Center, Washington, D.C. Wallin
    Papers, Box 1,50 Salvage Reports, Naval History Center, Washington, D.C.

United States Pacific Fleet Battle Force,
    n.d. USS *California*, Flagship, Memorandum No.7. Wallin Papers, Box 1, 50 Salvage
    Reports, Naval History Center, Washington, D.C.

Wallin, H.N. Cmdr.
    December 7, 1941 Memorandum Covering Apparent Damage to Vessels in Pearl As of
    1345 This Date. US Pacific Fleet, USS Pennsylvania, flagship. Wallin Papers, Box 1, 50
    Salvage Reports, Naval History Center, Washington, D.C.

    January 25, 1942 Progress of Salvage Work in Pearl Harbor. Wallin Papers, Box 1, 50
    Salvage Reports, Naval History Center, Washington, D.C.

    February 8, 1942 Present Situation with Respect to Salvage of Vessels in Pearl Harbor.
    3pp. Wallin Papers, Box 1,50 Salvage Reports, Naval History Center, Washington, D.C.

    1946 Rejuvenation of Pearl Harbor. Typescript sent to Admiral Nimitz and Navy
    Director of Public Information. Wallin Papers, Box 1,50 Salvage Reports, Naval History
    Center, Washington, D.C.

    1968 *Pearl Harbor: Why, How, Fleet Salvage and Final Appraisal.* Naval History
    Division, Washington, D.C.

CHAPTER 4

Dynamics of the Physical Environment on USS *Arizona*

Curt D. Storlazzi, M. Katherine Presto, Michael E. Field, and Matthew A. Russell

INTRODUCTION

A variety of factors have been identified that directly influence metal corrosion on shipwrecks, including water composition (dissolved oxygen, pH, salinity and conductivity), temperature and extent of water movement (North and MacLeod 1987:68).

Oxygen reduction is typically the main cathodic reaction occurring in steel exposed to seawater, so dissolved oxygen availability at the cathodic site controls the corrosion rate, with higher dissolved oxygen content resulting in higher corrosion. Water at the ocean's surface is generally oxygen-saturated, so overall dissolved oxygen content depends on the amount of mixing that occurs with surface water—increased water movement and mixing results in elevated dissolved oxygen levels. In addition, temperature and dissolved oxygen are inversely proportional, so lower temperature results in increased dissolved oxygen. The pH level is indicative of overall corrosion activity. In normal seawater, pH ranges from 7.5 to 8.2, but levels below 6.5 are found under concretion covering actively corroding metal. Lower pH levels (more acidic) typically characterize active or increased corrosion levels. Salinity is closely related to the corrosion rate of steel in water, so increased salinity usually results in higher corrosion rates. This is evident when comparing metal preservation in freshwater compared to seawater

environments—freshwater lakes typically exhibit better preservation of iron and steel. There are several ways that higher salinity affects corrosion, including increasing conductivity (which facilitates movement of ion between anodic and cathodic areas), increasing dissolved oxygen and supplying ions that can catalyze corrosion reactions, among others (North and MacLeod 1987:74). Higher conductivity can increase corrosion by increasing the movement of ions during the corrosion process.

In general, corrosion increases as temperature increases. Under controlled laboratory conditions, corrosion rate doubles for every 10°C rise in temperature. This relationship is complicated, however, by the effect of temperature on both dissolved oxygen and biological growth. Warmer water supports increased marine growth, which contributes to concretion formation on steel in seawater and that, in turn, generally reduces corrosion rates. In addition, as discussed above, lower temperature results in higher dissolved oxygen content, which consequently means increased corrosion (North and MacLeod 1987:74).

Water movement from waves and currents on a site affects corrosion in several ways, but generally high-energy environmental conditions results in higher corrosion rates. Active water movement can contribute to mechanical erosion of metal surfaces and can also impede development of protective concretion layers by removing accumulating ions before they can precipitate and begin the concretion formation process. Waves and currents also contribute to water mixing and aeration that result in increased dissolved oxygen levels (North and MacLeod 1987:74).

Factors that affect corrosion on metal shipwrecks are complicated and interrelated. Reducing one key factor can increase another, and the results are often unpredictable. It is clear, however, that in order to understand the corrosion history of an object, even a complex object like a World War II battleship, and to begin to define the nature and rate of deterioration affecting the object, an understanding of the various environmental factors at play is necessary. An important aspect of the USS *Arizona* Preservation Project was long-term monitoring of oceanographic and environmental parameters on the site. This was accomplished with *in situ* multiparameter instruments placed on the hull and on the seabed to the side of the vessel. Interior conditions were also measured using ROV-deployed instruments.

EXTERIOR DATA COLLECTION

LONG-TERM *IN SITU* MONITORING, 2002-2005

U.S. Geological Survey (USGS) and National Park Service (NPS) personnel collected long-term, high-resolution physical and chemical oceanographic measurements at the USS *Arizona* Memorial (USAR) in 2002–2005 to better understand the nature of the environment surrounding the mostly submerged historic ship, and to determine long-term, seasonal variability in key parameters that affect corrosion. Scientists used a number of bottom-mounted, multi-parameter instruments deployed in water depths less than 10 m to collect survey and time series environmental data.

Researchers calibrated and deployed a SonTek Triton Acoustic Doppler Velocimeter (ADV) wave-height and current meter and a YSI 6600 Multiparameter Sonde on *Arizona* in November 2002. These instruments have internal memory and batteries and can be left *in situ* for up to 60 days, recording data multiple times an hour. The instruments were retrieved and downloaded, then recalibrated and deployed every 60 days by USAR staff. The data were sent to the SRC in Santa Fe, New Mexico, and the USGS in Santa Cruz, California, for compilation and analysis. The instruments collected baseline data including wave height and direction and current velocity and direction around the vessel, and basic environmental parameters including pH, temperature, salinity, dissolved oxygen, oxygen reduction potential and conductivity. The purpose of these measurements was to collect hydrographic data to better constrain the nature of the physical and chemical environment on the submerged vessel hull and near the Memorial to determine temporal and spatial variability. Two RD Instruments 600 kHz Acoustic Doppler Current profilers (ADCP) were later deployed for a one-month period in April–May 2005 in the same locations as the SonTek instrument for additional data collection.

Project Objectives

The objective of the instrument deployments was to understand how waves, currents and water column properties such as water temperature, salinity, pH, turbidity, oxygen reduction potential and dissolved oxygen in the vicinity of the Memorial vary spatially and temporally.

These data were collected to support the NPS-SRC research to understand and characterize the nature and rate of natural processes affecting deterioration of USS *Arizona.* To meet these objectives, flow and water column properties close to *Arizona*'s hull were investigated. The first two instrument packages were deployed over a period spanning 14 months to investigate variability over daily-to-seasonal time scales. The objective of the third instrument deployments was to understand how currents and temperature in the vicinity of the Memorial vary over two spring-neap tidal cycles. These data supplemented the single-point measurements made between 2002–2004.

Study Area

       The instrument deployments were conducted adjacent to and on USS *Arizona*'s hull (Figure 4.1). The SonTek ADV was deployed in 10 m of water roughly 25 m southeast of *Arizona*'s port beam below the Number 1 turret from November 2002, through November 2003. In November 2003, the ADV was re-deployed in 10 m of water roughly 25 m northwest of USS *Arizona*'s starboard beam below the Number 1 turret and logged data at that location until January 2004. The seafloor at both of these sites is an organic-rich, very well sorted fine silt/mud. The YSI Sonde was deployed amidships on *Arizona*'s main deck just forward of the Number 3 barbette and just aft of the Memorial from January 2003 through January 2004. Vertical profiles of the water column using the Sonde were made off the USS *Arizona* Memorial's dock in February 2003. Two ADCPs were deployed concurrently at the two ADV sites to either side of the Number 1 turret from April 2005 through May 2005. All diving, mobilization and demobilization were based from the USS *Arizona* dock.

Operations

       This section provides information about personnel, equipment and vessels used during equipment deployments. See Tables 4.1 and 4.2 for personnel involved in this experiment and Tables 4.3 and 4.4 for complete deployment information for the instruments.
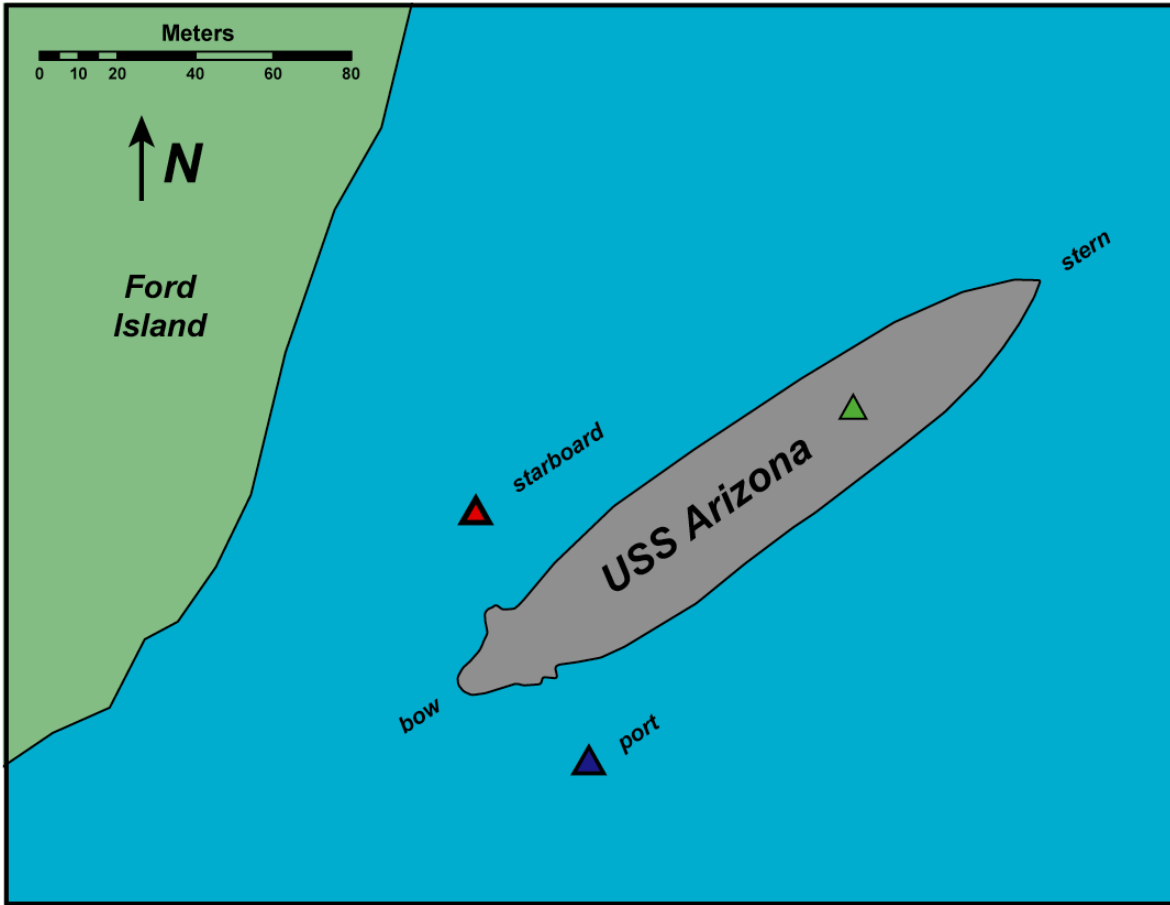
Figure 4.1. Map showing the spatial distribution of instrument packages in the study area relative to the USS *Arizona*'s hull and Ford Island.

Person	Affiliation	Responsibilities
Curt Storlazzi	USGS	Chief scientist, scuba diver
Matthew Russell	NPS-SRC	Co-chief scientist, led scuba diving operations
Marshall Owens	NPS-USAR	USAR Memorial curator, led refurbishment operations
Michael Field	USGS	Scientist, scuba diver
Larry Murphy	NPS-SRC	Scientist, scuba diver
Michael Freeman	NPS-USAR	Scuba diver

Table 4.1. Personnel involved in long-term instrument deployments, 2002–2004.

Person	Affiliation	Responsibilities
Curt Storlazzi	USGS	Chief scientist, scuba diver
Matthew Russell	NPS-SRC	Co-chief scientist, led scuba diving operations
Kathy Presto	USGS	Scientist, lead instrument technician
Jennifer Burbank	NPS-USAR	USAR Memorial ranger, diver, led recovery operations
Joshua Logan	USGS	Scientist, scuba diver, GIS Technician
Thomas Reiss	USGS	Scientist, dive safety officer

Table 4.2. Personnel involved in instrument deployment, 2005.

Instrument	Depth (m)	Date Deployed	Date Recovered	Latitude (dd)	Longitude (dd)
SonTek Triton	10	11/21/2002	1/30/2003	21.36415	-157.95054
SonTek Triton	10	1/30/2003	3/7/2003	21.36415	-157.95054
YSI 6600 Sonde	3	1/30/2003	3/7/2003	21.36494	-157.94986
SonTek Triton	10	3/21/2003	5/7/2003	21.36415	-157.95054
YSI 6600 Sonde	3	3/21/2003	5/7/2003	21.36494	-157.94986
SonTek Triton	10	5/15/2003	7/2/2003	21.36415	-157.95054
SonTek Triton	10	7/8/2003	8/29/2003	21.36415	-157.95054
SonTek Triton	10	8/29/2003	10/10/2003	21.36415	-157.95054
YSI 6600 Sonde	3	8/29/2003	10/10/2003	21.36494	-157.94986
SonTek Triton	10	10/23/2003	11/5/2003	21.36415	-157.95054
YSI 6600 Sonde	3	10/24/2003	11/20/2003	21.36494	-157.94986
SonTek Triton	10	11/20/2003	1/13/2004	21.36415	-157.95054
YSI 6600 Sonde	3	11/20/2003	1/22/2004	21.36494	-157.94986

Table 4.3. Instrument package deployment log, 11/2002–1/2004.

Instrument	Depth (m)	Date Deployed	Date Recovered	Latitude (dd)	Longitude (dd)
Starboard	9	4/2/2005	5/1/2005	21.364684	-157.950756
Port	10	4/2/2005	5/1/2005	21.364206	-157.95055

Table 4.4. ADCP deployment log, 4/2005–5/2005

Equipment and Data Review

Three primary instruments acquired data during the deployments. The first instrument was a SonTek Triton wave/tide gauge (Figure 4.2a). The primary sensor on this package is an upward-looking 10 MHz Acoustic Doppler Velocimeter (ADV), which collects three-dimensional single-point measurements of current velocity and acoustic backscatter data. A pressure sensor on the Triton provided tide data and spectral wave information. The Triton employed two different sampling schemes: First, it sampled the mean currents by averaging the current speeds over a 1-min window every 10 min. Second, it sampled the surface wind waves by collecting current and water depth data over an 8.5-min window every 2 hours.

The second primary instrument employed was an YSI 6600 Multi-parameter Sonde (Figure 4.2b). The YSI Sonde collected single-point measurements on water temperature and salinity, pH, dissolved oxygen and oxygen-reduction potential when deployed on the hull 3 m below the surface; the YSI was also used in profiling mode, collecting vertical profiles of water temperature and salinity, pH, dissolved oxygen and oxygen-reduction potential. When used in profiling mode, the YSI was lowered from the surface to the seafloor in the early morning and
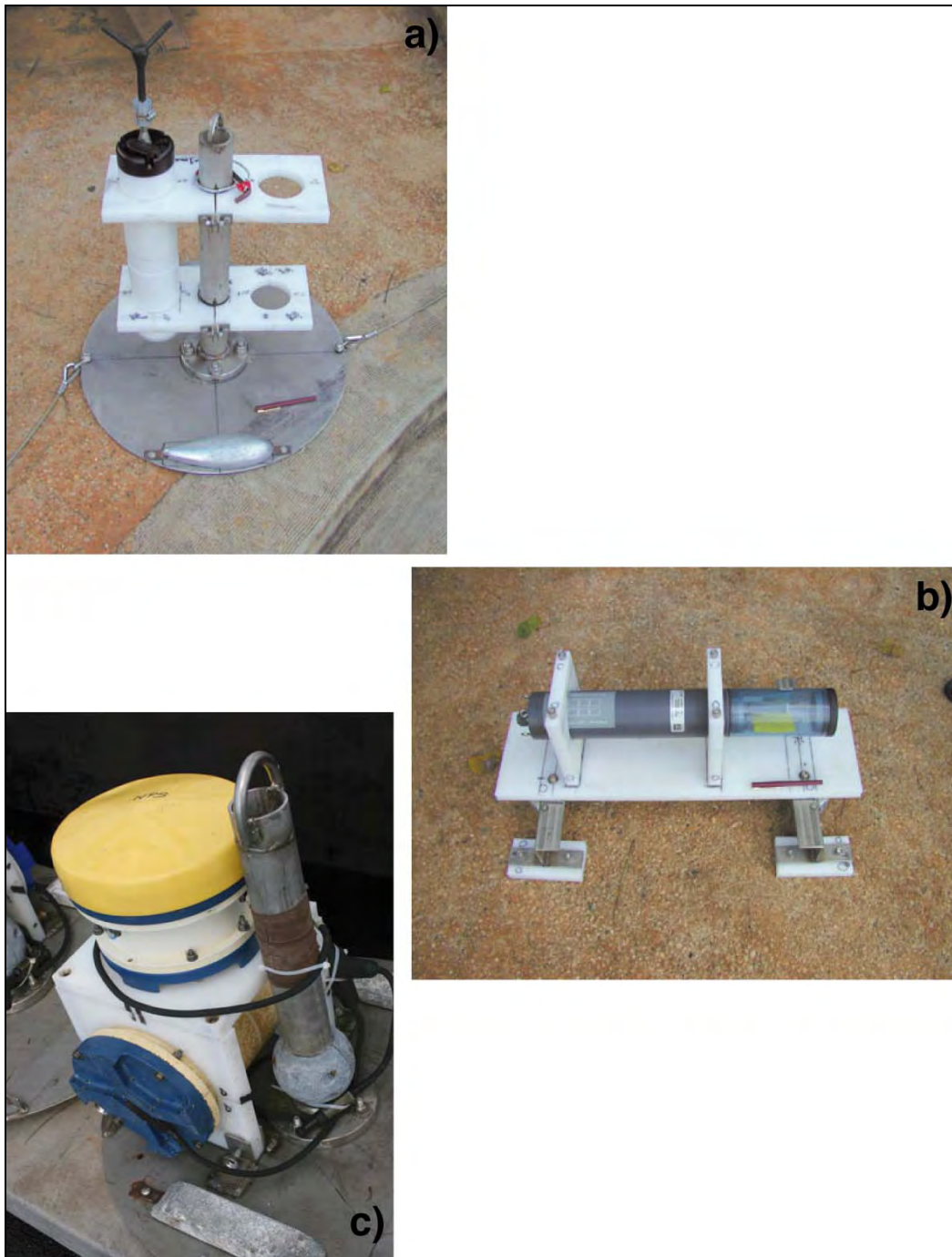
Figure 4.2. Photographs of instrument packages and their mounts. a) The Sontek Triton ADV and sea bed mount. This mount was designed to be able to simultaneously deploy the YSI 6600 Sonde in the empty bracket on the right side of the photograph; note the pen for scale. b) The YSI 6600 Sonde and hull mount; note the pen for scale. c) RD Instruments ADCP and its sea bed mount. The ADCP transducers and the pressure and temperature sensors are under the yellow protective cap (~20 cm diameter for scale).

the late afternoon for three consecutive days. During these profiles all the sensors on the YSI sampled at once per second.

The third primary instrument used to acquire data during the deployments were two RD Instruments 600 kHz Acoustic Doppler Current profilers (ADCP) (Figure 4.2c). These collected three-dimensional vertical profile measurements of current speed and direction in 0.5 m bins (sampling volumes) every 0.5 m from 1.0 m above the seafloor up to the water surface and single-point measurements of water temperature 0.5 m above the seafloor; a pressure sensor on the ADCP measured water level data. The ADCP sampled mean currents, water level and water temperature by averaging over a 1-min window every 4 min.

The first two instrument packages were typically deployed for approximately one- to two month periods, as limited by the power consumption and sensor sampling rates, while the third was deployed for only a one-month period (see Tables 4.3 and 4.4). The instrument specifics and sampling schemes are listed in Appendix A for the SonTek Triton ADV, Appendix B for the YSI 6600 Sonde, and Appendix C for the RD Instruments ADCP (Storlazzi, et al. 2004; Storlazzi, et al. 2005). Daily data on meteorologic forcing over the study period were recorded at the Honolulu International Airport roughly 5 km southeast of the study site. These digital data were downloaded and compiled from the National Climate Data Center (2005).

Deployment/Recovery Operations

Prior to installation of the SonTek ADV in 2002, diving scientists established a secure guideline from *Arizona*'s hull out to the location where it would be deployed. The ADV and its semi-permanent mount were initially deployed by lowering it just below the water's surface where scuba divers attached a lift bag and detached the lifting line. The divers followed a marker line to the sea floor to move the instrument package into place. The divers secured the instrument package with cables attached to sand anchors embedded in the seafloor (Figure 4.3). The same procedure was followed for the later ADCP deployment in 2005. The YSI Sonde was placed in its semi-permanent mount by researchers who swam it out from the USAR dock for deployment in 2002. Periodic recovery and redeployment operations for the ADV and Sonde between 2002–2004 involved researchers removing the instruments from their mounts,

Figure 4.3. The SonTek ADV in place on the harbor bottom adjacent to USS *Arizona*
(NPS Photo by Brett Seymour).

swimming them back to the dock for download and battery replacement; they were then redeployed (Figure 4.4). The vertical profiles collected with the YSI Sonde were done from the USAR dock. These entailed lowering the YSI Sonde to just below the surface for a minute to allow all of the sensors to equilibrate, then slowly lowering the YSI Sonde from the surface, down to the sea floor, then bringing it slowly back up to the surface.

Data Acquisition and Quality

SonTek Triton ADV data were acquired on 362 days during the 14-month period between November 2002 and January 2004, for more than 85% data coverage over the entire experiment period. Instrument refurbishment and battery failure accounted for the 64 days during these 14 months when no data were recorded. The ADV produced almost 77,750 observations from each sensor. Data quality was generally very high. Scientists archived the raw Triton data, and copies of the data were post-processed to remove spurious data whenever the beam correlation dropped below 70%. The post-processed data were saved and copies were

Figure 4.4. USS Arizona Memorial diver retrieving YSI Sonde (NPS Photo by Brett Seymour).

de-sampled to hourly intervals to better visualize longer-term variability; these desampled copies of the data were also saved and archived (Storlazzi, et al. 2004).

The YSI Sonde produced data on 59% of days deployed (215 out of 362 days), which resulted in just over 23,000 observations from each sensor. Data quality was generally good, exceptions were from improperly calibrated sensors or when fouled by biologic growth. The post-processed data were saved and copies were de-sampled to hourly intervals to better visualize longer-term variability; these de-sampled copies of the data were also saved and archived. Six vertical profiles were collected using the YSI 6600 Sonde, with 100% data recovery from the temperature, conductivity, and dissolved oxygen sensors. Due to sensor malfunction, no pH or oxygen-reduction potential data were recorded during any of the six profiles (Storlazzi, et al. 2004).

The RD Instruments ADCPs acquired current speed, current direction and near-bed water temperature data for 30 days between April 2 and May 1, 2005, yielding 100% coverage over the entire experiment period. Each ADCP made more than 10,400 observations of current speed, current velocity and acoustic backscatter from each of the 28 bins (>290,000 total samples per instrument) over the study period. Data quality was very high. The ADCP data near the surface

displayed slightly lower correlation due to bubble interference with the transducers. This loss of data from the bins closest to the surface is common to most upward-looking ADCPs and was expected. The raw ADCP data were archived and copies of the data were post-processed to remove all "ghost" data from above the surface. All data collected when the beam correlation dropped below 70% were discarded for visualization and analysis. Post-processed data were saved and copies were desampled to hourly intervals to identify longer-term variability; these desampled copies of the data were also saved and archived (Storlazzi, et al. 2005).

Results

This section reviews data collected by all systems during deployments and addresses significance of the findings to characterizing local oceanographic conditions in the study area.

Meteorologic Forcing

The Hawaiian Islands, situated at roughly 21° North, are in the Trade wind belt. Consequently, the study area is dominated by very low wind variability during the summer periods when the Trade winds blow consistently; insolation (solar heating) and thus air temperatures are high and precipitation is low. During the winters, when extratropical lows and frontal systems propagate through the Hawaiian Islands causing precipitation, weaker and more variable winds, decreased insolation and, thus, lower air temperatures occur. Based on oceanographic measurements made at USAR, decreased air temperatures and precipitation typically reduce water temperature and salinity in Pearl Harbor. The Trade winds, which generally cause the highest sustained wind speeds (excluding tropical cyclones) during the spring, summer and fall, are topographically steered around the Koolau Range to the east of Pearl Harbor, often approaching the south shore of Oahu from the south or southeast and resulting in strong winds to the north or northwest over USAR. During the winter months, passage of fronts and extratropical lows to the north of the Hawaiian Islands results in strong northerly winds being funneled south between the Waianae Range to the west of Pearl Harbor and the Koolau range to the East, resulting in strong winds to the south over USAR. These winds can drive surface currents and cause mixing of the water column at USAR.

Waves

Waves in Pearl Harbor during the study were generally extremely small, with significant wave heights (*Hsig*) on the order of cm's, with a range of 0.01 m to 0.08 m and a mean *Hsig* ± one standard deviation of 0.03 ± 0.01 m. Dominant wave periods (*Td*) are in a very narrow range between 19.85 and 20.38 sec, with a mean *Td* ± one standard deviation of 20.19 ± 0.08 sec; these low height, long period waves all were observed to come out of the southern quadrant (160º-200º). This narrow band range and corresponding low wave heights suggest that the pressure sensor along the 10-m isobath is at or near its resolution limits relative to the incident wave frequency. Because the depth of penetration of wave-induced pressure fluctuations and orbital motions decreases exponentially with depth and is dependant on wave height and period, it appears that the SonTek ADV's pressure sensor is only able to resolve longer period motions at these small wave heights. Thus, the shorter period wind waves typically observed in the afternoon when the Trade winds are blowing 10-20 m/sec are too small in height and too short in period for the pressure sensor to resolve from its depth of 10 m. The 20-sec period waves that are resolvable by the pressure sensor are likely long period ground swell (North Pacific winter swell or South Pacific summer swell) that has enough energy to propagate up the entrance channel of Pearl Harbor and into the East Loch past USAR.

In addition to these natural small, long-period swells, the pressure sensor record was often overwhelmed by high-amplitude, short-period (2-8 sec) modulations. These modulations appear to be due to large vessels passing over or by the Sontek instrument package, for they are anomalously large and have southeasterly (90º-150º) or northwesterly (270º-330º) directions, likely the result of incident waves and waves reflected off *Arizona*'s hull, respectively.

Tides

Pearl Harbor tides are of the mixed, semi-diurnal type with two uneven high tides and two uneven low tides per day; thus the tides change just over every 6 hours. The mean daily tidal range during the study was roughly 0.6 m, while the minimum and maximum daily tidal ranges are 0.4 m and 0.9 m, respectively (Figure 4.5). The lunar tidal cycle drives the magnitude of the tidal currents, with the highest tidal current speeds occurring during the spring tides (new and
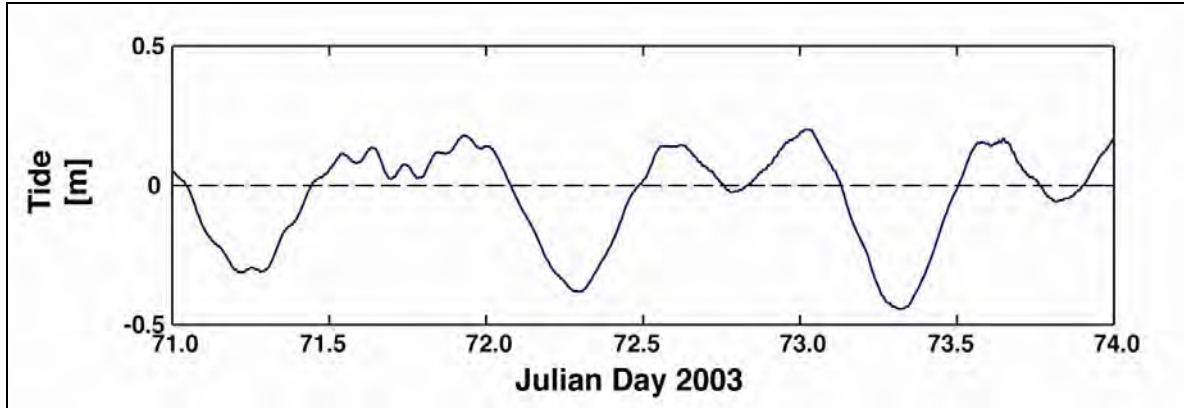
Figure 4.5. Typical tidal data from USS *Arizona*.

full moons) and the weakest during the neap tides (quarter moons). While tides control the majority of the variability in current speed and direction, insolation-driven trade wind intensification also appears to slightly influence daily variability. When the trade winds blow at high speed in the early to late afternoon, the net flow at the 10-m site appears to take on a more northwesterly component. This shift might be due to an upwelling-type of phenomena, oceanic water being drawn into the harbor to replace the surface water flushed offshore by the trade winds. We do not have information at this time that indicates which process or combination of processes is responsible for the observed intensification of northeasterly flow during the afternoon.

Currents

Most daily variability in current speed and direction at the study site is due to the semi-diurnal (12.4 hour) and diurnal (24.8 hour) tides. As the tide rises (floods), currents in Pearl Harbor flow to the north; conversely, as the tide falls (ebbs), the currents flow to the south. Mean current speeds ± one standard deviation approximately 1 m below the water surface are 0.028 ± 0.019 m/s off the starboard (northwestern) side of the hull and 0.023 ± 0.013 m/s off the port (southeastern) side of the hull. Close to the bottom, mean current speeds ± one standard deviation 1 m above the seafloor are 0.010 ± 0.007 m/s off the starboard (northwestern) side of the hull and 0.027 ± 0.015 m/s off the port (southeastern) side of the hull. Of note are the slightly different orientations in both instantaneous and net flow to the port and starboard sides of the USS *Arizona*'s hull. Off the starboard side, the flow is predominantly oriented north-

northeast or south-southwest, roughly parallel Ford Island's shoreline in the vicinity of the USS *Arizona*. Off the port side, however, the flow is predominantly oriented east-northeast or west-southwest, roughly parallel to the main trend of the East Loch of Pearl Harbor. These differences in orientation imply steering, not only by the bathymetry, but also by the USS *Arizona*'s hull (Figure 4.6).

Net flow at the surface along both sides of the USS *Arizona*'s hull was to the southeast at roughly 0.02 m/s. Assuming near-surface flow remained constant through this section of Pearl Harbor, the mean current speed of 0.02 m/s would result in a total replacement of water along the 185-m length of the hull in just over 2.6 hours. Net flow 1 m below the surface and 1 m above the seafloor along both sides of the USS *Arizona*'s hull were to the northwest at approximately 0.02 m/s and 0.01 m/s, respectively. Assuming near-bed flow remained constant through this section of Pearl Harbor, these mean current speeds would result in a total replacement of water along the 185-m length of the hull in just over 2.6 hours and 5.2 hours, respectively. However, because oscillatory tidal flows enhance these mean flow speeds, the actual replenishment time would typically be shorter.

The differences in current speed, both vertically and from one side of the hull to the other, result in velocity shear, which, in turn, likely increases turbulence and mixing. The values of vertical shear varied from 0.025 ± 0.015 1/s off the starboard (northwestern) side of the hull and 0.038 ± 0.023 1/s off the port (southeastern) side of the hull. The shear was generally highest during the falling tides. The vertical velocity shear, by moving seawater of a given density, would impart a vertical variation in current-induced force on the hull. Seeing that seawater in Pearl Harbor has a density around 1023 kg/m^3 (temperature~25 °C and a salinity~33 Practical Salinity Units, PSU, or parts per thousand), the mean current-induced force on the starboard (northwestern) side of the hull is 0.175 ± 0.131 N/m^2 and 0.291 ± 0.259 N/m^2 on the port (southeastern) side of the hull (Figure 4.7).

Water Column Properties

The water column properties collected include variations in acoustic backscatter (dB), temperature (ºC), salinity (PSU), pH, oxygen-reduction potential (mV), and dissolved oxygen (%). Their ranges, variability and potential causes for their variability are discussed here.
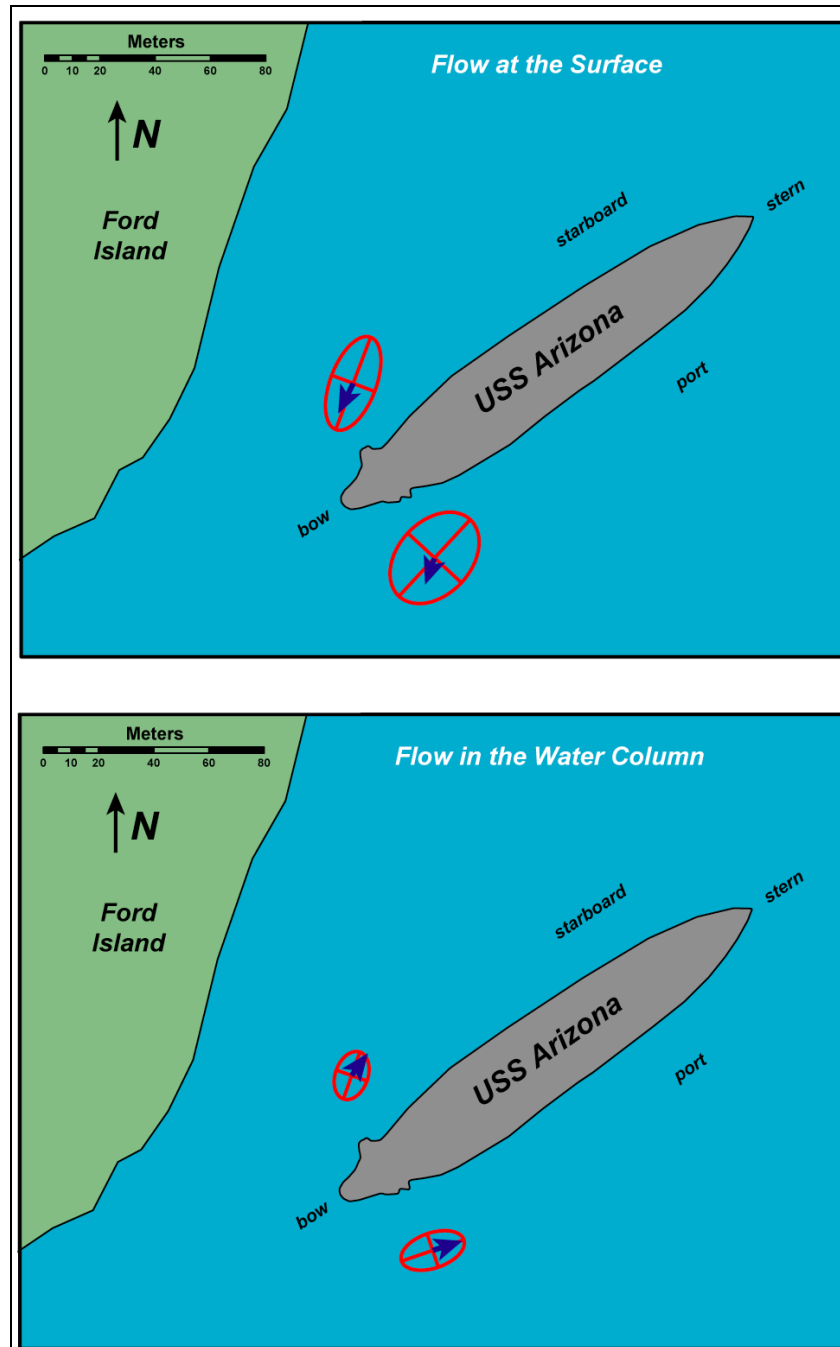
Figure 4.6. The orientation of mean flow and its variability in the water column adjacent to the *Arizona*. TOP: Flow at the surface. BOTTOM: Flow in the water column. The red ellipses denote the magnitude of major and minor axes of variability in flow; the blue vectors denote the magnitude and direction of mean flow. Note that surface flow is stronger and oriented to the southwest while flow within the water column is weaker and is oriented to the northeast. Off the starboard side, the flow is predominantly oriented north-northeast or south-southwest, roughly parallel Ford Island's shoreline; off the port side, however, the flow is predominantly oriented east northeast or west-southwest, roughly parallel to the main trend of the East Loch of Pearl Harbor.
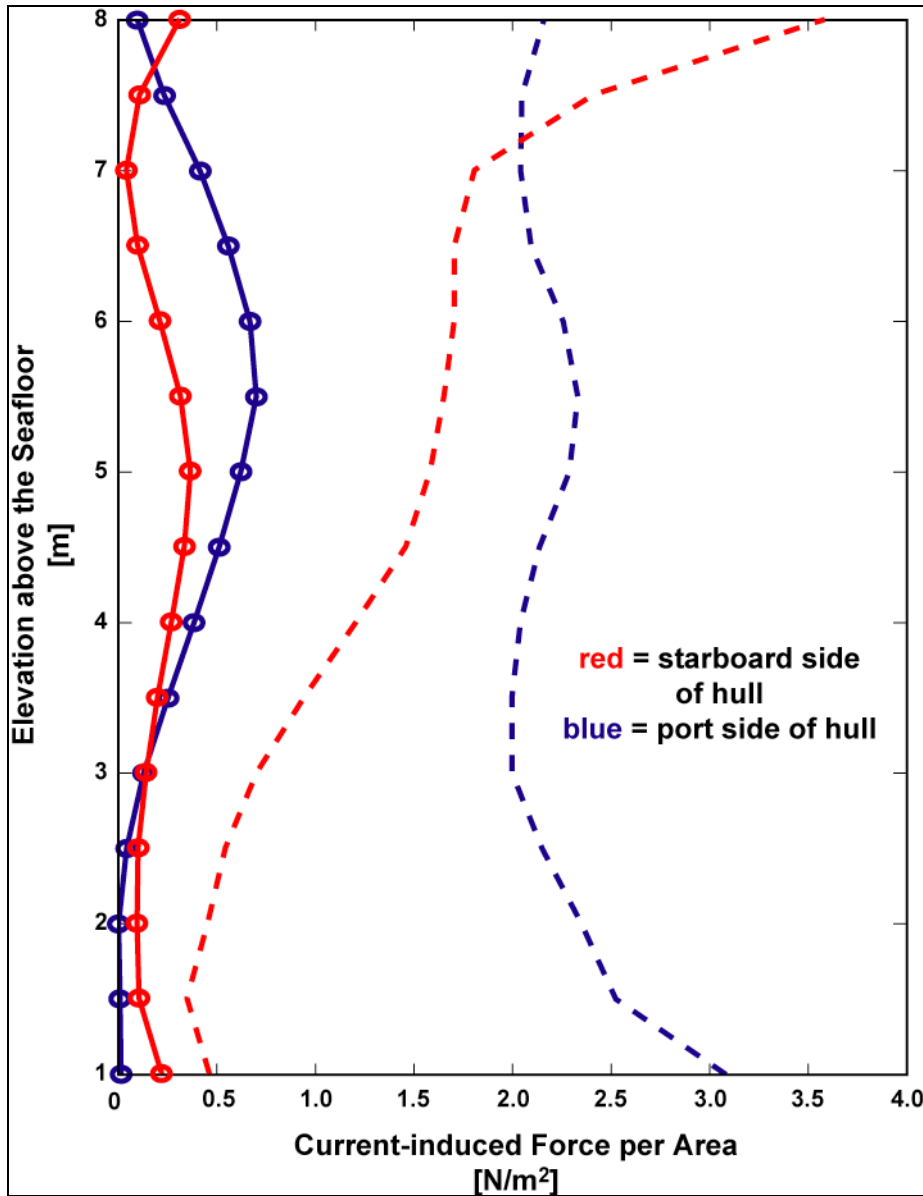
**Figure 4.7. Vertical profiles of the current-induced force on the USS *Arizona*'s hull.
Dashed lines are ± 1 standard deviation. Note that the force generally is at a maximum
6 m above the seafloor (4 m below the surface).**

Acoustic Backscatter

Over the period of study, the acoustic backscatter, which is a function of the particulate
matter in the water column, 0.6 m above the seabed at the site along the 10-m isobath ranged
between 145.48 dB and 281.52 dB, with a mean backscatter ± one standard deviation of 179.86 ±
20.64 dB. In general, highest acoustic backscatter measurements occurred during winter months

and the lowest during the summer months. This peak in acoustic backscatter suggests that wintertime phenomena causes increased particulate matter concentrations in the area around USS *Arizona*. Potential reasons for this increase in backscatter include: precipitation and runoff in other regions of Pearl Harbor that would introduce fine-grained particulate matter into the harbor that is advected into the area around *Arizona*, or nutrients introduced into Pearl Harbor from runoff might cause algal blooms that increase acoustic backscatter.

Acoustic backscatter was generally higher when the flow was to the south, likely caused by fine particulate matter being drawn down from the shallow regions of the northern half of the harbor. Acoustic backscatter also appeared to slightly increase during the early to mid-afternoon and decrease through the night (Figure 4.8); this suggests that either: (a) daily insolation-induced Trade wind intensification during the day creates larger Trade wind-driven waves that suspend more fine-grained sediment that is then advected by the sensor, or (b) more vessel traffic and prop wash during the day in the harbor tends to suspend more of the fine-grained bed sediment, which settles during the evening and night when vessel traffic subsides. We do not have information at this time that indicates which process or combination of processes is responsible for the observed intensification of acoustic backscatter during either the wintertime or in the afternoons and evenings.
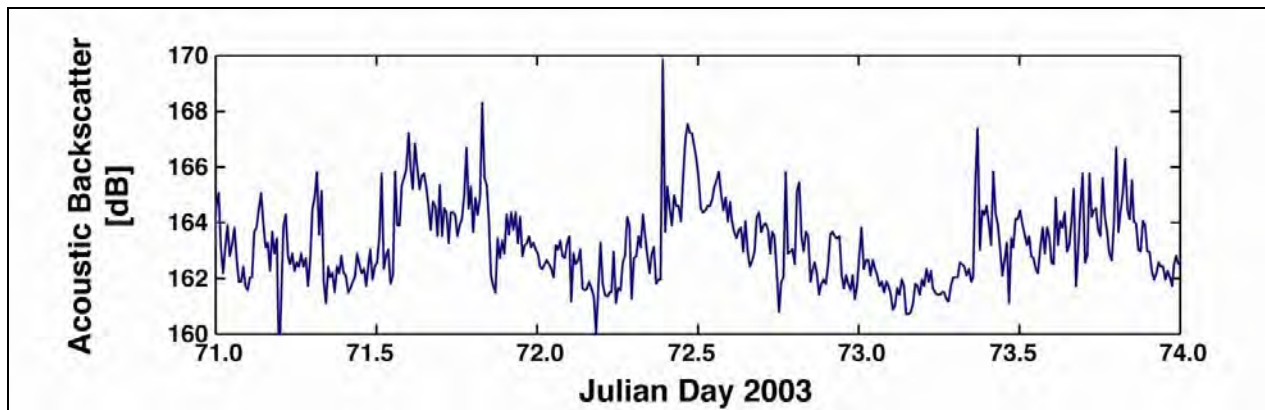
Figure 4.8. Typical acoustic backscatter data from USS *Arizona*.

Temperature

Over the period of study, water temperatures at the site along the 10-m isobath ranged between 23.14 °C and 27.52 °C, with a mean temperature ± one standard deviation of 26.03 ± 1.17 °C. The water temperature atop USS *Arizona*'s hull along the 3-m isobath ranged between 29.42 °C and 19.15 °C, with a mean temperature ± one standard deviation of 24.55 ± 2.08 °C. At both sites, insolation typically warmed the water, often more than 0.7 °C atop USS *Arizona*'s hull, but only 0.1-0.3 °C along the 10-m isobath. Thermal stratification, measured as the temperature difference between the sensor on the hull (depth~3 m) and the temperature sensor along the 10-m isobath, ranged between 0 and 2.5 °C, which reflects a distinct thermocline in the harbor's waters (Figure 4.9). This general trend of warmer water overlying cooler near-bed water causes the water column to be thermally stratified and stable, reducing interaction of the near-bed waters with the surface waters due to density contrasts.

Along the 10-m isobath, the variability in water temperature was greater off the starboard (northwestern) side of the hull between the USS *Arizona's* hull and Ford Island. In general, the near-bed water off the starboard (northwestern) side of the hull was slightly (0.02 ± 0.10 °C) warmer that off the port (southeastern) side of the hull (Figure 4.10). The greater stability off the port (southeastern) side of the USS *Arizona*'s hull is likely caused by greater mixing due to currents, which act to minimize temperature fluctuations caused by insolation or submarine groundwater discharge. We do not have information at this time that indicates that these processes are the cause of the temperature differences between the two sites.

Salinity

Over the period of study, the salinity at the site along the 3-m isobath ranged between 16.78 PSU and 42.56 PSU, with a mean salinity ± one standard deviation of 34.33 ± 4.25 PSU. Salinity tended to correlate positively with water temperature. This correlation is clearly seen when probable large surface runoff or groundwater effluences are advected by the YSI Sonde during the winter months, causing the temperature and salinity to rapidly drop. Gradual increases back to prevent levels over the course of a few days, likely due to current-induced mixing, follow these sharp decreases.
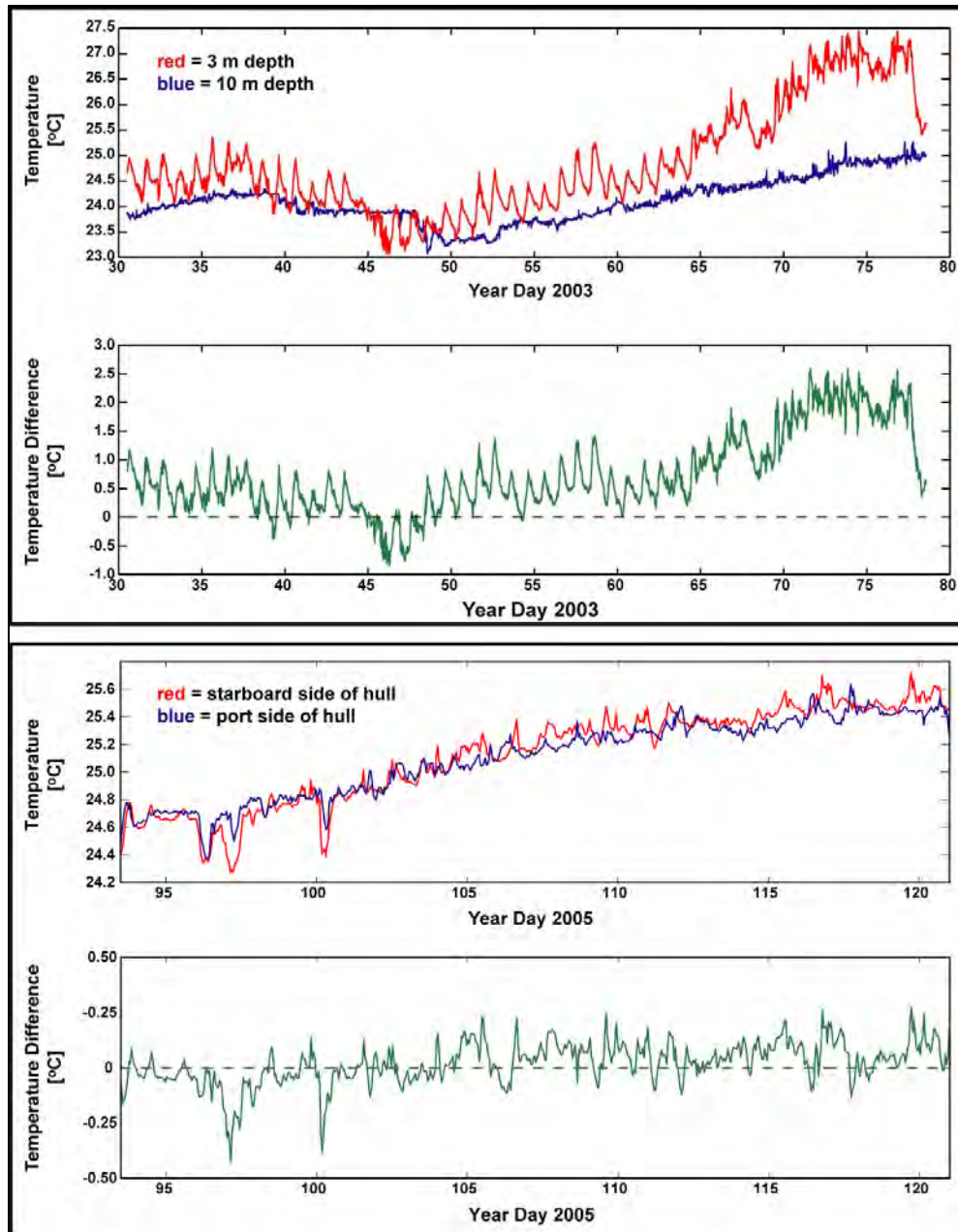
Figure 4.9. Differences in water temperature around the USS *Arizona*. TOP: Near-bed (10 m) and near-surface (3 m) temperatures and the resulting thermal stratification. BOTTOM: Concurrent water temperatures off the port and starboard sides of the hull and the resulting thermal gradient. While both the port and starboard temperatures both follow the same long-term trends, note the greater fluctuations in water temperature off the starboard side; this likely results from less mixing of the water column off the starboard side.

pH

Over the period of study, water pH at the site along the 3-m isobath ranged between 7.60 and 9.10, with a mean pH ± one standard deviation of 8.04 ± 0.15. Most variability in pH is at daily timescales; pH tends on average to rapidly increase from approximately 7.9 at roughly 09:00 each morning to more than 8.1 around 13:00, then decrease down to nominal levels of 7.9 by 21:00 (Figures 4.10 and 4.11). This daily increase, which is often on the order of 0.05 to 0.35, suggests that pH levels at the study site are related to daily insolation-driven warming or insolation-driven Trade wind intensification and Trade-wind wave-induced mixing.

Oxygen-Reduction Potential

Over the period of study, the oxygen-reduction potential at the site along the 3-m isobath ranged between 150.0 mV and 397.2 mV, with a mean oxygen-reduction potential ± one standard deviation of 289.2 ± 50.6 mV. Oxygen-reduction potential had an *inverse* relationship with pH and the percentage of dissolved oxygen during the summer months, with oxygen-reduction potential decreasing during the daytime and increasing into the night, attaining it greatest values just before sunrise. However, during the winter months when temperature and salinity were more variable, oxygen-reduction potential had more variable *positive* relationship with pH and the percentage of dissolved oxygen, suggesting that changes in salinity due to precipitation and/or submarine groundwater discharge might be impacting the data (Figures 4.10 and 4.11).

Dissolved Oxygen

Over the period of study, the dissolved oxygen levels in the water at the site along the 3-m isobath ranged between 0% and 288.5%, with a mean dissolved oxygen level ± one standard deviation of 69.5 ± 58.8%. Similar to the pH levels, most variability in dissolved oxygen levels is at daily timescales; dissolved oxygen tends to rapidly increase at roughly 09:00 each morning, peak around 13:00, then decrease down to nominal levels by 21:00 (Figures 4.10 and 4.11). This daily increase of 5-20% suggests that dissolved oxygen levels at *Arizona* are related to daily
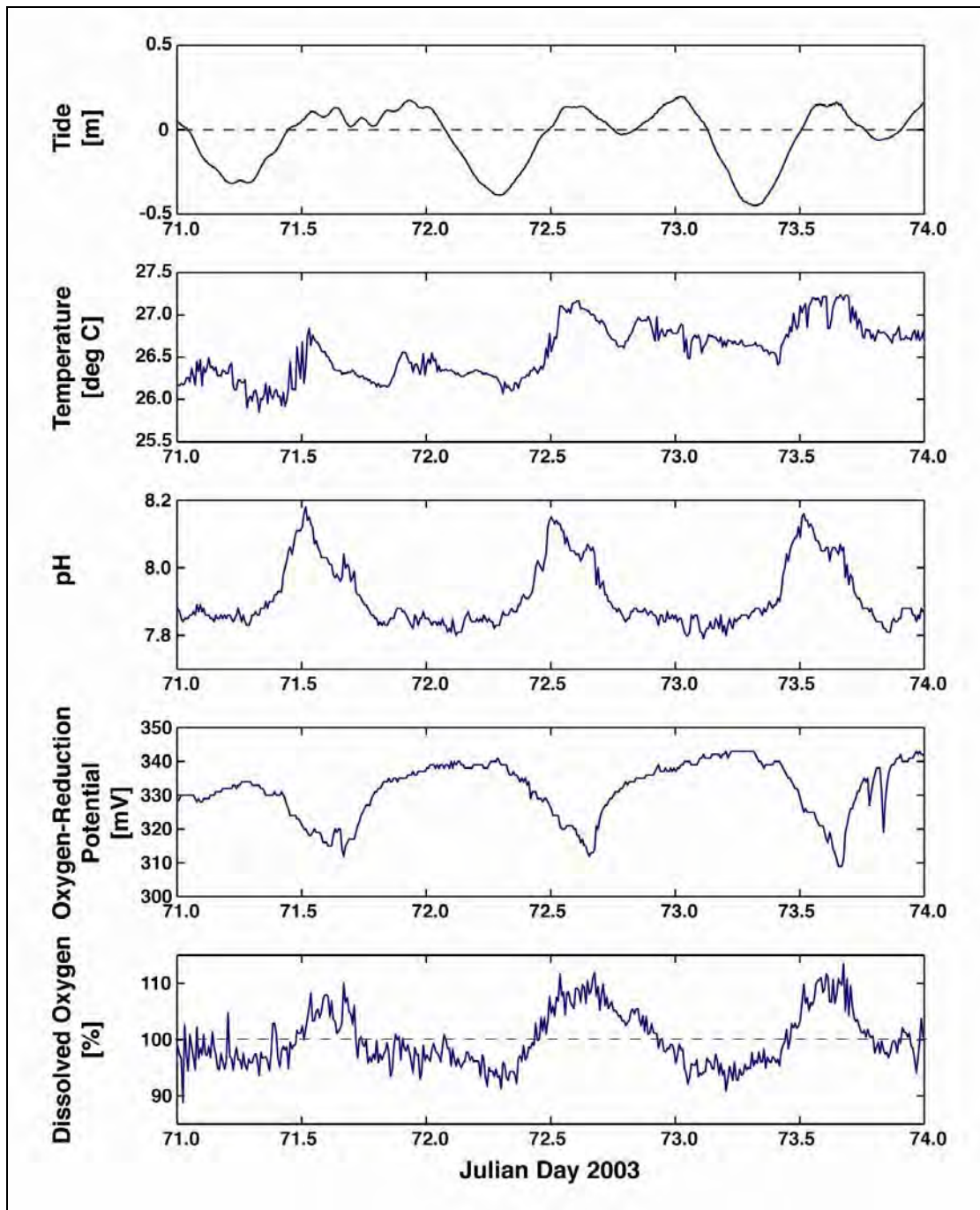
Figure 4.10. Graphic illustrating positive correlation between tide, temperature, ph, and dissolved oxygen; and an inverse correlation with oxygen reduction potential on the USS *Arizona* over a several day period.
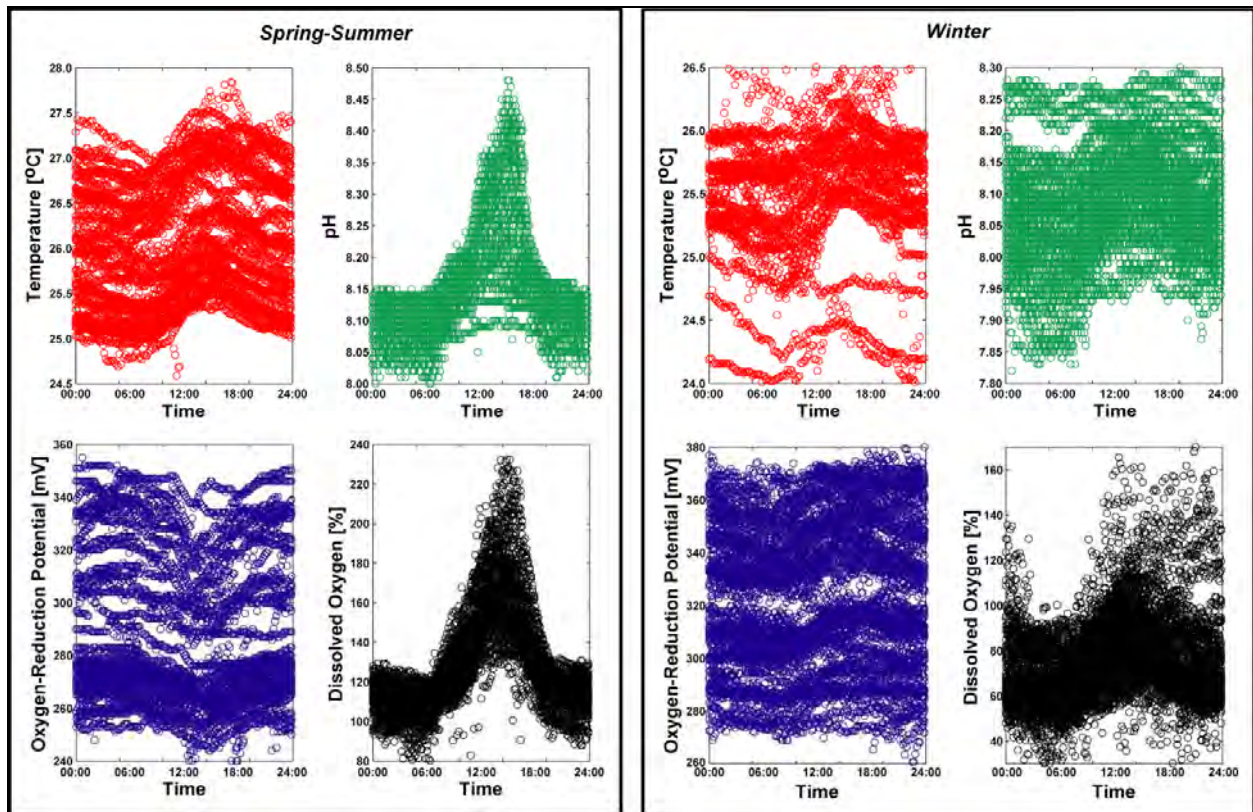
Figure 4.11. Phasing of pH, oxygen-reduction potential and dissolved oxygen relative to the time of day. These plots show how pH, dissolved oxygen and oxygen-reduction potential increase towards early afternoon and decline through the night into the early morning.

insolation-driven warming or insolation-driven Trade wind intensification and Trade-wind wave-induced mixing.

Vertical Variability

The temperatures during the vertical profiles taken in the early morning varied between 27.83 °C and 28.72 °C, with the near-surface temperatures on average roughly 0.74 °C warmer than the near-bed temperatures. The salinities during these profiles varied between 33.47 PSU and 34.38 PSU, with the near-surface temperatures roughly 0.79 PSU less saline on average than the near-bed salinities. The dissolved oxygen levels during these profiles varied between 15.3% and 91.2%, with the near-surface dissolved oxygen levels on average roughly 41.1% higher on average than the near-bed dissolved oxygen levels (Figure 4.12). The temperatures during the

vertical profiles taken in the late afternoon varied between 27.85 °C and 29.51 °C, with the near-surface temperatures roughly 1.32 °C warmer on average than the near-bed temperatures. The salinities during these profiles varied between 33.21 PSU and 34.35 PSU, with the near-surface temperatures roughly 0.91 PSU less saline on average than the near-bed salinities. The dissolved oxygen levels during these profiles varied between 11.7% and 104.4%, with the near-surface dissolved oxygen levels roughly 46.6% higher on average than the near-bed dissolved oxygen levels (Figure 4.12).

While mean near-bed temperatures did not vary significantly between the early morning and late afternoon vertical profiles, it is quite apparent that not only did the mean near-surface water temperatures increase significantly, but that a thermocline stretching to 6 m below the surface warmed on average approximately 0.8 °C. Neither salinity nor dissolved oxygen showed significant variations in the mean vertical profiles taken in the early morning versus those taken in the late afternoon.

DISCUSSION

Water movement and water column properties combine to affect steel hull corrosion. Water movement contributes to increased steel corrosion through at least two mechanisms: mechanical abrasion and causing increased dissolved oxygen in the disturbed water. The water movement data collected during this study suggest that the prevailing weather patterns, diurnal tides, and small, long-period swells that dominate Pearl Harbor likely have no extraordinary effects on hull corrosion. The anomalous, high-amplitude, short-period modulations from the southeasterly (90º-150º) or northwesterly (270º-330º) directions, however, may differentially affect *Arizona*'s hull. These swells are likely due to large vessels or possibly Navy tour boats moving past the Memorial, and may contribute to the increased deterioration and corrosion rates noted on the upper parts of the hull, in shallow water (see Chapter 5). As indicated by the corrosion data, due to hull orientation, these anomalous waves have a greater impact on the port side of the hull than the starboard side. In addition, greater current speed on the surface relative to the near bottom also contributes to increased corrosion in the shallower water (see Figure 4.3). The vertical velocity shear, caused by moving seawater of a given density, also imparts a vertical variation in current-induced force on the hull that is relatively greater on the port side than the
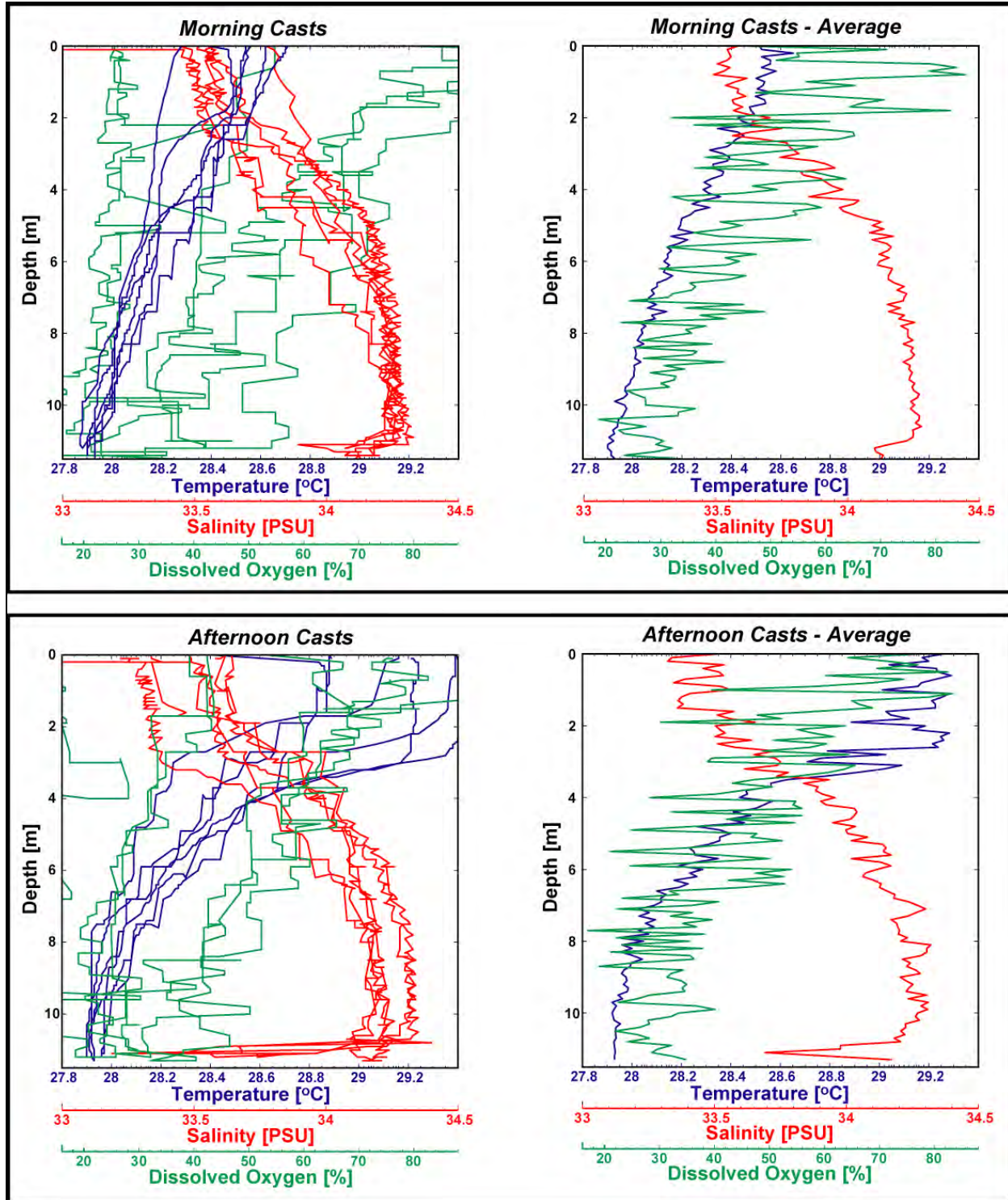
Figure 4.12. Vertical profiles of temperature, salinity and dissolved oxygen off the USS *Arizona* dock. These plots show how these parameters vary vertically from just below the water's surface down to the sea floor and how the vertical variation in these parameters changes over the course of a day.

starboard side of the ship (see Figure 4.4). This vertical velocity shear is also reflected in the corrosion data, with hull metal loss greatest on the port side between the surface and approximately 20 ft. water depth, based on direct measurement of midship hull samples. This differential corrosion is consistent with greater flow velocities on the port side. Below approximately 20 ft. water depth, metal loss is nearly the same on both sides of the hull.

With regard to the second variable, water column properties, it is unknown if acoustic backscatter has any direct effect on hull corrosion, but backscatter is likely a by-product of forces that do have an effect, such as current and other water movement. Water temperature in Pearl Harbor is consistently greater near the surface than near the seafloor, which contributes to the higher corrosion rates measured in shallow water. The temperature difference between the port and starboard sides of the ship is small enough that it likely has no effect on differential corrosion. Salinity, pH, oxygen-reduction potential, and dissolved oxygen vary somewhat over the course of each day and throughout the year, but the long-term data from the YSI Sonde does not offer any comparative data that might address hull corrosion variability. Vertical variability recorded during vertical profiling with the YSI Sonde and dissolved oxygen meter, however, is more illuminating. Corroborating the long-term data recorded with the SonTek ADV and YSI Sonde, temperature was found to be warmer at the surface and cooler near the harbor bottom. In an expected inverse relationship with temperature, salinity was slightly lower at the surface and higher near the bottom. The most important factor recorded, however, is dissolved oxygen, which was found to be on average 41–46% higher near the surface than at the harbor bottom. This strongly contributes to the higher corrosion rates found in shallower portions of *Arizona*'s hull. To determine if the same vertical variability in water column properties occurs inside *Arizona*'s hull as outside of it, comparative interior measurements were recorded. These are discussed in the next section.

INTERIOR DATA COLLECTION

INTERIOR MEASUREMENTS, 2002-2004

Environmental monitoring was conducted within *Arizona*'s interior cabins to determine internal environmental conditions. Internal conditions can be compared to external conditions to

infer interior corrosion nature and rate. These data are critical to developing a viable Finite Element Model that takes into account both interior and exterior hull corrosion. Interior investigations began in 2002 and used an YSI dissolved oxygen meter to obtain dissolved oxygen concentration inside selected core drill holes after removal of steel hull samples (see Chapter 5 for details of core sample operations). Investigations of interior spaces in 2003 used a VideoRay Remotely Operated Vehicle (ROV) equipped with a YSI 600XLM Multiparameter Sonde (a smaller version of the YSI Model 6600 Sonde described above) to measure temperature, salinity, pH, dissolved oxygen, and oxygen-reduction potential—with the exception of acoustic backscatter, the same parameters recorded externally (Figures 4.13 and 4.14). This survey focused on second deck cabins accessible to the ROV via open portholes, as well as inside Barbette No. 3, which is accessible from the surface. Subsequent investigations in 2004 recorded environmental parameters in Third Deck spaces—although very few of these areas were accessible to the ROV.

Operations

Interior Dissolved Oxygen Measurements, 2002

An YSI dissolved oxygen meter was used to obtain dissolved oxygen concentration inside selected core drill holes after removal of steel hull samples during 2002 sampling operations. First, ambient seawater was measured on the exterior of the sample location. Next, the dissolved oxygen probe was attached to the end of a 6 ft. section of PVC pipe and inserted into the hole after removal of a plug seal, which had been inserted into each drill hole after the core was removed. The probe was inserted 1–2 ft. and the readings were allowed to stabilize before recording. A total of five locations were sampled in this way.

Interior ROV-based Measurements, 2003–2004

For ROV operations in 2003–2004, the YSI Sonde was used in profiling mode to take continuous measurements. The VideoRay ROV manufacturers integrated the YSI Sonde with the ROV so that data could be received on the surface from the Sonde through the ROV tether,

Figure 4.13. VideoRay ROV equipped with YSI Sonde outside on open porthole on USS *Arizona*'s Second Deck (NPS Photo by Brett Seymour).
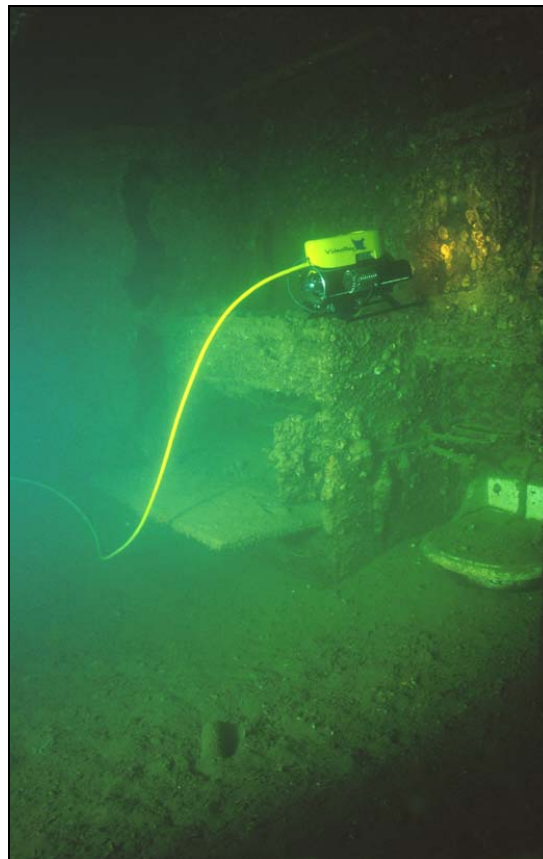
Figure 4.14. VideoRay ROV conducting interior investigations on USS *Arizona*'s Second Deck (NPS Photo by Brett Seymour).

and the Sonde could be controlled from the surface via a laptop computer. This allowed researchers to record separate data files for each location sampled. In addition, a continuous log of ROV movements was recorded and the timestamp on the ROV video could be correlated with the timestamp on the YSI data stream to allow precise interpretation of ROV location within each cabin.

In total, 23 separate interior spaces were measured using the YSI Sonde-equipped VideoRay ROV. These spaces included 20 cabins and hallways on the Second Deck accessible through a combination of open portholes, exterior hatches, and accessible bulkheads; two interior spaces on the Third Deck that are only accessible via vertical hatches, including one that can only be reached after a long run down a Second Deck hallway; and the interior of Barbette No. 3, which reaches down to the First Platform level (just below the Third Deck) (Figure 4.15).

Results

Interior Water Column Properties

Interior water column properties collected include variations in temperature (ºC), salinity (PSU), pH, oxygen-reduction potential (mV), and dissolved oxygen (%). Their ranges, variability and potential causes for their variability are discussed here. In total, 9,203 measurements were taken from Second Deck spaces; 2,160 measurements from Third Deck spaces, and 423 measurements at the First Platform level of Barbette No. 3.

Temperature

Temperatures recorded in Second Deck cabins varied from 26.3–27.5ºC, with an average of 27.2ºC; on the Third Deck, temperatures were steadier at 27.3–27.5ºC with a 27.4ºC average; inside Barbette No. 3 at the First Platform level, water temperatures were slightly cooler, ranging from 24.7ºC to 26.7ºC, with an average of 26.6ºC. All interior temperatures fall within the seasonal and/or daily range of variability recorded on *Arizona*'s exterior.
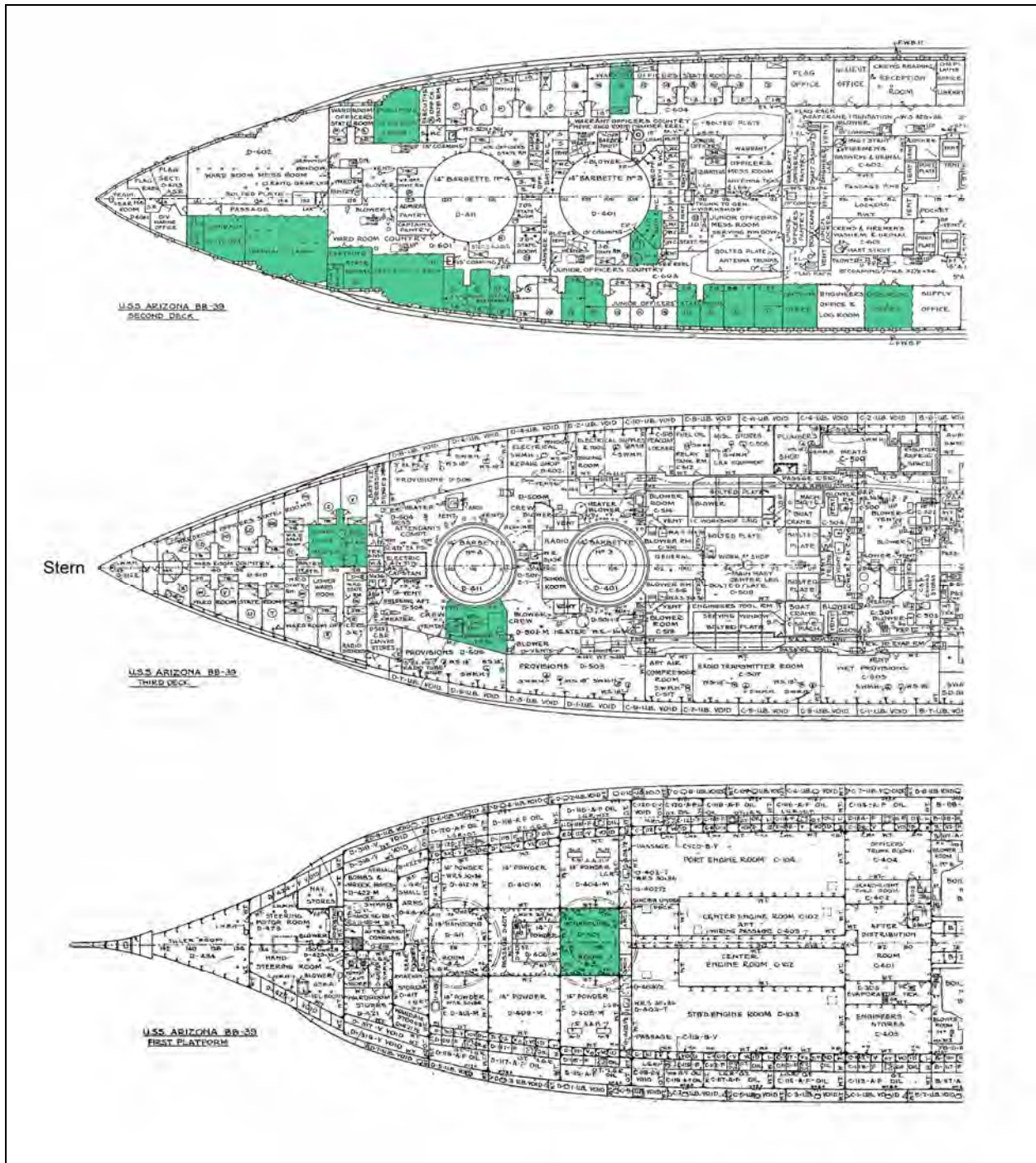
Figure 4.15. Interior spaces measured using the YSI Sonde-equipped VideoRay ROV.

Salinity

Inside Second Deck cabins, salinity ranged from 31.1–35.1 PSU, with an average of 34.0 PSU; on the Third Deck, salinity was 30.2–32.4 PSU with a 32.2 PSU average; inside Barbette No. 3 at the First Platform level, salinity was slightly higher (likely due to less seawater exchange and evaporation from the open top of the barbette), ranging from 35.3–35.0 PSU, with an average of 34.3 PSU. Like temperature, all interior salinity measurements fall within the long-term range of variability recorded outside *Arizona*'s hull, although the more enclosed Third Deck has a salinity that is slightly under 2 parts per thousand lower than more exposed interior spaces.

pH

Within Second Deck cabins, pH varied from 7.05–9.36, with an average of 7.69; on the Third Deck, pH was steadier at 7.90–8.07 with a 8.01 average; inside Barbette No. 3 at the First Platform level, pH was slightly higher, ranging from 8.18–9.36, with an average of 8.41. All interior pH measurements are close to the seasonal and/or daily range of variability recorded on *Arizona*'s exterior, and are within the normal range of variability for seawater, although enclosed interior spaces have slightly higher pH levels.

Oxygen-Reduction Potential

Oxygen-reduction potential recorded in Second Deck cabins varied from 125–912 mV, with an average of 775 mV; on the Third Deck, oxygen-reduction potential readings were anomalous, ranging from -237–307 mV with a -129 mV average; inside Barbette No. 3 at the First Platform level, oxygen-reduction potential ranged from 281–733 mV with a 642 mV average. Oxygen-reduction potentials fall well outside the seasonal and/or daily range of variability recorded on *Arizona*'s exterior, and (with the exception of the Third Deck readings) are much higher on average (see Chapter 5 for a more extensive discussion of oxygen-reduction potential)

Dissolved Oxygen

The data from interior dissolved oxygen measurements through hull steel sample holes taken in 2002 are shown in Table 4.5. Exterior measurements in ambient seawater before inserting the dissolved oxygen meter into the hull varied from 4.74 to 5.68 mg/L (Note: mg/L is an alternative unit of measure for dissolved oxygen, but one not easily converted to percent saturation after the fact). Once inserted into the hull through the core sample holes approximately 1–2 ft., the readings dropped, varying between 0.0 and 3.99 mg/L once they stabilized. These interior spaces reveal a wide range of oxygen concentrations depending upon access to ambient seawater. For the sample locations on the second deck (USAR-02-002 and USAR-02-008), which have some seawater exchange through open port holes, dissolved oxygen concentration dropped an average of 27% below ambient, exterior seawater measurements. For the sample locations in the torpedo blisters (USAR-02-003, USAR-02-004, and USAR-02-009), the dissolved oxygen concentration varied from 2.47 to 0.0 mg/L depending on proximity to breaches in the otherwise sealed torpedo blister, 56–100% less than ambient exterior measurements. Dissolved oxygen levels dropped to zero or near-zero in the two locations where the torpedo blister was completely sealed and had no seawater exchange.

From the YSI Sonde-equipped VideoRay ROV, inside Second Deck cabins dissolved oxygen ranged from 45.0–104.1%, with an average of 64.0%; on the Third Deck, dissolved oxygen levels were 0.0–12.6% with a 4.1% average; inside Barbette No. 3 at the First Platform level, dissolved oxygen was 40.4–80.6%, with an average of 47.8%. Interior dissolved oxygen measurements fall within the long-term range of variability recorded outside *Arizona*'s hull, although the Third Deck has much lower dissolved oxygen saturation than other interior spaces. In general, dissolved oxygen saturation decreases significantly as active seawater exchange is reduced. This observation is significant when considering interior steel hull corrosion rates.

Sample Number	Location	Exterior DO (mg/L)	Interior DO (mg/L - lowest)
USAR-02-002	Second Deck - Limited Seawater Exchange	4.74	3.99
USAR-02-003	Torpedo Blister - No Seawater Exchange	5.52	0
USAR-02-004	Torpedo Blister - No Seawater Exchange	4.82	0.01
USAR-02-008	Second Deck - Limited Seawater Exchange	5.4	3.35
USAR-02-009	Torpedo Blister - Limited Seawater Exchange	5.68	2.47

Table 4.5. Dissolved oxygen measurements inside the hull steel sample core holes.

Vertical Variability

One of the more interesting observations is that interior cabin water on the Second Deck is stratified by a subtle thermocline of about 0.2ºC. Dissolved oxygen levels, however, change significantly across this thermocline, from nearly 70% saturation above to about 50% saturation below the thermocline. This observation was noted throughout all Second Deck cabins. Although interesting, this phenomenon likely has a negligible effect on overall corrosion, and the observation was not repeated on the Third Deck at the First Platform level.

DISCUSSION

Except for dissolved oxygen and oxygen-reduction potential, water column properties from interior spaces of USS *Arizona* vary only slightly from exterior conditions. In general, Second Deck measurements vary little from Third Deck measurements. The amount of variation observed is considered negligible for all variables, with the single exception of dissolved oxygen. Interior measurements of temperature, salinity, and pH all fall within the seasonal or daily variation recorded on *Arizona*'s exterior and the norms expected for Pearl Harbor seawater. Salinity was slightly less on average in the lower, more enclosed portions of the hull's interior, while pH slightly higher; both of these would contribute to slightly lower corrosion rates. Significant differences in dissolved oxygen were observed on the hull's' interior, however, compared to baseline measurements outside the ship. As mentioned previously, dissolved oxygen is also the most important variable contributing to steel corrosion in seawater (see Chapter 5), and this is therefore a significant observation.   The higher overall oxygen-reduction potential measurements may reflect lower overall active corrosion, which would be consistent with other observations.

CONCLUSION

In all, more than 1,000,000 external observations of currents, waves and water-column properties were collected per day for 393 days between November 2002, and April 2005, in Pearl Harbor. Significant findings based upon these measurements and analyses include:

(1) Tides are of mixed, semi-diurnal type with a minimum, mean and maximum tidal range of 0.4 m, 0.6 m and 0.9 m, respectively.

(2) Waves are not an important factor in the vicinity of USS *Arizona*'s hull. Those observed were, while long period (~20 s), very small (order of cm's) and likely due to open-ocean long-period swell. Vessels passing close to the study site are likely responsible for the high-amplitude, low-period motions that were observed.

(3) Flow along the 10-m isobath is dominated by semi-diurnal and diurnal tidal motions, which are modulated to some degree by what appears to be wind forcing during the mid-to late afternoon. Flow at the surface is down-wind to the southwest. Flow throughout most of the water column is primarily parallel to the USS *Arizona*'s hull at 0.01-0.02 m/sec and net flow is to the northeast. Flow closer to the seafloor, however, is weaker and more variable in direction.

(4) Flow speeds are faster off the port side than the starboard side, and thus the water replenishment times on the port side of the hull are shorter than off the starboard side. Shear, both vertically in the water column and across the hull, was observed. This results in vertical variations in replenishment times and current-induced forces on the hull. This shear also likely increases vertical mixing of the water column.

(5) Acoustic backscatter was generally higher in the winter months and during the falling tide, suggesting advection of material introduced into the northern sections of Pearl Harbor due to winter precipitation and its movement south past the hull by ebbing tidal currents. Higher measurements of acoustic backscatter often occurred in the afternoon, suggesting increased trade wind-induced mixing or, perhaps, increased vessel activity, which facilitates water column mixing and fine-grained particulate resuspension.

(6) Water temperatures were generally slightly higher (mean = 26.03 °C) and less variable (standard deviation = 1.17 °C) along the 10-m isobath than along the 3-m isobath (mean

= 24.55 °C, standard deviation = 2.08 °C). A thermocline was often present in the

harbor's waters, with the shallower (3 m) and deeper (10 m) water temperatures often

differing by more than 2 °C. Water temperatures along the 10-m isobath were generally

cooler and less variable off the port side of the hull than off the starboard side, possibly

due to faster replenishment times and greater mixing of the water column.

(7) Salinity ranged from 16.78 PSU and 42.56 PSU, with a mean ± one standard deviation of

34.33 ± 4.25 PSU. Salinity appears to positively correlate with water temperature and

suggests that Pearl Harbor's waters are influenced by freshwater runoff or groundwater

effluence in the winter months.

(8) pH ranged between 7.60 and 9.10, with a mean ± one standard deviation of 8.04 ± 0.15

and dissolved oxygen 0% and 288.5%, with a mean ± one standard deviation of 69.5 ±

58.8%. Both pH and dissolved oxygen tended to correlate with the daily insolation cycle,

increasing during the morning into the early afternoon followed by decreasing through

the night to minimum levels just before sunrise.

(9) Oxygen-reduction potential ranged between 150.0 mV and 397.2 mV, with a mean ± one

standard deviation of 289.2 ± 50.6 mV. Oxygen-reduction potential had an *inverse* with

pH and the percentage of dissolved oxygen during the summer months and a *positive*

relationship with pH and the percentage of dissolved oxygen during the winter months

when temperature and salinity were more variable.

(10) During the vertical profiling, near-surface temperatures were on average roughly 1.03

°C warmer than the near-bed temperatures, near-surface temperatures were roughly 0.85

PSU less saline on average than the near-bed salinities and near-surface dissolved oxygen

levels were on average roughly 43.9% higher than the near-bed dissolved oxygen levels.

These data provide us with a much clearer picture of the nature of and controls on the

physical environment around USS *Arizona*'s hull. The complexity of the physical environment

surrounding and influencing *Arizona* is reflected in the number of interesting phenomena

observed during this study. The next step is to correlate these environmental aspects with active corrosion processes affecting *Arizona* to refine the predictive model of the ship's deterioration.

On *Arizona*'s interior, in general, most parameters recorded with the YSI Sonde-equipped VideoRay ROV were very similar inside the ship as outside. Temperature, salinity, and pH were all within a normal range of variability. Dissolved oxygen and oxygen-reduction potential, on the other hand, varied significantly from baseline measurements outside the hull. The most significant observation is that dissolved oxygen decreased to near-zero within interior spaces that do not receive active seawater exchange. Most significantly, on the Third Deck, which has no direct access to exterior seawater except through a single vertical hatch, dissolved oxygen averaged only 4.1% saturated. With the exception of a small portion of the First Platform accessible through Barbette No. 3, there is no access to any interior spaces below the Third Deck. However, based on data from the Third Deck and within the torpedo blisters, which indicate that dissolved oxygen can reach 0.0% saturated in spaces that do not have seawater exchange, it is probable that *Arizona*'s interior spaces below the Third Deck have extremely low levels of dissolved oxygen, and may even be at 0.0% saturated. Because all of *Arizona*'s original oil storage spaces are below the Third Deck, and the majority of *Arizona*'s remaining oil is likely still stored in those spaces, it is probable they are undergoing very low corrosion rates. This topic will be discussed in more detail in Chapter 5.

REFERENCES

National Climate Data Center, National Oceanographic and Atmospheric Administration
        2005 NCDC Hourly Surface Climate Data for Hawaii, Online Dataset,
        http://www.ncdc.noaa.gov/oa/climate/climatedata.html#hourly

North, N. A. and I. D. MacLeod
        1987 Corrosion of Metals. In *Conservation of Marine Archaeological Objects*, edited by
        C. Pearson, pp. 68-98. Butterworth & Co., London.

Storlazzi, C. D., M. A. Russell, M. D. Owens, M. E. Field and L. E. Murphy
        2004 *Dynamics of the Physical Environment at the USS Arizona Memorial: 2002-2004*.
        U.S. Geological Survey Open-File Report 2004-1353,
        http://pubs.usgs.gov/of/2004/1353/.

Storlazzi, C. D., M. A. Russell, M. K. Presto and J. E. Burbank
        2005 *Flow Patterns and Current Structure at the USS Arizona Memorial: April, 2005*.
        U.S. Geological Survey Open-File Report 2005-1334,
        http://pubs.usgs.gov/sir/2005/1334/.

CHAPTER 5

Steel-Hull Corrosion Analysis of USS *Arizona*

Donald L. Johnson, Brent M. Wilson, John D. Makinson, Robert De Angelis, William N. Weins, and James D. Carr

INTRODUCTION

Corrosion research on USS *Arizona* focused on understanding and characterizing the specific nature of corrosion occurring on the vessel and determining the corrosion rate for different structural elements of the ship. The goal was to establish a curve of deterioration and "plot" where *Arizona* currently falls on that curve. Predictive modeling of USS *Arizona* hull deterioration was accomplished by developing a Finite Element Model (FEM), constructed by the National Institute of Standards and Technology (NIST) in Gaithersburg, MD (see Chapter 6). The FEM was designed to model *Arizona*'s structural deterioration and eventual collapse—information critical for developing a sound, scientifically-based management plan and for determining when, or if, intervening in the vessel's natural deterioration should be considered. The FEM, however, was designed to model increasing hull stress as a function of decreasing percentage of remaining hull steel, and therefore lacks a specific time element. Corrosion analysis reported in this chapter supplies the necessary corrosion rate to make the FEM predictive. A key first-step in determining the steel-hull corrosion rate was to determine the remaining thicknesses of surviving steel-hull components. This could then be compared to as-

built steel thicknesses from surviving ship's plans. Because direct measurement of remaining

steel thickness could only be completed in limited areas, a corrosion rate model had to be created

for application to areas of *Arizona*'s hull in different environmental conditions, including

exterior, interior, above the harbor bottom, and below the harbor bottom. Because the battleship

is a large, complex three-dimensional structure, and it is impossible to directly measure corrosion

rates for all critical elements, there was necessarily some generalizing and use of inferential data

to derive rates of deterioration, particularly for inaccessible internal structures. In order for a

general corrosion rate model to be accurate, the overall corrosion process must be recognized

and described, including identifying relevant environmental variables that affect the corrosion

process.

This chapter presents a comprehensive synthesis of 1998–2007 research on corrosion of

USS *Arizona*'s steel-hull. It begins by describing the background necessary to evaluate the

corrosion process taking place on *Arizona*'s hull, including a review of parameters relevant to

electrochemical corrosion of steel in seawater, a discussion of hull steel chemistry and

microstructure, and seawater chemistry. The chapter then describes the corrosion process in

detail through a combination of theoretical and direct experimental applications, such as *in situ*

corrosion measurements and constituent analysis of concretion covering the ship. Finally, the

chapter details current understanding of hull corrosion rate variability (including factors which

control the rate) and presents an analysis of *Arizona*'s long-term structural integrity, with a

particular focus on primary oil containment spaces within the hull.

ELECTROCHEMICAL CORROSION OF STEEL IN SEAWATER

CORROSION PROCESS

Corrosion is an electrochemical process, which means that direct current, though very

small (on order of microamperes), flows in a cell made up of three necessary components: (1)

areas of opposing polarity; (2) an electrolyte; and (3) a return electrical circuit path. If any one

of the three electrochemical components is missing, corrosion will not occur.

As in a battery, positive and negative poles define areas that exhibit a potential difference

that constitute the driving force for the flow of current. Potential, or voltage, is the difference in

electrical charge between two points in a circuit expressed in volts or millivolts (mV). Two modes of current are used to explain the corrosion process. Current flowing from the negative pole or anode, through the electrolyte to the positive pole or cathode, and returning to the anode via a metallic return circuit path is referred to as positive current, and is associated with the flow of ions in the electrolyte. Current flowing in the opposite direction from the anode through the metallic circuit to the cathode is referred to as negative current, and is associated with the flow of electrons. To put this into perspective, adjacent regions on the metal hull act separately as anode and cathode, and the hull metal between the anode and cathode completes the metallic circuit needed to conduct electrons between them. The electrolyte in contact with hull metal conducts ions in solution in the opposite direction. Corrosion always occurs at areas where positive current leaves the structure and enters the electrolyte or corroding medium, and is identified as the anode (Figure 5.1).

Opposing polarity or potential difference between two areas is created in a variety of ways: the most obvious is the relative activity of elements in the electromotive force (EMF) series when any two (or more) are immersed in an aqueous solution saturated with that metal's ions (Table 5.1). It should be noted that the reactions are written as reduction reactions, for example, $Fe^{+2} + 2e = Fe$, where the reduction potentials are given in Table 5.1 as the Standard Hydrogen Electrode (SHE). Reduction potentials match the polarity of experimentally measured potentials, in accordance with the Stockholm convention. When comparing potentials in a given system, the higher potential is cathodic to the lower potential. For example, comparison of copper (Cu) and iron (Fe) shows a potential difference of 789 millivolts (mV). Assuming that both metals are placed in an electrolyte, such as sea water, and connected to each other by a conductor, Fe will corrode because it is more negative than Cu, and Cu will act as the opposing pole, or cathode, and will not corrode. This is the basis for the principle of cathodic protection, since the Fe in effect protects the Cu (see below for a more detailed analysis of cathodic protection). Zinc (Zn) is often connected to Fe structures to purposely cause the Zn to corrode and render the Fe a cathode; in this case the Zn is known as a sacrificial anode. In sea water, an alloy of aluminum is normally chosen to protect Fe (and steel) structures because it performs better than Zn in the presence of chloride ions present in sea water. The EMF series is based on concentrations of one mole per liter of that metal ion in the solution. In real situations,
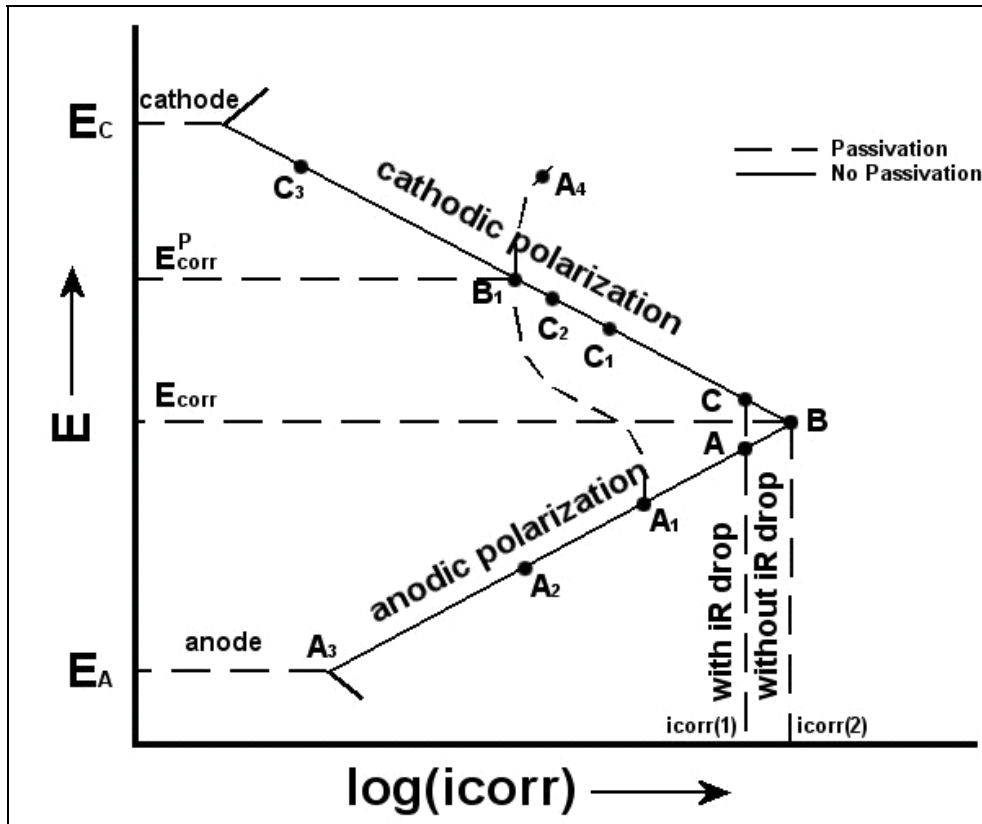
Figure 5.1. Typical polarization diagram with passivation superimposed (dashed).

Element E^0	Potential (millivolts) Relative to hydrogen electrode
Au/Au+	1498
Ag/Ag+	799
Cu/Cu+	342
Hydrogen	0
Fe/Fe++	-447
Zn/Zn++	-762
Al/Al+++	-1,662

Table 5.1. EMF Series for Selected Elements.

concentrations are much lower and correction for concentration and temperature is made by applying the Nerst equation:

$$E = E^0 + 2.3 \ (RT \ / \ nF) \ [\log \ (C)] \qquad\qquad [1]$$

where

E^0 (SHE) is standard potential at 1 mole/liter concentration of metal ion

R is the gas constant 8.314 J/mole °K

T is temperature (° K)

n is valence

F is Faraday constant, 96,500 Coulombs/equivalent (One coulomb = one ampere second and one equivalent = atomic wt./ valence)

C is concentration of oxidized species, Fe^{+2} (mole/liter)

While a bi-metallic (or two metal) cell is operative in many complex structures, there are a variety of cells which can cause corrosion without the existence of a second metal. First, oxygen cell corrosion is common in situations where the oxygen is not uniformly distributed over the surface. The areas low in oxygen corrodes faster than the area higher in oxygen—in such a case the area lower in oxygen is anodic to the area higher in oxygen. A specific class of metals forms an inherently thin yet very stable, uniform and protective layer in oxidizing environments. The metals in this class "passivate" readily and are corrosion resistant in the presence of oxygen. Examples of such metals include stainless steels and aluminum alloys. Steel will passivate in strong oxidizing solutions such as dilute nitric acid, but normally not in seawater. Second, temperature differential cells develop when a temperature difference occurs across a metal structure. An area at higher temperature is theoretically predicted to be anodic or negative to an area at lower temperature as Equation [1] indicates. Due to the very small shift in potential occurring at ordinary temperatures, this effect is often masked by other variables. Third, microconstituent corrosion cells, another form of corrosion cell, are common since most structural materials are alloys made up of a combination of other metals or non-metals. For example, mild steel used in ship construction may contain less than 0.2 % carbon yet undergo corrosion because the compound iron carbide, formed during cooling after fabrication, is

cathodic to the adjacent nearly pure iron making up the matrix. This is particularly significant when the pH is low or acidic. It should be noted that iron carbide is not an impurity since it imparts added strength to the steel. Fourth, a stress cell is often evident on steel where the metal has been stressed at sharp bend areas. The stressed area becomes anodic to the remaining structure. Finally, the differential electrolyte cell is typical of corrosion in which the composition of the electrolyte varies over the metal surface. In theory, the area lowest in concentration of oxidized species (Fe^{+2}) is anodic to the area higher in concentration. In practical terms, the most common differential cell is oxygen cell corrosion, in which the oxygen concentration varies on the surface on a micro-scale.

An aqueous solution of water combined with other ions is normally the corroding medium or electrolyte. An electrolyte is ion conductive and will provide transport for cations (positively charged ions) and anions (negatively charged ions). In the case of steel, iron cations enter the solution at a rate proportional to the current flow, usually in the range of microamps per square centimeter ($\mu A/cm^2$). If the electrolyte is distilled water with no impurities or dissolved oxygen, corrosion will not occur because the electrolyte will not conduct positive current.

The return circuit path must be an electron conductor. For a bi-metallic (galvanic) cell, such as a steel hull in structural contact with copper alloy propellers, the hull will corrode, in part, because steel is anodic to copper. Since the hull (anode) is much larger than the propellers (cathode), the corrosion caused by the galvanic cell would be minimal because the corrosion current supported by the small propellers is spread over a much larger hull surface. If the propeller were made of aluminum, however, the propeller would be anodic to the hull and would corrode in a very short time because it is small relative to the hull, and a high current supported by a large cathodic hull would be focused on a small anodic propeller (high current density). A non-conducting insulator is sometimes used to isolate areas of opposing polarity by interrupting the electron conducting metallic circuit. In most cases it impossible to isolate such areas physically. For example, microconstituent corrosion between iron (alpha iron) and iron carbide in the steel microstructure cannot be prevented by electrical isolation because the two microconstituents in steel cannot be insulated from each other.

When iron or steel is placed in seawater, corrosion begins as a reaction in which the oxidation of metal is the anodic or corroding portion of a corrosion cell. Chemical reactions at the anode are usually fairly simple and involve the release of electrons and conversion of metal

from a solid to an ion that is soluble in aqueous solutions. Since the corrosion process in this discussion involves steel, the anode reaction is illustrated by the oxidation of iron:

$$Fe = Fe^{+2} + 2e^{-} \qquad \qquad [2]$$

where

> Fe is iron in steel
>
> Fe^{+2} is iron ions in solution (oxidized specie)
>
> 2 electrons ($2e^{-}$) are released per gram-atom of iron

The cathode reaction can take many different forms depending upon the corroding electrolyte, flow conditions and temperature. Whatever form it takes, cathode reactions serve the purpose of consuming electrons produced at the anode. Since charge balance must be maintained, the rate of production and consumption of electrons must be equal. The two most common reduction reactions occurring at the cathode are hydrogen formation and oxygen consumption. Therefore, the rate of electron consumption, proportional to the corrosion rate, is typically governed in seawater by one or both of the following reactions:

$$\tfrac{1}{2}\,O_2 + H_2O + 2e^{-} = 2OH^{-} \qquad \text{(Oxygen consumption)} \qquad [3]$$
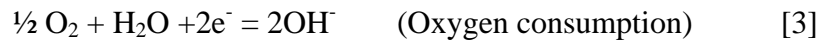
where

> OH^{-} is the hydroxyl ion

 or

$$2H^{+} + 2e^{-} = H_2 \qquad \qquad \text{(Hydrogen evolution)} \qquad [4]$$
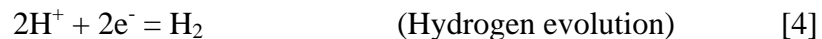
where

> H^{+} is the hydrogen ion

The corrosion product is loosely attached and does not become a diffusion barrier to oxygen. Combining equations [3] and [4], the overall corrosion reaction is given by:

$$Fe + \tfrac{1}{2}\,O_2 + H_2O = Fe(OH)_2 \qquad \qquad [5]$$

$$4Fe(OH)2 + O2 = 2H2O + 2Fe2O3 \cdot H2O \qquad \qquad [6]$$
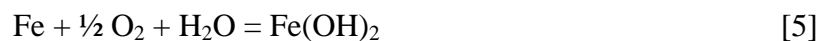
The iron oxide formed in equation [6] is red brown and is the familiar rust on cars and buildings.

In areas where oxygen has limited access, chlorine ions, if present in the electrolyte, diffuse into those areas to maintain charge balance. On *Arizona*, limited oxygen is caused by the presence of concretion loosely bonded to the metal surface and acting as a diffusion barrier to the influx of oxygen to the metal. The thicker the barrier, the slower the diffusion and a condition is reached in which the iron consumes oxygen faster than it is replenished. The resulting process is termed hydrolysis and creates acidic conditions that promote hydrogen discharge. Such reactions may also occur at crevices and pits on metal surfaces. A typical hydrolysis reaction is given by Jones (1996):

$$Fe^{+2} + 2\ H_2O + 2Cl\text{-} = Fe(OH)_2 + 2HCl \tag{7}$$
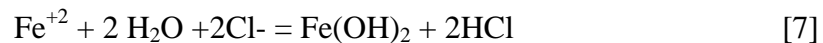
Charge balance is maintained in reactions [5], [6] and [7], thus electrons no longer appear in the reactions. The product $Fe(OH)_2$ converts to green hydrated magnetite or black magnetite in areas where oxygen is limited, such as the interface between metal steel hull and concretion.

Iron is not a biologically toxic metal, so when immersed in seawater it will be colonized by marine organisms. As a result, the formation of calcareous concretions on the surfaces of iron-based alloys such as steel produces a barrier to oxygen (Jones 1996:59, 212, 447-448). With oxygen depletion in the microenvironment between the concretion and the metal surface, chloride ions diffuse inward, and the pH drops to 4 or less as a result of hydrolysis reactions given by equation [7]. The concretion acts like a semipermeable membrane with an electrical resistivity of approximately 2,000 Ω-cm when wet in seawater (MacLeod 1989). MacCleod (1982) suggests that as concretion thickness increases, cathodic reactions migrate into the concretion rather than remaining sited at the metal surface. However, since concretion electron conductivity is low, it is more plausible to assume that cathodic reactions as well as anodic reactions occur at the concretion/metal interface. The iron ions Fe^{+2} and Fe^{+3} diffuse into the marine organisms' skeletal material, which is predominately aragonite (CaCO3), to produce siderite (FeCO3), as well as oxides of iron. Concretion containing iron sulfide (FeS) and elemental sulfur indicate the presence of sulfate-reducing bacteria (SRB). Normally, hydrogen reduction in support of corrosion is a slow process, but is stimulated in the presence of SRB

(North and MacLeod 1987). The influence of microbiologically influenced corrosion (MIC) is discussed elsewhere (see Chapter 7).

CORROSION VARIABLES

Steel corrosion in seawater is extensively documented in the professional literature (Schumacher 1979). From an archaeological perspective, archeologists and conservation specialists in Australia conducted pioneering research on iron and steel shipwreck deterioration and have determined that the major factors affecting shipwreck corrosion are metal composition and metallurgical structure, water composition, temperature, extent of water movement, marine growth, seabed composition and depth of burial beneath the seabed (North and MacLeod 1987:68). Collecting data necessary to characterize critical corrosion processes on USS *Arizona* involved evaluating each of these factors, all of which are complex and interrelated, and affect corrosion in different ways. When attempting to evaluate the corrosion history of an object it must be considered individually—there are very few oceanographic and environmental parameters that are uniform between sites. An excellent review of corrosion fundamentals with applications to marine environments is presented by North and MacLeod (1987); the following discussion draws heavily on their work.

A variety of factors have been identified that directly influence metal corrosion on shipwrecks, including water composition (dissolved oxygen, pH, salinity and conductivity), temperature and extent of water movement (North and MacLeod 1987:68). Oxygen reduction is typically the most important cathodic reaction occurring in steel exposed to seawater, so dissolved oxygen availability at the cathodic site may control the corrosion rate depending on the thickness of the concretion, mass transport rate of oxygen and metal ions through the concretion and microbial activity at the interface. Water at the ocean's surface is generally oxygen-saturated, so overall dissolved oxygen content depends on the amount of mixing that occurs with surface water—increased water movement and mixing results in elevated dissolved oxygen levels. In addition, temperature and dissolved oxygen are inversely proportional, so lower temperature results in increased dissolved oxygen. The pH level is another indicator of corrosion activity. In normal seawater, pH ranges from 7.5 to 8.2, but levels below 6.5 are found under concretion covering actively corroding metal. Lower pH levels (more acidic) characterize

accelerated corrosion when sulfate reducing bacteria (SRB) are present. Salinity is closely related to the corrosion rate of steel in water since increased salinity usually results in higher corrosion rates. This is evident when comparing metal preservation in freshwater compared to seawater environments—freshwater lakes typically exhibit better preservation of iron and steel. There are several ways that higher salinity affects corrosion, including increasing conductivity (which facilitates movement of ions between anodic and cathodic areas), increasing dissolved oxygen and supplying ions that can catalyze corrosion reactions, among others (North and MacLeod 1987:74). Higher conductivity can increase corrosion by increasing the movement of ions during the corrosion process.

In general, corrosion rate increases as temperature increases. This is complicated, however, by the effect of temperature on both dissolved oxygen and biological growth. Warmer water supports increased marine growth, which contributes to concretion formation on steel in seawater and that, in turn, generally reduces corrosion rates. In addition, as discussed above, lower temperature results in higher dissolved oxygen content, which consequently means increased corrosion (North and MacLeod 1987:74).

Water movement from waves and currents on a site affects corrosion in several ways, but generally high-energy environmental conditions results in higher corrosion rates. Active water movement can contribute to mechanical erosion of metal surfaces and can also impede development of protective concretion layers by removing accumulating ions before they can precipitate and begin the concretion formation process. Waves and currents also contribute to water mixing and aeration that result in increased dissolved oxygen levels (North and MacLeod 1987:74).

Factors that affect corrosion on metal shipwrecks are complicated and interrelated. Reducing one key factor can increase another, and the results are often unpredictable. It is clear, however, that in order to understand the corrosion history of an object, even a complex object like a World War II battleship, and to begin to define the nature and rate of deterioration affecting the object, an understanding of the various environmental factors at play is necessary. An important aspect of the current research program is long-term monitoring of oceanographic and environmental parameters on USS *Arizona* (see Chapter 4).

CORROSION POTENTIAL (E_{corr}) AND POURBAIX DIAGRAMS

During the corrosion process, when the oxidation and reduction rates are equal, there will be a voltage that characterizes the specific reaction rate or corrosion rate for a particular system—that characteristic voltage is known as the corrosion potential (E_{corr}). E_{corr} is indicated by voltage (expressed in millivolts in the range of 0 to -1000 mV) and is measured using a reference electrode, which measures localized electron flow from different parts of a metal into and out of surrounding electrolyte, and displayed on a standard digital multimeter. Although there are exceptions, a more negative E_{corr} value generally indicates a lower corrosion rate, while a more positive E_{corr} indicates a higher corrosion rate (MacLeod 1987:49-50). In all cases, the negative electrode is the anode and the positive electrode is the cathode. Although practitioners in the pipeline and oil industry identify a more negative potential as indicative of a higher corrosion rate, the opposite is true for concreted steel in seawater because steel is in a film free state and does not passivate (Uhlig 1971:49, 93). E_{corr} does not translate directly to an absolute corrosion rate; however, it does yield a relative measurement that is proportional to corrosion rate for different parts of the same structure in the same electrolyte. In sea water, then, the area of the steel structure where E_{corr} is lowest (most negative) reflects the area where the corrosion rate is lowest.

The reference electrode is essentially a small battery which produces a characteristic potential. Since the steel hull of the ship likewise produces a characteristic potential, the difference between the potential at the hull and the potential produced by the reference electrode is measured and documented as the corrosion potential (E_{corr}). Since the choice of reference electrode depends upon the electrolyte and the test circumstances, it is often necessary to convert potentials to a common potential, the standard hydrogen electrode (SHE). Although the hydrogen reference electrode is not used in the field because of its complexity, it is arbitrarily chosen to have a potential of 0.0 volts. There are numerous kinds of reference electrodes used in the field. The most common is the copper/copper sulphate ($Cu/CuSO_4$) reference electrode, in which a copper rod is placed in a glass or plastic tube and filled with distilled water, then brought to saturation with excess copper sulphate crystals. This electrode is used primarily in fresh water. Two other electrodes, commonly used in sea water, are both silver/silver chloride (Ag/AgCl) electrodes. In these electrodes, a silver coated rod is placed in a solution of either

silver salt or sea water. We used normal Ag/AgCl reference electrodes on the USS *Arizona* Preservation project.

An important tool to use in corrosion analysis is the Pourbaix diagram (Figure 5.2) (Pourbaix 1974). The Pourbaix diagram is a two dimensional map of the oxidizing power (E) and acidity (pH) of a selected metal or other ions immersed in an aqueous solution. Pourbaix diagrams present stability fields of corrosion products in terms of the independent variables potential (hydrogen electrode) and pH. Since potential and pH are readily measurable in the field, Pourbaix diagrams become a very important tool in understanding corrosion for specific systems (see below). Lines on the diagram, calculated from the Nerst equation (equation [1]) identify regions where specific ions (charged elements or compounds) are stable. The way that a Pourbaix diagram is most often used is to transfer E_{corr} and corresponding pH to the diagram directly (in this case iron-water). The region in which the intersection point of the two variables is located identifies possible supporting cathodic reactions and the corrosion products that result at the location where the parameters are being measured (Figure 5.2). It should be emphasized that the Pourbaix diagram only predicts whether or not corrosion will occur and identifies the corrosion products. The rate of corrosion cannot be determined from the diagram.

As an example of how the Pourbaix diagram for the iron-water system can be used, consider the solid lines on the diagram first (Figure 5.3). Superimposing typical pH and E_{corr} field measurements as small solid dots, all points that appear in the area labeled Fe^{+2} indicate active corrosion. The points are well below the region of Fe^{+3} stability, so ferrous ions (Fe^{+2}) dominate. Below the line identified by $(Fe^{+2}) = 10^{-6}$, steel is said to be immune because the concentration of iron is extremely low corresponding to a region of insignificant corrosion. The concentration of (Fe^{+2}) continues to decrease as the potential decreases. In addition to the large cross-hatched region to the left, there is a small triangular cross-hatched region to the right in which corrosion occurs. The region defined as passivation means that corrosion product oxides form on the surface and become protective. Passivation only occurs under specific conditions for selected iron-based alloys but does not normally occur for steel in seawater. Consider next the two dotted lines labeled (a) on the bottom and (b) above it. On line (a), reaction [8] occurs:

$$2H_2O + 2e = H_2 + 2OH(-) \qquad\qquad [8]$$
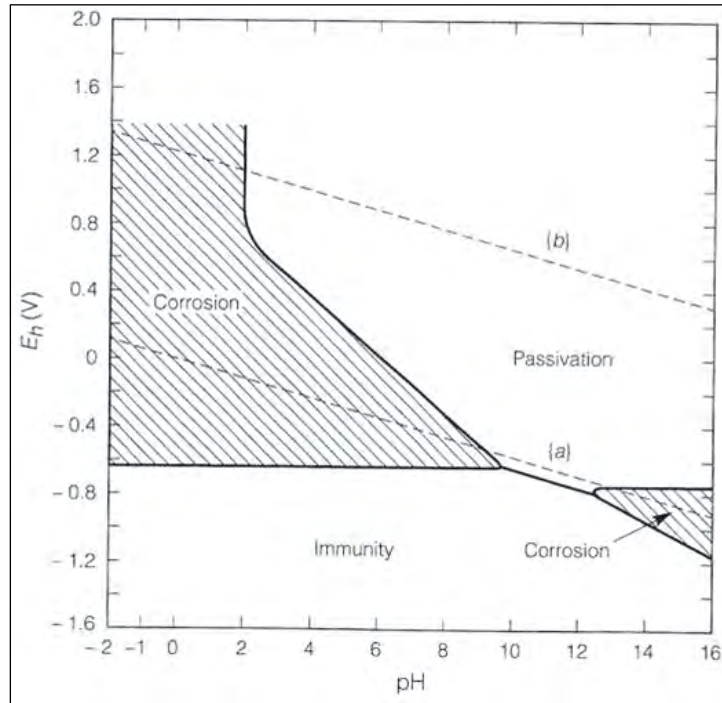
Figure 5.2. Simplified Pourbaix diagram for iron dissolved in water (Jones 1996:53).
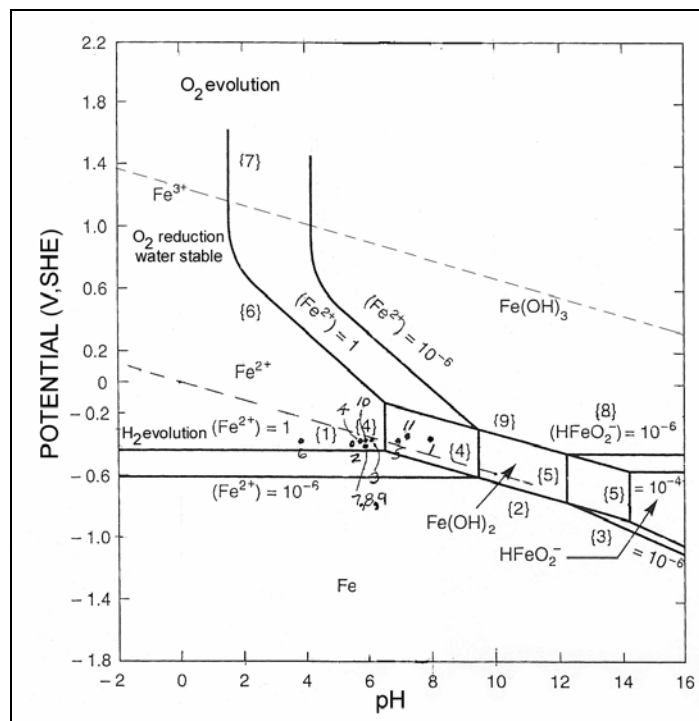
Figure 5.3. Pourbaix diagram for iron in water with E_{corr} / pH data taken on the USS *Arizona*, September 2000 (modified from Jones 1996:59).

135

Below line (a), water is unstable and hydrogen is evolved. Between lines (a) and (b), water is stable and oxygen is reduced to water or oxygen is consumed as a cathodic reaction in support of corrosion. On line (b), reaction [9] occurs:

$$O_2 + 4H^+ + 4e = 2H_2O \tag{9}$$

Above line (b), oxygen is stable and oxygen evolution takes place, although it seldom does because E_{corr} normally does not reach such a high potential. As will be noted later, the points appear to follow closely along the lower dotted line, hence, hydrogen evolution or oxygen consumption dominates the cathode reaction. At the lower pH values observed at the metal/concretion interface, the cathode reaction at or near the interface in the concretion involves hydrogen evolution as noted above (which explains the observation that initial penetration of the concretion sometimes releases gases and divers occasionally observe bubbles emerging from concretions in isolated locations on *Arizona*'s hull). The Pourbaix diagram for the carbon-water system (Figure 5.4) is also useful in identifying gases observed during diving operations. For example, at an E_{corr} of -400 mV, methane gas is stable in solution at a pH below about 6, carbon is stable between pH 6 to 8, and carbon dioxide is stable above pH 8. At E_{corr} of -300 mV, methane is stable below pH 4, carbon is stable between pH 6 to 7 and carbon dioxide is stable above pH 7. As will be discussed later, this diagram may be useful to explain why potentials suddenly rise in some interior compartments. While Figure 5.4 applies only at atmospheric pressure and temperature, extreme high pressure and low temperature at great depths result in very high solubility of methane gas. The result is solid hydrate, a stable form of methane under such conditions.

CORROSION RATE THEORY

The preceding discussion relates only to the potential for corrosion and does not address the issue of corrosion rate. Since corrosion produces or consumes electrons, the corrosion rate is directly proportional to current and inversely proportional to cross sectional area. A common expression for corrosion rate when expressed in terms of current is microamperes per centimeter squared ($\mu A/cm^2$). A more practical expression for corrosion rate incorporates metal loss into the expression and this can be accomplished by imposing Faraday's Law. The law states that
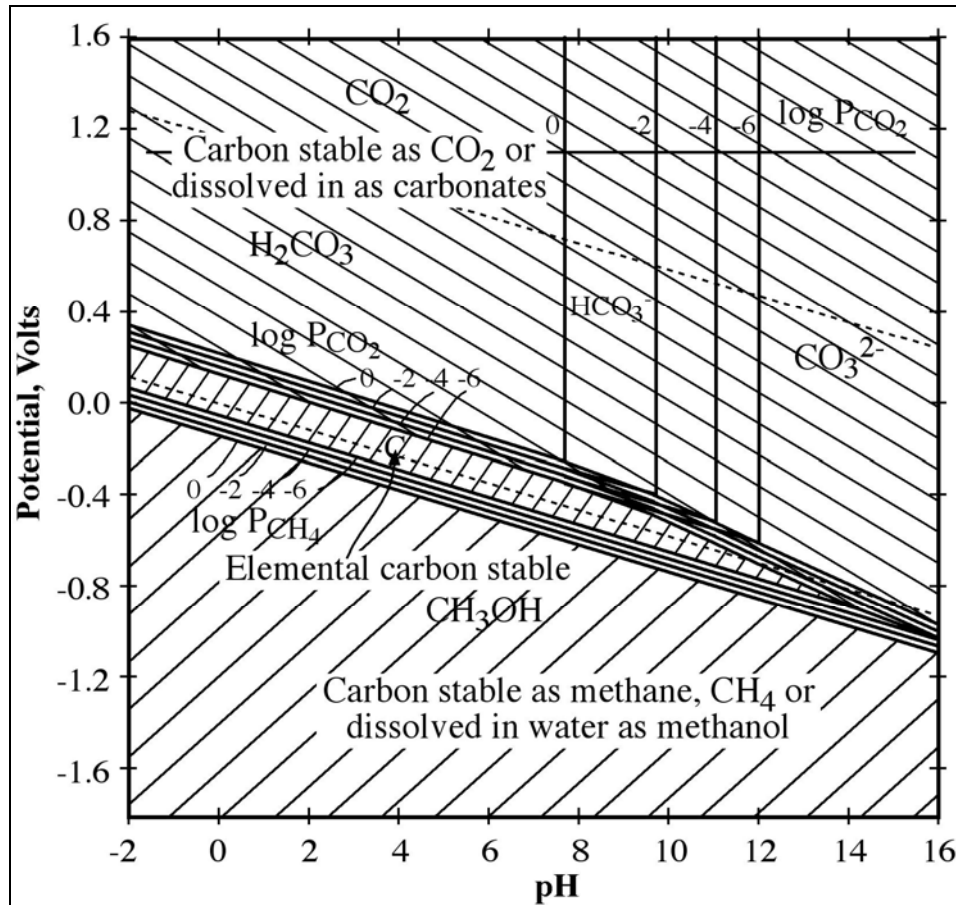
Figure 5.4. Pourbaix diagram for carbon in water system.

one equivalent weight of metal consumes 96,500 ampere seconds of current. Combining

physical and chemical properties of iron with Faraday's Law and using the appropriate constants,

expressions for corrosion rate are derived in following sections.

<u>Polarization</u>

Two types of polarization are identified in an electrochemical cell. The first type,

activation polarization, is related to corrosion product formation on the metal surface. As oxides

and gases begin to accumulate on that surface, the rate of electrochemical reactions reach a

steady state rate that depends on many factors, including the chemistry of the electrolyte, the

composition of the metal or alloy, the condition of the metal surface and temperature. The

second type, concentration polarization, is related to the rate at which reaction species reach the

metal surface. For example, if diffusion of oxygen is slower than corrosion reactions consuming

it, the corrosion rate is controlled by availability of oxidants rather than the rate at which the reactions themselves take place. As an analogy, the kinetic energy of a moving object is expended theoretically in proportion to the square of the velocity. At 30 mph, the kinetic energy is proportional to 30 x 30 = 900 and the moving object, such as an automobile, will reach speed with a specific fuel consumption rate. At 60 mph, the kinetic energy is proportional to 60 x 60 = 3600 and the consumption rate of fuel increases. According to kinetic theory, energy expended increases in this example by a factor of four although the speed only doubles. However, at a given speed, a dynamic equilibrium develops between wind resistance, engine and drive train friction and road resistance, and these factors can be thought of as polarizing in the sense that they effect the actual speed of the car and the kinetic energy actually expended. Although the above analogy is crude, it illustrates the fact that the process itself creates its own bias, and conditions change to meet these biases. In electrochemical processes, analogous effects are almost instantaneous and the transient condition is not measurable. What is measured are two empirical parameters, corrosion rate (i_{corr}) and corrosion potential (E_{corr}). Numerous environmental variables can also be measured such as pH, oxygen concentration, temperature, salinity and oxidation reduction potential. These parameters are used to better understand the corrosion processes reflected in i_{corr} and E_{corr}, and identify the type of polarization occurring. Since potential and pH are thermodynamic parameters, they combine to determine a point on a Poubaix diagram, as discussed earlier. The region where the point lies identifies the corrosion products and hence factors that control the process.

Activation Polarization

While the kinetic theory of corrosion is beyond the scope of this chapter, there are practical aspects of this theory that are necessary to interpret field corrosion data. Activation polarization reflects conditions, in which the corrosion rate is determined by the rate of electrochemical reactions such as hydrogen evolution (equation [4]) or oxygen consumption (equation [3]) occurring at the cathode surface. In practical terms, this means that oxidants (oxygen or hydrogen ions) are available in excess and impose no limit on the rate of corrosion. Dissolution of ions from the anode and their dispersal from the anode site, as in equation [2], is normally so fast that activation polarization is the rule at the anode. This concept is illustrated in

Figure 5.1, where potential is plotted on the vertical axis and corrosion rate (i_{corr}), expressed as the logarithm of the current density (log (i_{corr})), is plotted on the horizontal axis. The top descending solid line represents the path of cathodic polarization and the bottom ascending solid line represents the path of anode polarization for a hypothetical cell. It should be noted that the two lines converge to a point of intersection virtually instantaneously. At the point of intersection, i_{corr} is determined by projecting vertically downward to the horizontal (x) axis. E_{corr} is determined by projecting horizontally to the vertical (y) axis. According to activation or Tafel theory, a plot of E (potential) versus log (i_{corr}) is linear according to equation [10]:

$$y = mx + b \qquad\qquad [10]$$

In terms of potential and current, this equation is given by:

$$E = \beta(\log i_{corr}) + K \qquad\qquad [11]$$

where

> E is plotted on the vertical axis
>
> log (i_{corr}) is plotted on the horizontal axis.

The constant β is the Tafel constant and is expressed in millivolts (mV) per decade of current (mV per decade is defined as the potential change required to cause a 10-fold increase in the corrosion rate). β is an important parameter defining the corrosion process, as will be discussed later. Normally, the anode is under activation control, as mentioned above, but the cathode can be under either activation or concentration control. The constant K includes potential (E°) and exchange current density (i°). The vertical line between C and A corresponds to a potential difference between anode and cathode at the corrosion potential and referred to as an ohmic resistance drop. From Ohms Law:

$$I (\Delta E)/R \qquad\qquad [12]$$

where

> I is the total current (A)

Δ E is the potential difference between anode and cathode (volts)

R is the resistance (ohms)

The most significant feature of Figure 5.1 is the continuously decreasing i_{corr} along the anode line as the potential decreases. This is the theoretical basis for the experimental observation that i_{corr} decreases as anode E_{corr} becomes more negative (anode line B to A(3)). This observation was experimentally verified after acquisition and analysis of steel hull samples on *Arizona* in August 2002 (see below). If passivation were to occur, the sign would reverse such that an increasing potential would momentarily cause the corrosion rate to increase (corrosion product formation) but then suddenly decrease at a specific potential referred to as the passivation potential. A thin, stable and protective corrosion product layer forms and the corrosion rate decreases (dashed anode line A(3) to A(1) and on to B(1) and A(4)). The corrosion current, expressed in terms of microamperes per square centimeter (μA/cm^2), is converted to mils per year (mpy—a mil is 1/1000 of an inch) by applying Faraday's Law. The conversion constant is 0.46 for mild steel but varies depending on the metal or alloy:

$$1 \ \mu A/cm^2 = 0.46 \ mpy = 11.68 \ \mu mpy \qquad [13]$$

Concentration Polarization

Diffusion of oxidants to the cathode normally governs the consumption rate of electrons and, hence, the corrosion rate. The corrosion rate limiting equation [14] is expressed by:

$$i_L = \ i_{corr} = KDnFC/d \qquad [14]$$

where

i_L is limiting current density (mpy or μmpy)

i_{corr} is corrosion current (mpy or μmpy)

D is the diffusion coefficient for H$^+$ ion or O$_2$ through concretion barrier (cm^2/sec)

n is charge (valence)

F is Faraday's constant

C is concentration of H^+ ion or O_2 (mg/L)

d is diffusion thickness (cm)

K = 0.46 for mpy (11.68 for μmpy)

According to equation [14], the corrosion rate is directly proportional to the diffusion coefficient and concentration, and indirectly proportional to the thickness of the diffusion barrier (concretion) on the surface that impedes the diffusion of reactants, most commonly oxygen. Line l–l' in Figure 5.1 characterizes cathodic polarization and shows intersection with the anodic line at point B(1). It should be noted that if oxygen consumption were the only supporting cathode reaction, the corrosion rate could be determined knowing the consumption rate of oxygen—it would not be necessary to measure the corrosion rate directly. However, to measure the volume of oxygen consumed would be impossible to do in the field. Projecting vertically from point B(1) to the x axis, i_{corr} is determined. As will be noted later in this chapter, i(L), equation [14], reveals whether or not oxygen availability is sufficient to support corrosion.

CORROSION ANALYSIS OF USS *ARIZONA*

METHODOLOGY

Analysis of corrosion on USS *Arizona* includes determining corrosion rate, the most pertinent variable needed to address overall research questions regarding hull structural integrity and longevity. An evaluation of the corrosion process began by investigating *Arizona*'s steel metallurgy from initial construction to later reconstruction. Methods included chemical analysis, metallographic examination and Charpy impact testing—all standard metallurgical evaluations. Next, seawater chemistry and other environmental variables were collected over a two-year period to establish an environmental baseline for the site. Environmental parameters recorded during long-term deployment of water quality and oceanographic monitoring instruments includes dissolved oxygen, temperature, salinity, pH, oxygen reduction potential, conductivity, current speed and direction, and wave height and direction. In addition, water quality parameters were recorded inside *Arizona*'s hull periodically with a monitoring instrument deployed on a remotely operated vehicle (ROV). Specific dissolved oxygen measurements both inside and

outside the ship were also recorded on different occasions. A comprehensive analysis of oceanographic and water chemistry variables appears in Chapter 4; however, because of their importance to the corrosion process, they will be reviewed here. Because both properties of steel and environmental parameters directly affect the corrosion process, and therefore the corrosion rate, both need to be factored into an evaluation of *Arizona*'s overall corrosion.

After establishing background conditions, an evaluation of the corrosion process itself was accomplished by applying corrosion theory discussed above with specific experimental results from *in situ* corrosion measurements taken on *Arizona*'s hull, in combination with laboratory analysis of concretion samples. *In situ* values for E_{corr} and pH were measured at varying depths through the concretion from the exterior surface to metal/concretion interface. These measurements were taken over the course of multiple field seasons and in a variety of locations, and represent a comprehensive corrosion assessment of *Arizona*'s exterior hull. In addition, concretion samples from *Arizona*'s exterior hull were collected and analyzed using both x-ray diffraction and environmental scanning electron microscopy (ESEM). The former identified mineral species dominant in the concretion while the ESEM quantified the corresponding element concentrations in weight and atomic percent. These data provided evidence that it would be feasible to quantify the iron content in a given cross section of concretion and relate it back to corrosion rate.

The rate of *Arizona*'s steel hull corrosion fluctuates directly with numerous variables, and is somewhat different at various hull locations. Corrosion rate was investigated through a number of lines of inquiry, including direct metallographic and thickness measurements of steel hull samples, *in situ* ultrasonic thickness measurements, and correlating environmental parameters with limiting current density (i(L)). The minimum-impact method of choice for determining corrosion rate developed during the USS *Arizona* Preservation Project is the Concretion Equivalent Corrosion Rate (CECR). Corrosion rate of the interior and areas of the hull deep below the harbor bottom was estimated from environmental variables alone. Through multiple lines of evidence, an important understanding has been gained about conditions that exist on *Arizona*'s hull, interior and exterior, above the harbor bottom to just below it, and how they affect the steel-hull corrosion rate.

RESULTS

<u>Metallurgical Evaluation</u>

Because steel chemistry and microstructure have a direct effect on corrosion, steel samples from USS *Arizona* were examined by conventional metallurgical techniques, including optical metallography, Charpy impact and chemical analyses. Test work included both *Arizona*'s original 1913–1915 structural steels as well as steels used in 1929–1931 reconstruction. All test work was conducted in the Metallurgical Engineering Laboratories at the University of Nebraska–Lincoln (Johnson, et al. 2000). Analysis focused on steel collected from superstructure elements stored on land at Waipio Point in Pearl Harbor, which were removed from the battleship before Memorial construction began in 1960.

Chemical Analysis

Chemical analysis of steel samples taken from the ship used in the original construction beginning in 1913, and reconstruction from 1929–1931, were compared to hull steel from RMS *Titanic* (Felkins, et al. 1998) and a modern grade of ASTM A-36 steel (Anonymous 1975:49) (Table 5.2). Saveur (1935) reports impurities in early twentieth century steel varied for phosphorous (P) from a trace to 0.1%, silicon (Si) from a trace to 0.5% with most grades between 0.05–0.30 percent. Examination of Table 5.2 indicates that all of the steels contain less than 0.05% P and satisfy the maximum for Si. With one exception (*Titanic* steel), S contents are below 0.05%. Cook (1937) reports that in 1910, basic open hearth production was close to 17 million tons whereas Bessemer production was about 9.5 million tons. Based on the chemistries and statistics, it seems certain that USS *Arizona* structural steels were basic open hearth products. Somewhat higher S and P are reported for *Titanic* steel, most likely due to the fact that the steel used in the *Titanic* was an acid open hearth product, hence the reason for the higher sulfur. The higher copper content in W1-B2 is probably due to the addition of scrap to the open hearth during the production process. This is further evidence of open hearth production since the Bessemer process could not use scrap.

SAMPLE (wt %)							
Element	W3	W1-B2	WB2	WB3	WB5	Titanic	A36
	Rivet - 1913	Plate -1913	Main mast - 1929 -1931	Locker - 1913	Channel - 1913	1911	ASTM
C	0.207	0.102	0.226	0.450	0.228	0.210	0.200
P	0.031	0.046	0.013	0.028	0.006	0.045	0.012
S	0.043	0.023	0.039	0.024	0.046	0.069	0.037
Mn	0.510	0.450	0.502	0.521	0.435	0.470	0.550
Si	0.013	0.004	0.024	0.067	0.007	0.017	0.007
Cu	0.061	0.244	0.011	0.013	0.025	0.024	0.010
Al			0.029	0.006			

**Table 5.2. Steel Chemistry: USS *Arizona* Original Materials through 1913
and Reconstruction Materials 1929–1931.**

Metallography

Conventional metallographic methods were used to prepare specimens obtained from Waipio Point in March 1999 and again during a second field operation in September 2000 (Figures 5.5 and 5.6). Etching was done with 2% Nital after grinding and polishing. The microstructure of sample W1 consists of ferrite and pearlite, and the carbon content is estimated to be around 0.2%. The microstructure shows evidence of heavy banding—banded microstructure such as this is typical of plate steels from this time period (Figure 5.7).

Banding is a result of the solidification practices used for the ingot from which the steel was rolled and appears as a segregated structure of nearly parallel bands aligned in the direction of working (Yiming, et al. 1992). Photomicrographs of Sample W3 in the area around the rivet show the microstructure of both the rivet and the plate (Figure 5.8) and the plate (Figure 5.9) separately. The plate shows the same basic microstructure as W1, but the banding is less severe. The rivet has a microstructure which indicates that it was cooled rather quickly from the austenite range (Figure 5.10). The microstructure of the rivet consists of primary grain boundary ferrite and very fine pearlite interspersed with Widmanstatten ferrite. This microstructure would
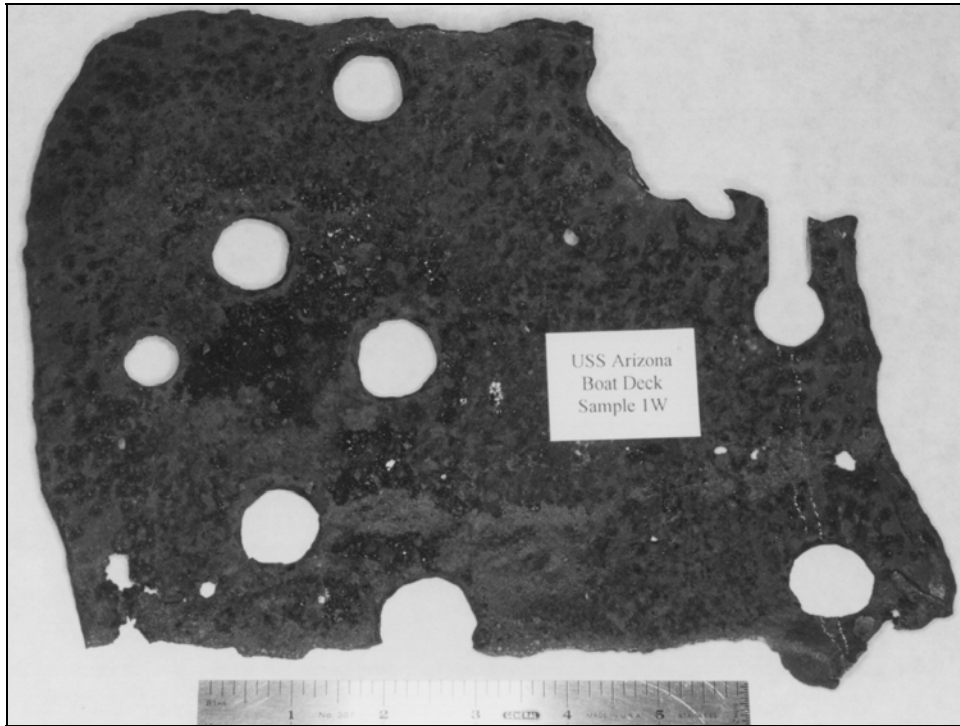
Figure 5.5. Sample W1, plate from boat deck with rivet holes.

Figure 5.6. Sample W3, section with rivet in place from boat deck.
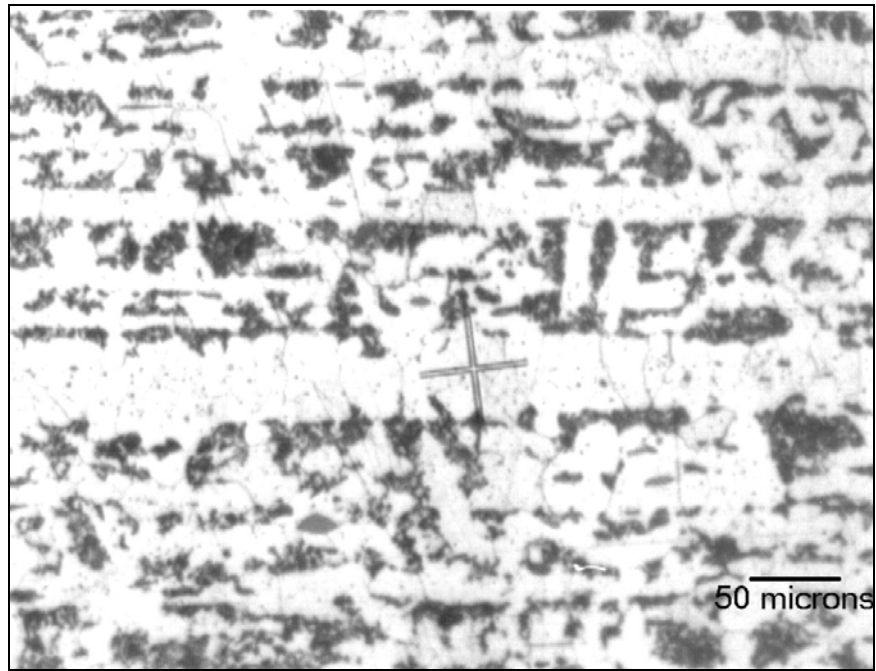
Figure 5.7.   Microstructure of W1, 175X, 0.2% Nital etch.
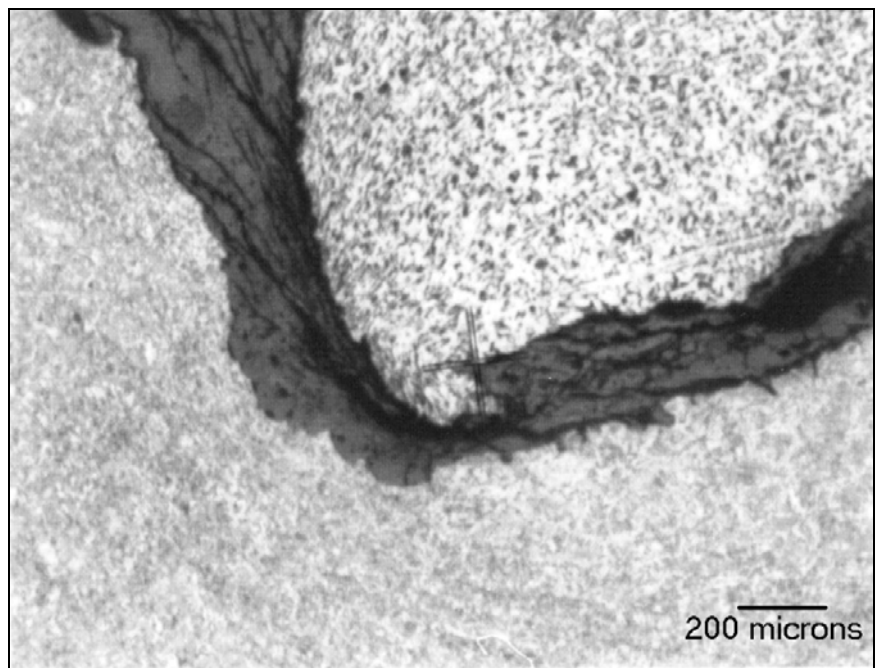
Figure 5.8. Microstructure of W3. Plate is at top right, rivet is at lower left. 45X, 2% Nital etch.
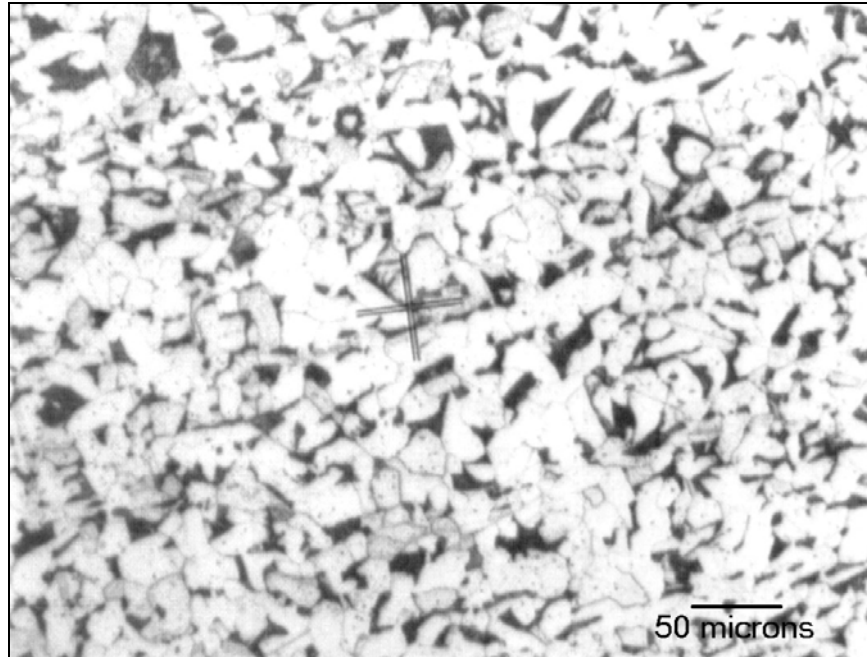
Figure 5.9. Microstructure of plate W3, 175X, 2% Nital etch.
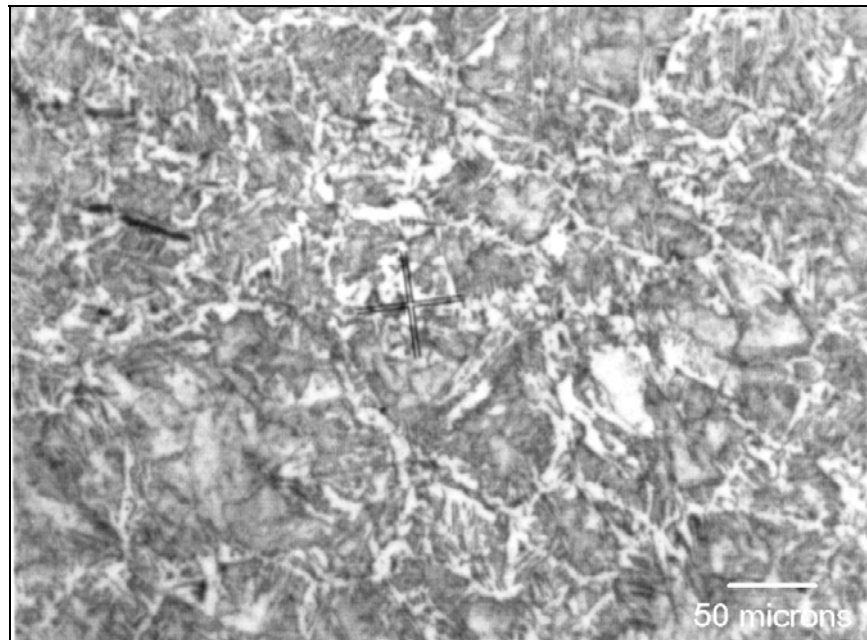
Figure 5.10. Microstructure of rivet in sample W3, 175X, 2% Nital etch.

be typical for hot riveting processes in which the rivets are heated red hot and swaged into place. The carbon content of the rivet is believed to be slightly higher than that of the plate.

The microstructure of samples W1 and W3 are typical for the time period and operations when this vessel was built. The banded microstructure seen in sample W1 can affect the rate and mechanism of corrosion of the steel over a period of time, but is not expected to be a significant factor. The fact that the microstructure of the rivet and plate (Figures 5.5 and 5.6) are different indicates that at least this part of the ship did not see extremely high temperatures. If it had seen temperatures above 1,340 °F (727 °C), the steel would have gone through a phase transformation and the microstructures of the rivet and plate would have been similar on cooling. Since banding appeared in sample W1, samples WB2, WB3 and WB5 from September 1999 were sectioned for examination in both the longitudinal and transverse directions.

Longitudinal and transverse sections of main mast tripod sample WB2 show Widmanstatten ferrite with slight evidence of banding (Figures 5.11 and 5.12). Microstructures are consistent with carbon content between 0.2–0.25%. Grain size of this material was measured to be ASTM 7.3

A longitudinal section of galvanized locker plate, WB3, has microstructure typical of medium carbon steel (Figure 5.13)(Table 5.2). Pearlite is resolved and grain size is finer than that of the much thicker walled mainmast. Galvanizing is still evident on the exterior of the plate. The reason for the use of medium carbon steel in this application is not clear, although this is believed to be an exterior panel in which medium carbon steel would offer some level of protection over low carbon grades. New York Navy Yard correspondence, however, does not identify galvanized sheet steel as being a medium carbon grade (New-York-Navy-Yard 1913).

A longitudinal section of boat deck channel member WB5 shows elongated MnS inclusions and oxide particle alignment clearly evident and also pronounced banding (Figure 5.14).

Charpy Impact

Charpy impact tests were performed on seven standard specimens obtained from the mainmast tripod sample WB2. Samples were machined with the specimen axis parallel to the longitudinal or rolling direction. Tests were performed on a Tinius Olsen instrumented impact
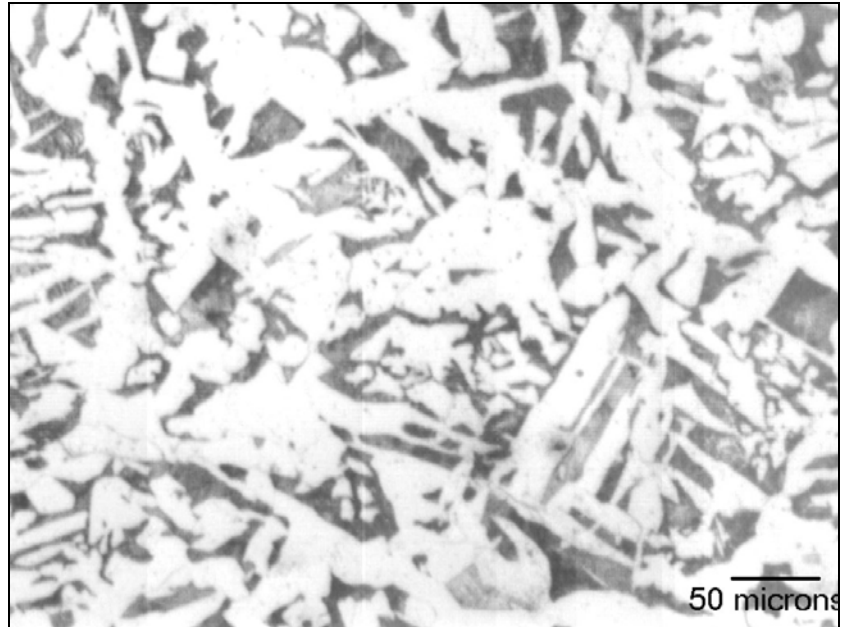
Figure 5.11. Microstructure of mainmast tripod leg, sample WB2, longitudinal, 175X, 2% Nital etch.
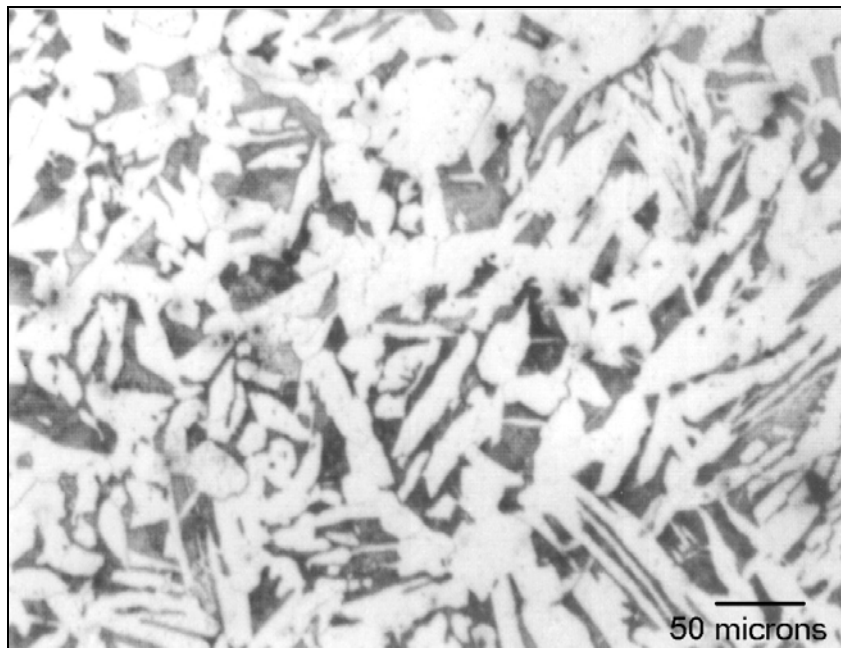
Figure 5.12. Microstructure of mainmast tripod leg, sample WB2, transverse, 175X, 2% Nital etch.
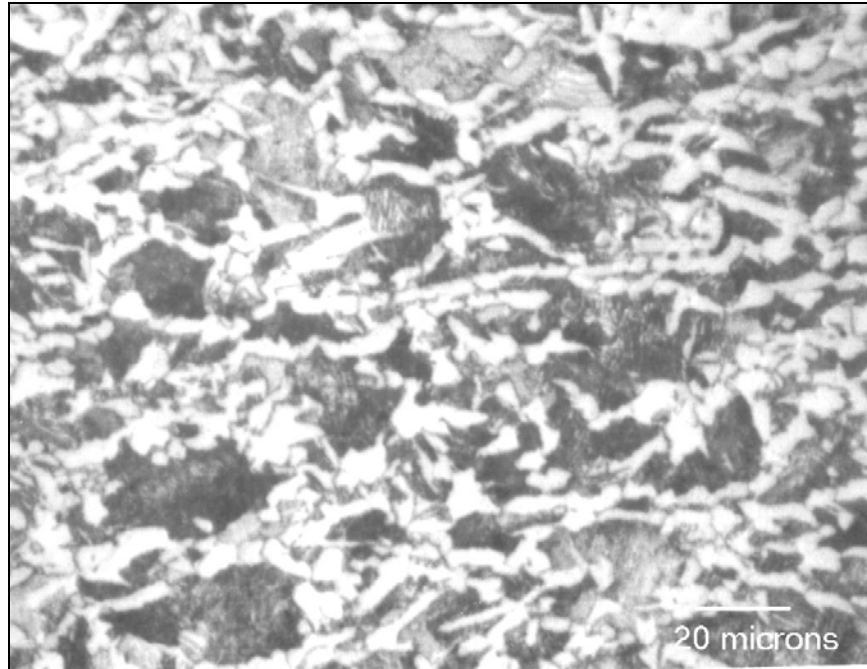
Figure 5.13. Boat deck locker sample WB3, longitudinal galvanized section, 450X, 0.2% Nital etch.
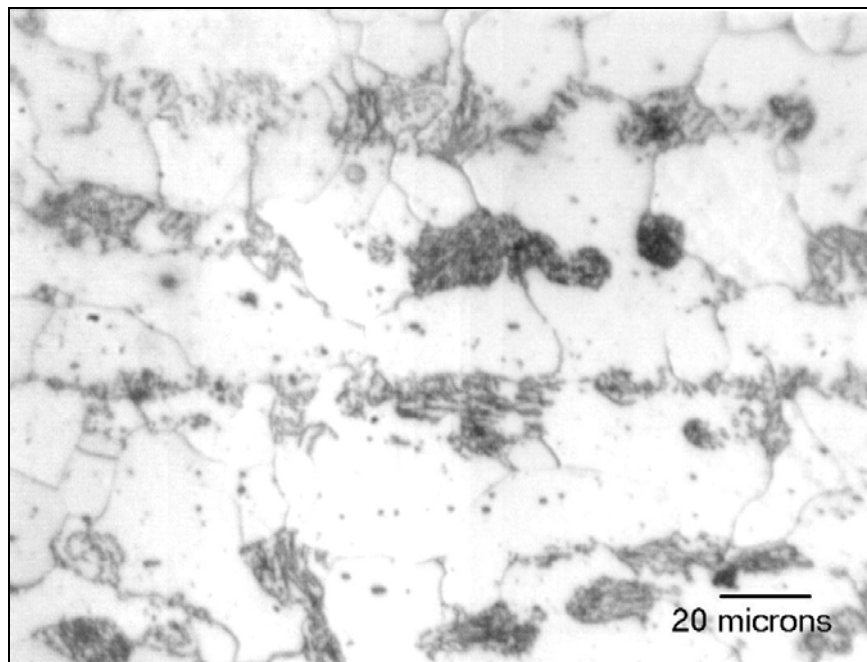
Figure 5.14. Microstructure of boat deck channel, sample WB5, longitudinal, 450X, 2% Nital etch.

tester using a Dynaup data acquisition system. Tests were run at temperatures of -196, -100, 25, 100 and 200 °C. Results from the Charpy impact testing are plotted using three commonly used reporting methods: temperature vs. energy absorbed, percent shear (ductile failure), and percent contraction at the fracture surface (Figure 5.15). Charpy impact curves for longitudinal plate from *Titanic*, *Arizona*, and A-36 grade were also compared using three common methods for comparing ductile vs. brittle fracture: the temperature at which the average of the upper and lower shelf occur at, the upper shelf energy and the temperature at which the material will absorb 20 J (15 ft.-lbs.) of energy (Figure 5.16)(Table 5.3) (Felkins, et al. 1998). Several factors are known to have significant effects on the toughness of steels, and in particular on the ductile to brittle transition behavior (Anonymous 1975:49).

The carbon content has the largest effect and raises the ductile to brittle transition temperature as measured by (DBTT) by 25 °F (14 °C) for every additional 0.1%. Manganese lowers the transition temperature by 10 °F (5.5 °C) for every 0.1% added whereas P raises it by 13 °F (7 °C) for every 0.1% added. Transition temperature is lowered as the grain size decreases by $D^{-1/2}$. These factors will also raise the upper shelf energy in conjunction with a lowering of the transition temperature. Using these guidelines for the effects of C, Mn, P and grain size, it can be calculated that the DBBT for *Arizona* and *Titanic* steels compared to the A-36 steel, measured by the average between the upper and lower shelf energies, should vary predictably (Table 5.4)—note that the A-36 and USS *Arizona* materials have essentially identical S contents (0.037% and 0.039% respectively) and P contents (0.012% and 0.013% respectively) whereas *Titanic* material has higher contents of 0.069% S and 0.045% P. The differences in transition temperature as computed between *Arizona* steels and A-36 grade can be explained through the C, Mn, P and grain size, whereas the differences between *Titanic* and A-36 grades takes into account of the higher S content in order to explain the differences. This is a direct result of the use of acid open hearth steelmaking practices which understandably were state-of-the art at that time in Europe. The mainmast steel from *Arizona* was of the same general quality from the metallurgical aspect as was the modern A-36 grade, with the differences being noted that the DBBT data were obtained from the mainmast steel manufactured in the late 1920s when cage masts were replaced with tripods.
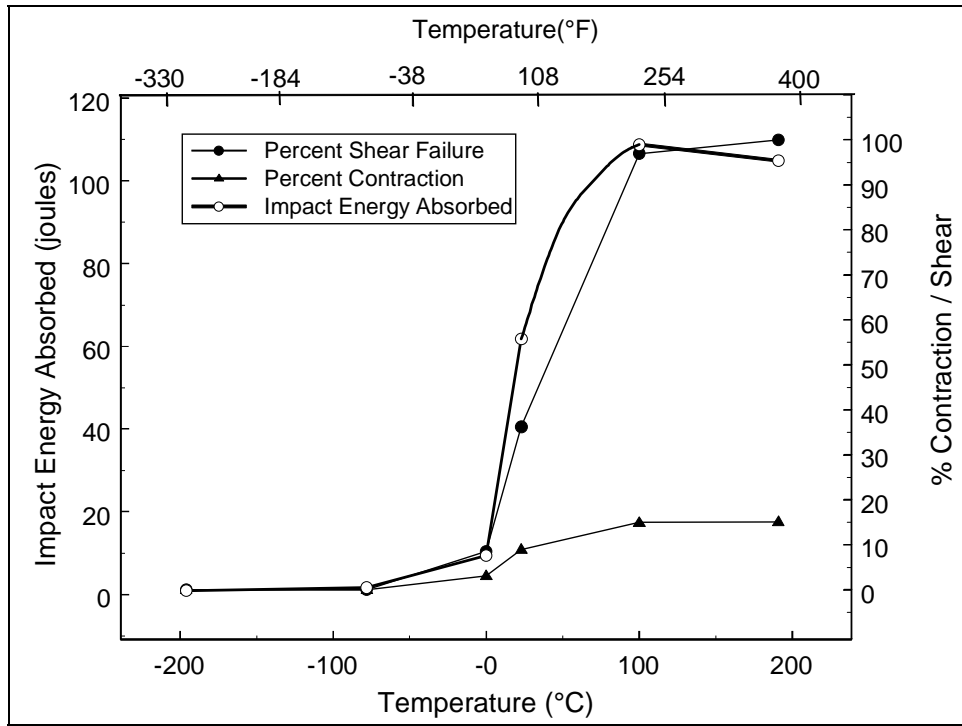
Figure 5.15. Charpy impact results plotted as temperature vs. energy absorbed, % shear failure, and % contraction for longitudinal steel samples taken from the mainmast of the USS *Arizona*.
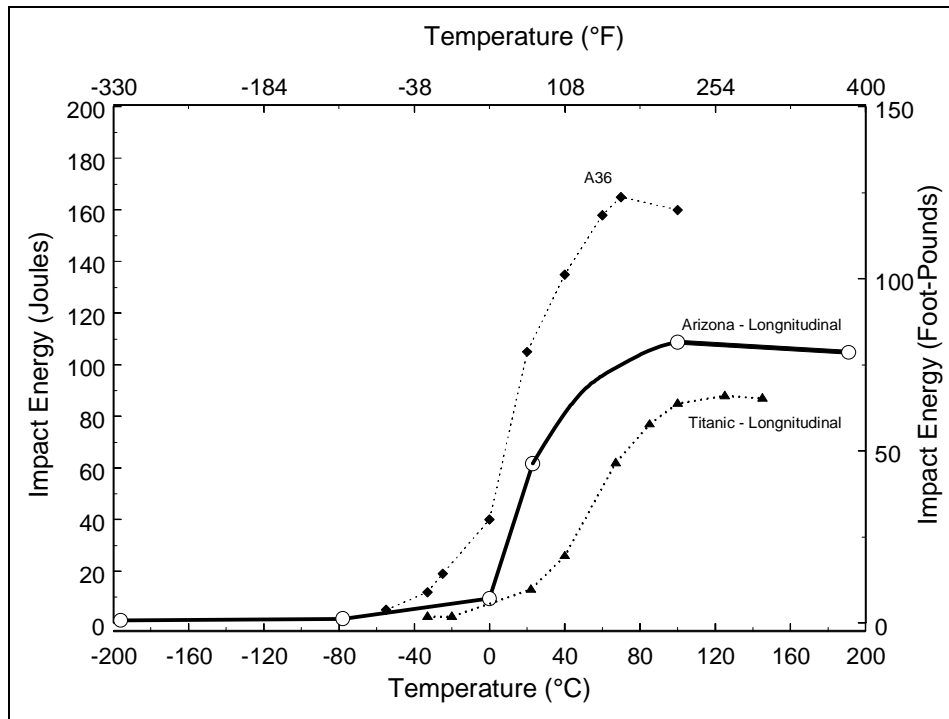
Figure 5.16. Charpy impact energy vs. temperature for longitudinal specimens from USS *Arizona*, HMS *Titanic*, and A36 steels.

152

Steel	DBTT	ΔT compared to A-36						Remarks
		Total	%C	%Mn	%P	G.S.	sum	
A-36	10°C / 50°F	0°C / 0°F	••					
USS AZ	20°C / 68°F	10°C/ 18°F	6.5	4.8	0	7	18.3	ok
Titanic	55°C / 131°F	45°C/ 81°F	2.5	8.0	4.2	31	55.7	(1)

Table 5.3. Comparison of the data for the impact results for USS Arizona tripod steel, titanic steel and a modern grade of A-36 steel.

	Arizona **Mast**	**A36**	**Rebar**	*Titanic*	**Effects**
Grain size (ASTM/ μm)	7.3 / 30	7.5 / 26	10.5 / 11	5-6 / 42 – 60	$d^{-1/2}$
Carbon (wt%)	0.226	0.20	0.26	.021	+25°F / 0.1%
Mn (wt%)	0.502	0.55	0.97	0.47	-10°F / 0.1%
P (wt%)	0.013	0.012	0.01	0.045	+13°F / 0.1%
S (wt%)	0.039	0.037	0.042	0.069	
Mn/S	12.8	15.0	23.0	6.8	(1)
T (°F) @ 20 joules	5°C / 41°F	-23°C / -10°F	-79°C / -110°F	29°C / 85°F	(2)
Upper Shelf (J)	110	165	90	85	(3)
DBTT as Average at ½ upper shelf	20°C / 68° F	10°C / 50°F	-20°C / -4°F	55°C / 131°F	(4)

(1) Measure of degree of free sulfur.
(2) Often used criterion for ship steel.
(3) Measure of toughness with 100% ductile failure.
(4) Often used measure for Ductile-Brittle Transition.

Table 5.4. Calculation of the DBTT for USS *Arizona* and *Titanic* steels as compared to A-36 as a function of C, Mn, P and grain size (GS).

Metallurgical Summary

Steel used to fabricate USS *Arizona* battleship during original construction, 1913–1915 and reconstruction, 1929–1931 were consistent with the best steel available during each time period. Due to the force of the forward magazine detonation, the best steel available today would not have had any impact on the outcome. Heavy banding in steels from both periods could adversely affect the corrosion resistance under anaerobic conditions that prevail during a corrosion cycle that developed under hard concretion layers that began to develop when the ship sank. Banding would have no effect on corrosion rate under aerobic conditions that may occur on local areas on the hull. In the part of the ship from which samples for this report were obtained, high temperatures above 1,340 °F (727 °C) did not occur.

The structural steel used in original construction was of surprisingly good quality for a basic open hearth steel technology that was only about 25 years old at the time the first materials were ordered for delivery to the New York Navy Shipyard. The somewhat lower quality of the early steel in terms of chemistry and microstructure had no measurable consequences on the damage that occurred on December 7, 1941 or on the results of the present investigation into the deterioration of the *Arizona*'s hull. Typical analysis and comparison with present day ASTM A-36 (Table 5.5) show minor differences in chemistry between the USS *Arizona*-era steel and present-day ASTM A-36 steel, however they are not considered significant with regard to corrosion response.

Environmental Evaluation

In all, more than 503,730 observations of currents, waves and water-column properties were collected on 362 days over the course of 14 months between November 2002 and January 2004, and an additional 580,000 observations of currents and near-bed water temperatures were collected during April 2005. As discussed in more detail in Chapter 4, oceanographic data indicate that tides are of a mixed, semi-diurnal type with a minimum, mean

	Carbon	Phosphorus	Sulpher	Silicon
USS Arizona	0.25	0.028	0.034	0.023
ASTM A36	0.20	0.012	0.037	0.007

Table 5.5. Chemistry of typical USS *Arizona* steel compared to modern day ASTM A36. All values wt %.

and maximum tidal range of 1.3 ft., 2.0 ft. and 3.0 ft. (0.4 m, 0.6 m and 0.9 m), respectively.
Waves are not an important factor in the vicinity of *Arizona*'s hull. Those observed were, long
period (~ 20 sec), but very small (order of cm's) and likely due to open ocean long-period swell.
Vessels passing close to the study site are likely responsible for the high-amplitude, low-period
motions that were also observed. Flow along the 33-ft. (10-m) isobath is dominated by semi-
diurnal and diurnal tidal motions, which are modulated to some degree by what appears to be
wind forcing during the mid- to late afternoon. Flow throughout most of the water column is
primarily parallel to the *Arizona*'s hull at ~ 0.065 ft./sec (~ 0.02 m/sec) and net flow is to the
northeast. Flow within a meter of the seafloor, however, is weaker and more variable in
direction. Flow velocities are greater off the port side than the starboard side, and thus the water
replenishment times on the port side of the hull are shorter than off the starboard side. Shear,
both vertically in the water column and across the hull, was observed. This results in vertical
variations in replenishment times and current-induced forces on the hull. This shear also likely
increases vertical mixing of the water column. Acoustic backscatter was generally higher in the
winter months and during the falling tide, suggesting advection of material introduced into the
northern sections of Pearl Harbor due to winter precipitation and its movement south past the
hull by ebbing tidal currents. Higher measurements of acoustic backscatter often occurred in the
afternoon, suggesting increased Trade wind-induced mixing or, perhaps, increased vessel
activity, which facilitates water column mixing and fine-grained particulate resuspension.

The water quality monitoring instruments indicate water temperatures along the 33-ft.
(10-m) isobath had a slightly higher mean of 78.85 °F (26.03 °C) and a less variable one standard
deviation of 1.17 °C than along the 10-ft. (3-m) isobath, which had a mean of 78.19 °F (24.55
°C) with one standard deviation of 2.08 °C. A thermocline was often present in the harbor's
waters, with the shallower (10 ft./3 m) and deeper (33 ft./10 m) water temperatures often
differing by more than 3.6 °F (2 °C). Water temperatures were generally cooler and less variable
off the port side of the hull than off the starboard side, possibly due to faster replenishment times
and greater mixing of the water column.

Salinity varied from 16.78 PSU and 42.56 PSU, with a mean ± one standard deviation of
34.33 ± 4.25 PSU. Salinity appears to positively correlate with water temperature and suggests
that Pearl Harbor's waters are influenced by freshwater runoff or groundwater effluence in the
winter months.

Open seawater pH varied between 7.60 and 9.10, with a mean ± one standard deviation of 8.04 ± 0.15 and dissolved oxygen 0% and 288.5%, with a mean ± one standard deviation of 69.5 ± 58.8%. Both pH and dissolved oxygen tended to correlate with the daily insolation cycle, increasing during the morning into the early afternoon followed by decreasing through the night to minimum levels just before sunrise.

Oxygen-reduction potential (ORP) varied between 150.0 mV and 397.2 mV, with a mean ± one standard deviation of 289.2 ± 50.6 mV. ORP often had an inverse relationship with pH and the percentage of dissolved oxygen, with oxygen-reduction potential decreasing during the daytime and increasing into the night, attaining it greatest values just before sunrise. During the vertical profiling, near-surface temperatures were on average 1.85 °F (1.03 °C) warmer than the near-bed temperatures, near-surface temperatures were 0.85 PSU less saline on average than the near-bed salinities and near-surface dissolved oxygen levels were on average roughly 43.9% higher than the near-bed dissolved oxygen levels.

A YSI dissolved oxygen instrument was used to obtain oxygen concentration at varying depths in the water column adjacent to *Arizona*'s hull, as well as internal measurements taken inside selected core drill holes during hull sample removal in 2002. During one measurement in August 2002, dissolved oxygen concentration varied as a function water depth in the water column from 6.47 mg/L at the surface to 5.08 mg/L at the harbor bottom at a depth of 30 ft. (Table 5.6; for additional data and analysis, see Chapter 4). For internal measurements, the instrument was attached to the end of a 6-ft. section of PVC pipe and inserted into the hole after removal of a plug seal inserted into each drill hole after the hull sample was removed. Exterior measurements in ambient seawater before inserting the dissolved oxygen meter into the hull varied from 4.74 to 5.68 mg/L (Note: mg/L is an alternative unit of measure for dissolved oxygen, but one not easily converted to percent saturation after the fact). Once inserted into the hull through the core sample holes approximately 1–2 ft., the readings dropped, varying between 0.0 and 3.99 mg/L once they stabilized. These interior spaces reveal a wide range of oxygen concentrations depending upon access to ambient seawater. For the sample locations on the second deck (USAR-02-002 and USAR-02-008), which have some seawater exchange through open port holes, dissolved oxygen concentration dropped an average of 27% below ambient, exterior seawater measurements. For the sample locations in the torpedo blisters (USAR-02-003, USAR-02-004, and USAR-02-009), the dissolved oxygen concentration varied from 2.47 to 0.0

Water Depth (ft.)	Dissolved Oxygen (mg/L)
0	6.47
2	6.36
4	6.33
6	6.41
8	6.3
10	6.16
12	6.28
14	6.14
16	6.04
18	5.92
20	5.57
22	5.55
24	5.16
26	5.1
28	5.07
30	5.08

Table 5.6. August 2002 dissolved oxygen data. Measurements taken 20-30 ft. off starboard side of *Arizona*'s hull, at approximately frame 75.

mg/L depending on proximity to breaches in the otherwise sealed torpedo blister, 56–100% less than ambient exterior measurements. Dissolved oxygen levels dropped to zero or near-zero in the two locations where the torpedo blister was completely sealed and had no seawater exchange. (see Table 4.5).

Finally, an ROV-deployed YSI water quality instrument recorded seawater parameters at selected locations within *Arizona*'s hull. In general, parameters recorded with the YSI sonde were nearly the same inside the ship, at least on the second deck level, as outside: pH = 8.0–8.1, temperature = 80–81° F, and salinity approximately 33.5 parts per thousand (ppt). Dissolved oxygen (DO%), however, dropped dramatically upon entering the ship. Outside, DO% = 86–88; typical inside DO% = 65–68 and in some instances dropped considerably lower. One of the more interesting observations is that interior cabin water is stratified by a subtle thermocline of about 0.5ºF however DO% changed significantly across this thermocline, from nearly 70 above to about 50 below the thermocline. This indicates very little water movement within interior cabins, even with open portholes. Researchers are also studying the extent of microbially-induced corrosion (MIC) in interior spaces of Arizona's hull (see Chapter 7).

Corrosion Analysis

An assessment of corrosion processes active on USS *Arizona*'s submerged hull consisted of theoretical evaluation, as well as both *in situ* and laboratory experimental measurements and analyses. Data collected relevant to a comprehensive investigation of corrosion process include *in situ* E_{corr} and pH measurements taken from 2000–2004.

In Situ Corrosion Potential (E_{corr}) and pH Measurements

E_{corr} /pH Measurements from Sequential Drilling through Concretion

In situ corrosion measurements taken systematically on *Arizona*'s hull include pH and E_{corr}. During this study. , *in situ* E_{corr} was obtained with Ag/AgCl reference electrodes giving a voltage measurement in mV. ThermoOrion (Beverly, MA) reference electrodes (Ag/AgCl, +200 mV to SHE) and Model 265A portable pH/mV meters with external ground adaptor were employed for primary data collection. In normal seawater, pH ranges from 7.5 to 8.2, but levels below 6.5 and as low as 4 are found under concretion covering actively corroding metal (North and MacLeod 1987:74). ThermoOrion pH electrodes were used in conjunction with the Model 265A portable meter. The general methodology for this procedure was developed by MacLeod (1995), who describes taking *in situ* E_{corr} measurements at the metal surface by drilling through the concretion, inserting pH and reference electrodes into the hole and taking sequential readings. During the present study, initial readings were made with ground contact made through a platinum disc on the bottom of the electrode. However, ground contact was modified, as discussed later, to avoid the possibility of poor contact at the bottom of the drilled hole. As an additional data set, a GMC-Staperm (Gardena, CA) Model AG-4-PT2 reference electrode (Ag/AgCl, seawater equivalent, +245 mV to SHE) with 200 ft. of #14 cable and 200 ft. of ground wire was used with a Wavetech HD-160 multimeter. The GMC electrode was deployed for exterior concretion surface measurements and was also used for ROV-mounted interior survey data collection.

At selected stations on the vessel, pH and E_{corr} were measured at various concretion-depths using reference electrodes inserted into holes drilled into the concretion. A drill rig

assembly and depth gage were constructed to drill ½-in. (1.3-cm)-diameter holes for inserting E_{corr} and pH probes (Figures 5.17 and 5.18). Hole depths were controlled by several depth jigs to provide uniform depths relative to the metal surface. Both E_{corr} and pH instruments were read out to the surface by 100 ft. cables; the topside recorder had voice communication with the diver. Multiple samples were drilled in a vertical transect at each station at varying water depths to characterize how the corrosion process changes with water depth and concretion thickness. These data have been collected in 14 transects arrayed from bow to stern, port and starboard, over several field seasons; however the largest cumulative data set of *in situ* corrosion measurements was collected between frame 70 and frame 90 (Figure 5.19). This 80-ft. hull section was chosen because the most complete original ship's plans, including original hull plate thickness was available between these frames. In addition, this hull section is the focus of the FEM completed by NIST (see Chapter 6).

In the first field season (2000), the focus was frame 85, completing vertical transects of *in situ* corrosion data on both the port and starboard sides of the ship (Figure 5.20). Only one E_{corr} measurement was taken for each drill sequence because the reference electrode was initially grounded through a platinum disc imbedded in the bottom of the electrode itself; no readings could be taken other than at the steel surface. Typical measurement procedures at a given water depth included surface pH; drilling to a depth of 0.4 in. (10 mm), taking pH reading at the bottom of the hole; drilling to 0.7 in. (18 mm), taking pH reading; and drilling to steel surface, where both pH and E_{corr} were obtained.

Data from the 2000 field season are tabulated (Table 5.7) and plotted in various graphs. A plot of pH vs. concretion depth shows that pH consistently decreases from a maximum at the exterior surface of the concretion to a minimum at the steel surface (Figures 5.21 and 5.22). The observation that pH decreases through the concretion from exterior to steel surface is consistent with reports on wrought and cast iron marine artifacts that note the cause for the decrease as similar to the crevice effect common in corrosion processes. Depletion of oxygen occurs as the concretion thickness increases and the low porosity of the concretion does not allow the oxygen to be replenished as fast as it consumed in the corrosion process (North 1976; North and MacLeod 1987). Chloride ions (Cl^-), with relatively high transport rates, migrate more rapidly than molecular oxygen through the concretion to the metal surface. The pH drops to as low as 4 at the metal surface as a result of hydrolysis reactions (equation [7]). The anodic reaction

Figure 5.17. Drilling through USS *Arizona*'s exterior concretion in preparation to measuring E_{corr} and pH (NPS Photo by Brett Seymour).

Figure 5.18. Measuring E_{corr} and pH through *Arizona*'s concretion (NPS Photo by Brett Seymour).
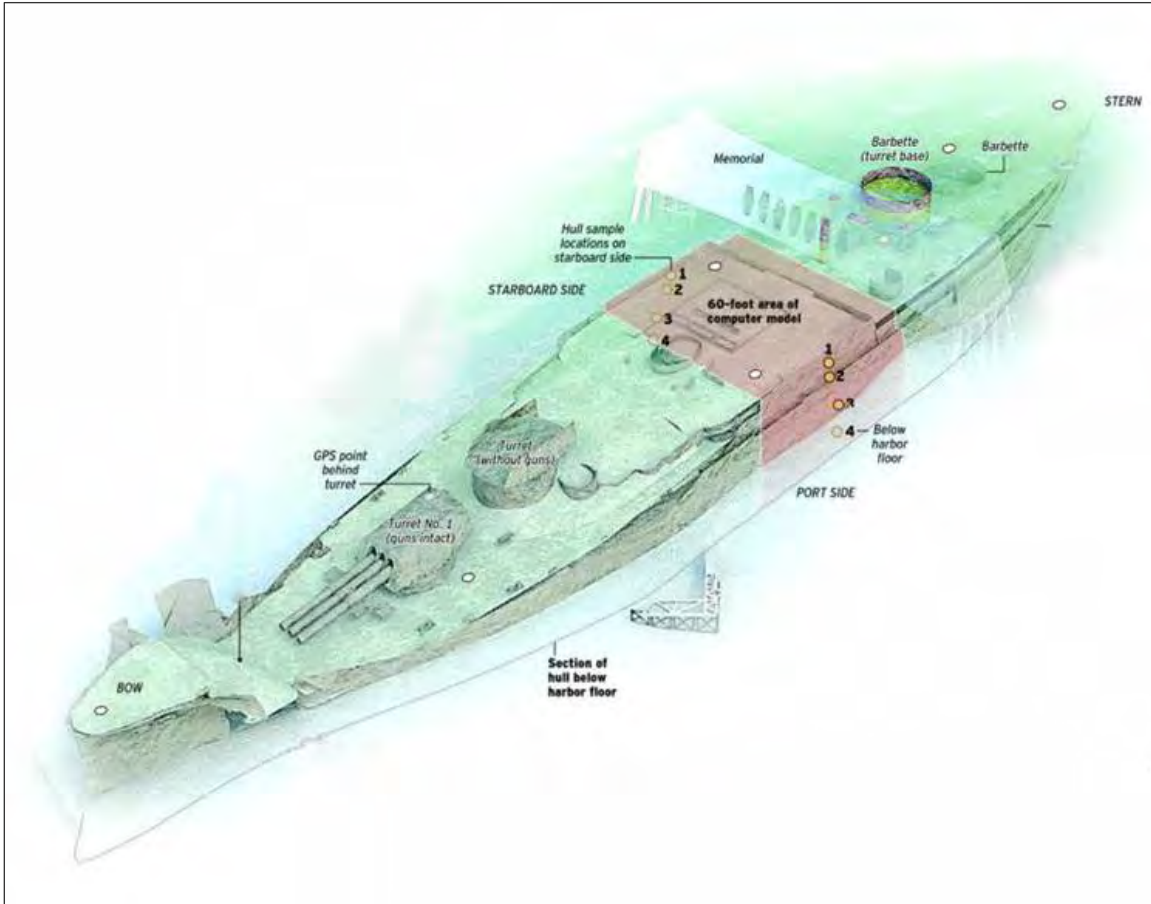
Figure 5.19. Graphic highlighting the 80-ft. long frame 70 to frame 90 section of USS *Arizona*'s hull (Graphic Courtesy of San Diego Union-Tribune).
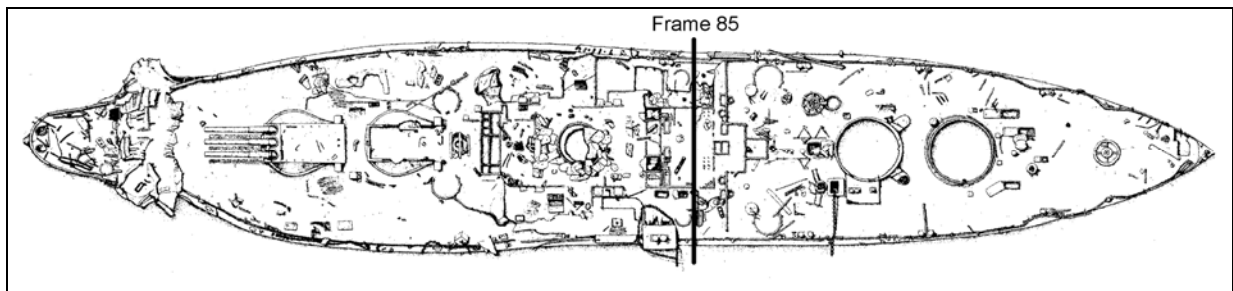
Figure 5.20. Frame 85 on USS *Arizona*'s hull, the focus for much of the corrosion analysis.

Sample	Vessel Side	Water Depth (ft.)	Drill Depth (mm)	Distance from Hull (mm)	pH	Ecorr (mV) vs. Ag/AgCl	Ecorr (mV) vs. SHE
+15C	Port	6	0	15	7.8		
+15C	Port	6	15	0	5.92	-591	-391
+14A	Port	7	0	8	8.05		
+14A	Port	7	8	0	7.99	-558	-358
+14B	Port	7	0	18	7.89		
+14B	Port	7	10	8	6.02		
+14B	Port	7	17	1	4.91		
+14B	Port	7	18	0	5.39	-590	-390
+14C	Port	7	0	18	7.89		
+14C	Port	7	13	5	7.39		
+14C	Port	7	18	0	6.09	-598	-398
+5A	Port	16	0	20.5	7.7		
+5A	Port	16	14	6.5	6.37		
+5A	Port	16	17	3.5	5.82		
+5A	Port	16	20.5	0	6.34	-564	-364
+5B	Port	16	0	17	n/a		
+5B	Port	16	13	4	6.46		
+5B	Port	16	15.5	1.5	6.07		
+5B	Port	16	17	0	5.77	-578	-378
-5A	Port	26	0	14	7.77		
-5A	Port	26	8	6	7.64		
-5A	Port	26	14	0	7.44	-572	-372
-5B	Port	26	0	17	7.69		
-5B	Port	26	11	6	6.09		
-5B	Port	26	12	5	3.83		
-5B	Port	26	17	0	3.86	-581	-381
+14D2	Starboard	3	0	15	7.64		
+14D2	Starboard	3	9	6	6.65		
+14D2	Starboard	3	15	0	5.85	-602	-402
+5D2	Starboard	12	0	20	7.62		
+5D2	Starboard	12	8	12	7.56		
+5D2	Starboard	12	20	0	5.48	-566	-366
-5D2	Starboard	22	0	10	7.03		
-5D2	Starboard	22	8	2	5.96		
-5D2	Starboard	22	10	0	7.26	-554	-354

Table 5.7. September 2000 *in situ* corrosion data. All data collected at frame 85 with Orion Ag/AgCl reference electrode using external ground. Elevation above (+) or below (-) top of torpedo blister. On port side, top of torpedo blister is at 21 ft. water depth; on starboard side, top of torpedo blister is at 17 ft. water depth
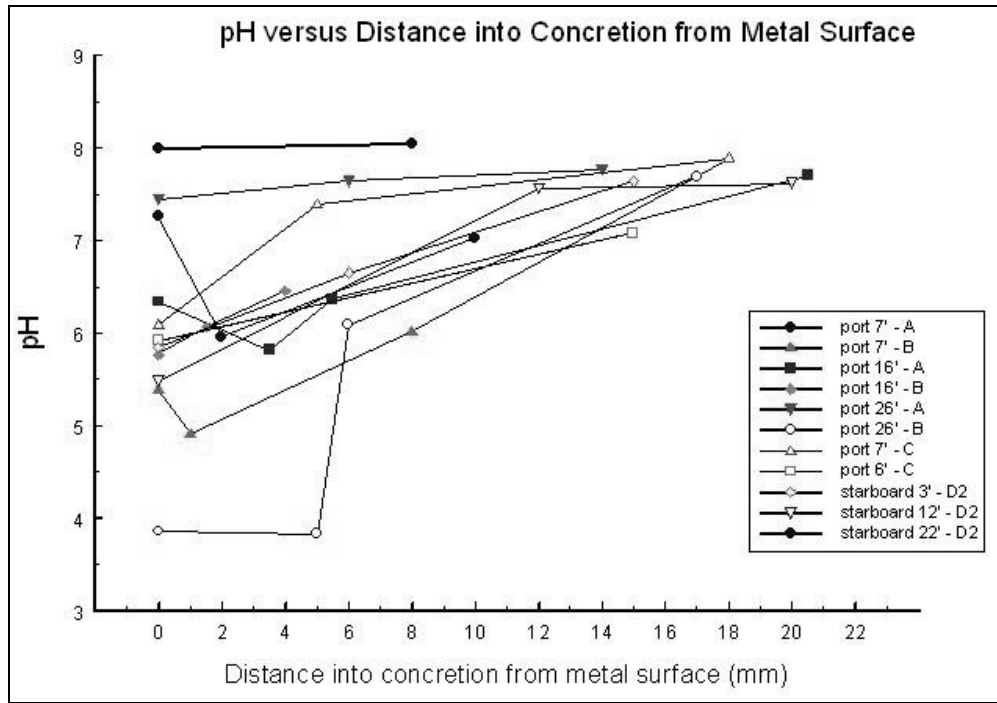
Figure 5.21. Relationship between pH and concretion thickness, based on September 2000 data in Table 5.7.
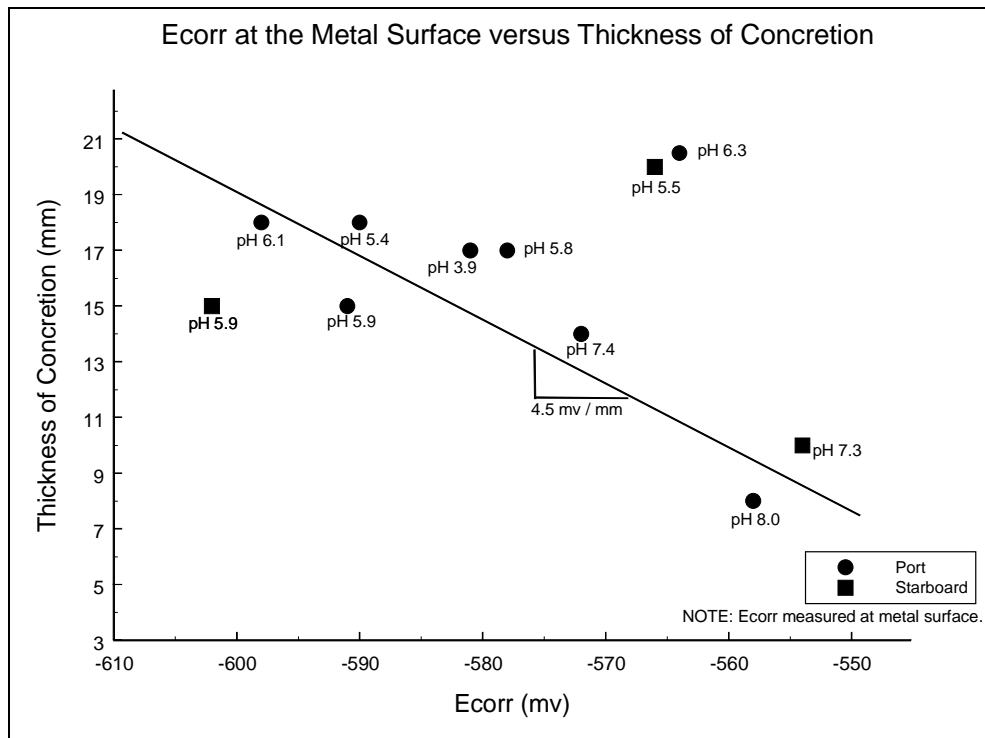
Figure 5.22. Relationship between E_corr, pH and concretion thickness, from data in Table 5.7.

163

continues at the steel surface and produces a solution rich in Fe^{+2}. Charge neutrality is maintained by outward diffusion of cations, mainly Fe^{+2} and H^+ ions as Cl^- ions continue their inward migration through the concretion to the underlying steel. Changes in the concretion's chemistry and stoichiometry (quantitative relationship between reactants and products in a chemical reaction) as a result of iron ion diffusion from the steel hull toward the concretion's exterior surface will be discussed below.

The lack of consistently good contact between the base of the probe and hull metal at the bottom of the drill hole resulted in inconsistent readings during the 2000 field season. As a result, it was decided to incorporate a separate ground connection to the hull, removed from the drill hole. A separate ground also had the advantage that E_{corr} readings could be taken at the concretion's exterior surface as well as at interior positions in the concretion, rather than just at the bottom of the drill hole on the steel surface.

E_{corr}/pH data from the 2000 field season is superimposed on the iron-water Pourbaix diagram in Figure 5.3. All of the points fall within the region of active corrosion because they appear in the area labeled Fe^{+2}, yielding iron ions in water solution. Note that the points are well below the region of Fe^{+3} stability, so ferrous ion (Fe^{+2}) dominates. Since the points appear to follow closely along the lower dotted line, the cathode appears to be dominated by equations [3] or [4]. Lower pH values observed at the steel/concretion interface suggests the cathode reaction involves hydrogen evolution, in addition to oxygen consumption, as observed by divers after the first penetration of the concretion.

Assuming that oxygen diffusion through the concretion is the single factor determining the corrosion rate, the corrosion rate is therefore proportional to the reciprocal of the concretion thickness (d), according to equation [14]. As concretion thickens, oxygen must diffuse through a longer path and the availability of oxygen at the metal/concretion interface decreases.

During the second field season collecting *in situ* corrosion data (2001), the external ground was incorporated using a large C-clamp attached to the end of the ground cable. As mentioned above, the external ground to the hull allowed both E_{corr} and pH to be measured at various depths into the concretion. As before, final readings were taken at the bottom of the drill hole in contact with hull steel. In addition to taking measurements at frame 85, *in situ* data collection was expanded to other areas of the hull including vertical transects of pH and E_{corr} data at frames 9, 28, 82, 128 and 148, on both the port and starboard sides of the ship (Figure 5.23).
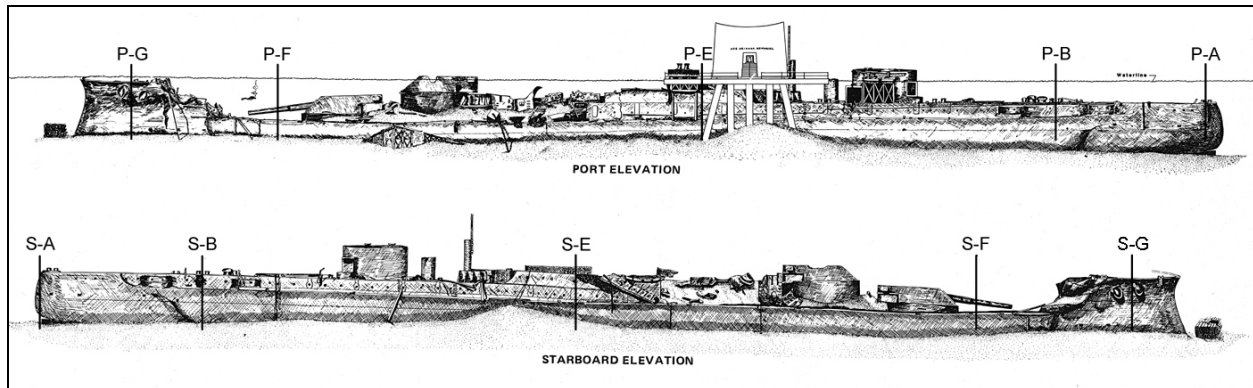
Figure 5.23. Location of *in situ* corrosion transects measured in June 2001.

Researchers in a small NPS launch recorded data relayed to them via hard wire communications from divers. Mobility allowed for attachment of the ground clamp in close proximity to the desired test site and easier deployment of test leads from meter readouts on the boat to diver positions. A comprehensive assessment of corrosion on *Arizona*'s hull was documented in terms of corrosion potential.

Data from the June 2001 field season were again tabulated (Tables 5.8–5.17) and plotted graphically. The most important observation from this data set is that E_{corr} is inversely proportional to water depth; that is, E_{corr} decreases (becomes more negative) as water depth increases (Figure 5.24). Figure 5.24 displays two values for each drill hole, appearing at the two ends of a vertical line—the top of the line corresponds to values taken at the steel hull surface, while the bottom of the line corresponds to values taken on the concretion's exterior surface. Visual observation indicates that E_{corr} decreases as the water depth increases. E_{corr} also decreases from the exterior surface of the concretion inward toward the steel hull, with the lowest E_{corr} value occurring at the steel surface (Figure 5.25). E_{corr} is most negative at the steel surface and the most positive at the concretion's exterior surface, as observed by North and MacLeod (1987).

Results of the June 2001 field season also clearly confirm that a decrease in pH, caused by reduced oxygen and increased choride ion, occurs as the steel surface is approached through the concretion (Figures 5.26 and 5.27). While this result is consistent at each location measured on *Arizona*'s hull, the effect is random with respect to water depth and frame location on the hull.

Sample	Location	Vessel Side	Water Depth (ft.)	Drill Depth (mm)	Distance from Hull (mm)	pH	E_{corr} (mV) vs. Ag/AgCL	E_{corr} (mV) vs. SHE
-5P-A	Frame 148	Port	13	0	27.5	8.03	-691	-491
-5P-A	Frame 148	Port	13	10	17.5	7.7	-675	-475
-5P-A	Frame 148	Port	13	21	6.5	6.25	-676	-476
-5P-A	Frame 148	Port	13	27.5	0	6.84	-674	-474
-18P-A	Frame 148	Port	29	0	15	5.09	-608	-408
-18P-A	Frame 148	Port	29	9	6	4.93	-608	-408
-18P-A	Frame 148	Port	29	15	0	3.08	-624	-424
-25P-A	Frame 148	Port	32	0	23	5.2	-597	-397
-25P-A	Frame 148	Port	32	16	7	5.22	-594	-394
-25P-A	Frame 148	Port	32	19	4	5.13	-594	-394
-25P-A	Frame 148	Port	32	23	0	3.54	-622	-422

Table 5.8. June 2001 *in situ* corrosion data, transect P-A. All data collected with Orion Ag/AgCl reference electrode using external ground. Elevation noted is distance below (-) gunwale, with gunwale depth at 8 ft.

Sample	Location	Vessel Side	Water Depth (ft.)	Drill Depth (mm)	Distance from Hull (mm)	pH	E_{corr} (mV) vs. Ag/AgCL	E_{corr} (mV) vs. SHE
-4.75S-A	Frame 148	Starboard	12	0	51	5.64	-548	-348
-4.75S-A	Frame 148	Starboard	12	11	40	5.8	-549	-349
-4.75S-A	Frame 148	Starboard	12	30	21	5.78	-562	-362
-4.75S-A	Frame 148	Starboard	12	51	0	5.58	-603	-403
-14.75S-A	Frame 148	Starboard	23	0	15	7	-545	-345
-14.75S-A	Frame 148	Starboard	23	8	7	5.93	-545	-345
-14.75S-A	Frame 148	Starboard	23	11	4	1.61	-548	-348
-14.75S-A	Frame 148	Starboard	23	15	0	5.26	-559	-359
-24.75S-A	Frame 148	Starboard	32	0	26	5.97	-544	-344
-24.75S-A	Frame 148	Starboard	32	17	9	6.12	-544	-344
-24.75S-A	Frame 148	Starboard	32	20	6	6.09	-544	-344
-24.75S-A	Frame 148	Starboard	32	26	0	5	-567	-367

Table 5.9. June 2001 *in situ* corrosion data, transect S-A. All data collected with Orion Ag/AgCl reference electrode using external ground. Elevation noted is distance below (-) gunwale, with gunwale depth at 7.25 ft.

Sample	Location	Vessel Side	Water Depth (ft.)	Drill Depth (mm)	Distance from Hull (mm)	pH	Ecorr (mV) vs. Ag/AgCL	Ecorr (mv) vs. SHE
+5P-B	Frame 128	Port	15	0	28	6.07	-542	-342
+5P-B	Frame 128	Port	15	n/a	16	5.62	-549	-349
+5P-B	Frame 128	Port	15	12	n/a	5.13	-565	-365
+5P-B	Frame 128	Port	15	28	0	4.85	-587	-387
-5P-B	Frame 128	Port	26	0	10	-	-546	-346
-5P-B	Frame 128	Port	26	10	0	5.55	-583	-383
-11P-B	Frame 128	Port	32	0	14	6.1	-547	-347
-11P-B	Frame 128	Port	32	12	2	6.01	-547	-347
-11P-B	Frame 128	Port	32	14	0	5.89	-558	-358

Table 5.10. June 2001 *in situ* corrosion data, transect P-B. All data collected with Orion Ag/AgCl reference electrode using external ground. Elevation noted is distance above (+) and below (-) torpedo blister.

Sample	Location	Vessel Side	Water Depth (ft.)	Drill Depth (mm)	Distance from Hull (mm)	pH	Ecorr (mV) vs. Ag/AgCL	Ecorr (mv) vs. SHE
+5S-B	Frame 128	Starboard	15	0	33	6.31	-542	-342
+5S-B	Frame 128	Starboard	15	10	23	6.73	-547	-347
+5S-B	Frame 128	Starboard	15	33	0	n/a	-570	-370
-5S-B	Frame 128	Starboard	25	0	14	n/a	-547	-347
-5S-B	Frame 128	Starboard	25	13	1	n/a	-572	-372
-5S-B	Frame 128	Starboard	25	14	0	n/a	-583	-383
-11S-B	Frame 128	Starboard	30	0	21	n/a	-548	-348
-11S-B	Frame 128	Starboard	30	10	11	n/a	-549	-349
-11S-B	Frame 128	Starboard	30	17	4	n/a	-551	-351
-11S-B	Frame 128	Starboard	30	21	0	n/a	-569	-369

Table 5.11. June 2001 *in situ* corrosion data, transect S-B. All data collected with Orion Ag/AgCl reference electrode using external ground. Elevation above (+) and below (-) torpedo blister, which is 20 ft.

Sample	Location	Vessel Side	Water Depth (ft.)	Drill Depth (mm)	Distance from Hull (mm)	pH	Ecorr (mV) vs. Ag/AgCL	Ecorr (mv) vs. SHE
+14P-E	Frame 82	Port	6	0	14.5	8.96	n/a	n/a
+14P-E	Frame 82	Port	6	11	3.5	8.6	n/a	n/a
+14P-E	Frame 82	Port	6	14.5	0	8.5	n/a	n/a
+5P-E	Frame 82	Port	18	0	26	8.09	-561	-361
+5P-E	Frame 82	Port	18	10	16	8.04	-552	-352
+5P-E	Frame 82	Port	18	18	8	5.67	-566	-366
+5P-E	Frame 82	Port	18	26	0	5.94	-614	-414
-5P-E	Frame 82	Port	26	0	21	4.54	-580	-380
-5P-E	Frame 82	Port	26	4	17	4.65	-560	-360
-5P-E	Frame 82	Port	26	11	10	2.97	-567	-367
-5P-E	Frame 82	Port	26	21	0	2.64	-584	-384

Table 5.12. June 2001 *in situ* corrosion data, transect P-E. All data collected with Orion Ag/AgCl reference electrode using external ground. Elevation above (+) and below (-) torpedo blister, which is 22 ft.

Sample	Location	Vessel Side	Water Depth (ft.)	Drill Depth (mm)	Distance from Hull (mm)	pH	Ecorr (mV) vs. Ag/AgCL	Ecorr (mv) vs. SHE
+14S-E	Frame 82	Starboard	3	0	>150	6.71	-542	-342
+14S-E	Frame 82	Starboard	3	10	140	6.72	-541	-341
+14S-E	Frame 82	Starboard	3	19	131	6.91	-538	-338
+14S-E	Frame 82	Starboard	3	>150	0	6.63	-533	-333
+5S-E	Frame 82	Starboard	12	0	63	6.48	-544	-344
+5S-E	Frame 82	Starboard	12	11	52	5.71	-547	-347
+5S-E	Frame 82	Starboard	12	52	11	3.89	-563	-363
+5S-E	Frame 82	Starboard	12	63	0	3.67	-562	-362
-5S-E	Frame 82	Starboard	23	0	14	6.24	-547	-347
-5S-E	Frame 82	Starboard	23	11	3	4.79	-551	-351
-5S-E	Frame 82	Starboard	23	14	0	5.04	-571	-371

Table 5.13. June 2001 *in situ* corrosion data, transect S-E. All data collected with Orion Ag/AgCl reference electrode using external ground. Elevation above (+) and below (-) torpedo blister, which is 18 ft. Sample +14S-E never reached metal, depth of concretion too great. At sample +5S-E, water flowed out of the hole, precipitating from black to red (see below).

Sample	Location	Vessel Side	Water Depth (ft.)	Drill Depth (mm)	Distance from Hull (mm)	pH	Ecorr (mV) vs. Ag/AgCL	Ecorr (mv) vs. SHE
0P-F	Frame 28	Port	27	0	23	6.14	No Data	No Data
0P-F	Frame 28	Port	27	10	13	6.21	No Data	No Data
0P-F	Frame 28	Port	27	23	0	4.1	No Data	No Data
-5P-F	Frame 28	Port	32	0	32	6.14	No Data	No Data
-5P-F	Frame 28	Port	32	12	20	6.14	No Data	No Data
-5P-F	Frame 28	Port	32	30	2	6.14	No Data	No Data
-5P-F	Frame 28	Port	32	32	0	4.75	No Data	No Data

Table 5.14. June 2001 *in situ* corrosion data, transect P-F. All data collected with Orion Ag/AgCl reference electrode using external ground. Elevation above (+) and below (-) torpedo blister, which is 27 ft.

Sample	Location	Vessel Side	Water Depth (ft.)	Drill Depth (mm)	Distance from Hull (mm)	pH	Ecorr (mV) vs. Ag/AgCL	Ecorr (mv) vs. SHE
0S-F	Frame 28	Starboard	23.5	0	21	6.14	-543	-343
0S-F	Frame 28	Starboard	23.5	8	13	6.28	-544	-344
0S-F	Frame 28	Starboard	23.5	18	3	5.51	-569	-369
0S-F	Frame 28	Starboard	23.5	21	0	5.85	-570	-370
-5S-F	Frame 28	Starboard	28.5	0	26	6.27	-537	-337
-5S-F	Frame 28	Starboard	28.5	17	9	5.93	-537	-337
-5S-F	Frame 28	Starboard	28.5	26	0	5.3	-547	-347

Table 5.15. June 2001 *in situ* corrosion data, transect S-F. All data collected with Orion Ag/AgCl reference electrode using external ground. Elevation above (+) and below (-) torpedo blister, which is 23.5 ft.

Sample	Location	Vessel Side	Water Depth (ft.)	Drill Depth (mm)	Distance from Hull (mm)	pH	Ecorr (mV) vs. Ag/AgCL	Ecorr (mv) vs. SHE
-5P-G	Frame 9	Port	10	0	18	6.71	-538	-338
-5P-G	Frame 9	Port	10	11	7	6.52	-538	-338
-5P-G	Frame 9	Port	10	18	0	5.12	-552	-352
-10P-G	Frame 9	Port	15	0	15	6.67	-540	-340
-10P-G	Frame 9	Port	15	10	5	6.45	-542	-342
-10P-G	Frame 9	Port	15	15	0	4.57	-568	-368
-15P-G	Frame 9	Port	20	0	19	6.62	-545	-345
-15P-G	Frame 9	Port	20	8	11	5.32	-551	-351
-15P-G	Frame 9	Port	20	17	2	3.64	-574	-374
-15P-G	Frame 9	Port	20	19	0	3.85	-566	-366
-19P-G	Frame 9	Port	24	0	21	6.53	-539	-339
-19P-G	Frame 9	Port	24	11	10	5.61	-539	-339
-19P-G	Frame 9	Port	24	21	0	4.97	-554	-354

Table 5.16. June 2001 *in situ* corrosion data, transect P-G. All data collected with Orion Ag/AgCl reference electrode using external ground. Elevation noted is distance below (-) gunwale, with gunwale depth at 5 ft.

Sample	Location	Vessel Side	Water Depth (ft.)	Drill Depth (mm)	Distance from Hull (mm)	pH	Ecorr (mV) vs. Ag/AgCL	Ecorr (mv) vs. SHE
-5S-G	Frame 9	Starboard	10	0	28	6.76	-541	-341
-5S-G	Frame 9	Starboard	10	11	17	6.63	-551	-351
-5S-G	Frame 9	Starboard	10	18	10	3.93	-568	-368
-5S-G	Frame 9	Starboard	10	28	0	3.52	-585	-385
-10S-G	Frame 9	Starboard	15	0	19	6.16	-550	-350
-10S-G	Frame 9	Starboard	15	16	3	5.57	-561	-361
-10S-G	Frame 9	Starboard	15	19	0	4.68	-561	-361
-15S-G	Frame 9	Starboard	20	0	11	6.15	-555	-355
-15S-G	Frame 9	Starboard	20	10	1	5.8	-562	-362
-15S-G	Frame 9	Starboard	20	11	0	4.7	-563	-363
-19S-G	Frame 9	Starboard	24	0	13	6.09	-551	-351
-19S-G	Frame 9	Starboard	24	12	1	5.98	-551	-351
-19S-G	Frame 9	Starboard	24	13	0	5.43	-551	-351

Table 5.17. June 2001 *in situ* corrosion data, transect S-G. All data collected with Orion Ag/AgCl reference electrode using external ground. Elevation noted is distance below (-) gunwale, with gunwale depth at 5 ft. At sample -5S-G, water flowed out of the hole, precipitating from black to red (see below).
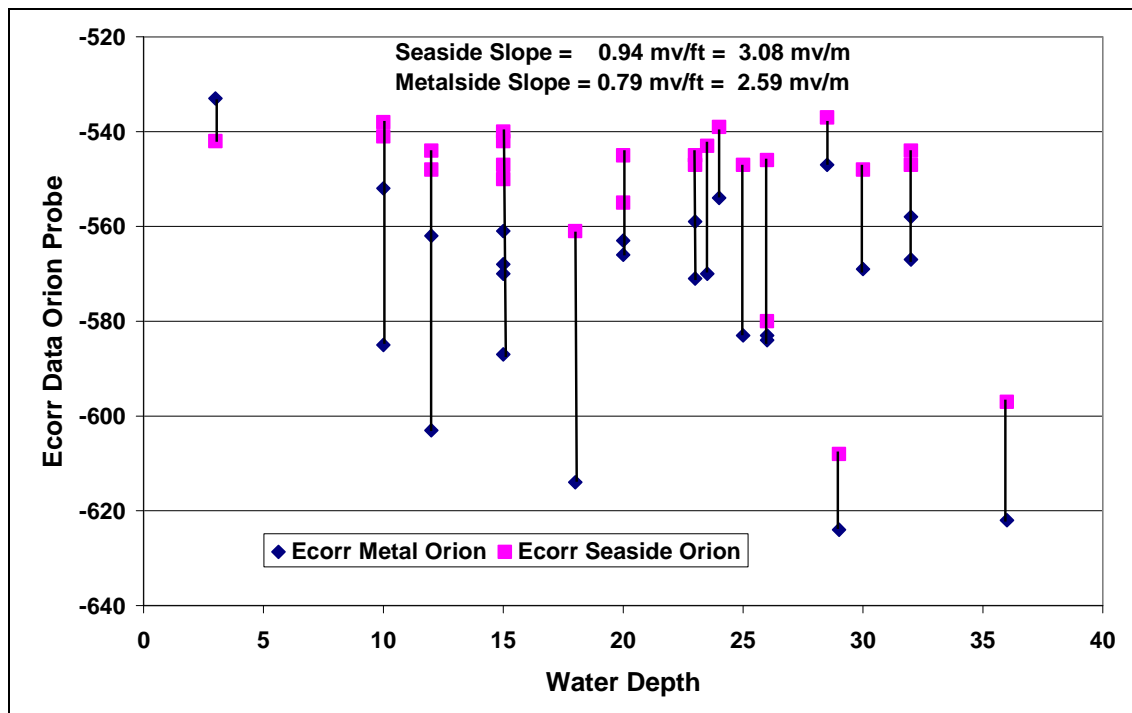
Figure 5.24. Corrosion potential as function of water depth, typical frames from June 2001 data set.
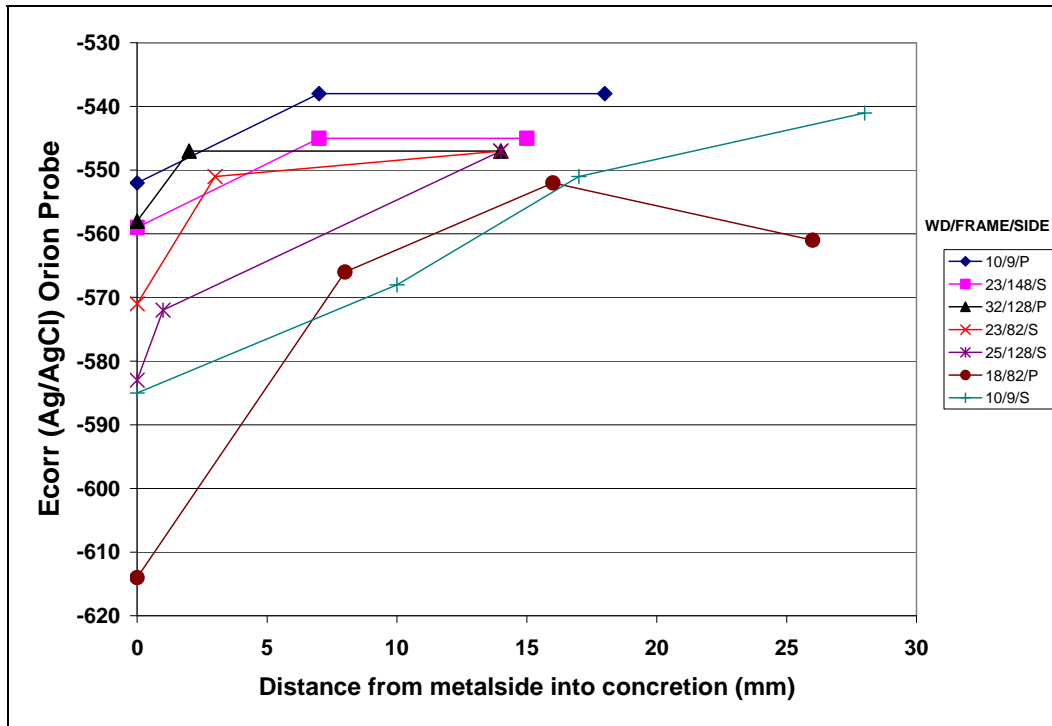
Figure 5.25. Corrosion potential as a function of distance from hull, into concretion to open seawater, typical frames from June 2001 data set.
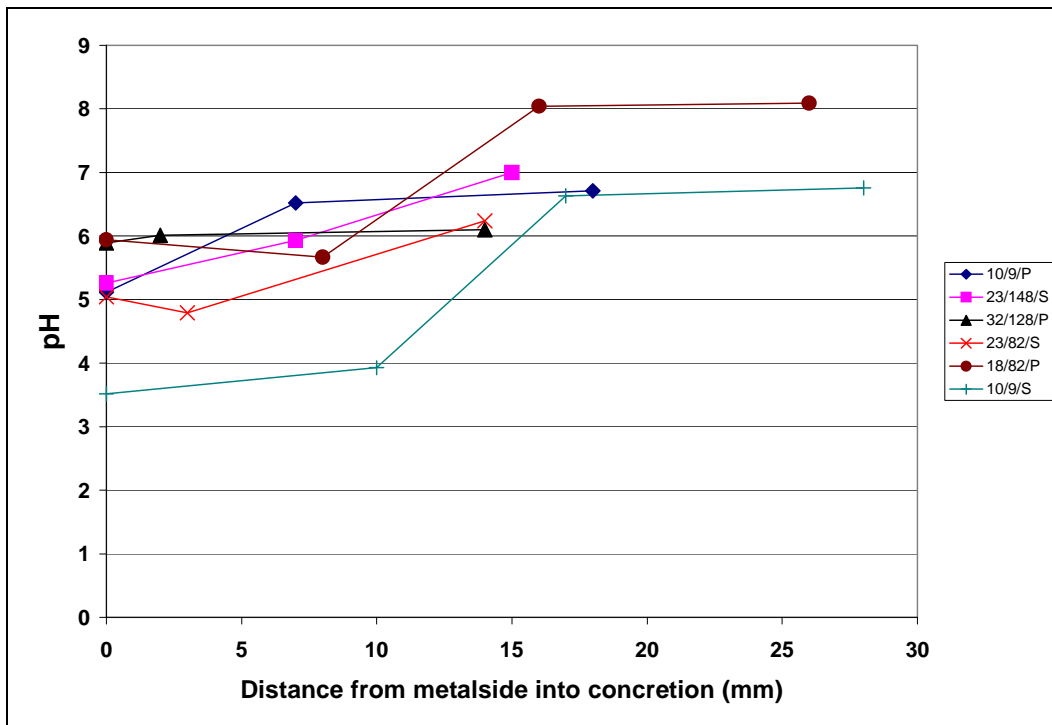
Figure 5.26. pH as a function of distance from hull surface, typical frames from June 2001 data set.

170
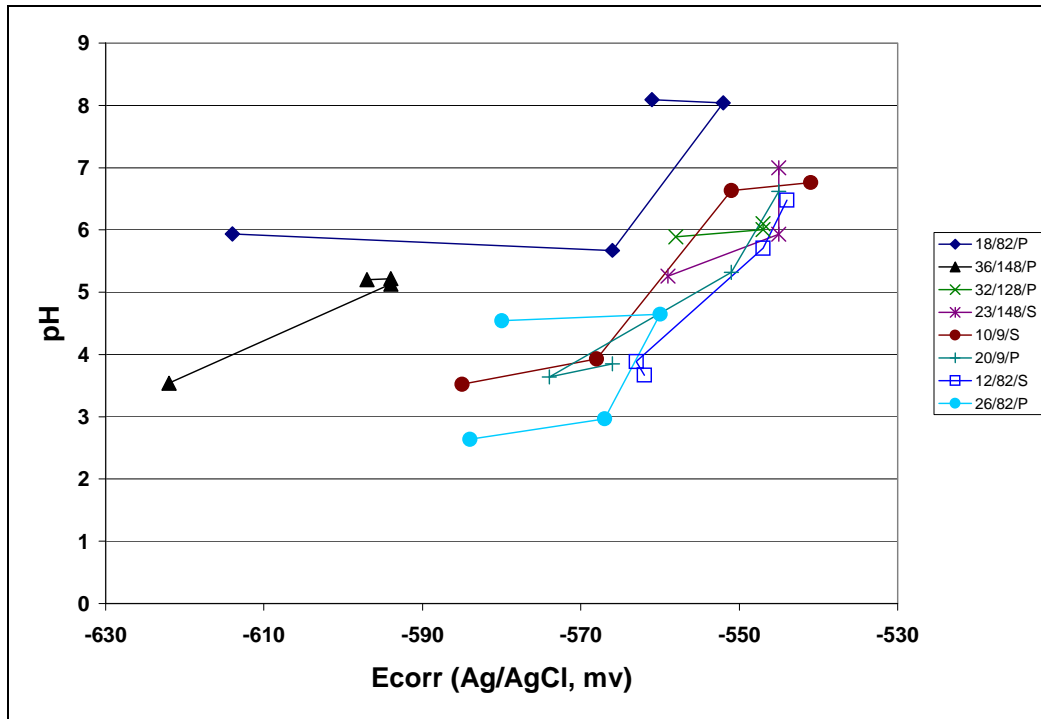
Figure 5.27. pH as a function of E_{corr}, typical frames from June 2001 data set.

The polarization diagram illustrates how the potential difference between points A and C prevents intersection of the cathode and anode polarization lines because of resistance between the E_{corr} probe and the metal surface (see Figure 5.1). From Ohms law:

$$i_{(corr\ IR\ drop)} = (E_{corr}\ (exterior) - E_{corr}\ (interior)) / (r)(d) \qquad [15]$$

where

r (Ω-cm) is the electrical resistivity

d (cm) is concretion thickness

E_{corr} is corrosion potential (volts)

$i_{(corr\ IR\ drop)}$ is concretion current density (amp/cm^2)

Using a value of r = 2000 Ω-cm for the electrical resistivity of the concretion (MacLeod 1982), and E_{corr} and d values for Frame 148, starboard, a typical calculation gives the following value for $i_{(corr,\ IR\ drop)}$ in mpy:

$$i_{(corr,\ IR\ drop)} = V/(\Omega\text{-cm x cm}) = 0.023 / (2000\ x\ 2.6)\ x\ 0.46 = 2.03\ mpy$$

171

Computation of $i_{(corr, IR\ drop)}$ for all of data in Tables 5.8–5.17, including E_{corr} values taken inside the concretion, resulted in a wide scatter of data. Figure 5.28 shows a plot of $i_{(corr, IR\ drop)}$ as a function of water depth after eliminating internal E_{corr} readings obtained from 22 sites over the entire hull. The trendline shows increasing $i_{(corr, IR\ drop)}$, just the opposite of i_{corr} obtained from metal samples taken from the hull. It is concluded that current distribution inside the concretion is complex and creates a voltage gradient across the concretion that cannot be related to i_{corr} in simple terms. Furthermore, the electrical resistivity of the concretion is not a constant as assumed in equation [15]. This observation is confirmed from x-ray diffraction results showing that the concretion is not homogeneous.

As discussed above, anodic polarization is shown as a solid line from A(3) to B or as a solid line from A(3) to A(1) and dotted from A(1) through B(1) to A(4) (Figure 5.1). From A(3) to B, the corrosion rate increases as E_{corr} increases and is typical of steel in seawater. For simplicity, anodic polarization is assumed to be linear to point B but in reality may deviate upward as the potential increases. From A(3) to A(4) along A(1) to B(1), passivation occurs as is typical for steel and aluminum in natural water. The metal passivates by initially corroding and
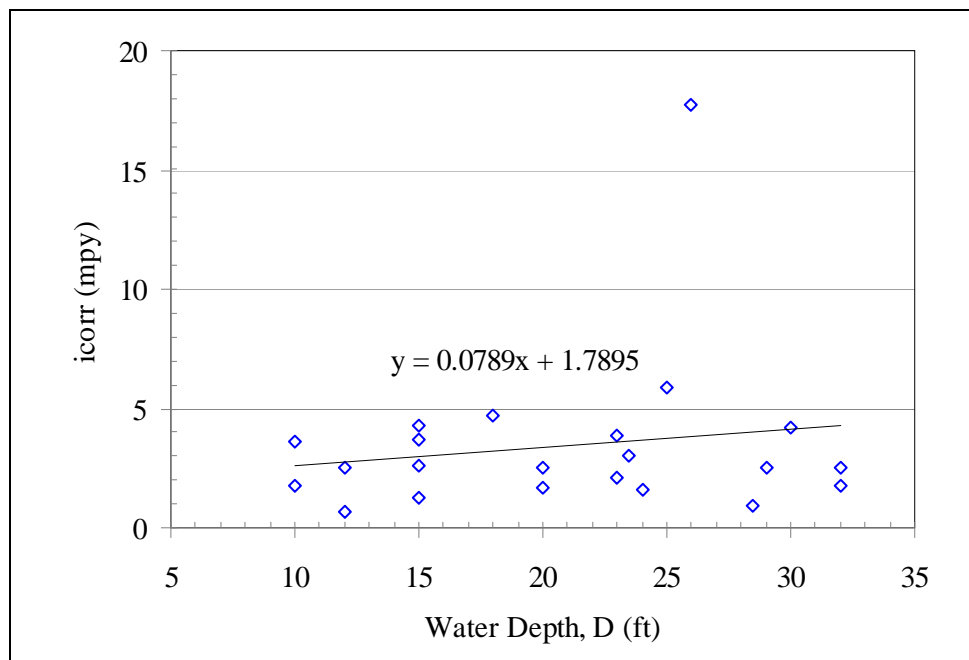
Figure 5.28. i_{corr} (IR Drop across concretion) as a function of water depth.

forming its own protective film. Approaching passivation, anodic polarization increases but peaks at around A(1) dropping to a lower current as the potential increases. Intersection with cathodic polarization at B(1) now occurs at a lower i_{corr} than that identified as i_{corr} (1). This illustrates how an increase in E_{corr} yields a lower rather than a higher i_{corr}. It is important to emphasize that steel does not normally passivate in seawater and anodic polarization continues to increase from A(3) to points A or B depending on the IR drop. The region between C and A, nearly point B, defines E_{corr} and the vertical line through C and A defines i_{corr}(1). The difference between E_{corr} (1) and E_{corr} (2) is small and usually neglected.

As an interesting aside, during concretion drilling at sites -5S-G (frame 9, starboard side, at a water depth of 10 ft.) and +5S-E (frame 82, starboard side, at a water depth of 13 ft.), clear water poured out of the drill hole upon removal of the drill. As it mixed with seawater, the outflow grew dark, then became cloudy and reddish in color and reduced visibility to a few feet. Outflow was strong and streamed out the drill hole approximately 8 in. Adjacent concretion had blistered away from the hull in this area, creating a gap between the steel hull and the concretion. One explanation for this phenomenon is hydrogen accumulation behind the concretion during hydrogen ion reduction as a result of equation [4] and equation [16].   Equation [16], derived from the Nerst equation [1], is useful to estimate the extent of pressure build up that can theoretically develop at the steel surface behind the concretion (Pourbaix 1974):

$$E^0 = E_{corr} = 0.000 - 0.0592pH - 0.0295 \log(P[H_2]) \hspace{2cm} [16]$$

The theoretical maximum gas pressure, equation [16], is over 950 atmospheres or 14,000 psi at pH = 4 and E_{corr} = 0.325 V (SHE). Obviously, the gas pressure could never reach such high values because hydrogen would slowly diffuse into the steel hull or escape through voids in the concretion before the pressure exceeded more than a few atmospheres. After the event, the hole was plugged. The next day the hole was reopened and clear water continued to pour out of the drill hole as the event was documented on underwater video.

Immediately before removing hull coupons in August 2002 (see below), E_{corr} and pH were obtained at each coupon sample location. Using the same procedure as in past field operations, pH and E_{corr} were measured in holes drilled close to the sample area. Initial E_{corr}/pH data was to be obtained through the concretion 6–8 in. above, forward, below and aft of the site

selected for each core sample before the pad was cleared of concretion. Due to time constraints, the number of readings was reduced as drill operations continued (Table 5.18).

The 2002 sample locations were revisited in November 2003 to once again collect E_{corr} and pH data (Table 5.19). This replication allows researchers to gauge the impact to the ship of removing the hull coupons and surrounding encrustation. Data collected were comparable to 2002 data from the same locations, indicating no negative impact to the ship resulted from coupon removal. The epoxy sealing had succeeded in preventing formation of local areas of increased corrosion during the year since coupon collection. The areas drilled for this data set were also the locations where preliminary ultrasonic thickness testing was conducted (see below).

Finally, in 2004 a final E_{corr}/pH data set was collected during expansion of the ultrasonic thickness survey (Table 5.20). These data continued to confirm earlier findings regarding E_{corr} and pH variability. E_{corr} as a function of water depth from Tables 5.19 and 5.20 are combined and plotted in Figure 5.29.

E_{corr} Transects at Concretion Exterior

In addition to sequential drilling and E_{corr}/pH measurements through the concretion, a potential survey was conducted in June 2001 at selected transects across *Arizona*'s hull using a GMC reference electrode and Wavetech HD-160 meter. Seven transects were selected for measurement from the harbor bottom on the starboard side of the ship, up the starboard side to the starboard gunwale, over exposed deck areas to the port gunwale, and down the port side of the ship to the harbor bottom (Figure 5.30). E_{corr} measurements were taken every 6 ft. along the transect on the exterior surface of the concretion. These transects were a quick, non-intrusive way to collect an additional data set that would complement and could be directly compared to the more detailed data obtained through sequential drilling. The transects indicate a consistent trend toward lower E_{corr} as the water depth increases (Figure 5.31). For example, the horizontal areas on Transects 1, 2, 3, and 4 are closer to the water surface nearer the stern than Transects 6 and 7, and as a result E_{corr} values in the latter two are from 15–25 mV more negative.

Transect 1, taken near the stern at approximately frame 148, reflects a drop in E_{corr} as the transect approaches the harbor bottom on both sides, particularly at and below the harbor bottom

Sample	Location	Vessel Side	Water Depth (ft.)	Drill Depth (mm)	Distance from Hull (mm)	pH	Ecorr (mV) vs. Ag/AgCl	Ecorr (mV) vs. SHE
USAR-02-001	Frame 76.5, 6 in. above sample	Port	5	0	15.4	7.64	-527	-327
USAR-02-001	Frame 76.5, 6 in. above sample	Port	5	9.4	6	6.12	-529	-329
USAR-02-001	Frame 76.5, 6 in. above sample	Port	5	15.4	0	6.51	-554	-354
USAR-02-001	Frame 76.5, 8 in. forward of sample	Port	5	0	23.5	7.7	-528	-328
USAR-02-001	Frame 76.5, 8 in. forward of sample	Port	5	11.3	12.2	7.7	-530	-330
USAR-02-001	Frame 76.5, 8 in. forward of sample	Port	5	23.5	0	6.53	-557	-357
USAR-02-001	Frame 76.5, 10 in. aft of sample	Port	5	0	26	7.43	-531	-331
USAR-02-001	Frame 76.5, 10 in. aft of sample	Port	5	10.2	15.8	6.68	-537	-337
USAR-02-001	Frame 76.5, 10 in. aft of sample	Port	5	26	0	6.5	-551	-351
USAR-02-002	Frame 76.5, 6 in. forward of sample	Port	19.5	0	17	7	-539	-339
USAR-02-002	Frame 76.5, 6 in. forward of sample	Port	19.5	10.5	6.5	6.58	-549	-349
USAR-02-002	Frame 76.5, 6 in. forward of sample	Port	19.5	17	0	5.95	-551	-351
USAR-02-002	Frame 76.5, 6 in. aft of sample	Port	19.5	0	42.5	7.49	-538	-338
USAR-02-002	Frame 76.5, 6 in. aft of sample	Port	19.5	8	34.5	7.24	-539	-339
USAR-02-002	Frame 76.5, 6 in. aft of sample	Port	19.5	42.5	0	5.5	-560	-360
USAR-02-003	Frame 76.5, 6 in. forward of sample	Port	26	0	17.4	6.99	-542	-342
USAR-02-003	Frame 76.5, 6 in. forward of sample	Port	26	7	10.4	7.43	-542	-342
USAR-02-003	Frame 76.5, 6 in. forward of sample	Port	26	17.4	0	6.34	-560	-360
USAR-02-004	Frame 76.5, 1 ft. aft of sample	Port	34	0	9	7.13	-509	-309
USAR-02-004	Frame 76.5, 1 ft. aft of sample	Port	34	6.5	2.5	5.51	-522	-322
USAR-02-004	Frame 76.5, 1 ft. aft of sample	Port	34	9	0	6.19	-523	-323
USAR-02-007	Frame 80.5, 6 in. aft of sample	Starboard	5	0	9.3	7.28	-550	-350
USAR-02-007	Frame 80.5, 6 in. aft of sample	Starboard	5	9.3	0	7.31	-562	-362
USAR-02-008	Frame 80.5, 6 in. forward of sample	Starboard	15	0	15.6	6.95	-549	-349
USAR-02-008	Frame 80.5, 6 in. forward of sample	Starboard	15	14.7	0.9	4.43	-563	-363
USAR-02-008	Frame 80.5, 6 in. forward of sample	Starboard	15	15.6	0	4.46	-561	-361
USAR-02-009	Frame 80.5, 6 in. forward of sample	Starboard	22	0	6.5	6.8	-552	-352
USAR-02-009	Frame 80.5, 6 in. forward of sample	Starboard	22	3.5	3	6.71	-553	-353
USAR-02-009	Frame 80.5, 6 in. forward of sample	Starboard	22	6.5	0	6.15	-557	-357
USAR-02-010	Frame 80.5, 6 in. forward of sample	Starboard	32.5	0	9	6.67	-689	-489
USAR-02-010	Frame 80.5, 6 in. forward of sample	Starboard	32.5	7	2	6.29	-695	-495
USAR-02-010	Frame 80.5, 6 in. forward of sample	Starboard	32.5	9	0	5.53	-699	-499

Table 5.18. *In situ* corrosion data collected August 2002 in location of each hull sample (coupon) collected. All data collected with Orion Ag/AgCl reference electrode.

Sample	Location	Vessel Side	Water Depth (ft.)	Drill Depth (mm)	Distance from Hull (mm)	pH	Ecorr (mV) vs. Ag/AgCl	Ecorr (mV) vs. SHE
USAR-03-001	Frame 76.5	Port	5	0	25	n/a	-547	-347
USAR-03-001	Frame 76.5	Port	5	7	18	n/a	-547	-347
USAR-03-001	Frame 76.5	Port	5	25	0	n/a	-587	-387
USAR-03-002	Frame 76.5	Port	19.5	0	12	n/a	-554	-354
USAR-03-002	Frame 76.5	Port	19.5	9	3	n/a	-555	-355
USAR-03-002	Frame 76.5	Port	19.5	12	0	n/a	-593	-393
USAR-03-003	Frame 76.5	Port	26	0	10	n/a	-555	-355
USAR-03-003	Frame 76.5	Port	26	6	4	n/a	-562	-362
USAR-03-003	Frame 76.5	Port	26	10	0	n/a	-580	-380
USAR-03-007	Frame 80.5	Starboard	5	0	15	n/a	-550	-350
USAR-03-007	Frame 80.5	Starboard	5	7	8	n/a	-559	-359
USAR-03-007	Frame 80.5	Starboard	5	15	0	n/a	-597	-397
USAR-03-008	Frame 80.5	Starboard	15	0	18	n/a	-552	-352
USAR-03-008	Frame 80.5	Starboard	15	8	10	n/a	-552	-352
USAR-03-008	Frame 80.5	Starboard	15	18	0	n/a	-562	-362
USAR-03-009	Frame 80.5	Starboard	22	0	12	n/a	-558	-358
USAR-03-009	Frame 80.5	Starboard	22	3	9	n/a	-558	-358
USAR-03-009	Frame 80.5	Starboard	22	8	4	n/a	-579	-379
USAR-03-009	Frame 80.5	Starboard	22	12	0	n/a	-585	-385

Table 5.19. *In situ* corrosion data collected November 2003 in same locations as the previous year, at the site of each hull sample (coupon) collected. All data collected with Orion Ag/AgCl reference electrode.

The plotted trend line is labeled $y = -0.2665x - 345.5$. The x-axis is "Water Depth, D (ft)" and the y-axis is "Ecorr (SHE, mv)".
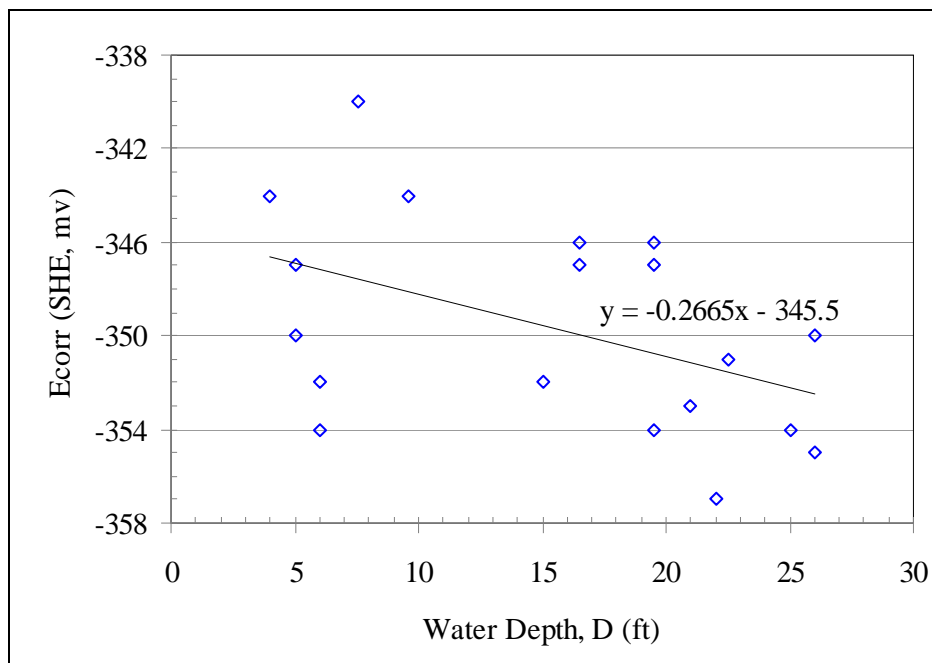
Figure 5.29. E$_{corr}$ as a function of water depth for in situ data collected in 2003 and 2004.

Sample	Location	Vessel Side	Water Depth (ft.)	Drill Depth (mm)	Distance from Hull (mm)	pH	Ecorr (mV) vs. Ag/AgCl	Ecorr (mV) vs. SHE
USAR-04-001a	Frame 88	Port	6	0	n/a	n/a	-597	-352
USAR-04-001a	Frame 88	Port	6	n/a	0	n/a	-600	-355
USAR-04-001b	Frame 88	Port	6	0	n/a	n/a	-599	-354
USAR-04-001b	Frame 88	Port	6	n/a	0	n/a	-600	-355
USAR-04-002	Frame 88	Port	19.5	0	21	n/a	-592	-347
USAR-04-002	Frame 88	Port	19.5	21	0	n/a	-596	-351
USAR-04-003	Frame 88	Port	25	0	19	n/a	-599	-354
USAR-04-003	Frame 88	Port	25	19	0	n/a	-601	-356
USAR-04-004	Frame 88	Starboard	4	0	n/a	n/a	-589	-344
USAR-04-004	Frame 88	Starboard	4	n/a	0	n/a	-593	-348
USAR-04-005	Frame 70	Port	7.6	0	18	n/a	-585	-340
USAR-04-005	Frame 70	Port	7.6	18	0	n/a	-588	-343
USAR-04-006	Frame 70	Port	19.5	8	18	n/a	-591	-346
USAR-04-006	Frame 70	Port	19.5	18	0	n/a	-591	-346
USAR-04-007	Frame 70	Port	26	0	14	n/a	-595	-350
USAR-04-007	Frame 70	Port	26	14	0	n/a	-598	-353
USAR-04-008	Frame 68	Starboard	9.6	0	24	n/a	-589	-344
USAR-04-008	Frame 68	Starboard	9.6	24	0	n/a	-591	-346
USAR-04-009	Frame 68	Starboard	16.5	0	20	n/a	-591	-346
USAR-04-009	Frame 68	Starboard	16.5	20	0	n/a	-592	-347
USAR-04-010	Frame 68	Starboard	22.5	0	13	n/a	-596	-351
USAR-04-010	Frame 68	Starboard	22.5	13	0	n/a	-598	-353
USAR-04-011	Frame 88	Starboard	16.5	0	22	n/a	-592	-347
USAR-04-011	Frame 88	Starboard	16.5	22	0	n/a	-594	-349
USAR-04-012	Frame 87	Starboard	21	0	17	n/a	-598	-353
USAR-04-012	Frame 87	Starboard	21	17	0	n/a	-601	-356

Table 5.20. *In situ* corrosion data collected November 2004 in location of each concretion sample collected during ultrasonic thickness testing. All data collected with Orion Ag/AgCl reference electrode.
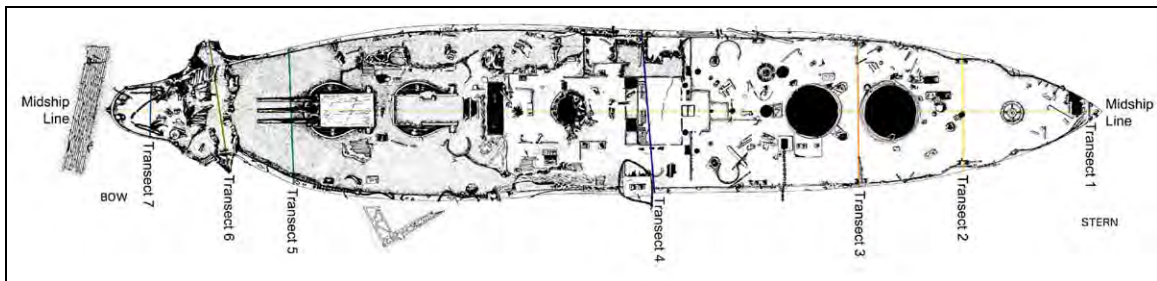
Figure 5.30. Transects for potential survey conducted in June 2001 at selected locations across *Arizona*'s hull using a GMC reference electrode.
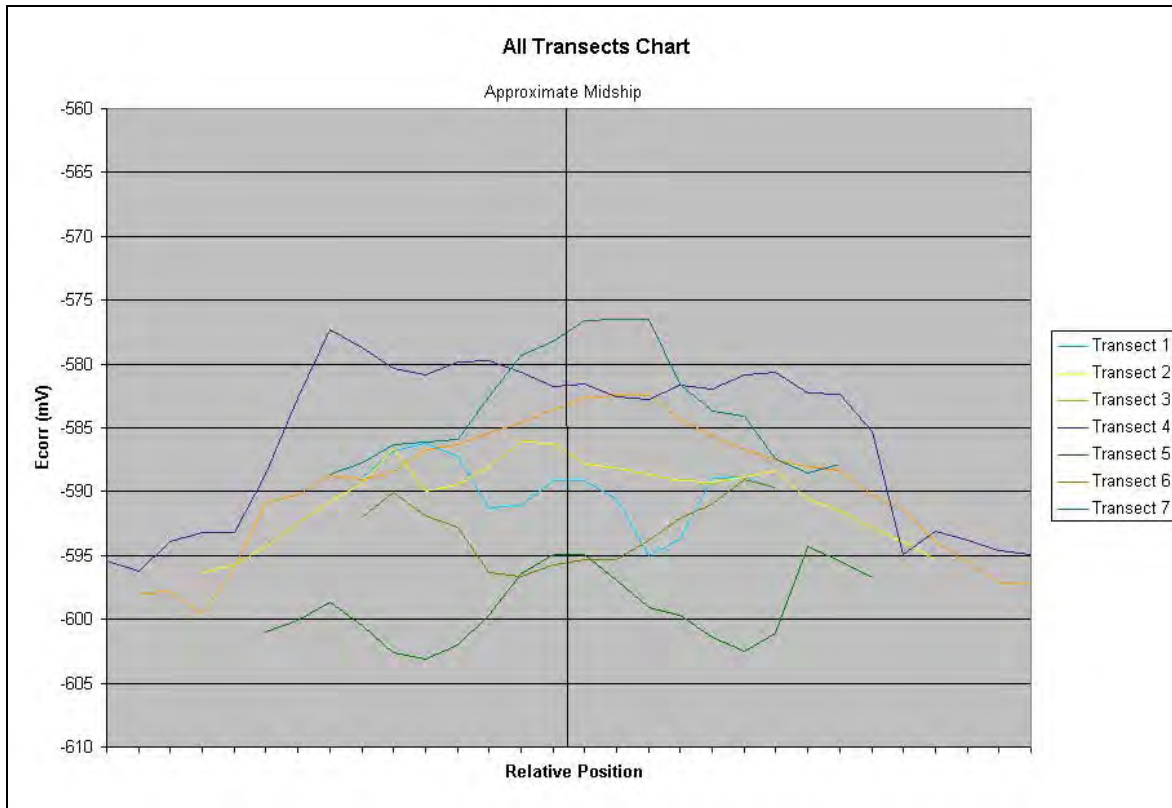
Figure 5.31. Compilation of E$_{corr}$ data from all seven transects from June 2001, plotted from harbor bottom on left, up and over Arizona's hull every 6 ft., to harbor bottom on right.

itself (Table 5.21)(Figure 5.32). Proximity to cuprous propellers may promote less negative readings at 12 ft. above the harbor bottom, port and starboard. The decrease near 24 ft. on both sides of the ship may reflect the initial drop off to the harbor bottom prior to the rise resulting from influence of the propellers. The drop in E$_{corr}$ as the transect approaches the harbor bottom is consistent with E$_{corr}$ data obtained from the ThermoOrion instrument inserted in holes drilled in concretion.

The next transect forward, transect 2, taken at approximately frame 128, shows a similar pattern in which from the gunwales to the harbor bottom E$_{corr}$ decreases on both sides but holds fairly steady across the main deck (Table 5.22)(Figure 5.33). The decrease to the harbor bottom is again attributed to the reduction in oxygen availability.

Transect 3, approximately frame 114, cuts across the main deck just forward of barbette no. 3, which extends about 6 ft. above the water surface and has accelerated water line corrosion vertically on its side. Because of this, E$_{corr}$ amidships on this transect is higher as compared to transects 2, 5, 7, and 6 (Table 5.23)(Figure 5.34).

Location	E_{corr} (mV) vs. Ag/AgCl (GMC Probe)	E_{corr} (mV) vs. Ag/AgCl (Orion Equiv.)	E_{corr} (mV) vs. SHE
Port mudline	-588.8	-543.8	-343.8
6 ft. above bottom	-586.8	-541.8	-341.8
12 ft. above bottom	-586.2	-541.2	-341.2
18 ft. above bottom	-587.2	-542.2	-342.2
24 ft. above bottom	-591.3	-546.3	-346.3
30 ft. above bottom	-591.1	-546.1	-346.1
Port gunwale	-589.2	-544.2	-344.2
6 ft. from port gunwale	-589.1	-544.1	-344.1
Starboard gunwale	-590.6	-545.6	-345.6
24 ft. above bottom	-595	-550	-350
18 ft. above bottom	-593.7	-548.7	-348.7
12 ft. above bottom	-588.9	-543.9	-343.9
6 ft. above bottom	-588.8	-543.8	-343.8
Starboard mudline	-589.8	-543.8	-343.8

Table 5.21. June 2001 *in situ* corrosion data, transect 1 (frame 148).
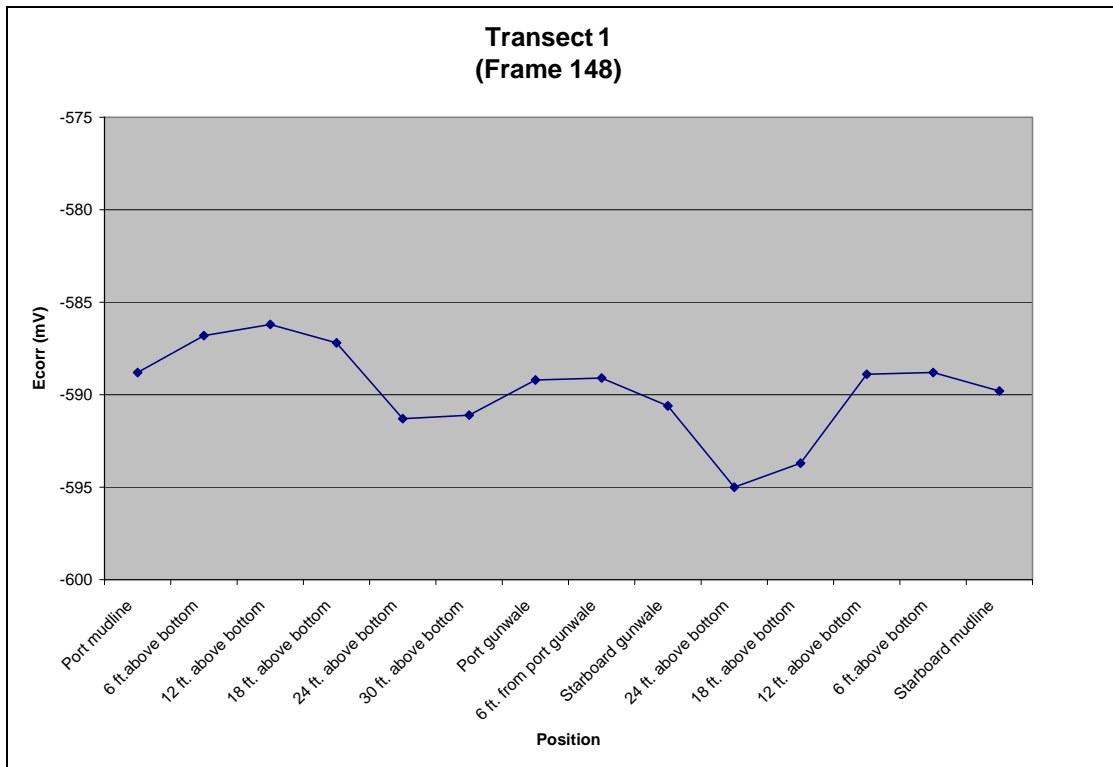
Figure 5.32. Graph of GMC data E_{corr} taken from Table 5.21, relative to hull position.

179

Location	E_{corr} (mV) vs. Ag/AgCl (GMC Probe)	E_{corr} (mV) vs. Ag/AgCl (Orion Equiv.)	E_{corr} (mV) vs. SHE
Port Mudline	-596.3	-551.3	-351.3
6 ft. above bottom	-595.7	-550.7	-350.7
12 ft. above bottom	-594.3	-549.3	-349.3
Torpedo blister	-592.5	-547.5	-347.5
6 ft. above torpedo blister	-590.8	-545.8	-345.8
Port gunwale	-589.4	-544.4	-344.4
6 ft. from port gunwale	-586.6	-541.6	-341.6
12 ft. from port gunwale	-590	-545	-345
18 ft. from port gunwale	-589.5	-544.5	-344.5
24 ft. from port gunwale	-588	-543	-343
30 ft. from port gunwale, by hatch	-586.1	-541.1	-341.1
36 ft. from port gunwale	-586.2	-541.2	-341.2
42 ft. from port gunwale	-587.8	-542.8	-342.8
48 ft. from port gunwale	-588.1	-543.1	-343.1
54 ft. from port gunwale	-588.6	-543.6	-343.6
60 ft. from port gunwale	-589.2	-544.2	-344.2
66 ft. from port gunwale, at starboard bitt	-589.3	-544.3	-344.3
72 ft. from port gunwale	-588.8	-543.8	-343.8
Starboard gunwale	-588.3	-543.3	-343.3
6 ft. above torpedo blister	-590.6	-545.6	-345.6
Torpedo blister	-591.5	-546.5	-346.5
12 ft. above bottom	-592.9	-547.9	-347.9
6 ft. above bottom	-593.9	-548.9	-348.9
Starboard mudline	-595.3	-550.3	-350.3

Table 5.22. June 2001 *in situ* corrosion data, transect 2 (frame 128).
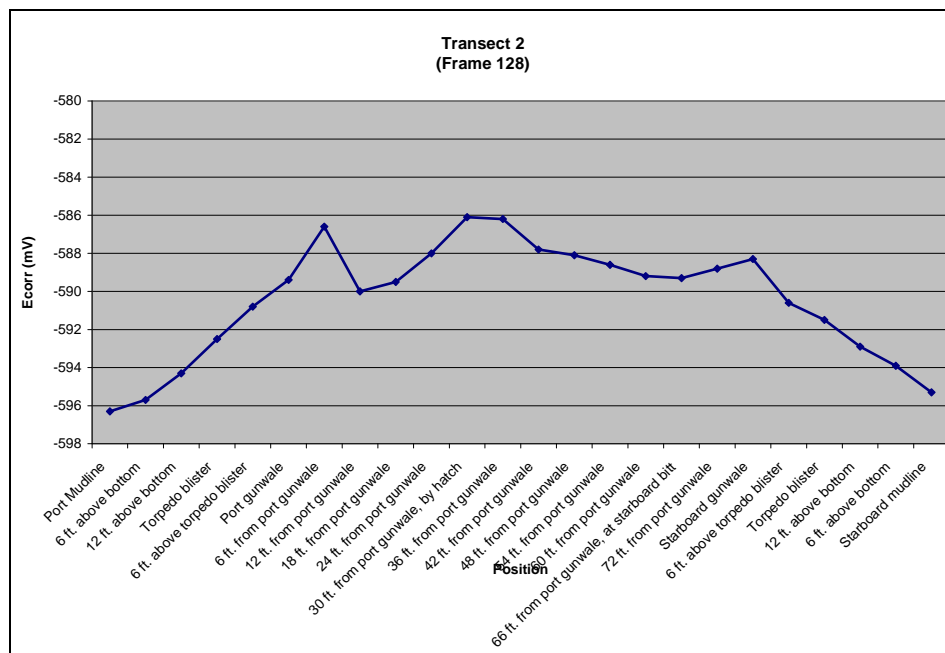
Figure 5.33. Graph of GMC data E_{corr} taken from Table 5.22, relative to hull position.

Location	E_{corr} (mV) vs. Ag/AgCl (GMC Probe)	E_{corr} (mV) vs. Ag/AgCl (Orion Equiv.)	E_{corr} (mV) vs. SHE
Port mudline	-598	-553	-353
6 ft. above bottom	-597.9	-552.9	-352.9
12 ft. above bottom	-599.6	-554.6	-354.6
Torpedo blister	-595.9	-550.9	-350.9
6 ft. above torpedo blister	-590.9	-545.9	-345.9
Port gunwale	-590.3	-545.3	-345.3
6 ft. from port gunwale	-588.7	-543.7	-343.7
12 ft. from port gunwale	-589	-544	-344
18 ft. from port gunwale	-588.4	-543.4	-343.4
24 ft. from port gunwale	-586.7	-541.7	-341.7
30 ft. from port gunwale	-586.3	-541.3	-341.3
36 ft. from port gunwale	-585.4	-540.4	-340.4
42 ft. from port gunwale	-584.6	-539.6	-339.6
48 ft. from port gunwale	-583.6	-538.6	-338.6
54 ft. from port gunwale	-582.7	-537.7	-337.7
60 ft. from port gunwale	-582.5	-537.5	-337.5
66 ft. from port gunwale	-582.5	-537.5	-337.5
72 ft. from port gunwale	-584.3	-539.3	-339.3
78 ft. from port gunwale	-585.6	-540.6	-340.6
84 ft. from port gunwale	-586.7	-541.7	-341.7
90 ft. from port gunwale	-587.5	-542.5	-342.5
96 ft. from port gunwale	-588	-543	-343
Starboard bitts	-588.3	-543.3	-343.3
Staboard gunwale	-590.3	-545.3	-345.3
6 ft. above torpedo blister	-591.4	-546.4	-346.4
Torpedo blister	-593.9	-548.9	-348.9
12 ft. above bottom	-595.5	-550.5	-350.5
6 ft. above bottom	-597.1	-552.1	-352.1
Starboard mudline	-597.2	-552.2	-352.2

Table 5.23. June 2001 *in situ* corrosion data, transect 3 (frame 114).
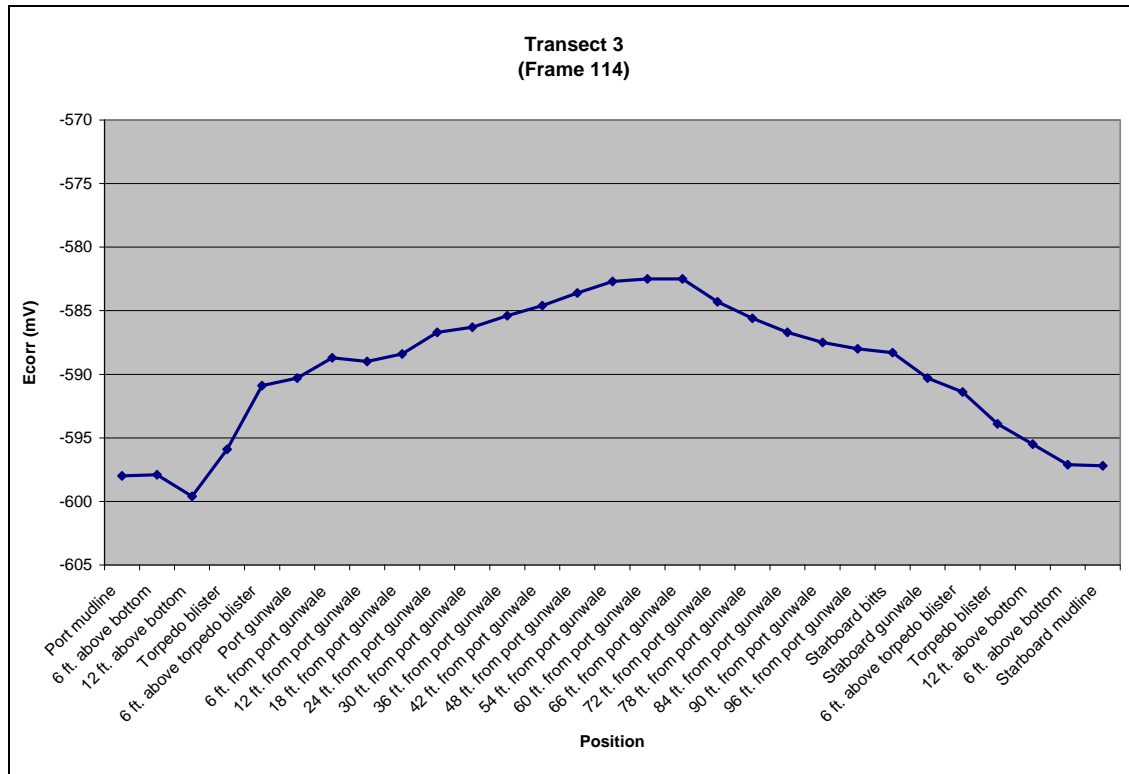
Figure 5.34. Graph of GMC data E$_{corr}$ taken from Table 5.23, relative to hull position.

Transect 4 crosses the upper deck in the crew galley area in shallow water forward of the Memorial, at approximately frame 82. E$_{corr}$ is -583 mV or higher over nearly the entire deck area—recent structural corrosion is consistent with higher E$_{corr}$ in this area (Table 5.24)(Figure 5.35).

Moving forward along the hull, transect 5, at approximately frame 28, has the lowest overall E$_{corr}$ values, which may be due to the fact that the deck is buried by several feet of sediment along the entire transect (Table 5.25)(Figure 5.36). The close proximity and exposure of the gun barrels of turret no. 1 above the harbor bottom may reflect a rise in E$_{corr}$ near the centerline of the hull. A drop in E$_{corr}$ from the torpedo blisters on either side to the harbor bottom is typical. Because the deck is collapsed in this area, the top of the torpedo blister and the gunwale are at about the same elevation.

As is the case for transect 5, transect 6 is in an area of maximum damage from the 1941 explosion that sank *Arizona*, at approximate frames 16–19. Blown out deck plates at what used to be the gunwales are exposed to increased sea water exchange and maximum oxygen

Location	E$_{corr}$ (mV) vs. Ag/AgCl (GMC Probe)	E$_{corr}$ (mV) vs. Ag/AgCl (Orion Equiv.)	E$_{corr}$ (mV) vs. SHE
Port mudline	-595.4	-550.4	-350.4
6 ft. above bottom	-596.2	-551.2	-351.2
Torpedo blister	-593.9	-548.9	-348.9
6 ft. above torpedo blister	-593.2	-548.2	-348.2
12 ft. above torpedo blister	-593.2	-548.2	-348.2
Port gunwale	-588.6	-543.6	-343.6
6 ft. from port gunwale	-582.7	-537.7	-337.7
12 ft. from port gunwale	-577.3	-532.3	-332.3
18 ft. from port gunwale	-578.7	-533.7	-333.7
24 ft. from port gunwale	-580.3	-535.3	-335.3
30 ft. from port gunwale	-580.8	-535.8	-335.8
36 ft. from port gunwale	-579.8	-534.8	-334.8
42 ft. from port gunwale	-579.7	-534.7	-334.7
48 ft. from port gunwale	-580.6	-535.6	-335.6
54 ft. from port gunwale	-581.8	-536.8	-336.8
60 ft. from port gunwale	-581.6	-536.6	-336.6
66 ft. from port gunwale	-582.6	-537.6	-337.6
72 ft. from port gunwale	-582.8	-537.8	-337.8
78 ft. from port gunwale	-581.7	-536.7	-336.7
84 ft. from port gunwale	-582	-537	-337
90 ft. from port gunwale	-580.9	-535.9	-335.9
96 ft. from port gunwale	-580.6	-535.6	-535.6
102 ft. from port gunwale	-582.3	-537.3	-337.3
Starboard bitts	-582.4	-537.4	-337.4
Starboard gunwale	-585.3	-540.3	-340.3
12 ft. above torpedo blister	-594.9	-549.9	-349.9
6 ft. above torpedo blister	-593.1	-548.1	-348.1
Torpedo blister	-593.8	-548.8	-348.8
6 ft. above bottom	-594.6	-549.6	-349.6
Starboard mudline	-594.9	-549.9	-349.9

Table 5.24. June 2001 *in situ* corrosion data, transect 4 (frame 82).
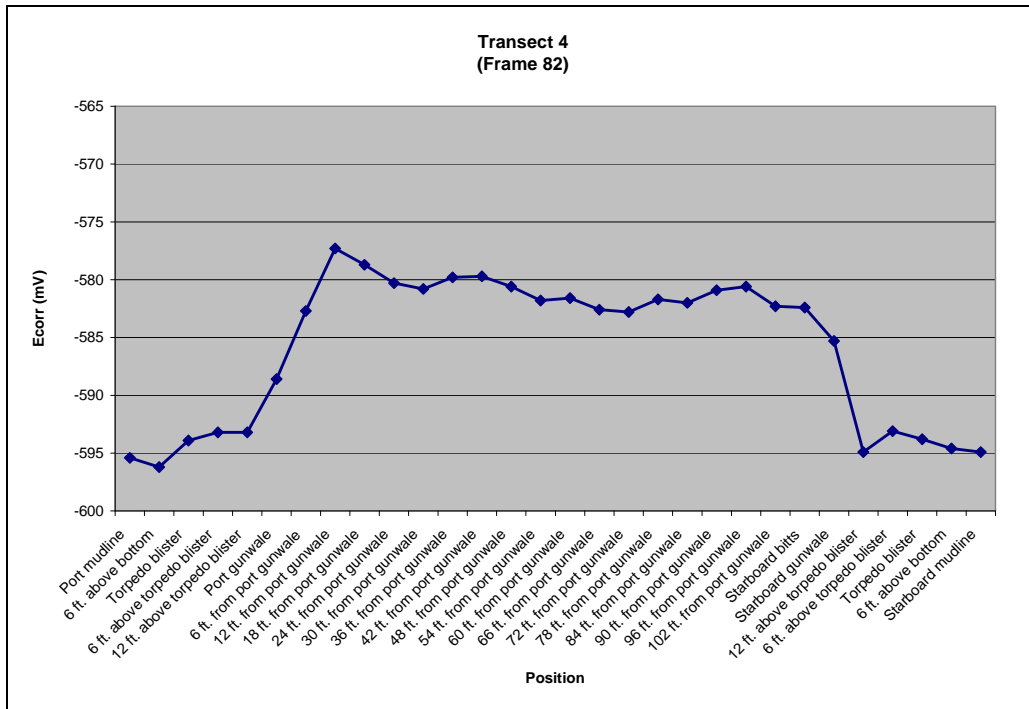
Figure 5.35. Graph of GMC data E_corr taken from Table 5.24, relative to hull position.

Location	E_corr (mV) vs. Ag/AgCl (GMC Probe)	E_corr (mV) vs. Ag/AgCl (Orion Equiv.)	E_corr (mV) vs. SHE
Port mudline	-601	-556	-356
6 ft. above bottom	-600.1	-555.1	-355.1
Torpedo blister	-598.7	-553.7	-353.7
6 ft. from port gunwale	-600.5	-555.5	-355.5
12 ft. from port gunwale	-602.6	-557.6	-357.6
18 ft. from port gunwale	-603.1	-558.1	-358.1
24 ft. from port gunwale	-602	-557	-357
30 ft. from port gunwale	-599.7	-554.7	-354.7
36 ft. from port gunwale	-596.4	-551.4	-351.4
42 ft. from port gunwale	-594.9	-549.9	-349.9
48 ft. from port gunwale	-594.9	-549.9	-349.9
54 ft. from port gunwale	-596.9	-551.9	-351.9
60 ft. from port gunwale	-599.1	-554.1	-354.1
66 ft. from port gunwale	-599.7	-554.7	-354.7
72 ft. from port gunwale	-601.4	-556.4	-356.4
78 ft. from port gunwale	-602.5	-557.5	-357.5
84 ft. from port gunwale	-601.1	-556.1	-356.1
Torpedo blister	-594.3	-549.3	-349.3
6 ft. above bottom	-595.4	-550.4	-350.4
Starboard mudline	-596.7	-551.7	-351.7

Table 5.25. June 2001 *in situ* corrosion data, transect 5 (frame 28).
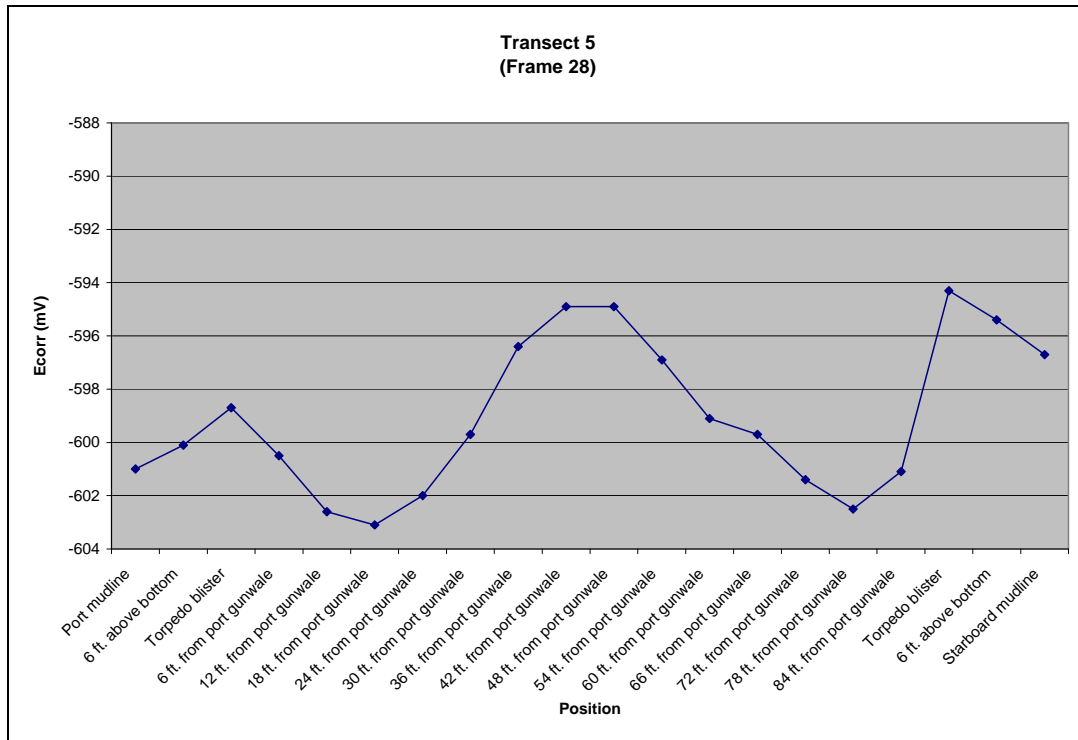
Figure 5.36. Graph of GMC data E$_{corr}$ taken from Table 5.25, relative to hull position.

availability. Because the plates flare out so much in this area, transects could not be taken to the harbor bottom. The lowest E$_{corr}$ appear near the centerline where silt has accumulated (Table 5.26)(Figure 5.37).

The final transect, transect 7, is near the bow, approximately frame 9, forward of the area of maximum damage, where the intact upper deck is in shallow water. As expected, E$_{corr}$ values are relatively high along the exposed upper deck, near -575 mV, and drop to near -590 mV at the harbor bottom (Table 5.27)(Figure 5.38). E$_{corr}$ transects with the GMC probe confirm the overall pattern produced by the sequential drilling and data collection through the concretion, that is that E$_{corr}$ decreases with increased water depth. E$_{corr}$ profiles generally tend to drop to lower potentials from stern (Frame 148) to bow (Frame 9) with maximum E$_{corr}$ near -330 mV (SHE) or -575 mV (Ag/AgCl, GMC) to a minimum approaching -360 mV (SHE) or -605 mV (Ag/AgCl, GMC)(Figure 5.31).

Location	E$_{corr}$ (mV) vs. Ag/AgCl (GMC Probe)	E$_{corr}$ (mV) vs. Ag/AgCl (Orion Equiv.)	E$_{corr}$ (mV) vs. SHE
Port edge	-592	-547	-347
6 ft. from port edge	-590.1	-545.1	-345.1
12 ft. from port edge	-591.9	-546.9	-346.9
18 ft. from port edge	-592.8	-547.8	-347.8
24 ft. from port edge	-596.3	-551.3	-351.3
30 ft. from port edge	-596.6	-551.6	-351.6
36 ft. from port edge	-595.7	-550.7	-350.7
42 ft. from port edge	-595.3	-550.3	-350.3
48 ft. from port edge	-595.3	-550.3	-350.3
54 ft. from port edge	-593.8	-548.8	-348.8
60 ft. from port edge	-592.1	-547.1	-347.1
66 ft. from port edge	-591	-546	-346
72 ft. from port edge	-589	-544	-344
Starboard edge	-589.7	-544.7	-344.7

Table 5.26. June 2001 *in situ* corrosion data, transect 6 (frames 16-19).
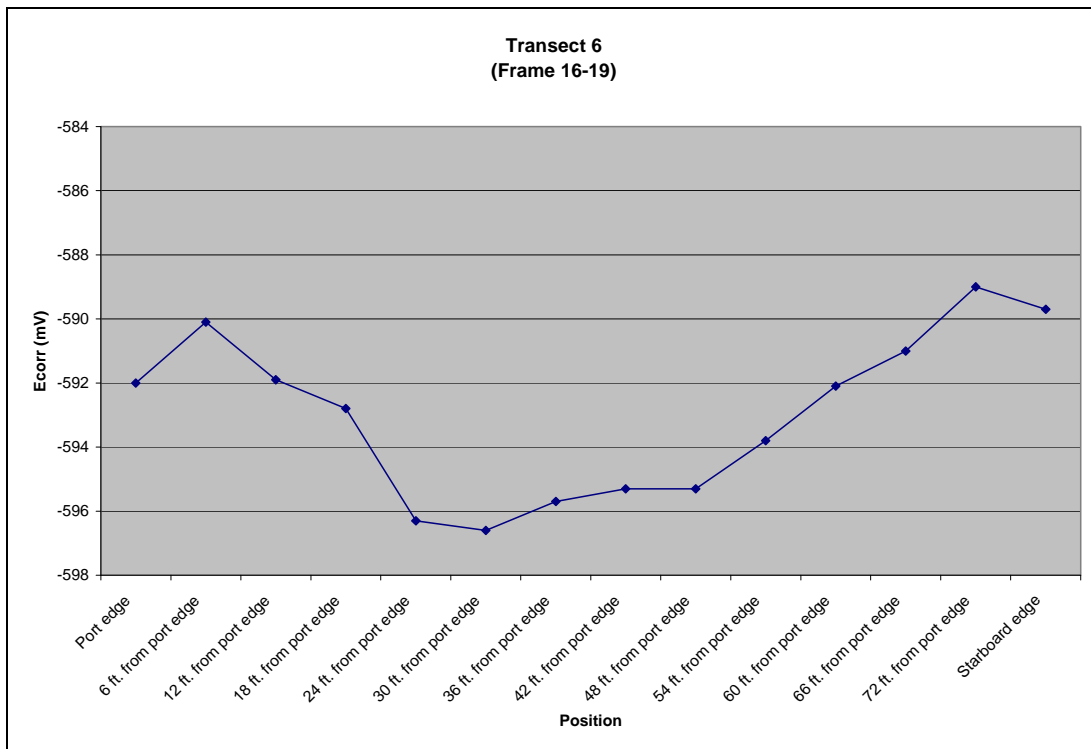
Figure 5.37. Graph of GMC data E$_{corr}$ taken from Table 5.26, relative to hull position.

Location	E_corr (mV) vs. Ag/AgCl (GMC Probe)	E_corr (mV) vs. Ag/AgCl (Orion Equiv.)	E_corr (mV) vs. SHE
Port mudline	-588.6	-543.6	-343.6
6 ft. above mudline	-587.7	-542.7	-342.7
12 ft. above mudline	-586.3	-541.3	-341.3
18 ft. above mudline	-586.1	-541.1	-341.1
24 ft. above mudline	-585.9	-540.9	-340.9
Port gunwale	-582.6	-537.6	-337.6
6 ft. from port gunwale	-579.3	-534.3	-334.3
12 ft. from port gunwale	-578.2	-533.2	-333.2
18 ft. from port gunwale	-576.6	-531.6	-331.6
24 ft. from port gunwale	-576.5	-531.5	-331.5
30 ft. from port gunwale	-576.5	-531.5	-331.5
Starboard gunwale	-581.6	-536.6	-336.6
24 ft. above mudline	-583.7	-538.7	-338.7
18 ft. above mudline	-584.1	-539.1	-339.1
12 ft. above mudline	-587.4	-542.4	-342.4
6 ft. above mudline	-588.5	-543.5	-343.5
Starboard mudline	-587.8	-542.8	-342.8

Table 5.27. June 2001 *in situ* corrosion data, transect 7 (frame 9).
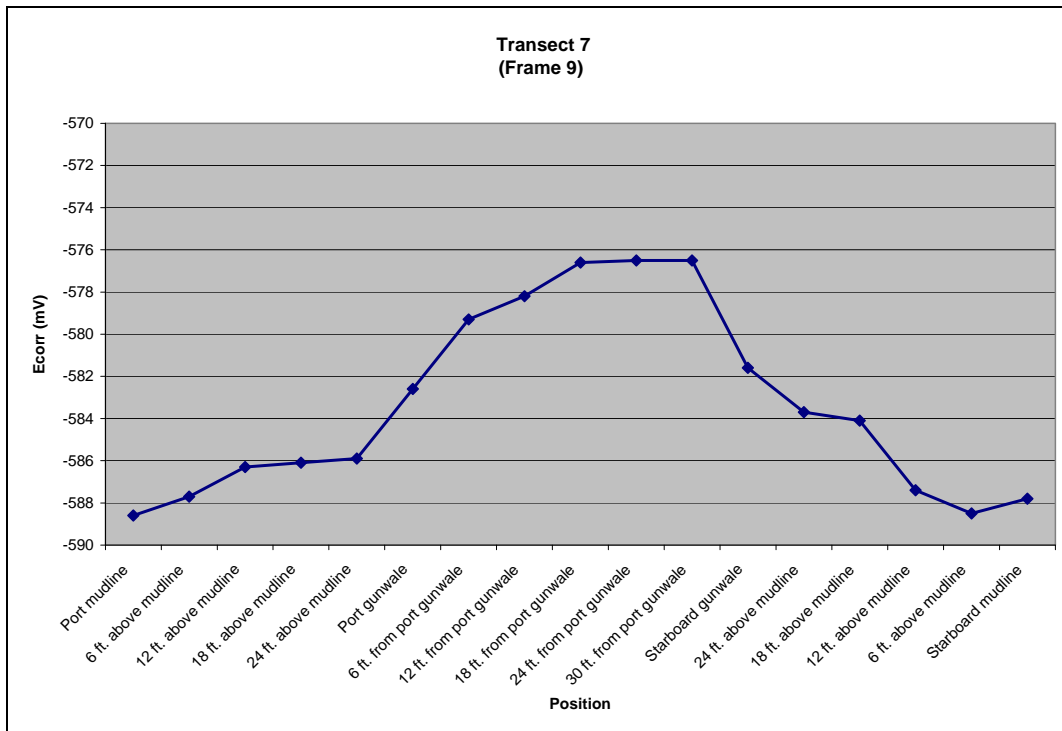
Figure 5.38. Graph of GMC data E_corr taken from Table 5.27, relative to hull position.

Interior E$_{corr}$ Measurements

Interior potential measurements were obtained by mounting a GMC reference electrode on a VideoRay ROV. The ROV was operated from the surface with a Wavetech HD-160 meter displaying E$_{corr}$ values alongside the operator. Because there was no direct access to the vessel's interior, E$_{corr}$ measurements were only taken on the exterior of concretion covering interior bulkheads. Interior spaces were entered through open portholes on *Arizona*'s second deck, as well as through open hatches on the main deck aft of the Memorial. E$_{corr}$ measurements were also taken on the inside of barbette no. 3. Methodology included taking baseline measurements outside the hull before entering the interior spaces. A running log of E$_{corr}$ values was recorded along with time displayed on the miniDV video deck, which recorded the video feed from the ROV, and a description of location and features within the interior cabin. In general, measurements were taken a various levels within the cabin interior, from floor to ceiling (silt-line to overhead).

On entry through open port holes, E$_{corr}$ increased from 8 to 18 mV, an average 13 mV; that is interior values are 8–18 mV more positive than baseline readings outside each cabin (Figures 5.39–5.47). This could indicate a slightly higher corrosion rate; however there are many variables at work. Translated to the Fe/H$_2$O Pourbaix diagram (Figure 5.2) this difference suggests that the corrosion potential is higher depending upon the pH in the compartments and the thickness of the concretion on interior surfaces. Knowledge of temperature, salinity, pH and oxygen concentration in interior compartments is important for contextualizing these results. Descent into hatches starboard of barbette no. 3 and barbette no. 4 to the third deck showed a similar increase in E$_{corr}$, though not as great (Figures 5.48 and 5.49).

The reason for the rise in E$_{corr}$ inside interior compartments is not fully understood. Perhaps the concretion, or what there is of it, is thin enough to change the balance between available oxygen and oxygen diffusion resistance in favor of higher effective oxygen availability at the interior surface. On the other hand, increased carbon or sulfur availability from overhead fuel oil may be the cause for the higher E$_{corr}$ readings. These and other possible explanations for the rise in E$_{corr}$ in interior compartments come from further examination of the carbon-water Pourbaix diagram (Figure 5.4). At a pH of 7 or lower, elemental carbon from oil trapped in the overheads is at equilibrium with water at slightly higher potentials. For example, carbon
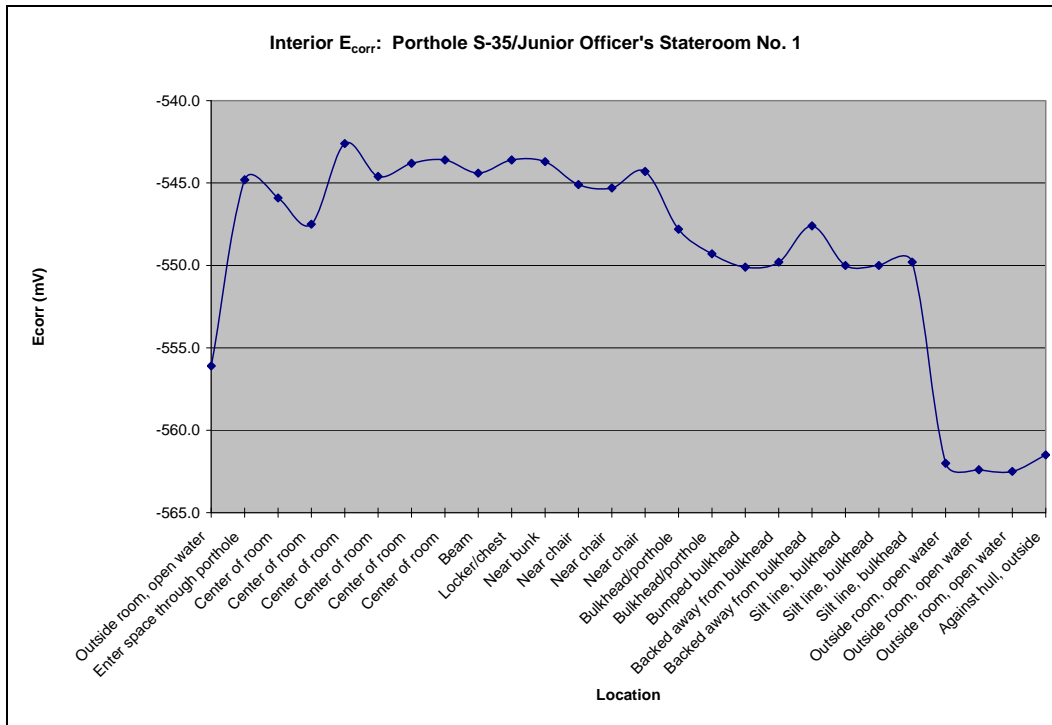
Figure 5.39. Graph of interior E_{corr} relative to location within Porthole S-35/Junior Officer's Stateroom No.1
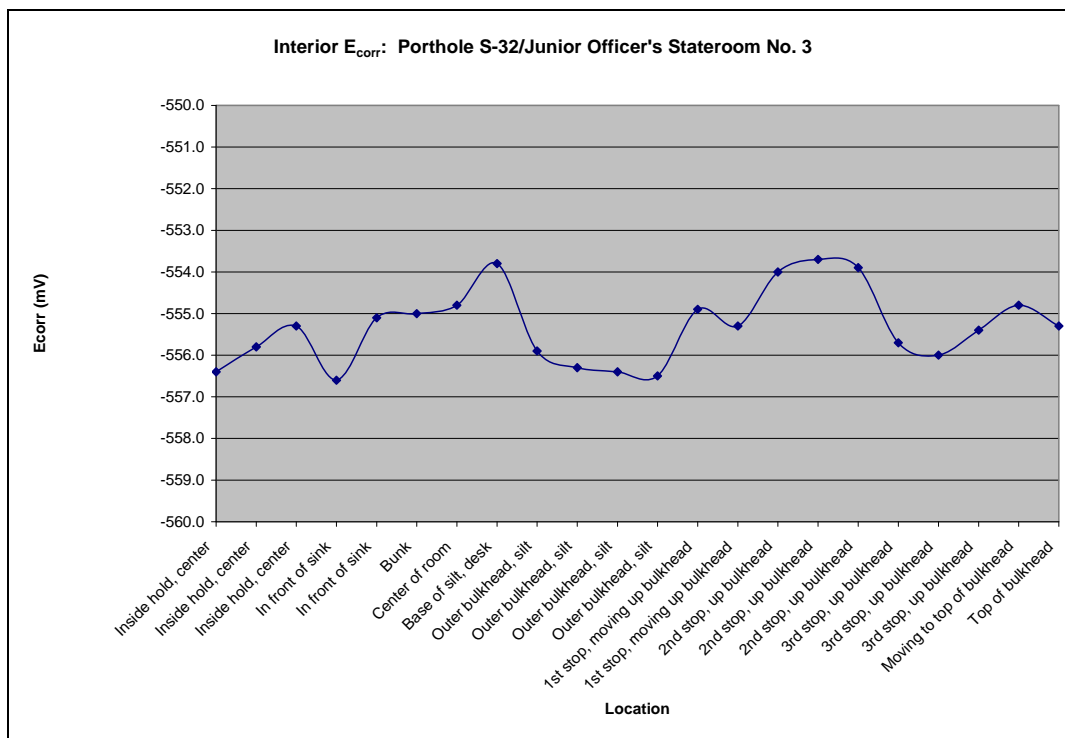
Figure 5.40. Graph of interior E_{corr} relative to location within Porthole S-32/Junior Officer's Stateroom No.3
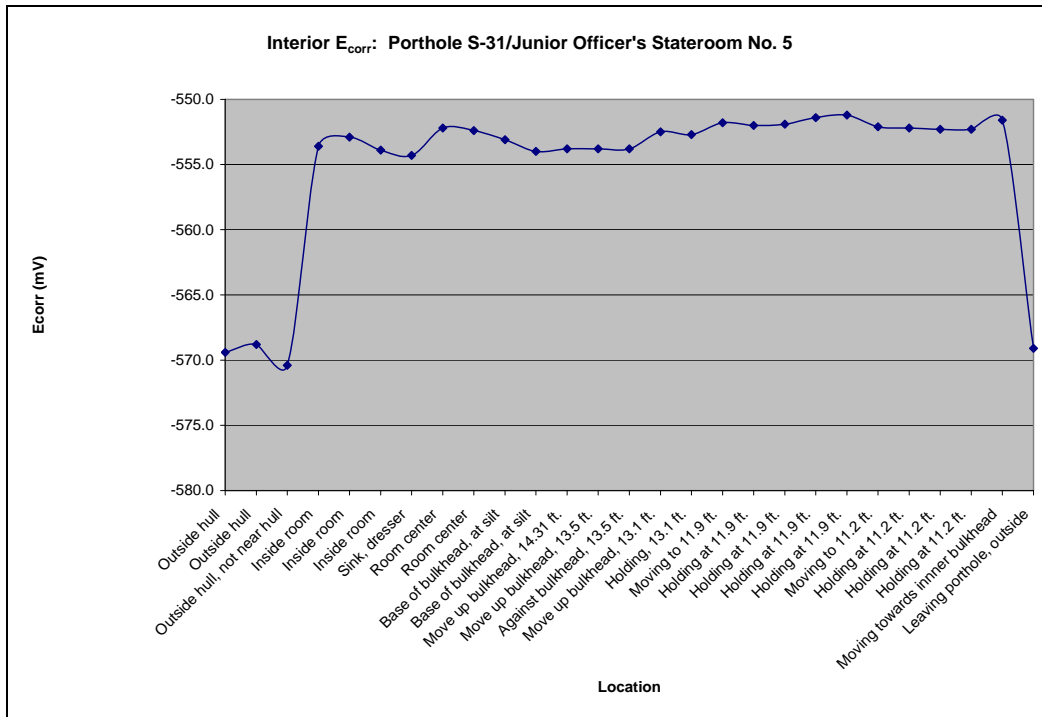
Figure 5.41. Graph of interior E_{corr} relative to location within Porthole S-31/Junior Officer's Stateroom No.5
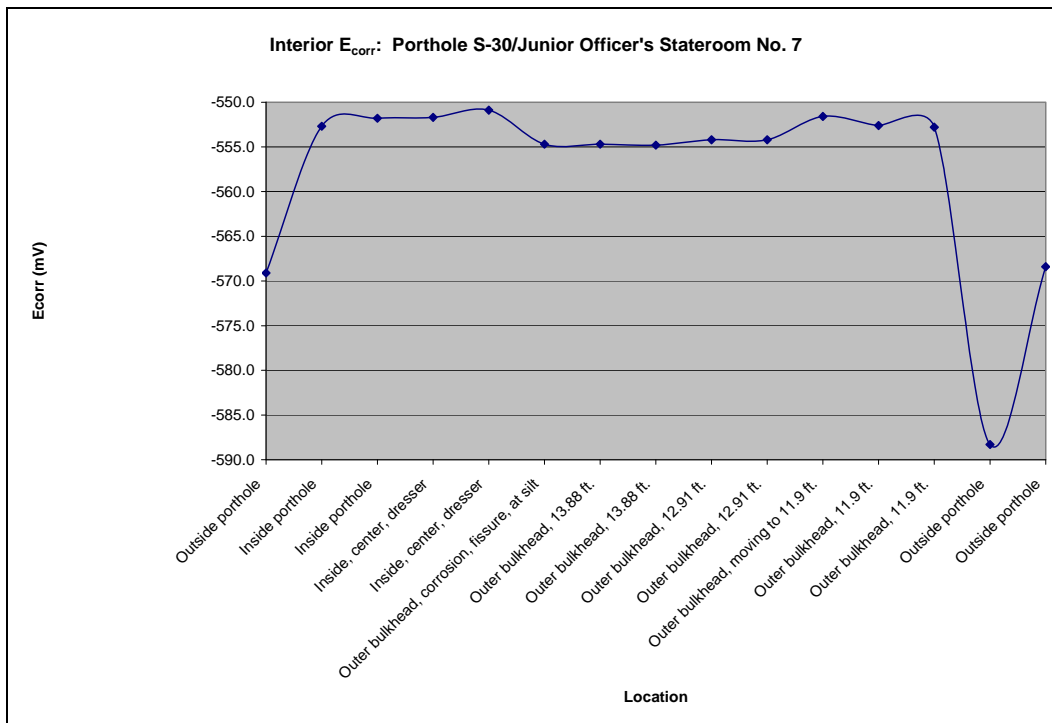
Figure 5.42. Graph of interior E_{corr} relative to location within Porthole S-30/Junior Officer's Stateroom No.7
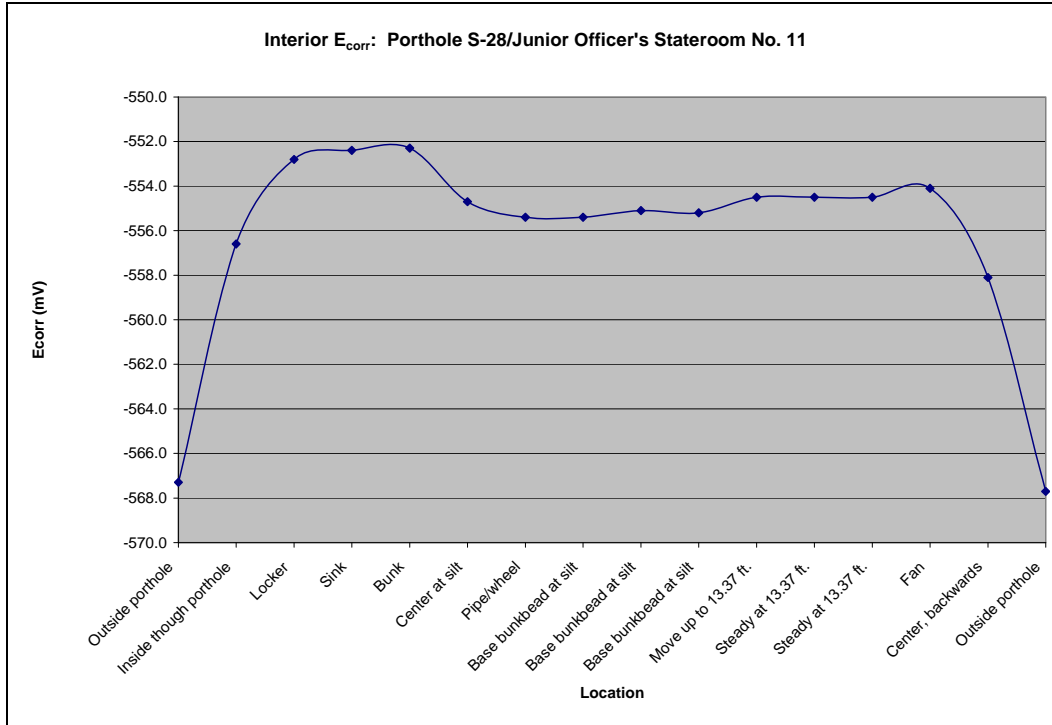
Figure 5.43.Graph of interior E_{corr} relative to location within Porthole S-28/Junior Officer's Stateroom No.11
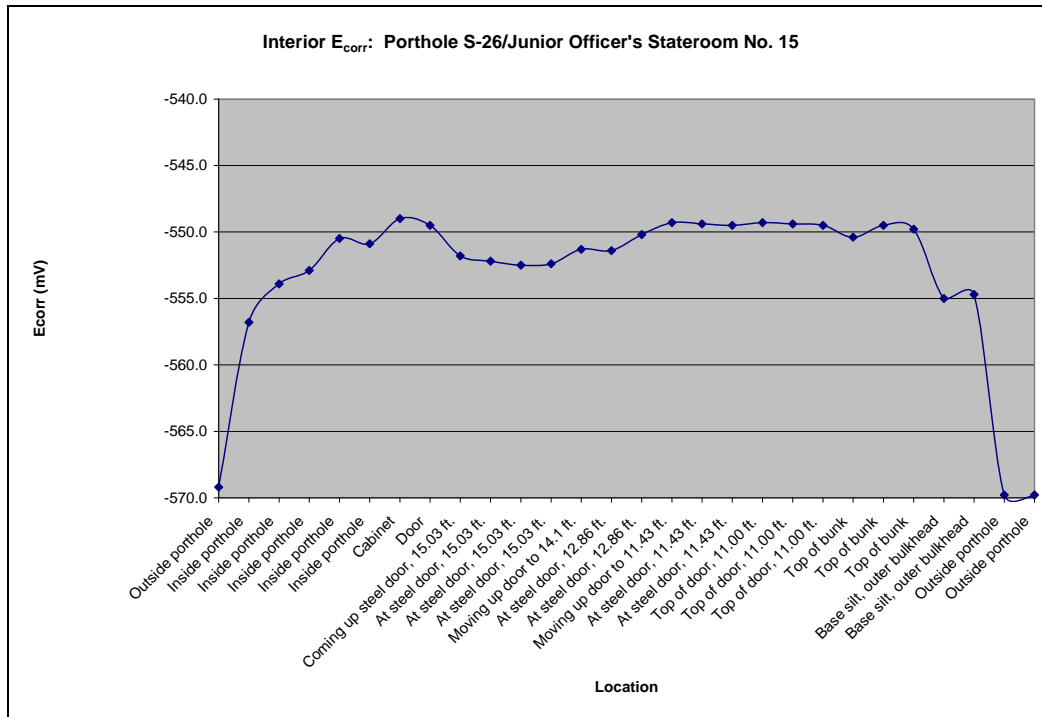
Figure 5.44.Graph of interior E_{corr} relative to location within Porthole S-26/Junior Officer's Stateroom No.15
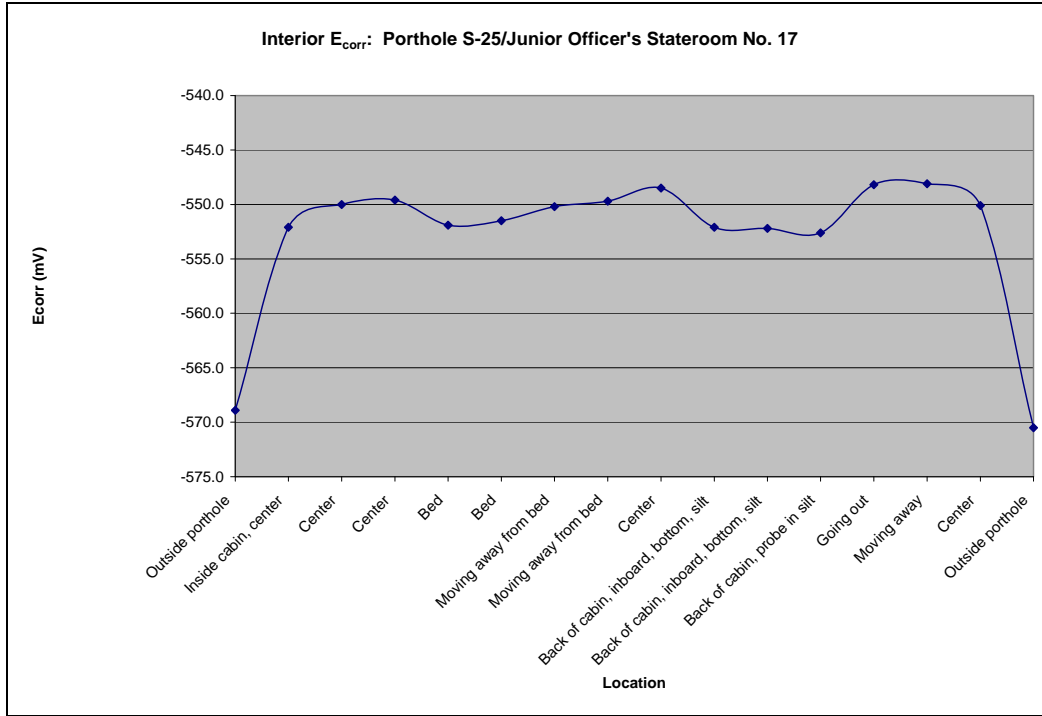
Figure 5.45.Graph of interior E_{corr} relative to location within Porthole S-25/Junior Officer's Stateroom No.17
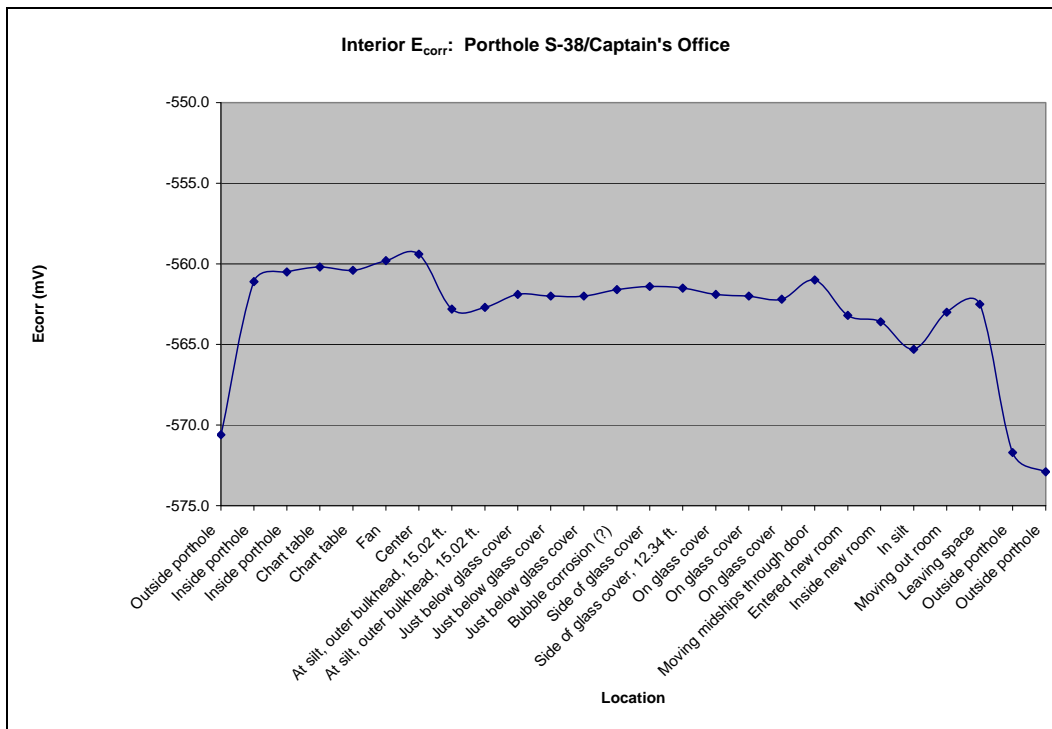
Figure 5.46. Graph of interior E_{corr} relative to location within Porthole S-38/Captain's Office
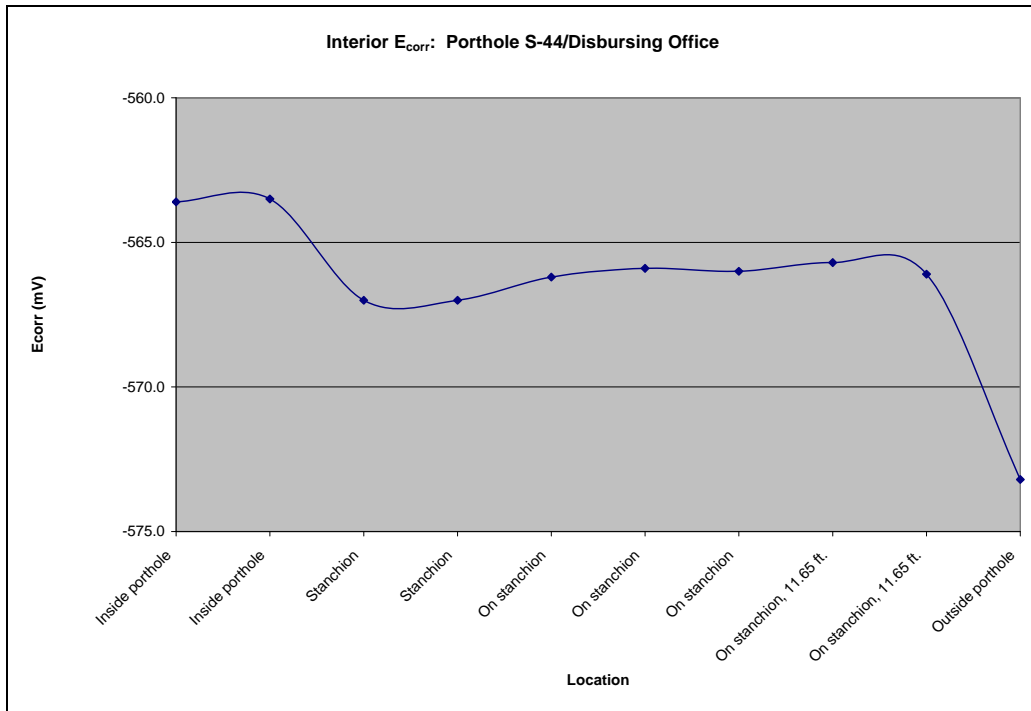
Figure 5.47. Graph of interior E_{corr} relative to location within Porthole S-44/Disbursing Office
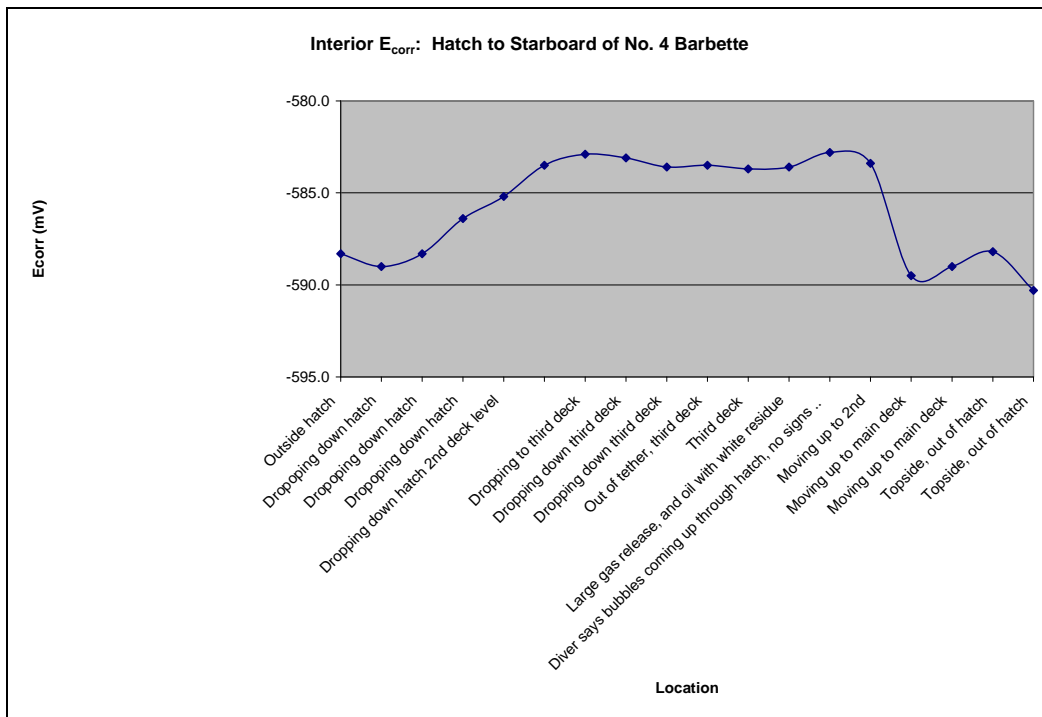
Figure 5.48. Graph of interior E_{corr} relative to location from Hatch to Starboard of No. 4 Barbette
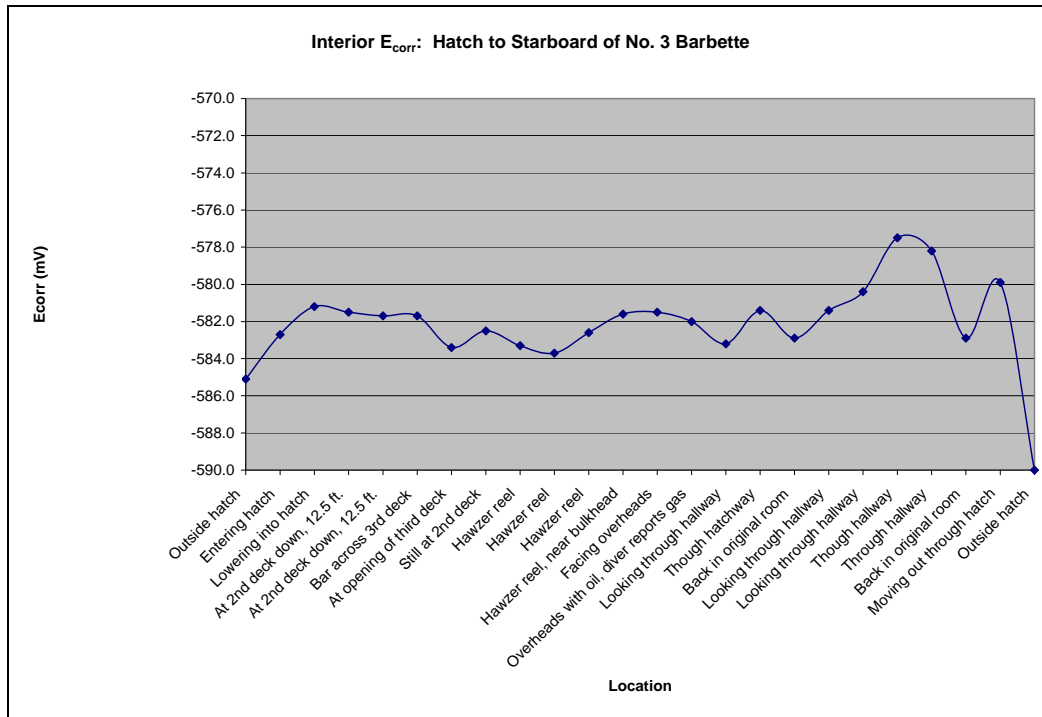
Figure 5.49. Graph of interior E_{corr} relative to location from Hatch to Starboard of No. 3 Barbette

promotes change in water chemistry with E_{corr} at a mixed potential involving more than just freely corroding iron. The carbon-water Pourbaix diagram (Figure 5.4) shows three regions that are of interest as related to interior E_{corr}. Elemental carbon is in equilibrium with water in a narrow diagonal band marked "C". Below the band are four diagonal lines that correspond to increasing partial pressures of methane ($p(CH_4)$ from 10^{-6} to 1 atm as the potential decreases), and above the diagonal band are four lines that correspond to increasing partial pressures of carbon dioxide ($p(CO_2)$ from 10^{-6} to 1 atm as the potential increases). Below the lower diagonal band, the entire region is stable methane or methane dissolved in water as methanol. Above the diagonal band, the entire region is stable carbon dioxide or carbon dioxide dissolved in water as carbonates. Extending a vertical line upward at pH 7, the line intersects the $p(CO_2) = 10^{-6}$ line at a potential of approximately -310 mV. Interior E_{corr} data averages about the same, hence it is feasible that an increase in potential of 8–18 mV is caused by a change in water chemistry in interior spaces as the partial pressure of carbon dioxide increases. In this connection, search for and application of the sulfur-water Pourbaix diagram may cast further light on the cause for the increase in potential. Chemical analysis of interior water samples is recommended to determine

whether or not this environment is more corrosive than exterior seawater and confirm the presence of carbonates and/or methanol predicted in the Pourbaix diagram (Figure 5.4). At greater depths and pressures in interior spaces, it may be possible that E_{corr} is lower, suggesting the presence of methane dissolved as methanol. The report of solid methane as hydrate at great ocean depths draws some interesting parallels. Chemical analysis of interior water would help clarify this issue. Another factor causing a potential increase in interior compartments is the existence of thermoclines (see Chapter 4 and above) and associated variation in oxygen content across them. Temperature or oxygen cells may also be operative.

The trend showing increasing (more positive) E_{corr} in interior compartments was not observed inside barbette no. 3 (Figure 5.50). A descent from the surface to 31 ft. below the surface to the bottom of the barbette (roughly equivalent to the harbor bottom outside the ship) showed a decrease in E_{corr}, similar to the trend for E_{corr} on the external hull. The E_{corr} values inside the barbette are consistent with readings on the external hull in that E_{corr} values decrease with depth. Both observations are consistent with a reduced tendency to corrode. In both cases, the water column is directly open to the atmosphere and gases such as carbon dioxide and methane would dissociate from water and outgas to the atmosphere. In interior compartments, with egress only at open port holes, outgassing is limited.

E_{corr} and pH Measurements Summary

Data clearly confirm the crevice effect at the hull's steel surface created by concretion coverage where the pH is the lowest, and gradually increases through the concretion to the concretion's exterior surface. In addition, results indicate that E_{corr} at both the steel surface and the concretion's exterior surface decrease with water depth.

Superposition of experimental steel surface E_{corr}/pH data on the iron-water Pourbaix diagram indicates active corrosion with hydrogen evolution or oxygen reduction depending on the pH. Hydrolysis causes a continuously lowering of pH in the concretion from exterior concretion surface to the steel surface. The carbon-water Poubaix diagram suggests that carbon presence from oil trapped in overheads may promote higher E_{corr} inside interior compartments. Depending on interior position, water depth, and proximity to fuel oil, either CH_4 as methanol or
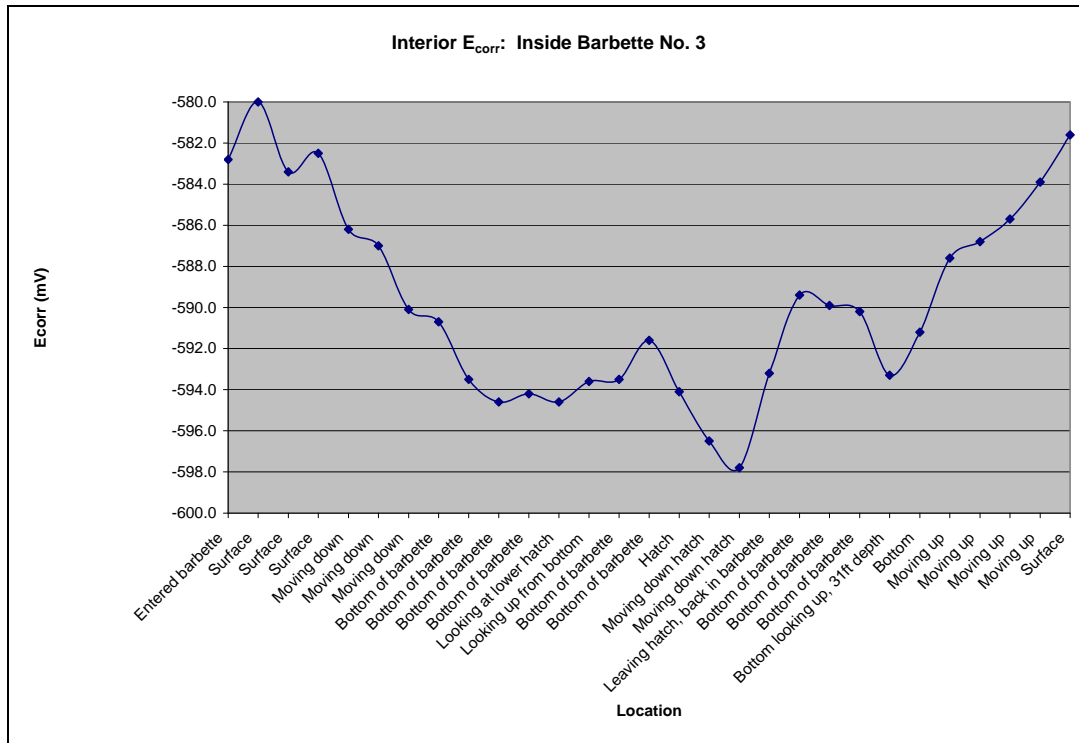
Figure 5.50. Graph of interior E_{corr} relative to location inside Barbette No. 3

CO_2 as carbonate dissolved in interior water cause a change in seawater chemistry and a resulting increase in E_{corr}.

Concretion Analysis

Fundamental research into the composition and characteristics of the concretion covering *Arizona*'s outer hull is being conducted to aid in understanding the kinetics and mechanisms of the corrosion process on the ship and to determine how concretion chemistry correlates with hull metal loss. The hard layer of concretion that forms on iron and steel objects in seawater is a combination of iron corrosion products and marine organisms, beginning with pioneering coralline algae that leave layers of calcium carbonate when they die. The calcium carbonate residue is overlaid by subsequent layers of coralline algae, and the increasing calcium carbonate layers forms a suitable substrate for secondary growth, such as soft corals and mollusks (North 1976:254). Outwardly diffusing iron ions replace some of the calcium resulting in a mix of iron

corrosion products, calcium carbonate and living marine organisms covering the iron or steel object. The concretion forms a semi-permeable barrier between the bare metal and seawater and has a significant influence on corrosion by reducing the amount of dissolved oxygen available for the corrosion reaction, increasing acidity at the metal-concretion interface and increasing the chloride ion concentration at the concretion/metal interface (North 1976:253).

Preliminary Concretion Examination

Fines residue from samples collected from *Arizona* in 1998 were collected for preliminary x-ray diffraction (XRD) analysis performed by the UNL laboratory. The results showed a high background, possibly caused by amorphous crystalline compounds which do not yield identifying peaks. Riding on the background were peaks corresponding to magnetite (Fe_3O_4) and other compounds that could not be identified because of the complexity of the x-ray pattern. In order to analyze a solid sample, a sample holder was installed in the x-ray machine that rigidly mounted a section of the sample. The sample was then milled in sequential 0.5 mil (0.0005 in.), or 12.7 μm (0.0127 mm), sections from the metal side into the concretion and scans run on each. Peaks revealed the same information as did the fines. This preliminary work confirmed the presence of iron in the concretion as reported in Lenihan (1989) and indicated that iron transport between the steel hull and concretion is significant in understanding marine corrosion.

X-Ray Diffraction and Environmental Scanning Electron Microscopy

Initial concretion investigation on USS *Arizona* focused on XRD to isolate and identify compounds that make up the concretion and on environmental scanning electron microscopy (ESEM) and x-ray fluorescence (XRF) to determine relative percentages of each element. The Air Force Research Laboratory, Eglin Air Force Base, conducted XRD and the Composite Materials and Structures Center at Michigan State University conducted the ESEM analysis. The University of New Mexico Analytical Chemical Laboratory in the Department of Earth and Planetary Sciences completed the XRF. In addition to these examinations, the Analytical Chemical Laboratory, Department of Chemistry, University of Nebraska-Lincoln conducted

direct chemical analyses.

A 2.2 in. (5.5 cm) diameter concretion sample (USAR-01-045) was used for XRD and ESEM. The concretion was collected by using an air-powered hole-saw and sectioned on a diamond saw using water containing a 3% TRIMSOL solution to produce the XRD and ESEM sample, which was from the upper half of the disc (Figures 5.51 and 5.52).

Preliminary results are consistent with North's (1976) findings that concretion formed on wrought and cast iron structures contains the mineral siderite, which is formed by the exchange of iron ions for calcium ions.   UNL scientists followed up on these findings with studies to determine the feasibility of translating iron content in the concretion to corrosion rate of the hull in the contact region between the metal and the concretion sample, which is presented in more detail below.

X-Ray Diffraction (XRD)

For XRD, the thin slice section was mounted in a Seimens x- ray diffractometer outfitted with a tube containing a copper anode and a graphite beam diffracted monochromator. The beam size at 60 degrees two theta was 0.079 in. x 0.39 in. (2 mm x 10 mm). X-ray patterns were collected over the angular range from 10 to 80 degrees two theta. A measurement was made every millimeter through the thickness of the specimen (Figure 5.53). Seimens search-match software determined the various phases present in the XRD patterns (Figure 5.54). Excellent fits to the observed XRD patterns were obtained with the combination of three phases: aragonite, siderite and magnetite (DeAngelis 2002). The integrated intensities of two Bragg peaks of siderite and aragonite, displayed as a function of position in the concretion indicate that the siderite ($FeCO_3$) was the major component in the concretion in the 0.5 in. (13 mm) of thickness nearest the steel surface (Figure 5.55). Aragonite ($CaCO_3$), almost absent in the first 0.5 in. (13 mm) from the metal surface, appears in the last 0.08 in. (2 mm) of concretion closest to the water/concretion interface. The distribution of magnetite was uniformly low in concentration through the 0.5 in. (13 mm) of concretion nearest the steel surface. The magnetite concentration increased in the last 0.08 in. (2 mm) of thickness (Figure 5.56). In addition to the concretion, a thin layer of oxide containing minerals is evident between the concretion and the hull metal. This layer is normally 0.08 to 0.20 in. (2 to 5 mm) thick and is identified as a mixture of

Figure 5.51. Top view of concretion sample.
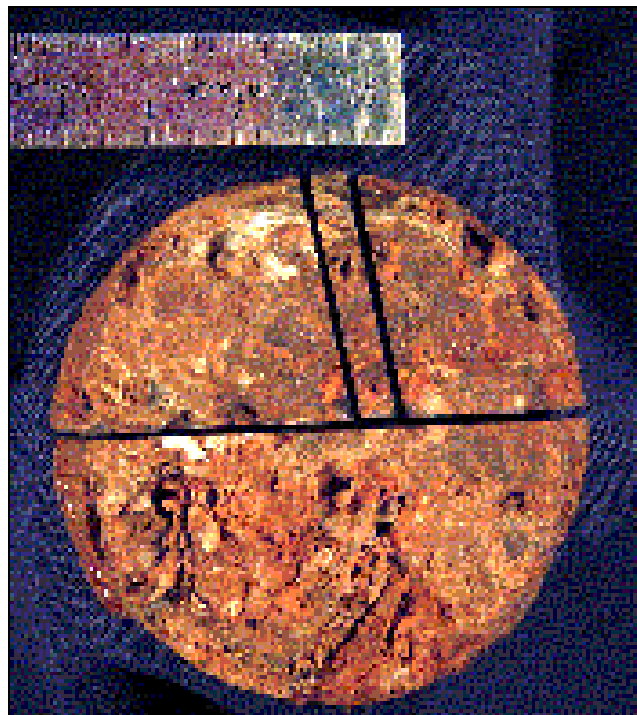
Figure 5.52. Concretion sample after sectioning.
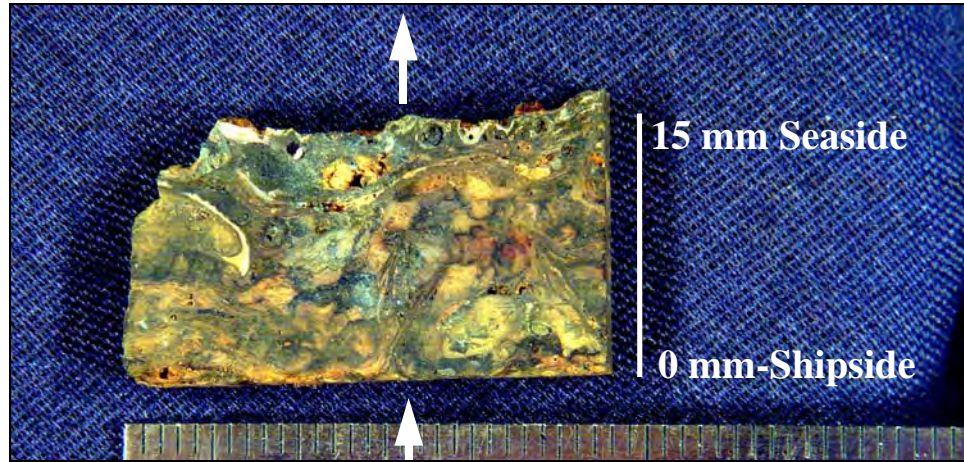
Figure 5.53. X-ray beam sampling path through the thickness of concretion.
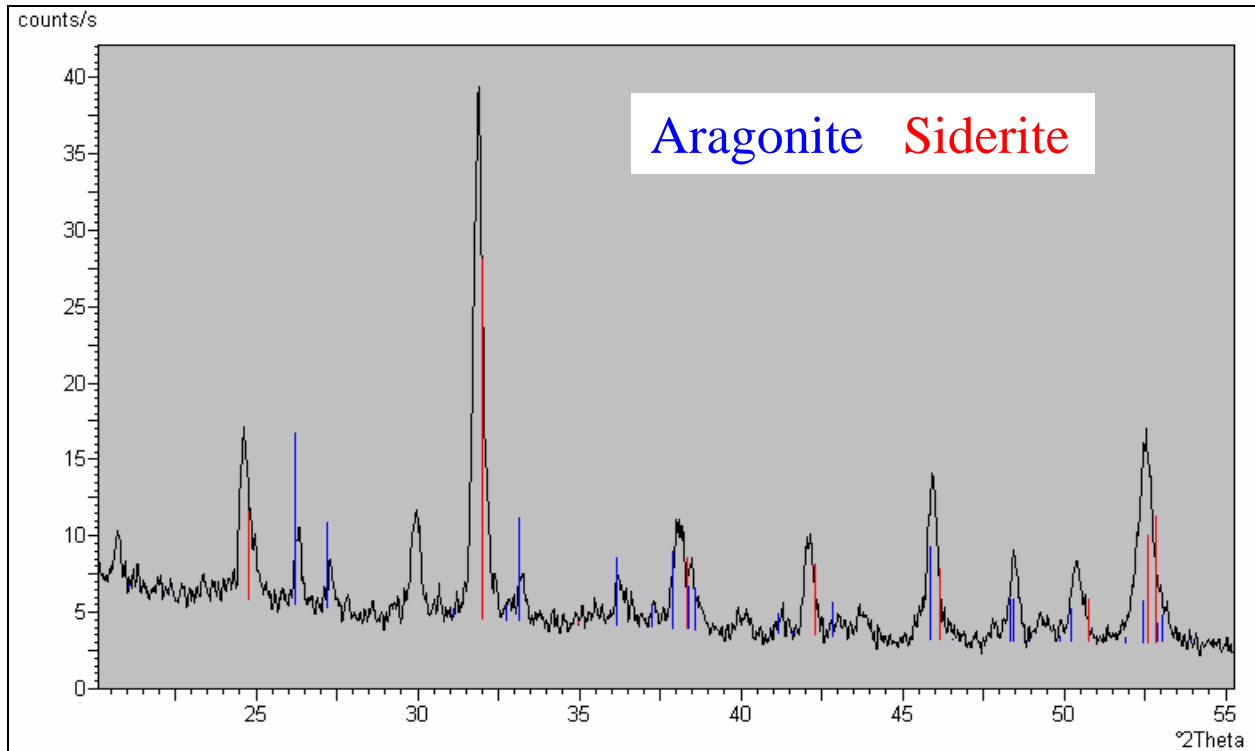
Figure 5.54. Typical experimental x-ray diffraction scan, 2mm from hull surface, 2-theta lines (red) from published standards for siderite, 2-theta lines (blue) from published standards for aragonite.
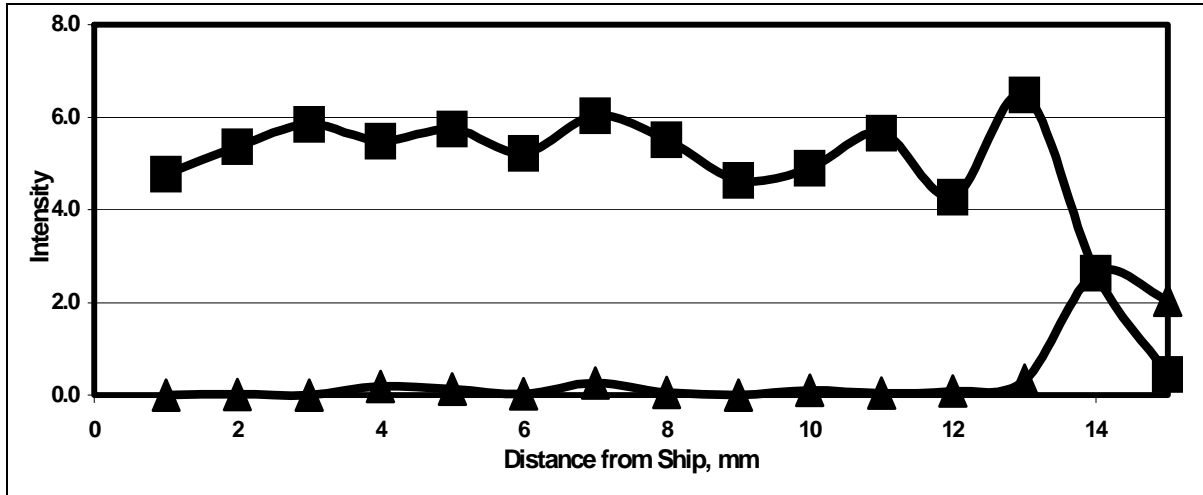
Figure 5.55. Average intensities of siderite and aragonite (lower numbers) peaks as function of distance from hull surface.
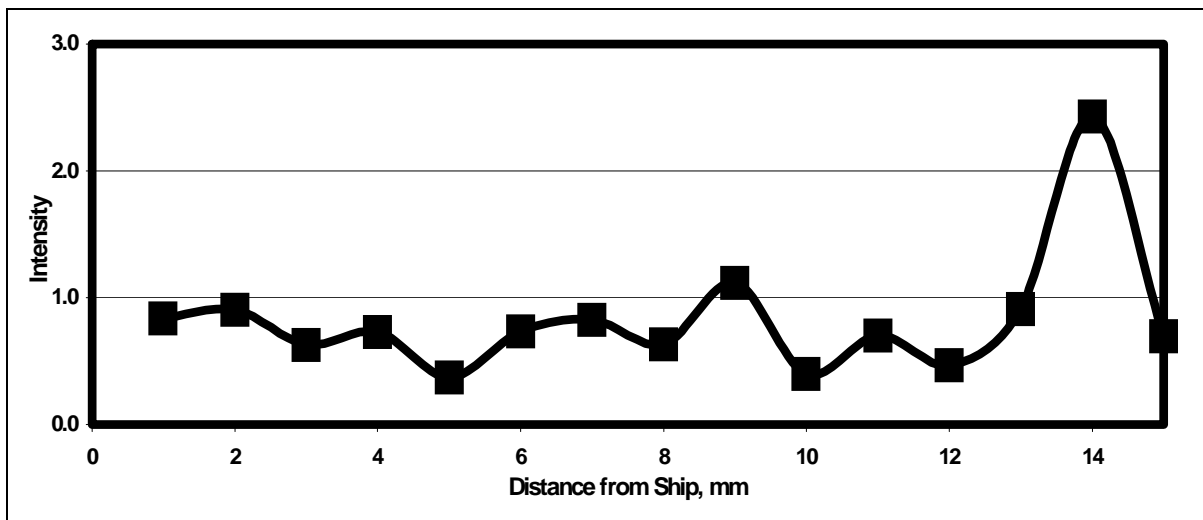
Figure 5.56. Average intensities of the magnetite x-ray diffraction peaks as a function of distance from hull surface.

compounds including chloride containing Akaganeite ($Fe_8(O,OH)_{16}C_{11.3}$, Iron Chloride Hydrate ($2FeCl_{3.7}H_2O$), as well as Goethite (FeO(OH), Lepidocrocite (FeO(OH), and Magnetite (Fe_3O_4).

The iron/water/carbon dioxide Pourbaix diagram (Figure 5.57) is useful to confirm XRD data since it incorporates stability fields for magnetite (Fe_3O_4), siderite ($FeCO_3$) and hematite (Fe_2O_3). Magnetite and siderite were identified by XRD although hematite is not stable in the range of E_{corr} and pH observed and was not identified. E_{corr}/pH data from data previously discussed is superimposed onto Figure 5.57. Starting from the left side of the diagram at a potential of about -0.4 V (SHE) and pH = 5.0, the green circled dots correspond to iron ions in solution predominantly as Fe^{+2} and exist in the region labeled "corrosion" on the iron/water Pourbaix diagram (Figure 5.2). In this region, the pH decreases slightly as E_{corr} increases. Next, magenta triangulated dots appear in the region labeled siderite at a potential of -0.32 V (SHE) and pH = 5.8. Siderite (with intensity proportional to concentration) exists throughout the concretion cross section, although the concentration is slightly higher at the metal surface, decreasing from a maximum 0.5 in (13mm) to near zero at the water/concretion interface (Figure 5.55). The green triangulated dots start at a potential of about -0.35 V (SHE) and pH = 6.5 and continue through the region labeled magnetite. Magnetite intensity is slightly lower near the steel surface and increases toward the concretion/water interface (Figure 5.56). Although there is some overlap between fields, pH increases as E_{corr} increases in the siderite region and levels off in the magnetite region. These observations are consistent with Figures 5.55 and 5.56 showing maximum siderite near the metal surface and maximum magnetite near concretion/water interface. The absence of hematite in XRD data was confirmed from E_{corr}/pH data since none of the points extend into that region.

Environmental Scanning Electron Microscopy (ESEM)

For ESEM, researchers selected 11 positions on the cross-section of the slice to probe with the electron beam (Figure 5.58). The initial seven of the 11 probe positions tracked the x-ray path and were at the following distances from the steel surface: (1) 0.03 in. (0.8 mm), (2) 0.2 in. (5.4 mm), (3) 0.1 in. (2.5 mm), (4) 0.27 in. (6.9 mm), (5) 0.33 in. (8.4 mm), (6) 0.37 in. (9.4 mm), and (7) 0.42 in. (10.7 mm). The last four probe positions were selected at interesting features in the structure of the concretion, and were located at the following distances from the
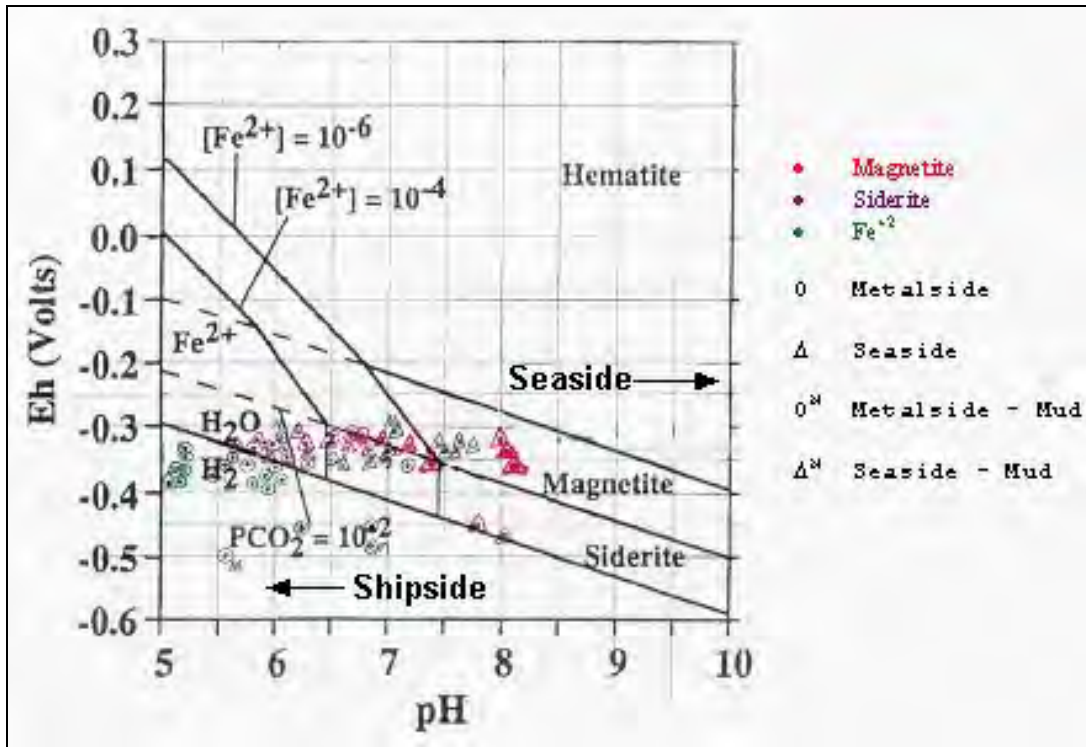
Figure 5.57. E_H - pH stability fields for hematite, magnetite and siderite in water-iron-CO_2 system at 25 °C and 1 atm pressure.
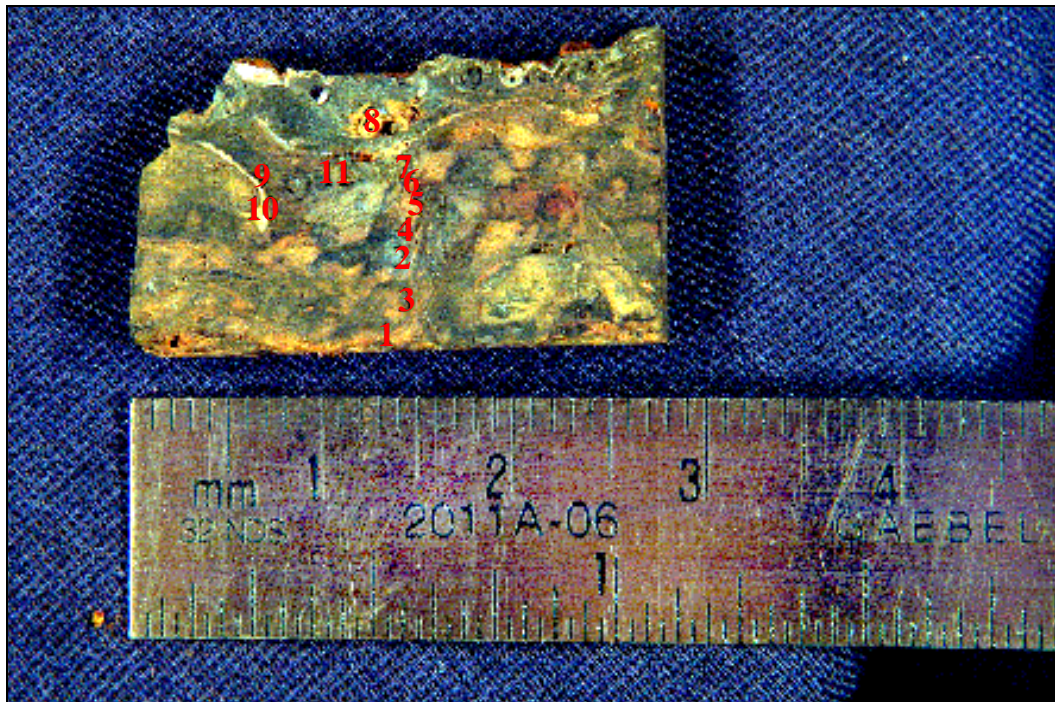
Figure 5.58. Positions of electron microscope probe.

steel surface: (8) 0.53 in. (13.5 mm), (9) 0.41 in. (10.4 mm), (10) 0.34 in. (8.6 mm), and (11) 0.42 in. (10.7 mm). Compositional scans were also made along lines about 10 mils (250 µm) in length to document the inhomogeneous structural characteristics of the concretion (DeAngelis 2002). The data collected consisted of structural images collected from back-scattered electrons and chemical images of the same areas collected from the florescence radiation of the particular element. The elements imaged were Fe, Ca, Ta, Al, Si, Br, O, Cl, C and S. Compositions at the 11 positions were then calculated from the total florescence x-ray spectrum obtained from each of the 11 probe positions (Table 5.28).

Discussion

Based on the positions of the electron microprobe readings and the wt % Fe at those positions, the mean Fe content in the concretion sample USAR-01-045 is calculated by graphical integration as follows:

$$\text{Fe (wt \%)} = \frac{1}{L}\int_0^x C_{Fe}dx \qquad\qquad [17]$$

where

> L is total thickness of concretion
>
> C_{Fe} is concentration of iron in weight % at position x
>
> x is distance into concretion in mm corresponding to C(Fe)
>
> Fe(wt%) = 1/15mm [798 wt %-mm] = 53 wt % Fe (mean) in concretion

An iron balance on a unit area through the metal/concretion for this sample shows that about 40% of the corroded iron is trapped in the concretion; the remaining iron remains as a thin oxide layer at the concretion/metal interface or is lost to seawater. DeAngelis also conducted XRD analysis of the thin oxide layer on metal coupon sample USAR-01-002. Dominant oxides were magnetite (Fe_3O_4) and Lepidocrocite (limonite) (FeO(OH)).

Based on ESEM results, UNL conducted direct chemical analysis on four concretion samples: USAR-03-001, USAR-03-002, USAR-03-003, USAR-03-007 and USAR-03-008. The average total iron content of these samples was 35 wt%. The University of New Mexico conducted XRF analysis on concretion samples USAR-01-042 and USAR-01-043. The average

Sample	Probe Pos.	C wt%	O wt%	Al wt%	Si wt%	S wt%	Cl wt%	Ca wt%	Fe wt%	Br wt%	Ta wt%
15	1		43.89		0.69	4.7	3.12	0.99	46.51	0	
16	2		25.14		0.35	3.28	4.04	1.87	65.31	0	
18	3		30.11		0.62	2.35	10.38	1.16	39.06	16.32	
16	2 thin part		19.31		0.25	1.73	9.35	2.39	55.78	11.18	
19	4		25.67		1.89	4.02	1.66	3.47	63.87	0	
20	5	5.3	10.41		0.95	1	0.95	1.73	78.2	0	1.45
21	6	4.07	9.67		1.25	1.22	0.54	1.9	60.84		0.52
22	7	6.68	15.21		0.6	9.05	0.32	10.36	57.7		0.07
23	8	9.07	28.31	2.5	3.16	1.59	0.42	3.95	51	0	0
24	8	7.08	24.76	1.68	2.19	1.23	0.49	1.51	61.07		
25	8	9.44	25.78	1.5	2.06	1.12	0.35	1.9	57.86		
26	9	6.64	38.74	0.18	0.53	1.59	0.78	33.49	18.04		
27	10	7.02	36.53	0.22	0.59	18.28	0.38	16.47	20.5		
28	11	8	26.99	1.98	4.45	9.2	0.77	1.59	47.03		
Sample	Probe Pos.	C at%	O at%	Al at%	Si at%	S at%	Cl at%	Ca at%	Fe at%	Br at%	Ta at%
15	1		71.11		0.64	3.8	2.28	0.64	21.54	0	
16	2		52.09		0.41	3.4	3.78	1.55	38.77	0	
18	3		58.76		0.69	2.29	9.14	0.9	21.84	6.38	
16	2 thin part		44.17		0.33	1.98	9.66	2.18	36.56	5.12	
19	4		52.32	0	2.19	4.08	1.53	2.82	37.29	0	
20	5	16.74	24.69		1.29	1.19	1.02	1.64	53.13	0	0.3
21	6	13.34	23.81		1.76	1.5	0.6	1.86	57.02		0.11
22	7	17.87	30.55		0.69	9.07	0.29	8.31	33.2		0.01
23	8	19.86	46.53	2.42	2.96	1.31	0.31	2.59	24.01	0	0
24	8	17.03	44.73	1.8	2.26	1.1	0.4	1.09	31.6		
25	8	21.5	44.09	1.52	2.01	0.96	0.27	1.3	28.35		
26	9	13.08	57.24	0.16	0.45	1.17	0.52	19.75	7.64		
27	10	13.74	53.64	0.19	0.49	13.4	0.25	9.66	8.63		
28	11	17.64	44.69	1.94	4.2	7.6	0.57	1.05	22.31		

Table 5.28. Chemical Compositions in Weight and Atomic Percent at the positions of the ESEM.

total iron content of these samples was 42.6 wt% (Table 5.29). Considering the heterogeneity through the cross section of the concretion, direct chemical analysis appeared to be an acceptable and much less expensive alternative to ESEM. Only minor amounts of other metallic oxides such as TiO_2, Al_2O_3, MnO and MgO are reported (Husler and Dodson 2003).

In addition to Fe, ESEM probe data shows the distribution of other elements (Table 5.28). It is interesting to note that carbon is below detectable levels until position (5) 0.33 in. (8.3 mm) into the concretion from the steel surface is reached. If a portion of this carbon is organic, there may be bacterial activity in the concretion as reported by North and MacLeod (1987). However, FeS was not detected as would be expected if SRB were active there. The level of detectability

Sample	%Fe	%Mg	%Ca
Direct Chemistry - UNL			
USAR-03-001	42.78	0.24	4.19
USAR-03-002	33.86	0.29	10.83
USAR-03-003	21.83	0.83	17.64
USAR-03-007*	48.10	1.49	0.57
USAR-03-008	29.15	1.67	19.0
XRF - UNM			
USAR-01-042	43.1		
USAR-01-043	42.1		
*results inconclusive			

Table 5.29. Wet chemistry and XRF concretion analysis, 2003.

is low; therefore, very low concentrations of sulphides could still exist and not be detected. In all but one case, there is sufficient iron to react with all of the sulphur to form FeS. This means that less than 4 at % of the Fe could be in the concretion in the form of FeS and possibly not be detected by XRD. Sufficient oxygen is available to form $FeCO_3$, $CaCO_3$, and Fe_3O_4, as identified by XRD with minor amounts of other oxides such as SiO_2, Al_2O_3 and Ta_2O_3. Other oxides of elements not reported in Table 5.28 are undoubtedly present. Probe positions (8), (9), (10), and (11) represent inhomogeneous features that were not part of the scan path. For example, analysis of position (8) reveals consistently higher than normal Si (SiO_2) and Al (Al_2O_3) and possible entrapment of silt in shell fragments. Position (9) shows abnormally high Ca in the same region as position (8). Position (10) shows an abnormally high sulfur content as well as high Ca. This indicates the possible presence of $CaSO_4$ or CaS.

From observation and analysis of data to date, oxygen availability determines the controlling corrosion process although equation [3] is not the directly dominant cathodic reaction.   Interface anaerobic conditions under and into the concretion, lead to the of SRB activity and microbial induced corrosion (Little, et al. 2000). Over time, as the concretion reaches $FeCO_3$ saturation, Fe^{+2} accumulates between the metal hull and concretion to further limit the corrosion rate.

Corrosion Rate (i_{corr})

During marine corrosion, unlike cast iron, the microstructure of steel (USS *Arizona* is low carbon steel, see Johnson et al., 2000 and Makinson *et al.,* 2002) does not result in a remnant

layer of graphite that preserves the original surface and allow for direct measurement of metal lost over time. Hence, it was impossible to use this technique to determine the iron corrosion rate, a technique pioneered in Australia and later applied elsewhere (e.g. Gregory 1999; MacLeod 1987; MacLeod 1995; McCarthy 1988). For steel vessels, the most accurate measure of metal loss is to determine actual steel thickness and subtract this value from original thickness specified on ship's plans. Once total metal loss is known, average corrosion rate can be calculated. With absolute corrosion rate determined, it is possible to calibrate electrochemical techniques such as linear polarization to determine instantaneous corrosion rate at any assessable location on the ship. Although this technique has not been pursued during this project, it is proposed for possible subsequent investigations (see concluding chapter). Measuring actual steel thickness can be accomplished by direct measurement or by using ultrasonic thickness instruments; however, the latter has serious limitations, as discussed below. Because *Arizona* is both a war grave and has international significance, as an alternative, a minimum-impact method to determine corrosion rate of the steel hull has been developed using density, thickness and total iron content of the concretion. The technique has been termed the Concretion Equivalent Corrosion Rate (CECR) and has provided the best combination of minimum impact and reliability. For interior spaces or other areas where it is impossible to collect concretion samples, an estimate of corrosion rate based on environmental parameters is the only alternative at the present time. However, linear polarization may be readily adaptable to interior as well as exterior corrosion rate measurement.

Previous Work

Initial work on corrosion rate began with an evaluation of previous data collected during the 1980s USS *Arizona* corrosion study. Specifically, Henderson (1989) was reviewed with particular attention to the data in Table 4.3 (Henderson 1989:128), which presents concretion thickness and weight vs. water depth for 12 vertical stations established on *Arizona*'s exterior hull. Concretion appeared in fairly distinct forms, dead and live. Dead, or hard, concretion is composed of skeletal marine organisms with an original high calcium carbonate composition and a maximum thickness of about 1 in. Accumulated live organisms on the exterior surface of the concretion measured up to about 3 in. in thickness. Table 4.3 (Henderson 1989:128) was

modified by Johnson et al. (2003:11) and reproduced here as Table 5.30 to show the original data analysis and conversion to the conventional expression of corrosion rate (i_{corr}) in terms of mpy. Column 1 in Table 5.30 locates (port or starboard) dual samples A and B. Column 2 is water depth. Column 3 is dry weight of corrosion product obtained after the concretion had been scraped from a 36-square inch area of the hull, dried at 100 °C for about 8 hours and the corrosion product separated from the bulk using a bar magnet. Column 4 is the weight of iron calculated assuming that the corrosion product was magnetite (Fe_3O_4) according to:

$$\text{Weight of Fe} = (\text{Dry Weight of Corrosion Product}) \times 0.724 \text{ gr}$$

where

$$(3 \times \text{molecular weight Fe})/\text{molecular weight } Fe_3O_4) = 3 \times 55.85/232 = 0.724$$

Column 5 is the i_{corr} in mpy calculated from the following equation:

$$i_{corr} = (\text{wt Fe}) \times (1/36) \times (1/2.54)^2 \times (1/7.87) \times (1/45) \times (1/2.54) \times 1000 = (\text{wt Fe}) \times 0.0048 \text{ mpy}$$

According to Henderson (1989:129), the data indicate that the "formation of corrosion products has been maximal at shallower depths and has occurred at lower rates at depths of 20-30 ft." In sea water, Uhlig and Revie (1985:93) note that passivity (thin, adherent protective

Station (Port/Starboard)	Water Depth (ft)	Dry Weight of Corrosion Products	Weight of Iron (gr./36sq.in)*	i_{corr} (mpy)*
17a/b	8	440/718	319/520	1.5/2.5
45a/b	9	161/568	117/411	0.6/2.0
11a/b	13	565/530	409/384	2.0/1.8
53a/b (avg)	17	99	72	0.4
61a/b	17	354/374	256/271	1.2/1.3
21a/b	22	5/25	4/81	0.0/0.1
2a/b	22	14/35	10/25	0.0/0.1
43a/b	24	376/118	272/85	1.3/0.4
12a/b (avg)	27	76	55	0.3
30a/b	27	198/164	143/119	0.7/0.6
33a/b	28	206/270	149/195	0.7/0.9
52a/b (avg)	28	138	100	0.5

Table 5.30. Calculated corrosion rate from original data from June 1986. Colums 4 and 5 adjust for approximately 2 years in dry dock prior to December 7, 1941.

film) of iron is not established and in such media, decreased oxygen concentration, as the water depth increases, results in a decrease in corrosion rate in the absence of concretion. As expected, i_{corr} in mpy (Table 5.30, column 5) is consistent with this observation although the presence of concretion, as discussed earlier, promotes lower pH and changes the chemistry at the concretion /metal interface.   As Henderson (1989:129) observes:

> Hard biofouling [concretion] at all stations was found to consist of entwined masses of oyster and vermetid shells. Hard biofouling extended beneath the bottom silt on the hull surfaces, and was exposed by digging holes about 3 feet into the silt at representative locations. The hard fouling layer had apparently grown on the lower hull areas before they were covered with silt by sedimentation or hull settling.

> No correlation was found to exist between water depth and thickness of hard biofouling, indicating that, over the long term, growth of oysters and vermetids had been relatively unaffected by depth and water motion. Hard biofouling averaged about ¾-inch thickness on vertical stations, where that layer serves as a primary barrier in protecting steel/oxides from corrosive effects of overlying water and, at present, appears to be stable and well bonded to the hull.

Korb (1987:1255-1256) further addresses this issue by noting that calcareous scale forms at cathode areas on the metal surface. A layer of hard shell and other biofouling restricts available oxygen at the metal surface, creates anoxic conditions and decreases the corrosion rate. However, increased stress on the structure occurs. Scale formation at cathode areas is confirmed by MacLeod (1982) and North and MacLeod (1987), who conclude that the main cathodic reactions take place in the concretion rather than at the metal surface because the metal surface becomes devoid of oxygen. The issue concerning the location of cathodic reactions will be continued below in a later section. On freshly exposed carbon steel surfaces, Fontana (1986:374) reports typical corrosion rates in sea water (Table 5.31).

Vertical Position On Structure	i_{corr} (mpy)
Marine atmosphere	3
Splash Zone	17
High Tide	8
Low Tide	5
Quite Sea Water	5-8
Mud Line	2 ½-3

Table 5.31. Typical Corrosion Rates for Mild Steel in Sea Water

A comparison of rates in Table 5.30 with those in Table 5.31 indicates that marine concretion attached to the hull significantly reduces the corrosion rate. Jones (1996:53, 59, 381) discusses macrofouling organisms and reports that they are often acidic, accelerating the corrosion of metal substrates but at the same time shelter the underlying metal from access to oxygen and create differential aeration cells which also accelerate corrosion. The oxygen free (anaerobic) environment beneath macro organisms can further host sulfate reducing bacteria, which can have further implications for corrosion rate.

Direct Measurements

As an initial control for corrosion rate research on USS *Arizona*, in August 2002 NPS-SRC partnered with the Naval Facilities Engineering Service Center-Ocean Construction Division, the U.S. Navy's Mobile Diving and Salvage Unit One (MDSU) and Titan Maritime Industries, Inc. to collect 4-in (10-cm) diameter hull plate samples ("coupons") from *Arizona*'s hull. MDSU surface-supplied divers removed each coupon from prescribed locations using a 4-in (10-cm) diameter proprietary hydraulic-powered hole-saw developed by Titan (Figure 5.59). This hole-saw did not utilize a pilot hole, which would compromise sample integrity. The coupons were removed from external, vertical hull locations marked by SRC archeologists. For analytic purposes, each sample had to be collected with concretion intact on both sides of the coupon (Figure 5.60), so a task-specific bit was designed to retain the coupon plus interior and exterior concretion. Eight coupons were removed from external, vertical hull locations on both port and starboard sides at frame 75 (Figure 5.61). On each side of the ship, one sample was taken from the upper deck level near the water line; from the second deck level above the torpedo blister; from the third deck level in the torpedo blister; and from the first platform level in the torpedo blister below the mud line. Ship plans were consulted for each location to ensure no compartments potentially containing oil would be penetrated. As a precaution, a half-inch hole was drilled near the sample location with a drill-tap that could be easily plugged should oil be encountered. Immediately after coupon removal, each location was plugged using a plumber's pipe plug and sealed with marine epoxy to prevent formation of localized corrosion cells and minimize exchange of interior and exterior water. Drilling operations were directed, monitored, filmed and photographed in-water by SRC personnel using scuba equipment.

Figure 5.59. U.S. Navy diver using Titan's hydraulic hole-saw to remove samples from Arizona's hull (NPS Photo by Brett Seymour).

Figure 5.60. Steel hull sample with intact interior and exterior concretion (NPS Photo by Brett Seymour).
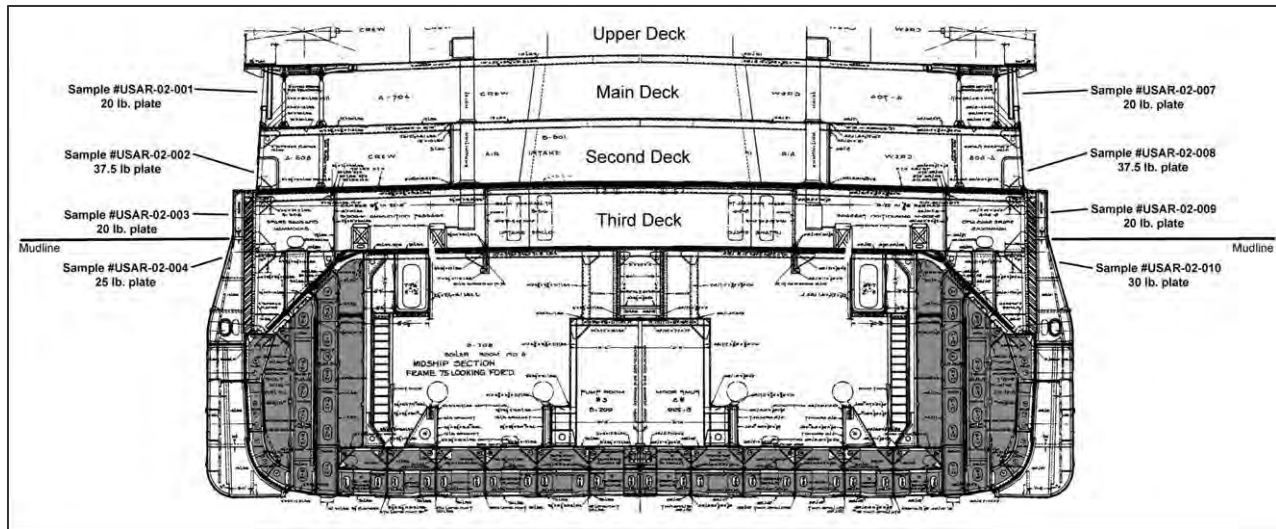
Figure 5.61. Location of samples removed from Arizona's hull at frame 75.

Hull coupon thickness was measured three different times. Preliminary field examination of each sample was performed as soon as the drill housing containing the coupon was detached from the drill and carried to the dock. This measurement is a rough field estimate using a millimeter scale. The second measurement was recorded at Rail Sciences, Inc. (RSI) in Omaha, Nebraska in September 2002 using calipers. Before the coupons were returned to SRC at Santa Fe, NM for long-term curation, UNL researchers removed a small chord from each sample for metallographic examination and optical measurement of plate thickness. The third measurement was obtained metallographically on a cross-section of each chord by Johnson at RSI laboratories (Johnson, et al. 2003:77). Because of some unevenness through the cross section of each chord, nine thickness measurements were obtained and combined to provide an average thickness for each coupon (Figures 5.62-5.69)(Table 5.32). Metallographic examination revealed that the most reliable thickness measurements were obtained from the polished cross sections, so it was decided to only use the optical data obtained at RSI for insertion into equation [19] (see below).

Averaged thickness of each coupon was compared to original steel thickness compiled from ship's plans to determine overall metal loss from December 1941 (it was assumed that minimal corrosion occurred during the ship's active use) to August 2002. The original ship cross-section at frame 75 provided as-built steel thickness in terms of theoretical weight, in pounds per square foot, at each location (Johnson, et al. 2003:82). Standard tables were used to convert theoretical weight to nominal thickness in inches—unfortunately, no thickness tolerances

Figure 5.62. Cross section photograph of steel hull sample #USAR-02-001.
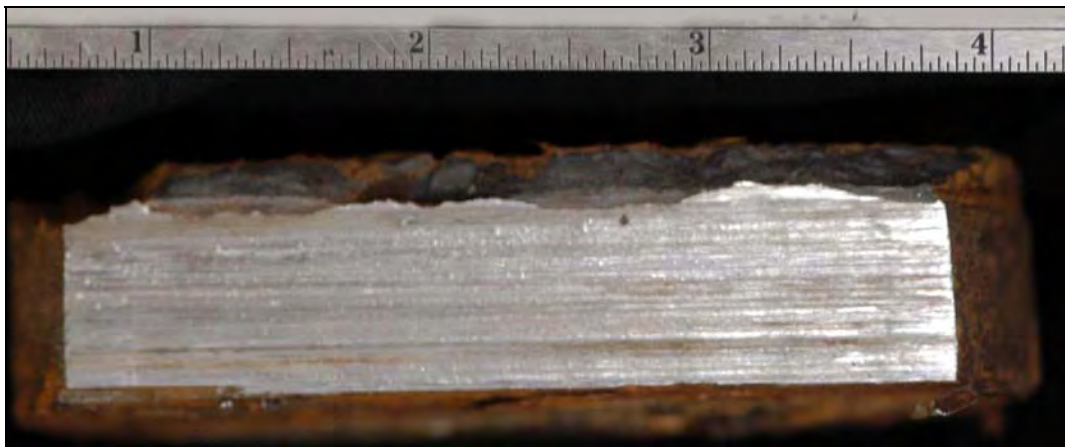
Figure 5.63. Cross section photograph of steel hull sample #USAR-02-002.

Figure 5.64. Cross section photograph of steel hull sample #USAR-02-003.
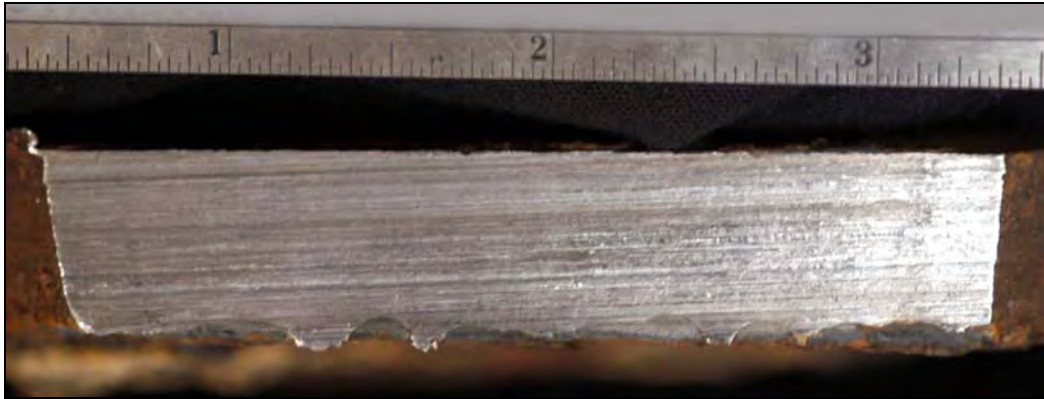
Figure 5.65. Cross section photograph of steel hull sample #USAR-02-004.
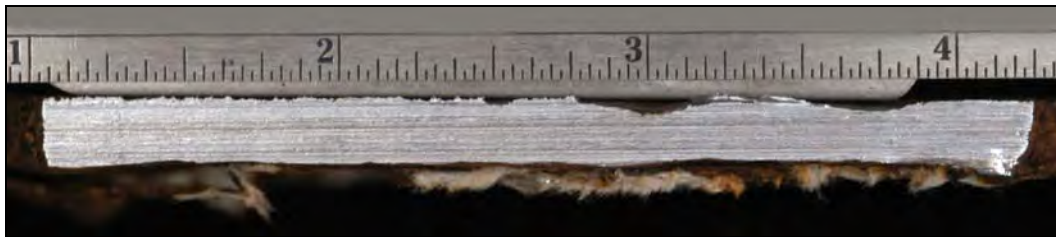
Figure 5.66. Cross section photograph of steel hull sample #USAR-02-005.

Figure 5.67. Cross section photograph of steel hull sample #USAR-02-006.

Figure 5.68. Cross section photograph of steel hull sample #USAR-02-007.
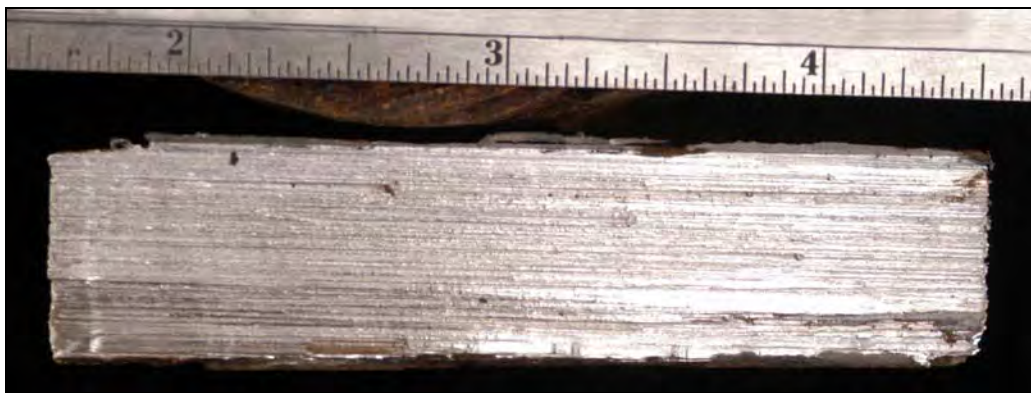
Figure 5.69. Cross section photograph of steel hull sample #USAR-02-008.

Measurement	USAR-02-001	USAR-02-002	USAR-02-003	USAR-02-004	USAR-02-007	USAR-02-008	USAR-02-009	USAR-02-0010
1	.116	.642	.4555	.5255	.223	.7755	.4545	.652
2	.1575	.6755	.4625	.597	.2015	.7845	.4845	.667
3	.087	.66	.4375	.5345	.201	.81	.4535	.6555
4	.1505	.683	.4225	.5554	.195	.807	.43	.663
5	.11	.6865	.4305	.579	.1895	.8005	.358	.654
6	.128	.642	.433	.5665	.177	.77	.3895	.658
7	.1165	.7095	.429	.553	.174	.792	.367	.6425
8	.178	.708	.4235	.5355	.1615	.7815	.36	.652
9	.174	.6325	.4125	.578	.241	.786	.33	.642
Average	.1323	.671	.4341	.5583	.1959	.7897	.403	.654

Table 5.32. Hull sample thickness measurements, in inches, from Rail Sciences Laboratory, March 2003.

are available. Assuming that the plate mill targets a nominal rather than a theoretical weight in lbs./ft.^{2}, the corresponding nominal thickness is shown in the top row of Table 5.33.

Data Analysis

With this data, corrosion rates are calculated according to the following:

$$\text{Metal loss} = T_o - T_a \qquad\qquad [18]$$

where

T_o is original thickness

T_a is actual thickness

The corrosion rate, (i_{corr}), in metal loss per unit of time, is given by:

$$i_{corr} = (T_o - T_a)/t \qquad\qquad [19]$$

When using English units, corrosion rate is given in mpy. In the International System of Units (SI), corrosion rate is given in microns per year (μm/yr) where one micron is 1/1000 of a millimeter. When the original and actual plate thicknesses are defined in either inches or millimeters, the corrosion rate equation becomes:

$$i_{corr} = \frac{T(o) - T(a)}{t} \times 1000 \qquad\qquad [20]$$

where

t is the exposure time in years (yr)

Nominal Thickness (Inches)	1/8	3/16	1/4	5/16	3/8	7/16	1/2	9/16	5/8	3/4	7/8
Theoretical Weight (lbs./sq. ft.)	6.15	8.7	11.25	13.8	16.35	18.9	21.45	24	26.55	31.65	36.75
Arizona Plate Weight (lb/sq.ft)							20		25	30	37.5

Table 5.33. Plate Thickness Conversion.

When metal loss is defined in inches, equation [20] expresses corrosion rate in mpy; when the metal loss is defined in millimeters, equation [20] expresses corrosion rate in µm/yr. This is a simplified expression that assumes a constant corrosion rate and essentially uniform corrosion. Although initial corrosion rates are high and decrease over time as concretion forms, it is assumed that corrosion rates stabilized fairly quickly (within a matter of a few years) and that for most of *Arizona*'s lifespan underwater, the rate has been nearly constant.

Results from equation [18] for each coupon are given in Figure 5.70 as a function of water depth, and the results from equation [20] are given in Table 5.34 and Figure 5.71. Because coupons were collected in 2002, t = 61 yr for these calculations. Note that for the two shallowest samples in Table 5.34 (USAR-02-001 and USAR-02-007, both in 5 ft. [1.52 m] water depth), i_{corr} was halved from the absolute value obtained from the direct measurement technique. Values were halved because, at those two locations, both the inside and outside of the hull are open to free-circulating seawater causing corrosion and concretion formation on both the interior and exterior sides of the hull at the same rate, effectively doubling the corrosion rate. On all other samples, there was little observable interior corrosion or concretion formation, and internal dissolved oxygen levels measured after coupon removal were at or near zero, indicating the majority of corrosion was taking place on the exterior side only.

It is significant to note that metal loss is greatest on the port side between the surface and about 20 ft. This is consistent with greater flow velocities on that side of the hull. Below about 20 ft., metal loss is nearly the same. An additional factor is the turbulence created by Navy launches and other port-side vessel traffic. The effect of water depth on corrosion rate is clearly evident in Figure 5.71 and Table 5.34. The two uppermost coupons, taken at the upper-deck level at approximately 5 ft. (1.52 m) water depth, incur the highest hull steel loss to corrosion (i.e. highest corrosion rate) of close to 3.0 mpy for the port side coupon (USAR-02-001) and 2.5 mpy for the starboard side coupon (USAR-02-007). To put this into perspective, 6 mpy (actual corrosion rate from both sides) corresponds to an average loss of 360 mils (0.009 µm) or 0.360 in. (9 mm) in 61 years, or the loss of nearly 75% of thickness on a ½ in. (12.7 mm) steel plate. Two reasons for the relatively high corrosion rate near the surface is maximum availability of oxygen and corrosion attack from both sides of the hull plate. Neither of these locations, however, is structural in nature nor supports any critical vessel elements.
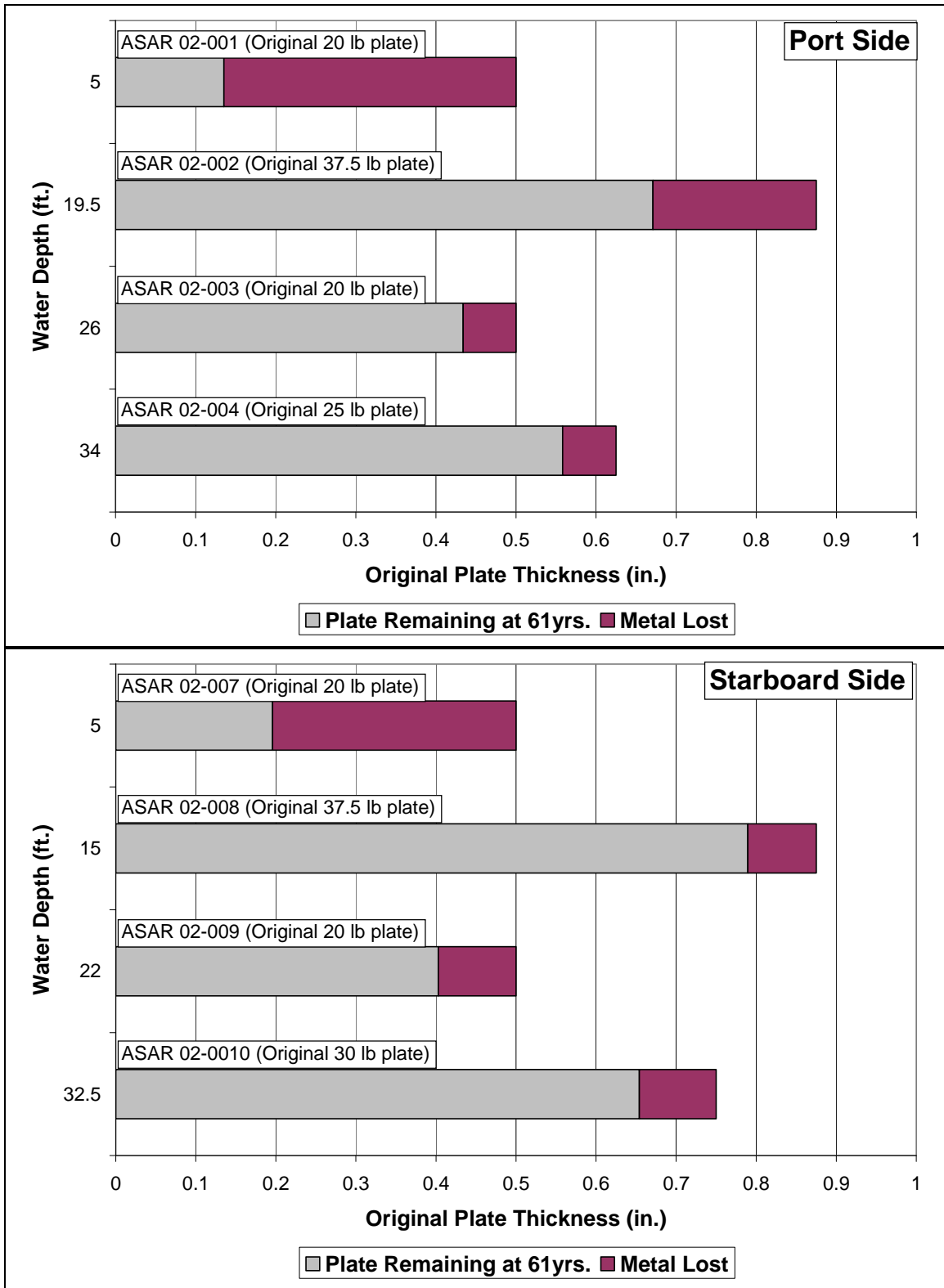
Figure 5.70. Metal loss as a function of original plate thickness and water depth

Sample	Original Thickness		Average Thickness (2002)		Water Depth		i_{corr}	
	in	mm	in	mm	ft	m	mils/yr	µm/yr
USAR-02-001	0.500	12.70	0.135	3.43	5.00	1.52	2.99*	75.98*
USAR-02-002	0.875	22.20	0.671	17.04	19.50	5.94	3.34	84.59
USAR-02-003	0.500	12.70	0.434	11.02	26.00	7.92	1.08	27.54
USAR-02-004	0.625	15.90	0.558	14.17	34.00	10.36	1.10	28.36
USAR-02-007	0.500	12.70	0.196	4.97	5.00	1.52	2.49*	63.36*
USAR-02-008	0.875	22.20	0.790	20.07	15.00	4.57	1.39	34.92
USAR-02-009	0.500	12.70	0.403	10.24	22.00	6.71	1.59	40.33
USAR-02-010	0.750	19.05	0.654	16.61	32.50	9.91	1.57	40.00
								*values halved

Table 5.34. Corrosion rate as a function of water depth from direct coupon measurement.

$$y = -0.0509x + 2.956$$
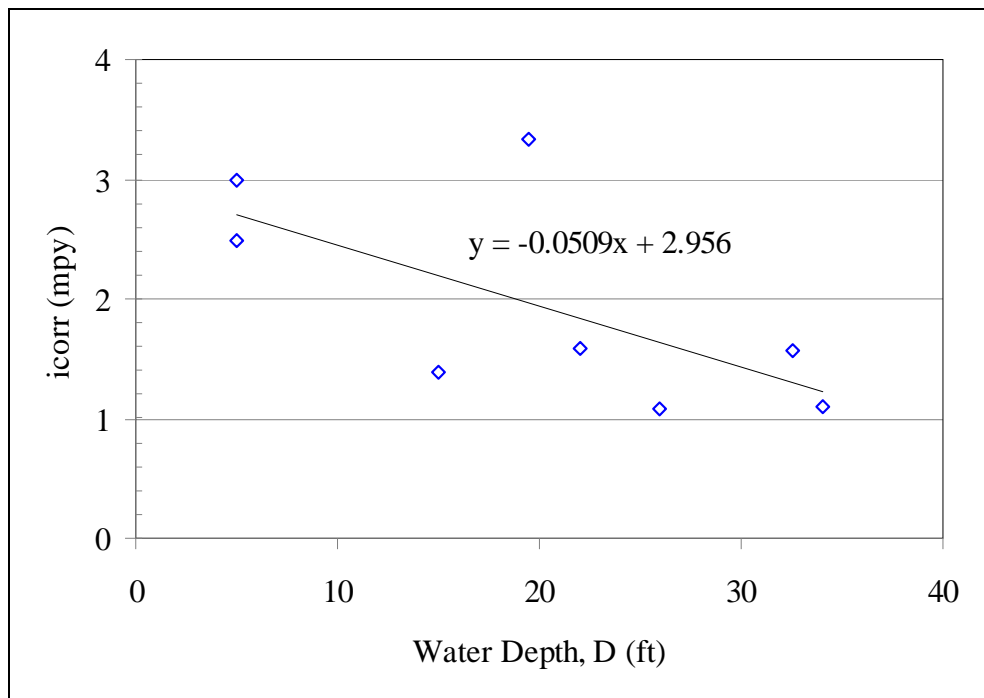
Figure 5.71. Corrosion rate (i_{corr}) of hull samples as a function of water depth.

219

Hull corrosion rate at the second-deck level varies from 3.3 mpy on the port side at a depth of 19.5 ft. (5.9 m) (USAR 02-002) to 1.4 mpy on the starboard side at a depth of 15 ft. (4.5 m) (USAR 02-008) (Table 5.34)(Figure 5.71). Examination of each of these coupons reveals a very thin layer of interior concretion, indicating limited marine activity on the interior side just above the torpedo blister. Average oxygen concentration of the interior spaces adjacent to the interior side of each sample was about 4.25 mg/L or 65% of the maximum at the surface. This was determined by inserting an oxygen probe into the interior space water immediately after removing the sample. Corrosion on interior surfaces of the hull likely contributes to the total metal loss in spaces where there is some exchange with fresh seawater, concretion is minimal, and oxygen is available to support corrosion in accord with equation [3]. However, such seawater exchange seems to be limited in this area.

Similarly, coupons removed from the torpedo blister above the harbor bottom vary from 1.1 mpy at a depth of 26 ft. (7.9 m) on the port side (USAR-02-003) to 1.6 mpy at a depth of 22 ft. (6.7 m) on the starboard side (USAR-02-009). Interior spaces at this level are inside the torpedo blister rather than inside the ship's hull. Dissolved oxygen on the interior side approaches zero on the portside and 2.5 mg/L (approximately half the exterior levels) on the starboard side, and the interior surface of the coupons are generally smooth with virtually no contribution to metal loss. The torpedo blisters at these locations are sealed from the exterior environment, so oxygen replenishment is negligible.

From the torpedo blister coupons removed from just below the harbor bottom (USAR-02-004 and USAR-02-010), the corrosion rate is unchanged at 1.1 and 1.6 mpy, respectively. It was only possible to measure the port side sample interior torpedo blister space for dissolved oxygen. The readings were near zero, indicating that available oxygen has been consumed, likely during initial corrosion, and not replenished through exchange with fresh seawater. Historically, it is interest to note that while the original intent of the torpedo blister addition during reconstruction in 1929-1930 was to provide added protection from torpedo attack, it now provides additional corrosion protection to the original external hull of the ship in lower regions of the hull where oil bunkers are still intact.

Just below the harbor bottom, i_{corr} appears to hold steady or increase slightly. This may be related to the fact that the maximum bacterial populations are found in the upper 1.6 ft. (0.5 m) of the seabed sediment according to MacLeod (1982). With oxygen depletion into the mud

and E_{corr} falling below the hydrogen evolution potential, hydrogen reduction becomes dominant according to equation [4] as sulphate reducing bacteria (SRB) catalyze the discharge of hydrogen and i_{corr} accelerates. When bacteria break down organic matter, they use the energy stored in their chemical bonds and subsequently shuttle electrons to dissolved oxygen. Since oxygen disappears deeper than a few inches into the mud, the bacteria use sulfate ion in sea water by chemically reducing sulfate to sulfide (Kerr 2001). Little (personal communication, 2003) notes that iron sulfide formed below the harbor bottom is cathodic to the iron oxide directly above it in sea water and could be the cause of accelerated corrosion at or near the harbor bottom. The depth of maximum bacterial activity is variable but is known to be active at interfacial sites such as that represented at the harbor bottom. For example, in the Gulf of Mexico, the depth of maximum activity is only a few millimeters. Based on these observations, i_{corr} may decrease substantially with increasing depth into the mud. Corrosion well below the harbor bottom is not fully understood, and may be investigated further in the future. It should be noted that SRB may also be present at the metal/concretion interface, and as such, may have an impact on corrosion over the entire hull of the ship.

Corrosion rate gradient (change in corrosion rate relative to water depth) is 0.05 mpy/ft. or 0.17mpy/m (Figure 5.71). MacLeod (2002:703) reports that the corrosion rate gradient of pre-steel-era iron shipwrecks, determined from annualized depth of corrosion as measured by penetration of graphitization into cast iron, is 0.36 mpy/m. The difference can be explained in terms of microstructural and chemical differences between cast iron and low carbon steel, as well as differences in environmental variables such as temperature, oxygen concentration, salinity, tidal conditions and marine organism activity.

Further Considerations – Relating Direct Measurements to E_{corr} and Limiting Current (i(L))

Experimental observation clearly indicates that E_{corr} and i_{corr} are each linear when plotted as a function of water depth (Figures 5.24, 5.29 and 5.71), hence a plot of i_{corr} as function E_{corr} is also linear. By eliminating water depth as a variable and combining the results with equation [11], Tafel equations are derived for each frame location (Table 5.35).

The Tafel constant β is the slope of the anodic polarization line (Figure 5.1). A high value of β means that the electrode is highly polarized, the line steeply increases and the

Frame	Tafel Expression*	β (mV/decade)
9	$E_{corr} = 42 \log(i_{corr})$ 358	42
75	$E_{corr} = 30 \log(i_{corr})$ 354	30
82	$E_{corr} = 22 \log(i_{corr})$ 352	22
76-88	$E_{corr} = 23 \log(i_{corr})$ 356	23
128	$E_{corr} = 28 \log(i_{corr})$ 352	28
*E_{corr} (SHE,mV), i_{corr} (mpy)		

Table 5.35. Corrosion Rate as a Function of Corrosion Potential

corrosion current is relatively low. If β is low, polarization is limited and the corresponding corrosion rate is relatively high. The ability of iron ions to go into solution in seawater and be removed from hull metal is variable depending upon the proximity of concretion to hull metal, its thickness, oxygen permeability and flow patterns at the concretion/metal interface. Observations indicate the Tafel constants β for each frame location is highest near the bow, decrease uniformly aft towards midships, and then increase somewhat towards the stern (Table 5.35). The Tafel equations provide an alternative method to determine corrosion rate, where E_{corr} is substituted into the equation closest to the location where E_{corr} is taken and solved for i_{corr}. Although not as accurate as other methods, these equations provide a corrosion rate estimate at frame locations outside of the midships area.

Below the harbor bottom, significant shifts in E_{corr} both port and starboard occur to suggest that bacteria are active in the interface area near the harbor bottom. For example, a comparison of coupon sample locations USAR-02-003 and USAR-02-004 on the port side indicate that E_{corr} values are more positive in the latter case by more than 40 mV. However, i_{corr} is identical at 1.1 mpy. A similar comparison of coupon sample locations USAR-02-009 and USAR-02-010 on the starboard side show that E_{corr} values are more negative in the latter case by more than 130 mV. However, i_{corr} is identical at 1.6 mpy. It is apparent that corrosion data are not consistent from just above to just below the harbor bottom. This inconsistency above and below the harbor bottom may be due to accelerated bacterial activity near the water/harbor bottom interface (Brenda Little, personnal communication, 2003). According to Little et al. (2000), bacteria consume oxygen and anoxic conditions are created in this area. Sulphate is reduced to sulphide and iron sulfide formed below the harbor bottom is cathodic to the oxide above it. With significant change in conditions at the harbor bottom, acid forming bacteria and SRB are likely active all over the hull. Hydrogen evolution occurs as bacterial activity

accelerates hydrogen discharge. It is difficult, however, to separate hydrolysis effects (equation [7]) from bacterial effects. Corrosion measurements below the harbor bottom are limited and more data is needed to elucidate corrosion behavior in this complex environment. In addition, E_{corr} acquisition needs to extend to well below the harbor bottom to better elucidate the effect of low oxygen content deep in the mud to that of much higher oxygen in water above. A further understanding of bacterial activity is also needed to relate E_{corr} and i_{corr}, not only at the harbor bottom and below but at the metal/concretion interface in other parts of the hull.

Oxygen availability directly or indirectly controls corrosion of steel in seawater, and equation [14] incorporates the significant variables necessary to evaluate oxygen transport rate across the surface barrier (in this case, the concretion). If oxygen consumption according to equation [3] were the only cathodic reaction, then the corrosion rate would be directly proportional to both the diffusion coefficient and oxygen concentration gradient across the concretion, and indirectly proportional to the concretion thickness. Hence, in such a circumstance, the corrosion rate could be determined knowing the amount of oxygen consumed according to equation [14], rather than resorting to the more difficult method of determining the amount of metal lost. However, corrosion seldom involves a single cathodic reaction, such as oxygen consumption, and equation [14] is utilized instead as an important diagnostic tool in assessing the complex role of oxygen. This is particularly true for *Arizona* since hydrolysis underneath the concretion creates an entirely different environment at the metal surface where corrosion actually takes place. As will be noted later, equation [14] incorporates numerous environmental variables either directly or indirectly to evaluate oxygen concentration and diffusivity, including salinity, temperature, viscosity and concretion permeability.

The E_{corr} gradient across the concretion for each of the hull coupon sites varies depending on the coupon site, but is typically about 1 mV/mm (Figure 5.72). pH also decreases through the thickness of the concretion (Figure 5.73)(Makinson, et al. 2002), the cause related to hydrolysis given by equation [7]. Bacterial activity may also be a cause of reduced pH, but the extent that each contributes is complex and variable from one site to another (Brenda Little, personal communication, 2003). As mentioned earlier, SRB accelerates the formation of hydrogen gas and hence has been shown to accelerate corrosion at low pH. Applying equation [14] to a typical set of data corresponding to coupon #USAR-02-008:
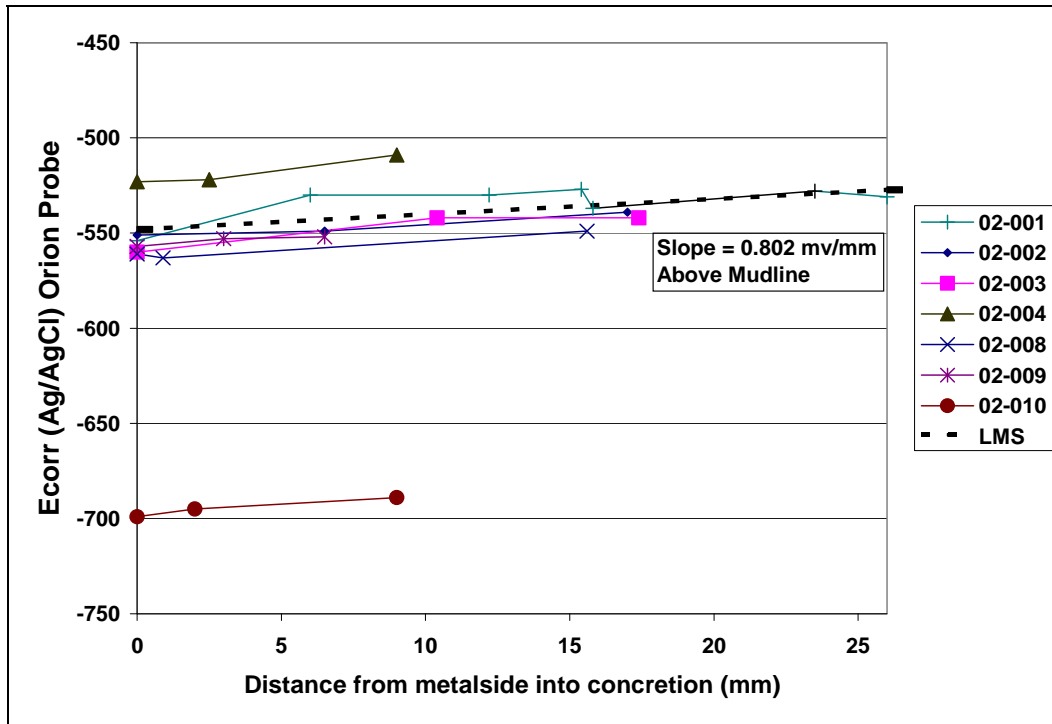
Figure 5.72. Corrosion potential as a function of distance from hull surface into concretion, August 2002.
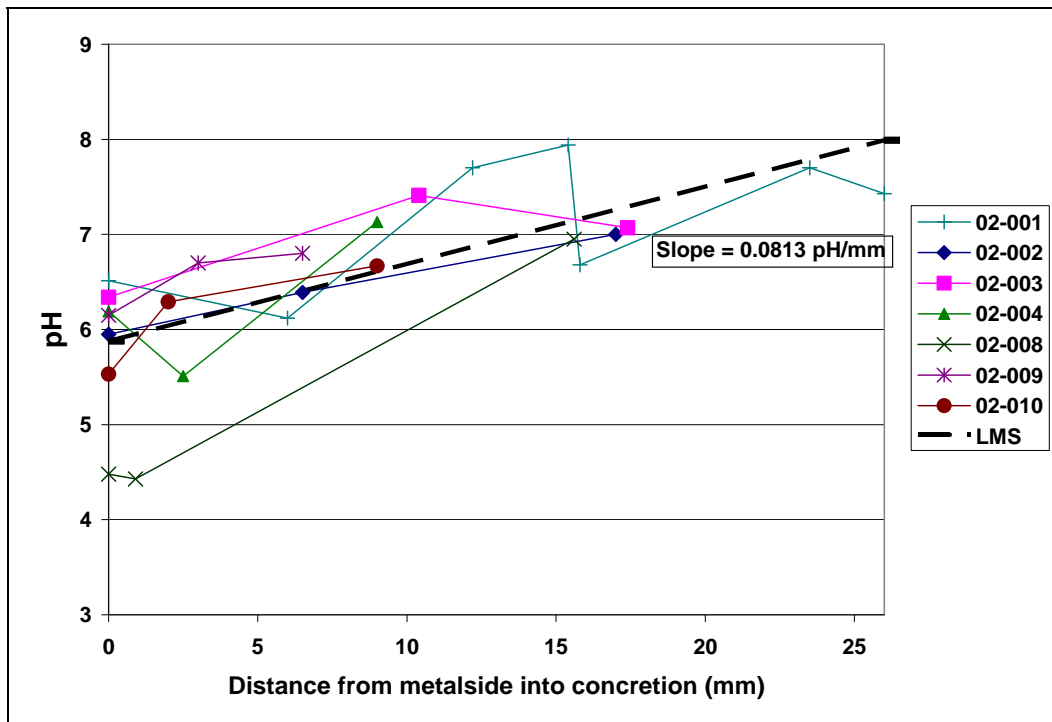
Figure 5.73. pH as a function of distance from hull surface into concretion, August 2002.

$$i(L) = i_{corr} = 0.46 \, DnFC/d \qquad\qquad\qquad [21]$$

where

$D(O_2)= 2.45 \times 10(\exp [-5])(\, cm/sec^2)*$

$n = 4/gr \, mole \, O_2 = 4/32gr \, O_2 = 0.125$

$F = 96,500$ (coulomb/equivalent, coulomb is amp sec)

$CO_2 = 6.1 \, mg/L$

$d = 1.56 \, cm$

* Diffusivity of oxygen in water

then

$i_{corr} = 0.5 \, mpy$

The actual corrosion rate, i_{corr}, obtained from coupons removed from hull is 1.4 mpy or 3.04 microamps/cm^2 (Figure 5.71). Since this value of i_{corr} is higher by a factor of about three than that calculated from equation [21], hydrogen discharge in addition to oxygen reduction must occur to support a corrosion rate of 1.4 mpy. On the other hand, if the cathodic reaction occurs in the concretion, d could be as low as 0.6 cm near the concretion/water surface, thus the calculated corrosion rate would agree with the rate determined from coupon measurements. The latter would seem to be a simple solution if the cathodic reaction did indeed occur in the concretion.

Ultrasonic Thickness Evaluation

Because of the intrusive nature of the direct measurement technique, it is impractical to remove hull coupons at multiple locations around *Arizona*'s hull. The eight coupons removed in 2002 provided direct measure of corrosion rate in eight representative locations, and became control sites for applying less intrusive methods for measuring hull thickness to reliably predict corrosion rate. A major project goal was to test nondestructive hull thickness measurement techniques. In June 2001, an ROV-mounted Cygnus ultrasonic thickness gauge attached to a VideoRay ROV was used in an attempt to measure interior compartment bulkhead thickness.

Prior to mounting on the ROV, the gauge was calibrated to a 0.5 in steel test block in air. Since bulkhead readings varied from less than 0.2 in. to nearly 0.75 in. (on the same bulkhead, sometimes in the same location), it was concluded that the data were not accurate either because the unit could not compensate for marine corrosion deposits on the surface of the metal or there was electrical interference between the sensor and the ROV. In December 2001, NPS-SRC tested a diver-deployed Cygnus 1 Underwater Multiple Echo Ultrasonic Digital Thickness Gauge on *Arizona*'s hull at frame 85, in the location where concretion samples were removed during in situ E_{corr} and pH data collection (see above). This instrument proved to be unreliable (consistent, reproducible readings were unobtainable), even with significant grinding, polishing, and other surface preparation.

Because precise hull thickness is known in the location of each of the eight hull coupons collected in 2002, those locations were selected for further ultrasonic thickness (UT) instrument testing. For 2003 fieldwork, another instrument was tested. Dr. Art Leach from Krautkramer Ultrasonic Systems (Lewiston, PA, now GE Inspection Technologies) recommended their UT products, and arranged for Mr. Jay Schraan from Inspection Technologies, Inc. (Pomona, CA) to demonstrate their technology on *Arizona*. In October 2003, before beginning fieldwork in Hawaii, Dr. Leach visited NIST in Gaithersburg, Maryland, to calibrate the instrument on the hull coupons collected from *Arizona* in August 2002. This direct calibration with *Arizona* plate material allowed precise speed-of-sound measurements to be made from actual hull steel taken from the *in situ* locations to be tested.

For field operations in November 2003, a Krautkramer USN 58L ultrasonic portable flaw detector was deployed with 5 MHz composite penetration probe. The intent was to revisit the sites of five of the above-harbor bottom hull coupons collected in August 2002—because the exact hull thickness at each of these locations based on measurements made by UNL researchers was known, these locations made ideal test sites for the UT instrument. During UT operations, NPS researchers worked underwater to prepare the hull's surface and deploy the probe, while Johnson and Schraan worked topside with the instrument's user interface. The readings were again widely variable. In a final effort, surface preparation of hull metal included chipping off the strongly adhering inner oxide layer between the concretion and steel surface, and using a pneumatic grinding wheel to flatten the steel surface. The readings were still inconsistent with coupon data, even at locations where the surface was ground shiny and smooth. It was then

thought that concretion on the interior side had some effect on the readings. This issue has not been resolved, but the data does have promising application.

Eliminating extreme data, an error of less than 10% is the best that can be expected from this technology (Table 5.36). A 10% error translates to an error of 0.1 mpy at a 1.0 mpy corrosion rate, or 0.3 mpy at a 3 mpy corrosion rate, which is as good as coupon sampling could produce. The wide variation between sample location USAR-03-001 and USAR-03-007 reflect the roughness due to corrosion from both sides in each case. However, pitting or roughness is shallow and, as a result, corrosion on *Arizona* was uniform. Based on the above limitations, the trend line relating i_{corr} to water depth from UT is given by:

$$i_{corr} = 6.04 - 0.23D \text{ (mpy)} \tag{22}$$

For comparison, the trend line relating i_{corr} to water depth from coupon data is:

$$i_{corr} = 2.956 - 0.05D \text{ (mpy)} \tag{23}$$

Researchers from Inspection Technologies, Inc. returned to *Arizona* in November 2004 to apply new methodology to UT measurements, and to expand the survey beyond the original data points. Different probes were used, including a KBA 560 and an ISS probe. Because of the focus on frames 70–90 for the FEM, UT data were obtained in vertical transects as close to frames 70 and 90 as possible—three test points were selected in each vertical transect. Although better, more consistent results were obtained, the data were still ambiguous (Table 5.37). Although UT techniques look promising, further investigation is required. It is now evident that removal of the concretion and significant surface preparation (buffing and grinding to make the surface as smooth as possible) of the steel hull is essential before consistent, repeatable readings can be obtained. In some cases, even after extensive surface preparation, there are locations where UT measurements are unreliable because of unevenness of the surface due to corrosion (Figure 5.74). Uneven coupling of the face of the UT probe against the hull has been a continuing problem.

Sample	Location	Vessel Side	Water Depth (ft.)	Original Hull Thickness (in.)	Actual Thickness from Coupons (in.)	Ultrasonic Thickness (in.)	Error (%)
USAR-03-001	Frame 76.5	Port	5	0.5	0.135	0.159	+17
USAR-03-002	Frame 76.5	Port	19.5	0.875	0.671	0.73	+8.8
USAR-03-003	Frame 76.5	Port	26	0.5	0.434	0.457	+5.4
USAR-03-007	Frame 80.5	Starboard	5	0.5	0.196	0.178	-9.1
USAR-03-008	Frame 80.5	Starboard	15	0.875	0.79	0.84	+6.4

Table 5.36. Ultrasonic measurements corresponding to hull samples, 2003.

Sample	Location	Vessel Side	Water Depth (ft.)	Original Hull Thickness (in.)	Ultrasonic Thickness (in.)
USAR-04-001a	Frame 88	Port	6	0.5	0.428
USAR-04-001b	Frame 88	Port	6	0.5	0.474
USAR-04-002	Frame 88	Port	19.5	0.875	0.588
USAR-04-003	Frame 88	Port	25	0.5	0.423
USAR-04-004	Frame 88	Starboard	4	0.5	0.31
USAR-04-005	Frame 70	Port	7.6	0.5	0.19
USAR-04-006	Frame 70	Port	19.5	0.875	0.802
USAR-04-007	Frame 70	Port	26	0.5	0.442
USAR-04-008	Frame 68	Starboard	9.6	1	0.713
USAR-04-009	Frame 68	Starboard	16.5	0.875	0.753
USAR-04-010	Frame 68	Starboard	22.5	0.5	0.277
USAR-04-011	Frame 88	Starboard	16.5	0.875	0.466
USAR-04-012	Frame 87	Starboard	21	0.5	0.411

Table 5.37. Ultrasonic measurements corresponding to hull samples, 2004.

Figure 5.74. Steel surface of Arizon's hull after extensive preparation. Part of the strongly adhering layer below the concretion remains at top. Uneven steel surface is due to corrosion (NPS Photo by Brett Seymour).

Concretion Equivalent Corrosion Rate (CECR)

Because determining hull corrosion rate through direct measurement as described above is destructive and impractical, and because determining steel hull thickness with ultrasonic technology has proved unreliable, alternative indirect indicators of steel hull corrosion rate have been sought. The most promising indirect method for determine *Arizona*'s steel hull corrosion rate is correlation between hull iron loss and concretion iron gain, as measured through concretion analysis. External hull concretion analysis and its relationship to corrosion on USS *Arizona* began in the late 1980s. Henderson (1989) scraped samples of concretion from the hull, dried and weighed them, and separated the magnetic corrosion products with a bar magnet. In 1998, Johnson converted the data generated by Henderson (1989) to corrosion rate in mpy to illustrate that analysis of the concretion may have merit as a way to determine corrosion rate (Johnson, et al. 2003). Based on these observations, x-ray diffraction (XRD) and environmental scanning electron microscopy (ESEM) studies on USS *Arizona* concretion were initiated in 1999 at UNL to better understand in what form the iron exists in the concretion and how the metal hull and the concretion interact. Subsequently, x-ray studies were continued at Eglin Air Force Base, Florida and the University of Florida. Using XRD data, De Angelis (2002) identified the iron minerals siderite ($FeCO_3$), with lower residuals of aragonite ($CaCO_3$) and magnetite (Fe_3O_4), as the primary constituents in the concretion (Johnson, et al. 2003:91-92; Johnson, et al. 2006a, 2006b)(see above). Measuring distribution of iron in the concretion cross-section using ESEM and x-ray fluorescence (XRF), Johnson used graphical integration to determine the mean (total) iron content, the result, 40% to 50% by weight, was close to the same iron content obtained from chemical analysis of a sample representing the total thickness of the concretion (Johnson, et al. 2003:96-97). Data from *Arizona* concretion analysis revealed that the specific weight of the concretion per unit area (density x thickness) and total iron in concretion in weight percent (%Fe) decreases with water depth (Figure 5.75). The equation expressing the relationship between weight %Fe and water depth is given by:

$$\text{Wt\% iron} = -1.0621D + 50.12 \qquad\qquad [24]$$
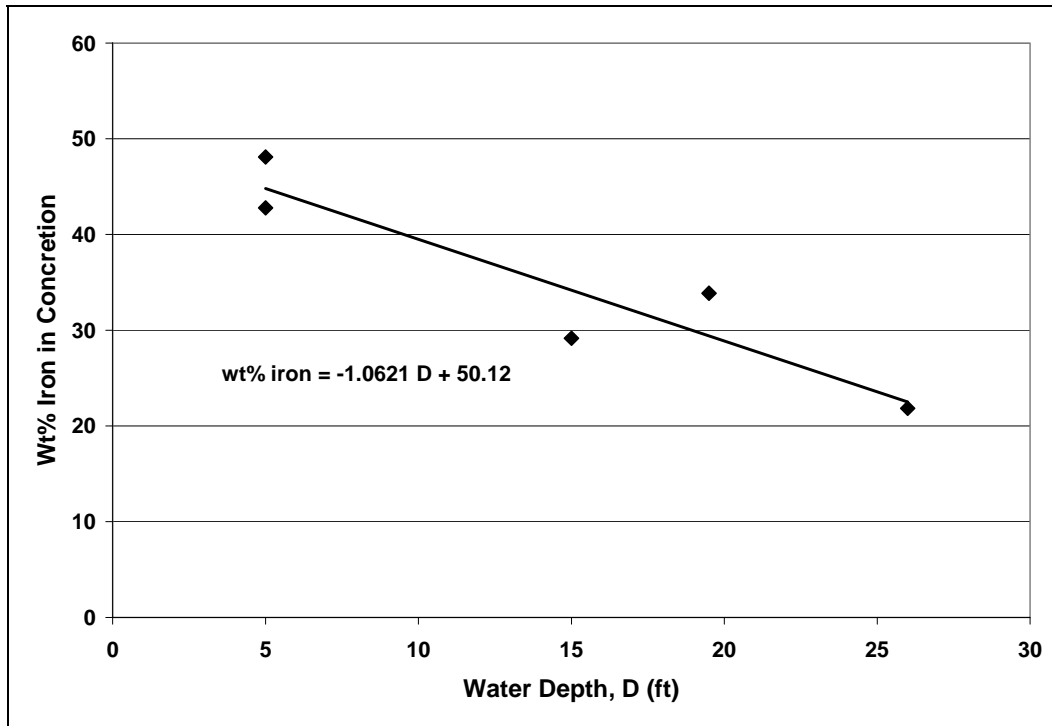
Figure 5.75. Weight % iron vs. water depth.

At the same time, concretion density, measured using standard methodology described in ASTM D572-00, also decreases with water depth, as expressed by the equation:

$$\rho = 2.3903 - 0.0027D \text{ (gr/cm2)} \qquad [25]$$

Corrosion rate, based on direct measurement analysis of hull coupons, shows a similar trend—corrosion rate decreases with water depth (Figure 5.71 and Table 5.34). Based on these results, Johnson developed a quantitative expression relating the metal lost in a specific cross-section of steel hull, and the metal gained by the concretion in the same overlying cross-sectional area (Russell, et al. 2006). The technique was refined using samples of concretion obtained from *Arizona*'s hull in 2003 and 2004. Concretion samples from 2003 and 2004 were acquired using a 3-in (7.5-cm) hole saw bit with a pneumatic drill. After the samples were removed, each location was sealed with a pH-neutral marine epoxy—others have recommended hydraulic cement (see Mardikian 2004:147).

The Concretion Equivalent Corrosion Rate (CECR) expresses corrosion rate determined from iron content, density and thickness of the concretion. This equation is based on the assumption that iron ions generated at the concretion/metal interface are captured by the concretion as $FeCO_3$ by replacement of calcium in calcium carbonate. The specifics of the exchange of calcium for iron are not well understood and are under study. To a lesser extent, iron also forms magnetite and other oxides and oxychlorides, as discussed in an earlier section. Combination of density, thickness and iron content yield the following equation in English units (mpy) as derived by Johnson:

$$i_{corr} = \frac{0.5 \times p \times wt\% \ Fe \times d}{t} \qquad [26]$$

where

i_{corr} is corrosion rate (mpy)

% Fe is weight percent iron in concretion (dry basis)

p is concretion density (gr/cm^3)

d is concretion thickness (cm)

t is exposure time in years (yr)

0.5 is a unit conversion constant

Using SI units in µm/yr, the equation becomes:

$$i_{corr} = \frac{12.7 \ x \ p \ x \ wt\% Fe \ x \ d}{t} \qquad [27]$$

where the variables in equation [26] are defined, but with a unit conversion constant of 12.7.

Physical and chemical properties for 16 concretion samples and corresponding corrosion rates calculated from equations [26] and [27] are tabulated in Table 5.38. Corrosion rates from direct measurement of hull coupons and concretion analysis are compared in Figure 5.76. The actual corrosion rate obtained from metal coupons is higher than that predicted by concretion analysis using equation [26], as indicated by the separation between the two trend lines. The reasons for the difference are: (1) higher initial (pre-concretion) corrosion rates that produced

Sample	Thickness	Density*	Total Iron**	Water Depth		$i_{corr(conc)}$	
	cm	g/cm3	%Fe	ft	m	mils/yr	µm/yr
USAR-02-005	0.51	2.26	22.20	34.00	10.36	0.21	5.33
USAR-02-006a	1.15	2.25	26.00	34.00	10.36	0.55	14.01
USAR-02-006b	0.95	2.41	45.20	34.00	10.36	0.85	21.50
USAR-03-001	2.50	2.53	42.78	5.00	1.52	2.18	55.40
USAR-03-002	1.20	2.34	33.86	19.50	5.94	0.77	19.48
USAR-03-003	1.00	1.92	21.83	26.00	7.92	0.34	8.59
USAR-03-008	1.80	2.44	29.15	15.00	4.57	1.03	26.22
USAR-04-002	2.10	2.43	42.09	19.50	5.94	1.70	43.30
USAR-04-003	1.89	2.39	46.95	26.00	7.92	1.68	42.75
USAR-04-005	1.82	2.30	29.88	5.00	1.52	0.99	25.21
USAR-04-006	1.84	2.55	43.77	19.50	5.94	1.63	41.40
USAR-04-007	1.39	2.29	41.23	26.00	7.92	1.04	26.46
USAR-04-008	2.36	2.41	45.86	5.00	1.52	2.07	52.58
USAR-04-009	1.95	2.47	48.16	15.00	4.57	1.84	46.76
USAR-04-010	1.34	2.47	34.75	22.00	6.71	0.91	23.19
USAR-04-011	2.19	2.34	46.69	15.00	4.57	1.90	48.23
USAR-04-012	1.71	2.43	34.25	22.00	6.71	1.13	28.69

*Density measurements were made in accordance with ASTM D792-00

**Dry basis

Table 5.38. Physical and chemical properties of concretion as a function of water depth.
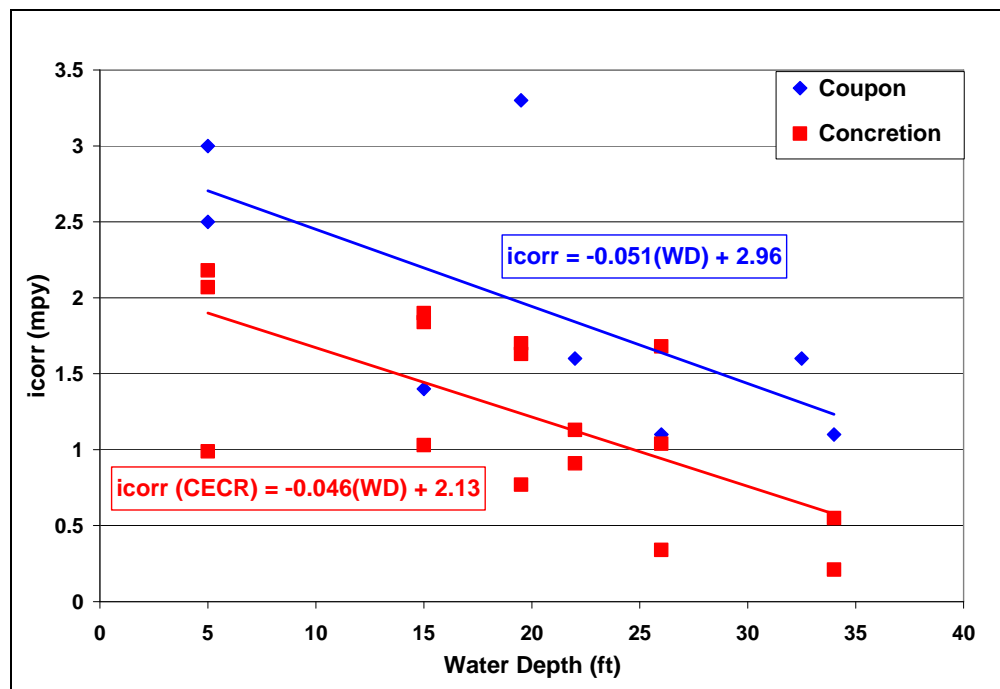
Figure 5.76. Comparison of the corrosion rate on *Arizona* compiled from both coupon data and concretion iron content measurements as a function of water depth.

232

soluble iron that was not incorporated into concretion; (2) formation of an oxide layer between the steel surface and the concretion, which is not captured during concretion removal and therefore the iron within it is not included in the analysis; and (3) possible corrosion on the interior side of the hull plates. Analysis of the ratios of the two trend lines in Figure 5.76 reveals that corrosion rates obtained from the coupons using the direct measurement technique is higher than corrosion rates predicted by the concretion constituent analysis by a factor of 1.6. With this ratio factored in, a general equation for estimating corrosion rate directly from physical and chemical concretion properties is given in equation [28], where the constants in equations [26] and [27] are multiplied by 1.6 for English and SI units respectively to yield an expression for the actual corrosion rate, defined as the Concretion Equivalent Corrosion Rate (CECR):

$$CECR = \frac{K \times p \times wt\% \ Fe \times d}{t} \qquad [28]$$

where

$$K = \quad 0.8 \text{ for units in mpy}$$
$$K = \quad 20.32 \text{ for units in } \mu m/yr$$

Note: Density is given on a wet basis whereas iron content is given on a dry basis. The correction factor 1.6 takes this into account.

Based on the results to date, concretion constituent analysis appears to be a viable proxy, minimum-impact method for estimating corrosion rates for steel vessels in seawater. Calculated CECRs between frame numbers 70 and 90 on *Arizona*'s hull are consistent with coupon analysis at frame 75. Although CECR (equation [28]) is based on analyzing concretion from the *Arizona*, further analysis continues at other sites to confirm the correction factor of 1.6 where variables such as temperature, flow velocity, organic activity, pH, salinity, and oxygen concentration may be different (Wilson, et al. 2007). A correction factor for other sites may be derivable from such variables on-site where testing is ongoing, and further refinements to the equation may be necessary.

Correlation with Environmental Parameters and Application to Interior Compartments

The preceding work focused on correlating corrosion rates obtained from direct measurement techniques from hull coupons with corrosion rates calculated from physical and chemical concretion properties on *Arizona*'s outer hull near frame 85. These correlations allow prediction of corrosion rates in other external hull areas directly accessible to researchers for concretion sample removal. A methodology for predicting corrosion rates in inaccessible hull areas, such as the outer hull below the harbor bottom and interior spaces, is also necessary to create a viable FEM of *Arizona*'s hull. While previous work correlates corrosion rate with water depth, it is believed that depth is likely a characteristic that actually represents numerous other physical and chemical properties more directly determinative of the corrosion process itself. Direct correlation with other known corrosion parameters, such as dissolved oxygen concentration, pH, temperature, the ratio of oxygen concentration to concretion thickness, and oxygen and iron mobility through the concretion, is the next step in a holistic evaluation of corrosion on *Arizona*.

Initial work in this area began with preliminary analysis of interior water chemistry data collected with the YSI sonde deployed on the VideoRay ROV. For example, average oxygen levels in Warrant Officers State Rooms 12 and 14 on the second deck, as well as the hallway between them, was about 3 mg/L. Equation [14] gives the corrosion rate as a function of oxygen concentration, diffusion layer thickness and oxygen diffusivity where oxygen reduction is assumed to be the only cathodic reaction. The latter may be a reasonable assumption since concretion is apparently limited in interior compartments and may not support hydrolysis and evolution of hydrogen to the extent that it does on exterior surfaces. Collecting the constants in equation [21]:

$$i_{corr} \text{ (O}_2 \text{ reduction, mpy)} = 5{,}550 \text{ D(cm}^2\text{/sec)[C[O}_2\text{] mg/L]/ [d(cm)]} \qquad [29]$$

where

$$J \text{ (O}_2 \text{ flux, gr/cm2/sec)} = DC(O2)/d$$

Assuming a constant value of d = 0.2 cm for diffusion thickness, D = 2.45 x 10^{-5} and C[O$_2$] = 3 mg/L, the corrosion rate in interior spaces on the second deck, estimated from equation [29], is 2 mpy.

Over a 61 year period, 0.002 x 61 = 0.12 in., indicating that slightly more than 0.1 in. of bulkhead thickness has corroded away. On 10 lb/ft.^{2} bulkhead plate (¼ in.), this would mean that on average 60% of the plate remains, and within about 15 years, one-half plate thickness will remain. This is a rough estimate but the numbers illustrate the utility of this approach if better information can be obtained with regard to oxygen concentration and concretion thickness in interior compartments.

Oxygen availability is the primary variable driving corrosion and has led the authors to arrive at to two different models related to the role of oxygen in the corrosion process. The first model assumes that both anode and cathode reactions occur at the metal surface and have a direct correlation to oxygen concentration, pH and bacterial activity at the metal/concretion interface and an indirect correlation to numerous environmental parameters at the concretion/seawater interface. The second model, according to MacLeod (1982), assumes that while the anode reaction occurs at the metal surface, the cathode reaction(s) occur in the concretion at or near the concretion/water interface. The basis for these interpretations centers on the concretion and its role as a barrier to the transport of oxygen to the metal surface. Limiting current density (equation [14]) is useful in this discussion to predict the corrosion rate based on local environmental conditions. It should be noted that diffusivity values used in equations [21] and [29] are those of molecular oxygen (O$_2$) in water assuming that the void spaces are filled with water and allow diffusion of O$_2$ through a tortuous yet continuous path from sea water to the metal hull surface. The accuracy of the calculated corrosion rate is dependent on the accuracy of the diffusion coefficient (D). For the *Arizona* site, the published value of D at 25° C is used directly. At other sites, however, such as that of the Japanese Midget Submarine submerged off the coast of Oahu in deep, cold water, a correction for D must be made, as outlined above, that includes knowledge of several environmental parameters, including oxygen saturation, salinity, temperature, oxygen concentration, and viscosity. Limiting current density is used in this study as a quantitative methodology to estimate corrosion rate by incorporating a variety of environmental variables mentioned above.

Model 1: Cathode Sited at the Metal Surface

Assuming that the cathode reaction occurs at the metal surface, the value of d or length of the diffusion path for oxygen is approximately equal to the thickness of the concretion. These measurements are obtained *in situ* on the hull or measured later in the laboratory after concretion samples are removed and transported to UNL laboratories. In a typical example given by equation [21], the result for the external hull concludes that the corrosion rate predicted by oxygen consumption is lower than that actually observed by a factor of three. Since oxygen is depleted at the surface and does not satisfy the total demand for electron consumption, the difference is associated with influx of chlorine ions, the formation of HCL, and the lowering of pH. The hydrogen ions gain electrons from iron as it corrodes, and hydrogen gas is released as a result of the combination of two neutralized atoms (equation [4]). Hydrogen accumulates between the concretion and the hull and gradually migrates through the concretion to sea water either by diffusion or by migration through fissures in the concretion. Hydrogen discharge is relatively slow but accelerates in the presence of SRB as discussed above.

These theoretical considerations are summarized in Figure 5.77, a polarization diagram that characterizes Model 1, in which potential (E, SHE, mV) is plotted versus corrosion current or rate (mpy). Anodic polarization (Fe to $Fe^{+2} + 2e$) is derived from a composite of Tafel expressions (Table 5.35). The composite expression is given by equation [31] and plotted as line (d):

$$E_{corr} = 30 \log(i_{corr}) - 354 \tag{31}$$

Cathodic polarization resulting from hydrogen discharge is expressed by equation [11] with data derived from Jones (1996:99) where $E° = -59.2$ pH (mV), $\beta = 100$ mV/decade and $i° = 0.46$ mpy. The result is plotted on Figure 5.77 at pH = 3, 4, 5 and 6, typical values at the metal/concretion interface from Tables 5.7–5.18 and identified by span (c). Span (a) defines the region corresponding to limiting current density or calculated corrosion rate (equation [14]) resulting from   oxygen consumption shown by the vertical lines between 0.35 to 1.3 mpy. The actual corrosion rates from coupon data (Figure 5.71) are identified in span (b) between vertical
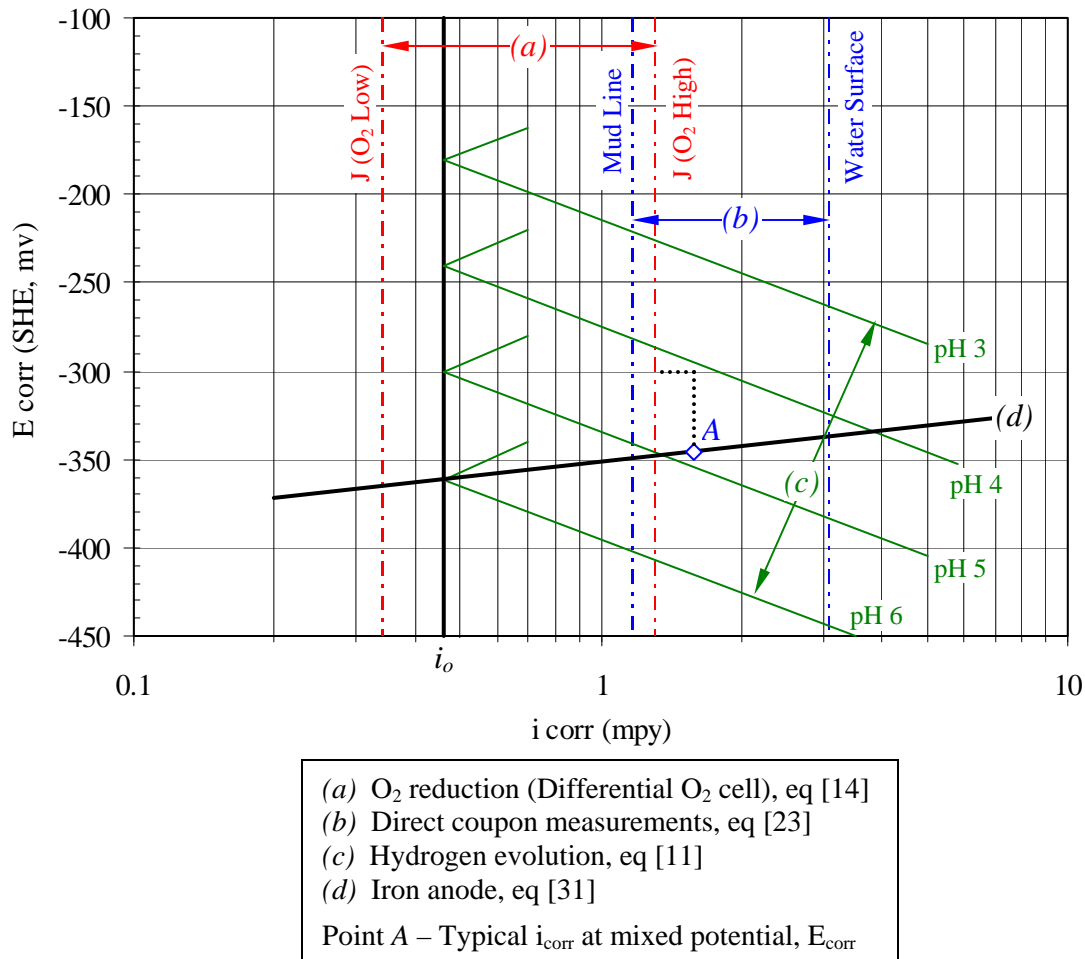
Figure 5.77. A polarization diagram plotting corrosion potential versus corrosion rate.

lines at near 1.2 and 3 mpy. Two cathodic reactions support corrosion and mixed potential

theory shows a typical corrosion rate at point A. Point A lies on the dotted line representing

interaction between oxygen reduction and hydrogen discharge at its point of intersection with

anodic polarization, line (d). At the mixed potential, resulting typical values of E_{corr} and i_{corr} are

shown in span (b). There is a wide variation in concretion thickness from the surface to the

harbor bottom (Figure 5.78). According to equation [14], i(L) is inversely proportional to

concretion thickness, hence oxygen concentration at the surface is highly variable from point to

point promoting differential oxygen cell corrosion. As a result, oxygen flux (J) is identified

corresponding to low and high availability of oxygen (Figure 5.77). The result is differential

oxygen cell corrosion as discussed in an earlier section. There is a wide variability in pH at the

The chart shows Concretion Thickness, d (mm) on the y-axis (0 to 35) versus Water Depth (ft) on the x-axis (0 to 40), with the equation y = -0.066x + 19.41.
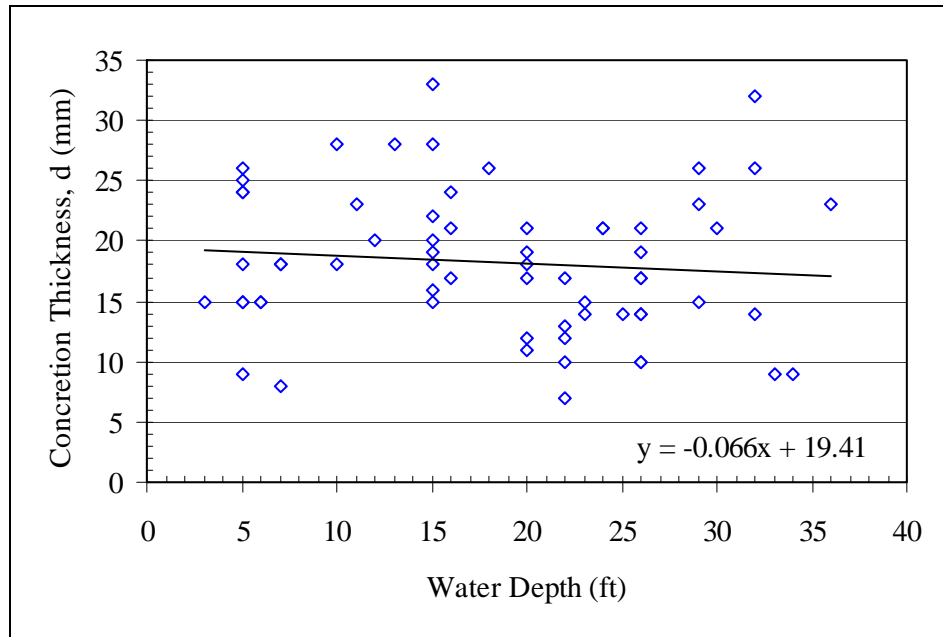
Figure 5.78. Concretion thickness as a function of water depth.

metal concretion interface with minimum pH at the sites where the concretion thickness is greatest (Figure 5.79). As oxygen consumption continues, the net oxygen level remains low on the metal surface and hydrolysis continues to maintain acidic conditions at the metal surface.

In review, oxygen consumption alone does not support the actual corrosion rates of between 1 and 3 mpy. The result concluded from this analysis is that hydrogen discharge is significant in controlling the rate of corrosion at a majority of sites on *Arizona*, although the driving force is the availability of oxygen at the concretion/metal interface as dictated by the oxygen concentration and thickness of the concretion at a particular location on the hull. The evidence for hydrogen discharge is quite evident from on-site observations of gaseous bubbles emerging from concretion and from the low pH values obtained from *in situ* data collected at numerous sites around the hull. During one field operation, a drill hole through concretion resulted in a significant flow outward of water as the bit was withdrawn. As the water poured out of the hole, it made contact with surrounding water at a pH of approximately 8. The result was immediate precipitation of iron as iron hydroxide (discussed above).
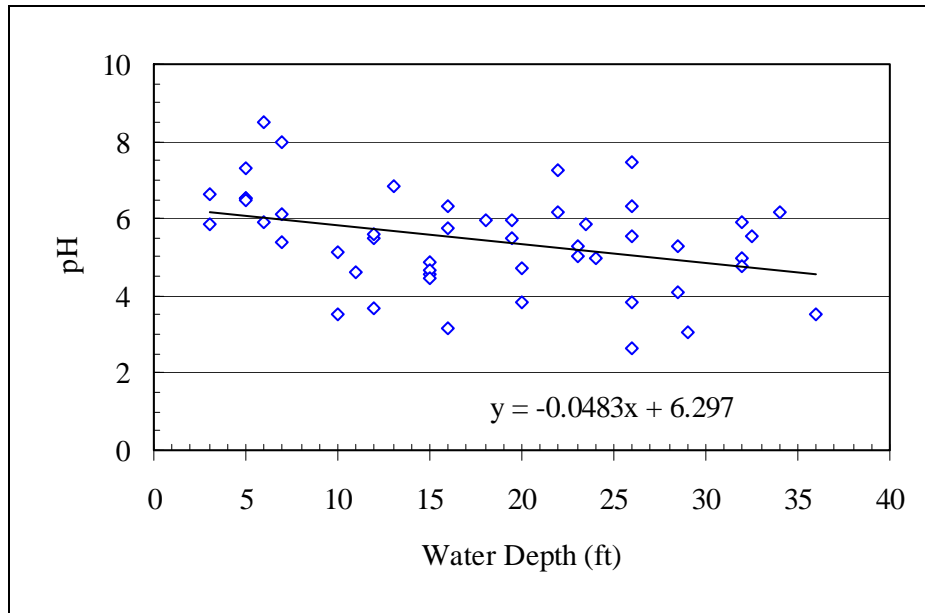
Figure 5.79. pH at metal/concretion interface as a function of water depth.

Model 2: Cathode Sited in Concretion

As mentioned above, MacLeod (1982) and North (1976) identify the concretion/seawater interface as the site for cathodic oxygen reduction. To carry this concept a step further, if the cathodic reaction takes place inside the concretion, a value of d can be determined from equation [14] that will satisfy a known value of i_{corr}. For example, solving equation [14] for d knowing C and i(L) (i_{corr}) in mpy, a diffusion thickness of $d = 0.6$ cm allows adequate oxygen diffusion to support a corrosion rate of 1.4 mpy without hydrogen discharge. There are several issues that make this model attractive in addition to the calculations above. Based on readings taken during *in situ* drilling and measurement sequences, the steel surface E_{corr} is consistently negative to readings taken inside the concretion and at the seawater/concretion interface. This would suggest that cathodic oxygen reduction could occur at the concretion/sea water interface or inside the concretion. Based on concretion properties, it has been determined that retained water is on the order of 20-30 wt %. Assuming there is continuity of path from open seawater to the hull surface, the concretion is an ionic conductor, and hence iron ions can migrate from the hull surface through the concretion to seawater, with chlorine ions migrating in the opposite direction. What is missing in this model is the ability of the concretion to conduct electrons.

Electrons are released during corrosion, and in order to maintain charge balance during oxidation of iron to Fe^{+2}, these electrons must be consumed at cathode sites. Since neither water nor concretion minerals conduct electrons, the cathode and anode must be located adjacent to each other on the metal surface or connected electrically somehow through a conducting path. The former seems to be the only feasible explanation.

Summary

Model 1, preferred by the authors, was not considered for some time as a reasonable explanation of factors controlling corrosion of *Arizona*, and Model 2, proposed by MacLeod, prevailed. Model 1 was reconsidered, however, upon a detailed analysis of a Japanese Midget Submarine, submerged in 1300 ft. of water just outside the entrance to Pearl Harbor (Wilson, et al. 2007). Applying the environmental parameters specific to that site to equation [14], it was concluded that oxygen does satisfy the demand for electron consumption in deep water at the Midget Submarine site, whereas just the opposite is the case on *Arizona* in shallow water. The major difference between the two is concretion thickness. On *Arizona*, concretion thickness averages about 2 cm, but with wide variability, whereas the Midget Submarine concretion thickness averages 0.4 cm, with much less variability. Based on equation [14] and XRD data, it has been proposed that the corrosion rate on the Midget Submarine is limited by the formation kinetics of minerals in the concretion (Wilson, et al. 2007). As a result of data comparisons on these submerged vessels, i(L) (equation [14]) has become an important marker to determine controlling factors at differing geographical and sea depth locations. Oxygen availability is the primary variable that determines how fast corrosion will proceed. For relatively short term exposure to sea water, oxygen concentration at the steel surface is the same as oxygen concentration in the open water and dictates the corrosion rate. However, for long term exposure at moderate water depth where marine organisms exist, concretion accumulation creates a barrier to oxygen permeation and the chemistry at the metal surface beneath the accumulating concretion becomes much different that it would be in the absence of concretion. pH and E_{corr} have been determined at the interface by drilling through the concretion to the metal surface. Although there are limitations to this approach because of unavoidable dilution in the drill hole, the results provide insight into the corrosion process and have lead to the conclusion that three

processes occur to establish a steady state corrosion rate. Cathodic reactions include hydrogen discharge and oxygen reduction or consumption. The two combine to create a mixed corrosion potential and corresponding corrosion rate. As oxygen consumption continues, low oxygen is maintained at the metal surface. Differential oxygen cell corrosion is a contributing factor because of locally large variations in concretion thickness (Figure 5.78). An attempt has been made to characterize these processes on the polarization diagram (Figure 5.77). To further understand these interactions, a spectroscopic study of metal/concretion interface chemistry is recommended for future study.

CONCLUSIONS

CONCRETION ANALYSIS

Concretion acts as a sink for iron corroded from the adjacent steel hull, accounting at one location for about 60% of the iron lost from the hull. Based XRD data, iron appears primarily as iron carbonate with lesser amounts of magnetite. These observations are confirmed from *in situ* E_{corr} and pH measurements by superimposing the data on a calculated potential/pH Pourbaix diagram. The data corresponds to fields stable with respect to iron carbonate and magnetite.

Based on a variety of data and methods of analysis, a comprehensive understanding of corrosion processes occurring on the hull above the harbor bottom has been accomplished. With this information as background, analysis of corrosion at and below the harbor bottom and in interior compartments can be inferred, however, research should continue to further refine calculated corrosion rates on inaccessible hull components.

XRD of concretion reveals the compounds $FeCO_3$, $CaCO_3$ and Fe_3O_4. A mean iron content of 53% is calculated from ESEM data while XRF reveals 43% on a different sample. Direct chemical analysis of the same sample used for XRD reveals comparable iron content. Superposition of E_{corr}/pH data on the water-iron-CO_2 system confirms the presence of siderite and magnetite from the steel hull through the concretion cross-section to sea water. Results indicate that concretion characteristics vary as a function of water depth. Studies continue to correlate these properties with iron content and corrosion rate. The relationship between CECR

and the limiting current corrosion rate (equation [14]) have lead to a more comprehensive understanding of the corrosion process on *Arizona*.

CORROSION RATE

Sufficient data at exterior hull locations are now available to determine corrosion rates from the water surface to the harbor bottom, port and starboard. While hull coupon sampling was only undertaken at frame 75, previous E_{corr} transect surveys indicate that this data is typical of corrosion rates anywhere along the hull in contact with sea water above the harbor bottom. Corrosion rate data in Table 5.34 suggest that the corrosion rate is slightly higher on the port side above about 20 ft.—below that, the rates converge to equivalent values. On the exterior hull, the corrosion rate follows the empirical equation derived from the best fit for combined data, port and starboard, which is valid to just above the harbor bottom:

$$i_{corr} = \ 2.956 - \ 0.050 \ WD) \hspace{3cm} [31]$$

where

i_{corr} is the corrosion rate in mpy

WD is water depth in ft.

As a heuristic device, based on this data, time interval from August 2002 until the plate thickness is reduced to one–half its original thickness can be determined. One–half original thickness was arbitrarily taken as a thickness below which structural integrity is severely compromised, although the FEM provides a more precise value (see Chapter 6). At 5 ft., port, 27% of 20 lb. plate remains whereas at 5 ft. starboard, 40% of 20 lb. plate remains. Both sides have exceeded the one-half thickness criteria. At 19½ ft., port, 77% of 37½ lb. plate remains whereas at 15 ft., starboard, 90% of 37½ lb. plate remains. These data translate to time to one–half thickness of 130 years, port, and nearly twice that time, starboard. At 26 ft., port, 87% of 20 lb. plate remains whereas at 22 ft., starboard, 81% of 20 lb. plate remains. These data translate to time to one–half thickness of 160 years, port, and about 90 years, starboard. Below the harbor bottom at 34 ft., port, 90% of 25 lb. plate remains whereas at 32½ ft. starboard, 87%

of 30 lb. plate remains. These data translate to time to one–half thickness of 220 years port, and 170 years starboard.

Based on metal coupon analysis at frame 75, the corrosion rate on the USS *Arizona*'s exterior hull is approximately 3.0 mpy near the surface and decreases by nearly one third to about 1.0 mpy just below the harbor bottom. By comparison, corrosion rates for unconcreted steel in open seawater at the surface are reported to be in the 4–8 mpy range (Schumacher 1979:xx). Lower than predicted corrosion rates are directly related to metal concretion interaction, and subsequent decreased oxygen availability.

Oxygen availability, as related to direct cathodic oxygen reduction and differential oxygen cell corrosion, is the most significant variable in the corrosion process on the hull. Electrical conductivity and cation/anion transport through the concretion are also important variables. Depletion of oxygen at the steel/concretion interface leads to hydrolysis and a decrease in pH. At numerous sites, E_{corr} relative to SHE is below the potential required for hydrogen reduction, so it is not surprising to observe hydrogen evolution around the hull. Corrosion rate and E_{corr} decrease with water depth, as is consistent with a decreasing oxygen concentration to the harbor bottom. The observation that E_{corr} increases as i_{corr} increases confirms the original observation made by MacLeod (2002). Oxygen concentration inside the torpedo blister decreases into the harbor bottom, suggesting the same behavior occurs beneath the harbor bottom. Calculated limiting current density is used as a diagnostic tool to identify the role of oxygen consumption and hydrogen discharge in the corrosion process. For assessing corrosion rate of *Arizona*'s hull, direct measurement of hull thickness and comparing to original thickness is the most accurate methodology, but obviously it is impractical for quick and cost effective assessment. An alternative methodology developed on USS *Arizona* by University of Nebraska –Lincoln researchers, CECR, is beginning to prove itself in this and other applications as a minimum-impact approach for assessing corrosion rate.

The deterioration rate of *Arizona*'s hull will increase with time because corrosion from both sides of hull plate will accelerate due to the entry of fresh sea water from the top down. Steel-hull coupon samples USAR-02-001 and USAR-02-007 have reached the one-half thickness criteria and there is evidence that this is already beginning to occur on USAR-02-002. The predictions of corrosion to one-half thickness in 200 years or more on the originally thickest plate are probably optimistic in view of the accelerated corrosion that will occur with time from

the top down. It should be emphasized that corrosion rates are reported as uniform average values although localized shallow pitting is evident.

At the harbor bottom and below, where most of the fuel oil is bunkered, steel-hull coupon samples USAR-02-004 and USAR-02-010 show that the corrosion rate remains constant or increases somewhat, consistent with potential increased bacterial activity in this region. How far this region extends into the harbor bottom is unknown, although current evidence suggests that corrosion rates below the harbor bottom and in interior compartments of *Arizona* remain low.

REFERENCES

Anonymous
    1975 *Metals Handbook, Failure Analysis and Prevention*. 8th ed 10. American Society for Metals.

Cook, E.
    1937 *Open Hearth Steel Making*. ASM International, Cleveland.

DeAngelis, R.
    2002 *X-Ray Diffraction and Environ mental Scanning Electron Microscope Investigation of Concretion from the USS Arizona*. Manuscript on File at National Park Service, Santa Fe.

Felkins, K., J. Leighly, H.P and A. Jankovic
    1998 The Royal Mail Ship Titanic: Did a Metallurgical Failure Cause a Night to Remember? *Journa of Metals* 50(1):12-18.

Fontana, M. G.
    1986 *Corrosion Engineering*. 3rd ed. McGraw-Hill, New York.

Gregory, D.
    1999 Monitoring the Effect of Sacrificial Anodes on the Large Iron Artefacts on the Duart Point Wreck, 1997. *International Journal of Nautical Archaeology* 28(2):164-173.

Henderson, S.
    1989 Biofouling and Corrosion Study. In *Submerged Cultural Resources Study: USS Arizona Memorial and Pearl Harbor National Historic Landmark*, edited by D. J. Lenihan, pp. 117-156. Submerged Resources Center Professional Papers No. 9. National Park Service, Santa Fe.

Husler, J. and C. Dodson
    2003 *X-Ray Fluorescence Analysis of Concretion*. Manuscript on File at National Park Service, Santa Fe.

Johnson, D. L., J. D. Makinson, R. DeAngelis, B. M. Wilson and W. N. Weins
    2003 *Metallurgical and Corrosion Study of Battleship USS Arizona, USS Arizona Memorial, Pearl Harbor*. Manuscript on File at National Park Service, Santa Fe.

Johnson, D. L., W. N. Weins and J. D. Makinson
    2000 Metallographic Studies of the U.S.S. Arizona. In *Microstructural Science Vol. 27: Understanding Processing, Structure, Property, and Behavior Correlations*, edited by W. N. Weins, pp. 85-91. ASM International, New York.

Johnson, D. L., B. M. Wilson, J. D. Carr, M. A. Russell, L. E. Murphy and D. L. Conlin
2006a Corrosion of Steel Shipwrecks in the Marine Environment: USS Arizona - Part 1. *Materials Performance* 45(10):40-44.

2006b Corrosion of Steel Shipwrecks in the Marine Environment: USS Arizona - Part 2. *Materials Performance* 45(11):54-57.

Jones, D. A.
1996 *Principles and Prevention of Corrosion*. 2nd ed. Prentice Hall, New York.

Kerr, R. A.
2001 Life-Potential, Slow, or Long Dead. *Science* 294(5548):1820-1821.

Korb, L. J.
1987 *Metals Handbook: Volume 13, Corrosion*. 9th ed. American Society for Metals.

Lenihan, D. J. (editor)
1989 *Submerged Cultural Resources Study: USS Arizona Memorial and Pearl Harbor National Historic Landmark*. Submerged Resources Center Professional Papers No. 9. National Park Service, Santa Fe.

Little, B. J., R. I. Ray and R. K. Pope
2000 Relationship Between Corrosion and the Biological Sulfur Cycle: A Review. *Corrosion* 56(4):433-443.

MacLeod, I. D.
1982 The Electrochemistry and Conservation of Iron in Sea Water. *International Journal of Nautical Archaeology and Underwater Exploration* 2(4):267-275.

1987 Conservation of Corroded Iron Artifacts – New Methods for On-Site Preservation and Cryogenic Deconcreting. *International Journal of Nautical Archaeology and Underwater Exploration* 16(1):49-56.

1989 Electrochemistry and Conservation of Iron in Sea Water. *Chemistry in Australia* 56(7):227-229.

1995 *In Situ* Corrosion Studies on the Duart Point Wreck, 1994. *International Journal of Nautical Archaeology* 24(1):53-59.

2002 In Situ Corrosion Measurements and Management of Shipwreck Sites. In *International Handbook of Underwater Archeology*, edited by C. V. Ruppe and J. F. Barstad, pp. 697-714. Kluwer Academic/Plenum Publishers., New York.

Makinson, J. D., D. L. Johnson, M. A. Russell, D. L. Conlin and L. E. Murphy
2002 In situ corrosion studies on the battleship USS Arizona. *Materials Performance* 41(10):56-60.

Mardikian, P.
  2004 Conservation and Management Strategies Applied to Post-Recovery Analysis of the American Civil War Submarine H. L. Hunley (1864). *International Journal of Nautical Archaeology* 33(1):137-148.

McCarthy, M.
  1988 S.S. Xantho: The Pre-Disturbance, Assessment, Excavation and Management of an Iron Steam Shipwreck off the Coast of Western Australia. *International Journal of Nautical Archaeology and Underwater Exploration* 17(4):339-347.

New-York-Navy-Yard
  1913 Correspondence. National Archives and Records Administration, North East Region, New York.

North, N. A.
  1976 Formation of Coral Concretions on Marine Iron. *International Journal of Nautical Archaeology and Underwater Exploration* 5(3):253-258.

North, N. A. and I. D. MacLeod
  1987 Corrosion of Metals. In *Conservation of Marine Archaeological Objects*, edited by C. Pearson, pp. 68-98. Butterworth & Co., London.

Pourbaix, M.
  1974 *Atlas of Electrical Chemical Equilibria in Aqueous Solutions*. National Association of Corrosion Engineers, Houston.

Russell, M. A., D. L. Conlin, L. E. Murphy, D. L. Johnson, B. M. Wilson and J. D. Carr
  2006 A Minimum-Impact Method for Measuring Corrosion Rate of Steel-Hulled Shipwrecks in Seawater. *International Journal of Nautical Archaeology* 35(2):310-318.

Saveur, A.
  1935 *The Metallography and Heat Treatment of Iron and Steel*. McGraw-Hill, New York.

Schumacher, M. (editor)
  1979 *Sea Water Corrosion Handbook*. Noyes Data Corporation, Park Ridge, NJ.

Uhlig, H. H. and R. W. Revie
  1985 *Corrosion and Corrosion Control*. 3rd ed. John Wiley & Sons, New York.

Wilson, B. M., D. L. Johnson, H. Van Tilburg, M. A. Russell, L. E. Murphy, J. D. Carr, R. J. DeAngelis and D. L. Conlin
  2007 Corrosion Studies on the USS Arizona with Application to a Japanese Midget Submarine. *Journal of Metals* 59(10):14-18.

Yiming, X., W. N. Weins and A. Dhir
      1992 A Metallographic Investigation of Banding Diffusion of Phosphorous in Steels. In
        Microstructural Science 20. ASM International, New York.

CHAPTER 6

Finite Element Modeling of USS *Arizona*

Timothy J. Foecke and Li Ma

INTRODUCTION

A computer-based engineering model has been constructed of an 80-ft. midships section of the wreck of USS *Arizona* in an attempt to determine the current condition of the wreck and predict its future strength as it continues to corrode. This model incorporates the findings from other components of the study, corrosion rates, structural surveys, soil testing and analysis of the concretion, into a single tool that can be used to predict how the wreck will continue to degrade.

FINITE ELEMENT MODELING

The methodology chosen for this work is finite element analysis (FEA), also known as finite element modeling (FEM). In this technique, the body under study is mathematically divided into many thousands of smaller pieces called elements. Each element is given a location, a proximity to other elements, its own mechanical properties and details about how it is connected to its neighbors and how it is allowed to deform and move. Once the structure is built of these elements in the computer, loads are applied to the model and boundary conditions are set to restrain movement. The results of the model are predictions of the deformations and

deflections that will result from that loading, as well as predictions of the stresses that each element, and thus each piece of the body, will experience.

BUILDING THE MODEL

Rather than model the entire ship at a much coarser level, it was decided to choose a representative section of the ship to model with higher precision. The section of the wreck adjacent to the monument, between frames 70 and 90, was selected for several reasons. First, as will be seen, detailed original ship's plans are readily available for this portion of the ship. Accurate original plans are a necessary starting point for constructing a viable, accurate model. Second, the blast from the bomb detonated in the forward magazines and sank the ship, at least in film evidence examined, seems to have primarily vented up the main stack as it moved aft, and thus the region from frames 70 to 90 were likely less damaged below decks than regions further forward, although historical evidence suggests there was damage evident as far back as frame 78 (see Chapter 3). Nonetheless, this region of the ship likely experienced effects from the blast and subsequent fire, which may elevate corrosion rates compared to unaffected areas (see Chapter 5). Modeling this section of the ship therefore builds an element of conservatism into the model. Finally, this region of the ship is primarily composed of engine spaces below and working spaces above, and it is free from massive structures such as main gun barbettes that would make the results more difficult to generalize to other regions of the ship.

The National Park Service (NPS) Submerged Resources Center (SRC) provided the National Institute of Standards and Technology (NIST) with as many blueprints of *Arizona*'s design as available that showed the main construction details and layout of the load-bearing elements and interior spaces (Figure 6.1). Many more drawings of the smaller details of junctions and fittings were not used, as at the scale of the model the connections between major parts of the ship would need to be idealized and not modeled at the rivet level. Unfortunately, several pieces of information regarding the internal configuration of the ship, particularly the detailed placement of floor beams and wall columns and their dimensions, were not found in the drawings. Transverse sections of the ship at frames 75 and 93 gave some finer structural details (Figure 6.2), and these combined with the individual deck plans and the midships longitudinal
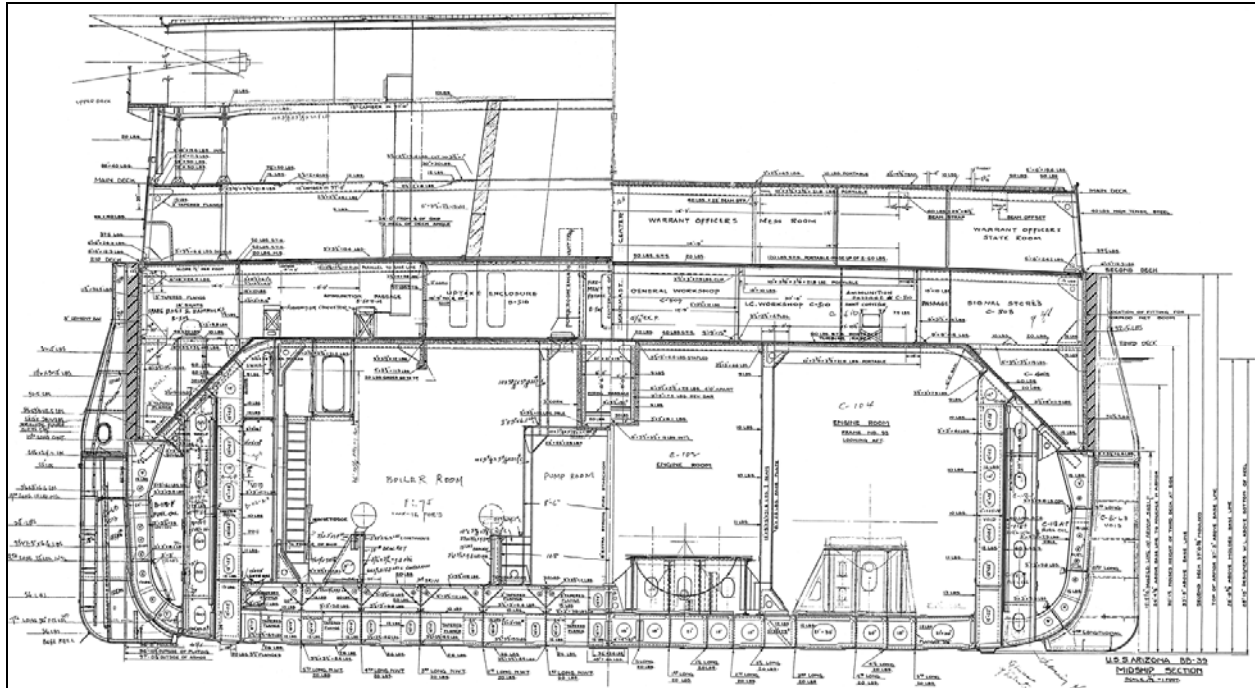
Figure 6.1. Example of as-received blueprint showing a composite frame section of frame 75 looking forward (left) and frame 93 looking aft (right) (USS *Arizona* Memorial Archive).
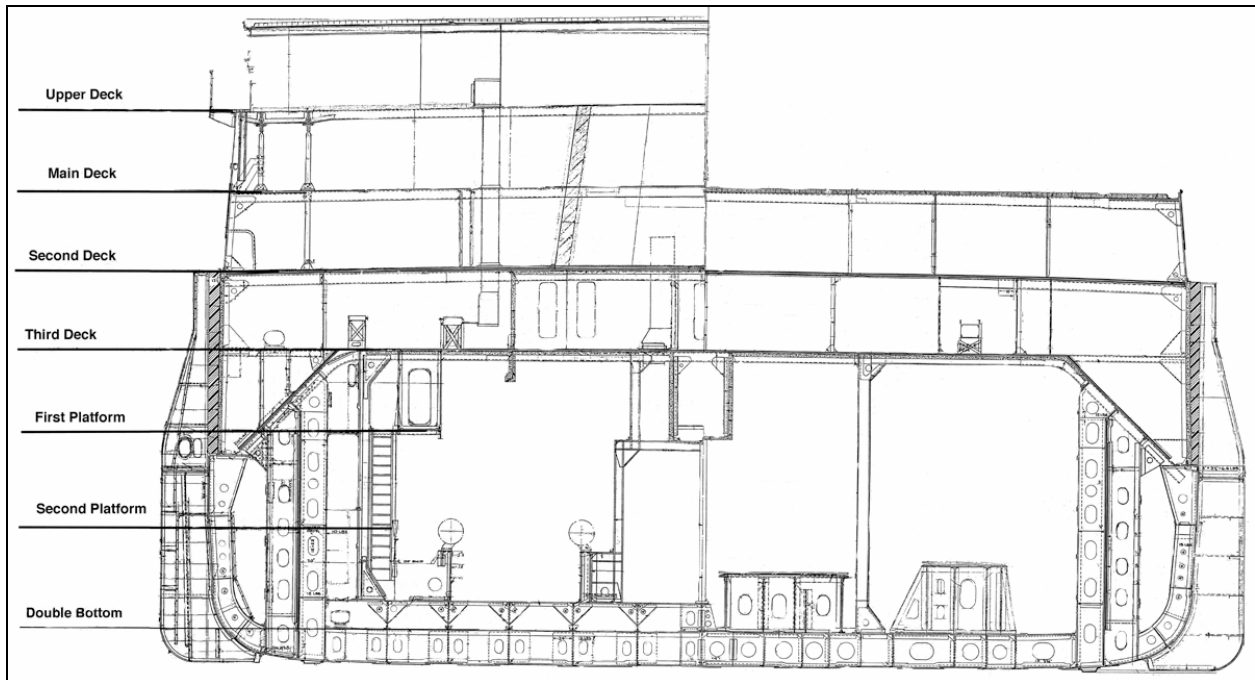
Figure 6.2 Example of cleaned blueprint showing a composite frame section of frame 75 looking forward (left) and frame 93 looking aft (right) with decks indicated (NIST Graphic).

section (Figure 6.3) allowed for reasonable assumptions about the location and dimensions of all load-bearing components to be made. As mentioned, the connections between these components were idealized to speed running of the model. In effect, the component connections were entered as if two components being joined were simply made of one piece of metal. Because riveted connections are designed to be stronger than either constituent that makes up the joint, this is a reasonable assumption. Details from archeological surveys of the wreck as to broken connections, missing deck plate and any other damage to the load bearing structures were added as modifications to the as-built design in the model. This process brought the model from its as-built state to approximate its present condition.

The model was meshed at a level of detail that can be seen in Figure 6.4. After initial runs of the FEM, if certain areas of the model were found to not converge to a satisfactory result, the area was remeshed more finely until the solutions converged. If there were areas that did not show large changes in stress as the ship corroded, these could be remeshed with coarser elements, again saving computational time. The sequence of layers of the model build is shown in Figures 6.5–6.21.
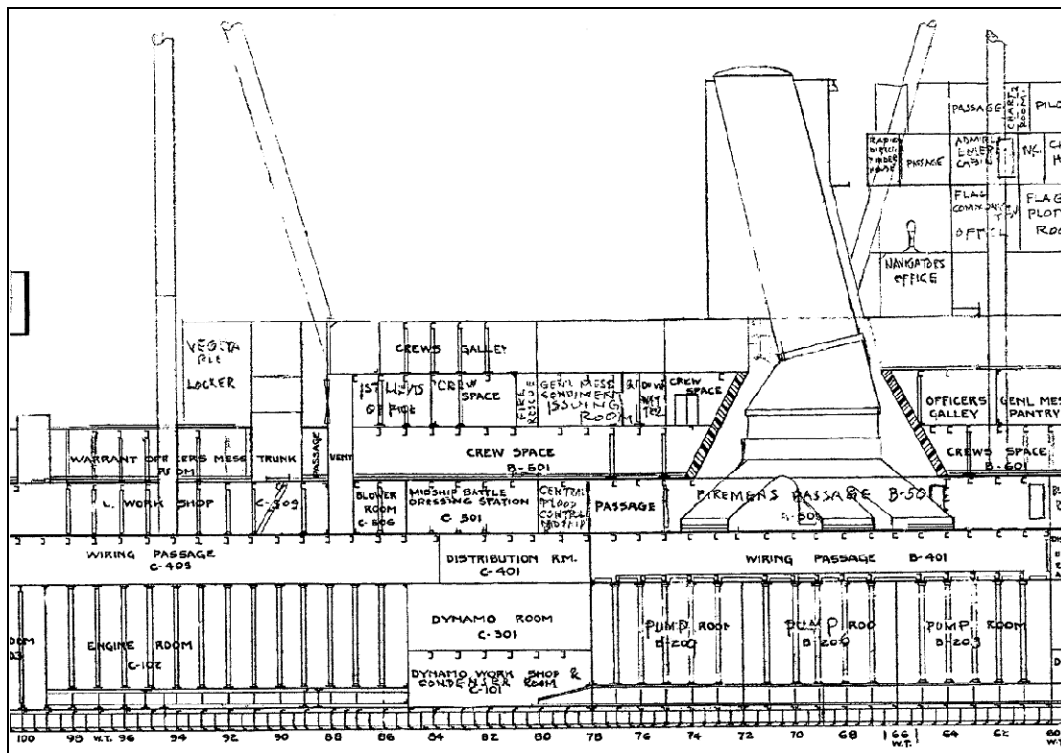
Figure 6.3. Midsection cutaway of the region from frame 60 to 100, showing beams and girders (USS *Arizona* Memorial Archive).
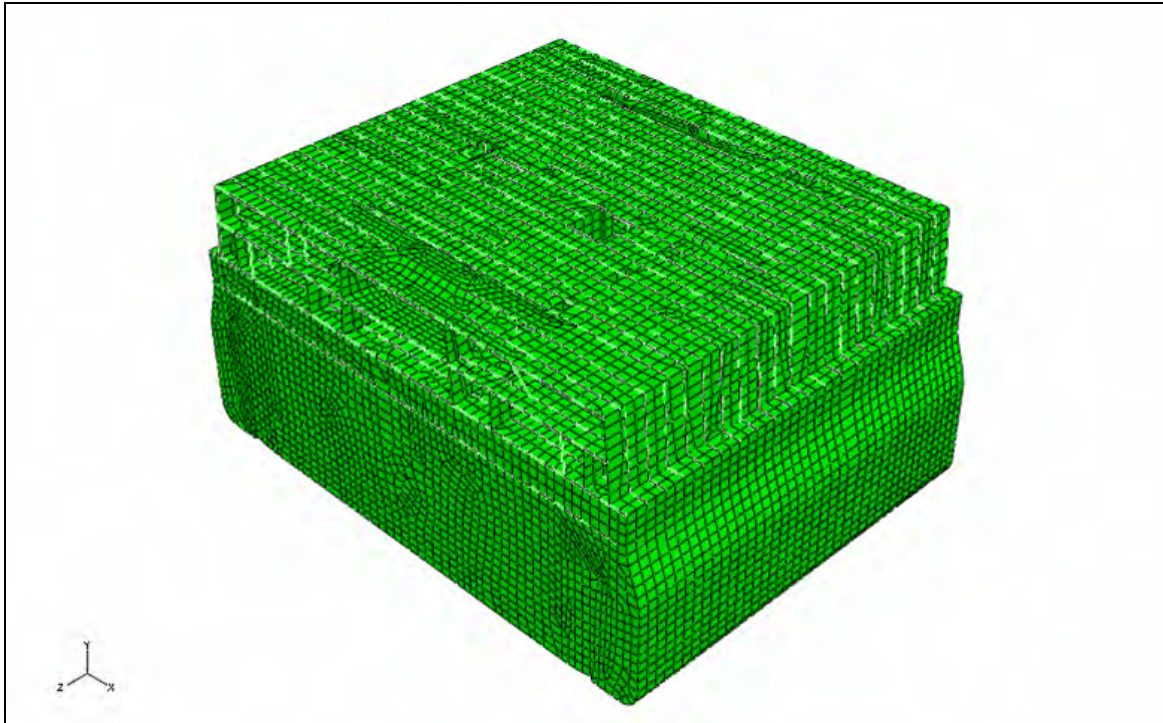
Figure 6.4. Image showing the level of meshing on the FEM. The model contains roughly 57,000 elements and 255,000 degrees of freedom, roughly equivalent to the NIST models of the collapse of World Trade Center towers 1 and 2 (NIST Graphic).
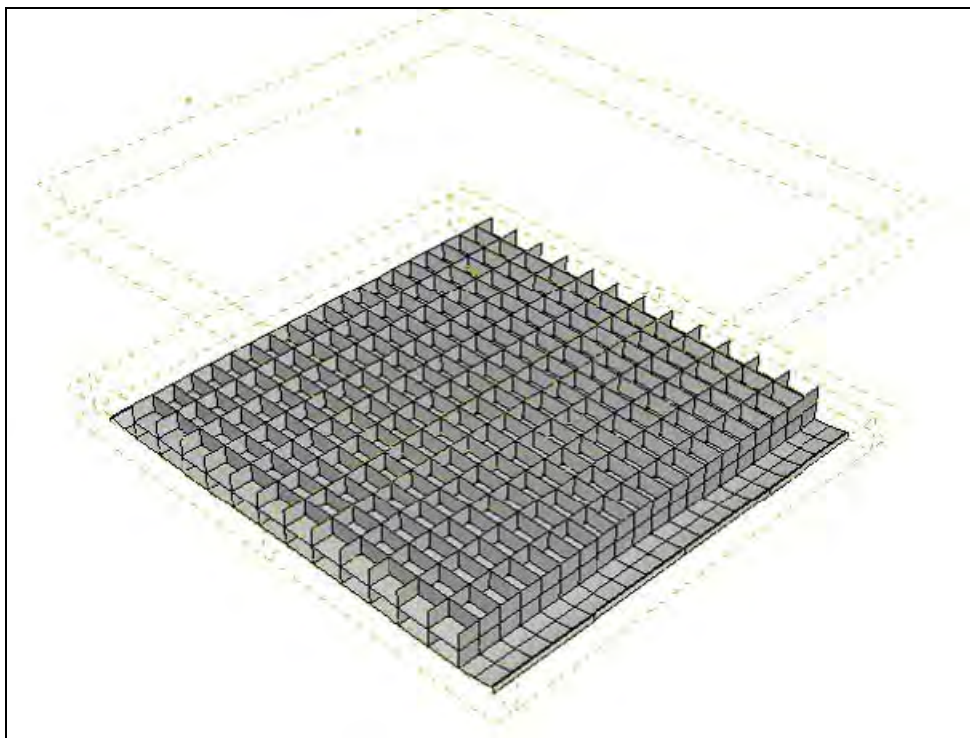
Figure 6.5. Model cutaway showing addition of double bottom framing to hull bottom (NIST Graphic).
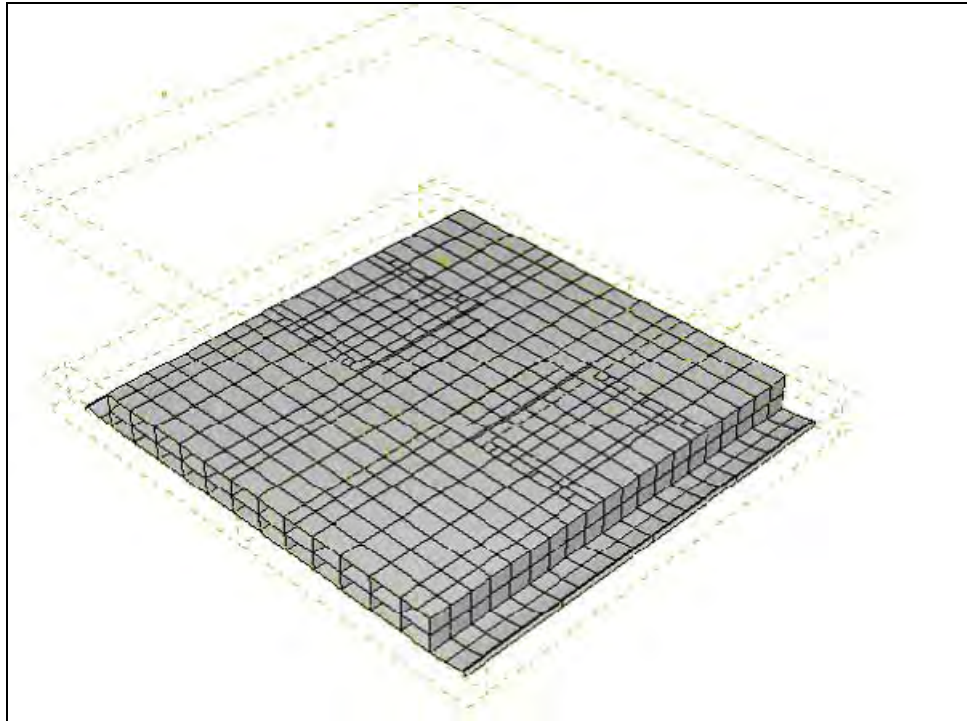
Figure 6.6. Model cutaway showing addition of hold platform decking to double bottom framing (NIST Graphic).
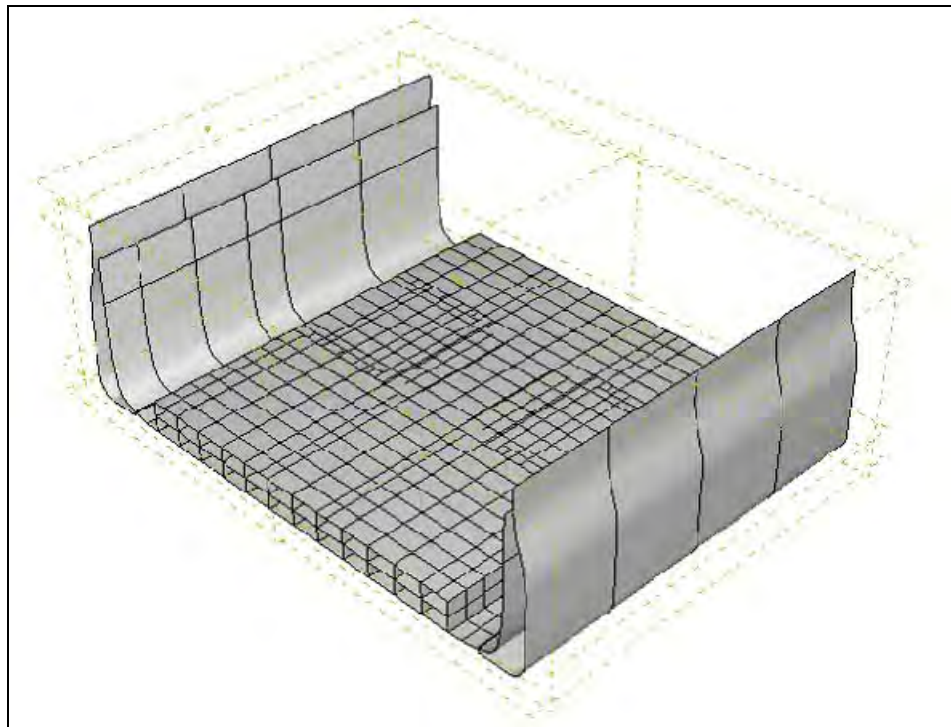
Figure 6.7. Model cutaway showing addition of side shell and torpedo blisters (NIST Graphic).
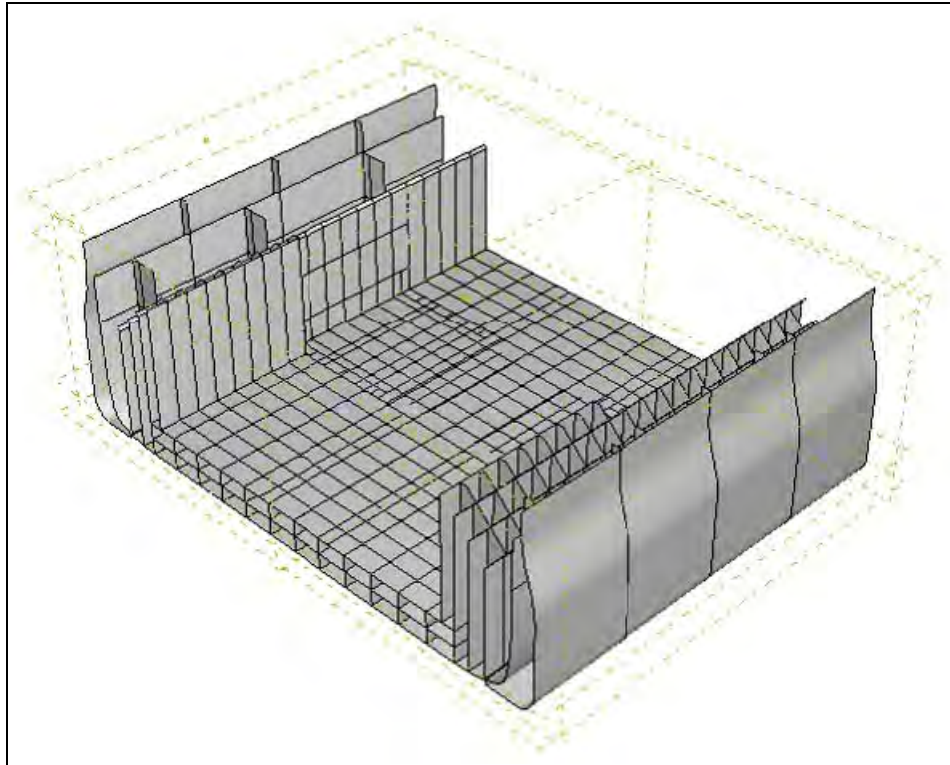
Figure 6.8. Model cutaway showing addition of side oil tanks (NIST Graphic).
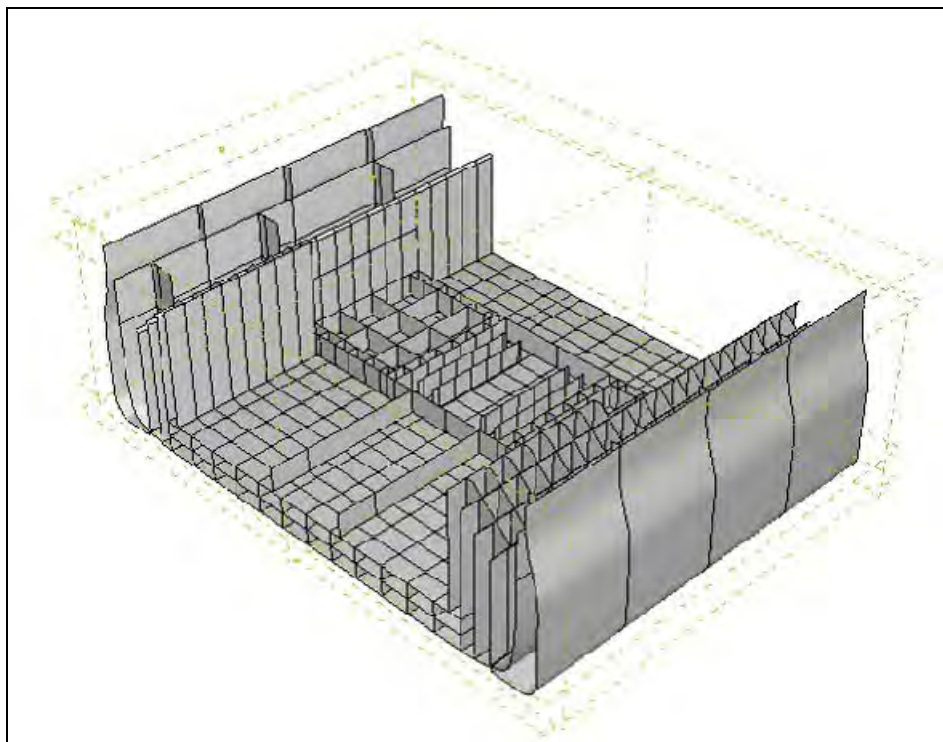
Figure 6.9. Model cutaway showing addition of bulkheads between hold platform and second platform (NIST Graphic).
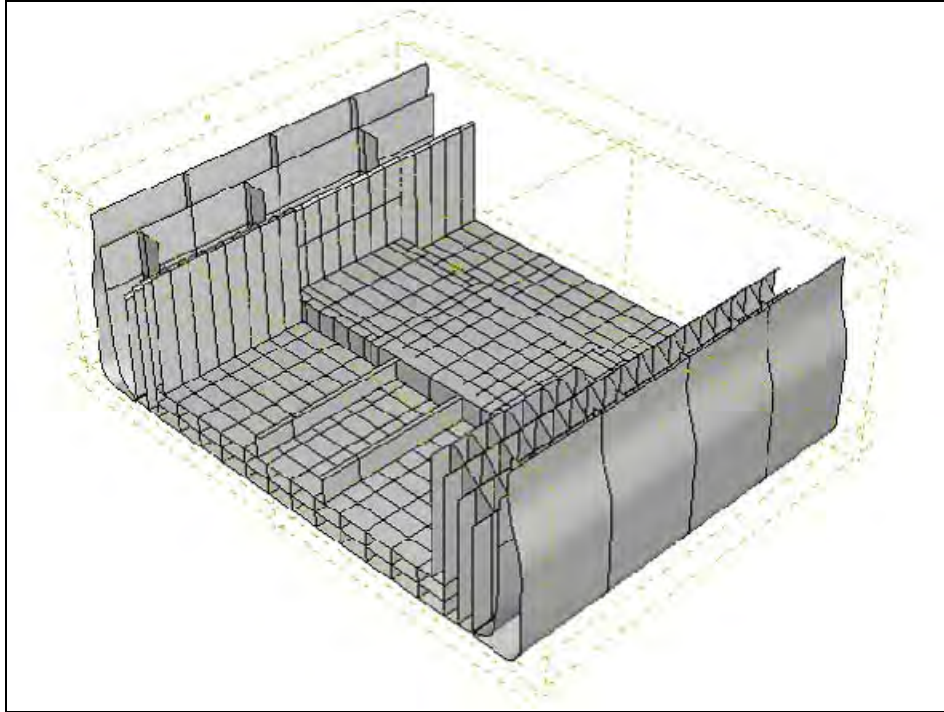
Figure 6.10. Model cutaway showing addition of second platform decking (NIST Graphic).
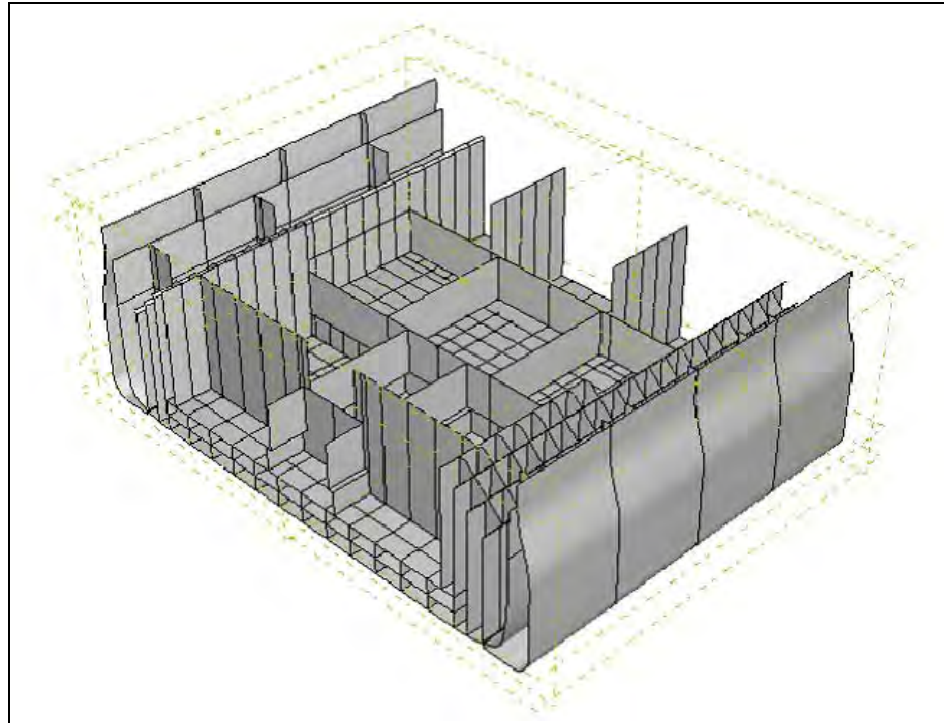
Figure 6.11. Model cutaway showing addition of bulkheads on the first platform and the third deck (NIST Graphic).
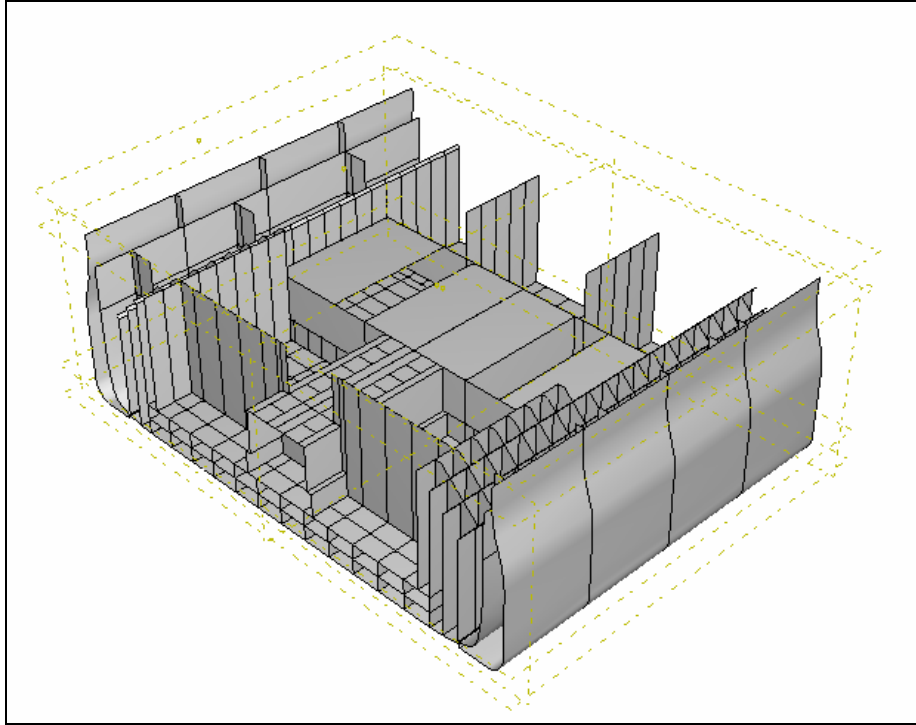
Figure 6.12. Model cutaway showing addition of first platform deck plating (NIST Graphic).
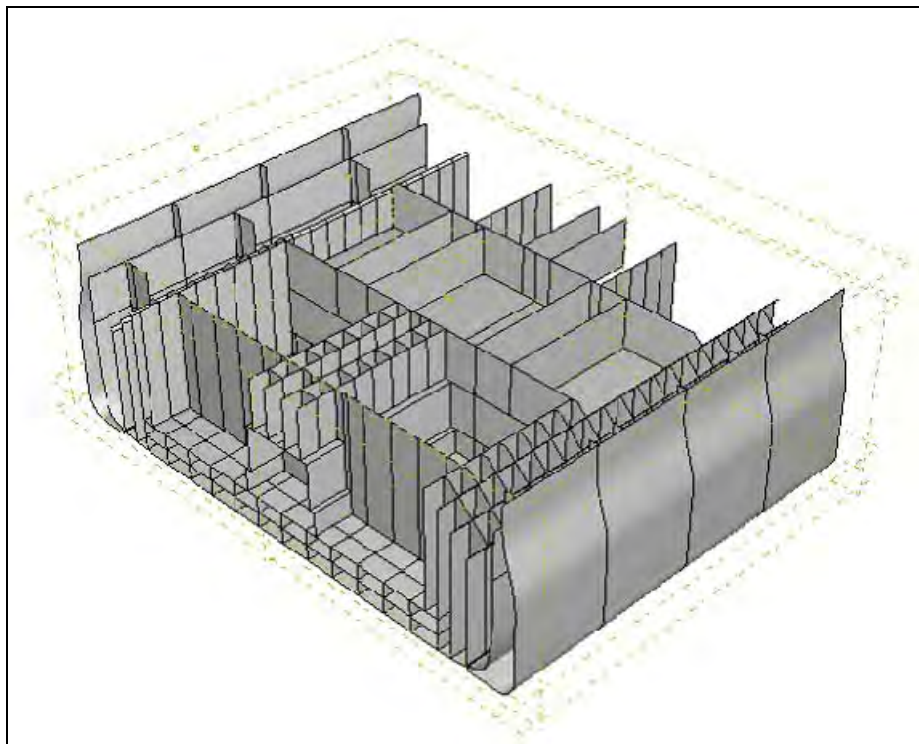
Figure 6.13. Model cutaway showing addition of bulkheads between first platform and the third deck (NIST Graphic).
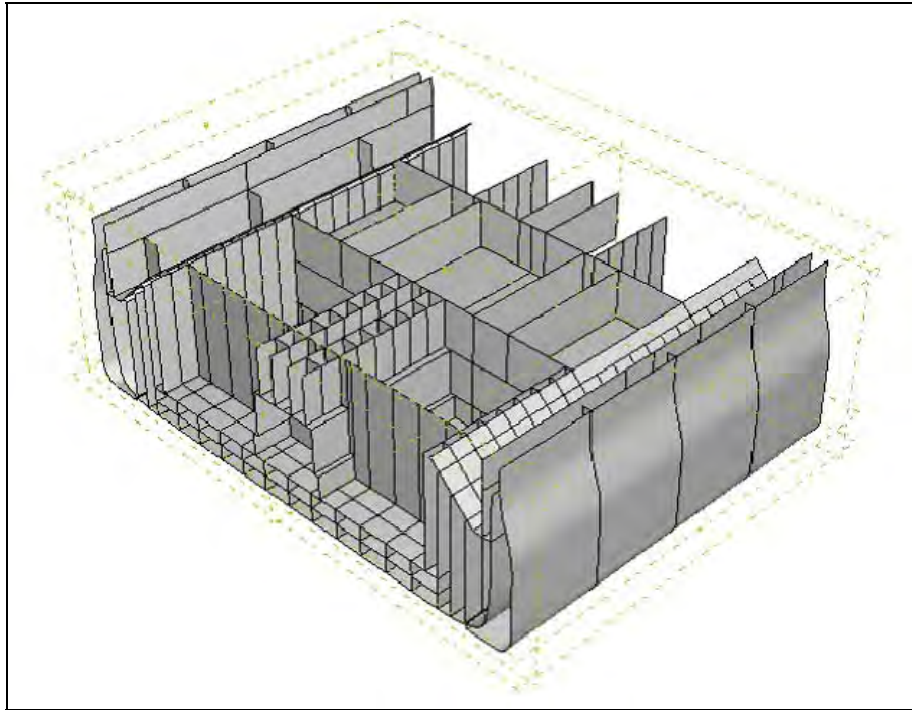
Figure 6.14. Model cutaway showing addition of the side shell armor belt and the tops of the side oil tanks (NIST Graphic).
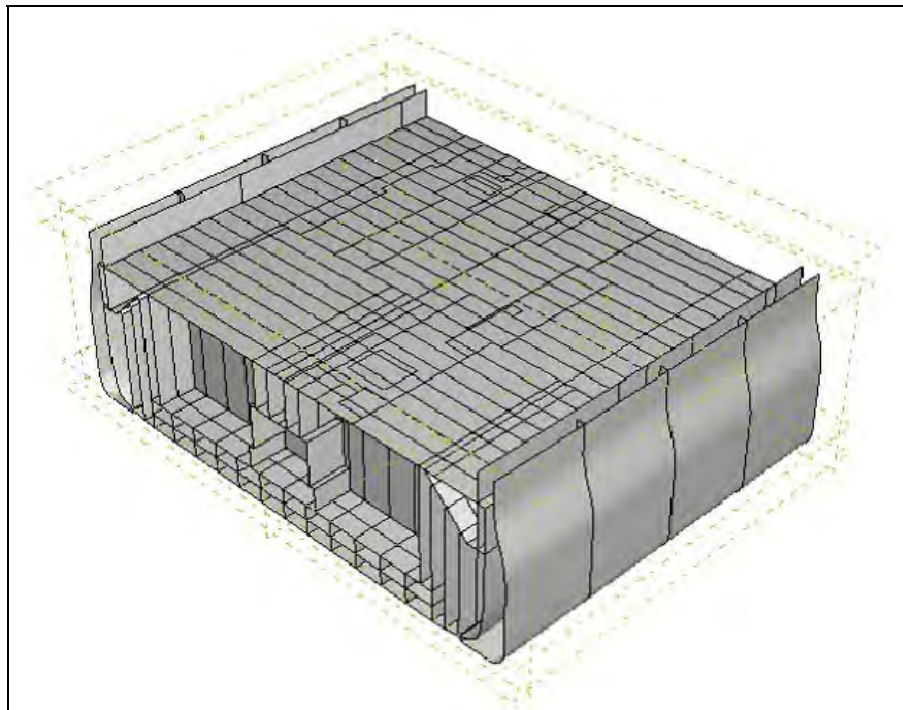
Figure 6.15. Model cutaway showing addition of third deck plating (NIST Graphic).
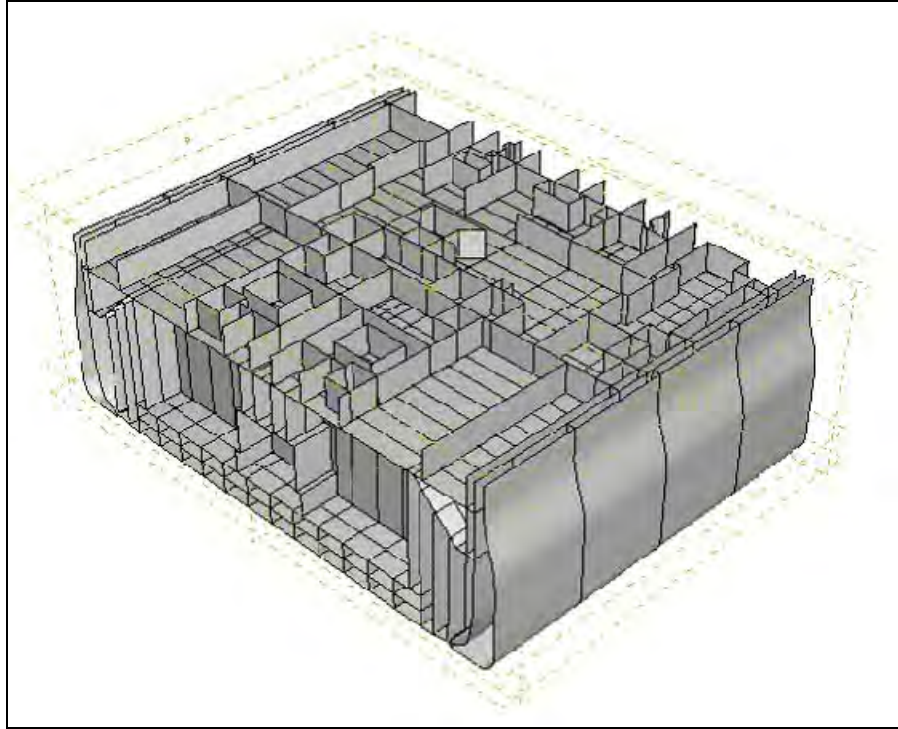
Figure 6.16. Model cutaway showing addition of bulkheads between third and second decks (NIST Graphic).
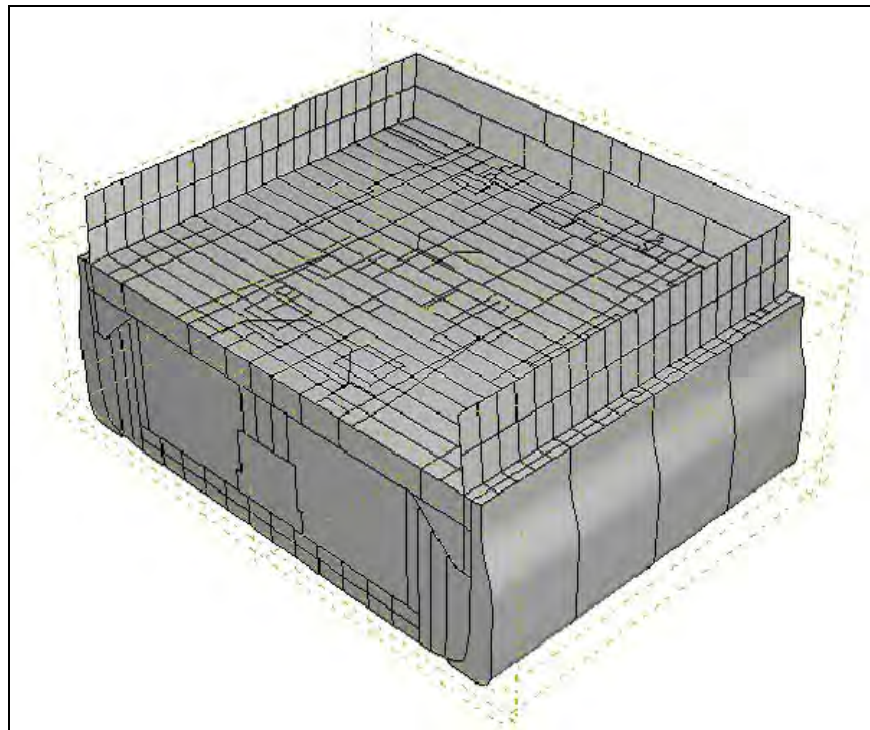
Figure 6.17. Model cutaway showing addition of second deck plating, exterior bulkheads between second and main decks, and virtual bulkheads at frames 70 and 90 to establish proper boundary conditions (NIST Graphic).
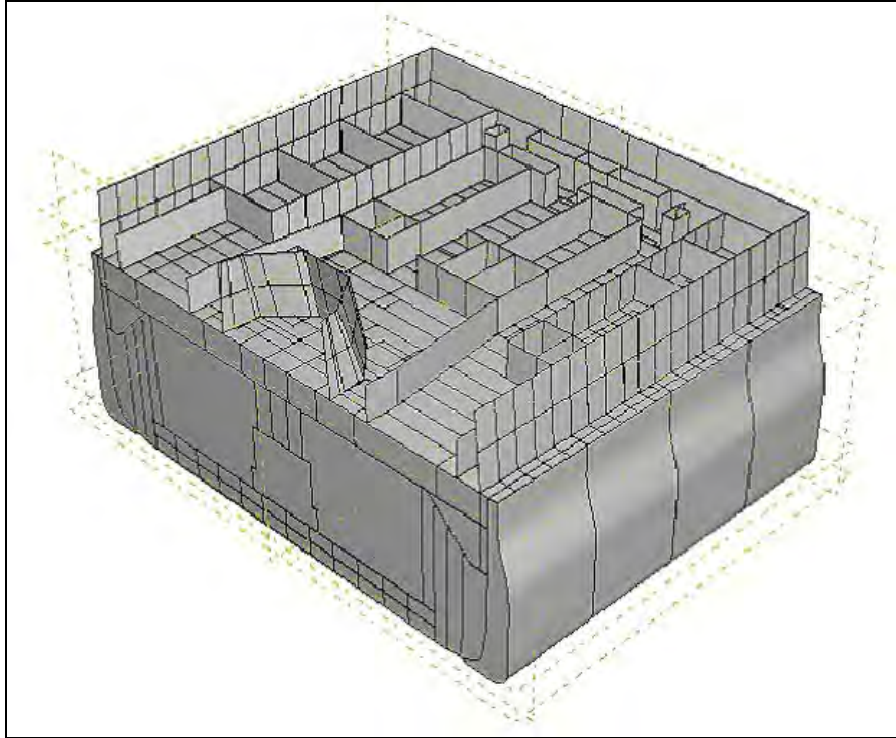
Figure 6.18. Model cutaway showing addition of internal bulkheads between second and main decks and first layer of stack armor plate (NIST Graphic).
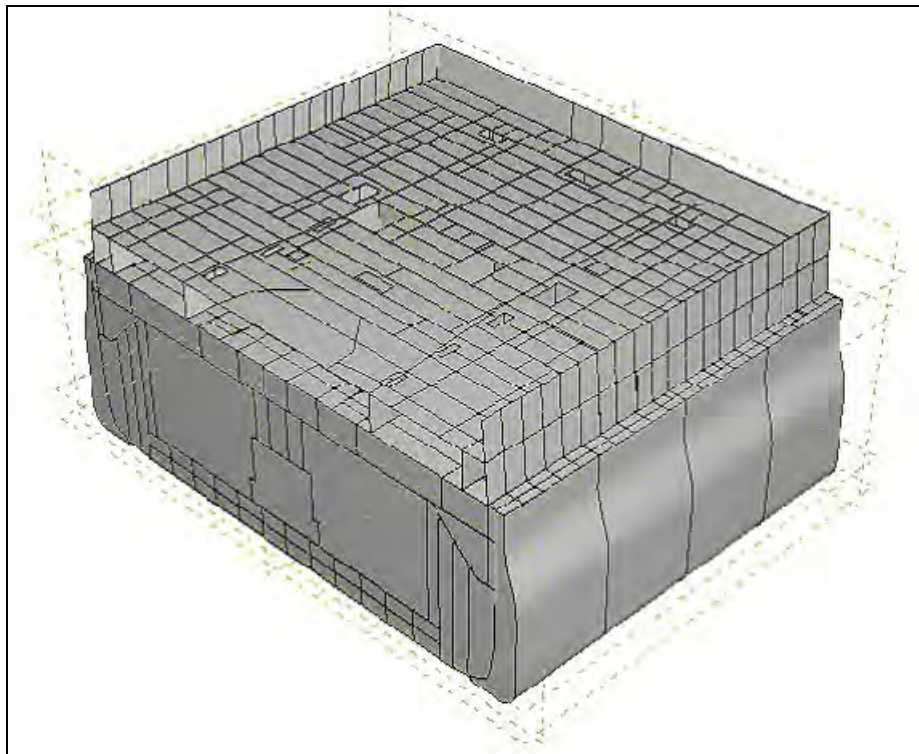
Figure 6.19. Model cutaway showing addition of main deck plating (NIST Graphic).
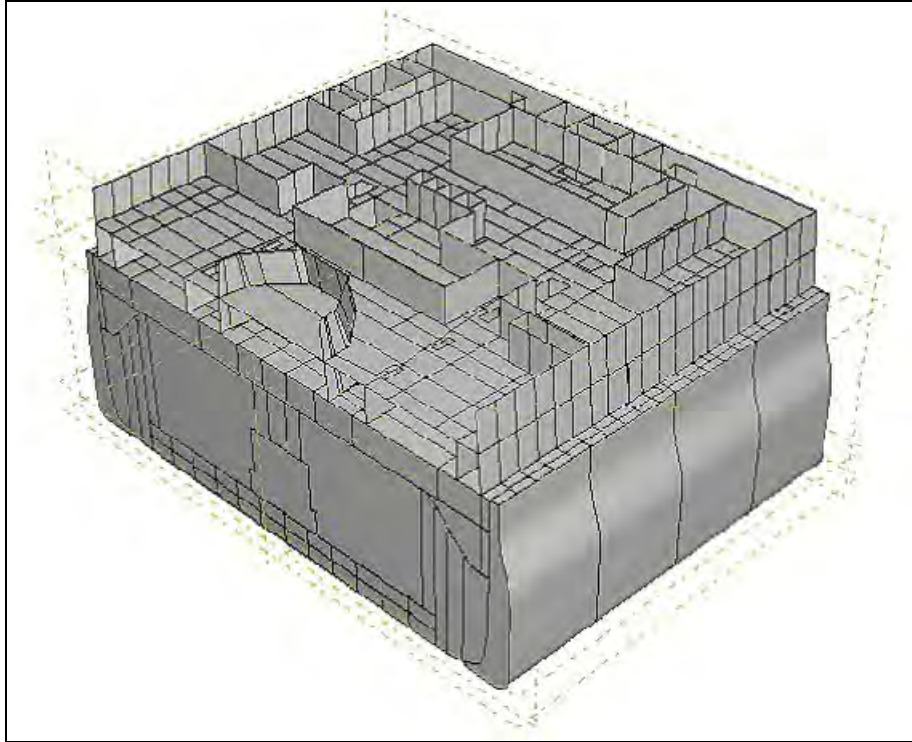
Figure 6.20. Model cutaway showing addition of interior and exterior main deck bulkheads and additional stack armor plate (NIST Graphic).
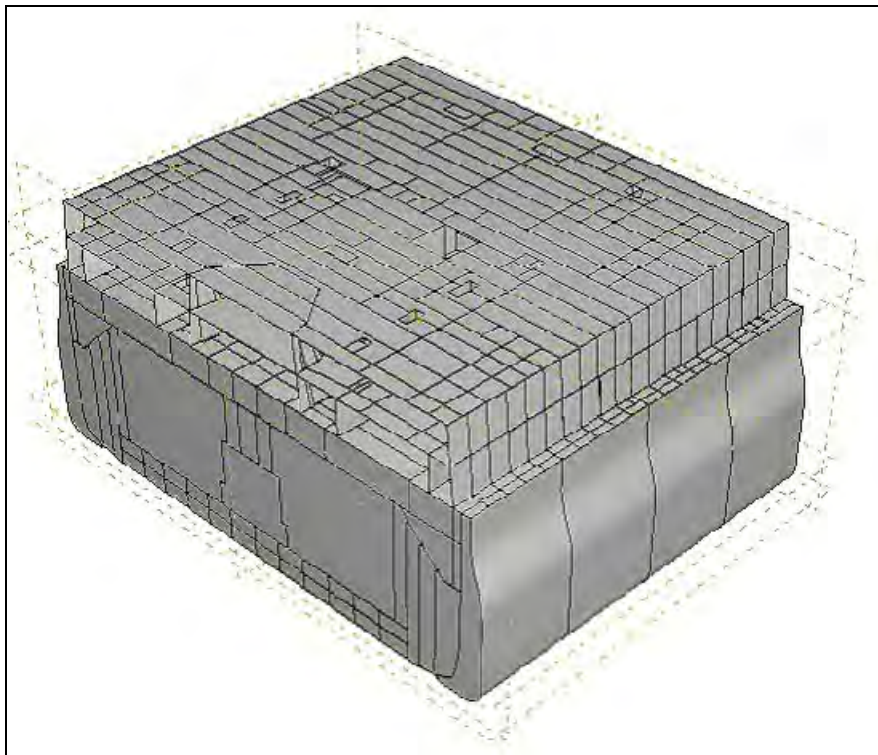
Figure 6.21. Model cutaway showing addition of upper deck plating (NIST Graphic).

The steel of the hull and structure was modeled as an isotropic elastic plastic continuum, with a linear work hardening rate from the yield strength to the ultimate tensile strength. The values of specific properties used (density: 7800 kg/m^3, Young's modulus: 200 GPa, Possion's ration: 0.3, yield stress: 309 MPa, ultimate stress: 563 MPa) are all standard literature values or measured using tensile tests on coupons of steel taken from *Arizona*.

The viscoplastic properties of the sediment upon which the wreck sits have been measured by the U.S. Geological Survey (USGS), as reported in Chapter 10. These properties were used in the model as part of the lower boundary condition, where the steel of the outer hull was proscribed to be in contact with the mud, allowing both load transfer and for the mud/steel interface to slip as the ship settles and deforms.

The concretion on *Arizona* has been found to have a fairly dramatic impact on the decay and eventual collapse of the wreck. The layer of biomass, shells, mud, sand and corrosion product that is encasing the wreck has been described and discussed in Chapter 5. The encrustation layer, while stiff and fairly hard, is also quite brittle, with the constituents being poorly bonded to both each other and the surface of the steel. The mechanical effect of the encrustation on the collapse of the wreck is in its weight. As the wreck's steel components corrode, they lose thickness and weight. But overall the encrustation grows faster than the steel corrodes, and thus over time the wreck gains mass. This deadweight must be added to the self-weight of the steel, and it is both together that is driving the collapse of the wreck.

The oil that fueled *Arizona*, Bunker C fuel oil, has a density of 0.97 that of sea water at 25 degrees C. It has been reported that *Arizona* contained as much as one million gallons of oil just prior to the attack, and it is estimated that much as one-half million gallons may still remain within the wreck. It is unknown whether the oil is primarily contained within the original fuel cells or whether a significant portion has leaked out and lies underneath the decks. Because the oil is more buoyant than sea water, it will exert a lifting force on the wreck structure wherever it is located. As a worst case estimate, we calculated the lifting force of a half-million gallons of Bunker C as if it was located at one spot, and the result was approximately 62 tons of lift. This equates to 2 pounds per square inch if the oil were idealized as a cube of liquid under a single deck. This is an insignificant loading on the structure, and it would not contribute in any way to the eventual failure in comparison to the self-weight and the weight of the encrustation, as will be seen. Thus, the mechanical effect of the lifting force of the oil is not considered further.

To facilitate changes in properties and/or boundary conditions within the model, it was divided into zones, or collections of elements, that could have their properties changed in unison. These generally consisted of pairs of decks within the structure, as the main parameter to be varied is the density, reflecting changes in corrosion in the steel plates and members at different water depths and under the mudline, and thus differences in steel thicknesses.

Once the model is developed in geometry and element placement, a definition of the boundary conditions needs to be imposed (Figure 6.22). The open ends at frames 70 and 90 were constrained from motion along a line parallel to the long axis of the ship. The steel elements in contact with the first layer of mud elements were prescribed to remain in contact as both are allowed to deform. The extent of the mud was set at a dimension that would ensure that all of the mud deformation that results from the motion of the wreck was entirely contained within the volume of the mud in the model. The boundary of the mud was constrained from motion in all three axes. Each element was given a self-weight with a density that can be independently set or changed as part of a zone, and the surfaces of the elements were allowed to bear additional loads from the concretion.
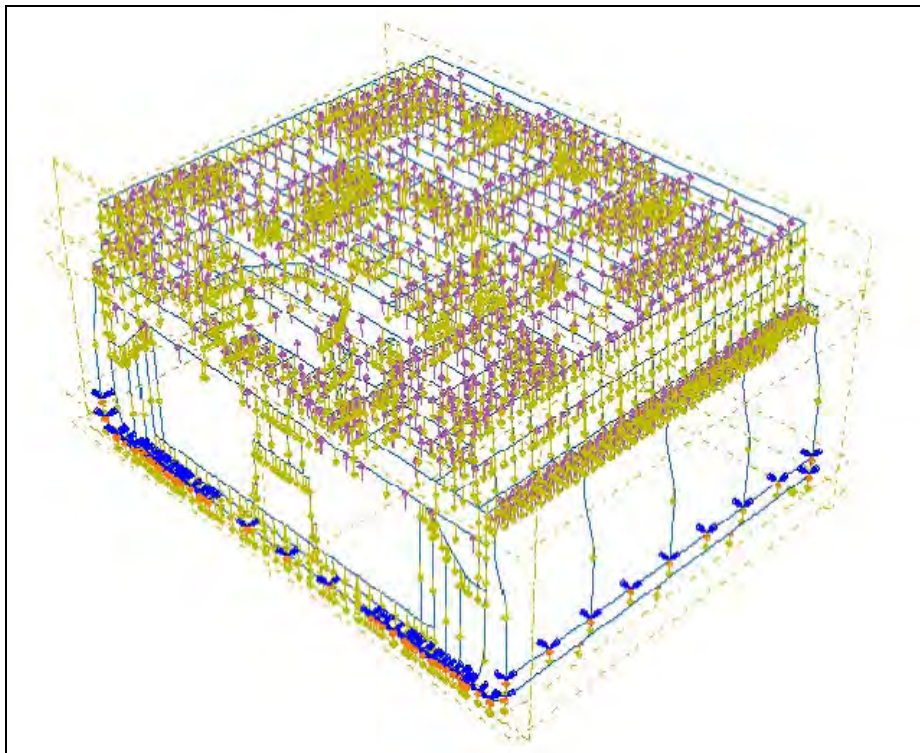
Figure 6.22. Diagram of boundary conditions and loadings in the model. Gold - weight, purple - encrustation, blue - no longitunal motion, orange - support from mud (NIST Graphic).

A major limitation of the finite element method involves the fact that the geometry of the body being studied is fixed, while the loads, boundary conditions and material properties are changed, to study how a design performs under different conditions. This works very well for design issues, which is where FEA is commonly used. In the present study, the inverse problem is being studied: the loads and material properties are fixed, while the geometry is changing with time due to corrosion of the steel. Under ordinary circumstances, the entire model would need to be re-meshed with the new measurements for every state of the wreck to be studied. In order to be able to run a parameter study, where the variables that can be changed are varied in a systematic way to evaluate the stability of the system, a model was developed where the density of the elements was changed.

The critical parameter in this study is the stress that any given component experiences under the weight of itself, what it is attached to, and the concretion. Stress is load divided by cross-sectional area. The stress increases if the area decreases (due to corrosion) or the load increases (due to, in this case, increasing density). Using this technique, the physical dimensions of the element are kept constant, but the density is increased such that the stress in the component increases as it "thins" in the model. There is a small error introduced using this method, as the bending moment of inertia is being kept constant in the model with the constant dimensions of the load bearing sections, while thinning by corrosion would decrease the bending moment of inertia, allowing for collapse sooner than the model predicts. This effect is believed to be small, and is being checked by performing an actual remesh of the model using the new, corroded thicknesses and directly comparing the stresses from this model to the original results.

RESULTS

It is perhaps most illustrative to present the results from the model in chronological order as the wreck decays, describing issues that develop and warrant examination. In the figures to follow, stresses are shown in a color scale ranging from dark blue through green, yellow, orange and red. These roughly correspond to stress levels of less than 10%, 10-25%, 25-50%, 50-75%, and more than 75% of the breaking stress of the steel, respectively. Once an element has reached the breaking stress, it is defined as having no strength in the model, and is removed. The results presented are those where the steel not covered by mud is allowed to degrade 3 times faster than

the buried steel, which appears from corrosion analysis (Chapter 5) to be a reasonable scenario. The approximate equivalent dates were determined by assuming a linear corrosion rate from 1941 through the dates of the actual thickness measurements on the wreck, and extrapolating into the future. Since the corrosion rate is most likely non-linear, being affected by many factors such as the presence and thickness of the encrustation, this is only an approximation that will need to be refined in future work. For the purposes of this chapter, the approximation is useful for fixing the "age" of the wreck for planning purposes at the present day at 20% degredation.

Stresses in the Structure—As Built

Figure 6.23 shows the computed stresses in the model when dimensions of the ship are taken directly from the design blueprints, and thus as the ship was built. The stresses everywhere are very low, which is to be expected as this is a warship and it was considerably overbuilt to be able to withstand battle damage. The stresses are higher in the vertical walls in the lower levels, as expected, since these walls are supporting much of the weight of the ship above.
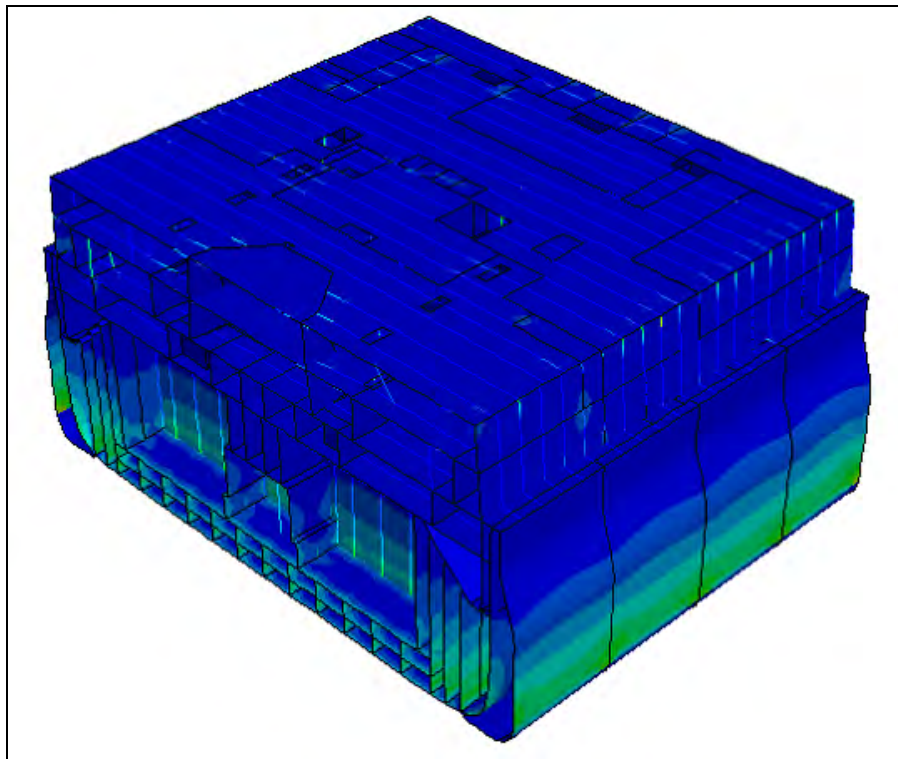
Figure 6.23. Self-weight stresses in as-built condition (NIST Graphic).

Stresses in the Structure—10% Corrosion Thickness Loss (rough equivalent to 1980)

Overall the stress distribution is very similar to the as-built condition, with the overall stress levels somewhat higher. It is noteworthy that the deck beams in the upper deck have jumped significantly in stress, and the second, first and main decks remain almost unstressed (Figure 6.24).

Stresses in the Structure—20% Corrosion Thickness Loss (rough equivalent to 2020)

The upper deck is now showing sagging of the beams and deck plates as they continue to thin. Stresses at the turn of the bilge of the torpedo blisters are approaching the tensile strength of the steel. Stresses in the vertical members continue to increase (Figure 6.25).

Stresses in the Structure—30% Corrosion Thickness Loss (rough equivalent to 2050)

The turn of the bilge area of the torpedo blister, as well as the connections of the lower bulkheads to the hold platform are very close to critical. There is additional sagging in the upper deck, as well as increased stresses in the bulkheads of the lower deck (Figure 6.26).

Stresses in the Structure—50% Corrosion Thickness Loss (rough equivalent to 2120)

Localized collapse events have begun to appear, including the torpedo blisters, double bottom vertical wall segments, upper deck beams and the region around the stack armor, undoubtedly collapsing under the weight of this very thick steel (Figure 6.27).

Stresses in the Structure—60% Corrosion Thickness Loss (rough equivalent to 2150)

There is general collapse of the deck plating on the upper and main decks, collapse of the outer hull plating and torpedo blisters, very high stresses in the bulkheads at the hold platform in the engine spaces. Buckling of the hull shell plating has begun (Figure 6.28).
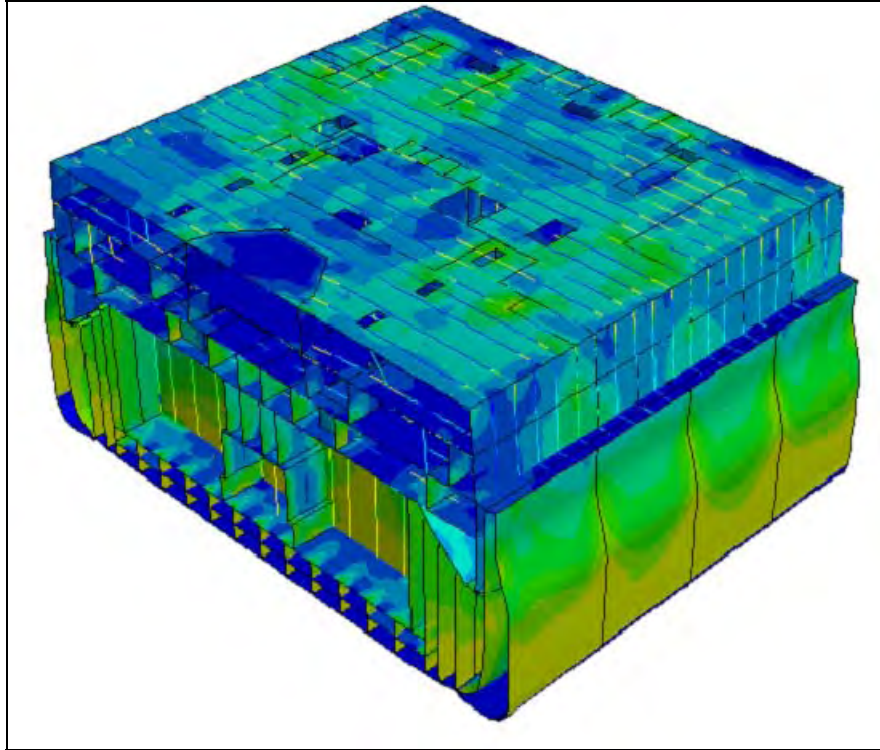
**Figure 6.24. Self-weight stresses after 10% thickness loss due to corrosion,
approximate date = 1980 (NIST Graphic).**
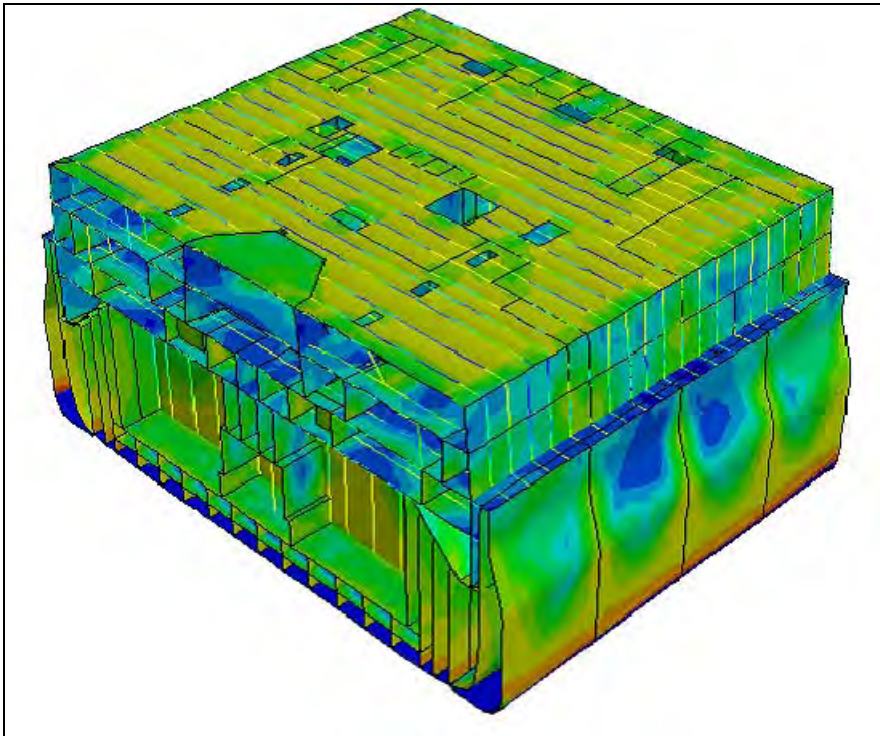
**Figure 6.25. Self-weight stresses after 20% thickness loss due to corrosion,
approximate date = 2020 (NIST Graphic).**
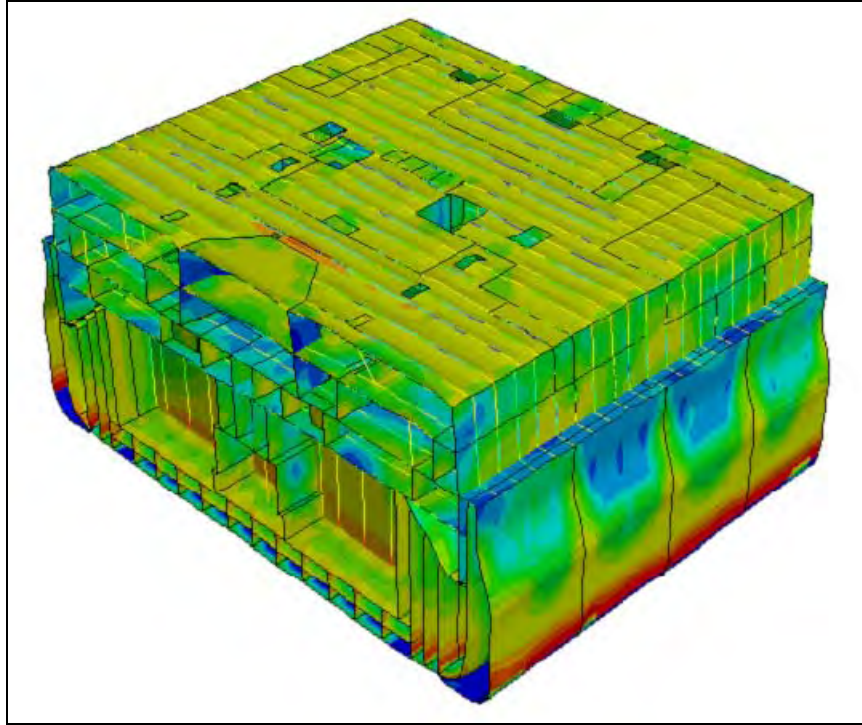
**Figure 6.26. Self-weight stresses after 30% thickness loss due to corrosion,
approximate date = 2050 (NIST Graphic).**
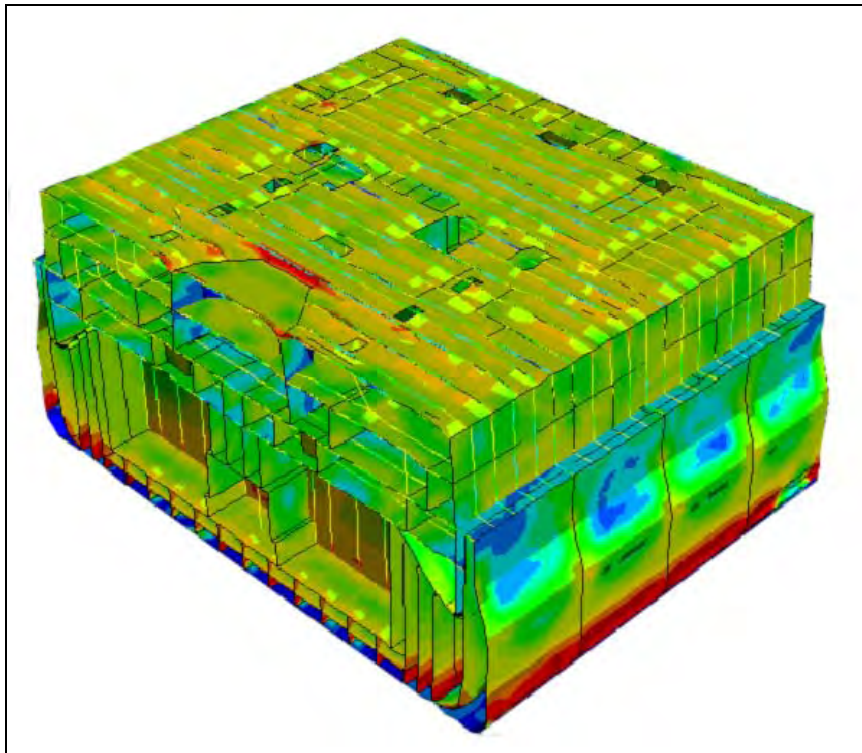
**Figure 6.27. Self-weight stresses after 50% thickness loss due to corrosion,
approximate date = 2120 (NIST Graphic).**
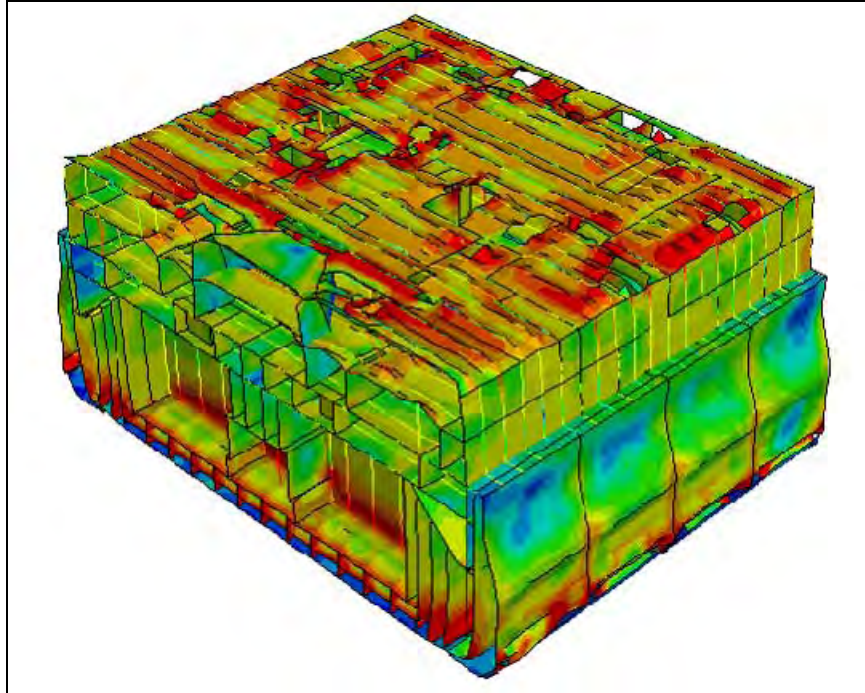
**Figure 6.28. Self-weight stresses after 60% thickness loss due to corrosion,
approximate date = 2150 (NIST Graphic).**

Stresses in the Structure—70% Corrosion Thickness Loss (rough equivalent to 2180)

The upper deck is now unrecognizable, and much of the deck plating and deck beams
will have fallen onto and accelerated the collapse of the main deck and those further below. The
hull shell and torpedo blister continue to collapse, as does now the double bottom (Figure 6.29).

Stresses in the Structure—80+% Corrosion Thickness Loss (rough equivalent to 2210 and
beyond)

The decks of the superstructure (upper, main, and second) can be expected to further
collapse and pancake onto the third deck. The double bottom has now completely collapsed.
Note however that the core cylinder of the wreck, consisting of the volume bounded by the third
deck, the inner bottom and the side oil tanks is still relatively intact (Figure 6.30–6.32).
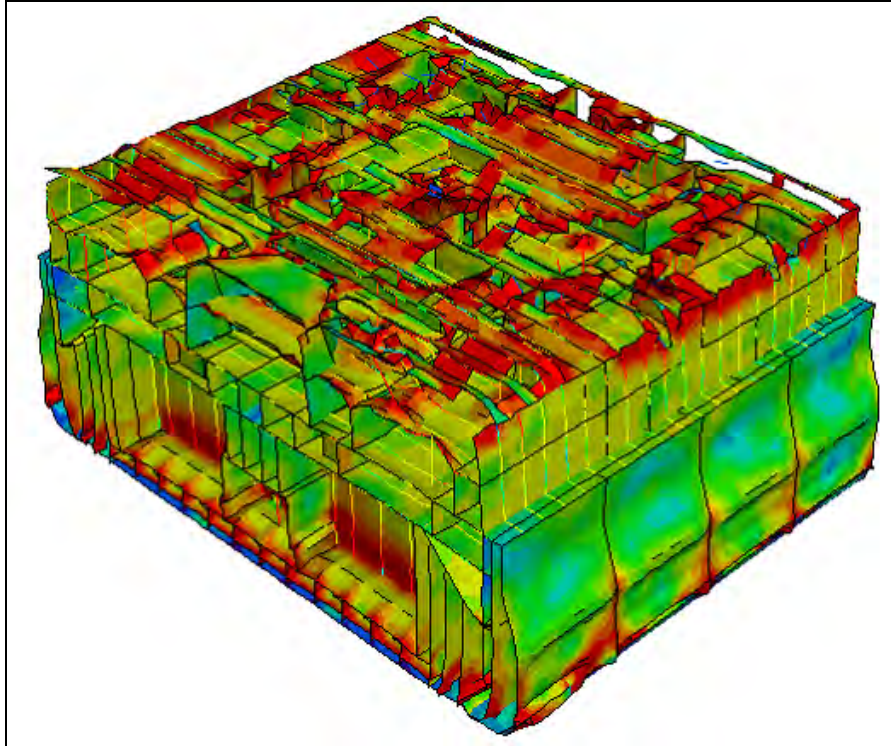
Figure 6.29. Self-weight stresses after 70% thickness loss due to corrosion, approximate date = 2180 (NIST Graphic).
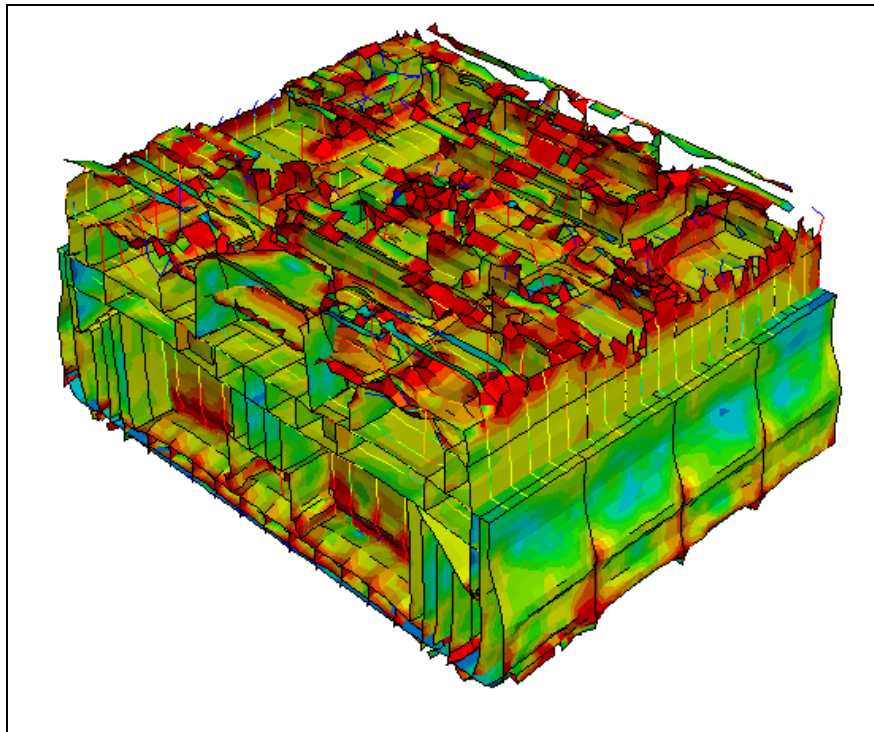
Figure 6.30. Self-weight stresses after 80% thickness loss due to corrosion, approximate date = 2210 (NIST Graphic).
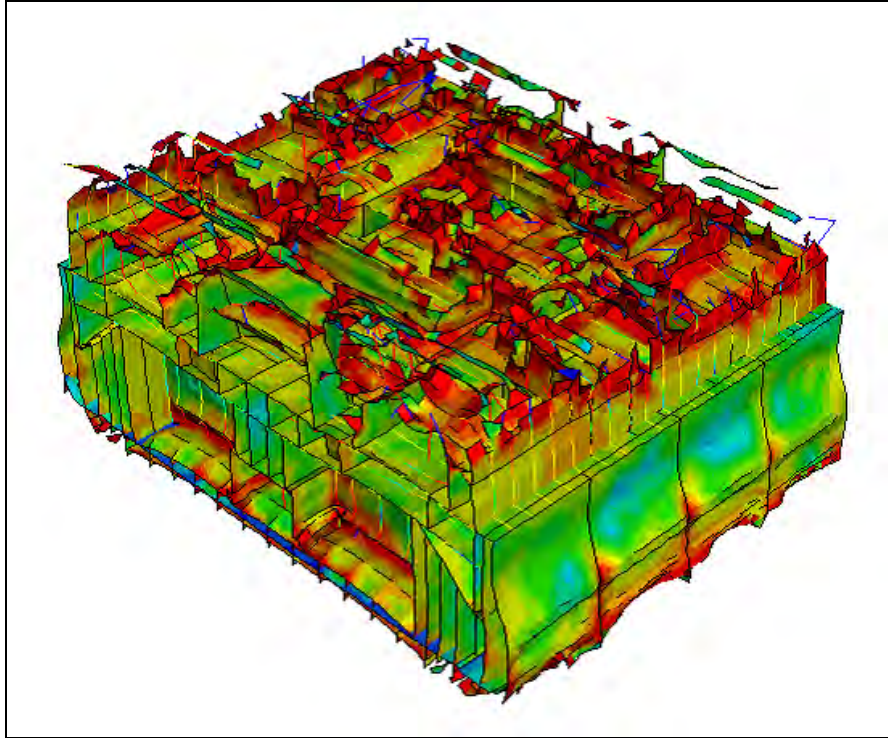
Figure 6.31. Self-weight stresses after 90% thickness loss due to corrosion, approximate date = 2240 (NIST Graphic).
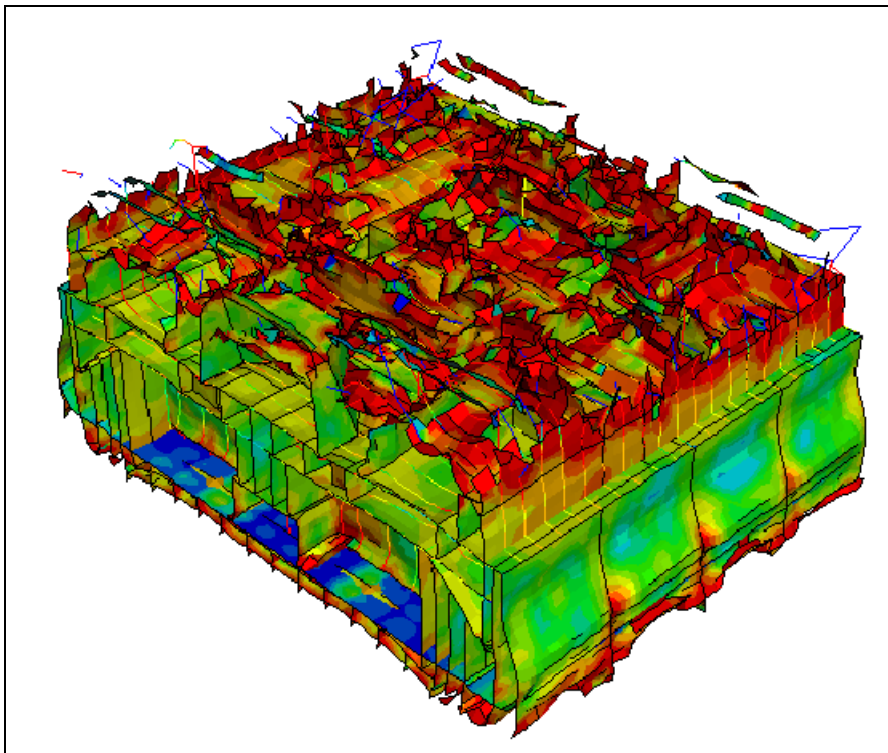
Figure 6.32. Self-weight stresses after 95% thickness loss due to corrosion, approximate date = 2250 (NIST Graphic).

OBSERVATIONS AND CONCLUSIONS

The results of this FEA of the wreck of USS *Arizona* seem to indicate that the wreck is approximately one fifth to one fourth of the way to an eventual collapse due to corrosion. A surprising aspect of the results is that collapse is predicted to initiate in the side and bottom of the hull before any significant collapse events in the exposed regions of the upper decks. This is likely due to the fact that the boundary condition of the wreck is that it rests on a viscoplastic solid representing the mud, rather than a pure fluid of sea water. The mud will rather quickly compress and become quite hard, concentrating the load on the bottom of the hull rather than distributing it more generally.

FURTHER WORK

Many refinements and extensions to this analysis of the wreck of *Arizona* are possible, and will be performed on a time-available basis by staff at NIST. Now that the methodologies for simulating the degredation and eventual collapse of a submerged steel-hulled ship using FEA have been developed, this work can be easily extended to answer several key questions concerning the future of USS *Arizona*.

First, this model can, in a very straightforward way, be extended to the entire length of the ship. Of course, this would increase the calculation time needed dramatically, but key insights into the behavior of structural elements in the present study can be used to cut down the computation time. For example, once it is determined how a section of deck plating and supporting deck beam deform as the members thin, and it is found to be consistent across the model, this region can be replaced with a single element that has hybrid parameters calculated from the model. Thus, instead of performing calculations on thousands of connected elements, one could be used.

One large unknown in this study is the damage to the internal load-bearing structures in the lower decks due to the events on December 7, 1941. It is almost certain that the region forward of the main stacks suffered significant damage, but since submersibles and divers cannot reach these regions for direct observations, we must speculate and make best and worst case scenario assumptions for our analyses. These assumptions could be fine-tuned with input from

experts in blast damage in the naval community, perhaps at the Naval Surface Warfare Center in Carderock, Maryland. Initial contacts with researchers at that facility indicated interest but inability to assist due to lack of funding.

The wreck is listing slightly to port, and this causes the self-load to be directed slightly off of vertical onto the load bearing structures. Elastic-plastic collapse of columns and stanchions will be significantly affected by deviations from vertical, and the effect of the list will be for some structures to collapse sooner than predicted in this model. The effect of the list and how it is changing over time is a factor that could be added to refine the model, based on analysis by USGS.

Corrosion data has been collected on the wreck by the NPS-SRC since the early 1980s. These data, coupled with the direct measurements of corrosion via coupon removal from the wreck, has allowed modeling of the corrosion rate at many locations on the wreck. In the present study, the differences in corrosion rates were only modeled as differences between whole decks above and below the mud line. A further refinement to the model that would allow for more accurate spatial location of potential developing weak points would be to map the measured differences in corrosion rate onto the structure.

The eventual goal of this model is to construct a tool that can not only give some predictions as to eventual collapse of the wreck, but also be able to virtually test out potential remediation techniques before going through the time, expense and intrusion of working on the ship. One of the easier things that can be controlled is the accumulation of concretion. If it is found that the corrosion rate is significantly reduced by the presence of this layer, as it appears to be the case, then encouragement of its formation would be useful. Conversely, if the FEA model is expanded to test the effect of having more or less mass on the wreck surfaces from concretion, a removal or preventative routine would be of value. This would be a straightforward extension of the current study.

Finally, Pearl Harbor is an active naval base, with ship traffic constantly entering and exiting. Each of these ships produces a wake that can, depending on the distance from the wreck, deliver a significant impact to the hull. In the case of *Nimitz*-class carriers, nearly the entire water column under the ship is being displaced as they pass in salute, delivering a mini-tsunami. The present model deals with slow, steady-state decay of the structure, attempting to predict the timeframe of collapse. It is more likely that a significant failure will be precipitated

by a more sudden event such as a wave or a large storm. Using new modules developed to study the effect of landslide-induced waves within reservoirs upon dams, a study could be conducted looking at the magnitude of stress spikes in the wreck with the passing of ships or during large storms.

CHAPTER 7

Microbiological Research on USS *Arizona*

Christopher J. McNamara, Kristen Bearce Lee, and Ralph Mitchell

INTRODUCTION

The purpose of this research is to investigate the possible role of microorganisms in USS *Arizona* corrosion and concretion formation. Specific goals include isolating and identifying microorganisms from Pearl Harbor, especially within the concretion covering *Arizona*'s steel hull; determining the organisms within the community responsible for corrosion of steel similar to that found in USS *Arizona*; and investigating environmental parameters that may influence the rate of corrosion by microrganisms (e.g., temperature, nutrients, and redox).

POTENTIAL FOR MICROBIOLOGICALLY INFLUENCED CORROSION OF USS *ARIZONA* STEEL

BACKGROUND AND PREVIOUS WORK

Biofilms are communities of microorganisms attached to an interface and embedded in a polysaccharide matrix produced by the microorganisms. Biofilms are ubiquitous in nature (Costerton et al. 1995) and are a common cause of medical infections (Costerton et al. 1999) and

275

industrial biofouling (Costerton et al. 1995). In the latter two situations, biofilms present persistent problems because of their inherent resistance to antibiotics and disinfectants (Anwar et al. 1992).

Biofilm formation is a multistage, complex process that begins with the initial adhesion of microorganisms to a surface. Surface adhesion is facilitated by a variety of factors. Biotic factors include motility as well as cell surface features such as capsules, fimbrae, and hyrdophobicity (McEldowney and Fletcher 1987). Abiotic factors that affect attachment include surface hydrophobicity, and the presence of polycations and organic coatings (van Loosdrecht et al. 1990).

Once microorganisms have attached to a surface, cell division occurs producing masses of cells referred to as microcolonies (Costerton et al. 1999). In addition, biofilm organisms produce large amounts of exopolymer, which consist mainly of polysaccharides (Christensen and Characklis 1990). The exopolymer serves a variety of functions, including protection from desiccation, erosion, antibiotics, and disinfectants as well as nutrient and energy storage (Costerton et al. 1995).

The polymer matrix may also limit the movement of materials through the biofilm. The result is the formation of microhabitats within the biofilm caused by gradients in factors such as pH, O_2, nutrients, and organic carbon (Whitfield 1988, Rittmann et al. 1999). Areas within the polymer matrix may differ dramatically from the adjoining sections of the biofilm and from the overlying bulk fluid (de Beer et al. 1994). The polymer matrix may be able to limit the transport of gases to the extent that anoxic areas can form within biofilms in aerobic habitats. The depletion of oxygen from microhabitats within biofilms has important consequences for the corrosion of metals. The metal surface under the exopolymer becomes anodic relative to nearby areas with higher O_2 concentrations. Electrons flow from the anodic site to the cathode where they combine with O_2 and H^+, resulting in dissolution of the metal at the anode (Ford and Mitchell 1991, Gu et al. 2000).

Consumption of O_2 by microbial respiration and limitation of O_2 diffusion into the biofilm by the polymer matrix can lead to the formation of completely anaerobic microhabitats within and beneath the biofilm. Anaerobic conditions can result in the growth of sulfate-reducing bacteria (SRB), a frequent cause of microbiologically influenced corrosion (MIC).

Metal corrosion is driven by the hydrogenase activity of the SRB. Electrons flow from

the anodic site to the cathodic site, where they combine with H^+ produced from the dissociation of H_2O to form H_2. SRB remove H_2 and reduce SO_4^{2-} to S^{2-}, which reacts with dissociated Fe^{2+} to produce an FeS precipitate (Ford and Mitchell 1991, Gu et al. 2000). Prevention of microbial growth on the metal surface can effectively reduce rates of corrosion (Ford and Mitchell 1991, Gu et al. 2000).

Recent work in the Harvard University Mitchell laboratory has focused on microbial corrosion of aircraft fuel tanks. Microorganisms frequently contaminate jet fuel and cause corrosion of fuel tank metals. Little is known about the microbial community currently found in aircraft fuel tanks. We examined the composition of the microbial community found in fuel tanks containing jet fuel to determine the potential of this community to cause corrosion of aluminum alloy 2024 (AA2024). The microbial community of these fuel tanks is composed almost entirely of Bacillus and a small number of fungi (Figure 7.1). These microorganisms grew abundantly using hydrocarbons in the fuel as the sole carbon source. Electrochemical impedance spectroscopy and open circuit potential measurements indicated that the Bacillus-dominated community accelerated corrosion of AA2024 (Figure 7.2). This was confirmed by metallographic analysis. Despite the limited taxonomic diversity of microorganisms recovered from jet fuel, the bacterial community has the potential to corrode fuel tanks.

CURRENT WORK

We examined the potential role of microorganisms from Pearl Harbor in corrosion of the steel. Water samples from Pearl Harbor were collected by Ralph Mitchell and plated onto Difco nutrient agar. Isolates were collected and are being screened for the ability to use Bunker C fuel oil as a carbon source by inoculating cultures into minimal salt medium (0.22 g l^{-1} $(NH_4)_2SO_4$, 1.20 g l^{-1} KH_2PO_4, 0.23 g l^{-1} $MgSO_4 \cdot 7H_2O$, 0.25 g l^{-1} $CaCl_2$, 0.024 g l^{-1} yeast extract) with 1% Bunker C fuel oil.

As a surrogate for steel from USS *Arizona*, we used A36 steel which is similar to some steel on the *Arizona* (Johnson et al. 1999, see Chapter 5). Coupons were polished to 320 grit and inserted into corrosion cells containing minimal salt medium with 1% Bunker C fuel oil. One-half of the cells were inoculated with bacteria isolated from water in Pearl Harbor and the remaining cells were uninoculated controls. One hour after construction and weekly thereafter,
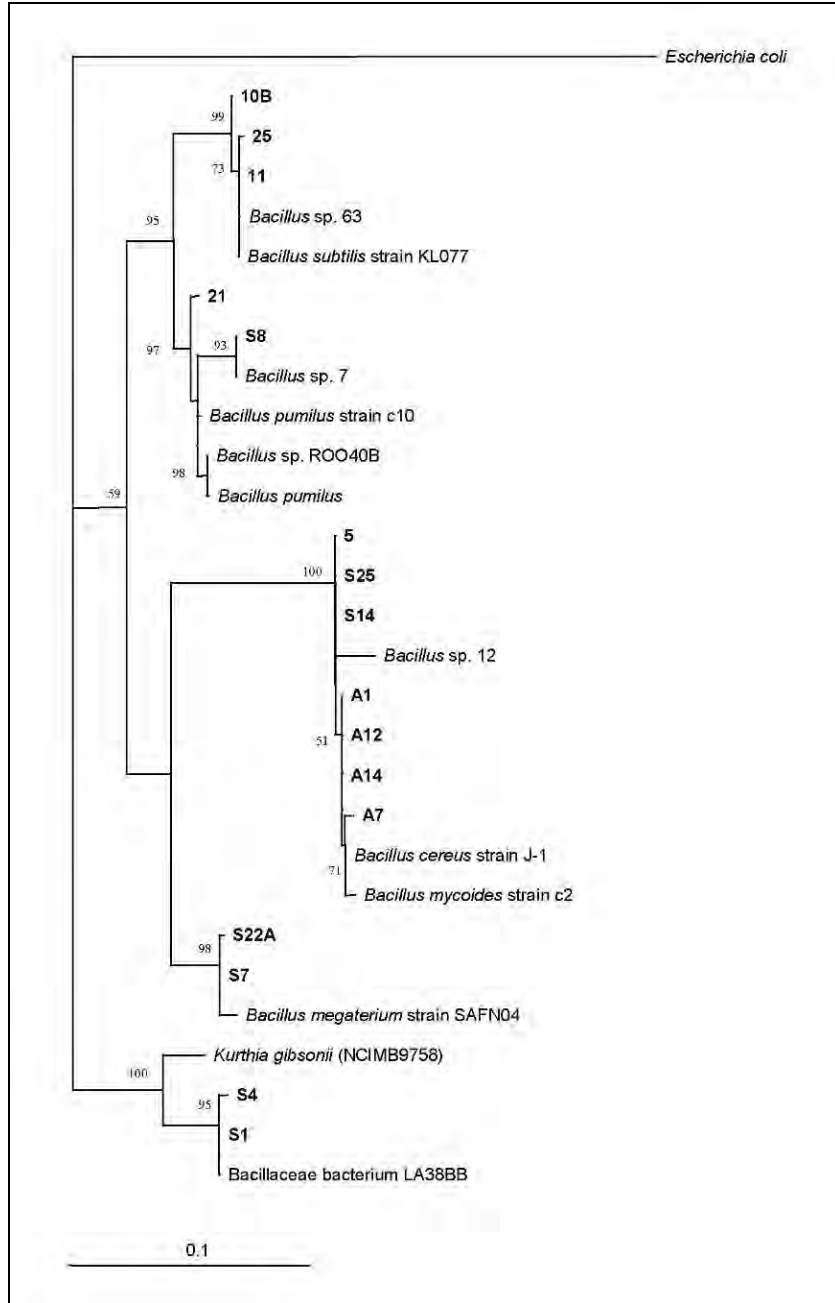
Figure 7.1. Phylogenetic relationships based on partial 16S rDNA sequences of bacterial isolates from aircraft fuel tanks and closely related sequences from the GenBank database. Neighbor joining tree; bootstrap values based on 1000 replicates are indicated for branches supported by >50% of trees. Scale bar represents 0.1 nucleotide changes per position.
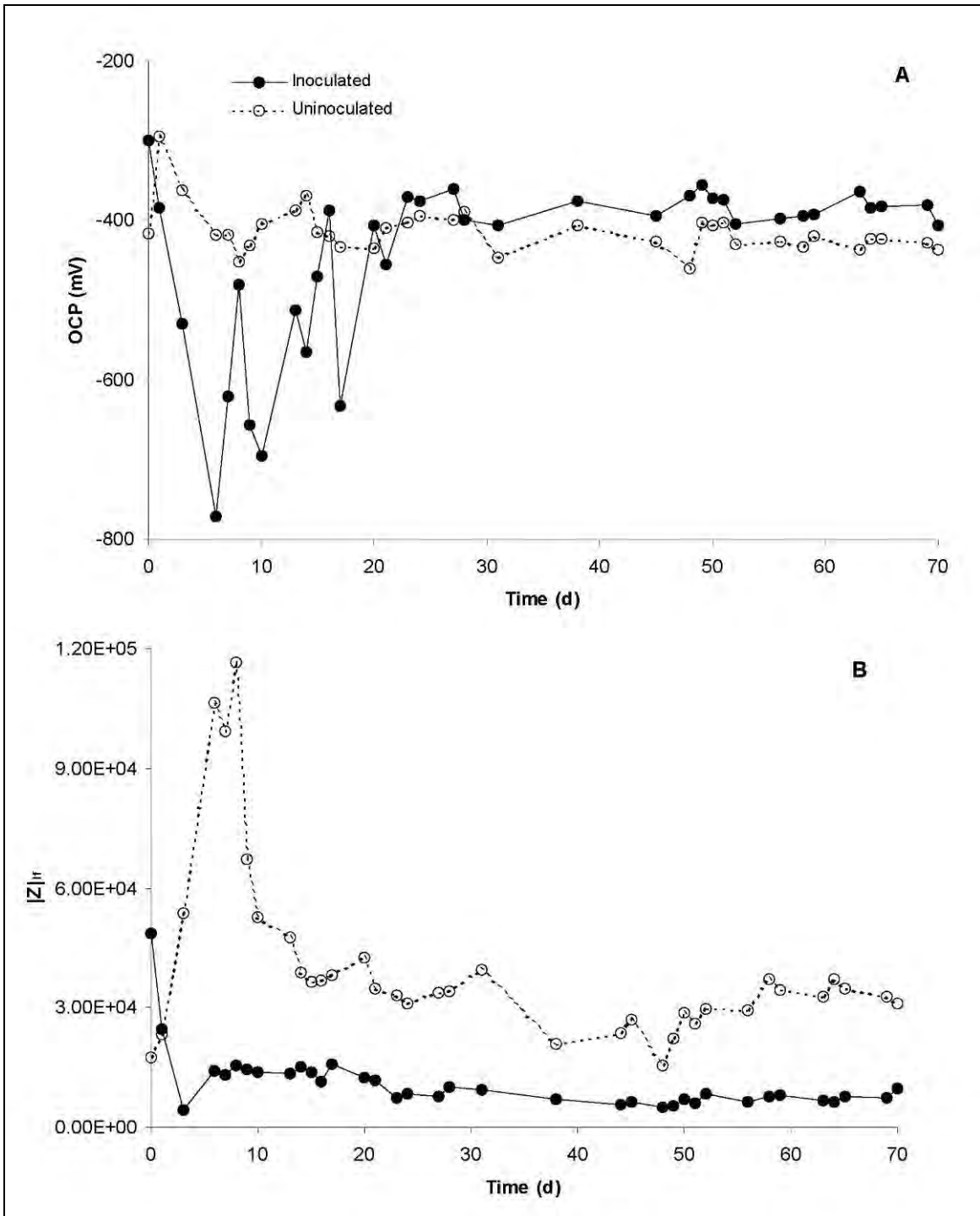
Figure 7.2. Open circuit potential (OCP) of aluminum alloy 2024 (AA2024) coupons (A).
Low frequency impedance (|Z|lf, 50 mHz) response of AA2024 coupons (B).

 the open circuit potential was measured, followed by a cyclic polarization (CP) scan (Figure

7.3). Coupons were polarized from –0.25 V vs. open circuit potential (OCP) to a vertex potential

of 1.0 V vs. OCP, and then a final potential of 0.0 V vs. OCP. The scan rate was 5.0 mV s^{-1}. All

measurements were made using a saturated calomel reference electrode.

Initial CP scans of the A36 stainless steel coupons were similar (Figures 7.4A and 7.5A).

After 1 week incubation inoculated and uninoculated cells are still similar (Figures 7.4B and

7.5B). Hysteresis of the curves is negative, there is no distinct primary passivation potential

(E_{pp}), and there appears to be a transpassive region and a breakdown potential (E_b). In addition,

the OCP is located within the passive region and is lower than the repassivation potential (E_{rp}).

After 3 weeks, differences between cyclic polarization (CP) scans for the inoculated and

uninoculated cells are apparent. The uninoculated cell did not change substantially from week 1

(Figure 7.4C). However, in the inoculated cell the E_{rp} decreased ~200 mV and while the

hysteresis was still negative, it was shifted in the positive direction. A passive film is damaged

when the potential is raised into the transpassive region. Negative hysteresis indicates that the

film repairs itself and pits do not initiate, while positive hysteresis indicates that the film is not

repaired and may indicate pit formation. Additionally, when the OCP is less than E_{rp} it is

believed that pits will not grow, while in the opposite case it is believed that pits will continue to

grow. Movement of the hysteresis in the positive direction and the decrease in the E_{rp} in the

inoculated cell may indicate a trend toward pitting corrosion caused by the biofilm.
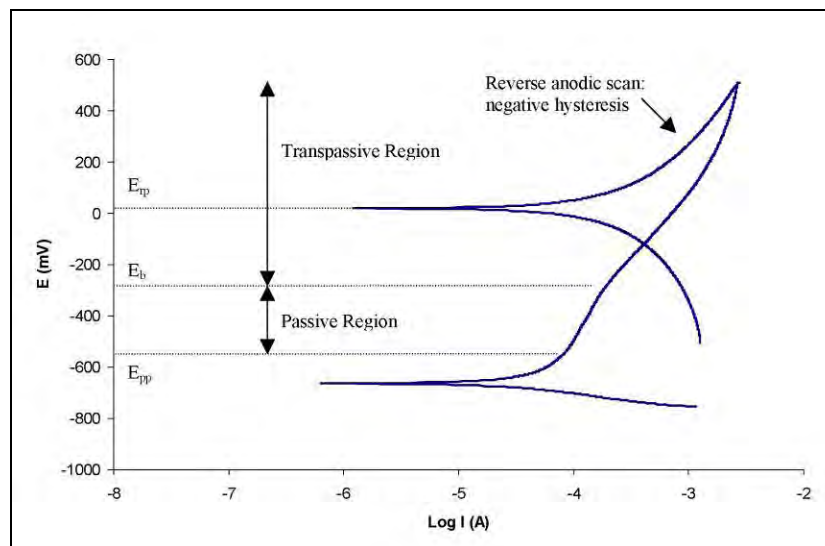
Figure 7.3. Generalized cyclic polarization scan illustrating characteristics of the curve.
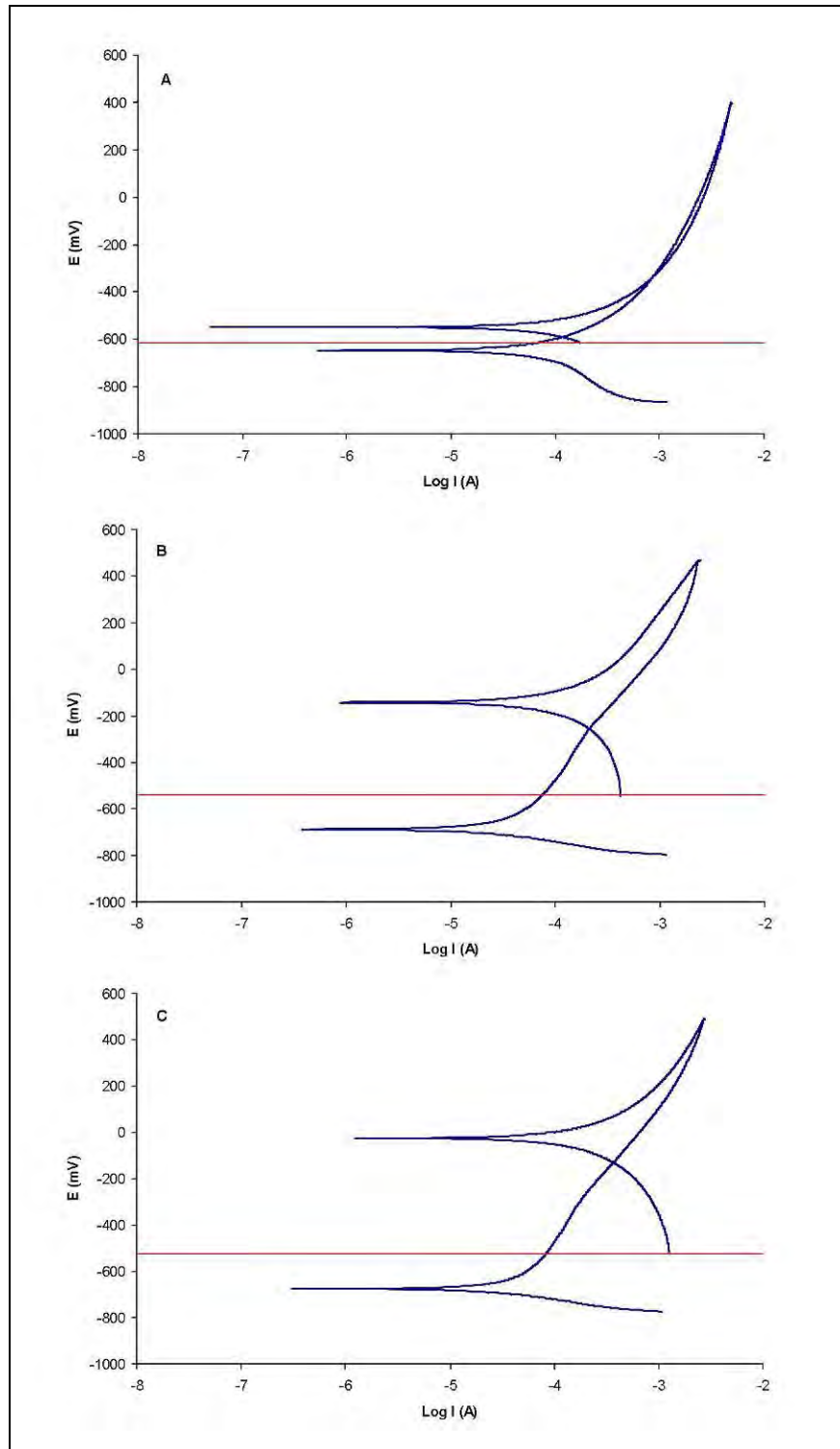
Figure 7.4. Cyclic polarization scans of uninoculated cells after 0 (A), 1 (B), and 3 (C) weeks. The open circuit potential is indicated by the horizontal line.
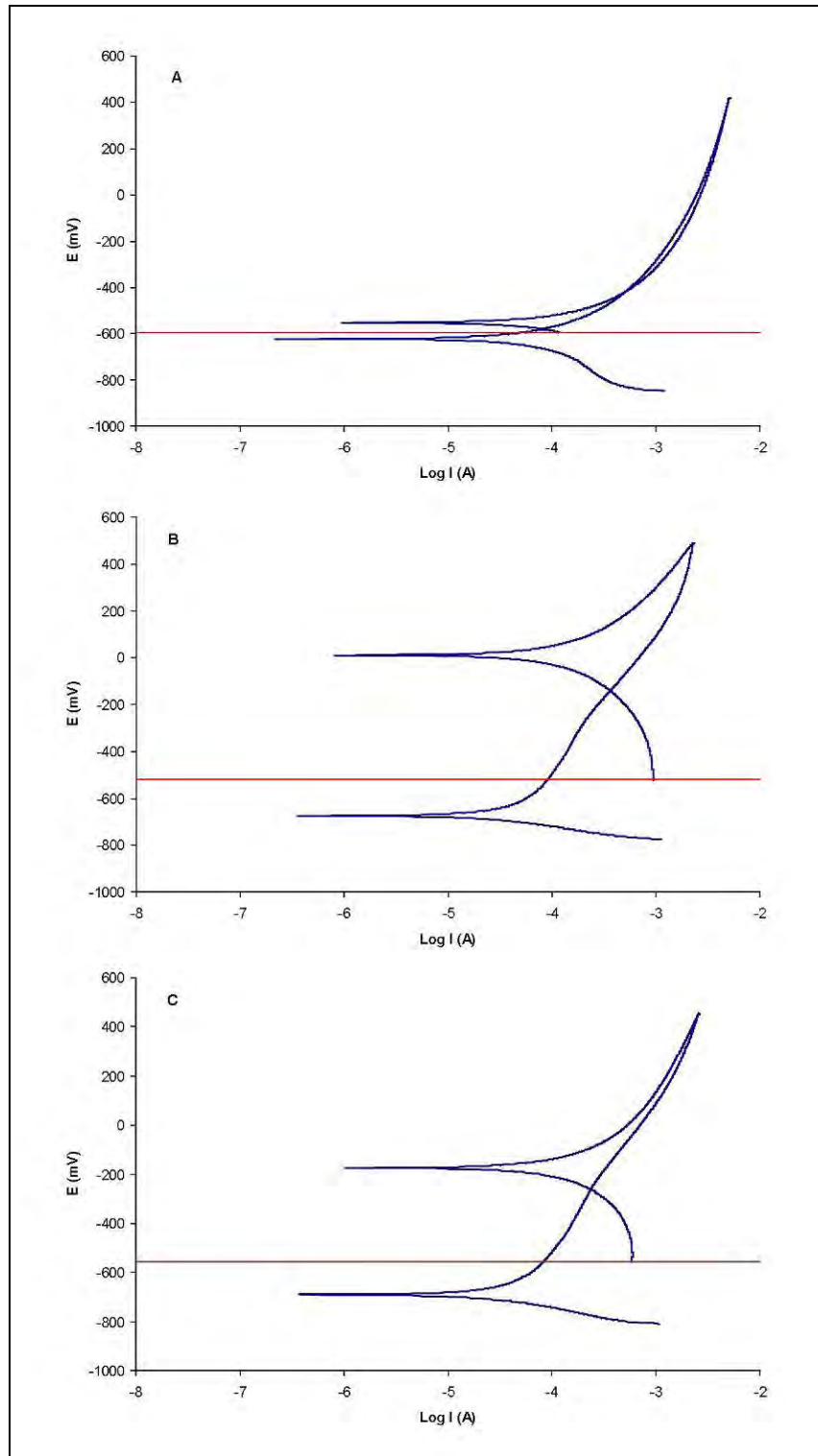
Figure 7.5. Cyclic polarization scans of inoculated cells after 0 (A), 1 (B), and 3 (C) weeks. The open circuit potential is indicated by the horizontal line.

ANALYSIS OF BACTERIAL COMMUNITY COMPOSITION IN USS *ARIZONA* CONCRETIONS

Invertebrate fouling communities called concretions form on archaeological metals submerged in marine environments. The concretions are inhabited by bacteria that play a role in formation and persistence of the concretion layer. We analyzed the bacterial community in concretion samples collected from the external hull of USS *Arizona* in Pearl Harbor, HI. Variability in the size of the bacterial community was high, and the concretions appear to harbor approximately 10^6 bacteria/g. Analysis of 16S rDNA clones indicated that the community consisted of bacteria related to three phyla: Firmicutes, Bacteroidetes, and Proteobacteria. The low bacterial diversity may indicate a late-succession stage community within the stable concretion. Alternatively, the low diversity could be the result of residual antifouling chemicals applied to the ship hull. It is likely that the bacterial community detected in these concretions plays an important role in the continuing corrosion of USS *Arizona*.

Thick biofouling layers referred to as concretions or encrustations form on archaeological materials in marine environments (Makinson et al. 2002). North (1976) characterized concretions formed on iron from the *Batavia* wreck, which sank in 1629 off the coast of Western Australia. The concretions consisted of a multilayered mixture of iron oxides (e.g., goethite and magnetite) and fragmented shell or skeletal material with an outer layer of living organisms that was indistinguishable from surrounding reef material.

Formation of concretion layers begins with the adhesion of bacteria to surfaces, which occurs rapidly in marine environments (Marshall et al. 1971). Attached bacteria subsequently impact the settlement and attachment of marine invertebrates (Maki et al. 1989). The invertebrate assemblages undergo a succession of organisms that begins with tunicates, bryozoans, amphipods, sponges, and barnacles, and is dominated in later stages by barnacles, sponges, and mussels (Bram et al. 2005).

Other locations where these communities have been studied include offshore oil and gas platforms, where fouling layers 10 - 20 cm thick have been found (Page et al. 1999). On these platforms, biofouling causes increased structural loads and wave resistance, and increased corrosion rates (e.g., within cracks and crevices or due to reduction in cathodic protection)

(Zvyaginstev 1990; Zvyaginstav and Ivin 1995). Concretions may have similar impact on archaeological materials.

The purpose of this study was to investigate the bacterial composition of concretions on USS *Arizona*. USS *Arizona*, a national shrine, war grave and naval memorial located in Pearl Harbor, Hawaii, is visited annually by more then 1.5 million people. In addition to the remains of more than 900 sailors and marines, the ship contains an estimated minimum 2,300 tons of fuel oil. Corrosion and deterioration of the ship both threaten an important national monument and represent a severe environmental hazard. This study is part of a larger effort by the National Park Service Submerged Resources Center to analyze the current condition of USS *Arizona*, to predict the future course of deterioration of the ship, and to preserve the site for future generations (Russell et al. 2004).

EXPERIMENTAL METHOD

Concretion samples were collected from two locations on the exterior hull of USS *Arizona* in November 2004. Samples were collected with a pneumatic drill fitted with a 7.6 cm diameter hole saw. Sample 14 was collected on the ship's port side near the stern at a depth of 5.9 m below the water surface. Sample 15 was collected on the ship's starboard side near the stern at a depth of 4.7 m below the water surface. Samples were shipped on ice overnight to Harvard University (Figure 7.6).

In the Mitchell Laboratory, samples were wrapped in sterile aluminum foil and pulverized with a hammer, sonicated (Branson model 2510 Ultrasonic Bath, Danbury, CT) for 5 min. to detach bacteria, and preserved with 1% formaldehyde. Bacteria were concentrated by filtration (15 kPa vacuum) onto 0.22 µm pore size black polycarbonate membranes (Poretics, Livermore, California), stained for 5 min. with 1.0 ml of 1.0 µg/ml 4',6-diamidino-2-phenylindole (DAPI), and rinsed with 1.0 ml deionized water (Porter and Feig 1980). Bacteria were then enumerated in three subsamples from each concretion using epifluorescence microscopy. Cells were counted in randomly selected fields at 1000X magnification until between 300 and 400 cells were enumerated.

DNA was extracted from concretions using the UltraClean Soil DNA Kit (MoBio Labs, Carlsbad, CA). The 16S rDNA was amplified using the polymerase chain reaction (PCR) as
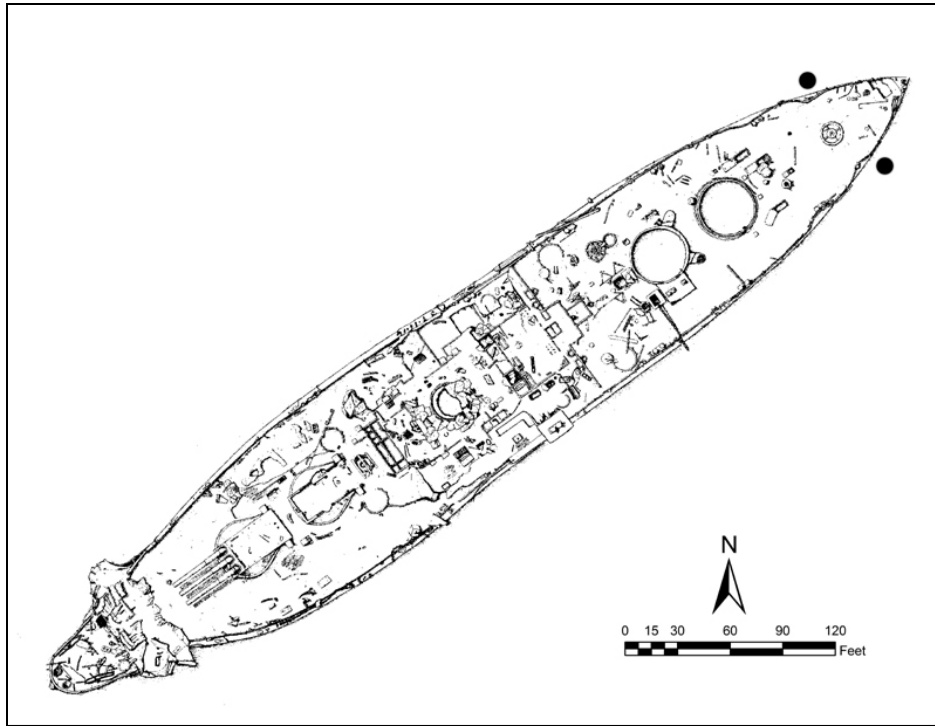
Figure 7.6. Points at the stern indicate sample locations on the exterior hull of USS *Arizona*. Sample 14 was collected on the port side of the ship and sample 15 on the starboard side (Drawing by NPS-SRC).

previously described (Perry et al. 2005) with primers 27f and 1492r (Lane 1991). The size of PCR products was verified by agarose gel electrophoresis. PCR products were purified using the QIAQuick PCR Purification Kit (Qiagen, Valencia, CA), cloned into the pCR 2.2-TOPO vector, and transformed into competent *Escherichia coli* as described in the manufacturer's instructions (TOPO TA Cloning Kit K4500-01, Invitrogen, Carlsbad, CA).

Clone inserts were PCR amplified from lysed colonies with vector specific primers. PCR products were simultaneously digested with *Msp*I and *Hha*I (Mills et al. 2003). Restriction digests contained 1.0 μg DNA and 5 units of each enzyme and were incubated at 37°C for three hours. Clones were grouped according to restriction fragment length polymorphism (RFLP) banding patterns and rarefaction curves were calculated for the RFLP patterns (Simberloff 1978). The diversity of sample 15 was estimated using Chao1 (Hughes et al. 2001).

Representative clones from each RFLP group were sequenced at the Dana Farber/Harvard Cancer Center High-Throughput DNA Sequencing Facility (Cambridge, MA) using a 3700 DNA Analyzer (Applied Biosystems, Foster City, CA) as described in the

manufacturer's instructions. Unaligned sequences were compared to the National Center for Biotechnology Information database using the Basic Local Alignment and Search Tool (BLAST) to find closely related sequences (Altschul et al. 1997). Alignments were constructed using Clustal X (Thompson et al. 1997) and phylogenetic analysis was performed using Paup 4.0 beta 10 (Swofford 2003). Sequences were deposited in the National Center for Biotechnology Information (NCBI) GenBank database.

RESULTS

We examined the bacterial community from two concretion samples removed from the exterior hull of USS *Arizona*. Bacterial numbers were not significantly different between samples (sample 14: $1.6 \times 10^6 \pm 7.6 \times 10^4$ bacteria/g; sample 15: $6.9 \times 10^6 \pm 1.4 \times 10^6$ bacteria/g; mean±se). Rarefaction analysis of RFLP patterns indicated that bacterial diversity of the concretion samples was low (Figure 7.7). Only six different RFLP patterns were found in sample 14, and 12 different RFLP patterns were observed in clones from sample 15. Using Chao1, the estimated diversity of sample 15 was 14.7.

Representative clones from each RFLP pattern were sequenced and compared to the NCBI database using BLAST (Table 7.1). The closest BLAST matches to all sequences were from organisms isolated from marine environments. All clones, with the exception of clone 15-1, contained sequences that were $\geq 96\%$ similar to the closest BLAST match. Clone 15-1 was 92% similar to the 16S rDNA of an uncultured bacterium from a hypersaline endoevaporitic microbial mat.

All clones were closely related to sequences obtained from bacteria belonging to three Phyla: Firmicutes, Flavobacteria, and Proteobacteria (Figure 7.8). Two of the clones (11% of all clones) were affiliated with the Firmicutes. Both clones were phylogenetically associated with organisms that are endospore forming anaerobes (i.e., *Alkaliphilus*, *Clostridum*, and *Tepidibacter*). Six of the clones (33% of all clones) were affiliated with the Proteobacteria. Three of these clones were closely associated with α-Proteobacteria and three were closely associated with γ-Proteobacteria. The majority of clones that were sequenced (10 clones or 55%) were phylogenetically affiliated with the Bacteroidetes.
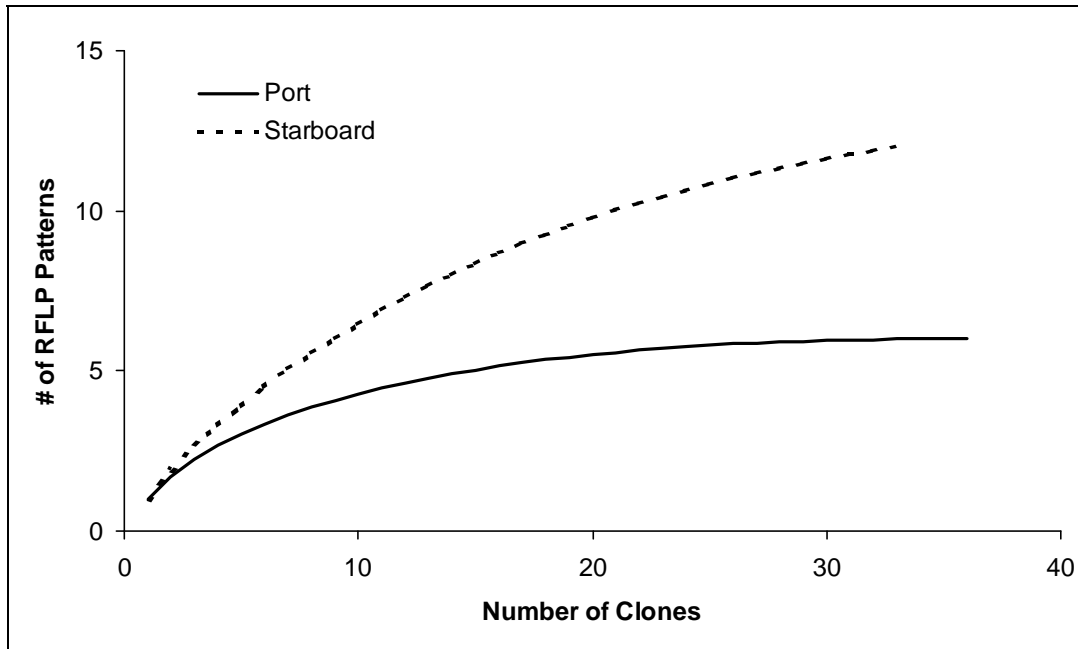
Figure 7.7. Rarefaction analysis of RFLP patterns from concretion samples.

DISCUSSION

Bacterial abundance in the concretions was similar to abundances typically reported for aquatic communities and for bacteria associated with stone and mineral formations (Linley 1983; McNamara et al. 2006). Despite the rather typical densities of microorganisms, the diversity of bacteria in the concretion was quite low, consisting of 18 different RFLP patterns representing bacteria from just three Phyla. The low bacterial diversity of the concretion communities was unexpected given the high diversity commonly found in marine systems (Giovannoni et al. 1990; Bernard et al. 2000).

All of the sequenced clones were similar to bacteria from seawater or marine invertebrates (based on the BLAST results). Phylogenetic affiliation of two clones with class Clostridia in the Firmicutes (anaerobic endospore formers) may indicate that there are anoxic microhabitats within the concretion. On the other hand, their presence could be due to the persistence of endospores in the concretion. The three clones that were phylogenetically associated with the α-Proteobacteria clustered with sequences from the genera *Roseobacter* and *Hyphomonas*, which are common in sea water and have been found associated with shellfish

(Jannasch and Wirsen 1981; Prabagaran et al. 2007). Among the γ-Proteobacteria-affiliated clones, *P. eurosenbergii* is associated with corals and coral bleaching (Thompson et al. 2004) while *H. venusta* is a moderate halophile that may be associated with fish (von Graevenitz et al. 2000). Within the Bacteroidetes, almost all clones were affiliated with the class Flavobacteria, which is extremely common in many environments, including seawater (Weeks 1981).

Sample Location	Clone	Putative Group	Closest BLAST Match (GenBank Accession No.)	% Similarity	No. of Clones (% Representation)[a]	Accession No.
Port	14-2	Bacteroidetes	*Formosa* sp. 5IX/A01/134 (AY576730)	100	3 (13)	EF173601
Port	14-3	γ-Proteobacteria	*Photobacterium eurosenbergii* strain LMG 22223T (AJ842344)	99	2 (8)	EF173602
Port	14-9	Bacteroidetes	*Flavobacterium* sp. V4.MO.31 (FSP244697)	97	4 (17)	EF173603
Port	14-14	α-Proteobacteria	*Roseobacter* sp. H454 (AY368572)	99	2 (8)	EF173604
Port	14-27	Bacteroidetes	*Flavobacterium* sp. V4.BO.21 (FSP244691)	97	12 (50)	EF173605
Port	14-29	Bacteroidetes	*Winogradskyella poriferorum* strain UST030701-295 (AY848823)	99	1 (4)	EF173606
Starboard	15-1	Bacteroidetes	Uncultured bacterium clone E2aA01 (DQ103638)	92	1 (3)	EF173607
Starboard	15-2	Bacteroidetes	*Formosa* sp. 5IX/A01/134 (AY576730)	100	1 (3)	EF173608
Starboard	15-4	Bacteroidetes	*Muricauda aquimarina* strain SW-72 (AY445076)	99	1 (3)	EF173609
Starboard	15-8	Firmicutes	Uncultured Gram-positive bacterium isolate MZ-31.NAT (AJ810555)	99	3 (9)	EF173610
Starboard	15-14	Bacteroidetes	*Salegentibacter* sp. 6-16 (AJ783959)	99	11 (33)	EF173611
Starboard	15-18	Bacteroidetes	*Gillisia mitskevichiae* (AY576655)	96	3 (9)	EF173612
Starboard	15-23	α-Proteobacteria	*Roseobacter* sp. JL-126 (AY745859)	100	3 (9)	EF173613
Starboard	15-25	α-Proteobacteria	*Hyphomonas jannaschiana* strain ATCC 33883 (T) (HJJ227814)	97	1 (3)	EF173614
Starboard	15-30	γ-Proteobacteria	*Halomonas* sp. BYS-1 (AY062217)	99	2 (6)	EF173615
Starboard	15-31	Firmicutes	Uncultured Gram-positive bacterium clone LR-39 (DQ302459)	98	2 (6)	EF173616
Starboard	15-39	Bacteroidetes	Marine bacterium KMM 3909 (AF536383)	96	3 (9)	EF173617
Starboard	15-40	γ-Proteobacteria	*Vibrio* sp. V261 (DQ146982)	98	2 (6)	EF173618

[a]Percent representation within each sample.

Table 7.1. Summary of 16S rRNA gene sequences identified in the clone library.
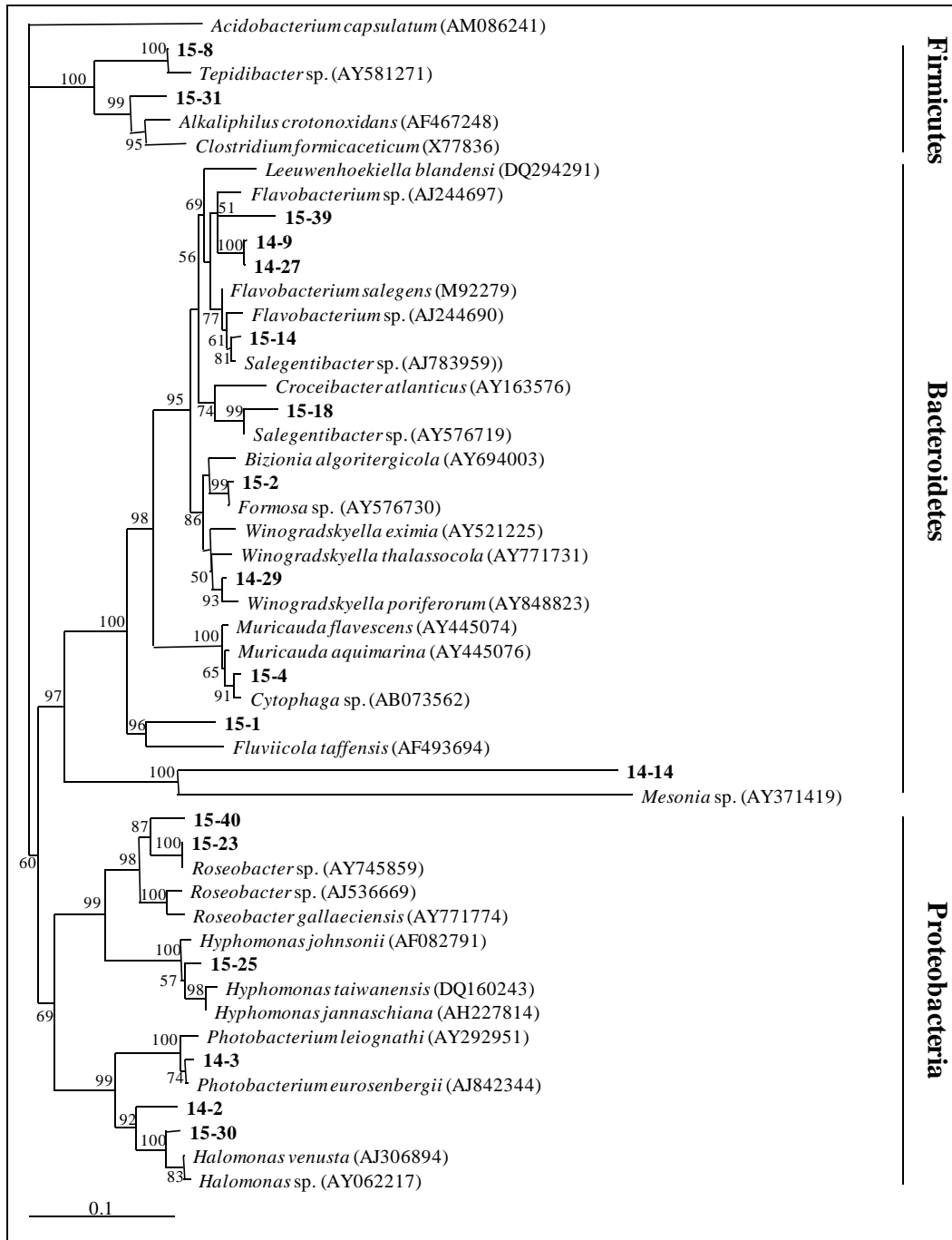
Figure 7.8. Neighbor joining tree based on 16S rDNA sequences of clones isolated from USS *Arizona*.
Bootstrap values based on 1000 replicates are indicated for branches supported by >50% of trees. Scale bar
represents 0.1 nucleotide changes per position.

There are similarities between the concretion communities from USS *Arizona* and other biofouling communities. For example, Moss et al. (2006) found that large percentages of estuarine biofilms were composed of Proteobacteria. Shikuma & Hadfield (2005) examined changes in biofilms in Pearl Harbor and found a stable community, composed mainly of Proteobacteria, which persisted over time at increasing densities. Similarities between these early-stage fouling communities and the bacterial community observed in concretions on USS *Arizona* suggest that the concretion community may be a stable, late successional-stage community that has developed from earlier attached communities.

Alternatively, the low diversity in concretions could result from residual antifouling paint on the hull. USS *Arizona* was completely retrofitted in March 1939. At that time, the U.S. Navy used copper or mercuric oxides contained in a variety of binders as antifoulants (Candries 2000). Many groups within the Bacteroidetes, a significant component of USS *Arizona* clones, are metal resistant (Jackson et al. 2005). The toxic antifouling paint may have limited early colonization and survival by bacteria, thereby resulting in low diversity in the mature fouling layer.

CONCLUSIONS

The bacterial community in concretions on the hull of USS *Arizona* is dominated by organisms from three groups: Firmicutes, Flavobacteria, and Proteobacteria. To our knowledge, this is the first study to examine the bacterial community of a late stage marine fouling concretion on archaeological materials. Further investigations of concretion microorganisms are needed to determine if the results obtained here are applicable to concretions on other submerged heritage sites and to determine the effect of the microorganisms on corrosion of the underlying metal.

Ultimately, this research is a work in progress. Because key elements remained unfunded during the USS *Arizona* Preservation Project, few conclusions can be made regarding the role of microorganisms in *Arizona*'s corrosion rate. Future work to be done on this project includes further study of the potential of microorganisms to cause corrosion of A36 steel, determining the effects of environmental factors such as temperature, nutrient levels and redox on MIC, and examining microbial corrosion rates on other types of steel that may be found both in hull structural steel and oil bunkers on both the sea water side and on the interior oil/steel interface.

REFERENCES

Altschul S.F., T.L. Madden, A.A. Schäffer, J. Zhang, Z. Zhang, W. Miller, and
D.J. Lipman
1997 Gapped BLAST and PSI-BLAST: a New Generation of Protein Database Search
Programs, *Nucleic Acids Research* 25:3389-3402.

Anwar, H., J.L. Strap, and J.W. Costerton
1992 Establishment of Aging Biofilms: Possible Mechanism of Bacterial Resistance to
Antimicrobial Therapy. *Antimicrobial Agents and Chemotherapy* 36:1347-1351.

Bernard L., H. Schäfer, F. Joux, C. Courties, G. Muyzer, and P. Lebaron
2000 Genetic Diversity of Total, Active and Culturable Marine Bacteria in Coastal Sea
Water, *Aquatic Microbial Ecology* 23:1-11.

Bram J.B., H.M. Page, and J.E. Dugan
2005 Spatial and Temporal Variability in Early Successional Patterns of an Invertebrate
Assemblage at an offshore oil Platform, *Journal of Experimental Marine Biology and
Ecology* 317:223-237.

Candries M.
12 December 2000 Paint Systems for the Marine Industry, *Notes to Complement the
External Seminar on Antifoulings*, Department of Marine Technology, University of
Newcastle-upon-Tyne, http://www.geocities.com/maxim_candries

Christensen, B.E. and W.G Characklis
1990 Physical and Chemical Properties of Biofilms, In *Biofilms*, edited by W.G.
Characklis and K.C. Marshall, John Wiley and Sons Inc., New York.

Costerton, J.W., Z. Lewandowski, D.E. Caldwell, D.R. Korber, and H.M. Lappin-Scott.
1995. Microbial Biofilms. *Annual Review of Microbiology* 49:711-745.

Costerton, J.W., P.S. Stewart, and E.P. Greenberg
1999. Bacterial biofilms: A Common Cause of Persistent Infections.
Science 284:1318-1322

de Beer, D., P. Stoodley, F. Roe, and Z. Lewandowski
1994. Effects of Biofilm Structures on Oxygen Distribution and Mass Transport.
Biotechnology and Bioengineering 43:1131-1138.

Ford, T.E. and R. Mitchell
1991. The Ecology of Microbial Corrosion. In *Advances in Microbial Ecology,* Vol.
11, edited by K.C. Marshall, Plenum Press, New York

Giovannoni S.J., T.B. Britschgi, C.L. Moyer, and K.G. Field
      1990 Genetic Diversity in Sargasso Sea Bacterioplankton, *Nature* 345:60-63

Gu, J.-D., T.E. Ford, and R. Mitchell
      2000 Microbial Corrosion of Metals. In *Uhlig's Corrosion Handbook, Second Edition,*
      edited by R. Winston Revie, John Wiley and Sons Inc., NY.

Hughes J.B., J.J. Hellman, T.H. Ricketts, and J.M. Bohannan
      2001 Counting the Uncountable: Statistical Approaches to Estimating Microbial
      Diversity, Applied Environmental Microbiology 67:4399-4406.

Jackson CR, KG Harrison, and S.L. Dugas
      2005 Enumeration and Characterization of Culturable Arsenate Resistant Bacteria in a
      Large Estuary, *Systematic Applied Microbiology* 28:727-734.

Jannasch H.W., and C.O. Wirsen
      1981 Morphological Survey of Microbial Mats Near Deep Sea Thermal Vents, Applied
      Environmental Microbiology 41:528-538.

Johnson, D.L., W.N. Weins, J.D. Makison, and D.A. Martinez
      1999 Metallographic Studies of the USS *Arizona*. Proceedings of the International
      Metallographic Society.

Lane D.J.
      1991 16S/23S rRNA Sequencing, In *Nucleic Acid Techniques in Bacterial Systematics*,
      edited by E. Stackebrandt, and M. Goodfellow, pp. 115-175, John Wiley and Sons, New
      York

Linley E.A.S., R.C. Newell, and M.I. Lucas
      1983 Quantitative Relationships Between Phytoplankton, Bacteria, and Heterotrophic
      Microflagellates in Shelf Waters, *Marine Ecology Progress Series* 12:77-89.

Maki J.S., D. Rittschof, A.R. Schmidt, A.G. Snyder, and R. Mitchell
      1989 Factors Controlling Attachment of Bryozoan Larvae: A Comparison of Bacterial
      Films and Unfilmed Surfaces, *Biology Bulletin* 177:295-302.

Makinson J.D., D.L. Johnson, M.A. Russell, D.L. Conlin, and L.E. Murphy
      2002 *In situ* Corrosion Studies on the Battleship USS *Arizona*, *Materials Performance*
      41:56-60.

Marshall K.C., R. Stout, and R. Mitchell
      1971 Mechanism of the Initial Events in the Sorption of Marine Bacteria to Surfaces.
      Journal of General Microbiology 68:337-348.

McEldowney, S. and M. Fletcher
    1987 Adhesion of Bacteria from Mixed Cell Suspensions to Solid Surfaces. *Archives of Microbiology* 148:57-62.

McNamara C.J., T.D. Perry, K. Bearce, G. Hernandez-Duque, and R. Mitchell
    2006 Epilithic and Endolithic Bacterial Communities in Limestone from a Mayan Archaeological Site, *Microbial Ecology* 51:51-64.

Mills H.J., C. Hodges, K. Wilson, I.R. MacDonald, and P.A. Sobecky
    2003 Microbial Diversity in Sediments Associated with Surface-Breaching Gas Hydrate Mounds in the Gulf of Mexico, *FEMS Microbiology and Ecology* 46:39-52.

Moss J.A., A. Nocker, J.E. Lepo, and R.A. Snyder
    2006 Stability and Change in Estuarine Biofilm Bacterial Community Diversity, *Applied Environmental Microbiology* 72:5679-5688.

North N.A.
    1976 Formation of Coral Concretions on Marine Iron, *International Journal of Nautical Archaeology and Underwater Exploration* 5:253-258.

Page H.M., J.E. Dugan, D.S. Dugan, J.B. Richards, and D.M. Hubbard
    1999 Effects of an Offshore Oil Platform on the Distribution and Abundance of Commercially Important Crab Species, *Marine Ecology Progress Series* 185: 45-57.

Perry IV T.D., V. Klepac-Ceraj, X.V. Zhang, C.J. McNamara, M.F. Polz, S.T Martin., N. Berke, and R. Mitchell
    2005 Binding of Harvested Bacterial Exopolymers to the Surface of Calcite, *Environmental Science and Technology* 39:8770-8775.

Porter K.G., and Y.S. Feig
    1980 The Use of DAPI for Identifying and Counting Aquatic Microflora, *Limnology and Oceanography* 25:943-948.

Prabagaran S.R., R. Manorama, D. Delille, and S. Shivaji
    2007 Predominance of Roseobacter, Sulfitobacter, Glaciecola, and Psychrobacter in Seawater Collected off Ushuaia, Argentina, Sub-Antarctica, *FEMS Microbiology and Ecology* 59:342-355.

Rittman, B.E., M. Pettis, H.W. Reeves, and D.A. Stahl
    1999 How Biofilm Clusters Affect Substrate Flux and Ecological Selection. *Water Science and Technology* 39:99-105.

Russell M.A., L.E. Murphy, D.L. Johnson, T.J. Foecke, P.J. Morris, and R. Mitchell
    2004 Science for Stewardship: Multidisciplinary research on *USS Arizona*, *Marine Technology Society Journal* 38:54-63.

Shikuma N.J., and M.G. Hadfield
    2005 Temporal Variation of an Initial Marine Biofilm Community and its Effects on
    Larval Settlement and Metamorphosis of the Tubeworm *Hydroides elegans*,
    Biofilms 2:231-238.

Simberloff D.
    1978 Use of Rarefaction and Related Methods in Ecology, In *Biological Data in Water
    Pollution Assessment: Quantitative and Statistical Analysis*, edited by K.L. Dickson, J.
    Cairns Jr., and R.J. Livingston, ASTM STP 652, American Society for Testing and
    Materials.

Swofford D.L.
    2003 *PAUP*. Phylogenetic Analysis Using Parsimony (*and Other Methods),* Ver. 4,
    Sinauer Associates, Sunderland, Massachusetts.

Thompson F.L., T. Iida, and J. Swings
    2004 Biodiversity of Vibrios, *Microbiology And Molecular Biology Reviews* 68:403-431.

Thompson J.D., T.J. Gibson, F. Plewniak, F. Jeanmougin, and D.G. Higgins
    1997 The ClustalX Windows Interface: Flexible Strategies for Multiple Sequence
    Alignment Aided by Quality Analysis Tools, *Nucleic Acids Research* 24:4876-4882.

von Graevenitz A., J Bowman., C. Del Notaro, and M. Ritzler
    2000 Human infection with *Halomonas venusta* Following Fish Bite, *Journal of Clinical
    Microbiology* 38:3123-3124.

van Loosdrecht, M.C.M., J. Lyklema, W. Norde, and A.J.B. Zehnder
    1990 Influence of Interfaces on Microbial Activity. *Microbiological Reviews* 54:75-87.

Weeks O.B.
    1981 The Genus Flavobacterium, *In The Prokaryotes: a Handbook on Habitats,
    Isolation, and Identification of Bacteria*, edited by M.P. Starr, H. Stolp, H.G. Trüper, A.
    Balows, pp. 1365-1370, H.G. Schlegel, Springer-Verlag, New York.

Whitfield, C.
    1988 Bacterial Extracellular Polysaccharides. *Canadian Journal of Microbiology*
    34:415-420.

Zvyaginstev A.Y.
    1990 Fouling and Corrosion Damage to Supporting Pillars of Oil Platforms in the South
    China Sea, *Soviet Journal of Marine Biology* 15:392-397.

Zvyaginstav A.Y., and V.V. Ivin
    1995 Study of Biofouling of the Submerged Structural Surfaces of Offshore Oil and Gas
    Production Platforms, *Marine Technology Society Journal* 29:59-62.

CHAPTER 8

An Environmental Study of USS *Arizona* Bunker C Fuel Oil

Amanda M. Graham

INTRODUCTION

USS *Arizona* was originally commissioned in 1916 as an oil-burning Pennsylvania-class battleship (Lenihan 1990). The ship was a member of Battle Division 8 in Norfolk, VA, where it served through World War I. Because of oil shortages during World War I the ship served as a gunnery training vessel and patrolled the North American Atlantic coast rather than joining other U.S. Navy vessels in Europe (Lenihan 1990). Following World War I and until 1929, USS *Arizona* served in various capacities including acting as a transport vessel and serving in the Pacific Ocean.

In 1929, USS *Arizona* was docked in Norfolk, VA, in order to modernize the vessel. Modernization included an increase in oil capacity from 2,332 to 4,630 tons of oil, adding increased protection from enemy fire, the addition of a modern power plant, and engine upgrades. Blisters were added to the outer hull for additional protection from torpedoes, and armor was added to the upper hull to minimize damage from anti-aircraft fire. The new power plant and engine upgrades allowed the vessel to maintain fleet speed and offset the increased weight load from the addition of more armament (Lenihan 1990). In 1940, post modernization, the ship sailed to the Pacific and was stationed in Pearl Harbor, HI.

On December 7 1941, USS *Arizona* along with other battleships stationed in Pearl Harbor, were attacked. Enemy fire that struck USS *Arizona* penetrated the upper deck armor and exploded near the forward magazine, which sympathetically detonated the magazines. The explosion caused the bow to collapse and the ship to sink while burning for two days following the attack (Lenihan 1990). The ship's bunkers, which hold 4,630 tons oil, had been filled with Bunker C fuel oil prior to the attack, helping to fuel the fire following the explosion. During the days following the attack, USS *Arizona*, USS *West Virginia*, USS *Tennessee*, USS *Maryland*, USS *Oklahoma*, and USS *California* leaked Bunker C fuel oil into the surrounding harbor. Other battleships stationed near USS *Arizona* sustained less damage during the attack and went on to serve during World War II. In comparison, USS *Arizona* was not usable for World War II, but instead the ship was scavenged for parts. *Arizona* remains where it sank, and its significance in the 1941 Pearl Harbor attack is acknowledged physically by a memorial built over the remains of the ship The National Park Service currently manages the memorial.

Although oil was burned off following the Pearl Harbor attack, an unknown amount of oil remains trapped in the ship, and leaks from the ship continuously. The National Park Service Submerged Resources Center collected oil as it leaked from the ship and determined that at least 1 to 2 liters of oil per day leak from the ship into the surrounding harbor (Johnson et al. 2002; Murphy and Russell, personal communication). Little is known about the interior of the ship because of USS *Arizona*'s status as a memorial. Therefore, this study represents a unique opportunity to characterize oil leaking from the ship, determine whether the oil from the ship is present in surrounding sediments, and study the microbial degradation of fuel oil leaking from USS *Arizona*. This information is an important first step in understanding the influence of Bunker C fuel oil leaking from the ship on the surrounding environment, and will also contribute to management strategies for the ship. This study was conducted as part of USS *Arizona* Preservation Project and was designed to address several research domains that are directly concerned with the oil contained within *Arizona*'s hull, understanding its nature and the implications for inferring what is occurring within the hull, and the oil's impact on the environment.

BUNKER C FUEL OIL COMPOSITION AND PROPERTIES

During the crude oil refining process, different distillates are collected based on boiling temperatures (Hunt 1995). Bunker C is from the No. 6 petroleum distillation-boiling fraction, which is the highest distillation-boiling fraction (>400°F), and is sometimes referred to as "No. 6" fuel oil. Bunker C consists of saturates (i.e., *n*-alkanes, branched alkanes, and cycloalkanes), aromatics (i.e., naphthalenes and benzo[*a*]pyrene), heterocycles (i.e., benzothiophenes and naphthobenzothiophenes), asphaltenes, and resins (Irwin et al. 1997). The oil may also contain sulphur and nitrogen, contained in heterocycles, along with vanadium and nickel complexed to asphaltenes (Walker et al. 1976; Irwin et al. 1997; Lunel et al. 2000). Since Bunker C is from the highest petroleum distillation fraction, it contains increased concentrations of high molecular weight carbon molecules in comparison to other lower boiling fraction distillation oils (i.e., diesel) (Irwin et al. 1997). For example, in comparison to other lighter distillate oils, Bunker C contains a large concentration of high molecular weight molecules, especially $C_{12} - C_{34}$ *n*-alkanes and large polycyclic aromatic hydrocarbons (PAHs). Furthermore, approximately 5% of the total PAH concentration consists of four to six ring aromatic hydrocarbons (Irwin et al. 1997; Richmond et al. 2001). The American Petroleum Institute (API) gravity of Bunker C is 12.3° and it has a density of 971 kg/m^3 at 22°C along with a low water soluble fraction (WSF) <10 ppm.

The large concentration of high molecular weight molecules increases the viscosity of Bunker C fuel oil and makes it difficult to use. Therefore, to make the Bunker C more usable it may be blended with a lighter oil (i.e., diesel) (Irwin et al. 1997). Post-distillation additives, such as calcium, cerium, iron, or manganese, may also be added to increase combustion temperatures (Irwin et al. 1997). Thus, the actual composition of Bunker C is variable and dependent upon the distillation process along with any lighter oil blending and post-distillation additives (Irwin et al. 1997).

ENVIRONMENTAL FATE OF BUNKER C FUEL OIL

The original chemical composition of oil greatly influences its susceptibility to weathering processes following release into the environment. Weathering includes biotic (i.e.,

microbial degradation) and abiotic (i.e., evaporation) processes that alter oil composition. Weathering begins immediately following an oil spill and can be temperature and environment dependent (Atlas 1984; NRC 2003). Evaporation and dissolution are the first weathering processes to occur following an oil spill and the extent of both processes is dependent on the type of oil. Heavier oils (i.e., Bunker C fuel oil), which contain an increased concentration of higher molecular weight hydrocarbons are not as susceptible to evaporation and dissolution in comparison to lighter oils (i.e., diesel) containing few high molecular weight hydrocarbons (Atlas 1984; Irwin et al. 1997; NRC 2003). The extent of oil dispersion is also less extensive in heavier oils in comparison to lighter oils. Heavier oils have a much lower water soluble fraction than lighter oils; therefore, following a spill involving heavier oils, fewer hydrocarbons will enter the water column and become associated with suspended sediments or be available to microorganisms for degradation. Heavy fuel oils are less immediately bioavailable to organisms and less degradation or fewer toxic responses may occur (Atlas 1984; NRC 2003). However, heavier oils contain a greater concentration of PAHs, which may absorb into and accumulate in sediments, and remain there for years following an environmental release, making heavier oils a greater long-term environmental threat than lighter oils (Irwin et al. 1997; Bixiam et al. 2001).

Photooxidation is another type of weathering process and occurs when hydrocarbons are oxidized to ketones, aldehydes, alcohols and acids by energy transfer between molecules (Garrett et al. 1998; NRC 2003). Following photooxidation, hydrocarbon products are more water-soluble than their precursors and therefore become more bioavailable (Garrett et al. 1998; NRC 2003). Garrett and colleagues (1998) suggested aromatics were affected by photooxidation more than saturated compounds found in crude oil, indicating that oils with more aromatics have an increased susceptibility to photooxidation.

Emulsification and tarball formation are also important weathering processes. Oil will emulsify when water droplets are formed in oil, and emulsification is dependent on the percentage of resins and asphaltenes in spilled oil (NRC 2003). Heavier oils with higher concentrations of asphaltenes and resins will emulsify before lighter oils (NRC 2003). Tarballs are formed by recalcitrant high molecular weight hydrocarbons, which can sink in the water and deposit in sediments (NRC 2003). Both emulsification and tar ball formation increase the density and viscosity of oil and provide an increased surface area for microbial attachment (NRC

2003). These weathering processes are important in determining the environmental fate of spilled oil.

Following an environmental release, the chemical properties of Bunker C fuel oil make it more difficult to clean up and more likely to persist in the environment in comparison to lighter oils (Irwin et al. 1997; Lunel et al. 2000; Richmond et al. 2001; NRC 2003). Most hydrocarbons in Bunker C have a high molecular weight and therefore are not likely to evaporate (Irwin et al. 1997; Lunel et al. 2000). Following an environmental release of Bunker C, less than 10% of the oil will evaporate, in comparison to lighter oils such as diesel, in which 75% of the oil will evaporate (Irwin et al. 1997; Lunel et al. 2000; Richmond et al. 2001; NRC 2003). The high density, viscosity, and increased concentration of high molecular weight molecules of Bunker C also allow it to sink in freshwater and saltwater and form stable tar balls and emulsify in saltwater (Irwin et al. 1997; Lunel et al 2000; Richmond et al. 2001; NRC 2003). These chemical properties of Bunker C allow it to persist in the environment longer than lighter fuel oils following a spill, and Bunker C has been detected more than 20 years after an environmental spill (Vandermeulen and Singh 1994; Wang et al. 1994; Irwin et al. 1997; NRC 2003). Overall, the original make-up of oil is an important factor in its eventual environmental fate. In addition, utilization of hydrocarbons by microorganisms occurs at the oil-water interface, therefore the amount of oil in the water indicates the amount of oil that will be bioavailable for degradation or toxic response by organisms (Irwin et al. 1997; Barron et al. 1999; Baars 2002).

TOXICITY OF BUNKER C FUEL OIL

The high viscosity and high concentration of PAHs in Bunker C oil composition contributes to its toxicity in the environment (Irwin et al. 1997). However, it is considered to be less toxic than lighter petroleum products, such as diesel, because less Bunker C enters the water column immediately following an oil spill (NOAA 1994; Irwin et al. 1997; Barron et al. 1999; Baars 2002). As a result, the immediate danger to the environment in spills involving Bunker C is the coating of marine organisms as well as ingestion of the fuel oil by marine organisms (Irwin et al. 1997; Richmond et al. 2001; Baars 2002; Hir and Hily 2002). The stability of Bunker C fuel oil in water and its potential persistence in the environment (i.e., sedimentation of PAHs)

results in a long-term environmental persistence and increases the exposure of toxic components to the surrounding environment (Bixian, et al. 2001; Richmond et al. 2001).

Emulsification of Bunker C oil increases the threat of toxicity because it increase, the mobility of toxic compounds including (i.e., PAHs) entering the water column (Irwin et al. 1997; Richmond et al. 2001). Richmond et al. (2001) documented increased toxicity of emulsified Bunker C by using Microtox® assays to detect decreased light emission from bioluminescent bacteria exposed to emulsified Bunker C. The study found a decrease in the toxicity (by Microtox® assays) in microorganisms grown in chitin-amended pre-emulsified Bunker C media in comparison to microorganisms grown in pre-emulsified Bunker C media only. This decrease in toxicity was attributed to PAH adsorption to chitin (Richmond et al. 2001).

Bunker C toxicity to humans is associated with the presence of the 16 PAHs that are listed by the Environmental Protection Agency's (EPA) priority pollutants for remediation (Irwin et al. 1997; Baars 2002). These priority pollutants include naphthalene, acenaphthylene, acenaphthene, fluorene, phenanthrene, anthracene, flouranthene, pyrene, benzo[*a*]anthracene, chrysene, benzo[*b*]fluoranthene, benzo[*k*]fluoranthene, benzo[*a*]pyrene, benzo[*a,h*]anthracene, benzo[*g,h,i*]perylene, and indeno[*c,d*]pyrene (EPA 1984; Baars 2002). PAHs contained in the EPA's priority pollutant list are are 2-ring to 5-ring PAHs and individually suspected carcinogens, (i.e., bezno[*a*]pyrene) (Samanta et al. 2002). While the toxicity of individual PAHs has been demonstrated, PAHs in the environment are encountered as a mixture which may contribute to increased toxicity (Neilson 1994; Samanta et al. 2002). A human toxicity study was performed following a 2.8 million gallon spill of Bunker C by the *Erika* off the coast of Brittany, France in 1999 (Baars 2002; Samanta et al. 2002). Baars (2002) found no toxic effects to humans involved in the spill clean up and tourists in the area following the *Erika* spill. However, individuals that cleaned birds after the spill measured benzo[*a*]pyrene dermal exposure levels of 295 ng/cm^2, far above the human exposure limit value of 2 ng/cm^2 according to the Netherland National Institute of Public Health and the Environment (Baars 2002). Together these studies suggest Bunker C is of toxicologic concern.

BUNKER C FUEL OIL SPILLS IN THE MARINE ENVIRONMENT

Bunker C fuel oil is a major contributor to marine oil spills because of its frequent use and transport in marine vessels. The greatest environmental impact of spills in the open ocean results from the oil washing ashore and contaminating coastal environments. According to the United Kingdom National Environmental Technology Centre, 90-95% of heavy fuel oil spills in the open ocean are washed ashore (Lunel et al. 2000). Following the *Erika* spill in the Atlantic Ocean approximately 65 km south of Britanny, France, much of the oil was washed into coastal waters where it impacted coastal industries such as fishing (Baars 2002).

Bunker C fuel oil causes environmental problems for coastal habitats and has been shown to persist following a spill in coastal areas, including Chedabucto Bay, Nova Scotia, Canada, for over 20 years because of its high concentration of high molecular weight components (Vandermeulen and Singh 1994; Wang et al. 1994). The *Arrow* spilled 528,344 gallons of Bunker C fuel oil near the Chedabucto Bay of Nova Scotia, Canada in 1970. By comparing the oil samples taken in 1990 from beaches considered to have low ecological energy inputs by ocean action to the original *Arrow* oil Vandermuelen and Singh (1994) confirmed that degraded petroleum residues of *Arrow* oil were still present. These authors also demonstrated that *Arrow* oil was still present in samples taken from Jargon Lagoon and Black Duck Cove south of Chedabucto Bay and on the North Atlantic Coast (Vandermeulen and Singh 1994). Furthermore, oil samples taken from Black Duck Cove were in a relatively unweathered form still containing an *n*-alkane profile similar to the original *Arrow* Bunker C oil (Vandermeulen and Singh 1994). PAHs from Black Duck Cove were also similar to the original *Arrow* Bunker C oil and some lower molecular weight aromatics (i.e., naphthalene) were still present (Vandermeulen and Singh 1994). Biomarker profiles, which are used for oil identification, were used to compare oil samples from Jargon Lagoon and Black Duck Cove to original *Arrow* biomarker profiles (Vandermeulen and Singh 1994). Oil samples from both areas had similar biomarker profiles when compared to original *Arrow* Bunker C oil (Vandermeulen and Singh 1994). These biomarker results suggest the unweathered oil present in Black Duck Cove is *Arrow* Bunker C oil that had persisted for over 20 years, from 1970 to 1994. However, not all Bunker C spills exhibit the long-term environmental persistence of the *Arrow* oil spill because of varying coastal conditions.

On December 23 1988, *Nestucca* spilled approximately 230,000 gallons of Bunker C fuel oil in the Pacific Ocean contaminating Washington and Vancouver c oastal areas (Strand et al. 1992). In comparison to the *Arrow* oil, there was little persistence of *Nestucca-* spilled petroleum by the third sampling period in February 1990 (Strand et al. 1992). The contrast in petroleum persistence between the Washington and Vancouver coastline (*Nestucca* spill) and the Nova Scotia coast line (*Arrow* spill) can be explained by the differences in the ocean energy inputs (i.e., wave action, strength of local currents and wind) of the contaminated coastal areas, and in the amount of clean up following the spill (Atlas 1981; Strand et al. 1992; Vandermeulen and Singh 1994). Areas that had extensive Bunker C fuel oil persistence from the *Arrow* were low to medium energy coastal areas. Also, after the 1970 spill, the decision was made to allow these areas to recover naturally rather than clean up the sites (Vandermeulen and Singh 1994). Comparatively, the coastal areas studied from the 1988 *Nestucca* spill were higher energy coastal areas and improvements were made in the clean up of coastal oil spills by use of oil absorbing pads and pom-poms (Strand et al. 1992).

Tracking and monitoring environmental oil spills is difficult because of different weathering parameters, such as biodegradation by microorganisms, that can change components of oil. Therefore, components in oil that are conserved and resistant to biotic and abiotic weathering processes can be used as references to monitor biotic and abiotic weathering (Prince et al. 1994; Frontera-Suau et al. 2002). This is generally accomplished using a conserved suite of compounds found in oil referred to as biomarkers.

<div align="center">OIL BIOMARKERS</div>

Biomarkers (i.e., hopanes) are complex organic molecular fossils that share structural similarity to parent biological precursors, and tend to be resistant to weathering processes (Peters and Moldowan 1993). Biomarker profiles are unique to each oil and can be used to link crude oil to its source (Hunt 1995). Therefore, biomarkers are used extensively for identifying the source of an oil spill along with assessing the extent of oil weathering (Mackenzie 1984; Peters and Moldowan 1993; Kvenvolden et al. 1995; Whittaker and Pollard 1997; Wang et al. 2001b). Biomarkers are derived from environmental inputs during oil formation and closely resemble the parent molecules from which they were formed (Mackenzie 1984; Peters and Moldowan 1993;

Kvenvolden et al. 1995; Whittaker and Pollard 1997; Wang et al. 2001b). For example, pristane and phytane (Figure 8.1) are branched acyclic isoprenoids that are derivatives of phytol, which is associated with chlorophyll (Mackenzie 1984; Peters and Moldowan 1993). Hopane (Figure 8.1) is a pentacyclic triterpane and originates from bacteriohopane, a component of bacterial membranes (Mackenzie 1984; Peters and Moldowan 1993; Prince et al. 1994). Steranes, in comparison, originate from eukaryotic sterols (Peters and Moldowan 1993). Because of their predecessor molecules, pristane, phytane, hopanes and steranes are ubiquitous in oil and therefore are the most commonly used biomarker ratios for oil identification and internal references to determine the extent of weathering (Whittaker and Pollard 1997). Hopanes and steranes are more persistant than pristane and phytane which are prone to microbial degradation and may be degraded within days of a spill (Blumer and Sass 1972; Prince et al. 1994). Therefore, pristane and phytane are only useful for identification and weathering ratios prior to extensive microbial degradation and weathering (Blumer and Sass 1972; Prince et al. 1994; Whittaker and Pollard 1997; Wang et al. 1999; Frontera-Suau et al. 2002). Hopane and sterane ratios have been used as identification and weathering ratios for oil up to 25 years following the original spill (Wang et al. 1998b).

Pristane   Phytane

C$_{30}$ 17α,21β(H)-Hopane   18α(H)-Oleanane
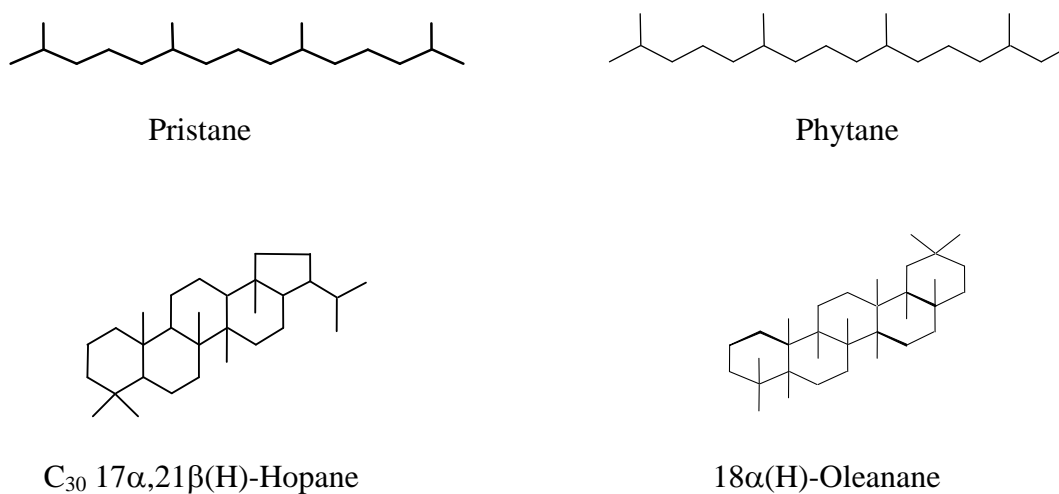
Figure 8.1. Selected biomarker chemical structures.

Biomarker ratios are used as a tool for oil identification and also to determine the extent of oil biodegradation (Peters and Moldowan 1993; Prince et al. 1994; Bost et al. 2001; Frontera-Suau et al. 2002). For example, maturity and source correlation ratios indicate the thermal maturity of oil and the original bedrock source. These ratios can be used as identification tools to relate unknown oils to the original source and as a chemical fingerprint for oil to oil relatedness (Peters and Moldowan 1993). For example, Kvenvolden and colleagues (1995) used hopane and sterane ratios to identify an oil source in Prince William Sound, Alaska as input other than the Alaskan North Slope crude oil spilled on March 24 1989 from the *Exxon Valdez*. Furthermore $17\alpha,18\alpha,21\beta$(H)-28,30-bisnorhopane $17\alpha,18\alpha,21\beta$(H)-25,28,30-trisnorhopane, and 18α(H)-oleanane were also detected, and these are three biomarkers compounds not present in Alaskan North Slope crude oil from the *Exxon Valdez*. (Kvenvolden et al. 1995). In addition, other studies have used similar ratios to correlate fresh or weathered oil with its original source (Vandermeulen and Singh 1994; Wang et al. 1994; Wang et al. 1995; Munoz et al. 1997; Wang et al. 1998a; Wang et al. 2001a; Wang et al. 2001b; Zakaria et al. 2001).

Biomarkers can also be used as an internal reference to observe the extent of degradation. Laboratory and field studies have focused on 17α(H),21β(H)-hopane as an internal reference for weathering and degradation studies because it is found in all oils (Peters and Moldowan 1993). In addition, 18α(H)-oleanane (Figure 8.1) is also important for oil weathering and degradation studies, because no laboratory studies have shown it to be degraded although it is found only in oils formed with angiosperm input and therefore is not a ubiquitous biomarker (Peters and Moldowan 1993; Alberdi and Lopez 2000). Prince and colleagues (1994) found 17α(H),21β(H)-hopane to be resistant to microbial degradation, and not produced during oil degradation using Alaskan North Slope crude oil in a laboratory study at 15°C. Pollard et al. (1999) quantified oil degradation in laboratory microcosms containing Fuel oil No. 6 by using biomarker ratios. They found the Σn-alkanes to 17α(H),21β(H)-hopane ratio to be the most sensitive to degradation compared to the ratio of Σn-alkanes to branched alkanes pristane and phytane. Aerobic degradation of 17α(H),21β(H)-hopane has been observed in laboratory studies by using a 18α(H)-oleanane to 17α(H),21β(H)-hopane ratio of Bonny Light crude (Frontera-Suau et al. 2002) and Venezuelan crude oils (Bost et al. 2001).

Degradation of 17α(H),21β(H)-hopane has also been observed in field studies. For example degradation of 17α(H),21β(H)-hopane was observed in an oil spill of Arabian Light crude into a tropical ecosystem of Guadeloupe, France in 1986 (Munoz et al. 1997) and also in the Gulf of Quintero Bay, Chile, where the *Metulla* spilled Arabian Light crude and Bunker C fuel oil in 1974 (Wang et al. 2001a). The results of these studies suggest some microorganisms are capable of degrading 17α(H),21β(H)-hopane and therefore a suite of biomarkers should be used to monitor microbial oil degradation.

AEROBIC OIL DEGRADATION

Microorganisms are capable of utilizing many of the compounds in oil as their sole carbon source. Aerobic degradation of oil proceeds by utilizing the saturates in the order of increasing *n*-alkanes, branched alkanes and finally cycloalkanes. Concurrent with *n*-alkane degradation, the aromatics are degraded in order of size, with lower molecular weight aromatic degradation occurring before higher molecular weight aromatics.

Aerobic microbial degradation studies have shown *n*-alkanes are the easiest component of oil to degrade, and degradation of *n*-alkanes has been demonstrated with increasing chain length up to *n*-C_{44} (Haines and Alexander 1974; Atlas 1981). Utilization of *n*-alkanes for growth of microorganisms may proceed by β oxidation (Figure 8.2) with an initial monoterminal attack by monooxygenase forming an alcohol, followed by the formation of an aldehyde. Finally, a monocarboxylic acid is formed (Atlas 1981; Widdel and Rabus 2001). Further utilization of the monocarboxylic acid can be achieved by β-oxidation and the formation of two-carbon unit fatty acids and acetyl coenzyme A, which eventually results in the formation of CO_2 (Schaeffer et al. 1979; Atlas 1981; Salanitro et al. 1997). Branched isoprenoids, such as pristane and phytane, are more difficult for microorganisms to utilize as a carbon source because of methyl branching (Schaeffer et al. 1979; Atlas 1981; Salanitro et al. 1997). Microbial attack of isoprenoids is dependent on the position of methyl branching and strategies other than β oxidation can be utilized if branching occurs in the β-position (Schaeffer et al. 1979). For example, utilization of branched alkanes (i.e., pristane) by an alternate strategy, for example, ω oxidation, forms dicarboxcylic acids and continues until mineralization by β-oxidation (Atlas

1981). Examples of other initial methods of attack by microorganisms are α oxidation or β alkyl group removal (Pirnik 1977).

In contrast to straight and branched alkanes, cycolalkanes are more resistant to microbial attack. Cycloalkanes are found throughout the environment from natural sources (i.e., oil, plants and microbes) along with synthetic sources (Trudgill 1978; Atlas 1981; Perry 1984). Furthermore, cycloalkanes are often used as biomarkers (i.e., hopane) in oil (Peters and Moldowan 1993). Microbial cycloalkane metabolism occurs more readily in cycloalkanes containing a side chain (i.e., methylcyclohexane) than in unsubstituted cycloalkanes (i.e., cyclohexane) (Trudgill 1978; Atlas 1981; Perry 1984).

Utilization of unsubstituted cycloalkanes proceeds by oxidation of the ring forming an intermediate alcohol or ketone. These intermediates can be further utilized by ring cleavage and subsequent β, α, or ω oxidation (Trudgill 1978; Atlas 1981; Perry 1984). Although few microbial cultures have been able to metabolize unsubstituted cycloalkanes, Stirling and colleagues (1977) were able to isolate a *Nocardia* sp. with different cycloalkanes (i.e.,
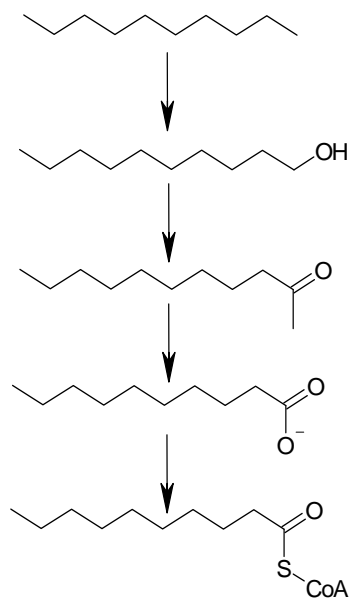
Figure 8.2. β-oxidation pathway for microbial utilization of *n*-alkanes (Adapted from Atlas 1984).

dodecylcyclohexane and heptadecylcyclohexane) as the sole carbon sources. Metabolism of cycloalkanes with a side chain is initiated by β-oxidation of the *n*-alkane, yielding a cyclohexane carboxylic acid (Beam and Perry 1974; Atlas 1981).

Degradation of aromatic hydrocarbons in oil is of special interest because of persistence and carcinogenicity associated with PAHs, which increases with increasing ring size (Cerniglia 1992; Kanaly and Harayama 2000; Dean-Ross et al. 2002). Bunker C fuel oil is made up of 25% aromatics, with approximately 5% of the total PAH concentration consisting of four to six ring aromatic hydrocarbons (Irwin et al. 1997; Richmond et al. 2001). Microbial degradation pathways differ with the amount of substitution and the number of rings present, but are initiated by dioxygenation of an aromatic ring forming *cis*-dihydrodiol (Figure 8.3) (Atlas 1981; Neilson 1994). Pathways for microbial growth with PAHs up to three rings (i.e., naphthalene and phenanthrene) as the sole carbon source have been elucidated in the laboratory (Figure 8.3), indicating that individually these molecules can be readily degraded (Cerniglia 1992). Co-oxidation is an important degradation pathway for high molecular weight PAH molecules with four or more rings (i.e., flouranthene and benzo[*a*]pyrene) (Atlas 1981; Cerniglia 1992; Juhasz and Naidu 2000; Kanaly and Harayama 2000). Few laboratory bacterial cultures have utilized high molecular weight PAHs as a sole carbon source, although there are exceptions for the four ring molecules pyrene, chrysene, and flouranthene. Microorganisms capable of utilizing PAHs with more than four rings (i.e., benzo[*a*]pyrene) as the sole carbon source have not been isolated, although degradation by co-oxidation has been demonstrated in the laboratory and the field (Cerniglia 1992; Juhasz and Naidu 2000; Kanaly and Harayama 2000). Although studies using individual PAHs are important for pathway elucidation, studies observing degradation of mixed PAHs are also important because this is how PAHs occur environmentally. Thus far, studies using PAH mixtures have shown both enhanced (Beckles et al. 1998) and inhibitory (Dean-Ross et al. 2002) degradation effects, which indicates more research is needed to understand microbial degradation of PAH mixtures.

ANAEROBIC OIL DEGRADATION

Anaerobic degradation of oil is important in contaminated sediments, in oil reservoirs and during oil refining and transport. For example, sulfate reducing bacteria are found in oil refining sites where their growth causes corrosion of machinery because of H_2S formation during

Figure 8.3. Representative pathway for microbial utilization of naphthalene (Adapted from Neilson 1994).

anaerobic metabolism of petroleum (Postgate 1979). Studies since have shown that anaerobic

bacteria utilizing different electron acceptors, such as sulfate, nitrate, and ferric iron, are able to

degrade hydrocarbons, including aromatics (i.e., toluene) and longer chain *n*-alkanes (i.e.,

hexadecane) (So and Young 1999; Anderson and Lovely 2000; Elshahed et al. 2001; Boll et al.

2002). Both anaerobic alkane and aromatic degradation are initiated by the same step, the

addition of a functional group (i.e., methyl or fumarate) to the respective substrate (Spormann

and Widdel 2000). Two sulfate reducing strains, Hxd3 and Pnd3, were found to utilize *n*-alkanes

by the addition of a C_1 functional group to the *n*-alkane substrate (Aeckersberg et al. 1998;

Rabus et al. 2001; Widdel and Rabus 2001). Anaerobic degradation of toluene, a monoaromatic

hydrocarbon, has been widely studied and can be degraded by pure anaerobic cultures utilizing

sulfate, nitrate, and ferric iron as an electron acceptor (Spormann and Widdel 2000). The toluene

degradation pathway is initiated by fumarate addition to the methyl group by benzylsuccinate

synthase which yields benzylsuccinate (Spormann and Widdel 2000; Rabus et al. 2001; Widdel

and Rabus 2001; Boll et al. 2002). These studies indicate anaerobic degradation pathways are

important to consider in oil degradation.

MICROBIAL INFLUENCE ON SHIPWRECKS

Aerobic and anaerobic microbial metabolism can contribute to the deterioration of a sunken ship by physically influencing the surrounding environment (i.e., pH change) or by degrading materials in or on the ship. For example, studies have shown bacterial communities can physically influence pH and increase deterioration rates of wood, bone and iron (Gregory 1995; McLeod 1995). Other studies have shown that canvas deterioration in a shipwreck was due to microbial degradation (Gregory 1995; Wheeler 2001). This indicates microbial processes can effect shipwrecks chemically (i.e., pH influence) and biologically (i.e., degradation). There is a need to better understand how microbial populations affect the integrity of a shipwreck.

A better understanding of microbial interactions within a shipwreck is specifically important for USS *Arizona* because the ship is made of steel and lies in a temperate saltwater environment, making it very susceptible to corrosion. The ship also contains and is leaking Bunker C oil that can be used as a carbon source for microbial growth, suggesting that microbial metabolic activities may be extensive. Anaerobic degradation of the oil may cause H_2S formation, increasing the ship's corrosion rate (Postgate 1979). Future studies can build upon the need to understand how oil degrading microbial communities influence metal corrosion and USS *Arizona* provides an excellent site for this type of scientific research.

SIGNIFICANCE AND OBJECTIVES OF THIS RESEARCH

Since the sinking of USS *Arizona* in 1941, it has been estimated that 1-2 liters of oil are released per day from the ship into the surrounding Pearl Harbor waters (Murphy and Russell, personal communication). The ship rests in a warm saltwater environment, which is conducive to structural corrosion. Further corrosion of the ship may ultimately result in the remaining amount of oil located in the ship to be released into the surrounding Pearl Harbor environment at a faster rate. This study will characterize oil leaking from USS *Arizona* to determine the extent of oil weathering prior to its release into the environment. Furthermore, this study will compare biomarker fingerprints of oil leaking from the ship to biomarkers of oil in sediments. This will determine if oil leaking from the ship is present in surrounding sediments. We will also determine if microorganisms from sediments on and surrounding the ship can degrade oil leaking

from the ship. This study will not only contribute to the overall understanding of the biodegradation and weathering of Bunker C oil in the marine environment, but it will also provide a foundation upon which future management decisions are made by the National Park Service regarding the ship and the surrounding environment. Therefore, the objectives of this study are:

1.   To chemically characterize oil leaking from the ship, including the hopane and sterane biomarkers.

2.   To characterize and fingerprint oil in sediments collected adjacent to and surrounding USS *Arizona*.

3.   To determine if aerobic microorganisms associated with USS *Arizona* sediments are capable of degrading Bunker C fuel oil leaking from the ship and if they influence Bunker C biomarker profiles.

MATERIALS AND METHODS

SEDIMENT AND OIL SAMPLES

Sediment and oil samples were collected from USS *Arizona* located in Pearl Harbor, HI, during 2000 and 2001 by underwater archaeologists from the National Park Service's Submerged Resources Center (Figures 8.4 and 8.5). Sediment samples were collected underwater by divers using 500 ml glass Erlenmeyer flasks. Sediment-filled flasks were brought to the surface, flushed with N_2, capped with black rubber stoppers, and sealed with electrical tape. Flasks were immediately placed in a cooler on ice. Samples of oil leaking from various USS *Arizona* locations (designated A and B) were collected using PVC pipes equipped with 50 ml conical polypropylene tubes attached to the end of the pipe. Conical tubes were brought to the surface, flushed with N_2, capped, and sealed with electrical tape. Samples were shipped on ice from Pearl Harbor to the laboratory in South Carolina and stored at 4°C.

Bow

Port   **Starboard**

Location B

01-029 Starboard Porthole S-43
(second deck, Disbursing Office)

01-018 Starboard Porthole S-38 (second
deck , Captain's Officer Stateroom)

01-026 Starboard Porthole S-34
(Junior Officer Stateroom)

00-004, 00-005, 00-006, 00-007
Starboard Porthole S-31

01-032 Midship's Galley

00-008, 01-019 Starboard Hatch

01-012 Starboard Porthole S-20

01-027 Starboard Captain's cabin

Location A

00-009 A hatch starboard of
Barbette No. 4

01-015 A hatch starboard of
Barbette No. 4

00-034 A hatch starboard of
Barbette No. 4

Barbette No. 4

Port   **Starboard**

Stern

**Figure 8.4. USS *Arizona* sample locations for oil leaking from the ship. Location A
(stern starboard hatches) and B (stern starboard portholes) represent two different
general areas of the ship.**

311

Bow

Port   **Starboard**

01-041 Sediment
collected port side of
gun turret no. 1.

01-031 Sediment
collected near gun turret
no. 1.

00-032, 00-033 Sediment
collected port side 10 ft. from
hull

00-001, 00-00Table 8.2. Oil
leaking from USS *Arizona*
hopane biomarker ratios.
2, 00-003 Sediment collected
starboard side 12 ft. from hull

00-030 Sediment collected from
the bottom of barbette no. 4

Port   **Starboard**

Stern

Figure 8.5. USS *Arizona* sediment sample locations.

USS *ARIZONA* OIL EXTRACTIONS

To characterize oil leaking from different areas of the ship, oil samples (that included a mix of oil and seawater) were extracted using dichloromethane (GC Grade, EM Science, Gibbstown, NJ) and NaCl (2% in distilled water). After extracts became clear, five more fractions were collected to ensure good recovery for each sample, and all extracts were combined. Following extraction, samples were evaporated at 50ºC under vacuum to approximately 3 ml. Samples were then transferred to pre-weighed scintillation vials, air-dried, and weighed.

SEDIMENT EXTRACTIONS

To characterize hydrocarbons in sediments collected on the ship and in adjacent sediments, wet sediments were extracted using a Soxhlett apparatus. For each sediment sample, a sub-sample (approximately 2 g) was placed in a cellulose thimble (33 mm x 80 mm, Whatman, Maidstone, England) and extracted with a combination of the following three solvents placed in a round bottom flask: 30 ml acetone (GC Grade, Fisher Scientific, Fair Lawn, NJ), 30 ml hexane (GC Grade, Burdick & Jackson, Muskegon, MI), and 180 ml dichloromethane (GC Grade, EM Science, Gibbstown, NJ). After continuous Soxhlet extraction for 16 h, the extracts were evaporated and weighed.

USS *ARIZONA* ENRICHMENT CULTURES

To enrich for oil degrading microbial communities from USS *Arizona* sediments, Bunker C oil-degrading enrichment cultures were initiated using 1 g of USS *Arizona* wet sediments, 24 ml of GP2 medium, a synthetic saltwater medium supplemented with potassium nitrate (Chang, et al. 2000) that was amended with 2 mg/ml USS *Arizona* 00-034 oil. Oil sample 00-034 was chosen for the enrichment study because it was less weathered in comparison to other samples of USS *Arizona* oil. Enrichments were maintained in the dark at 30°C at 200 rpm and were transferred after 30 days using a 4% inoculum transfer. Samples for oil and microbial community analysis were not taken until after three monthly transfers had occurred. Aliquots (1

ml) were removed from the third monthly transfer at day 30 and stored at –80°C for microbial community structure analysis. The remaining contents of each culture flask were extracted for oil analysis.

USS *ARIZONA* ENRICHMENT CULTURE EXTRACTIONS

To remove oil from USS *Arizona* enrichment cultures, oil was extracted by shaking the entire contents of the culture flasks 5 times with approximately 100 ml of dichloromethane. Extracts were dried with anhydrous sodium sulfate (12-60 mesh, J.T. Baker, Phillisburg, NJ) and evaporated under vacuum to approximately 3 ml at 50ºC. Samples were then transferred to pre-weighed scintillation vials, air-dried and weighed.

OIL ANALYSIS

For all oil analyses, extracted oil (from both oil samples leaking from USS *Arizona* and aerobic enrichment cultures) and sediment solvent-extractable materials were first shaken for 6 h with hexane, and allowed to sit overnight to precipitate the asphaltenes. Deasphaltened samples were analyzed with a Hewlett-Packard Model 5890 Series II *Plus* gas chromatograph using a flame ionization detector and HP-5 column (25 m, 0.32 mm i.d.x 0.17 υm). The initial temperature was 50°C with a 5°C/min rate change to a final temperature of 310°C where it was held for 20 min. The injector temperature was 290°C and the detector temperature was 315°C. Helium was used at the carrier gas at 20.0 psi (Bost et al. 2001). Extractable materials were run at the same time as Bonny Light crude (BLC) oil, an oil that has been thoroughly characterized in the laboratory (Frontera-Suau et al. 2001; Norman et al. 2002), for peak comparisons. An additional peak was further examined in sediment solvent-extractable materials since it was predominant and ubiquitous in all sediment samples. This peak was analyzed collaboratively with Dr. Kevin Crawford (The Citadel, Charleston, SC) using a ThermoQuest gas chromatograph coupled to a Polaris Q mass spectrometer (full scan, EI mode).

PAH AND BIOMARKER ANALYSIS

PAHs and their alkylated homologues, as well as biomarkers (refer to Table 8.1 for a complete list) were analyzed by Dr. Tom McDonald (Texas A&M University, College Station, TX) using a Hewlett-Packard 5890 II gas chromatograph coupled to a Hewlett-Packard mass spectrometer in selected ion monitoring mode (SIM) according to the method of McDonald and Kennicutt (1992). Calibration standards were prepared at five concentrations (from 0.02 – 1 µg/ml) by diluting a commercially available standard (NIST SRM 2266). For each compound of interest, a relative response factor (RRF) was determined for each calibration level, and the 5 RRFs averaged to produce a relative response factor for each compound.

BIOMARKER QUANTITATION

Following analysis, biomarkers concentrations were calculated using peaks from m/z=191 to identify terpanes and m/z=217 to identify steranes (Bost et al. 2001). Peak concentrations were determined by multiplying the area under the peak by the calculated standard. Following concentration calculation, ratios were determined. C_{30} $17\alpha(H),21\beta(H)$-hopane was divided by $18\alpha(H)$-oleanane for the hopane to oleanane ratio. This ratio was used to determine if C_{30} $17\alpha(H),21\beta(H)$-hopane was being degraded (Bost et. al. 2001; Frontera-Suau et. al. 2002). C_{27} $17\alpha(H)$-22,29,30-trisnorhopane (Tm) and C_{27} $18\alpha(H)$-22.29,30-trisnorneohopane (Ts) were used for the Ts/(Ts + Tm) ratio. The concentration of Ts was divided by the sum of Ts and Tm concentrations. This ratio can be used as a maturity and source rock ratio (Peters and Moldowan 1993). The concentrations of C_{31} $17\alpha(H)$-homohopane (22*S* and 22*R*) were used for the C_{31} 22*S*/(22*S* + 22*R*) ratio. The concentration of 22*S* was divided by the sum of 22*S* and 22*R* concentrations. This ratio was used to determine if the 22*R* epimer was being degraded in comparison to the 22*S* epimer (Peters and Moldowan 1993). Tricyclic terpane ratios were also calculated from mass chromatograms m/z=191 using the peak areas of C_{28} $13\beta,21\alpha(H)$-tricyclic terpane 22*R* and 22*S* and C_{29} $13\beta,21\alpha(H)$-tricyclic terpane 22*R* and 22*S,* respectively to compare with the peak area of C_{30} $17\alpha,21\beta(H)$-hopane. These ratios were calculated to determine if C_{28}

PAHs and Heterocycles

Compound	Abbreviation	Compound	Abbreviation
Naphthalene	C0N	Fluoranthene	Fl
C1-Naphthalenes	C1N	Pyrene	C0Py
C2-Naphthalenes	C2N	C1-Fluoranthenes/Pyrenes	C1Py
C3-Naphthalenes	C3N	C2-Fluoranthenes/Pyrenes	C2Py
C4-Naphthalenes	C4N	C3-Fluoranthenes/Pyrenes	C3Py
Benzothiophene	C0B	Naphthobenzothiophene	C0Nbf
C1-Benzothiophenes	C1B	C1-Naphthobenzothiophenes	C1Nbf
C2-Benzothiophenes	C2B	C2-Naphthobenzothiophenes	C2Nbf
C3-Benzothiophenes	C3B	C3-Naphthobenzothiophenes	C3Nbf
Biphenyl	Bph	Benz(a)anthracene	BaA
Acenaphthylene	Acl	Chrysene	C0C
Acenaphthene	Ace	C1-Chrysenes	C1C
Dibenzofuran	Dbf	C2-Chrysenes	C2C
Fluorene	C0F	C3-Chrysenes	C3C
C1-Fluorenes	C1F	C4-Chrysenes	C4C
C2-Fluorenes	C2F	Benzo(b)fluoranthene	BbF
C3-Fluorenes	C3F	Benzo(k)fluoranthene	BkF
Anthracene	An	Benzo(e)pyrene	BeP
Phenanthrene	C0P	Benzo(a)pyrene	BaP
C1-Phenanthrene/Anthracenes	C1P	Perylene	Pe
C2-Phenanthrene/Anthracenes	C2P	Indeno(1,2,3-c,d)pyrene	IP
C3-Phenanthrene/Anthracenes	C3P	Dibenzo(a,h)anthracene	DA
C4-Phenanthrene/Anthracenes	C4P	C1-Dibenzo(a,h)anthracenes	C1DA
Dibenzothiophene	C0D	C2-Dibenzo(a,h)anthracenes	C2DA
C1-Dibenzothiophenes	C1D	C3-Dibenzo(a,h)anthracenes	C3DA
C2-Dibenzothiophenes	C2D	Benzo(g,h,i)perylene	BP
C3-Dibenzothiophenes	C3D		

Cycloalkanes

Compound	Abbreviation
C_{30} 17α(H),21β(H)-hopane	C29-Hopane
18α-Oleanane	18α-Oleanane
C_{30} 17α(H),21β(H)-hopane	C30-Hopane

Table 8.1 PAHs, alklyated PAHs and cycloalkanes analyzed by GC-MS.

13β,21α(H)-tricyclic terpanes or C_{29} 13β,21α(H)-tricyclic terpanes were being degraded in comparison to C_{30} 17α,21β(H)-hopane.

Mass chromatogram peak areas of C_{27} 5α(H),14α(H),17α(H)-sterane (20*S* and 20*R*), C_{27} 5α(H),14β (H),17β (H)-sterane (20*S* and 20*R*) and C_{30} 17α(H),21β(H)-hopane were calculated for the $C_{27}S/C_{30}H$ ratio. This ratio was used to determine if C_{27} -steranes were being degraded in comparison to conserved C_{30} 17α(H),21β(H)-hopane. Mass chromatogram peak areas C_{28} 5α(H),14α(H),17α(H)-sterane (20*S* and 20*R*), C_{28} 5α(H),14β (H),17β (H)-sterane (20*S* and 20*R*) and C_{30} 17α(H),21β(H)-hopane were calculated for the $C_{28}S/C_{30}H$ ratio. This ratio was used to determine if the C_{28}-steranes were being degraded in comparison to conserved C_{30} 17α(H),21β(H)-hopane. Mass chromatogram peak areas of C_{29} 5α(H),14α(H),17α(H)-sterane (20*S* and 20*R*), C_{29} 5α(H),14β (H),17β (H)-sterane (20*S* and 20*R*) and C_{30} 17α(H),21β(H)-hopane were calculated for the $C_{29}S/C_{30}H$ ratio. This ratio was used to determine if the C_{29}-steranes were being degraded in comparison to conserved C_{30} 17α(H),21β(H)-hopane.

DNA EXTRACTION AND ANALYSIS

DNA extractions from aerobic enrichment cultures were performed according to Bost (2001). Aliquots (1 ml) of each enrichment culture were centrifuged for 10 min at 14,000 rpm. The resulting pellet was resuspended in 556 μl of TE buffer (10 mM Tris-HCl, pH 7.5; 1 mM EDTA, pH 8.0) and treated with 11 μl of lysozyme (50 mg/ml, Sigma, St. Louis, MO). After a 30 min incubation at 37°C, proteinase K (3 μl) and SDS (30 μl) were added, and the mixture was incubated for 1 h at 65°C. Following incubation 100 μl of 5 M NaCl and 80 μl hexadecyltrimethylammonium bromide (10% CTAB in O.7 M NaCl, J.T. Baker, Phillipsburg, NJ) were added, and the mixture was incubated for 10 min at 65°C. The mixture was extracted consecutively with chlorform:isoamyl alcohol (24:1), phenol:chloroform:isoamyl alcohol (25:24:1), and chlorform:isoamyl alcohol (24:1) at room temperature, and the supernatant was recovered at each step. Recovered supernatant was resuspended in 450 μl of chilled isopropanol to precipitate DNA and stored at -20°C for at least two hours. The mixture was centrifuged for 10 min at 14,000 rpm and 4°C, then the supernatant was removed. The DNA pellet was washed with 500 μl of chilled 70% ethanol for 30 min. DNA pellet and 70% ethanol were centrifuged for

15 min at 14,000 rpm and 4°C. Supernatant was removed and the DNA pellet was air dried, then resuspended in 50 μl of TE buffer.

DNA AMPLIFICATION

To amplify extracted DNA 16s rDNA was amplified by polymerase chain reaction (PCR), targeting a 323 base pair fragment, using two primers common to the *Bacteria* domain (Ferris et. al. 1996). The forward primer used for amplification was (5570F), *E. coli* positions 1055 to 1070; 5'-ATGGCTGTCGTCAGCT-3', and the reverse primer used for amplification was (9206GCR); *E. coli* positions 1392 to 1406 5'-CGCCCGCCGCGCCCCGCGCCCGGCCCGCCGCCCCCGCCCCACGGGCGTGTGTAC-3'. DNA aliquots of 0.5 ml were added to PCR master mix containing 1x PCR buffer (Promega, Madison, WI), 5 mM MgCl$_2$ (Promega, Madison, WI), 5570F and 9206GCR 10 pM/μl each (Foster City, CA), dNTPs (dGTP, dTTP, dATP, dCTP) 0.2 mM each (Applied Biosystems) 2.5 u/μl Taq Polymerase (Promege, Madison, WI), and 0.1 mg/ml Bovine Serum Albumin (New England Biolabs, Beverly, MA) to a final volume of 50 μl. DNA amplification was performed on the GeneMATE Thermal Cycler (ISC BioExpress, Kaysville, UT). The template DNA was initially denatured for 5 min at 94°C. After the initial denaturation, the PCR cycle was denaturation for 15 s at 94°C, primer extension for 2 min. at 72°C, and annealing for 30 s. The temperature during annealing was decreased by 1°C from 53°C to 43°C, upon reaching 43°C 20 supplementary annealing cycles were performed. Finally, primer extension was performed at 72°C for 6 min. DNA product was confirmed on an agarose gel in 1xTAE (20mM Tris actate [pH7.4] 10 mM sodium acetate 1mM Na$_2$-EDTA) and stained with ethidium bromide. DNA was visualized using a UV transilluminator and photographed.

DENATURING GRADIENT GEL ELECTROPHORESIS

Amplified DNA of two 45 μl reactions was combined and purified with the QIAquick PCR purification kit (Qiagen, Chatsworth, CA). Purified DNA in 30 μl aliquots were loaded onto 1X TAE 6% polyacrylamide gels (Fisher Scientific, Fair Lawn, NJ) with a 40% to 60% gradient consisting of 40% (v/v) formamide (Fisher Scientific, Fair Lawn, NJ) and 7 M urea (J.T.

Baker, Phillipsburg, NJ). Denaturing gradient gel electrophoresis (DGGE) was performed using

a Dcode Universal Detection System (Bio-Rad, Hercules, CA) for 16 h at 50 volts and 60ºC.

Following electrophoresis, gels were stained with 50 ml SYBR Green I (Molecular Bio-Probes,

Eugene, OR) for 1 h and visualized using a Bio-Rad VersaDoc system (Bio-Rad, Hercules, CA).

CHARACTERIZATION OF OIL LEAKING FROM USS *ARIZONA*

INTRODUCTION

USS *Arizona* remains in the same place where it sank after the December 7, 1941 attack,

and a memorial was built over the site in 1980. The ship's bunkers had been filled with 4,630

tons of Bunker C fuel oil prior to the attack and not all of the oil was burned off during and after

the attack. Oil continues to leak from the ship into Pearl Harbor at an estimated rate of 1-2 L per

day as determined by collecting oil as it bubbled out of the ship (Lenihan, 1990; Johnson et al.,

2002; Murphy and Russell, personal communication). Characterization of the oil leaking from

USS *Arizona* can provide an indication of the extent of oil weathering. Oil weathering can occur

by abiotic processes (i.e., photodegradation or dissolution into saltwater) or biotic process (i.e.,

microbial degradation). In addition, examining the compositional changes between oil leaking

from different locations may contribute to decisions involving conservation and management of

USS *Arizona* by providing indirect information about the environmental conditions in the interior

environment of the ship.

GAS CHROMATOGRAPHIC ANALYSIS OF OIL LEAKING FROM USS *ARIZONA*

Samples of oil leaking from 15 locations were collected in 2000 and 2001 from USS

Arizona (Figure 8.4). The samples contained a mixture of oil and seawater, so they were

extracted with dichloromethane and air-dried overnight. Initial gas chromatographic analysis

provided a means of monitoring the overall extent of oil weathering, specifically the depletion of

n-alkanes and the branched alkanes, pristane and phytane. Gas chromatographic traces of oil

leaking from the ship differed depending on location (Figures 8.6–8.8). Overall, oil leaking from

location A (Figure 8.6) still contained *n*-alkanes and branched alkanes in comparison to oil
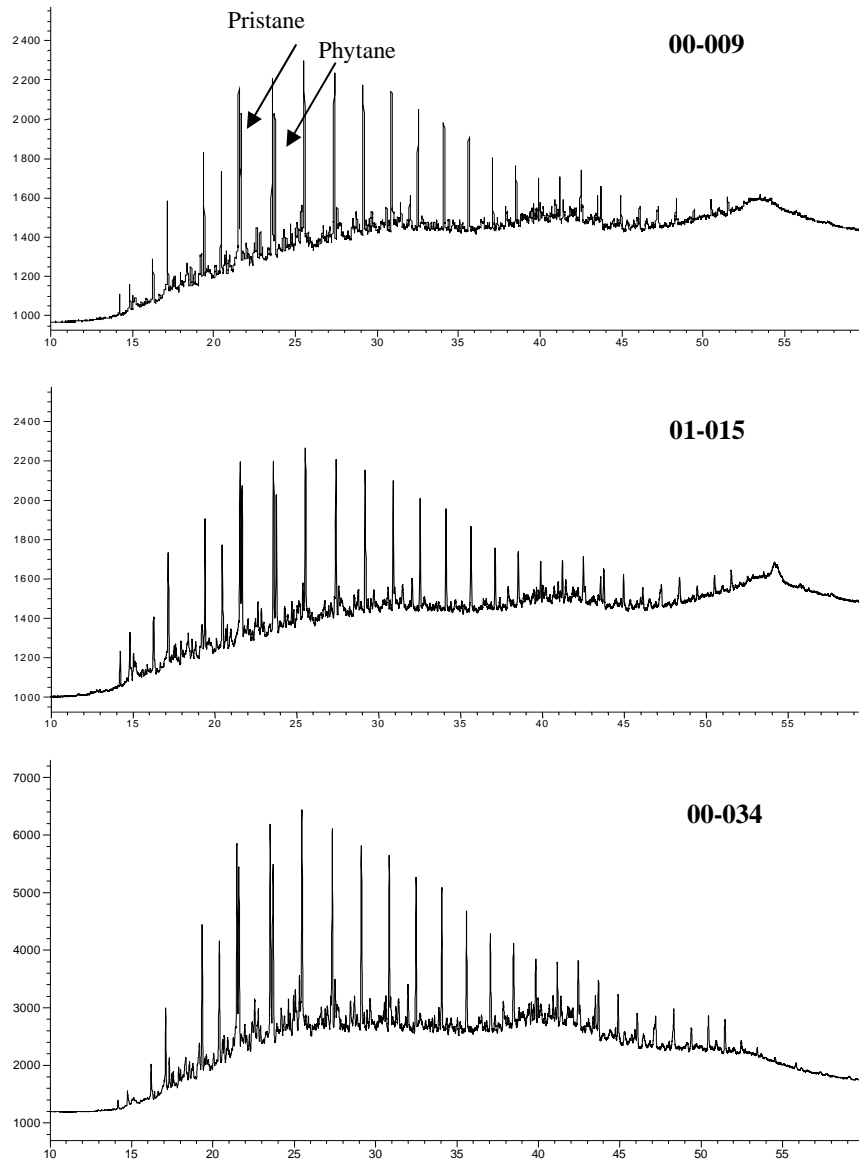
Figure 8.6 GC-FID traces of *USS Arizona* oil samples representative for oil leaking from location A. Oil leaking from location A still contains *n*-alkanes and the branched alkanes, pristane and phytane. In the above chromatograms, the y-axis is the detector response and the x-axis is the retention time in minutes. Detector response for the y-axis is not the same scale for each chromatogram.
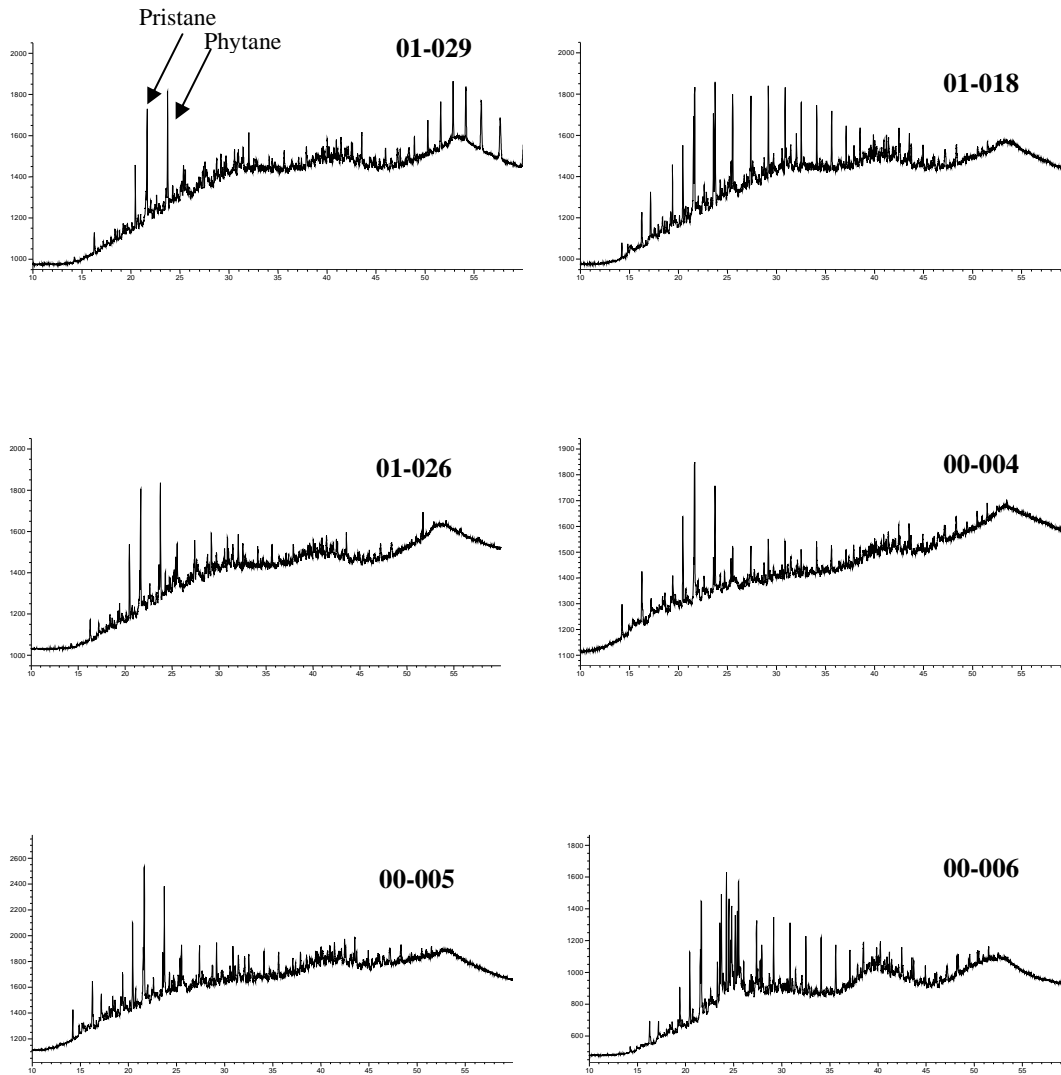
**Figure 8.7 GC-FID traces of *USS Arizona* oil samples representative of location B.
Oils leaking from location B show significant weathering, most noticeably depletion
of *n*-alkanes in comparison to oil leaking from location A. The branched alkanes,
pristane and phytane, are still present. In the above chromatograms, the y-axis is the
detector response and the x-axis is the retention time in minutes. Detector response
for the y-axis is not the same scale for each chromatogram.**
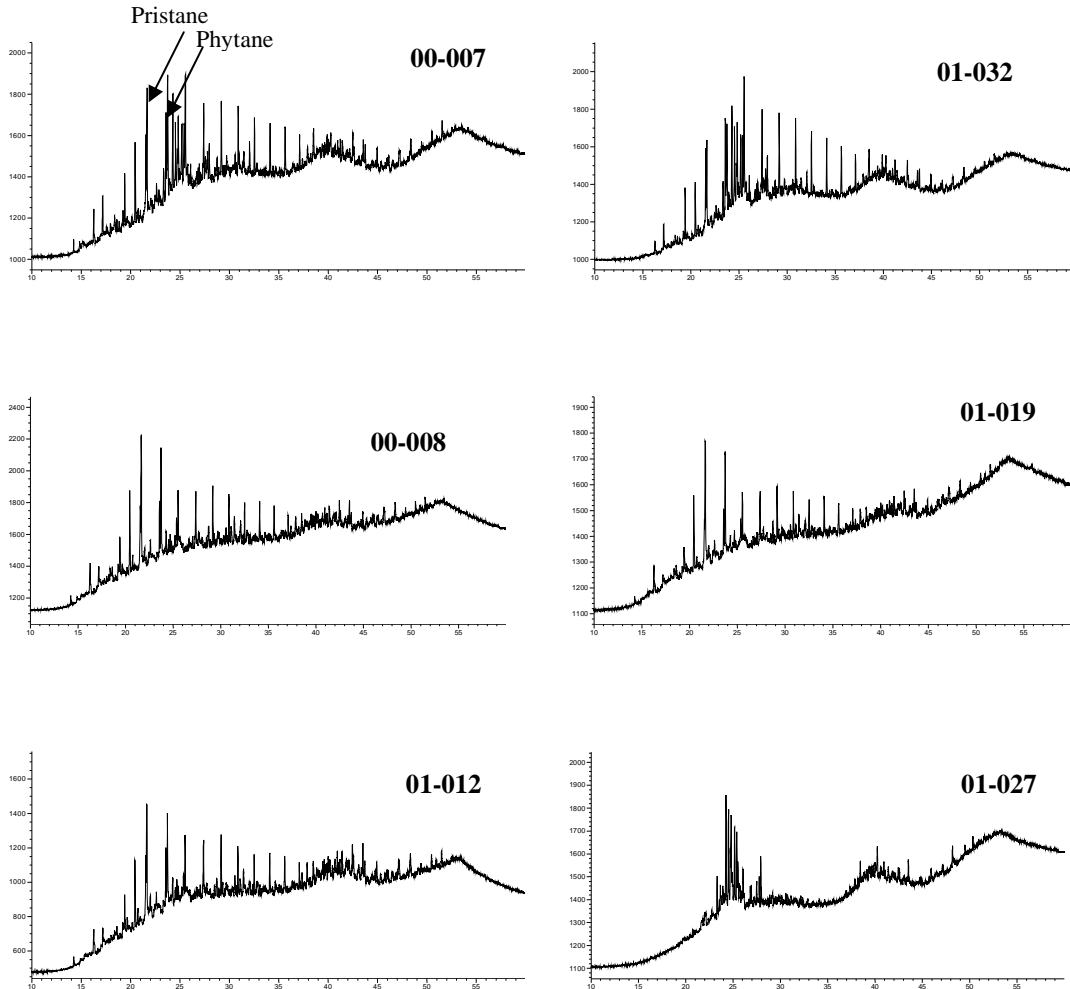
Figure 8.8 GC-FID traces of *USS Arizona* oil samples representative of location B. Oils leaking from location B show significant weathering of the oil, most noticeably depletion of *n*-alkanes in comparison to oil leaking from location A. In the above chromatograms, the y-axis is the detector response and the x-axis is the retention time in minutes. Detector response for the y-axis is not the same scale for each chromatogram.

leaking from location B (Figures 8.7 and 8.8). Gas chromatographic traces for 00-009, 01-015 and 00-034 are from location A and contain *n*-alkanes, along with pristane and phytane (Figure 8.6). In comparison, traces for 01-029, 01-018, 01-026, 00-004, 00-005, 00-006, 00-007, 01-032, 00-008, 01-019, 01-012 and 01-027 (Figures 8.7 and 8.8) are from location B and show a depletion of *n*-alkanes but still contain pristane and phytane. Overall, this suggests that oil leaking from location B has undergone more weathering (either biotic or abiotic) than oil leaking from location A.

INDIVIDUAL PAH ANALYSIS OF OIL LEAKING FROM USS *ARIZONA*

Mass spectrometry was utilized to monitor the concentration of 53 target PAHs (including heterocycles) (Table 8.1) in samples of oil leaking from different locations of USS *Arizona*. Triplicates of three oil samples, 01-015 and 00-034 (from location A) and 01-029 (from location B), were chosen for PAH analysis because they showed the least weathering (01-015 and 00-034) or the most weathering (01-029). Overall, mass spectrometry analysis indicated PAHs were still present in all three analyzed samples of oil (Figure 8.9). For oil sample 00-034, one of the three triplicates exhibited a different PAH pattern, causing large standard error bars. Mass spectrometry indicated oil samples 01-029 (location B) and oil sample 00-034 (location A) had fewer low molecular weight PAHs than sample 01-015 (location A) (Figure 8.9). For example, sample 01-029 and 00-034 contained less 2-ring naphthalene, and C_1-C_4 naphthalenes than sample 01-015 leaking from location A. Differences in high molecular weight hydrocarbons from locations A and B were not observed (Figure 8.10).

PAHS COMPARED TO CONSERVED BIOMARKERS

Mass spectrometry also provided data for analysis of the biomarkers $C_{30}17\alpha(H),21\beta(H)$-hopane and $18\alpha(H)$-oleanane present in oil leaking from the ship. The ratio of $C_{30}17\alpha(H),21\beta(H)$-hopane to $18\alpha(H)$-oleanane was calculated for oil extracts to determine if $C_{30}17\alpha(H),21\beta(H)$-hopane was being degraded. Ratios were similar (e.g., 6.17) in all oil samples from USS *Arizona* (Table 8.2), indicating no degradation of $C_{30}17\alpha(H),21\beta(H)$-hopane.
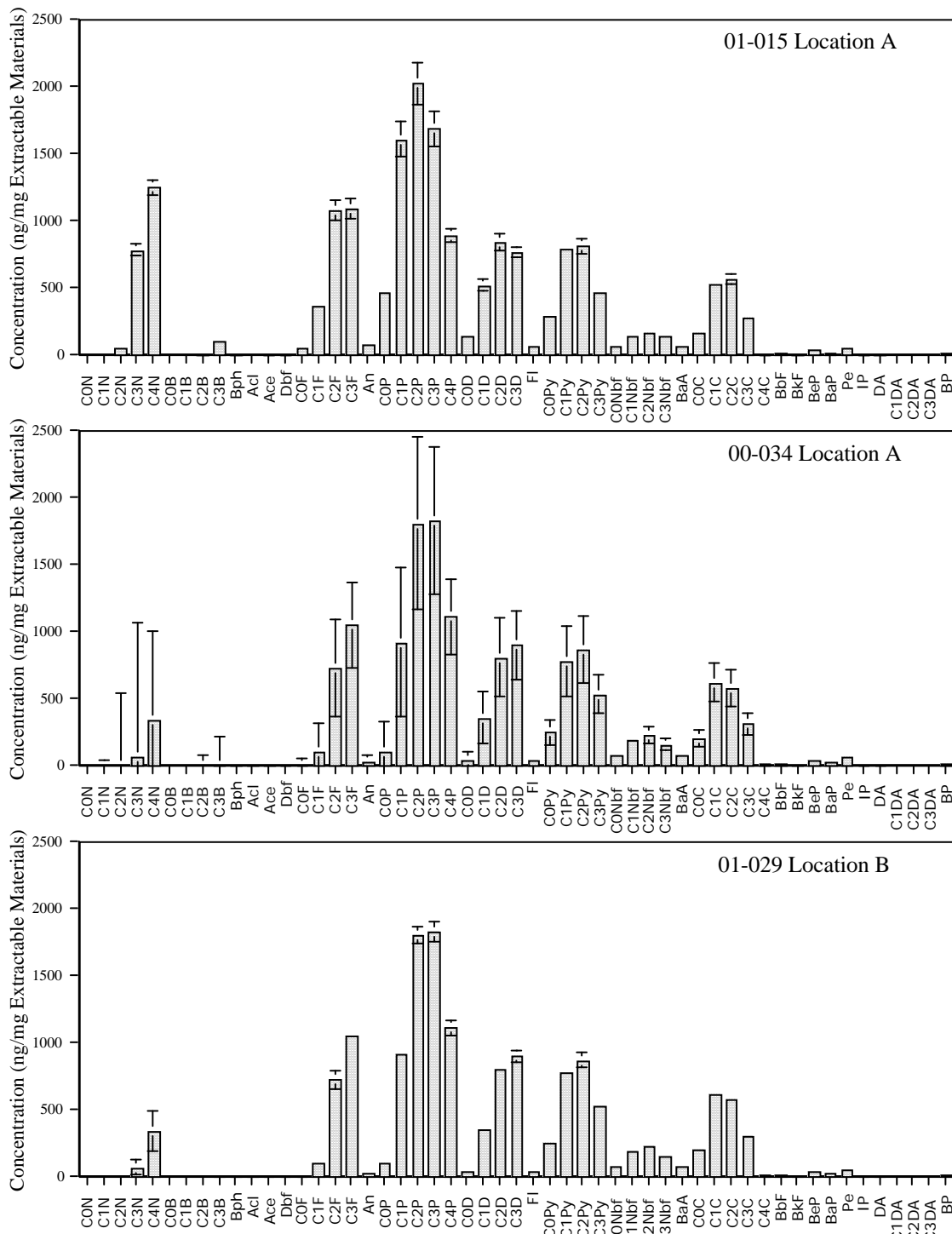
Figure 8.9 Individual PAH analysis for oil leaking from USS *Arizona*. Oil leaking from 00-034 and 01-029 shows a depletion of lower molecular weight PAHs in comparison to oil leaking from 01-015. Abbreviations are defined in Table 8.1 and locations of leaking oil are defined in Figure 8.4.
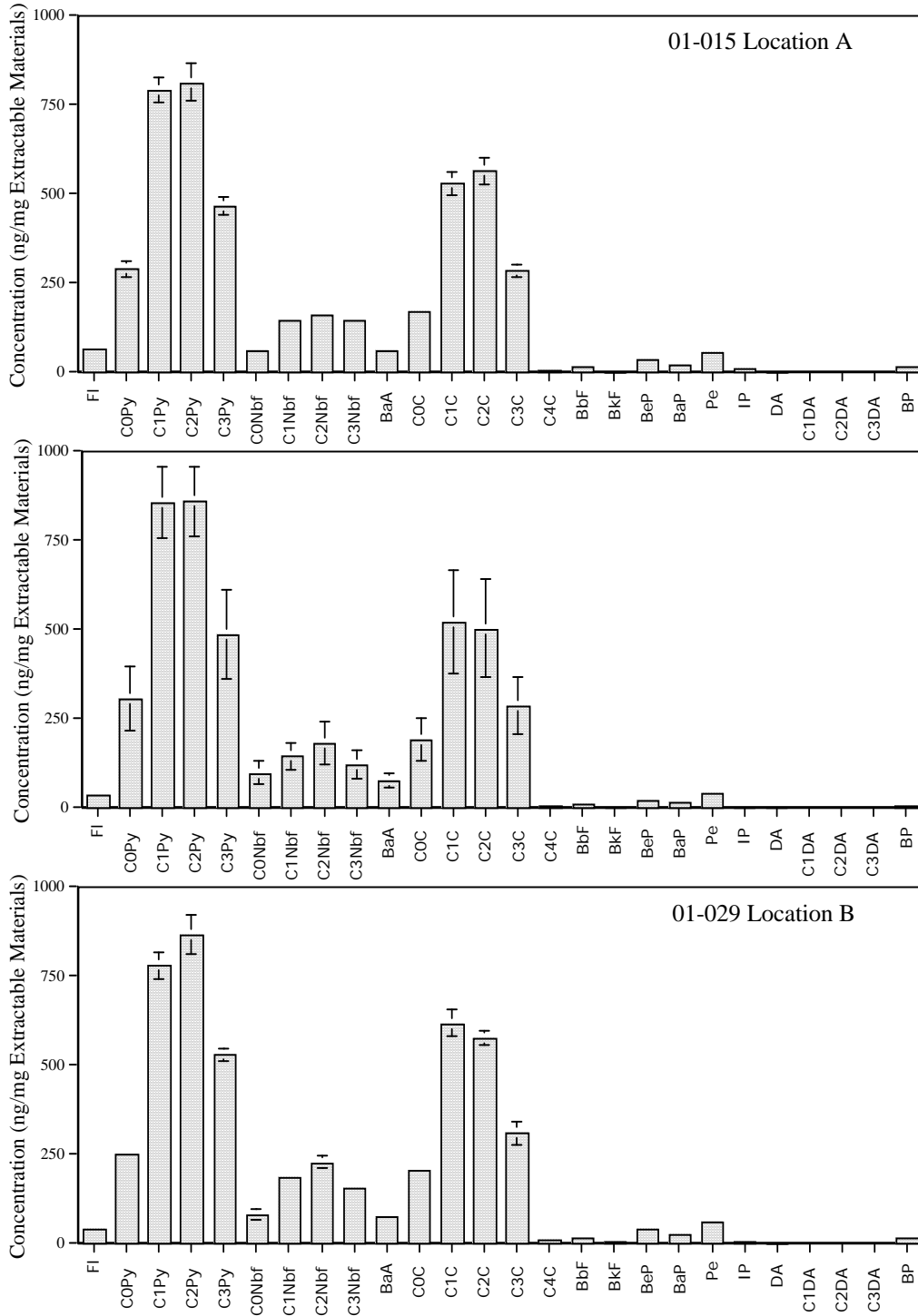
Figure 8.10. Individual PAH analysis of high molecular weight PAHs for oil leaking from USS *Arizona*. Abbreviations are defined in Table 8.1 and locations of leaking oil are defined on Figure 8.4.

Oil	Location	$C_{30}H/18\alpha$ Oleanane [a]	$Ts/(Ts+Tm)$ [b]	$C_{31}S/(C_{31}R + C_{31}S)$ [c]	$C_{28}TT/C_{30}H$ [d]	$C_{29}TT/C_{30}H$ [e]
01-015	A	6.20±0.09	0.53±0.03	0.50±0.01	0.36±0.02	0.36±0.02
00-034	A	5.93±0.25	0.43±0.01	0.50±0.01	0.45±0.01	0.43±0.01
01-029	B	6.25±0.15	0.56±0.01	0.50±0.01	0.31±0.01	0.31±0.01

All values are the means and standard error of triplicate samples.

[a] Calculated from m/z=191 mass chromatogram peak areas of C_{30} 17α(H),21β(H)-hopane and 18α(H)-oleanane.

[b] Calculated from the m/z=191 mass chromatogram peak areas of C_{27} 17α(H)-22,29,30-trisnorhopane (Tm) and C_{27} 18α(H)-22,29,30-trisnorneohopane (Ts).

[c] Calculated from the m/z=191 mass chromatogram peak areas of C_{31} 17α(H)-homohopane (22S and 22R).

[d] Calculated from the m/z=191 mass chromatogram peak areas of C_{28} 13β,21α(H)-tricyclic terpanes and C_{30} 17α(H)21β(H)-hopane.

Table 8.2. Selected biomarker ratios of oil leaking from USS *Arizona*.

The results indicate that 18α(H)-oleanane and C_{30}17α(H),21β(H)-hopane can be used as conserved biomarkers to monitor PAH degradation.

The ratios of total PAHs to the conserved biomarkers were calculated in order to determine relative total PAH ratio changes between oil leaking from different locations of the ship (Table 8.3). Overall, the ratios of total PAHs to conserved biomarkers were greater in oil leaking from location A in comparison to oil leaking from location B (Table 8.3). Total PAHs to conserved C_{30}17α(H),21β(H)-hopane values were higher in sample 00-034 (from location A) and were lowest in sample 01-029 (from location B) (Table 8.3). Total PAHs to conserved 18α(H)-oleanane values were also higher in sample 00-034 (from location A) and the lowest ratio was observed in sample 01-029 (from location B) (Table 8.3). For oil sample 00-034, 1 of the 3 triplicates exhibited different PAH concentrations, causing a large standard error for the total PAHs to the conserved biomarkers C_{30}17α(H),21β(H)-hopane and 18α(H)-oleanane ratios.

The ratios of low molecular weight total napthalenes to conserved biomarkers C_{30}17α(H),21β(H)-hopane and 18α(H)-oleanane were calculated to observe any total naphthalenes ratio changes between oil leaking from different locations of the ship. The ratios of total naphthalenes to conserved biomarkers were greater in oil leaking from location A in comparison to oil leaking from location B (Table 8.3). For example, total naphthalenes to conserved C_{30}17α(H),21β(H)-hopane values were the greatest in sample 00-034 (from location A) which had a ratio of 18.15±8.24 and were the lowest in sample 01-029 (from location B) which had a ratio of 0.18±0.01 (Table 8.3). The ratio of total naphthalenes to 18α(H)-oleanane

Oil	Location	Total PAHs:C$_{30}$-hopane[a]	Total PAHs:18α-oleanane	Total naphthalenes:C$_{30}$-hopane[a]	Total naphthalenes:18α-oleanane
01-015	A	38.65$\pm$0.55	239.65$\pm$7.21	4.37$\pm$0.29	27.16$\pm$2.18
00-034	A	97.70$\pm$21.27	590.07$\pm$145.05	18.15$\pm$8.24	110.60$\pm$53.95
01-029	B	25.87$\pm$0.99	161.56$\pm$6.22	0.18$\pm$0.01	4.56$\pm$2.46

All values are the means and standard error of triplicate samples.
[a] C$_{30}$-hopane represents C$_{30}$ 17α(H),21β(H)-hopane.

Table 8.3. USS *Arizona* oil ratios of total PAHs and total naphthalenes to conserved biomarkers.

values were also the greatest in sample 00-034 (from location A) which had a ratio of 110.60$\pm$53.95 and decreased to the lowest ratio in sample 01-029 (from location B) which had a ratio of 4.56$\pm$2.46 (Table 8.3). One of the oil samples for 00-034 had 1 of the 3 triplicates exhibited a different PAH pattern, causing large standard error for the total naphthalenes to conserved biomarkers C$_{30}$17α(H),21β(H)-hopane and 18α(H)-oleanane ratios.

BIOMARKER ANALYSIS OF AEROBICALLY DEGRADED BUNKER C CRUDE OIL

Mass spectrometry was used to determine biomarker profiles of oil leaking from USS *Arizona* and determine if weathering processes such as degradation are influencing biomarker profiles. Triplicates of three oil samples 01-015 and 00-034 (from location A) and 01-029 (from location B) were chosen for analysis. Mass chromatograms for *m/z*=191 for hopanes and *m/z* 217 for steranes were analyzed. Mass chromatograms *m/z*=191 for oil leaking from USS *Arizona* showed no discernable differences between oil leaking from different locations 01-015, 00-034 (from location A) and 01-029 (from location B). (Figures 8.11 and 8.12). Mass chromatograms for the *m/z*=217 sterane trace also showed no discernable differences between oil leaking from different locations 01-015, 00-034 (from location A) and 01-029 (from location B). (Figures 8.11 and 8.12).

Biomarker ratios were calculated from mass chromatograms *m/z*=191 as described in section 2 (Table 8.2). Briefly, mass chromatogram peak areas of C$_{30}$ 17α(H),21β(H)-hopane and 18α-oleanane were calculated for the hopane to oleanane ratio. Peak areas of C$_{27}$ 17α(H)-22,29,30-trisnorhopane (Tm) and C$_{27}$ 18α(H)-22,29,30-trisnorneohopane (Ts), were calculated
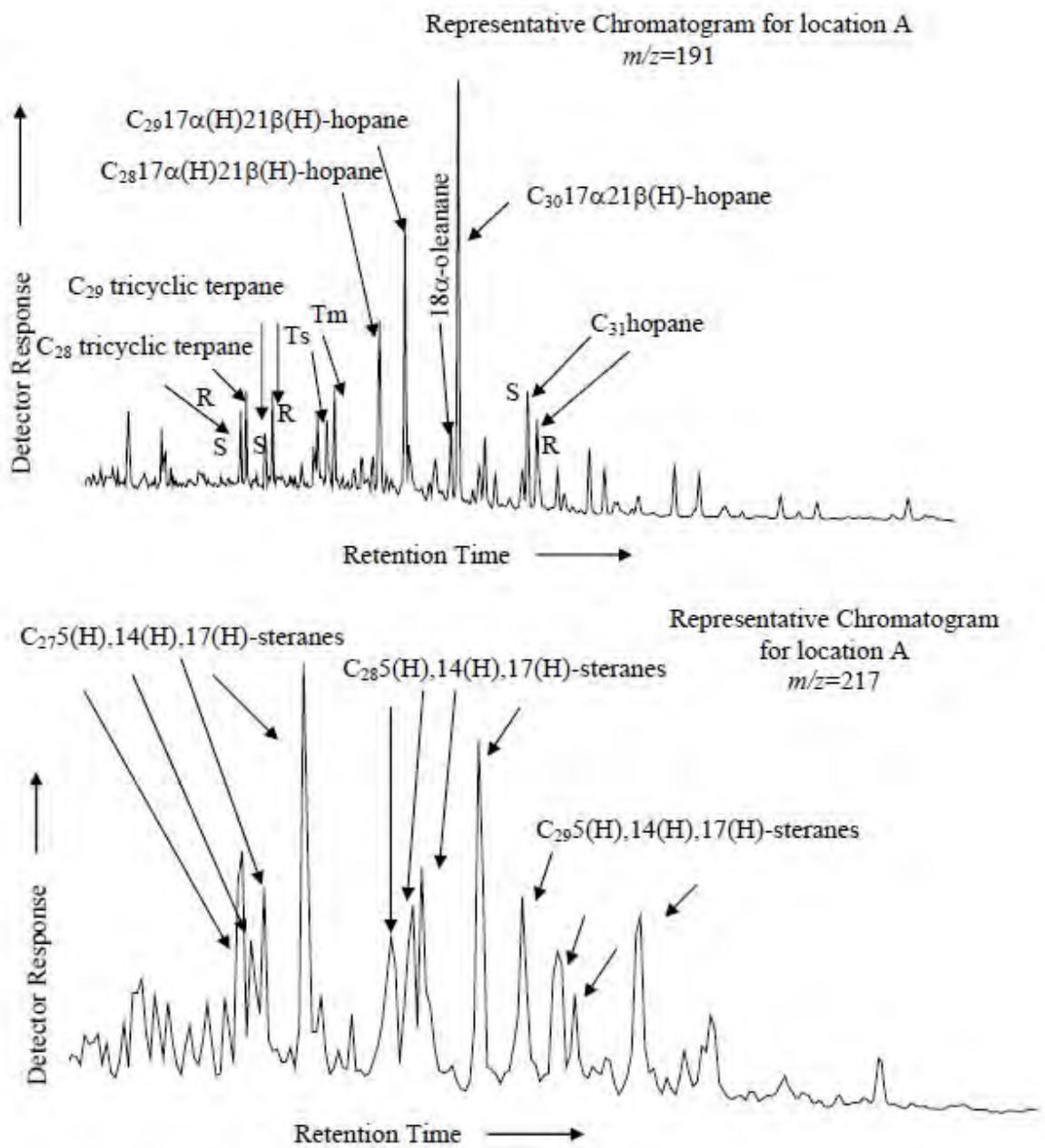
Figure 8.11. **Representative mass chromatograms for 01-015 and 00-034 oil leaking from location A of USS *Arizona* for *m/z*=191 (hopanes) and *m/z*=217 (steranes).**
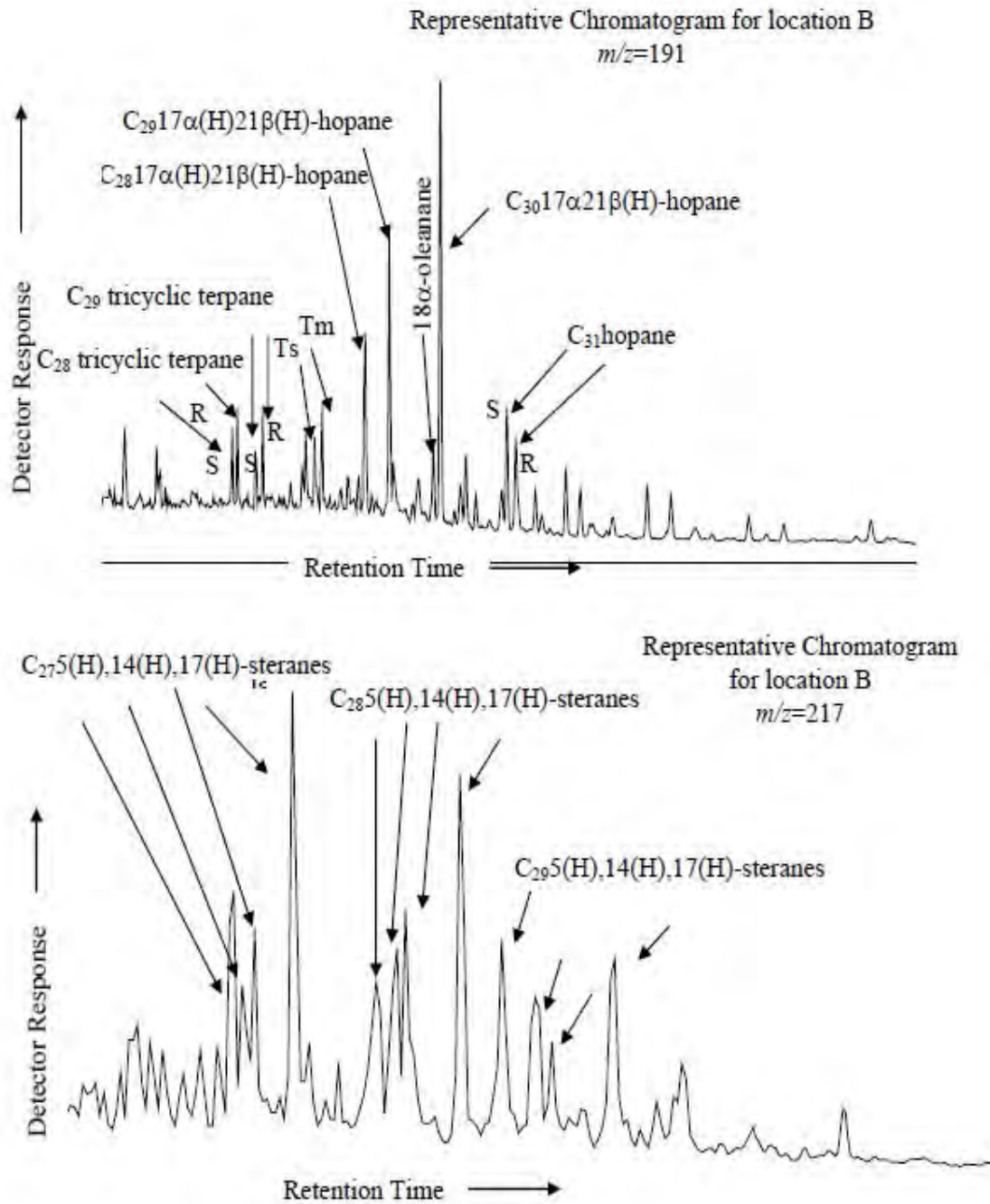
Figure 8.12. Biomarkers mass chromatograms for 01-029 oil leaking from location B of USS *Arizona* for *m/z*=191 (hopanes) and *m/z*=217 (steranes).

for the Ts/(Ts + Tm) ratio. Mass chromatogram peak areas of C_{31} $17\alpha(H)$-homohopane ($22S$ and $22R$) were calculated for the C_{31} $22S/(22S + 22R)$ ratio. Tricyclic terpane ratios were also calculated from mass chromatograms m/z=191 using the peak areas of C_{28} $13\beta,21\alpha(H)$-tricyclic terpane $22R$ and $22S$ and C_{29} $13\beta,21\alpha(H)$-tricyclic terpane $22R$ and $22S$, respectively to compare with the peak area of C_{30} $17\alpha,21\beta(H)$-hopane ($C_{28}TT/C_{30}H$ and $C_{29}TT/C_{30}H$, respectively). Ratios calculated from mass chromatograms m/z=191 for oil 01-015, 00-034, and 01-029 had little variability (Table 8.2). For example, ratios for the Ts/(Ts+Tm) ratio ranged from 0.43 ± 0.01 for oil sample 00-034 (from location A) to 0.56 ± 0.01 for oil sample 01-029 (from location B) (Table 8.2). In comparison, the ratio of $C_{31}S/(C_{31}R + C_{31}S)$ was 0.50 ± 0.01 for all oil samples (01-015, 00-034 and 01-029) (Table 8.2). The ratios of $C_{28}TT/C_{30}H$ for samples of oil leaking from the ship ranged from 0.31 ± 0.01 for sample 01-029 to 0.45 ± 0.01 for sample 00-034 (Table 8.2). The ratio of $C_{29}TT/C_{30}H$ for oil samples ranged from 0.31 ± 0.01 for sample 01-029 to 0.43 ± 0.01 for sample 00-034 (Table 8.2).

Biomarker ratios were also calculated from mass chromatograms m/z=217 (Table 8.4). Details for calculation are in section 2. Briefly, mass chromatogram peak areas of C_{27} $5\alpha(H),14\alpha(H),17\alpha(H)$-sterane ($20S$ and $20R$), C_{27} $5\alpha(H),14\beta(H),17\beta(H)$-sterane ($20S$ and $20R$) and C_{30} $17\alpha(H),21\beta(H)$-hopane were calculated for the $C_{27}S/C_{30}H$ ratio. Mass chromatogram peak areas C_{28} $5\alpha(H),14\alpha(H),17\alpha(H)$-sterane ($20S$ and $20R$), C_{28} $5\alpha(H),14\beta(H),17\beta(H)$-sterane ($20S$ and $20R$) and C_{30} $17\alpha(H),21\beta(H)$-hopane were calculated for the $C_{28}S/C_{30}H$ ratio. Mass chromatogram peak areas of C_{29} $5\alpha(H),14\alpha(H),17\alpha(H)$-sterane (20S and 20R), C_{29} $5\alpha(H),14\beta(H),17\beta(H)$-sterane ($20S$ and $20R$) and C_{30} $17\alpha(H),21\beta(H)$-hopane were calculated for the $C_{29}S/C_{30}H$ ratio.

Following calculation, sterane biomarker ratios for oil leaking from the ship were compared. Overall oil sample 01-015 and 01-029 ratios were similar to each other and were less than sample 00-034 (Table 8.4). For example, the ratio of $C_{27}S/C_{30}H$ for sample 00-034 was 2.62 ± 0.11. In comparison, the ratios for samples 01-015 and 01-029 were 1.96 ± 0.04 and 1.91 ± 0.06, respectively (Table 8.4). The same ratio pattern is true for $C_{28}S/C_{30}H$. The ratio for sample 00-034 was 2.13 ± 0.26 in comparison, the ratios for samples 01-015 and 01-029 were 1.58 ± 0.01 and 1.56 ± 0.01, respectively (Table 8.4). The same pattern is also present in the

$C_{29}S/C_{30}H$ ratio. The ratio of for sample 00-034 was 1.77 ± 0.07 and, the ratios for samples 01-015 and 01-029 were $1.62\pm0.09$and 1.58 ± 0.01, respectively (Table 8.4).

CHARACTERIZATION OF HYDROCARBONS IN SEDIMENTS COLLECTED FROM USS *ARIZONA*

INTRODUCTION

USS *California*, USS *Maryland*, USS *Oklahoma*, USS *Tennessee*, USS *West Virginia*, and USS *Arizona* were attacked in Pearl Harbor on December 7, 1941. Every ship was assaulted and released Bunker C fuel oil into the immediate area (Lenihan, 1990). Following the Pearl Harbor attack, USS *Arizona* sank and unlike the other ships it was not recovered for use during World War II (Lenihan, 1990). Instead, USS *Arizona* remains in the same place it sank, continually leaking Bunker C fuel oil into the environment (Lenihan, 1990). During 1961, a memorial was built over the ship to commemorate the lives lost during the Pearl Harbor attack (Lenihan, 1990; Pearl Harbor Natural Resources Trustees, 1999). The ship and memorial are both managed by the National Park Service. Because the ship is considered a memorial, oil remaining inside cannot be physically removed, therefore oil continues to leak into Pearl Harbor.

Oil	Location	$C_{27}S/C_{30}H$ [a]	$C_{28}S/C_{30}H$ [b]	$C_{29}/C_{30}H$ [c]
01-015	A	1.96 ± 0.04	1.58 ± 0.01	1.62 ± 0.09
00-034	A	2.62 ± 0.11	2.13 ± 0.26	1.77 ± 0.07
01-029	B	1.91 ± 0.06	1.56 ± 0.01	1.58 ± 0.01

All values are the means and standard error of triplicate samples.
[a]Calculated from *m/z*=217 mass chromatogram peak areas of $C_{27}5\alpha(H),14\alpha(H),17\alpha(H)$-sterane (20S and 20R), $C_{27}5\alpha(H),14\beta(H),17\beta(H)$-sterane (20S and 20R) and C_{30} $17\alpha(H),21\beta(H)$-hopane.
[b]Calculated from *m/z*=217 mass chromatogram peak areas of $C_{28}5\alpha(H),14\alpha(H),17\alpha(H)$-sterane (20S and 20R), $C_{28}5\alpha(H),14\beta(H),17\beta(H)$-sterane (20S and 20R) and $C_{30}17\alpha(H),21\beta(H)$-hopane.
[c]Calculated from *m/z*=217 mass chromatogram peak areas of of $C_{29}5\alpha(H),14\alpha(H),17\alpha(H)$-sterane (20S and 20R) $C_{29}5\alpha(H),14\beta(H),17\beta(H)$-sterane and C_{30} $17\alpha(H),21\beta(H)$-hopane.

Table 8.4. Oil leaking from USS *Arizona* sterane biomarker ratios.

USS *Arizona* is not the only source of contamination in Pearl Harbor. Another source is the nearby U.S. Navy facility, which contributes anthropogenic compounds (i.e., PAHs, PCBs, and metals) to the sediments (Ashwood and Olsen, 1988; U.S.Navy, 1998). In addition, Chevron released 41,244 gallons of Bunker C oil into Pearl Harbor during a refinery oil spill on May 4, 1996 (Pearl Harbor Natural Resource Trustees, 1999).

The objective of this study was to characterize hydrocarbons in the sediments adjacent to and surrounding USS *Arizona*. Sediment extracts were examined by GC-FID (for *n*-alkane and branched alkanes) and GC-MS for PAHs and their alkylate homologues as well as biomarkers (m/z-191 and m/z=217). The biomarker profiles of oil extracted from sediments can be compared to biomarker profiles of oil leaking from USS *Arizona*. Therefore, a comparison of patterns can be used to determine if oil leaking from the ship is present in Pearl Harbor sediments.

GAS CHROMATOGRAPHIC ANALYSIS OF SEDIMENT SOLVENT-EXTRACTABLE MATERIALS

Sediment samples from 8 locations were collected from Pearl Harbor during the summers of 2000 and 2001 (Figure 8.5). Solvent-extractable materials obtained from sediments by continuous soxhlet extraction averaged 1.79 ± 0.35 mg extractable material/g of dry sediment (Table 8.5). Following gravimetric measurement, GC-FID analysis of sediment extracts

Sediment	Location	Solvent-Extractable Material (mg/g)[a]
00-001	Stern section, starboard side, 12 ft. from hull	2.15 ± 0.58
00-002	Stern section, starboard side, 12 ft. from hull	0.99 ± 0.57
00-003	Stern section, starboard side, 12 ft. from hull	1.00 ± 0.11
00-032	Stern section, port side, 10 ft. from hull	1.23 ± 0.17
00-033	Stern section, port side, 10 ft. from hull	1.04 ± 0.29
00-030	Stern section, bottom of barbette No. 4	2.59 ± 0.11
00-031	Bow section, gun turret No. 1	0.99 ± 0.61
01-041	Bow section, port side of gun turret No. 1	1.37 ± 0.38

All values are the average of triplicate samples with the standard errors of those values.
[a]mg extractable material per gram of dry sediment.

Table 8.5. USS Arizona sediment solvent-extractable material

indicated the presence of *n*-alkanes along with the presence of several ubiquitous peaks (Figures 8.13–8.16). Bonny Light crude (BLC) oil was analyzed by gas chromatography during the same run as the sediment extracts, demonstrating peaks in sediment extracts that co-eluted with *n*-alkanes in BLC suggesting *n*-alkanes are present in the sediments (Figures 8.13–8.16).

The large ubiquitous peak (observed at a retention time of 26.821) found in all solvent-extractable materials was identified as butylated hydroxytoluene (BHT) (*m/z*=205) by GC-MS (Figure 8.17). In order to elucidate the source of the BHT, soxhlet extraction was conducted without sediments, containing only solvent, boiling chips, and a cotton thimble. BHT was detected in these extracts by GC-MS (Figure 8.18). However, BHT was also detected by GC-MS in oil sample 00-034 of oil leaking from USS *Arizona* that was not extracted using a soxhlet apparatus (Figure 8.19). A soxhlet extraction control with just solvents was not conducted.

PAH ANALYSIS OF SEDIMENT SOLVENT-EXTRACTABLE MATERIALS

Further analysis of sediment solvent-extractable material by GC-MS for 53 PAHs and their alklyated homologues (and heterocycles) was conducted. The higher standard error for PAHs detected in sediment extracts (as compared to GC-MS analysis of PAHs in oil leaking from the ship) may be due to inherent variability in the sediments sampled. Using mass spectrometry, low molecular weight PAHs, naphthalene and fluorene or their alkylated homologues, were not detected. However, a number of high molecular weight PAHs (i.e., pyrene, chrysene) were detected (Figures 8.20–8.22).

PAHS COMPARED TO CONSERVED BIOMARKERS

GC-MS analysis of the biomarkers $C_{30}17\alpha(H),21\beta(H)$-hopane and $18\alpha(H)$-oleanane present in USS *Arizona* sediments (Table 8.6) was also conducted. The total amount of PAHs was variable in sediments, ranging from 426.97 ± 236.71 to 16278.60 ± 10105.12 ng PAH/mg dry sediment. The ratios of total PAHs to conserved biomarkers $C_{30}17\alpha(H),21\beta(H)$-hopane ranged from 0.44 ± 0.09 to 10.43 ± 4.86. Total PAHs to $18\alpha(H)$-oleanane ranged from 1.38 ± 0.30 to 37.14 ± 20.14 (Table 8.7).
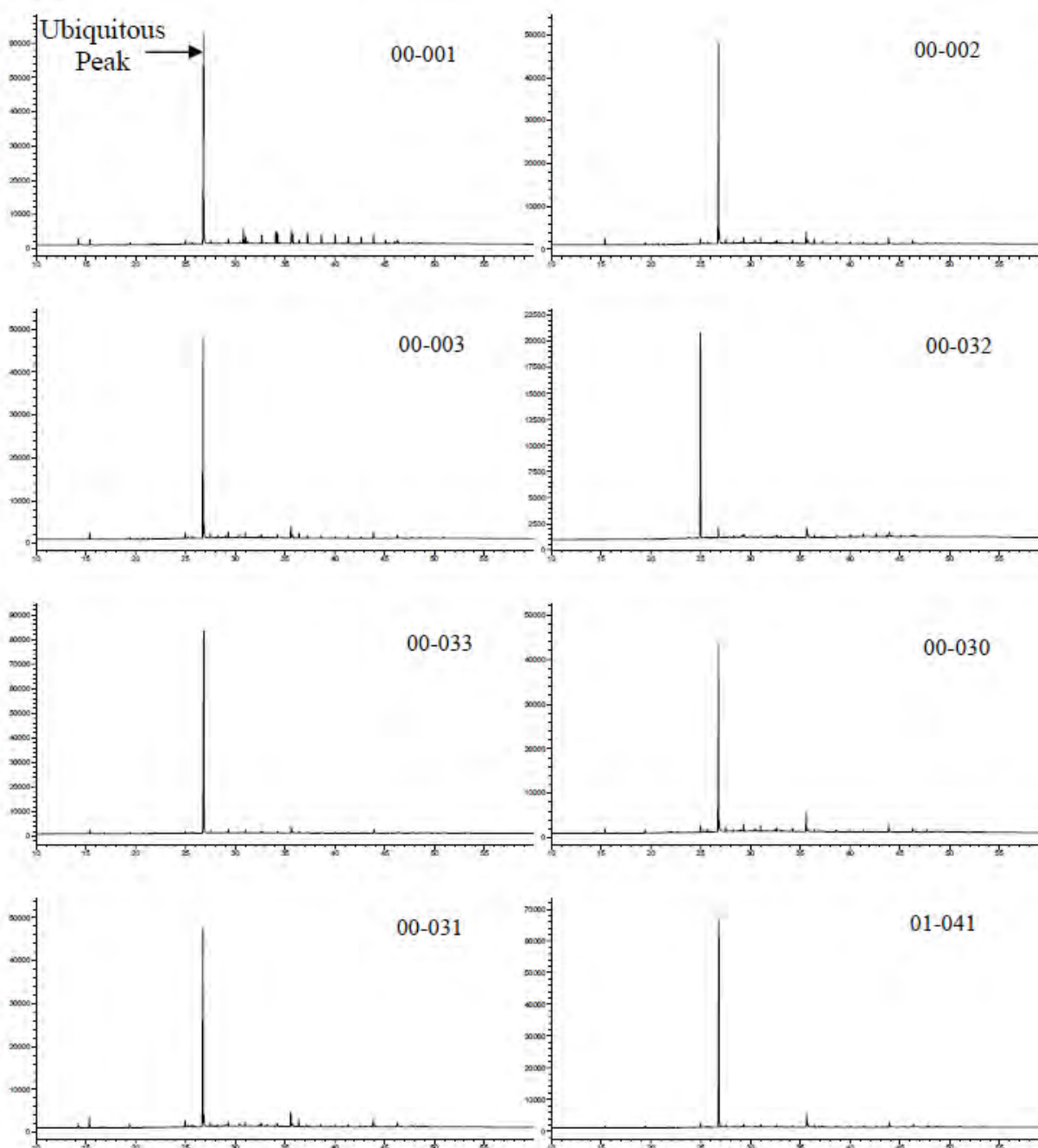
Figure 8.13. Gas chromatograms of solvent-extractable materials removed from sediments. There was a ubiquitous peak found in all sediments extracts. In the above chromatograms, the y-axis is the detector response and the x-axis is the retention time in minutes.
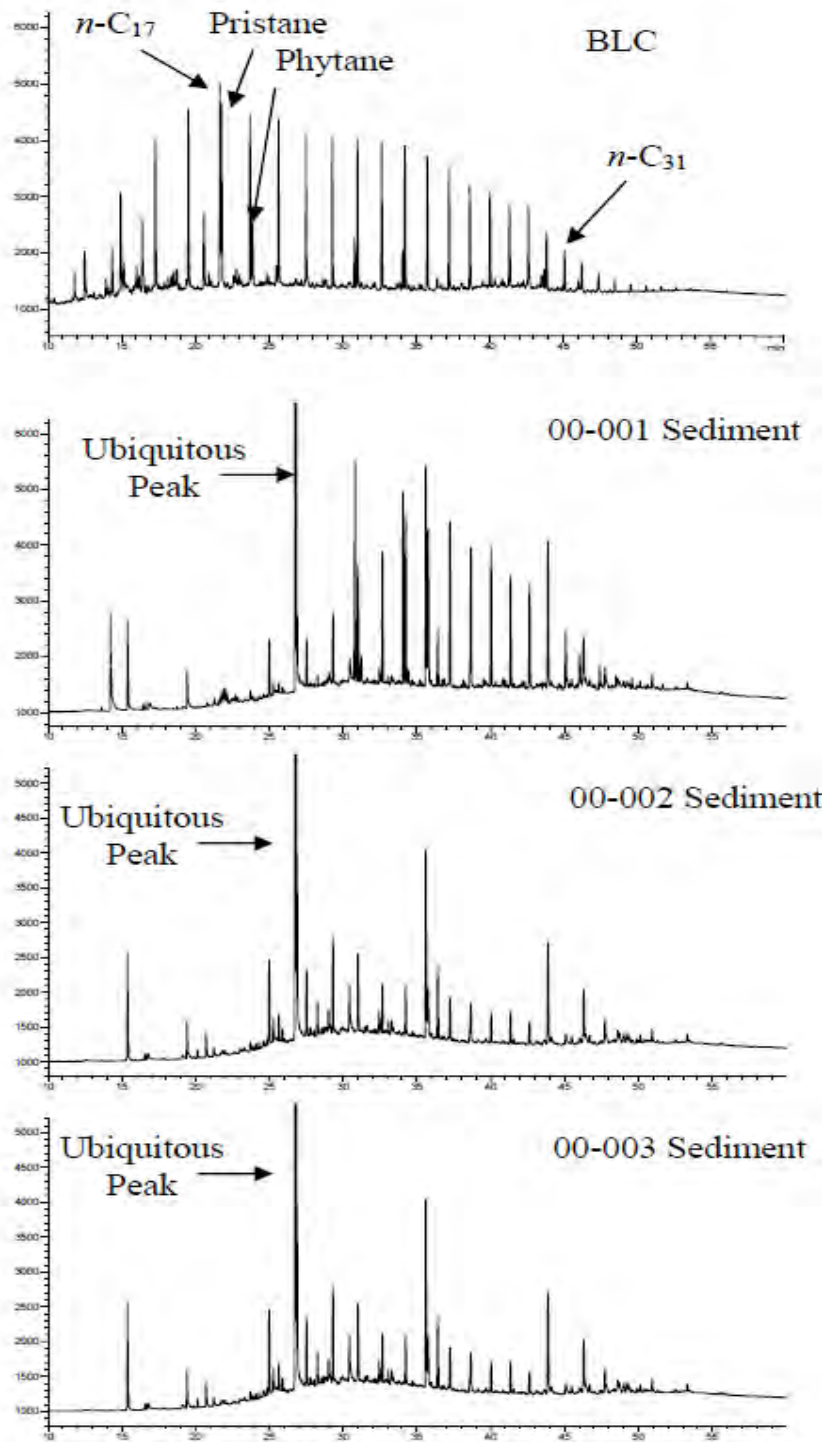
Figure 8.14. Gas chromatograms of solvent-extractable materials removed from sediments collected 12 ft. from the stern starboard hull. A GC trace for BLC (top trace) was conducted to compare retention times. Extracts contained *n*-alkanes and a ubiquitous peak found in all sediments. In the above chromatograms, the y-axis is detector response and x-axis is the retention time in minutes. The chromatograms have been scaled to a lower detector response than the highest peak to observe smaller peaks in the trace. The y-axis is not the same scale for each chromatogram.

335
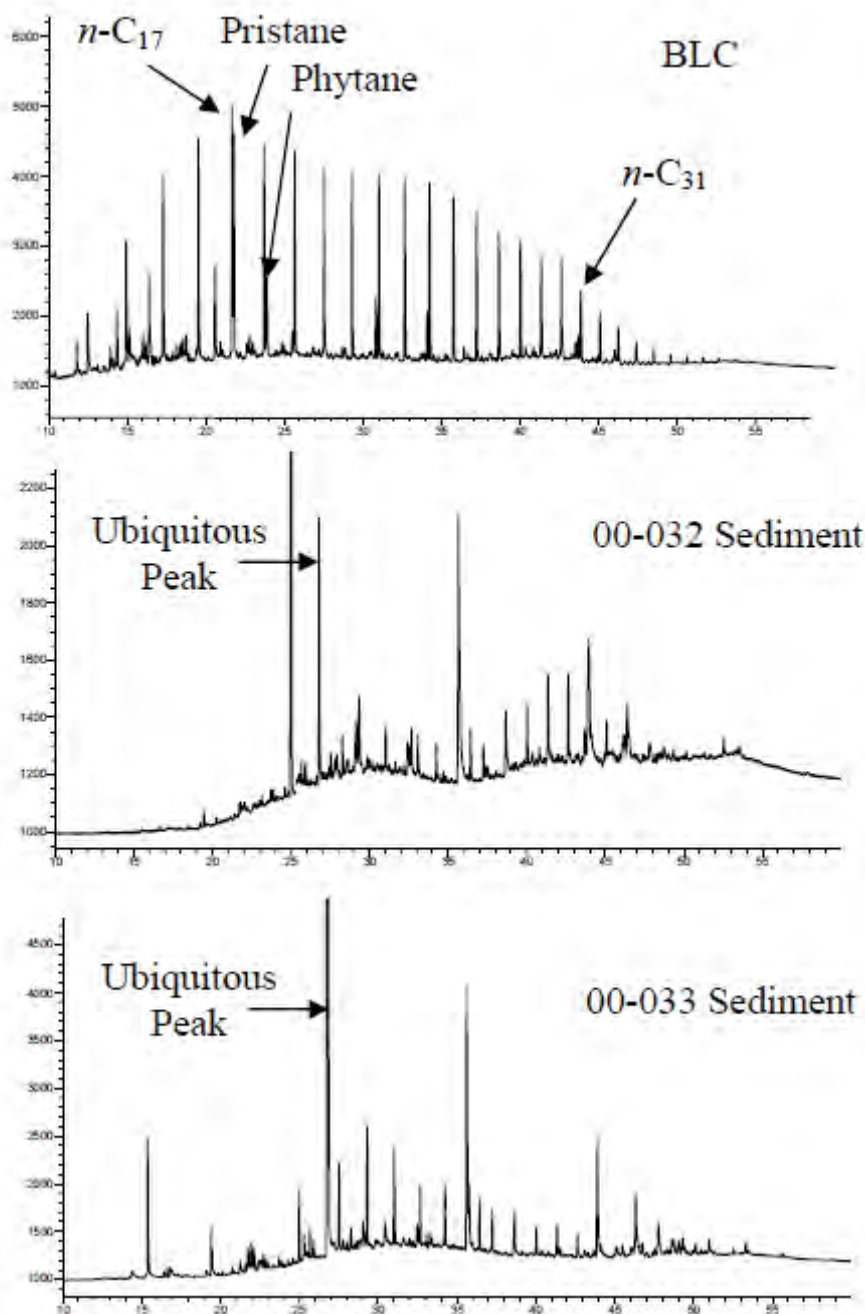
Figure 8.15. Gas chromatograms of solvent-extractable materials removed from sediments collected 12 ft. from the port starboard hull. A GC trace for BLC (top trace) was conducted to compare retention times. Extracts contained *n*-alkanes and a ubiquitous peak found in all sediments. In the above chromatograms, the y-axis is detector response and x-axis is the retention time in minutes. The chromatograms have been scaled to a lower detector response than the highest peak to observe smaller peaks in the trace. The y-axis is not the same scale for each chromatogram.
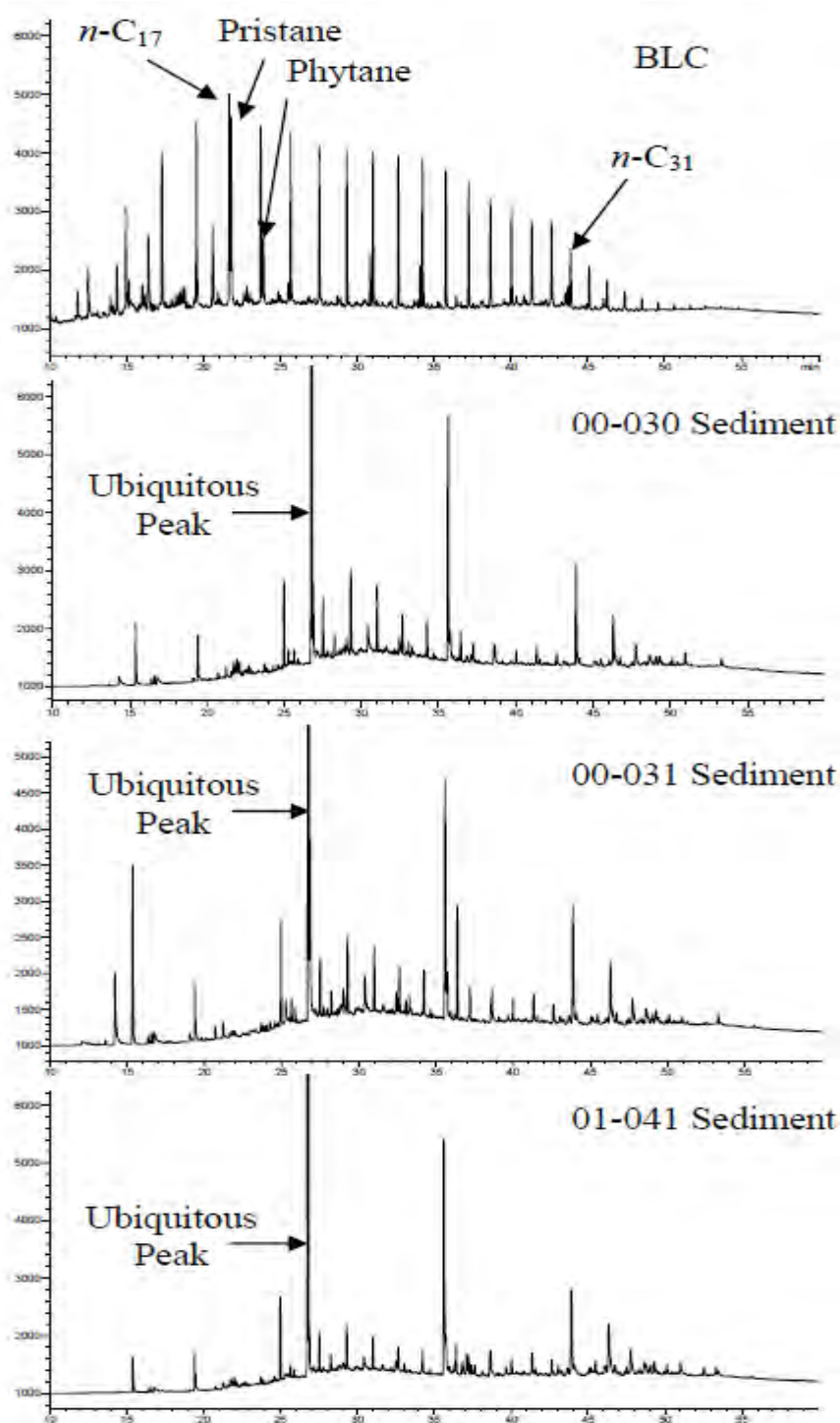
Figure 8.16. Gas chromatograms of solvent-extractable materials removed from sediments collected on top of the ship. A GC trace for BLC (top trace) was conducted to compare retention times. Extracts contained *n*-alkanes and a ubiquitous peak found in all sediments. In the above chromatograms, the y-axis is detector response and x-axis is the retention time in minutes. The chromatograms have been scaled to a lower detector response than the highest peak to observe smaller peaks in the trace. The y-axis is not the same scale for each chromatogram.
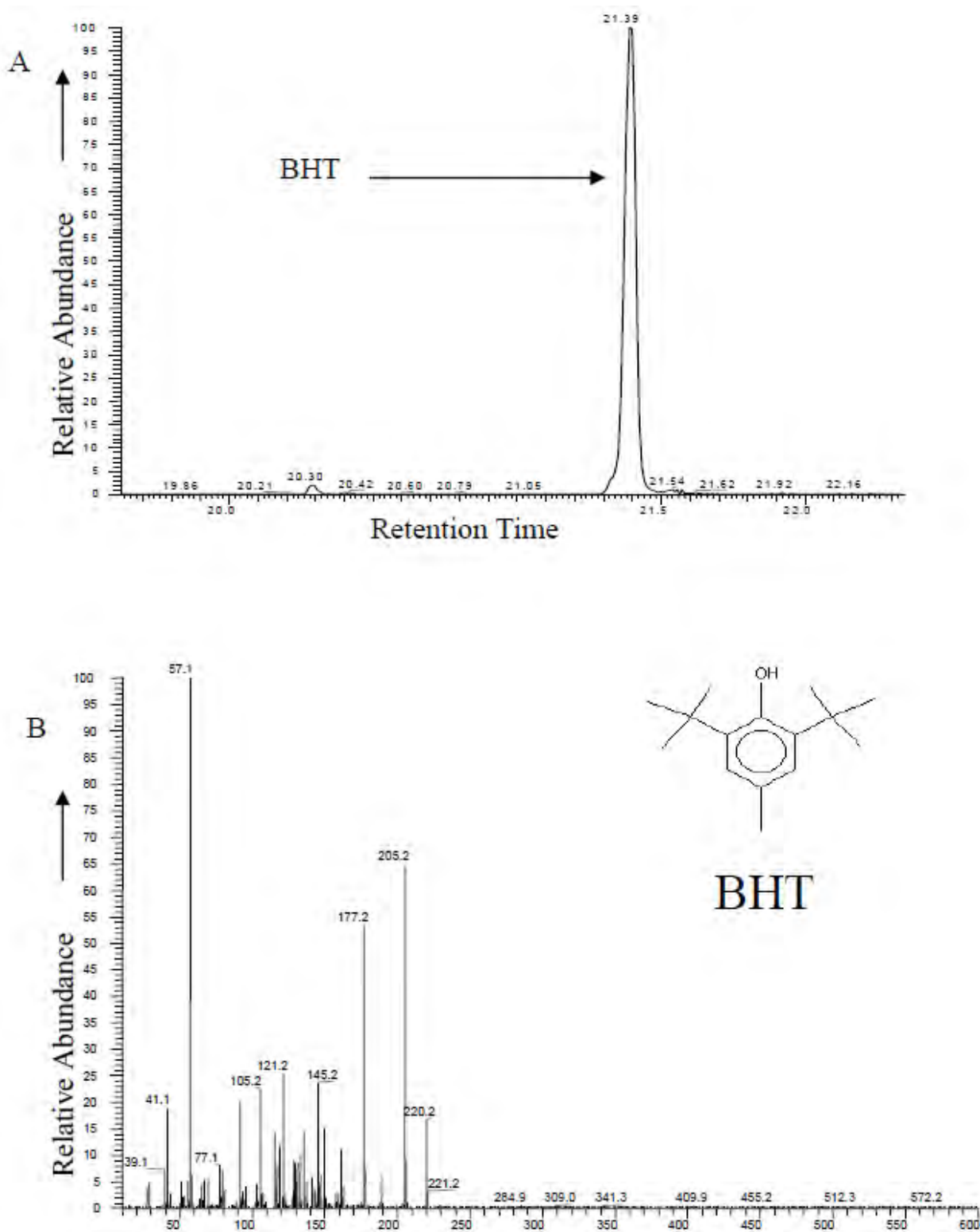
Figure 8.17. Total ion chromatogram (TIC) trace of the ubiquitous peak found in all sediment extracts (A). The mass spectra monitored at *m/z*=205 was identified as butylated hydroxytoluene (BHT) (B)
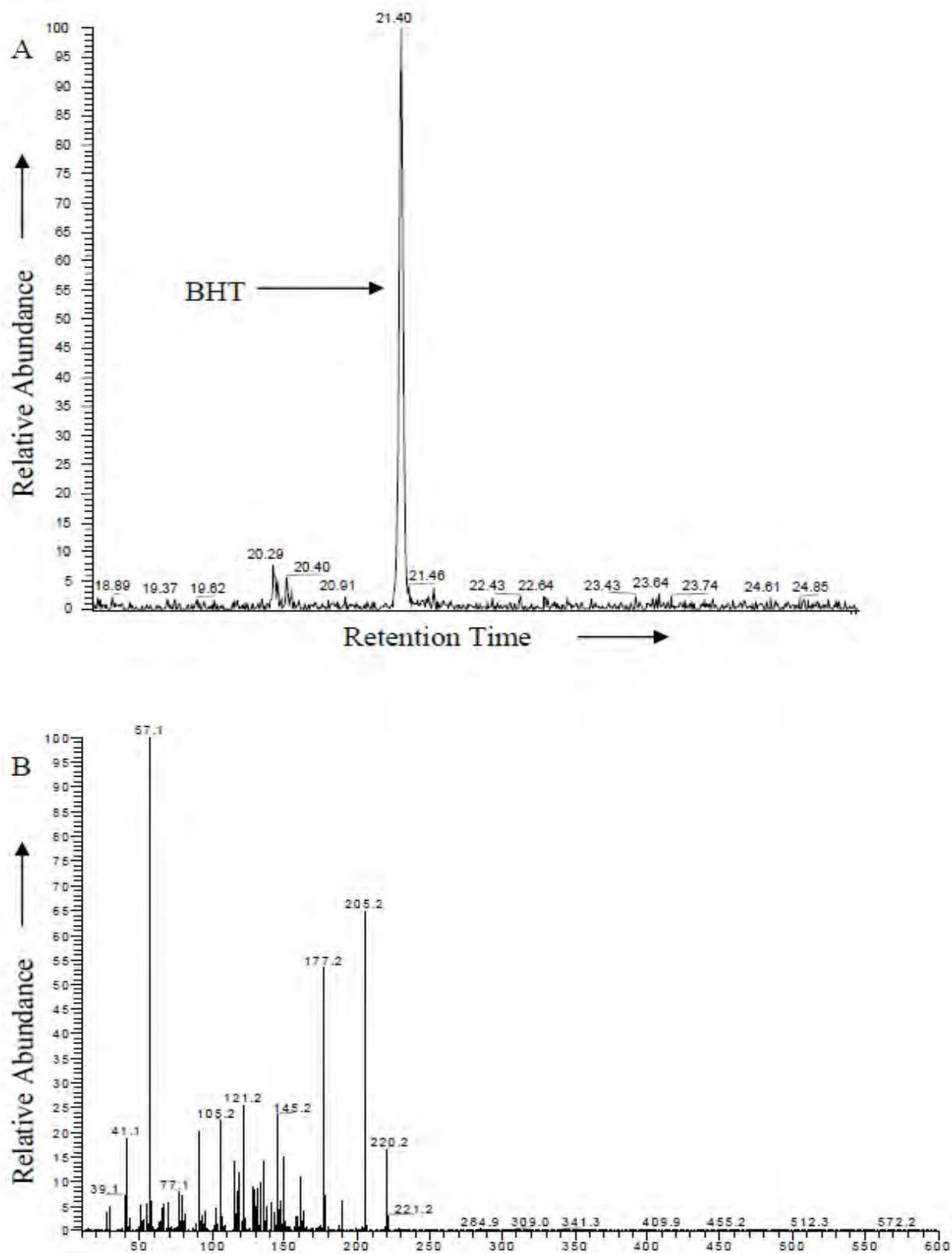
Figure 8.18. Total ion chromatogram (TIC) trace of BHT found in boiling chip and thimble extracts (A). The mass spectra monitored at *m/z*=205 was identified as BHT (B).
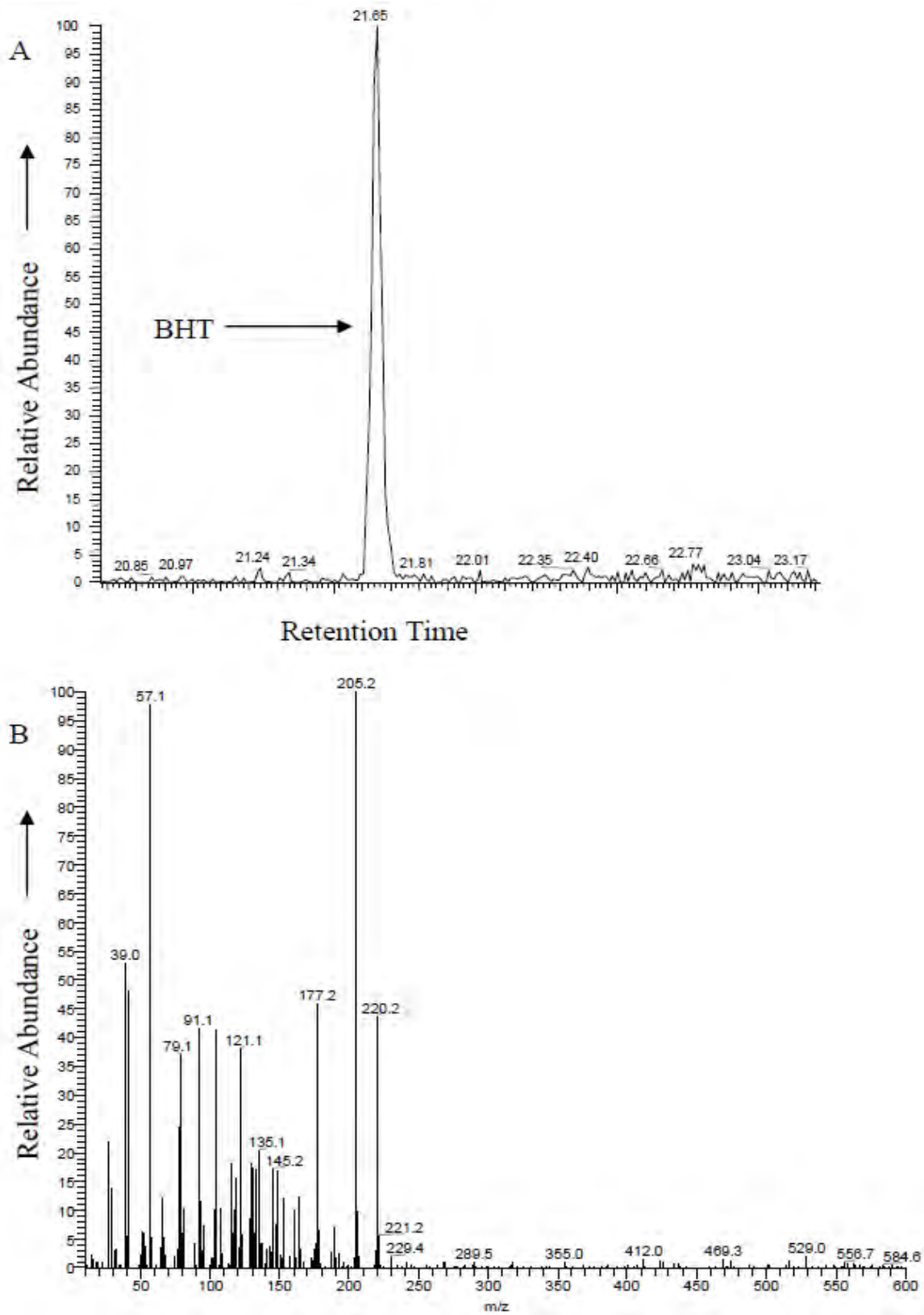
Figure 8.19. Total ion chromatogram trace of BHT found in oil sample 00-034 leaking from USS *Arizona* (A). The mass spectra monitored at *m/z*=205 was identified as BHT (B).
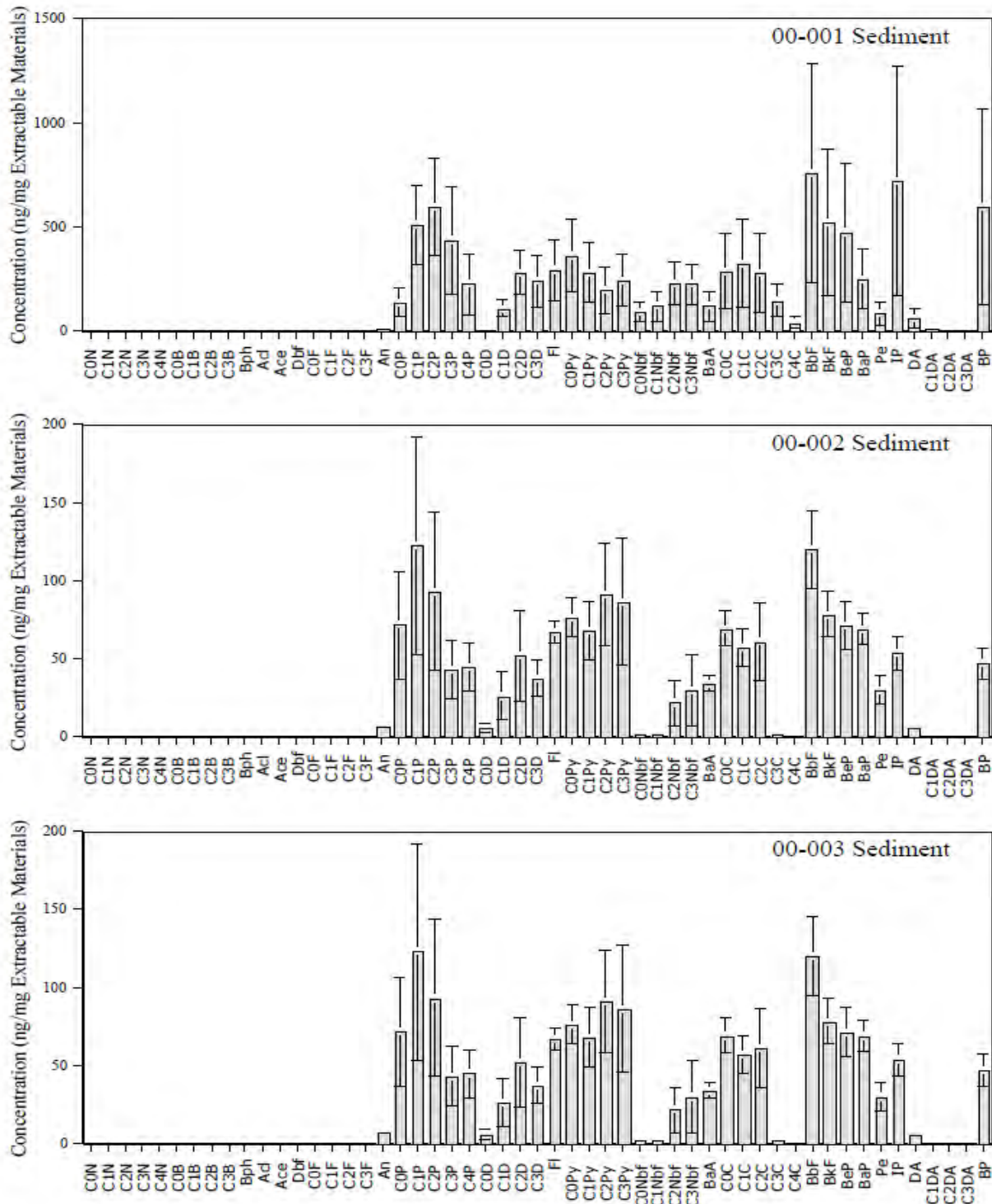
Figure 8.20. Individual PAH analysis for solvent-extractable materials from sediments collected 12 ft. off the stern starboard side of USS *Arizona*. There are no detectable amounts of low molecular weight PAHs (i.e., naphthalene), but high molecular weight PAHs (i.e., pyrene) were detected. Concentration (y-axis) is not the same scale for each histogram. Abbreviations are defined in Table 8.1 and locations of sediments are defined in Figure 8.5.
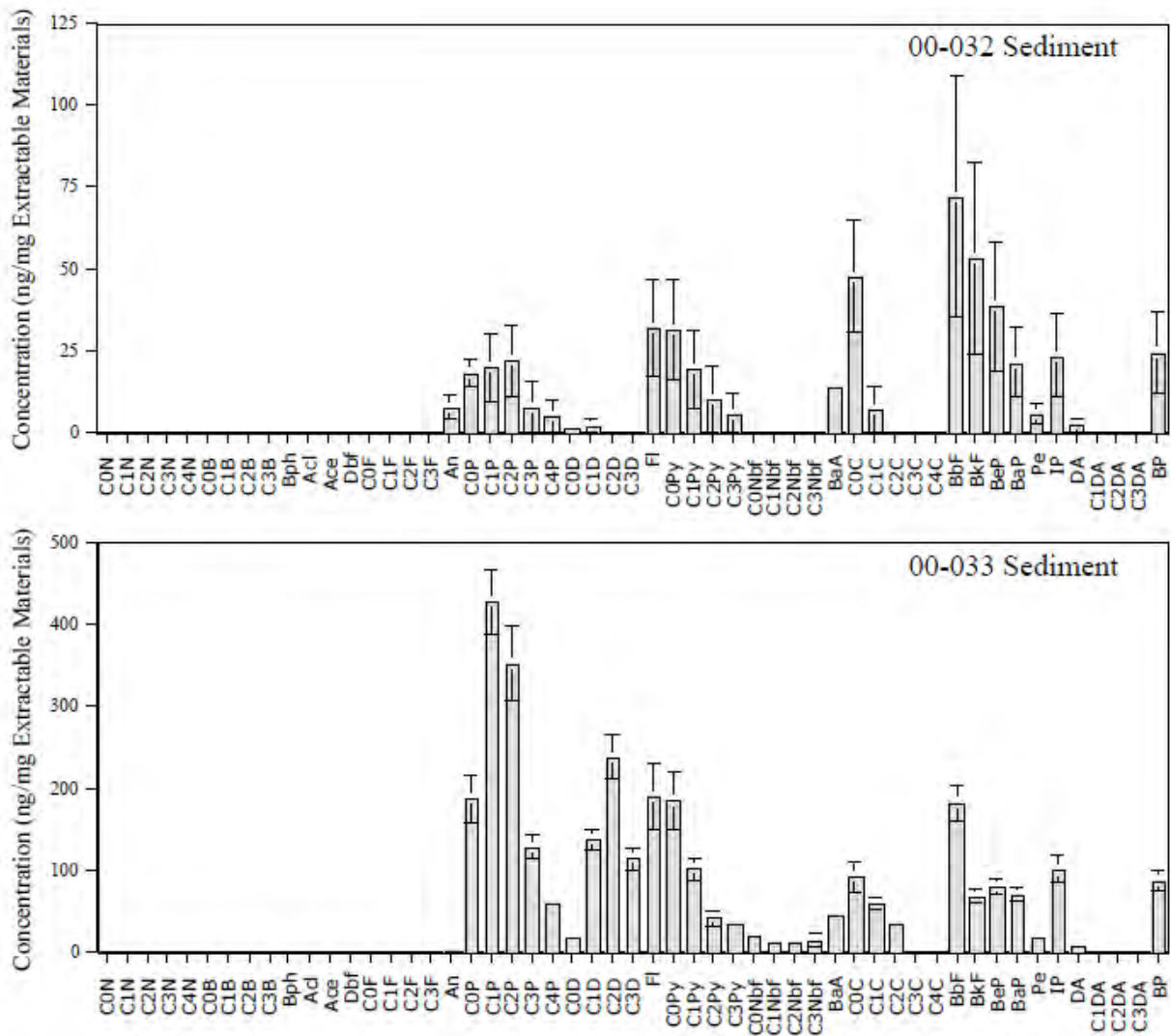
Figure 8.21. Individual PAH analysis for solvent-extractable materials from sediments collected 10 ft. off the port side of USS *Arizona*. There are no detectable amounts of low molecular weight PAHs (i.e., naphthalene), but high molecular weight PAHs (i.e., pyrene) were detected. Concentration for the y-axis is not the same scale for each histogram. Abbreviations are defined in Table 8.1 and locations of sediments are defined in Figure 8.5.
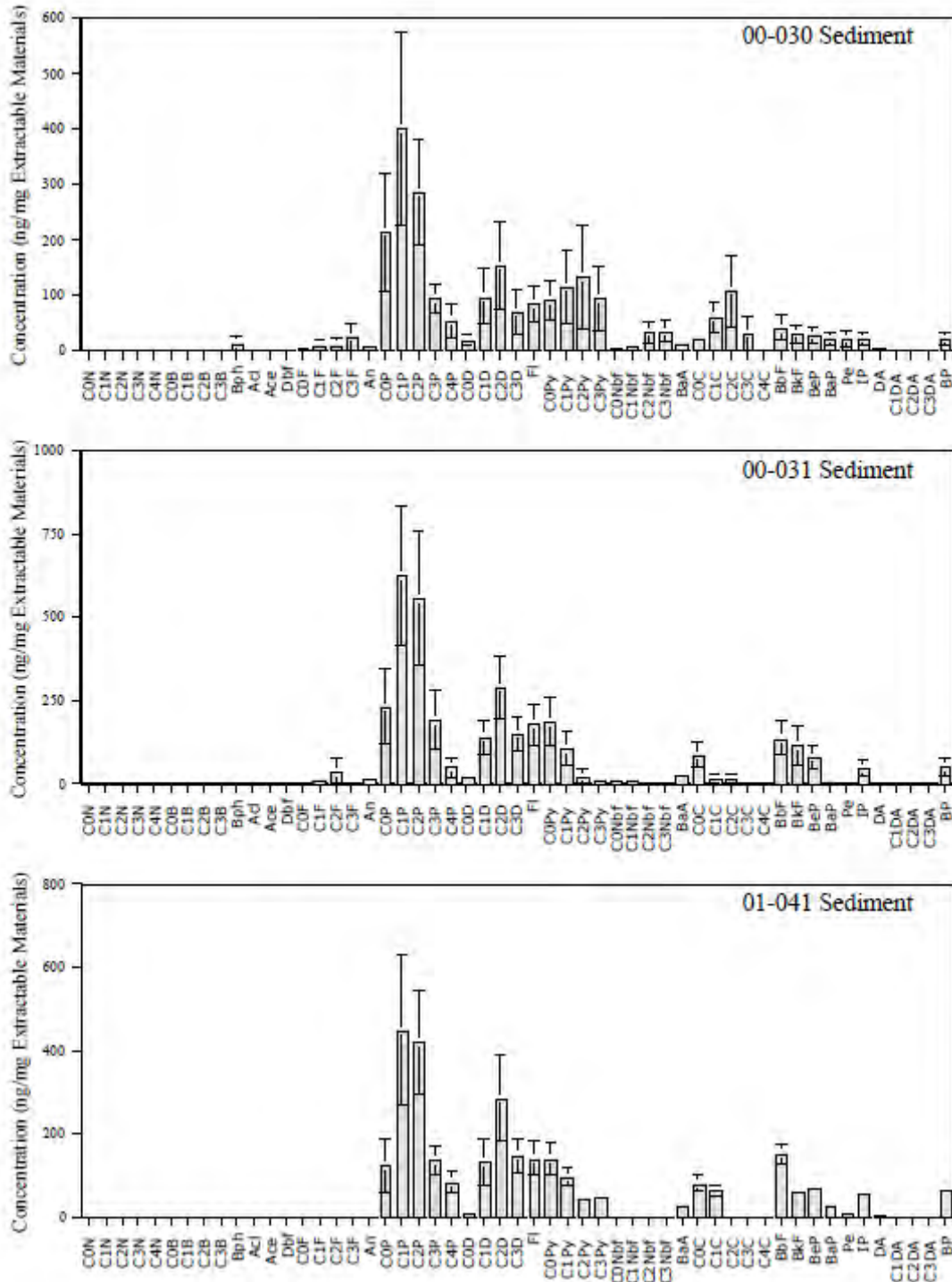
Figure 8.22. Individual PAH analysis for solvent-extractable materials from sediments collected on top of USS *Arizona*. There are no detectable amounts of low molecular weight PAHs (i.e., naphthalene), but high molecular weight PAHs (i.e., phenanthrene) were detected. Concentration for the y-axis is not the same scale for each histogram. Abbreviations are defined in Table 8.1 and locations of sediments are defined in Figure 8.5.

Sediment	$C_{30}H/18\alpha$ Oleanane[a]	$Ts/(Ts+Tm)$[b]	$C_{28}TT/C_{30}H$[c]	$C_{29}TT/C_{30}H$[d]
00-001	3.16+0.29	0.37+0.04	0.20+0.08	0.19+0.08
00-002	9.21+5.30	0.37+0.01	0.63+0.46	1.16+0.98
00-003	2.80+1.03	0.86+0.37	0.38+0.12	0.42+0.11
00-032	4.11+0.68	0.45+0.04	0.17+0.08	0.22+0.12
00-033	3.38+0.40	0.45+0.07	0.20+0.08	0.19+0.08
00-030	2.82+0.96	0.52+0.09	0.98+0.32	0.77+0.30
00-031	2.19+0.68	0.44+0.03	0.61+0.34	0.65+0.32
01-041	2.95+0.43	0.43+0.14	0.20+0.08	0.20+0.08

All values are means and standard error of triplicate samples.

[a]Calculated from m/z=191 mass chromatogram peak areas of $C_{30}17\alpha(H),21\beta(H)$-hopane and $18\alpha(H)$-oleanane.

[b]Calculated from the m/z=191 mass chromatogram peak areas of $C_{27}17\alpha(H)$-22,29,30-trisnorhopane (Tm) and $C_{27}18\alpha(H)$-22,29,30-trisnorneohopane (Ts).

[c]Calculated from the m/z=191 mass chromatogram peak areas of $C_{28}13\beta,21\alpha(H)$-trycyclic terpanes and $C_{30}17\alpha(H),21\beta(H)$-hopane.

[d]Calculated from the m/z=191 mass chromatogram peak areas of $C_{29}13\beta,21\alpha(H)$-trycyclic terpanes and $C_{30}17\alpha(H),21\beta(H)$-hopane

Table 8.6. Hopane biomarker ratios calculated for sediment solvent-extractable materials collected from different locations on and near USS *Arizona*.

Sediment	Total PAHs[a]	Total PAHs:$C_{30}H$[b]	Total PAHs:18α-oleanane
00-001	9286.36+5164.92	10.43+4.86	37.14+20.14
00-002	16278.60+10105.12	9.36+7.56	19.85+9.64
00-003	1661.33+369.16	9.51+7.44	21.68+9.22
00-032	426.97+236.71	1.57+1.38	3.67+6.35
00-033	3160.40+402.41	0.44+0.09	1.38+0.30
00-030	2484.10+1171.70	9.79+9.20	19.47+10.58
00-031	3476.83+1428.96	7.14+6.66	20.47+18.96
01-041	2915.63+823.17	9.04+5.32	22.70+10.36

All values are the means and standard error of triplicate samples.

[a]The ng amount of PAHs per mg of dry sediments.

[b]$C_{30}H$ represents $C_{30}17\alpha(H),21\beta(H)$-hopane.

Table 8.7. Ratio of total PAHs to biomarkers of USS *Arizona* sediment solvent-extractable material.

BIOMARKER ANALYSIS OF SEDIMENT SOLVENT-EXTRACTABLE MATERIALS

GC-MS was used to examine USS *Arizona* sediment biomarker profiles, focusing on mass chromatograms m/z=191 peak areas (for terpanes / hopanes) and m/z=217 (for steranes) (Figures 8.23–8.28). In m/z 191 mass chromatograms, C_{28-31} hopanes, Ts and Tm, as well as C_{28-29} tricyclics were detected. Biomarker ratios were then calculated from m/z=191 peak areas (Table 8.7). Peak areas of $C_{30}17\alpha(H),21\beta(H)$-hopane and 18α-oleanane were used to determine if $C_{30}17\alpha(H),21\beta(H)$-hopane was being degraded relative to the stable 18α-oleanane. Peak areas of $C_{27}17\alpha(H)$-22,29,30-trisnorhopane (Tm) and $C_{27}18\alpha(H)$-22,29,30-trisnorneohopane (Ts) were calculated for the Ts/(Ts + Tm) ratio.

Tricyclic terpane ratios were also calculated from mass chromatograms m/z=191 using the peak areas of $C_{28}13\beta,21\alpha(H)$-tricyclic terpane (22*R* and 22*S*) and $C_{29}13\beta,21\alpha(H)$-tricyclic terpane (22*R* and 22*S*) to compare with the peak area of $C_{30}17\alpha(H),21\beta(H)$-hopane. These ratios were calculated to determine if C_{28} and C_{29} tricyclic terpanes were being degraded in comparison to $C_{30}17\alpha,21\beta(H)$-hopane. Ratios calculated from mass chromatograms m/z=191 for solvent-extractable materials from sediments were variable and had no discernable differences between different sampling areas (Table 8.6). For example, the Ts/(Ts+Tm) ratio ranged from 0.37 ± 0.04 to 0.86 ± 0.37 (Table 8.6).

In sediment extracts, the C_{27}, C_{28}, and C_{29} steranes were detected by GC-MS (m/z=217). Biomarker ratios were also calculated from peak areas of mass chromatograms m/z=217 as decribed in section 2. Briefly, mass chromatogram peak areas of C_{27} - $C_{29}5\alpha(H),14\alpha(H),17\alpha(H)$-sterane (20S and 20R), C_{27} - $C_{29}5\alpha(H),14\beta(H),17\beta(H)$-sterane (20S and 20R), and $C_{30}17\alpha(H),21\beta(H)$-hopane were calculated for the $C_{27}S/C_{30}H$, $C_{28}S/C_{30}H$, and $C_{29}S/C_{30}H$ ratios. Sterane biomarker ratios for solvent-extractable materials from sediments had no discernable differences between different sampling areas because of large standard errors in the calculated ratios (Table 8.8).
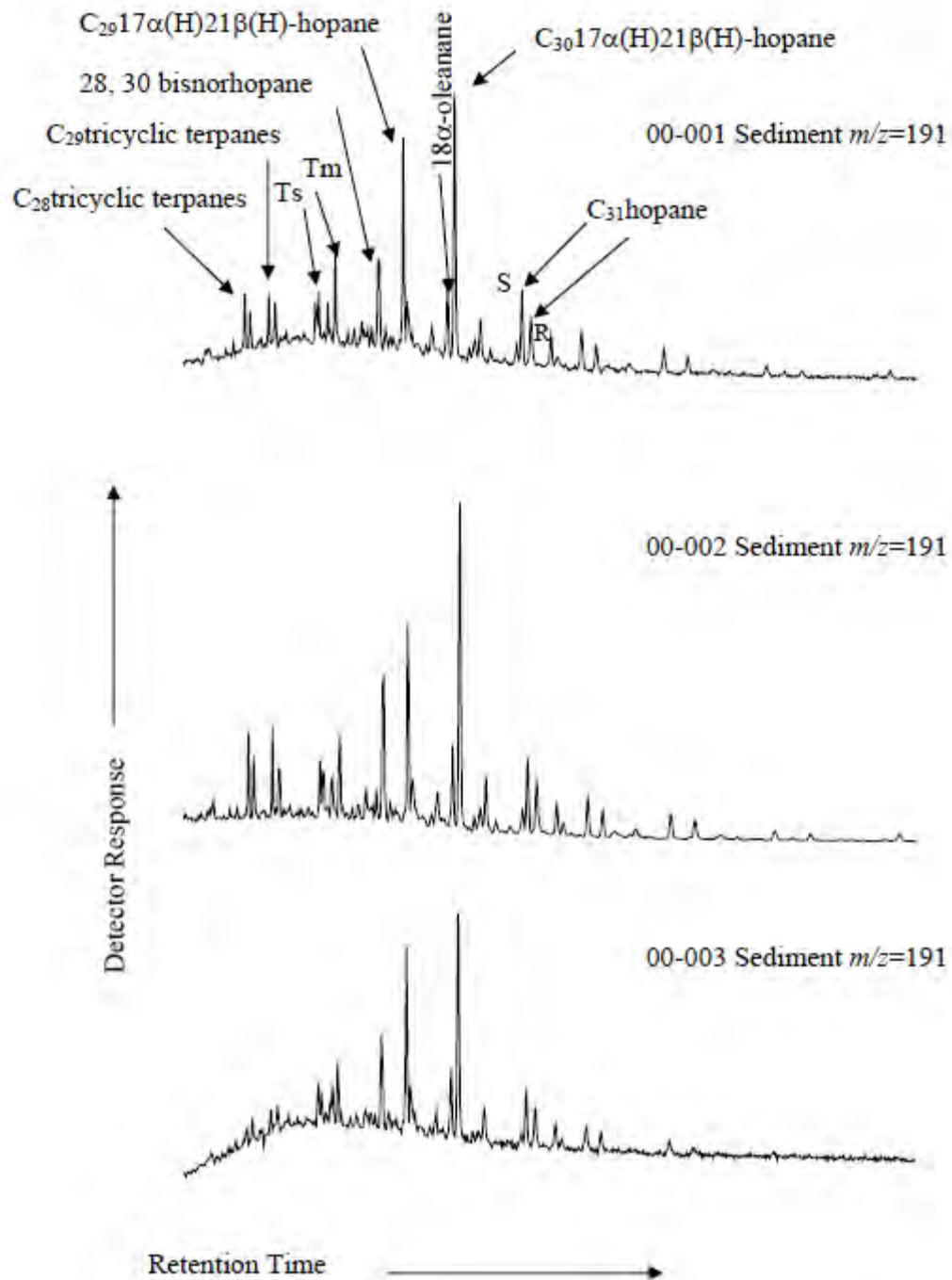
Figure 8.23. GC-MS chromatograms (*m/z*=191) of solvent-extractable material from sediments collected from the stern section, starboard side, 12 ft. from hull. Chromatograms are representative of triplicate samples.
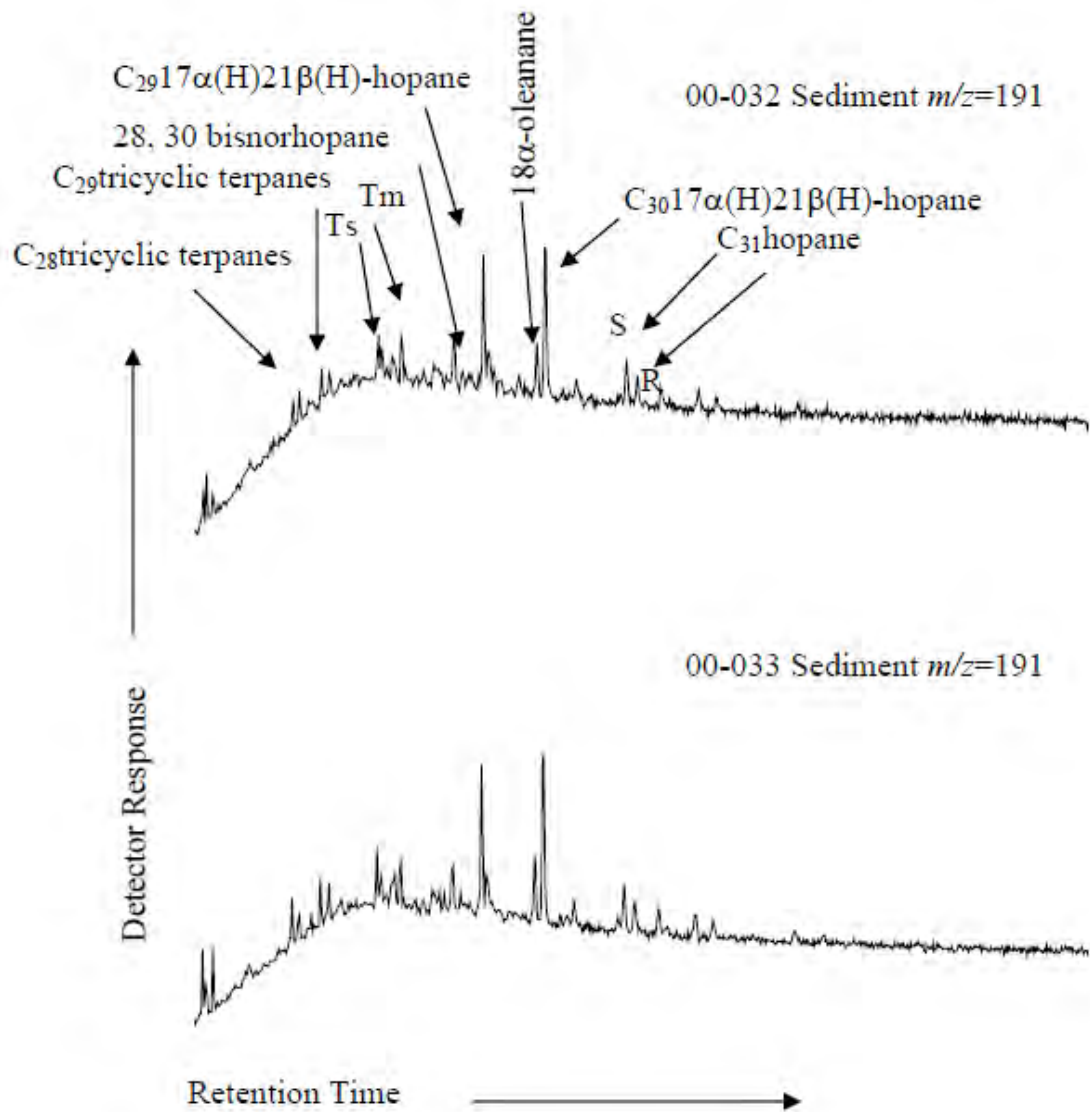
Figure 8.24. GC-MS chromatograms (*m/z*=191) of solvent-extractable material from sediments collected from the stern section, port side, 10 ft. from hull. Chromatograms are representative of triplicate samples.
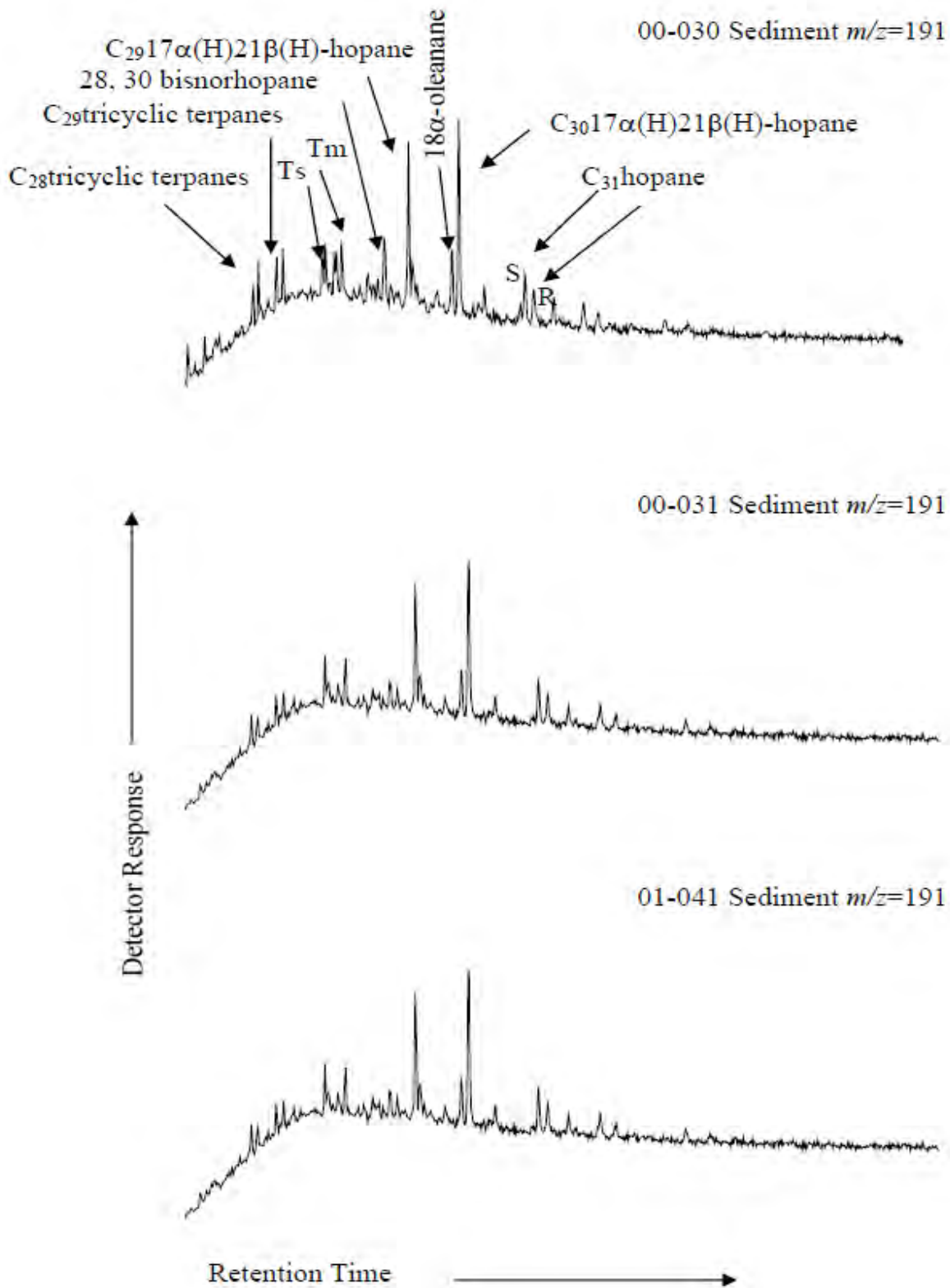
Figure 8.25. GC-MS chromatograms (*m/z*=191) of solvent-extractable material from sediments collected on top of the ship. Chromatograms are representative of triplicate samples.
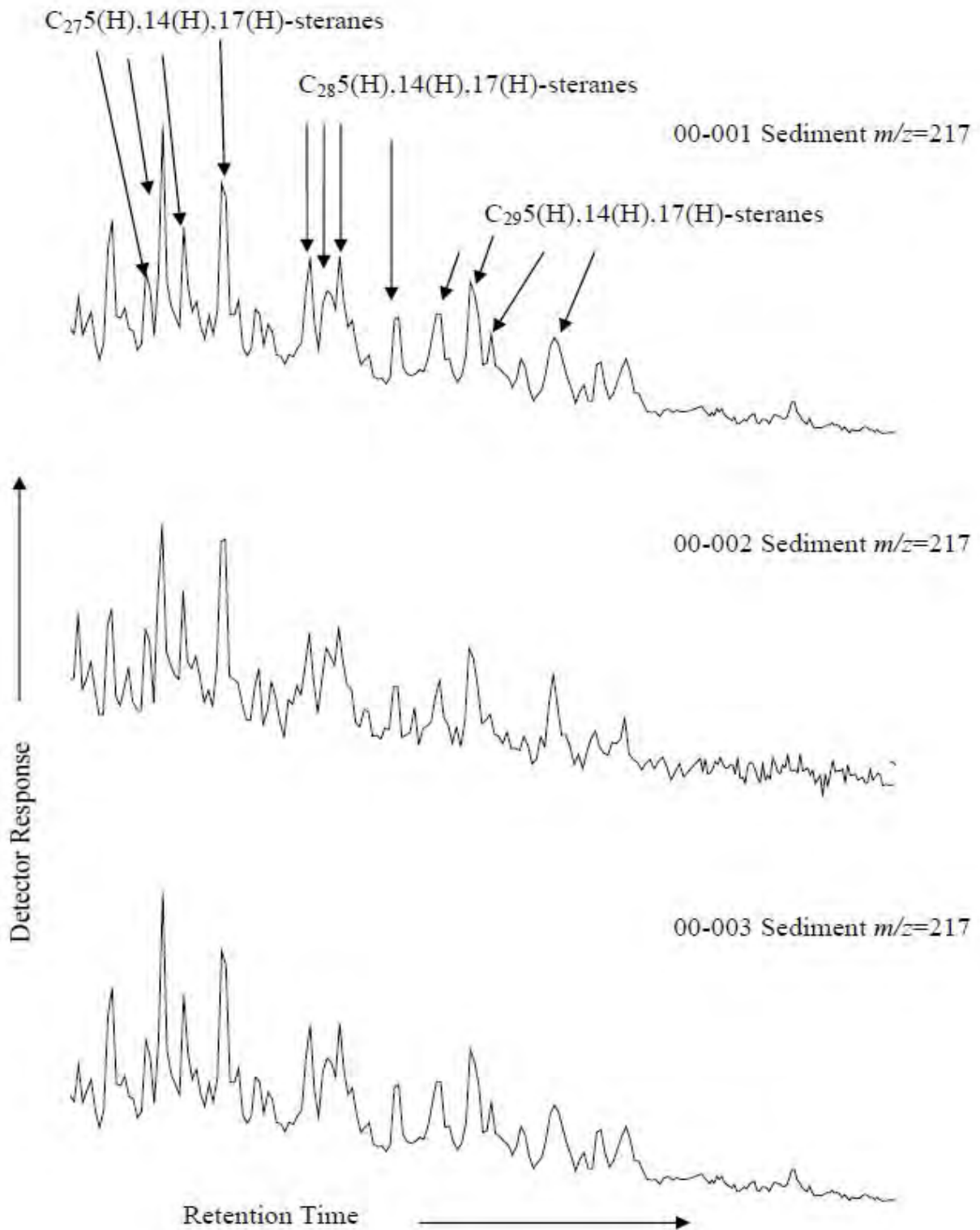
Figure 8.26. GC-MS chromatograms (*m/z*=217) of solvent-extractable material from sediments collected from the stern section, starboard side, 12 ft. from hull. Chromatograms are representative of triplicate samples.
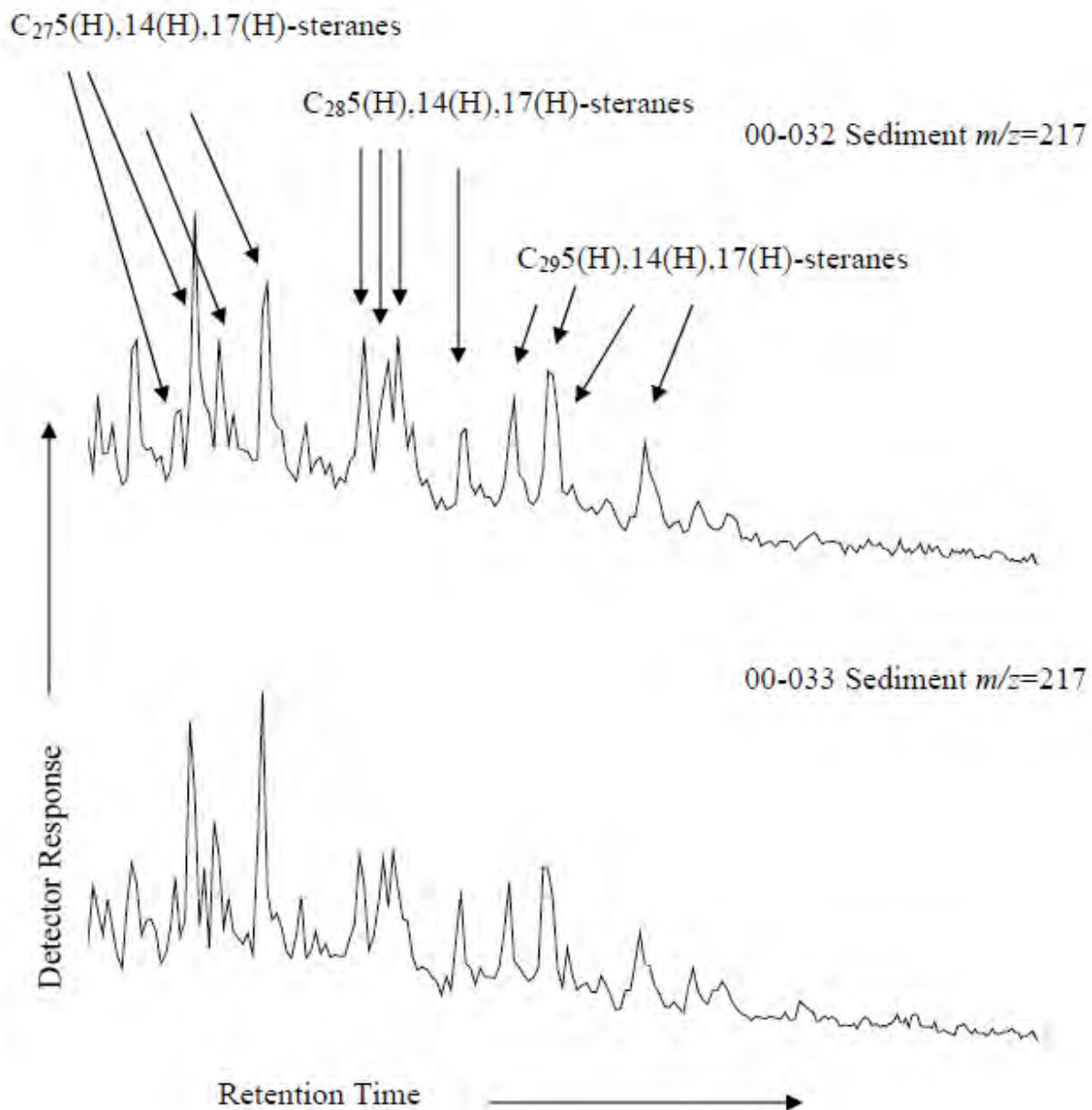
Figure 8.27. GC-MS chromatograms (*m/z*=217) of solvent-extractable material from sediments collected from the stern section, port side, 10 ft. from hull. Chromatograms are representative of triplicate samples.
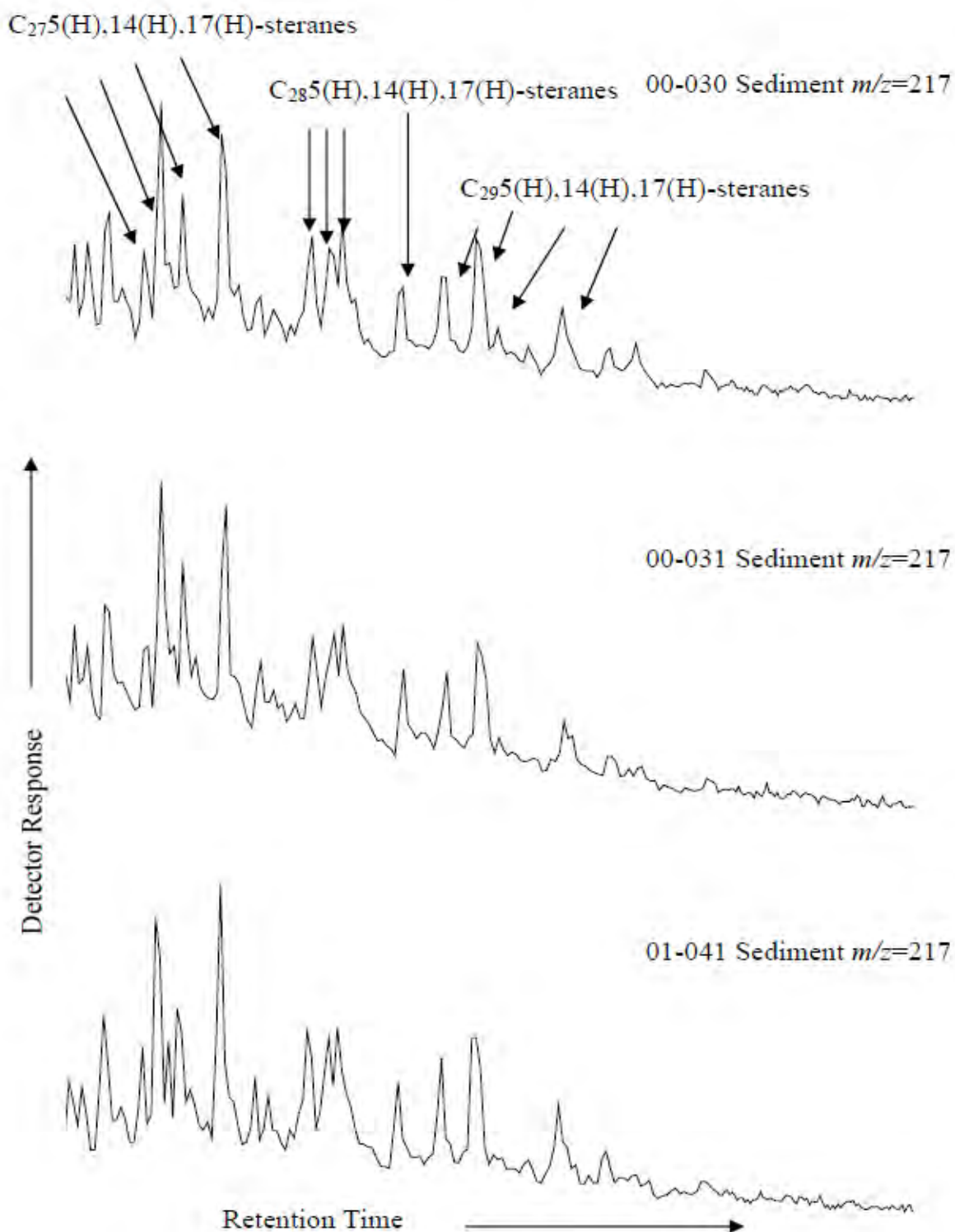
Figure 8.28. GC-MS chromatograms (*m/z*=217) of solvent-extractable material from sediments collected on top of the ship. Chromatograms are representative of triplicate samples.

Sediment	$C_{27}S/C_{30}H^a$	$C_{28}S/C_{30}H^b$	$C_{29}/C_{30}H^c$
00-001	0.98+0.01	0.68+0.06	0.74+0.05
00-002	1.15+0.66	1.84+1.44	1.58+1.10
00-003	1.27+0.15	0.75+0.13	0.83+0.14
00-032	1.24+0.35	0.79+0.20	0.66+0.07
00-033	1.17+0.10	0.57+0.01	0.70+0.04
00-030	1.59+0.19	1.09+0.34	1.07+0.18
00-031	1.95+0.19	1.60+0.56	1.19+0.32
01-041	1.28+0.05	0.58+0.01	0.65+0.01

All values are the means and standard error of triplicate samples.
[a]Calculated from m/z=217 mass chromatogram peak areas of $C_{27}5\alpha(H),14\alpha(H),17\alpha(H)$-sterane (20*S* and 20*R*), $C_{27}\alpha(H),14\beta(H),17\beta(H)$-sterane (20*S* and 20*R*) and $C_{30}17\alpha(H),21\beta(H)$-hopane.
[b]Calculated from m/z=217 mass chromatogram peak areas of $C_{28}5\alpha(H),14\alpha(H),17\alpha(H)$-sterane (20*S* and 20*R*), $C_{28}5\alpha(H),14\beta(H),17\beta(H)$-sterane (20*S* and 20*R*) and $C_{30}17\alpha(H),21\beta(H)$-hopane.
[c]Calculated from m/z=217 mass chromatogram peak areas of $C_{29}5\alpha(H),14\alpha(H),17\alpha(H)$-sterane (20*S* and 20*R*), $C_{29}5\alpha(H),14\beta(H),17\beta(H)$-sterane and $C_{30}17\alpha(H),21\beta(H)$-hopane.

Table 8.8. Sterane biomarker ratios calculated for sediment solvent-extractable materials collected from different locations on and near USS *Arizona*.

DEVELOPMENT OF BUNKER C FUEL OIL DEGRADING AEROBIC ENRICHMENT CULTURES

INTRODUCTION

Bunker C fuel oil is one of the most commonly spilled oils in the marine environment, and studies have shown the oil can persist in the environment for years (Strand et al., 1992; Irwin et al., 1997; Lunel et al., 2000). Bunker C was found in sediments examined twenty years after the *Arrow* spill in Chedabucto Bay, Novia Scotia, Canada (Vandermeulen and Singh, 1994). Studies have shown Bunker C fuel oil is degradable by microorganisms in laboratory enrichments, despite the increased concentrations of high molecular weight hydrocarbons (Mulkins-Phillips and Stewart, 1974; Minas and Gunkel, 1995; Wang et al., 1998a). In a laboratory study involving microbial degradation of Bunker C, gravimetric measurements showed enrichment cultures were able to degrade 30% to 85% of the non-asphaltenic components of the oil (Mulkins-Phillips and Stewart, 1974).

USS *Arizona* offers a unique opportunity to study the microbial degradation of Bunker C fuel oil. The sediments adjacent to the ship have been chronically exposed for over 60 years to

the oil leaking from the ship. In addition, hydrocarbon contaminants from other sources in Pearl Harbor, (i.e., US Navy facility and Chevron) may be present. Therefore, it would be expected that environmental conditions found in Pearl Harbor sediments may have enriched for microbial communities capable of degrading hydrocarbons (Floodgate, 1984; Frontera-Suau et al., 2002). In addition, structural differences in microbial communities from different sediment sampling locations may influence the extent of degradation.

In order to monitor petroleum degradation, internal components of oil that are resistant to biotic and abiotic weathering processes can be used as an internal reference to monitor the progression of degradation (Peters and Moldowan, 1993; Prince et al., 1994; Bost et al., 2001; Frontera-Suau et al., 2002). These compounds, referred to as internal markers or biomarkers, are more resistant to biotic and abiotic weathering than other components of oil. However, laboratory and field studies have shown that microbial communities are capable of influencing biomarker profiles by aerobically degrading various biomarkers that are generally considered to be conserved (Munoz et al., 1987; Moldowan et al., 1995; Bost et al., 2001; Wang et al., 2001a; Frontera-Suau et al., 2002). Possible degradation of biomarkers is an important consideration when using them as an internal reference to determine the extent of oil degradation.

The results presented in this section focus on determining if aerobic bacteria in sediments adjacent to and on top of USS *Arizona* can degrade the Bunker C fuel oil leaking from the ship. In addition, a molecular approach to examining microbial community structure, DGGE was used to determine if microbial enrichment cultures enriched from sediments were similar. Finally, analysis of biomarkers, specifically *m/z*=191 (for hopanes) and *m/z*=217 (for steranes), were examined to see if enrichment cultures were capable of degrading biomarkers found in oil leaking from the ship.

AEROBIC ENRICHMENT CULTURE DEGRADATION OF OIL LEAKING FROM USS *ARIZONA*

Eight different enrichment cultures (in triplicate) were initiated from sediments collected from USS *Arizona* sampling locations (Figure 8.4). For each aerobic enrichment culture initiated, triplicate Erlenmeyer flasks were inoculated with sediment from the different locations. Therefore, each of the triplicates is an independent (separate) culture. Following the third

monthly transfer, gravimetric measurements of oil extracted from the 8 enrichment cultures grown in triplicate and uninoculated controls, were determined after a 30 day incubation. The gravimetric measurements indicate the amount of oil lost during the 30 days of microbial growth and also includes abiotic losses of oil occurring during the incubation period. The uninoculated control showed a 6.13%$\pm$0.65% average decrease in the weight of recovered oil. In comparison, inoculated aerobic enrichment cultures averaged a 31.03%$\pm$4.58% decrease in the weight of recovered oil (Table 8.9). For enrichments 00-001, 00-030, and 00-033, 1 of the 3 triplicate cultures exhibited less degradation of oil. Therefore, these enrichments did not show as much oil loss and had larger standard errors than other enrichments throughout these experiments. For example, enrichment 00-001 had triplicates with gravimetric weights 14.71 mg, 5.24 mg, and 4.08 mg.

GAS CHROMATOGRAPHIC ANALYSIS OF OIL FROM ENRICHMENT CULTURES

Following gravimetric measurements, oil extracted from aerobic enrichment cultures following 30 days of growth were analyzed by gas chromatography utilizing flame ionization detection to determine the extent of *n*-alkane and branched alkane degradation in comparison to oil extracted from uninoculated controls. Gas chromatographic traces of oil extracted from the enrichment cultures demonstrated degradation of *n*-alkanes and branched alkanes along with a decrease in the unresolved complex mixture (UCM) in comparison to uninoculated control samples (Figure 8.29). The decrease in the UCM, which consists of unresolvable PAHs as well as heterocycles, indicates PAHs may be degraded also, although PAHs must be further resolved by GC-MS analysis.

PAH ANALYSIS OF OIL FROM AEROBIC ENRICHMENT CULTURES.

Mass spectrometry was conducted to determine concentrations of individual PAHs present in oil extracted from the aerobic enrichment cultures and uninoculated controls. Overall, mass spectrometry indicated a decrease of low molecular weight hydrocarbons (i.e., naphthalene, alkylated naphthalenes, flourene, and alkylated flourenes) in the enrichment cultures compared

Aerobic Enrichment	Inoculum Source	Percent Loss
Control	Uninoculated Control	6.13±0.65
00-001	Stern section, starboard side, 12 ft. from hull	28.99±9.92
00-002	Stern section, starboard side, 12 ft. from hull	39.37±1.50
00-003	Stern section, starboard side, 12 ft. from hull	32.36±1.37
00-032	Stern section, port side, 10 ft. from the hull	36.89±0.01
00-033	Stern section, port side, 10 ft. from the hull	22.22±2.44
00-030	Stern section bottom of barbette No. 4	32.53±10.52
00-031	Bow section, gun turret no. 1	36.48±1.53
01-041	Bow section, port side of gun turret no. 1	34.14±6.42

All values are the averages of triplicate samples with the standard errors of those values. The uninoculated control was maintained under the same conditions as aerobic enrichments for 30 days without microbial inoculum.

Table 8.9. Gravimetric analysis of oil extracted from USS *Arizona* aerobic enrichments.
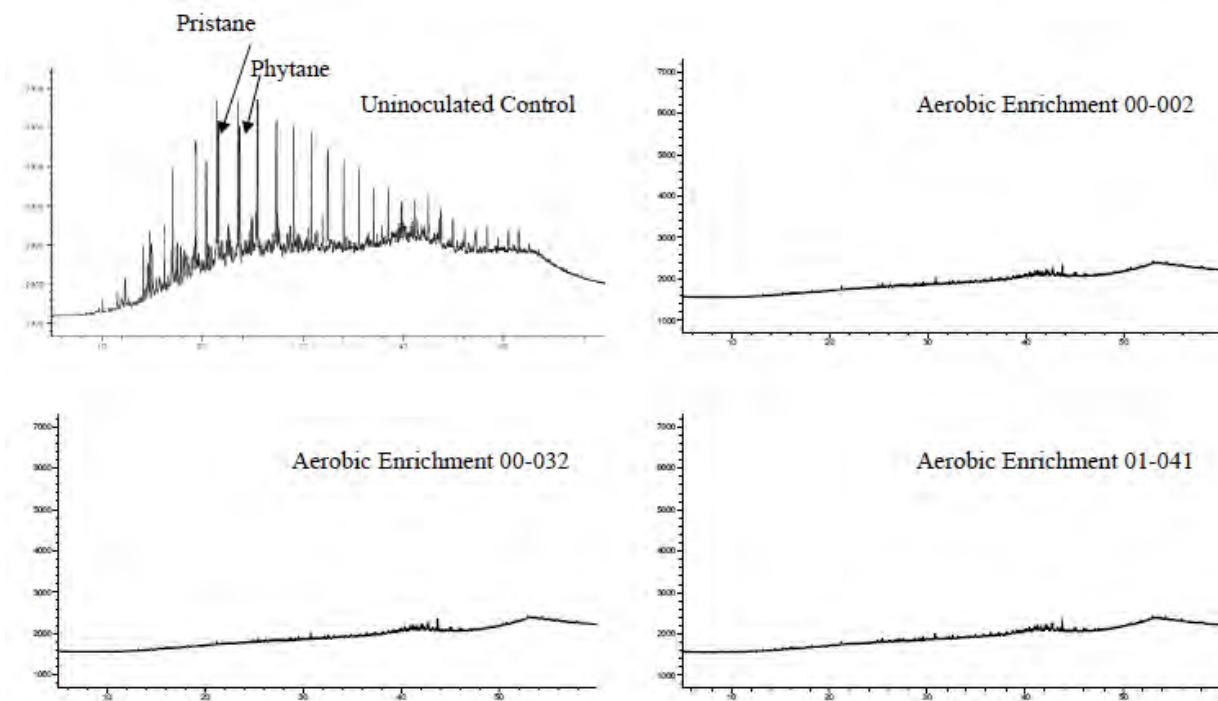
Figure 8.29. Gas chromatographic traces of oil extracted from USS *Arizona* aerobic enrichment cultures. The uninoculated control after 30 days still contains *n*-alkanes and branched alkanes. In comparison, following 30 days of microbial growth with Bunker C fuel oil as the only carbon source, loss of *n*-alkanes and the branched alkanes, pristane, and phytane, were observed. The y-axis is the detector response and x-axis is the retention time in minutes.

to the uninoculated controls (Figures 8.30 and 8.31). The concentration of higher molecular weight PAHs (i.e., perylene) were persistent relative to other PAHs when compared to the uninoculated control (Figures 8.32 and 8.33). It is important to note that during oil degradation, compounds that are not degraded will increase in concentration relative to the total amount of remaining oil. This occurrence does not indicate an increase in the absolute quantity of these compounds.

Enrichments 00-002, 00-003, and 01-041 had increased concentrations of C1-dibenzo(a,h)anthracene (C1DA) relative to other PAHs and the uninoculated control indicating no degradation of C1DA (Figures 8.34 and 8.35). Furthermore, enrichment 01-041 also did not demonstrate degradation of C2-phenanthrene/anthracene (C2Nbf) or C3-phenanthrene/anthracene (C3Nbf) relative to other USS *Arizona* aerobic enrichment cultures (Figures 8.34 and 8.35). Enrichment 01-041 also exhibited less pyrene degradation relative to other USS *Arizona* aerobic enrichment cultures (Figures 8.34 and 8.35).

PAHS COMPARED TO CONSERVED BIOMARKERS.

Gas chromatography coupled to mass spectrometry also provided $18\alpha(H)$-oleanane and $C_{30}\,17\alpha(H),21\beta(H)$-hopane concentrations in oil extracted from USS *Arizona* aerobic enrichment cultures and uninoculated controls after a 30 day incubation. Ratios for $C_{30}\,17\alpha(H),21\beta(H)$-hopane to $18\alpha(H)$-oleanane were calculated to determine if $C_{30}\,17\alpha(H),21\beta(H)$-hopane was being degraded relative to $18\alpha(H)$-oleanane. To date, no laboratory or field studies have shown degradation of $18\alpha(H)$-oleanane (Peters and Moldowan, 1993). Ratios of $C_{30}\,17\alpha,21\beta(H)$-hopane to $18\alpha(H)$-oleanane varied little between oil extracted from aerobic enrichments and uninoculated controls after 30 days of incubation, indicating no degradation of $C_{30}17\alpha(H),21\beta(H)$-hopane (Table 8.10).

The ratios of total PAHs to conserved biomarkers $18\alpha(H)$-oleanane and $C_{30}17\alpha(H),21\beta(H)$-hopane from aerobic enrichments with 30 days microbial growth in comparison to the uninoculated control decreased, indicating a loss of PAHs (Table 8.11). For example, the total PAH to $C_{30}17\alpha(H),21\beta(H)$-hopane ratio for the uninoculated control was

356
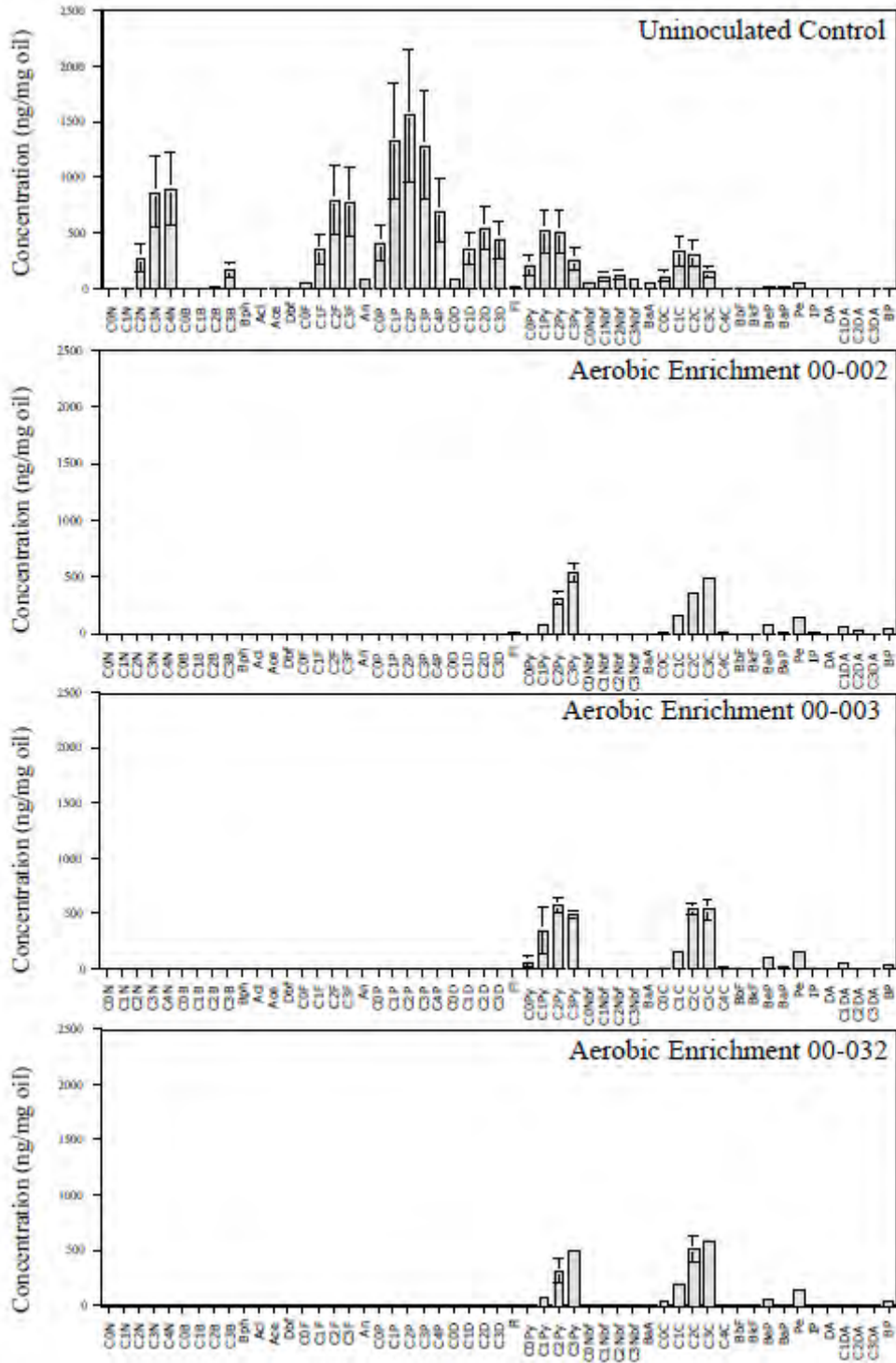
Figure 8.30. Individual PAH analysis for oil extracted from USS *Arizona* aerobic enrichments initiated from sediments surrounding the ship following 30 days growth indicates a substantial loss of PAHs in comparison to the uninoculated control. Abbreviations for PAH compounds are defined in Table 8.1 and locations for sediments used for aerobic enrichment inoculum are defined in Figure 8.5.
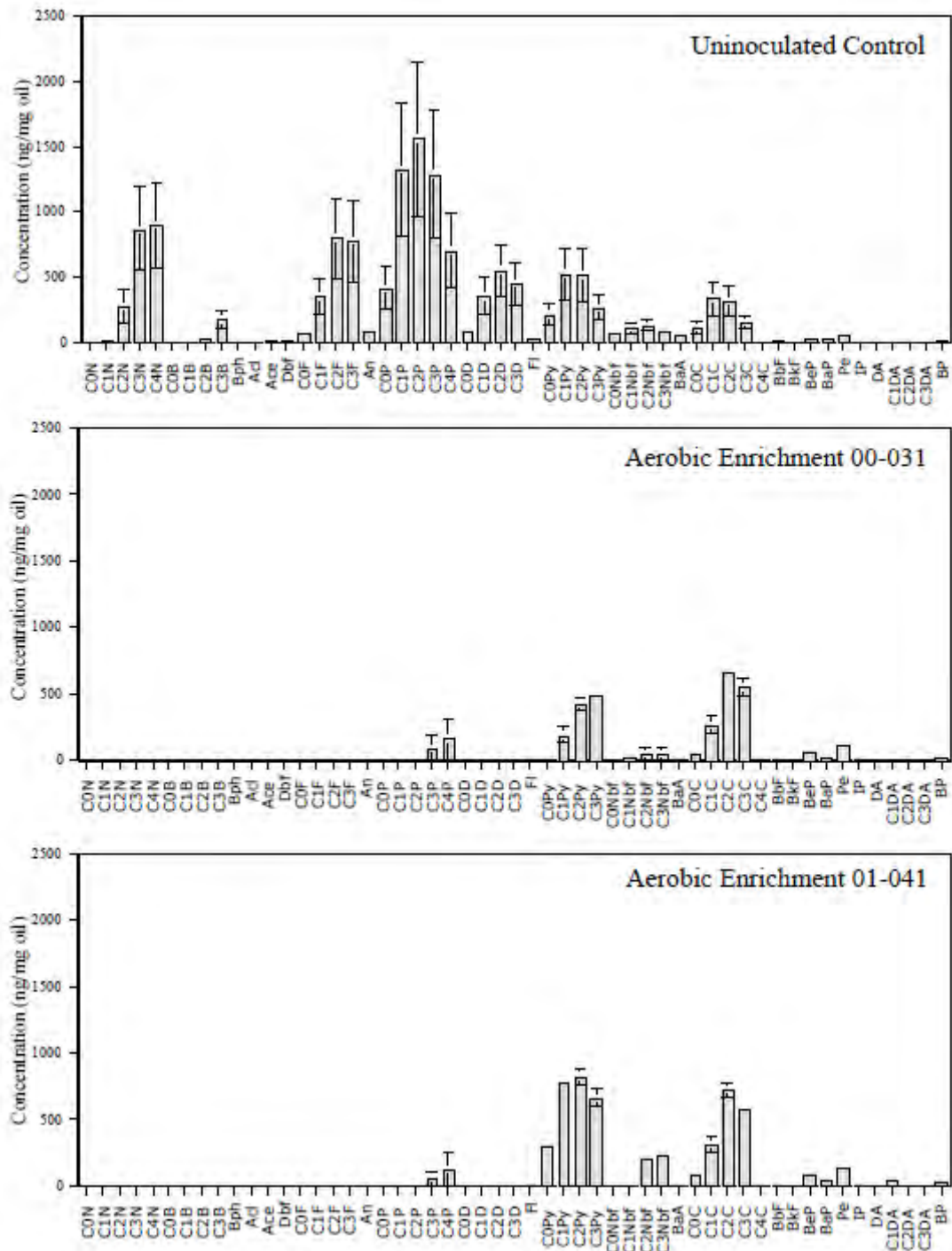
Figure 8.31. Individual PAH analysis for oil extracted from USS *Arizona* aerobic enrichments initiated from sediments on top of the ship following 30 days incubation indicates a substantial loss of PAHs in comparison to the uninoculated control. Abbreviations for PAH compounds are defined in Table 8.1 and locations for sediments used for aerobic enrichment inoculum are defined in Figure 8.5.
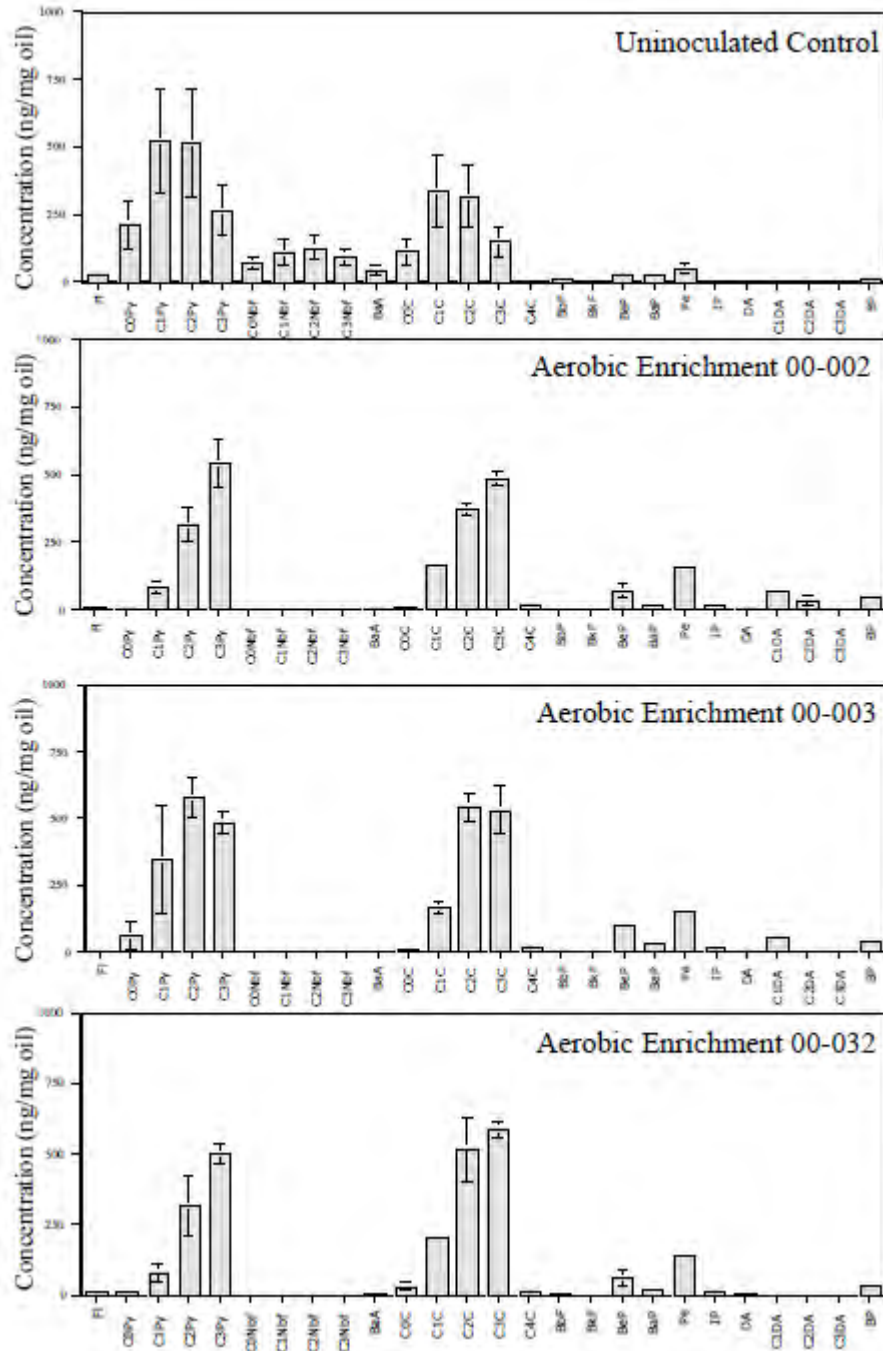
Figure 8.32. Individual PAH analysis of high molecular weight PAHs for oil extracted from USS *Arizona* aerobic enrichments initiated from sediments surrounding the ship following 30 days growth. Abbreviations for PAH compounds are defined in Table 8.1 and locations for sediments used for aerobic enrichment inoculum are defined in Figure 8.5.
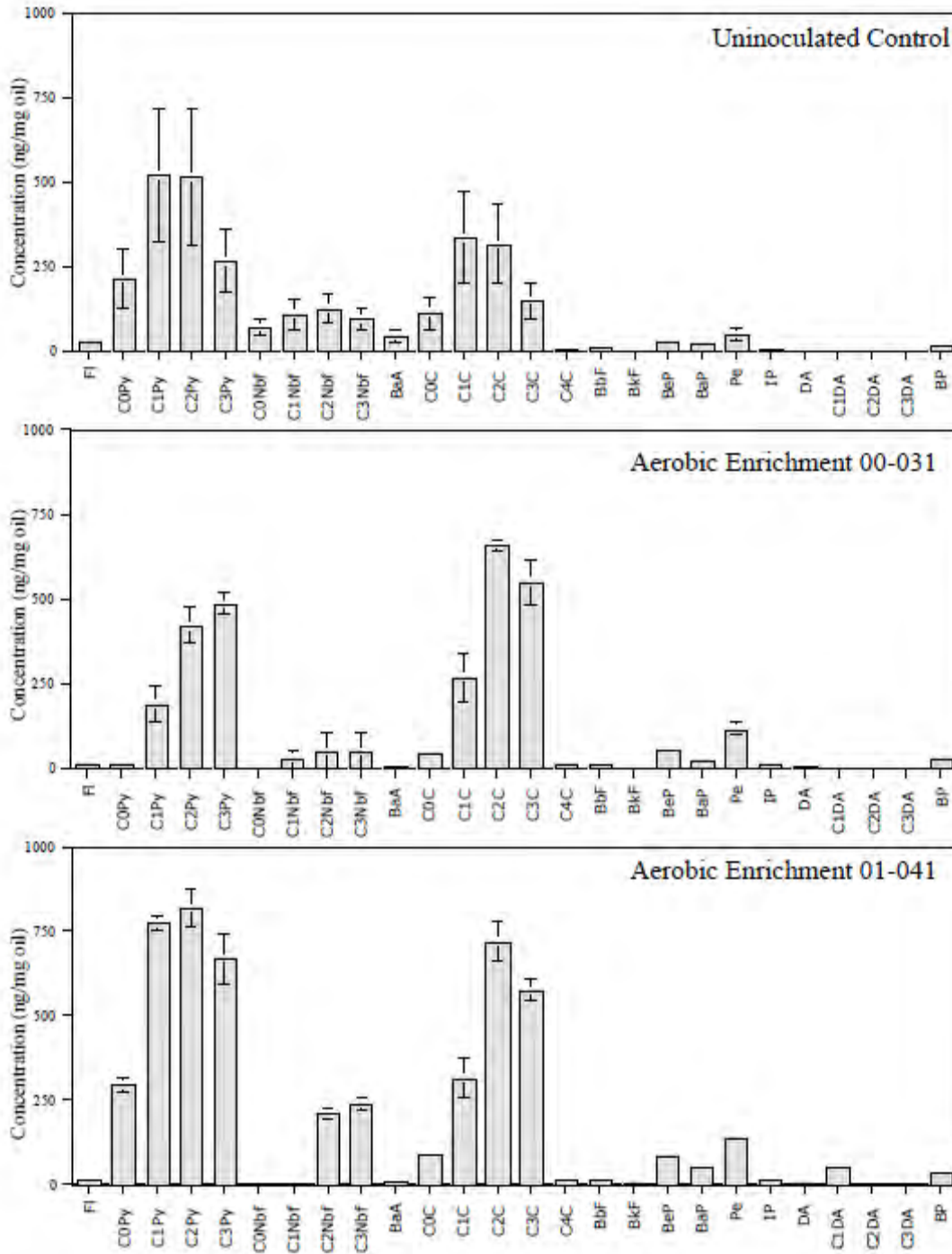
Figure 8.33. Individual PAH analysis of high molecular weight PAHs for oil extracted from USS *Arizona* aerobic enrichments initiated from sediments on top of the ship following 30 days growth. Abbreviations for PAH compounds are defined in Table 8.1 and locations for sediments used for aerobic enrichment inoculum are defined in Figure 8.5.
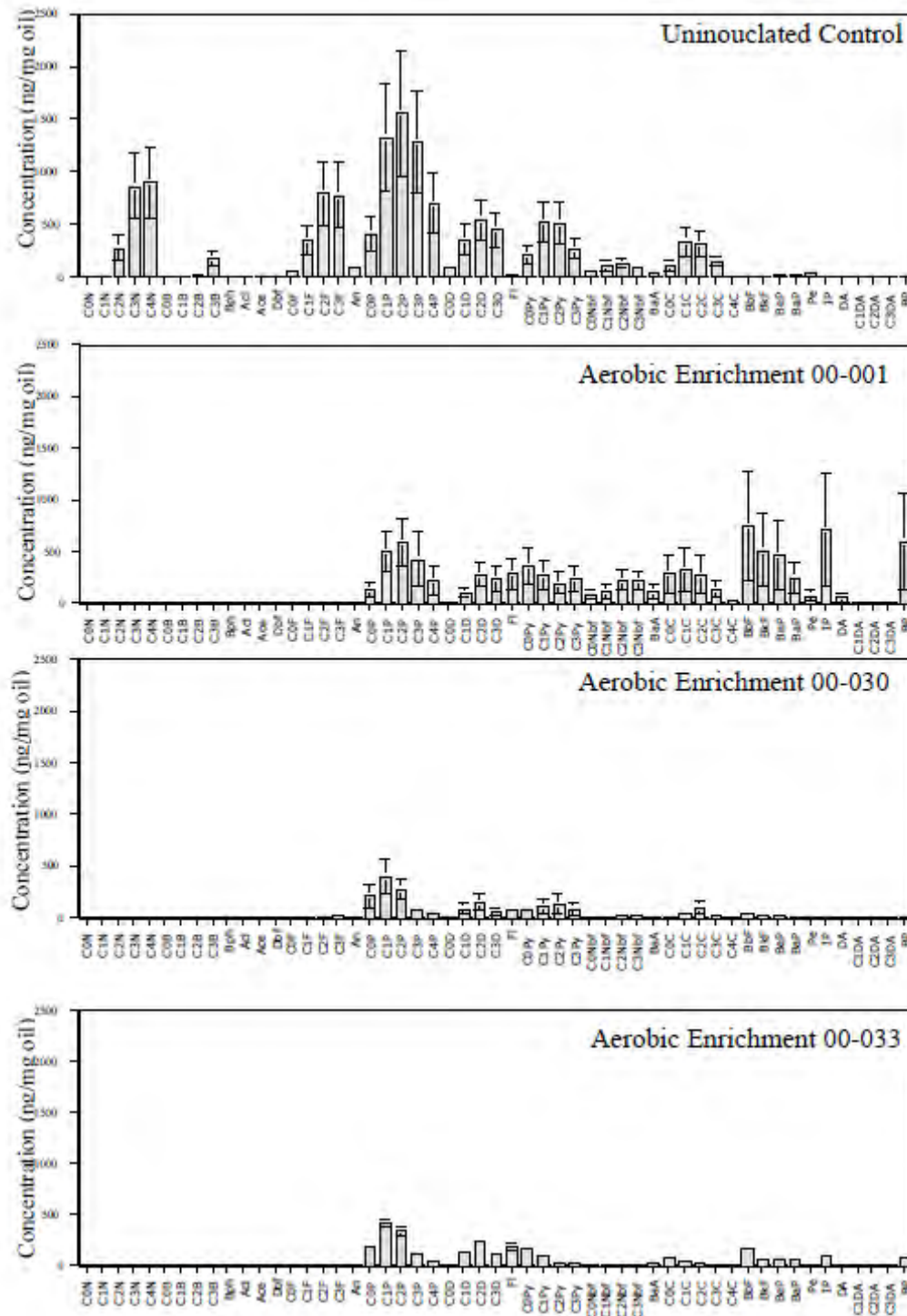
Figure 8.34. Individual PAH analysis for oil extracted from USS *Arizona* aerobic enrichments following 30 days incubation. These enrichments had one of the three triplicates that did not show oil degradation. Abbreviations for PAH compounds are defined in Table 8.1 and locations for sediments used for aerobic enrichment inoculum are defined in Figure 8.5.
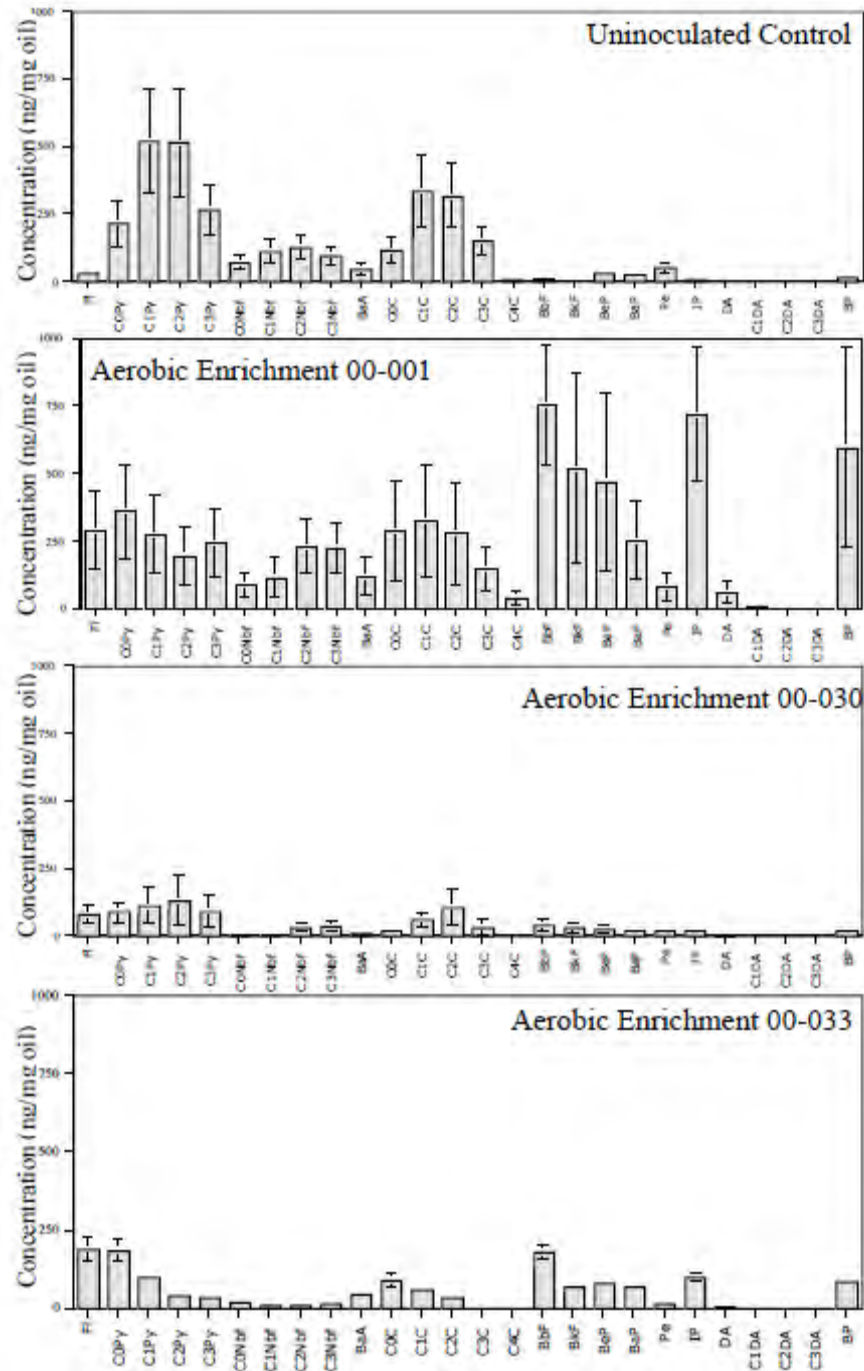
Figure 8.35. Individual PAH analysis of high molecular weight PAHs for oil extracted from USS *Arizona* aerobic enrichments following 30 days incubation. These enrichments had one of the three triplicates that did not show oil degradation. Abbreviations for PAH compounds are defined in Table 8.1 and locations for sediments used for aerobic enrichment inoculum are defined in Figure 8.5.

Aerobic Enrichment	$C_{30}H/18\alpha$ oleanane[a]	$Ts/(Ts+Tm)$[b]	$C_{31}S/(C_{31}R + C_{31}S)$[c]
Uninoculated Control	4.95±0.16	0.36±0.02	0.52±0.03
00-001	5.14±0.03	0.27±0.04	0.57±0.01
00-002	5.09±0.05	0.39±0.05	0.57±0.01
00-003	5.08±0.05	0.31±0.01	0.56±0.01
00-032	5.11±0.04	0.26±0.07	0.58±0.01
00-033	4.55±0.43	0.37±0.45	0.52±0.02
00-030	5.06±0.06	0.37±0.03	0.55±0.02
00-031	5.07±0.09	0.41±0.05	0.56±0.01
01-041	5.09±0.03	0.39±0.11	0.58±0.01

All values are the means and standard error of triplicate samples. The uninoculated control was maintained under the same conditions as aerobic enrichments for 30 days without microbial inoculum.
[a]Calculated from m/z=191 mass chromatogram peak areas of $C_{30}17\alpha(H),21\beta(H)$-hopane and $18\alpha(H)$-oleanane.
[b]Calculated from the m/z=191 mass chromatogram peak areas of $C_{27}17\alpha(H)$-22,29,30-trisnorhopane (Tm) and $C_{27}18\alpha(H)$-22,29,30-trisnorneohopane (Ts).
[c]Calculated from the m/z=191 mass chromatogram peak areas of $C_{31}17\alpha(H)$-homohopane (22*S* and 22*R*).

Table 8.10. Hopane biomarker ratios calculated for aerobic microbial enrichment cultures initiated from Pearl Harbor sediments after 30 days of biodegradation.

Aerobic Enrichment	$C_{30}H/18\alpha$ oleanane[a]	$Ts/(Ts+Tm)$[b]	$C_{31}S/(C_{31}R + C_{31}S)$[c]
Uninoculated Control	4.95±0.16	0.36±0.02	0.52±0.03
00-001	5.14±0.03	0.27±0.04	0.57±0.01
00-002	5.09±0.05	0.39±0.05	0.57±0.01
00-003	5.08±0.05	0.31±0.01	0.56±0.01
00-032	5.11±0.04	0.26±0.07	0.58±0.01
00-033	4.55±0.43	0.37±0.45	0.52±0.02
00-030	5.06±0.06	0.37±0.03	0.55±0.02
00-031	5.07±0.09	0.41±0.05	0.56±0.01
01-041	5.09±0.03	0.39±0.11	0.58±0.01

All values are the averages of triplicate samples with the standard errors of those values. The uninoculated control was maintained under the same conditions as aerobic enrichments for 30 days without microbial inoculum.
[a]$C_{30}H$ represents $C_{30}17\alpha(H),21\beta(H)$-hopane.

Table 8.11. USS *Arizona* aerobic enrichment ratios of total PAHs to biomarkers.

15.32$\pm$4.30 and the same ratio for USS *Arizona* aerobic enrichment cultures ranged from 1.66$\pm$0.14 for enrichment 00-002 to 15.32$\pm$12.89 for enrichment 00-001.

DGGE ANALYSIS OF AEROBIC ENRICHMENT CULTURE MICROBIAL COMMUNITIES.

DGGE analysis was performed to determine differences in the microbial community structure of the aerobic enrichment cultures. For each aerobic enrichment culture initiated, triplicate Erlenmeyer flasks were inoculated with sediments from the different locations. Therefore, each of the triplicates (designated A, B, and C) is an independent (separate) culture. Following 30 days of incubation, the microbial community DNA was extracted from each of the triplicates for each enrichment culture, and then amplified using a 323 bp region of the V9 region of the 16s rDNA. This is a region conserved in the domain *Bacteria*. Following DNA amplification, DNA was run on DGGE. DGGE separates DNA based on the sequence, therefore, each band has the potential to represent a single micoorganism. All DNA extracts were run on the same DGGE gel for band comparison. DGGE revealed multiple banding patterns with an average of 10 bands per enrichment lane (Figure 8.36). There was variability between banding patterns of enrichment culture triplicates and since each of the triplicates was incubated in a separate flask, some variability might be expected. Enrichments 00-001, 00-030, and 00-033, each had 1 of the 3 triplicate cultures that exhibited less degradation of oil, and these enrichments had fewer DGGE bands. For example, triplicate A in enrichment culture 00-001 contained 8 bands and less degradation of oil was observed than triplicates B and C (Figure 8.36). Triplicates B and C had 10 and 11 bands, respectively (Figure 8.36).

BIOMARKER ANALYSIS OF AEROBICALLY DEGRADED BUNKER C CRUDE OIL.

Analysis of oil from USS *Arizona* aerobic enrichments by GC-MS was used to determine if aerobic microbial degradation was influencing crude oil biomarker profiles, and to determine if biomarker profiles from aerobic enrichments were similar to biomarker profiles in sediments and oil leaking from the ship. Mass chromatograms for hopanes (m/z=191) and steranes (m/z 217) were examined. Chromatograms for (m/z=191) hopanes showed few changes in the key
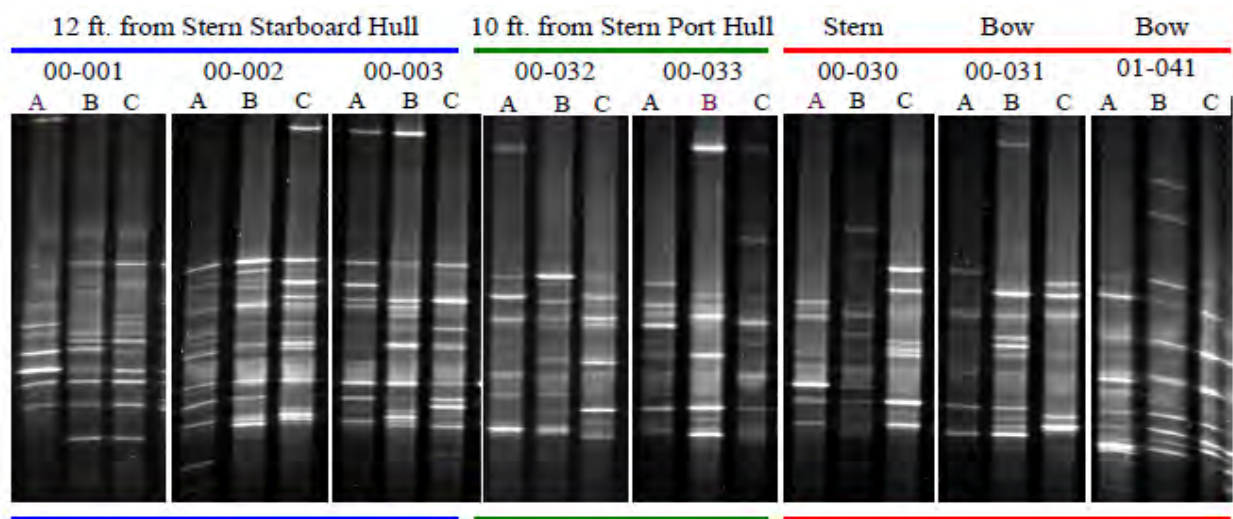
Figure 8.36. DGGE analysis of USS *Arizona* aerobic enrichment cultures. Triplicate cultures are designated by A, B and C. The blue bar denotes enrichment cultures that were inoculated with sediments collected from the stern section, starboard side, 12 ft. from the hull. The green bar denotes enrichment cultures that were inoculated with sediments collected from the stern section, port side, 10 ft. from the hull. The red bar denotes enrichment cultures that were inoculated with sediments collected from the top of the ship, and title above indicates the section they were collected from (bow or stern). The purple letters denotes enrichments that not did show degradation (00-001 A, 00-033 B and 00-030 A).

biomarkers (i.e., $C_{30}17\alpha(H),21\beta(H)$-hopane) compared to the uninoculated control (Figure 8.37). However, there was a decrease in the C_{28} - $C_{29}13\beta,21\alpha(H)$-tricyclic terpane 22R and 22S epimers in oil extracted from aerobic enrichment cultures in comparison to the uninoculated control (Figure 8.37).

Mass chromatograms for (m/z=217) sterane trace showed a decrease in C_{27} steranes in oil extracted from aerobic enrichment cultures in comparison to the uninoculated control (Figure 8.38). There was no decrease in C_{28} steranes and C_{29} steranes in aerobic enrichment cultures (Figure 8.38).

Biomarker ratios were calculated from mass chromatograms m/z=191 as detailed in section 2 to examine whether changes were occurring to biomarker profiles. Briefly, mass chromatogram peak areas of $C_{30}17\alpha(H),21\beta(H)$-hopane and 18α-oleanane were calculated for the hopane to oleanane ratio (Table 8.10). Peak areas of $C_{27}17\alpha(H)$-22,29,30-trisnorhopane (Tm) and $C_{27}18\alpha(H)$-22,29,30-trisnorneohopane (Ts), were calculated for the Ts/(Ts + Tm) ratio.
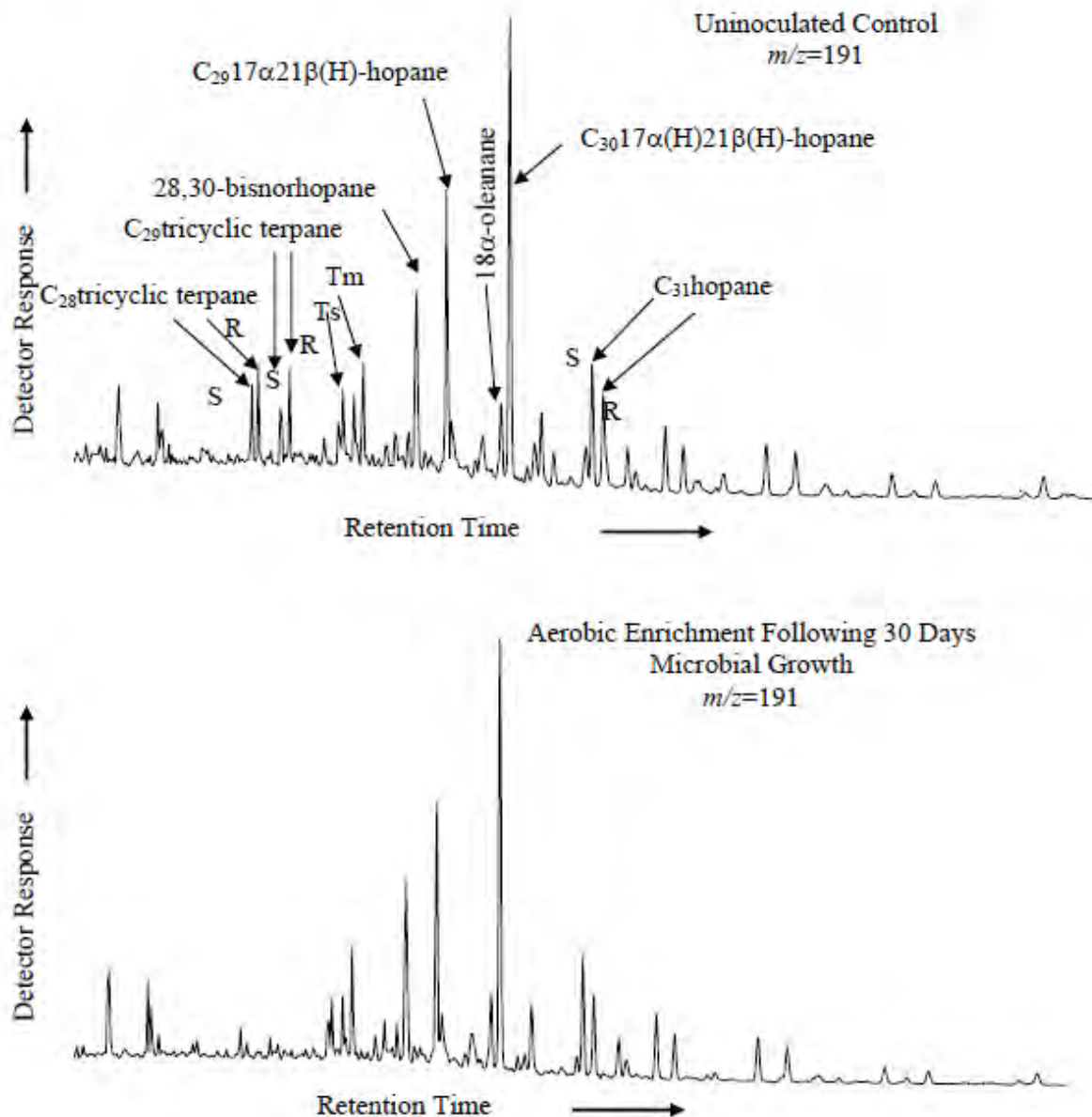
Figure 8.37. GC-MS chromatograms (*m/z*=191) of hopanes extracted from USS *Arizona* aerobic enrichments and uninoculated controls following 30 days of microbial incubation. Chromatograms are representative of triplicate samples.
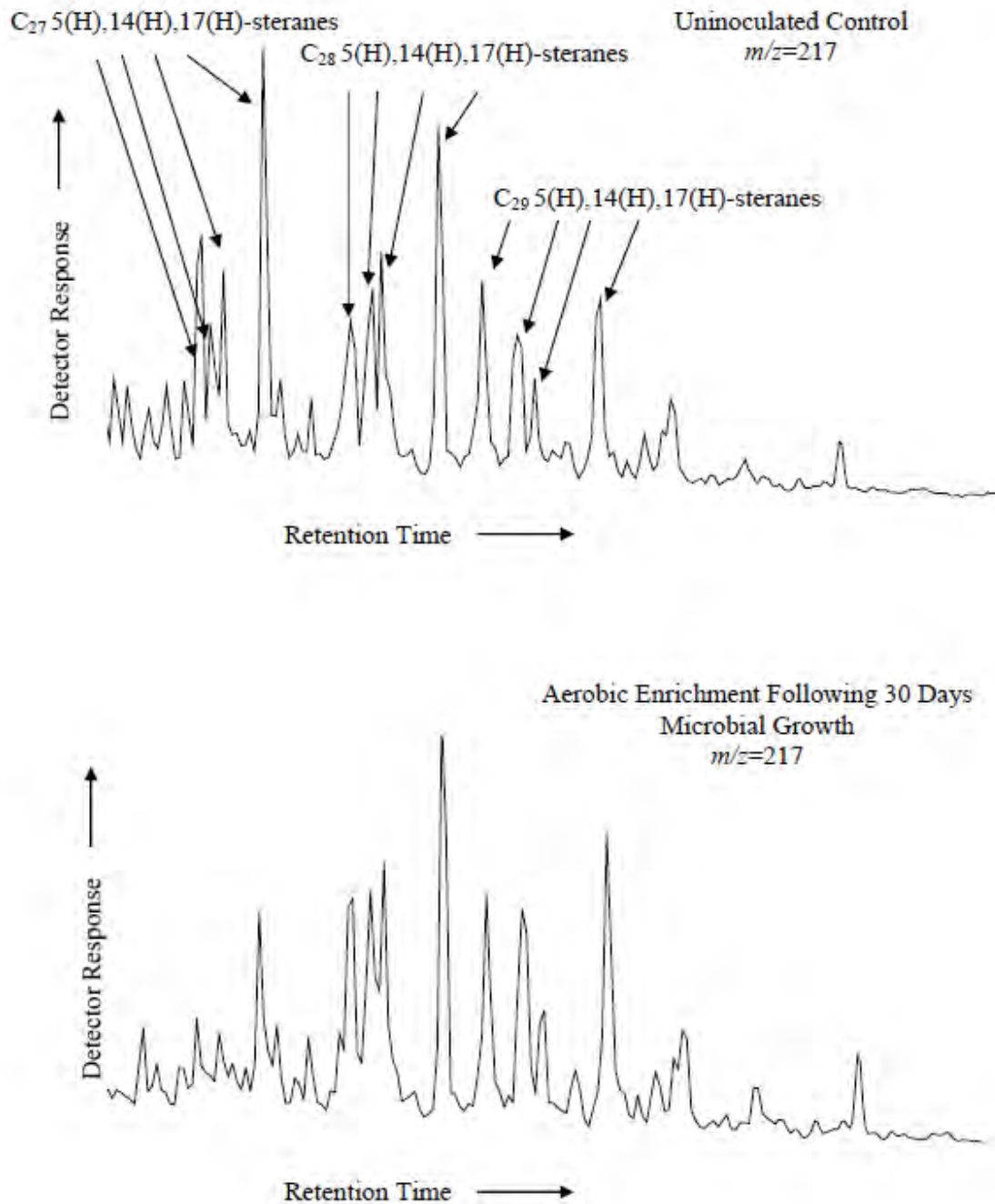
Figure 8.38. GC-MS chromatograms (*m/z*=217) of steranes extracted from USS *Arizona* aerobic enrichments and uninoculated controls following 30 days of microbial incubation. Chromatograms are representative of triplicate samples.

Aerobic Enrichment	$C_{27}S/C_{30}H^a$	$C_{28}S/C_{30}H^b$	$C_{29}S/C_{30}H^c$
Uninoculated Control	1.46±0.67	1.17±0.41	0.97±0.39
00-001	1.06±0.60	1.42±0.15	1.51±0.07
00-002	0.51±0.01	1.35±0.04	1.48±0.04
00-003	0.55±0.03	1.45±0.07	1.45±0.01
00-032	0.52±0.01	1.35±0.03	1.49±0.03
00-033	1.34±0.57	1.75±0.19	1.44±0.05
00-030	1.05±0.59	1.32±0.13	1.49±0.06
00-031	0.83±0.32	1.44±0.13	1.47±0.06
01-041	0.52±0.06	1.61±0.07	2.63±1.01

All values are the means and standard error of triplicate samples. The uninoculated control was maintained under the same conditions as aerobic enrichments for 30 days without microbial inoculum.
[a]Calculated from m/z=217 mass chromatogram peak areas of $C_{27}5\alpha(H),14\alpha(H),17\alpha(H)$-sterane (20$S$ and 20R), $C_{27}5\alpha(H),14\beta(H),17\beta(H)$-sterane (20$S$ and 20R) and $C_{30}7\alpha(H),21\beta(H)$-hopane.
[b]Calculated from m/z=217 mass chromatogram peak areas of $C_{28}5\alpha(H),14\alpha(H),17\alpha(H)$-sterane (20S and 20R), $C_{28}5\alpha(H),14\beta(H),17\beta(H)$-sterane (20$S$ and 20R) and $C_{30}17\alpha(H),21\beta(H)$-hopane.
[c]Calculated from m/z=217 mass chromatogram peak areas of $C_{29}5\alpha(H),14\alpha(H),17\alpha(H)$-sterane (20$S$ and 20R) $C_{29}5\alpha(H),14\beta(H),17\beta(H)$-sterane and $C_{30}7\alpha(H),21\beta(H)$-hopane.

Table 8.12. Sterane biomarker ratios calculated for aerobic microbial enrichment cultures initiated from Pearl Harbor sediments after 30 days of biodegradation.

Mass chromatogram peak areas of $C_{31}17\alpha(H)$-homohopane (22S and 22R) were calculated for the $C_{31}22S/(22S + 22R)$ ratio. Overall, these ratios did not change in USS *Arizona* aerobic enrichment cultures in comparison to the uninoculated control (Table 8.10).

Tricyclic terpane ratios were calculated from mass chromatograms (m/z=191) peak areas of C_{28} - $C_{29}13\beta,21\alpha(H)$-tricyclic terpane (22$R$ and 22S) to compare with the peak area of $C_{30}17\alpha,21\beta(H)$-hopane. These ratios were calculated to determine if the C_{28} and C_{29} tricyclic terpanes were being degraded in comparison to $C_{30}17\alpha,21\beta(H)$-hopane. For the uninoculated control, the ratio for C_{28} and $C_{29}13\beta,21\alpha(H)$-tricyclic terpane 22$R$ and 22S to $C_{30}17\alpha,21\beta(H)$-hopane was 0.20±0.08 and 0.19±0.08, respectively. For the enrichment cultures, this ratio could not be calculated because the tricyclic terpanes were below the detection limit.

Biomarker ratios were also calculated from mass chromatograms m/z=217 (Table 8.10). Details for calculation are in section 2. Briefly, mass chromatogram peak areas of $C_{27}5\alpha(H),14\alpha(H),17\alpha(H)$-sterane (20$S$ and 20R), $C_{27}5\alpha(H),14\beta(H),17\beta(H)$-sterane (20$S$ and 20R) and $C_{30}17\alpha(H),21\beta(H)$-hopane were calculated for the $C_{27}S/C_{30}H$ ratio. Mass chromatogram peak areas $C_{28}5\alpha(H),14\alpha(H),17\alpha(H)$-sterane (20$S$ and 20R), $C_{28}5\alpha(H),14\beta$

(H),17β (H)-sterane (20*S* and 20*R*) and C_{30}17α(H),21β(H)-hopane were calculated for the C_{28}S/C_{30}H ratio. Mass chromatogram peak areas of C_{29}5α(H),14α(H),17α(H)-sterane (20S and 20R), C_{29}5α(H),14β(H),17β (H)-sterane (20*S* and 20*R*) and C_{30}17α(H),21β(H)-hopane were calculated for the C_{29}S/C_{30}H ratio (Table 8.10)

Ratios for C_{27} steranes were lower in USS *Arizona* aerobic enrichment cultures in comparison to the uninoculated control. For example, the uninoculated control ratio for C_{27}S/C_{30}H was 1.46±0.67 (Table 8.10). In comparison, the C_{27}S/C_{30}H ratio ranged from 0.51±0.01 for enrichment 00-002 to 1.34±0.57 for enrichment 00-033 (Table 8.12). Enrichments 00-001, 00-030, and 00-033, had 1 of the 3 triplicate cultures with less degradation of oil, and these enrichments high higher C_{27}S/C_{30}H ratios in comparison to the uninoculated control and had larger standard errors than other enrichments. For example, enrichment 00-033 had triplicates with C_{27}S/C_{30}H ratios of 1.29, 2.36, and 0.39.

DISCUSSION

The National Park Service estimates that 2,200 tons of Bunker C fuel oil remain aboard USS *Arizona*, and it has been estimated that 1-2 L of the oil leaks each day from the ship to the surface seawater (Johnson et al., 2002; Murphy and Russell, personal communication). Oil leaking from the ship and in surrounding Pearl Harbor sediments has never been fully characterized. The objectives of this study were to obtain fundamental information on the oil leaking out of the ship, to compare oil from the ship to oil in surrounding sediments, and to determine the biodegradability of the oil leaking from the ship by microorganisms enriched from Pearl Harbor sediments. In addition, characterization of the biomarker profiles in these studies provided a foundation for additional comparisons. A better understanding of the abiotic and biotic weathering processes influencing the oil may contribute to USS *Arizona* management and conservation decisions in the future.

OIL LEAKING OUT OF USS *ARIZONA*

First, chemical characterization of the oil was conducted to determine the extent of abiotic and biotic weathering processes. Previous studies have shown that *n*-alkanes are the first

oil component to be lost by both biotic weathering processes (i.e., biodegradation) and abiotic weathering processes (i.e., evaporation) following an environmental spill (Wang et al., 1994; Whittaker and Pollard, 1997; Wang et al., 1998a; Prince, et al., 2002; NRC, 2003). Following loss of *n*-alkanes, a decrease in the branched alkanes (pristane and phytane) is generally observed (Blumer and Sass, 1972; Wang et al., 1994; Whittaker and Pollard, 1997; Wang, et al., 1998a; NRC, 2003). Characterization of oil leaking from USS *Arizona* by chromatography indicated *n*-alkanes were still present in oil leaking from the hatches near barbette no. 4 (location A). In comparison, oil leaking from the stern starboard portholes (location B) had a decrease in *n*-alkanes, suggesting that oil leaking from location B is more weathered than oil leaking from location A.

Further GC-MS characterization of the oil leaking from the ship was conducted to quantitatively characterize the PAHs present. High molecular weight PAHs (i.e., chrysene and pyrene) tend to be more resistant to microbial degradation in comparison to lower molecular weight PAHs (i.e., naphthalenes and flourenes) (Cerniglia, 1992; Dean-Ross et al., 2002; Wang et. al, 1998; NRC, 2003). Lower molecular weight PAHs are more readily degraded by microorganisms and are more susceptible to abiotic weathering processes such as dissolution and evaporation than high molecular weight PAHs (Wang et al., 1994; Wang et. al, 1998a; Michel and Hayes, 1999; NRC, 2003). PAHs were detected in all samples of oil leaking from USS *Arizona*. For example, sample 01-015 (from location A) contained low molecular weight naphthalenes and flourenes along with similar amounts of high molecular weight PAHs. The presence of higher concentrations of naphthalenes in sample 01-015 in comparison to lower concentrations of naphthalenes in sample 01-029 suggests sample 01-015 is less weathered. Naphthalene and its alkylated homologues are often the first PAHs to be lost by weathering following release of oil into the environment (Wang et al., 1994).

The similarity between the high molecular weight PAH histograms for all three samples of oil leaking from the ship suggests either no weathering of high molecular weight PAHs or the same extent of weathering for all three samples. Since there is no original sample of oil from USS *Arizona* available, we cannot definitively say that no weathering of the high molecular weight PAHs has occurred. Also, we cannot compare our PAH data directly to another Bunker C fuel oil sample because the oil is a complex mixture that may undergo post-distillation processes, including the addition of additives, therefore modifying its composition (Irwin et al.,

1997). Since some low molecular weigh PAHs are still present in all three samples and high molecular weight PAHs are weathered more slowly than low molecular weight PAHs, it is probable that little or no weathering of high molecular weight PAHs has occurred.

The ratios for total PAHs to conserved biomarkers indicated that oil leaking from location B had fewer total PAHs than oil leaking from location A, although these results are not definitive. Sample 00-15 from location A had a ratio value closer to sample 01-029 that may suggest that 00-015 is more weathered than 00-034 oil leaking from location A. PAH data for oil leaking from the ship does not support this observation. A more probable explanation for large ratio differences between sample 00-015 and 00-034 can be attributed to the large variation between replicates that resulted in a larger standard error in 00-034. By disregarding this triplicate, the ratio for total PAHs to $C_{30}17\alpha,21\beta(H)$ hopane for sample 00-034 became 118.97 ± 2.73 (compared to 97.70 ± 21.27 when all three triplicates are considered) which indicates more PAHs are present in 00-034 than 01-015.

The PAH results for oil leaking from USS *Arizona* in comparison to the GC-FID results suggests oil leaking from the ship differs primarily in *n*-alkanes. GC-FID results showed differences in *n*-alkanes from different locations, but branched alkanes pristane and phytane were present in samples from all locations. Furthermore, data for PAH analysis indicated that except for naphthalene, PAH concentrations were similar. Overall, this indicates that *n*-alkanes and naphthalenes are the only compounds decreasing in oil from location B in comparison to location A. This is consistent with oil weathering patterns, since *n*-alkanes and low molecular weight PAHs are the first to decrease after an environmental release of oil (Blumer and Sass, 1972; Wang et al., 1994; Wang et. al, 1998a; Michel and Hayes, 1999; NRC, 2003).

Overall, oil leaking from location A was less weathered than oil leaking from location B, indicating that perhaps oil leaking from location B has been exposed to an environment more favorable for weathering before it leaves the ship than oil leaking from location A. Another possibility is that conditions are more conducive to degradation in the reservoir (original ship location of oil that is leaking from location B). The ship has a total of four decks, with oil bunkers on the bottom of the ship and the sides of decks four (the lowest deck) and three (above deck four) (Lenihan, 1990; Murphy and Russell, personal communication). Oil leaking from location A may take a more direct path out of the ship to the surface or pool on the third deck of the ship (Murphy and Russell, personal communication). The third deck of the ship may have

less seawater exchange and dissolved oxygen, therefore the environment may be less conducive for oil weathering processes, especially microbial degradation (Murphy and Russell, personal communication). In comparison, it is possible that oil leaking from location B is taking more time to travel from the original bunker to the surface of the ship, allowing more time for chemical changes in the oil before leaking to the surface. Furthermore, oil leaking from location B could be leaking from the bunker to the second deck, which has seawater exchange, introducing nutrients and dissolved oxygen required for microbial degradation processes.

Components of oil that are resistant to abiotic and biotic forms of weathering, known as biomarkers, are useful internal indicators of degradation. Biomarkers can also be used as a fingerprint to identify oil (Peters and Moldowan, 1993). In this study, hopanes and steranes were analyzed in three samples of oil leaking from USS *Arizona*. Analysis of 01-015, 00-034, and 01-029 indicated that there were no statistical differences in biomarker profiles in oil leaking from different locations of the ship (ANOVA, $p=0.054$). The similarity between biomarker profiles and calculated biomarker ratios also suggested that biomarkers were not degraded in the samples of oil leaking from the ship. Furthermore, ratios for selected biomarkers were similar, suggesting that oil leaking from USS *Arizona* is from the same (or very similar) source.

OIL EXTRACTED FROM USS *ARIZONA* SEDIMENTS.

Crude oil can persist in sediments and is often identified years after its initial deposition (Wang et al., 1994; Vandermeulen and Singh, 1994; Wang et al., 1998b). To obtain information about the presence of petroleum hydrocarbons in sediments on or adjacent to USS *Arizona*, hydrocarbons were extracted by a continuous soxhlet extraction technique. In general, the amount of solvent extractable material per gram of sediment was low (1.79 mg extractable material/ g dry sediment) in comparison to other hydrocarbon-contaminated sediments studies in our laboratory (ranged from 1.91 – 84.08 mg extractable material/ g dry sediment) (Frontera-Suau et al., 2002).

Gas chromatographic traces of USS *Arizona* sediment solvent-extractable materials showed a common peak in all sediment extracts. This peak was identified using GC-MS as BHT, an antioxidant that is present in some foods, cosmetics, plastics, and rubber products (Fries and Puttman, 2002). Studies have detected BHT in rainwater, ground water, and sediments

across the world (Jungclaus et. al, 1978; Fries and Puttman, 2002), although degradation studies have shown that BHT is quickly broken down in the environment (Mikami et al., 1979; Inui et al., 1979). The source of BHT in Pearl Harbor sediments is unknown, and it is possible that some of the BHT observed in our samples was due to the thimble or boiling chips during the soxhlet extraction process. However, we did detect BHT in samples of the oil leaking from the ship. The concentration observed in extracts of sediments samples was high (as observed by relative detector response) suggesting that BHT was (or had been) deposited in USS *Arizona* sediments. Fries and Puttman (2002) attributed the concentrations of BHT observed in water and sediment samples, despite the ability of microorganisms to easily degrade BHT, to the fact that BHT is used in large quantities in many countries (i.e., USA, Germany, England).

In USS *Arizona* sediments, high molecular weight *n*-alkanes, ranging from approximately $C_{20} – C_{32}$, were observed on gas chromatographic traces. Shorter chain length *n*-alkanes, as well as pristane and phytane, were not readily observed. GC-MS analysis demonstrated that low molecular weight PAHs were below the detection limit in USS *Arizona* sediments, but high molecular weight PAHs were present. The low concentration of low molecular PAHs could be due to weathering, since these compounds are generally lost to biotic and abiotic weathering processes prior to high molecular weight PAHs.

The detection of hopane and sterane biomarkers in sediment solvent-extractable materials further suggests oil is present in the sediment samples collected from USS *Arizona.* Biomarker compounds from the *m/z*=191 trace were identified that are not ubiquitous in all oils. The biomarkers 28, 30 bisnorhopane (often referred to as C_{28}hopane) and 18α(H)-oleanane are not found in all oils, and together are characteristic of oil from Miocene Monterey Formation source rock in California (Peters and Moldowan, 1993; Kvenvolden et al., 1993; Kvenvolden et al., 2002). Both 28, 30 bisnorhopane and 18α(H)-oleanane were detected in oil leaking from the ship and in sediment solvent-extractable materials. This suggests that oil leaking from the ship may be depositing into surrounding sediments, although it is possible that an oil other than USS *Arizona* is contributing to the 28, 30 bisnorhopane and 18α(H)-oleanane biomarker profiles.

Since biomarker profiles and calculated biomarker ratios are often diagnostic for different oils, a comparison of key biomarker ratios between the oil leaking from the ship and the sediments can be made. The $C_{30}H/18α$ oleanane ratio ranged from 5.93$\pm$0.25 to 6.25$\pm$0.15 for samples of oil leaking from the ship, compared to 2.19$\pm$0.68 to 9.21$\pm$5.30 for the sediment

samples. In general, this ratio was lower for sediment samples, suggesting that either hopane was being degraded relative to oleanane, or that other hydrocarbon inputs were influencing the ratio.

USS *ARIZONA* AEROBIC ENRICHMENT CULTURES.

It is well documented that microorganisms can degrade petroleum (Haines and Alexander, 1974; Mulkins-Phillips and Stewart, 1974; Atlas, 1981; Atlas, 1984). In addition, studies have shown that Bunker C fuel oil is degradable, although less degradable than other lighter crude oils (i.e., Louisiana crude oil) (Walker, et al., 1976). The pattern of microbial degradation of different components of crude oil follows a predictable pattern. Degradation of the saturate fraction occurs first, with degradation of *n*-alkanes then branched alkanes. Concurrently and following saturate degradation, PAHs are degraded, depending on ring size and alkylation.   PAH degradation proceeds from non-alkylated to increasing alkylation ($C_0 > C_1 > C_2 > C_3 > C_4 >$) (Fedorak and Westlake, 1984; Wang et al., 1998a). Low molecular weight PAHs are degraded before high molecular weight PAHs (>3-rings) (Cerniglia, 1992; Dean-Ross et al., 2002; Wang et. al, 1998a).

To determine the degradability of oil leaking from the ship, aerobic enrichment cultures were initiated from sediments collected from different locations as the microbial inoculum source. Oil leaking from the ship was used as the sole carbon source for aerobic enrichment cultures. Following a 30-day growth period, oil was extracted from enrichments and gravimetric measurement showed an average oil loss of $31.03 \pm 4.58\%$. This was greater than the losses observed in uninoculated controls ($6.13 \pm 0.65\%$), suggesting that degradation of USS *Arizona* Bunker C crude oil was occurring. Gas chromatographic traces of the oil extracted from the aerobic enrichment cultures showed depletion of the *n*-alkanes and branched alkanes (pristane, phytane). Further analysis by GC-MS demonstrated degradation of low molecular weight PAHs (i.e., naphthalenes and fluorenes) and some high molecular weight PAHs (i.e., pyrene) in the aerobic enrichment cultures. It is important to note that high molecular weight PAHs (i.e., chrysene and pyrene) persisted. Chrysene and pyrene, along with other high molecular weight PAHs are thought to be mutagenic and carcinogenic (Samanta et al., 2002).

Our laboratory studies, using defined conditions, show oil leaking from the ship is

degradable by microbial communities enriched from sediments collected on and near the ship. Furthermore, degradation was not dependent on microbial communities from specific sediment collection locations around the ship. These results correlate with other studies that have examined microbial degradation of Bunker C crude oil. Minas and Gunkel (1995) determined that 25.6% of Bunker C was degraded in soil microcosms grown at 18°C. Wang and colleagues (1998a) observed a 23% loss of Bunker C in freshwater enrichments inoculated with 8 well-characterized petroleum-degrading bacteria. In the latter study, pristane and phytane were still present in oil extracted from enrichments. Comparatively, our study did show degradation of pristane and phytane.

The microbial community analysis of USS *Arizona* aerobic enrichment cultures was performed by DGGE. DGGE provide a fingerprint of the microbial community based on the specific amplification of a 323 bp fragment of the 16S rRNA of microorganisms contained in the domain *Bacteria* (Ferris et. al, 1996). DNA extracts from aerobic enrichments (in triplicate) were run on the same gel to allow comparisons between different enrichments. DGGE profiles of the aerobic enrichment cultures suggested some banding pattern differences between different enrichment cultures and for some triplicates of the same enrichment cultures. Differences in banding patterns may be due to different microorganisms present in the original sediment inoculum (since the sediments were from different locations), and by flask-to-flask variability between triplicate enrichment cultures. There were some similar bands observed between sediment inoculum location, but overall there was not a consistent pattern or microbial community fingerprint based on location. Future studies, collaborative with corrosion biologists, will focus on the characterization of the facultative bacteria in these enrichment cultures, and their ability to accelerate biocorrosion of the ship during hydrocarbon degradation.

Biomarkers are compounds that are more resistant to microbial degradation than other components of oil, and can be used as an internal reference to monitor weathering in oil (Peters and Moldowan, 1993; Prince et al., 1994; Whittaker and Pollard, 1997). Although these compounds are considered resistant to degradation, both laboratory (Bost et al., 2001; Frontera-Suau et. al, 2002) and field studies (Moldowan, et al., 1995; Munoz et al., 1997; Wang et al., 2001a) have demonstrated biomarker degradation.

Oil extracted from USS *Arizona* aerobic enrichment cultures was analyzed by GC-MS to monitor *m/z*=191 (hopanes/terpanes) and *m/z*=217 (steranes) biomarkers to determine if there

were any differences in the biomarker profile following 30 days of microbial growth. Results

showed a depletion of C_{28}-C_{29}13β,21α(H)-tricyclic terpanes (22*R* and 22*S*) and a decrease in the

C_{27} steranes. These results are of interest because previous biomarker degradation studies in our

laboratory have shown C_{30}17α(H),21β (H)-hopane degradation but no tricyclic terpane or sterane

degradation (Bost et al., 2001; Frontera-Suau et. al, 2002). Furthermore, tricyclic terpanes are

thought to be degraded following C_{30}17α(H),21β (H)-hopane degradation, which we did not

observe (Reed, 1977; Siefert and Moldowan, 1979; Peters and Moldowan, 1993). In the

laboratory, Chosson et al. (1991) demonstrated degradation of the C_{27} steranes preferentially

over the C_{28} and C_{29} steranes by seven Gram-positive bacterial strains; no Gram-negative

bacterial strains were found capable of degrading these compounds.

A field study by Wang and colleagues (2001a) observed alteration of biomarkers 24 years

following a spill of Arabian crude and Bunker C fuel oil in Banco Satelite, Chile in 1974. In the

study, biomarkers from samples collected in 2000 were compared to fresh Arabian crude. The

study showed biomarker alteration of oil still present in sediments proceeded by weathering of

diasteranes>C_{27} steranes>tricyclic terpanes>hopanes>norhopanes and C_{29}-αββ-steranes. This

procession of biomarker alteration is similar to the procession observed in this study. Oil leaking

from USS *Arizona* and used for the aerobic enrichment cultures did not contain diasteranes, but

we did observe C_{27} steranes and C_{28}-C_{29} tricyclic terpane degradation. However, we did not

observe hopane degradation, the next biomarker group to be degraded in the Wang (2001b)

study.

CONCLUSIONS

The objectives of this study included characterizing oil leaking from USS *Arizona*,

characterizing petroleum hydrocarbons in the sediments and determining if oil leaking from the

ship was degradable by microorganisms enriched from surrounding sediments. Oil characterized

from USS *Arizona* suggests that oil leaking from different ship locations are exposed to different

environments, based on the extent of *n*-alkane weathering for oil leaking from the stern starboard

hatches compared to oil leaking near barbette no. 4. Biomarkers in oil leaking from the ship

were also identified in sediments collected near and on top of the ship. Biomarkers 28, 30

bisnorhopane and 18α(H)-oleanane were of special interest because they are not found in all oils

and were detected in oil leaking from the ship and in surrounding sediments. It is probable that oil leaking from the ship is present in surrounding sediments, but it is also possible that hydrocarbons, including biomarkers, from other sources are present in the sediments as well. Aerobic enrichment cultures initiated from USS *Arizona* sediments were capable of degrading different components (i.e., *n*-alkanes, branched alkanes, and PAHs) of Bunker C leaking from the ship. Certain high molecular weight PAHs (i.e. perylene) remained in oil extracted from enrichment cultures and did not decrease in concentration. These enrichments were capable of degrading the biomarkers C_{28}-C_{29} tricyclic terpanes and C_{27} steranes. C_{28}-C_{29} tricyclic terpanes and C_{27} steranes were also present in sediments, although in varying concentrations. This is interesting because C_{28}-C_{29} tricyclic terpanes and C_{27} steranes were degraded by USS *Arizona* enrichment cultures in the laboratory. C_{28}-C_{29} tricyclic terpanes and C_{27} steranes

In summary, these studies have contributed to our fundamental understanding of the oil that is leaking from USS *Arizona*, and the potential of microorganisms indigenous to Pearl Harbor sediments in degrading this oil. In addition, we have conducted the first comprehensive hydrocarbon fingerprint of Pearl Harbor sediments adjacent to and surrounding the ship. The results of these studies will be shared with the National Park Service Submerged Resources Center, and contribute to future management decisions regarding the conservation and preservation of USS *Arizona.*

REFERENCES

Aeckersberg, F., F. A. Rainey, and F. Widdel
> 1998 Growth, Natural Relationships, Cellular Fatty Acids and Metabolic Adaption of Sulfate-Reducing Bacteria that Utilize Long Chain Alkanes Under Anoxic Conditions. *Archives Microbiology* 170: 361-369.

Alberdi, M., and L. Lopes
> 2000 Biomarker 18α(H)-oleanane: Ageochemical Tool to Assess Venezuelan Petroleum Systems. *Journal of South American Earth Sciences* 13:751-759.

Anderson, R. T., and D. R. Lovely
> 2000 Hexadecane Decay by Methanogenesis. *Nature* 404:722.

Ashwood, T. L., and C. R. Olsen
> 1988 Pearl Harbor Bombing Attack: A Contamination Legacy Revealed in the Sedimentary Record. *Marine Pollution Bulletin* 19:68-71.

Atlas, R. M.
> 1981 Microbial Degradation of Petroleum Hydrocarbons: An Environmental Perspective. *Microbiological Reviews* 45:180-209.

> 1984. *Petroleum Microbiology*. 1st ed. Macmillan Publishing Company. New York.

Baars, B. J.
> 2002 The Wreckage of the Oil Tanker *Erika* Human Health Risk Assessment of Beach Cleaning, Sunbathing and Swimming. *Toxicology Letters* 128:55-68.

Barron, M. G., T. Podrabsky, S. Ogle, and R. W. Ricker
> 1999 Are Aromatic Hydrocarbons the Primary Determinant of Petroleum Toxicity to Aquatic Organisms? *Aquatic Toxicology* 46:253-268.

Beam, H. W., and J. J. Perry
> 1974 Microbial Degradation and Assimilation of n-alkyl-Substituted Cycloparaffins. *Journal of Bacteriology* 118:394-399.

Beckles, D. M., C. H. Ward, and J. B. Hughes
> 1998 Effect of Mixtures of Polycyclic Aromatic Hydrocarbons and Sediments on Flouranthene Biodegradation Patterns. *Environmental Toxicology and Chemistry* 17:1246-1251.

Bixian, M., F. Jiamo, Z. Gan, L. Zheng, M. Yushun, S. Guoying, and W. Xingmin
> 2001 Polycyclic Aromatic Hydrocarbons in Sediments from Pearl River and Estuary, China: Sapatial and Temporal Distribution and Sources. *Applied Geochemistry* 16:1429-1445.

Blumer, M. and J. Sass
>1972 Oil Pollution: Persistence and Degradation of Spilled Fuel Oil. *Science* 176:1120-1122.

Boll, M., G. Fuchs, and J. Heider
>2002 Anaerobic Oxidation of Aromatic Compounds and Hydrocarbons. *Current Opinion in Chemical Biology* 6:604-611.

Bost, F. D., R. Frontera-Suau, T. J. McDonald, K. E. Peters, and P. J. Morris
>2001 Aerobic Biodegradation of Hopanes and Norhopanes in Venezuelan Crude Oils. *Organic Geochemistry* 32:105-114.

Cerniglia, C. E.
>1992 Biodegradation of Polycyclic Aromatic Hydrocarbons. *Biodegradation* 3:351-368.

Chang, Y. J., J. R. Stephen, A. P. Richter, A. D. Venosa, J. Bruggemann, S. J Macnaughton, G. A. Kowlachuk, J. R. Haines, E. Kline, and D. C. White
>2000 Phylogenetic Analysis of Aerobic Freshwater and Marine Enrichment Cultures Efficient in Hydrocarbon Degradation: Effect of Profiling Method. *Journal of Microbial Methods* 40:19-31.

Chosson, P., C. Lanau, J. Connan, and D. Dessort
>1991 Biodegradation of Refractory Hydrogen Biomarkers from Petroleum Under Laboratory Conditions. *Nature* 351(6328):640-642.

Dean-Ross, D., J. Moody, and C. E.Cerniglia
>2002 Utilization of Mixtures of Polycyclic Aromatic Hydrocarbons by Bacteria Isolated from Contaminated Sediment. FEMS *Microbiology Ecology* 41:1-7.

Elshahed, M. S., L. M. Gieg, M. J. Mcinerney, and J. M. Suflita
>2001 Signature Metabolites Attesting to the *in situ* Attenuation of Alkylbenzenes in Anaerobic Environments. *Environmental Science and Technology* 35:682-689.

Environmental Protection Agency [EPA]
>1984 *List of the Sixteen PAHs with Highest Carcinogenic Effect*. IEA Coal Research, London.

Ferris, M. J., G. Muyzer, and D. M. Ward
>1996 Denaturing Gradient Gel Electrophoresis Profiles of 16S rRNA-Defined Populations Inhabiting a Hot Spring Microbial Mat Community. *Applied and Environmental Microbiology* 62:340-346.

Floodgate, G. D.
>1984 The Fate of Petrolum in Marine Ecosystems. In *Petroleum Microbiology* (R. M. Atlas, Ed.), pp. 61-98. McMillan Publishing Co., New York, NY.

Fries, E. and W. Puttman
    2002 Analysis of the Antioxidant Butylated Hydroxytoluene (BHT) in Water by Means
    of Solid Phase Extraction Combined with GC-MS. *Water Research* 36:2319-2327.

Frontera-Suau, R., F. D. Bost, T. J. McDonald, and P. J. Morris
    2002 Aerobic Biodegradation of Hopanes and Other Biomarkers by Crude Oil-Degrading
    Enrichment Cultures. *Environmental Science and Technology* 36:4585-4592.

Garrett, R. M., I. J. Pickering, C. E. Haith, and R. C. Prince
    1998 Photooxidation of Crude Oils. *Environmental Science and Technology* 32:3719-
    3723.

Gregory, D.
    1999 Monitoring the Effect of Sacrificial Anodes on the Large Iron Artifacts on the Duart
    Point Wreck, 1997. *International Journal of Nautical Archaeology* 28(2):164-173.

    1995 Experiments into the Deterioration Characteristics of Materials on the Duart Point
    Wreck Site: An Interim Report. *The International Journal of Nautical Archaeology*
    24:61-65.

Haines, J. R., and M. Alexander
    1974 Microbial Degradation of High Molecular Weight Alkanes. *Applied Microbiology*
    28:1084-1085.

Hir, M. L., and C. Hily
    2002 First Observations in a High Rocky-Shore Community After the *Erika* Oil Spill
    (December 1999, Brittany France). *Marine Pollution Bulletin* 44:1243-1252.

Ho, K., Patton, J. S., Latimer., R. J. Pruell, M., Pelletier, R. McKinney, and S. Jayaraman
    1999 The Chemistry and Toxicity of Sediment Affected by Oil from the *North Cape*
    Spilled into Rhode Island Sound. *Marine Pollution Bulletin* 38:314-323.

Hughes, J. B.
    1999 Cytological-Cytogentic Analyses of Winter Flounder Embryos Collected from the
    Benthos at the Barge *North Cape* Oil Spill. *Marine Pollution Bulletin* 38:30-35.

Hunt, J. M.
    1995 *Petroleum Geochemistry and Geology*. 2nd ed. W.H. Freeman and Company, New
    York.

Inui, H., K. Itoh, M. Matsuo, and J. Miyamoto
    1979 Studies on Degradation of 2,6-di-*tert*-butyl-4-methylphenol (BHT) in the
    Environment. Part-II: Biodegradability of BHT with Activated Sludge. *Chemosphere*
    6:383-91.

Irwin, R. J., M. VanMouwerik, L. Stevens, M. D. Seese, and W. Basham
    1997 National Park Service, Water Resources Division Environmental Contaminants
    Encyclopedia, Fuel Oil No. 6 Entry.

Johnson, D. L., W. N. Weins, J. D. Makinson, L. E. Murphy, L. E. Conlin, M. A. Russell, and P.
    J. Morris
    2002 In situ *Corrosion Studies on the Battleship USS* Arizona *Part I. Corrosion*.

Juhasz, A. L. and R. Naidu
    2000 Bioremediation of High Molecular Weight Polycyclic Aromatic Hydrocarbons: A
    Review of the Microbial Degradation of benzo[*a*]pyrene. *International Biodeterioration
    and Biodegradation* 45:57-88.

Jungclaus, G. A., V. Lopez-Avila and R. A. Hites
    1978 Organic Compounds in Industrial Waste Water: A Case Study of Their
    Environmental Impact. *Environmental Science and Technology* 12:88-96.

Kanaly, R. A. and S. Harayama
    2000 Biodegradation of High-Molecular-Weight Polycyclic Aromatic Hydrocarbons by
    Bacteria. *Journal of Bacteriology* 182:2059-2067.

Kvenvolden, K. A., F.D. Hostettler, J. B. Rapp, and P. R. Carlson
    1993 Hydrocarbons in Oil Residues on beaches of Islands of Prince William Sound,
    Alaska. *Marine Pollution Bulletin* 26:24-29.

Kvenvolden, K. A., F. D. Hostettler, P. R. Carlson, J. B. Rapp, C. N. Threlkeld. and A. Warden
    1995 Ubiquitous Tar Balls with a California-Source Signature on the Shorelines of Prince
    William Sound, Alaska. *Environmental Science and Technology* 29:2684-2694.

Kvenvolden, K .A., F. D. Hostettler, R. W. Rosenbauer, T. D. Lorensen, W. T. Castle and S.
    Sugarman
    2002 Hydrocarbons in Recent Sediment of the Monterey Bay National Marine Sanctuary.
    Marine Geology 181:101-113.

Lenihan, D. J.
    1990 *USS Arizona Memorial and Pearl Harbor National Historic Landmark*. 2 ed. Vol.
    No. 23. Submerged cultural resources study. Santa Fe, NM: Southwest Cultural
    Resources Center Professional Papers.

Lunel, T., A. Crosbie, L. Davies, and R. P. J. Swannell
    2000 The Potential for Dispersing Bunker C (IFO-380) Fuel Oils: Initial Results.
    Prepared by: National Environmental Technology Centre, Culham, Abingdon
    Oxfordshire, United Kingdom. 12 pp.

Mackenzie, A. S.
  1984 Applications of Biological Markers in Petroleum Geochemistry. In *Advances in Petroleum Geochemistry* (J. Brooks, and D. Weite, Eds.), Vol. 1, pp. 115-213. Academic Press, London.

McDonald, T. J. and M. C. Kennicutt
  1992 Fractionation of Crude Oils by HPLC and Quantitative Determination of Aliphatic and Aromatice Biological Markers by GC-MS with Selected Ion Monitoring. *LC-GC* 10:935-938.

McLeod, I. D.
  1995 *In Situ* Corrosion Studies on the Duart Point Wreck, 1994. *International Journal of Nautical Archaeology* 24(1):53-59.

Mills, M. A., T. J. McDonald, J. S. Bonner, M. A. Simon, and R. L. Autenrieth
  1999 Method for Quantifying the Fate of Petroleum in the Environment. *Chemosphere* 39:2563-2582.

Michael, J. and M. O. Hayes
  1999 Weathering Patterns of Oil Residues Eight Years After the *Exxon Valdez* Oil Spill. *Marine Pollution Bulletin* 38:855-863.

Mikami, N., H. Gomi, and J. Miyamoto
  1979 Studies on Degradation of 2,6-di-*tert*-butyl-4-methylphenol (BHT) in the Environment. Part-I: Degradation of ^{14}C-BHT in soil. *Chemosphere* 5:305-310.

Minas, W. and W. Gunkel
  1995 Oil Pollution in the North Sea- A Microbiological Point of View. *Helgolander Meeresunters* 49:14-158

Moldowan, J. M., J. Dahl, M. A. Mcaffrey, W. J. Smith and J. C. Fetzer
  1995 Application of Biological Marker Technology to Bioremediation of Refinery By-products. *Energy and Fuels* 9:155-162.

Mulkins-Phillips, G. J., and J. E. Stewart
  1974 Effect of Environmental Parameters on Bacterial Degradation of Bunker C Oil, Crude Oils, and Hydrocarbons. *Applied Microbiology* 28:915-922.

Munoz, D., M. Guiliano, P. Doumenq, F. Jacquot, P. Scherrer, and G. Mille
  1997 Long Term Evolution of Petroleum Biomarkers in Mangrove Soil (Guadeloupe). *Marine Pollution Bulletin* 34:868-874.

National Oceanic and Atmospheric Administration [NOAA]
  1994 NOAA/ Hazardous Materials Response and Assessment Division Fact sheet: No. 6 fuel oil (Bunker C) spills.

National Research Council [NRC]
>   2003. Oil in the sea III: Inputs, Fates, and Effects.

Neilson, A. J.
>   *1994 Organic Chemicals in the Aquatic Environment: Distribution, Persistence, and Toxicity*. CRC Press, Boca Raton, FL.

Nishigima, F. N., R. R. Weber, and M. C. Bicego
>   2001 Aliphatic and Aromatic Hydrocarbons in Sediments of Santos and Cananeia, SP, Brazil. *Marine Pollution Bulletin* 42:1064-1072.

Norman, R. S., R. Frontera-Suau, and P. J. Morris
>   2002 Variability in *Psuedomonas aeruginosa* lipopolysaccharide Expression During Crude Oil Degradation. *Applied and Environmental Microbiology* 10:5096-5103.
.
Pearl Harbor Natural Resource Trustees.
>   1999 Restoration Plan and Environmental Assessment for the May 14, 1996 Chevron Pipeline Oil Spill into Waiau Stream and Pearl Harbor, Oahu, Hawaii. Prepared by: U.S. Department of Defense, U.S. Department of the Interior, National Oceanic and Atmospheric Administration, and State of Hawaii. 122 pp.

Perry, J. J.
>   1977 Microbial Metabolism of Cyclic Hydrocarbons and Related Compounds. *CRC Critical Reviews in Microbiology* 5:387-412.

>   1984 Microbial metabolism of cyclic alkanes. *In* "Petroleum Microbiology" (R. M. Atlas, Ed.), pp. 61-98. McMillan Publishing Co., New York, NY.

Peters, K. E., and J. M. Moldowan
>   1993 *The Biomarker Guide: Interpreting Molecular Fossils in Petroleum.* Prentice-Hall Inc., Englewood Cliffs, NJ.

Pirnik, M. P.
>   1977 Microbial Oxidation of Methyl Branched Alkanes. *Critical Reviews in Microbiology* 5:413-422.

Pollard, J. T., M. Whittaker, and G. C. Risden
>   1999 The Fate of Heavy Oil Wastes in Soil Microcosms I: A Performance Assessment of Biotransformation Indices. *The Science of the Total Environment* 226:1-22.

Postgate, J. R.
>   1979 *The Sulphate-Reducing Bacteria*. Cambridge University Press, Cambridge, Great Britain.

Prince, R. C., D. L. Elmendorf, J. R. Lute, C. S. Hsu, C. E. Halth, J. D. Senius, G. J. Dechert, G. S. Douglas, and E. L. Butler
1994 17α(H),21β(H)-Hopane as a Conserved Internal Marker for Estimating the Biodegradation of Crude Oil. *Environmental Science and Technology* 28:142-145.

Prince, R. C., R. T. Stibrany, J. Hardestine, G. S. Douglas, and E. H. Owens
2002 Aqueous Vapor Extraction: A Previously Unrecognized Weathering Process Affecting Oil Spills in Vigorously Aerated Water. *Environmental Science and Technology* 36:2822-2825.

Rabus, R., H. Wilkes, A. Behrends, A. Armstroff, T. Fischer, A. J. Pierik, and F. Widdel 2001 Anaerobic Initial Reaction of *n*-alkanes in a Denitrifying Bacterium: Evidence for (1-methylpentyl) Succinate as Initial Product and for Involvement of an Organic Radical in *n*-hexane Metabolism. *Journal of Bacteriology* 183:1707-1715.

Reed, W. E.
1977 Molecular Compositions of Weathered Petroleum and Comparison with its Possible Source. *Geochimica et Cosmochimica Acta* 41:237-247.

Richmond, S. A., J. E. Lindstrom, and J. F. Braddock
2001 Effects of Chitin on Microbial Emulsification, Mineralization Potential, and Toxicity of Bunker C Fuel Oil. *Marine Pollution Bulletin* 42:773-779.

Salanitro, J. P., P. B Dorn, M. H. Huesemann, K. O. Moore, I. A. Rhodes, L. M. R. Jackson, T. E. Vipond, M. M. Western, and H. L. Wisniewski
1997 Crude Oil Hydrocarbon Bioremediation and Soil Ecotoxicity Assessment. *Environmental Science and Technology* 31:1769-1776.

Samanta, S. K., O. V. Singh, and R. K. Jain
2002 Polycyclic Aromatic Hydrocarbons: Environmental Pollution and Bioremediation. *Trends in Biotechnology* 20:243-248.

Schaeffer, T. L., S. G. Cantwell, J. L. Brown, D. S. Watt, and R. R. Fall
1979 Microbial Growth on Hydrocarbons: Terminal Branching Inhibits Biodegradation. *Applied and Environmental Microbiology* 38:742-746.

Sierfert W. K. and J. K. Moldowan
1979 The Effect of Biodegradation on Steranes and Terpanes in Crude Oil. *Geochimica et Cosmochimica Acta* 43:111-126.

So, C. M., and L. Y.Young
1999 Isolation and Characterization of a Sulfate-Reducing Bacterium that Anaerobically Degrades Alkanes. *Applied and Environmental Microbiology* 65:2969-2976.

Spormann, A. M., and F. Widdel
    2000 Metabolism of Alkylbenzenes, Alkanes, and Other Hydrocarbons in Anaerobic
    Bacteria. *Biodegradation* 11:85-105.

Stirling, L. A., R. J. Watkinson, and I. J. Higgins
    1977 Microbial Metabolism of Alicyclic Hydrocarbons: Isolation and Properties of a
    Cyclohexane Degrading Bacterium. *Journal of General Microbiology* 99:119-125.
.
Strand, J. A., V. I. Cullinan, E. A. Crecelium, T. J. Fortman, R. J. Citterman, and M. L.
    Fleischmann
    1992 Fate of Bunker C Fuel Oil in Washington Coastal Habitats Following the December
    1988 *NESTUCCA* Oil Spill. *Northwest Science* 66:1-14.

Trudgill, P. W.
    1978 Microbial Degradation of Alicyclic Hydrocarbons. *In Developments in
    Biodegradation of Hydrocarbons* (J. R. Watkinson, Ed.), pp. 47-84. Marcel Dekker, Inc.,
    New York.

U.S. Navy
    1998 Fact Sheet No. 2: Pearl Harbor Sediment Remedial Investigation/Feasibility Study.

Vandermeulen, J. H., and J. G. Singh
    1994 *Arrow* Oil Spill, 1970-90: Persistence of 20-yr Weathered Bunker C Fuel Oil.
    Canadian Journal of Fisheries Aquatic Science 51:845-855.

Volkman, J. K., D.G. Holdsworth, G. P. Neill and H. J. Bavor, Jr.
    1992 Identitfication of Natural, Anthropogenic and Petroleum Hydrocarbons in Aquatic
    Sediments. *The Science of the Total Environment* 112:203-219.

Walker, J. D., L. Petrakis, and R. R. Colwell
    1976 Comparison of the Biodegradability of Crude and Fuel Oils. *Canadian Journal of
    Microbiology* 22:598-602.

Wang, Z., M. Fingas, S. Blenkinsopp, G. Sergy, M. Landriault, L. Sigouin, J. Foght, K. Semple,
    and D. W. S. Westlake
    1998a Comparison of Oil Compositional Changes Due to Biodegradation and Physical
    Weathering in Different Oils. *Journal of Chromatography* 809:89-107.

Wang, Z., M. Fingas, S. Blenkinsopp, G. Sergy, M. Landriault, L. Sigouin, and P. Lambert.
    1998b. Study of the 25-year-old *Nipisi* Oil Spill: Persistence of Oil Residues and
    Comparisons Between Surface and Subsurface Sediments. *Environmental Science and
    Technology* 32:2222-2232.

Wang, Z., M. Fingas, E. H. Owens, L. Sigouin, and C. E. Brown
    2001 Long-Term Fate and Persistence of Spilled *Metula* Oil in a Marine Salt Marsh
    Environment: Degradation of Petroleum Biomarkers. *Journal of Chromatography*
    926:275-290.

Wang, Z., M. Fingas, and S. P. Page
    1999 Oil Spill Identification. *Journal of Chromatography A.* 843:369-411.

Wang, Z., M. Fingas, and G. Sergy
    1994 Study of 22-Year Old *Arrow* Oil Samples Using Biomarker Compounds by
    GC/MS. *Environmental Science and Technology* 28:1733-1746.

Wang, Z., M. Fingas, and G. Sergy
    1995 Chemical Characterization of Crude Oil Residues from an Arctic Beach by GC/MS
    and GC/FID. *Environmental Science and Technology* 29:2622-2631.

Wang, Z., M. Fingas, and L. Sigouin
    2001 Characterization and Identification of a "Mystery" Oil Ppill from Quebec (1999).
    Journal of Chromatography A 909:155-169.

Wheeler, A. J.
    2002 Environmental Controls on Shipwreck Preservation: the Irish Context. *Journal of
    Archaeological Science* 29:1149-1159.

Whittaker, M., and J. T. Pollard
    1997 A Performance Assessment of Source Correlation and Weathering Indices for
    Petroleum Hydrocarbons in the Environment. *Environmental Toxicology and Chemistry*
    16:1149-1158.

Widdel, F., and R. Rabus
    2001 Anaerobic Biodegradation of Saturated and Aromatic Hydrocarbons. *Current
    Opinion in Biotechnology* 12:259-276.

Witt, G.
    1995 Polycyclic Aromatic Hydrocarbons in Water and Sediment of the Baltic Sea.
    Marine Pollution Bulletin 31:237-248.

Zakaria, M. P., T. Okuda, and H. Takada
    2001 Polycyclic Aromatic Hydrocarbons (PAHs) and Hopanes in Stranded Tar-balls on
    the Coasts of Peninsular Malaysia: Applications of Biomarkers for Identifying Sources of
    Oil Pollution. *Marine Pollution Bulletin* 42:1327-1366.

CHAPTER 9

Long-Term Monitoring Program: Structure, Oil, Artifacts and Environment

Matthew A. Russell and Larry E. Murphy

INTRODUCTION

The National Park Service's (NPS) Submerged Resources Center (SRC) developed monitoring protocols and began systematically monitoring changes to USS *Arizona*'s accessible external areas in 1986 (Henderson 1989) as part of the USS *Arizona* Documentation Project conducted from 1983–1989 (Lenihan 1989). This was among the first such efforts on sunken metal hulls, along with the Western Australian Maritime Museum's investigation of SS *Xantho* which began about the same time (McCarthy 2000). The 1986 *Arizona* project established 61 photo-monitoring stations affixed to the hull to mount a camera to document the growth and change of concretion and biological communities covering *Arizona*'s external hull. In addition, 55 stations were marked with short PVC pipes attached to weights to monitor changes in sediment accumulation on horizontal surfaces across the hull. Each pipe marked a location where depth of sediment was taken for each observation period. This early monitoring effort was conducted sporadically by the USS *Arizona* dive team from 1986 until 1990. The program ceased when personnel changes reduced the dive team, and the park was no longer able to collect

the monitoring information. The earlier monitoring program has been superseded by the present program.

While the earlier studies attempted to monitor visible changes on the hull and deck, the present study, The USS *Arizona* Preservation Project, is directed at characterizing processes affecting the hull and determining their rate. This data contributes to a predictive model whose attributes and variables can be altered to reflect changing conditions and incorporation of new data as they are developed. In addition to the structural changes and oil release measurements, artifact and environmental variables are included and measured as part of the monitoring plan. Most aspects of the current monitoring project are quantitative; however, some, like comparative biological-based environmental observations, are qualitative. This chapter presents the monitoring program and its rationale.

The current long-term monitoring program was developed primarily to directly measure changes in *Arizona*'s structural integrity and quantify the rate of change to revise and provide controls for the predictive Finite Element Model (FEM, see Chapter 6). The present monitoring program takes several different forms, but each is designed to allow researchers and managers to quantify physical changes to *Arizona*'s hull fabric and project a long-term deterioration curve.

The present research and monitoring program began in 1998 when an oil catchment device was fabricated to measure oil release. Previously, only the leak points for oil were recorded. Additional monitoring techniques have been developed and applied during the USS *Arizona* Preservation Project based on the research domains and investigations conducted during the project. The NPS, through a cooperative effort between the USS *Arizona* Memorial and the SRC and their collaborators, has committed to continuing the monitoring program into the future to provide the most accurate depiction of *Arizona*'s hull status. Continuation of the program and inclusion of additional monitoring methods will provide an important cumulative data base useful to determining threshold levels of hull structural changes and to revise the predictive model and evaluate its accuracy. To be most effective and to facilitate comparative analyses, these cumulative measurements are being incorporated into a Geographical Information System (GIS). This chapter reports on the methodology and results through 2006 for primary monitoring methods used for long-term structural and environmental impact evaluation: Global Positioning System (GPS) hull movement monitoring, galley-specific crack monitoring, oil-release rate monitoring, environmental monitoring of water quality and sediment contamination attributable

to *Arizona,* general environmental observations and the GIS program developed to incorporate cumulative data.

STRUCTURAL INVESTIGATIONS AND MONITORING

Monitoring for significant structural alterations over time depends on an understanding of the hull structure and the sediments that support it. There are two primary concerns addressed by structural monitoring: collapse of the hull, which alters its nature as a National Historic Landmark (NHL), naval memorial and war grave; and increasing concern for potential catastrophic oil release of the approximately half-million gallons of Bunker C fuel oil remaining aboard in the intact aft portion of the hull. Because the vessel's superstructure was completely removed during salvage operations (see Chapter 3), only the hull will be addressed. Removal of the superstructure has the effect of appreciably reducing the weight supported by hull structural elements, which extends their predicted time to structural alteration and collapse.

In this discussion, hull structure change over time is subsumed beneath the issue of oil release. Predictive modeling of hull changes in general is addressed in depth in Chapter 6. Knowledge of *Arizona*'s hull is also useful for understanding the difficulty and implications of the often suggested "Why don't you just pump the oil out of the hull?" question often posed to park employees and others.

Characterization of *Arizona*'s hull structure began with collection, digitization, indexing and collating more than 250 original hull construction blueprints and those of the 1929–1931 refit. The next steps were to describe the hull's constituent metal and establish a corrosion rate that incorporated both the corrosion that has taken place to date and the present corrosion rate for incorporation into the FEM. Corrosion characterization and measurements are presented in Chapter 5. A necessary component to full characterization of the hull in its present condition is a model of the blast damage from the forward magazine explosion and other bomb damage to be incorporated into the FEM. Funding has been insufficient to accommodate the development of the blast impact for incorporation into the FEM to date.

Focusing on oil release potential requires an understanding of where in the vessel oil was contained. Historical records indicate that *Arizona* was nearly fueled to emergency capacity immediately before the December 7, 1941 attack—emergency capacity was approximately 6,100

tons of fuel (see Chapter 3). Assuming that 40% of the stern hull remains intact, one can derive a general estimate that there could be as much as 600,000 gallons remaining aboard, less that lost during and since the attack (Figure 9.1).

There is very limited access to interior spaces, as determined through extensive exploration of the stern with a VideoRay Remote Operated Vehicle (ROV) during fieldwork conducted as part of this project. At the time of the attack, most of the hatches were secured, particularly in the lower deck areas, which normally maintained Material Condition "X-Ray" with doors and fittings closed. Some areas, shaft alleys, engine rooms, and fire rooms, were in Condition "Zed," the highest level of security, where doors were secured and locked to maximize watertight conditions in battle; some were in Condition Y, intermediate between the two. Upon the sounding of "General Quarters" at the outset of the attack, *Arizona*'s crew began moving all areas to Condition Zed. This level was only partially achieved due to the suddenness of the attack and *Arizona*'s early demise (see Chapter 3). The historical assessment of *Arizona*'s material condition has been found to be accurate for the accessible areas, particularly the third deck, which has very limited access. Closed and secured doors and hatches contribute to the hull's integrity.
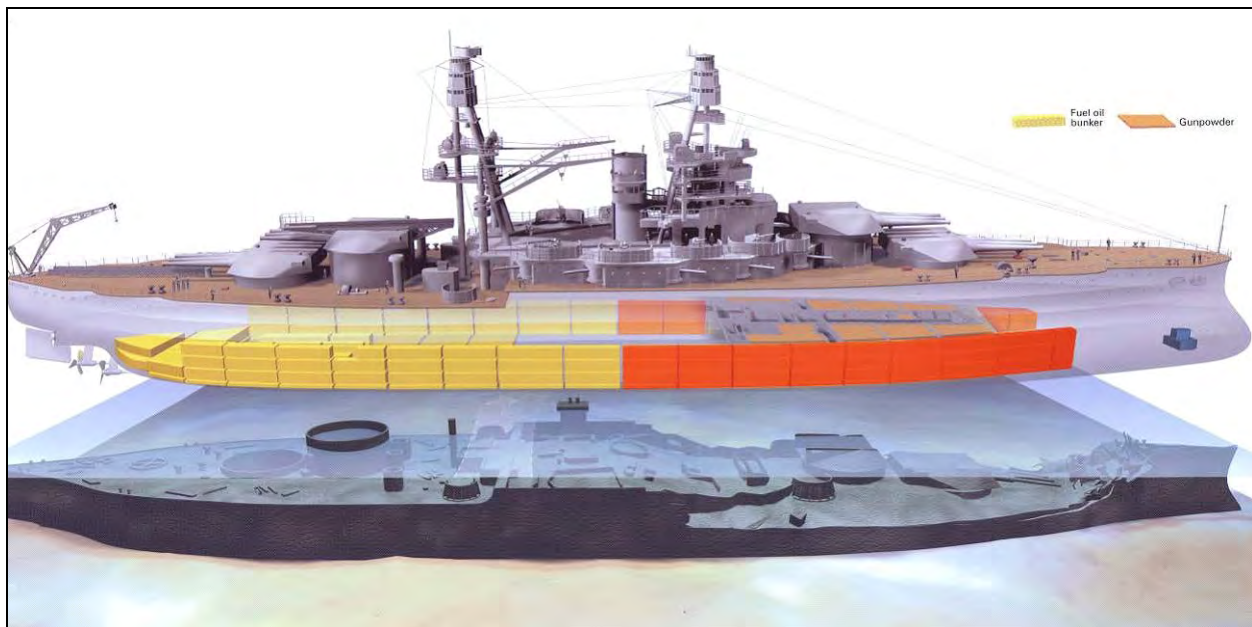
Figure 9.1. Graphic of oil bunker locations relative to hull damage. The yellow bunkers in the aft section (left) are presumed intact. This graphic depicts 50% of the hull remaining, rather than the more accurate 40% (Graphic by National Geographic Society).

Currently, only a small portion of the third deck is accessible, and a smaller yet portion of the first platform, which is the deck level above the topmost oil bunker. There is no direct access to any oil bunker in the hull. Access would have to be gained by cutting through many structural elements. At the amidships section, most of the bunkers are near the hull sides, again not directly accessible because of armor and the torpedo blister. The hull is buried to the level above its normal waterline (Figure 9.2). There is no present estimate of the amount of sediment that may be within the hull at the second platform level and below. Direct ROV observations in the second and third deck levels, which are accessible and have been explored, reveal they contain significant sediment, which decreases the deeper into the hull one goes. In undamaged areas or areas with few penetrations, there may be little sediment due to lack of access to suspended sediment transport and few open doorways. Any access to oil bunkers would require excavation, certainly on the exterior, cutting bulkheads, deck and hull structures, including splinter deck and side armor plate, which would compromise the integrity of the hull and weaken the whole structure, even with significant shoring of passages.

Another complicating factor in *Arizona* oil removal, unlike the several successful oil removals (such as USS *Mississinewa,* a World War II oiler sunk in Ulithi Harbor, Yap State, Federated States of Micronesia) is that large oil bunkers are not connected by a simple piping system. In the case of *Mississinewa*, which was not armored, the hull was inverted allowing easy
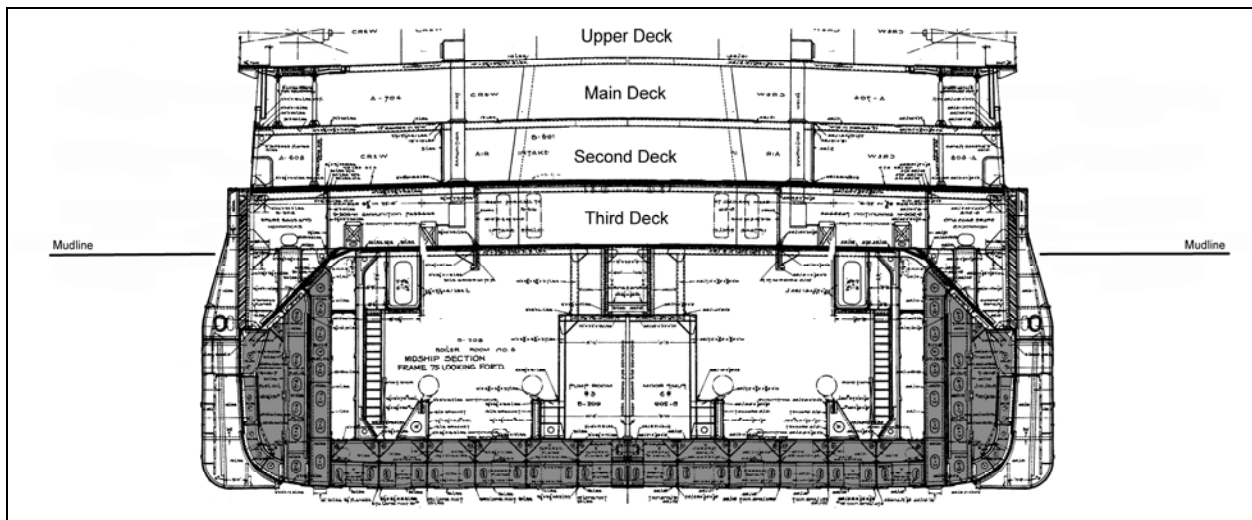
Figure 9. 2. *Arizona* **hull cross-section at frame 75. Dark areas are oil bunkers and the line indicates the current seabed level relative to the hull (Graphic by NPS-SRC).**

access to the single hull bottom greatly facilitating oil removal through a "hot tap process." In *Arizona*, bunkers are of varying size and are found throughout the ship: on the first platform, there are 30 bunkers; on the second platform, 34 bunkers; in the hold, 28 bunkers; and in the double bottom, 36 bunkers. The rationale for the large number of separate oil bunkers is that it is part of the defensive strategy of battleships. With more separated bunkers, the less likely a vessel could be put out of commission by sustaining damage to its fuel supply. Half or so of these bunkers remain and must be assumed to still contain oil. Approximately 50 to 60% of the oil bunkers in the forward hull were destroyed by the explosion that sank the ship. Each oil bunker is independently piped, suggesting that any oil removal plan could likely require accessing each bunker individually.

STRUCTURAL MONITORING

As internal and external structures of *Arizona*'s hull corrode and weaken, various parts of the vessel will differentially-experience shifting, settling and ultimately, collapse. All indications are that significant structural change is not imminent, and this is supported by the Finite Element Analysis (FEA, see Chapter 6). Since NPS presence on *Arizona* began in 1982, qualitative assessment by researchers observed that upper deck areas in and around the ship's galley (located amidships on the upper deck, just forward of the Memorial) show signs of change—widening cracks and some deck sagging and collapse were first observed by SRC researchers in 2000. This observation and the need to test and refine the FEM led to development of quantitative hull structural monitoring.

External GPS Monitoring

In order to determine whether internal collapse occurs in the hull, SRC researchers devised a monitoring protocol to quantitatively measure long-term stability across *Arizona*'s hull. The tool selected to monitor hull stability was high-resolution, survey grade, dual-frequency Global Positioning System (GPS). The SRC has been incorporating GPS and GIS into hydrographic survey since 1993, and adapted this nascent technology to underwater archeology (Murphy and Smith 1995, 1996; Shope et al. 1995). In recent years, this technology has reached

the point that extremely accurate, reliable instruments are available to the civilian survey market. Dual-frequency GPS receivers make it possible to collect positional data accurate to within a few millimeter Circle-of-Error Probable (CEP) at a 95% confidence level in three dimensions. This highly accurate GPS technology has been used to monitor movement of everything from historic buildings to mountain tops, and it is the most appropriate technology available for use on *Arizona*. At the same time, traditional "low-tech" methods for monitoring structural movement, such as simple, plastic crack monitors, were also used in specific locations.

The primary method used to monitor overall physical changes to USS *Arizona*'s hull is a network of discrete, real-world positions physically affixed to the ship whose three-dimensional coordinates are derived using very high-resolution GPS instruments. The GPS points were initially established on the vessel in June 2001. Eight datum points were selected to provide a network of monitoring points distributed longitudinally and transversly on the upper portions of *Arizona*'s hull on exposed horizontal structures (Figure 9.3). These points, when measured to high accuracy, provide information on internal hull structure changes. By plotting changes over time, both the quantity and direction (vector) of change in hull structure will be observable. Originally, the points were established by shooting hardened, pointed threaded bolts into the deck steel with a velocity tool adapted for underwater use. To limit corrosion of the stainless steel threaded bolts, a cone of pH-neutral epoxy was placed around each bolt with only the top of the bolt exposed (Figure 9.4). This technique was wholly unsuccessful; by 2003 the bolts had all but completely disappeared. In 2003, PVC pipe and fittings were used to replace the stainless steel bolts (Figures 9.5 and 9.6). The PVC was secured to the deck with epoxy at each of the eight monitoring points across *Arizona*'s exposed decks.
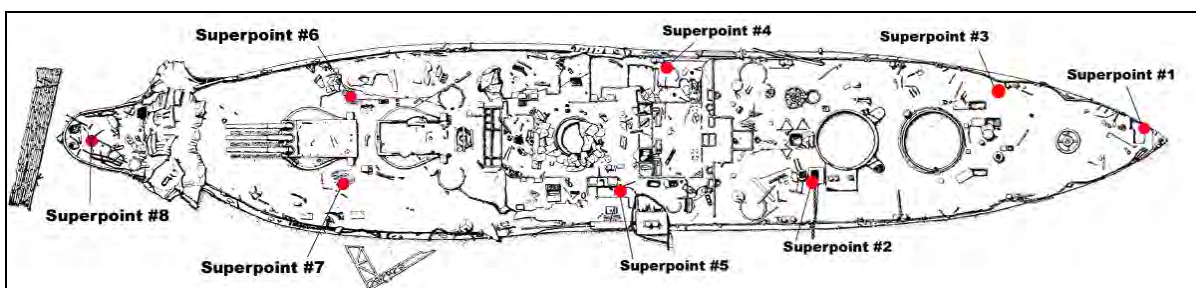
Figure 9.3. GPS monitoring points ("superpoints") on *Arizona* main and upper decks (Drawing by NPS-SRC).
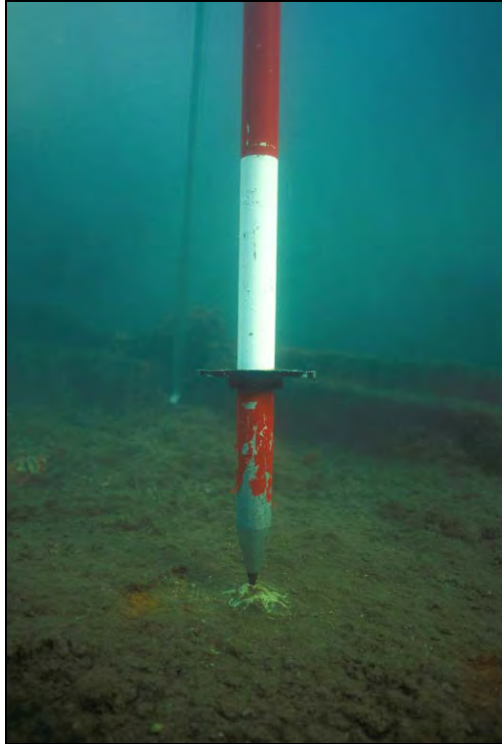
Figure 9.4. Surveying GPS monitoring points on *Arizona*, here using original velocity tool-set, stainless steel bolt surrounded by epoxy (NPS Photo by Brett Seymour).

Figure 9.5. Comparison of the original, left, and current GPS monitoring points. Note: 2001 epoxy covered by pioneering organisms (NPS Photo by Brett Seymour).

Figure 9.6. Surveying GPS monitoring points on *Arizona*, here using replacement PVC epoxyed to metal. This accommodates the point and facilitates set up. Note epoxy has been covered with pioneering organisms (NPS Photo by Brett Seymour).

Because GPS signals do not penetrate water, the GPS antenna had to be secured above the surface precisely above the survey datum point. SRC had earlier designed an underwater tripod, really a quadrapod, to accomplish this task. The tripod has three hollow aluminum legs that fill with water for stability when submerged and a fourth central leg filled with lead shot that is placed precisely on the point to be located. The underwater tripod has easily adjustable legs so that the center pole can be precisely positioned vertically above the datum point using a set of bull's eye levels attached (Figure 9.7). Divers add 5-ft. aluminum extension poles until they extend above the surface where a GPS antenna can be attached. Just as in terrestrial survey, the GPS receiver is programmed to account for the offset or Height of Instrument (HI) of the tripod and extension poles, which is exact because both the tripod's center leg and extension length have been manufactured to close tolerances and measured.

At each datum point, in-water NPS surveyors leveled the underwater tripod over the point using bull's eye levels affixed to the center pole (Figures 9.7–9.9). Once leveled, the GPS antenna is attached with a quick release to take the position reading. Using advanced survey data acquisition and post-processing techniques and software, data for each point were collected with sub-centimeter accuracy in three dimensions, or about the area of a pencil eraser. The structural monitoring points (nicknamed "superpoints") were scheduled to be re-surveyed every two years to determine if, and in what direction, the ship is moving, shifting, or settling.

Figure 9.7. Surveying GPS monitoring points on *Arizona*. Black object above diver's' mask on the survey pole is a set of bull's eye levels used to level the quadrapod (NPS Photo by Brett Seymour).
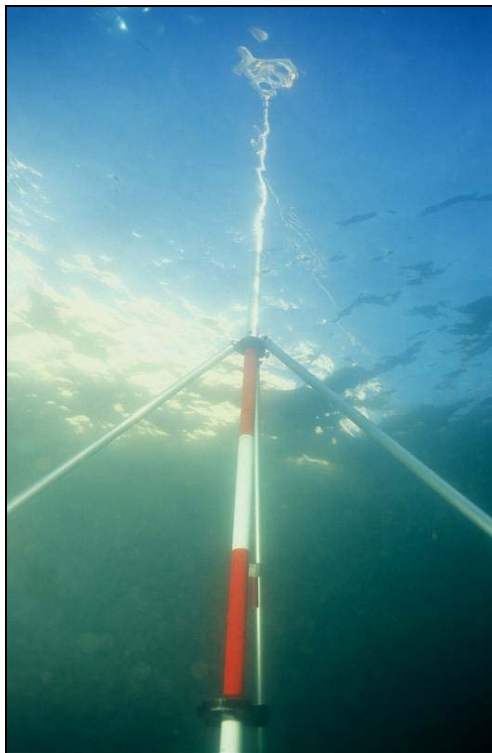
Figure 9.8. Surveying GPS monitoring points on *Arizona* using purpose-built quadrapod to support high-resolution GPS antenna above datum point (NPS Photo by Brett Seymour).

Figure 9.9. **GPS surveying "Superpoint #2," forward of barbette no. 3 (NPS Photo by Brett Seymour).**

During the 2001 field season when the initial occupation of the monitoring points took place, the NPS partnered with the U.S. Army's 29th Engineer Battalion Survey Platoon, who provided state-of-the-art, Trimble Navigation, Ltd. (Sunnyvale, CA) 4700 SSE survey grade, dual-frequency GPS receivers, and a survey team. At that time, NPS owned no survey grade GPS receivers. The occupation time of each point for the 4700 receivers is two minutes. Several points were positioned several times to verify accuracy and reproducibility. Results are presented in Table 9.1.

In the intervening two-year period, NPS acquired the necessary carrier-phase survey grade instruments to complete the survey in-house. Tim Smith, NPS GPS coordinator from the NPS Resources Inventory and Monitoring Division (RIMD) and Mark Duffy, GIS specialist from Assateague Island National Seashore, provided instruments and expertise to conduct the high-resolution underwater monitoring point reoccupation in 2003.

The 2003 reoccupation used a Trimble R8 Global Navigation Satellite System (GNSS) using 5700 Total Station Receivers. The Trimble R8 GPS system consists of a wireless base station, which is set up daily on an established survey monument near the park visitor center, and a field receiver, which mounted on the underwater tripod on site. The base station monitors its

Name	Description	Northing	Easting	Elevation (m)	Hori. Diff 2001-2003 (m)	Vert. Diff 2001-2003 (m)
USARSP001_01	June 2001 point	2362935.105	608919.734	-2.297		
USARSP001A_03	Nov. 2003 re-survey	2362935.115	608919.765	-2.254	0.032	0.043
USARSP001_03	New Nov. 2003 point	2362934.233	608918.321	-2.268		
USARSP001_06	June 2006 re-survey	2362934.259	608918.319	-2.271	0.027	0.003
USARSP002_01	June 2001 point	2362896.933	608879.359	-1.361		
USARSP002A_03	Nov. 2003 re-survey	2362896.939	608879.371	-1.385	0.014	0.024
USARSP002_03	New Nov. 2003 point	2362904.018	608897.789	-3.094		
USARSP002_06	June 2006 re-survey	2362904.02	608897.809	-3.051	0.021	-0.043
USARSP003_01	June 2001 point	2362925.038	608894.502	-2.36		
USARSP003A_03	Nov. 2003 re-survey	2362925.055	608894.522	-2.316	0.027	0.043
USARSP003_03	New Nov. 2003 point	2362926.047	608895.48	-2.208		
USARSP003_06	New June 2006 point	2362920.822	608890.76	-2.378		
USARSP004_01	June 2001 point	2362898.324	608848.58	-0.431		
USARSP004A_03	Nov. 2003 re-survey	2362898.341	608848.592	-0.433	0.021	0.002
USARSP004_03	New Nov. 2003 point	2362898.455	608848.344	-0.406		
USARSP004_06	June 2006 re-survey	2362898.452	608848.333	-0.372	0.012	-0.034
USARSP005_01	June 2001 point	2362878.249	608854.245	-2.077		
USARSP005A_03	Nov. 2003 re-survey	2362878.287	608854.237	-2.081	0.039	0.004
USARSP005_03	New Nov. 2003 point	2362878.116	608854.349	-2.015		
USARSP005_06	June 2006 re-survey	2362878.105	608854.356	-2.051	0.013	0.036
USARSP006_01	June 2001 point	2362864.903	608808.081	-6.52		
USARSP006A_03	Nov. 2003 re-survey	2362864.996	608808.115	-6.264	0.1	0.256
USARSP006_03	New Nov. 2003 point	2362865.352	608807.89	-6.46		
USARSP006_06	June 2006 re-survey	2362865.402	608807.799	-6.466	0.103	0.006
USARSP007_01	June 2001 point	2362850.831	608817.579	-7.842		
USARSP007A_03	Nov. 2003 re-survey	2362850.707	608817.458	-7.64	0.173	0.202
USARSP007_03	New Nov. 2003 point	2362850.872	608816.92	-7.671		
USARSP007_06	June 2006 re-survey	2362850.904	608816.948	-7.665	0.042	-0.006
USARSP008_01	June 2001 point	2362833.694	608779.754	-1.551		
USARSP008_03	New Nov. 2003 point	2362836.838	608780.678	-1.529		
USARSP008_06	June 2006 re-survey	2362836.839	608780.682	-1.529	0.004	0.000

Table 9.1. GPS survey data for USS *Arizona*.

reported monument position from various satellites in the GPS constellation—when satellites gave inaccurate locations for the base station, the base station generates a corrected position for those satellites and broadcasts the corrected differential signal to the field receiver via a radio operating at 450 mHz, thus eliminating the need for post-processing and greatly accelerating data acquisition. Shorter occupation time, in the case of dynamic environments like underwater precision surveying, reduces CEP. The 5700s only require a five-second occupation. Several readings can be taken in a short time, which minimizes any tripod movement from current or waves.

Collection software used was Trimble's TerraSync™. This software was selected because it is the first mobile GIS software to integrate GIS data collection capabilities with survey-grade GPS mapping. This software expedited the field data collection and increased overall accuracy. The dive team used the software to carry USS *Arizona* GIS Project location and map data with them from point to point using a Trimble Recon, an ultra-rugged, waterproof handheld computer or Personal Data Assistant (PDA) designed for field data collection. This expedited on site point location and reduced field time for the reoccupation.

During the 2003 reoccupation, the first problem encountered was that most of the epoxy encased stainless steel bolts had corroded away. The epoxy did not prevent electrolytic corrosion of the stainless steel embedded in the mild steel of the deck plates. Each point was reoccupied as best as possible, but new points not subject to corrosion had to be established. PVC was used, and each new point was established adjacent to the original point (see Figure 9.5). The diameter of the PVC datum point was selected to accommodate the point of the underwater tripod to both provide a solid support and facilitate deployment (see Figure 9.6). Each of these new points was then surveyed and became the permanent monitoring points or "superpoints" (see Table 9.1).

The second reoccupation of the GPS monitoring points occurred in June 2006. Tim Smith from RIMD again collected survey data, this time using dual-frequency GPS receivers supplied by Gateway National Recreation Area. The 2003 methodology was again used in 2006. One of the PVC points established in 2003 was dislodged during the survey because the wood to which it had been affixed had deteriorated, and it had to be re-established, this time on deck steel. This occupation of all eight superpoints was successful (see Table 9.1).

Although accuracy of each point was mathematically calculated to about 0.5 cm (CEP), it is necessary to apply a more conservative threshold of change to evaluation of future monitoring re-occupations as directly reflective of hull structural changes. We have determined the significant structural change threshold to be 10 cm because of environmental conditions and differences in equipment and stadia variations. Instrument error, set-up error, or most likely, nearly imperceptible antenna movement caused by water movement, which is generally averaged out during the longer occupation times than used on land surveys, can create cumulative errors of perhaps 5 cm or more. Consequently, we cannot reliably attribute any observed change that is less than 10 cm to vessel movement; however, corroborative evidence would be sought for any level of change observed. Because the GPS points exist as a network of positions, aggregate changes in the positions of more than one point, even if less than 10 cm, could potentially indicate net movement of hull structure. Horizontal and vertical differences recorded between 2003 and 2006 are consistently below the 5 cm circle of error (see Table 9.1). From this dataset, it can be concluded that no measurable movement occurred during the 2½ year period.

For this structural monitoring program to be valid there must be an important assumption made: that the sediments beneath *Arizona*'s hull are fully compressed and stable so that changes measured in survey point positions are the result of changes to the hull interior and not the result of support sediments beneath the hull compressing. To provide a control for geological conditions, an intensive investigation of the sediments around the hull was conducted in partnership with the U.S. Geological Survey. The conclusions of this investigation are that the sediments beneath USS *Arizona* are nearly fully compressed and stable (see Chapter 10).

<u>External Crack Monitoring</u>

Researchers in the 1980s observed the deck sagging forward of the galley area while mapping the hull. At the start of the USS *Arizona* Preservation Project, this midships-area was sagging and beginning to collapse. It represents the aft-most damage from the forward magazine detonation, and does not contribute to the battleship's overall structural integrity, especially oil-containing spaces. These upper deck areas were expected to be the first to show signs of weakening because they are most affected by the blast.

The galley-area on the second deck and those decks below have been damaged by the enormous explosion that sank the vessel, and they constitute the aft edge of the blast crater (Figures 9.10–9.12). The forward magazine blast force undercut the lower hull structure and the decks forward sufficiently for turret nos. 1 and 2 to have dropped more than 20 ft. The deck forward of the stack slopes down into the lower hull. The main deck and portions of the upper deck now are nearly even with the top of the 13-in. armor belt on the starboard side, and lower than it on the port side. Other deck areas were blown upward, and hull sides above the armor belt were blown outward nearly horizontal with the hull. The shell plate blown outward above the armor belt was removed during salvage of the superstructure in the 1940s. An indication of the extent and location of damage in this area can be derived from salvage reports (see Chapter 3). These salvage reports indicate divers were able to move forward within the hull during damage assessment dives to frame 76 on the main and second decks and not forward of frame 78 below the third deck. However, on the third deck in ammunition passageways A-504-M and A-505-M, access was possible as far forward as frame 66 (Paine 1943:5). This midships-area is the most damaged of the aft portion of the vessel, and it is here that most oil leaking occurs (see below). In addition to GPS, from 2001 to 2006 structural changes in the upper deck crew's galley (frames 80–88) were monitored using a series of plastic crack monitors normally used to measure crack movement in historic buildings (Figure 9.13). In June 2001, six plastic monitors were affixed over cracks in the upper deck galley where *Arizona*'s deck collapse had been qualitatively observed. These crack monitors were checked periodically to see if the cracks widened or shifted. After several years of monitoring, most of the gauges showed little movement, although at least one (#4) had fallen into an expanding hole on the starboard side of the galley floor as part of a limited upper deck collapse. The research team decided that the limited data they provided did not justify replacing the gauges as they broke or became dislodged, which happened frequently. Active monitoring of crack gauges ended in 2006, but they will be periodically checked as part of the ongoing monitoring project.

Internal Monitoring

Internal structural monitoring of USS *Arizona* has been a qualitative process primarily using the VideoRay ROV to visually examine and photographically document interior areas and
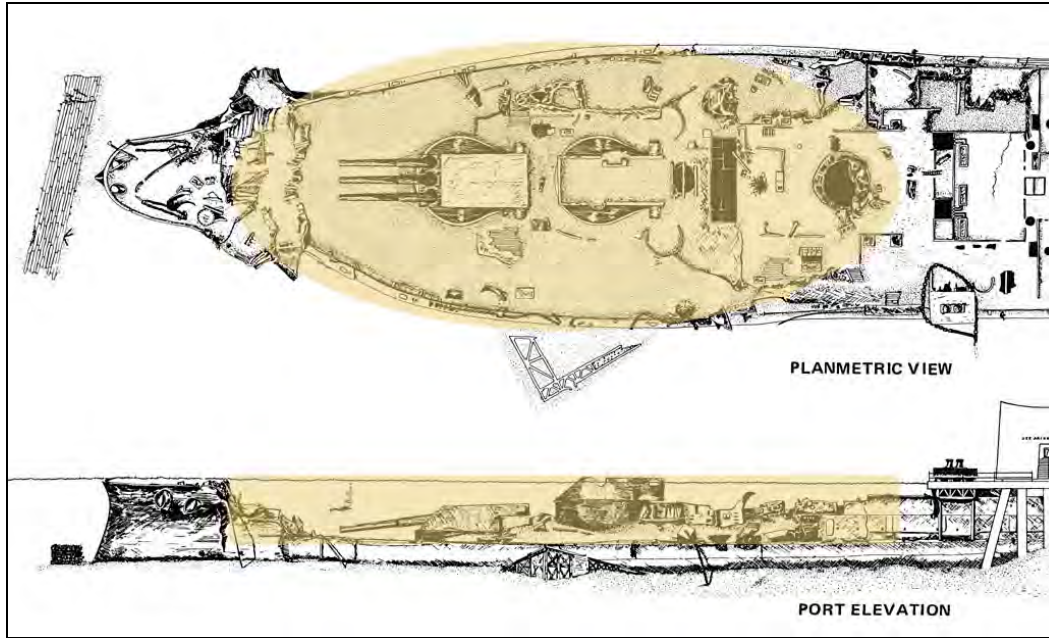
Figure 9.10. *Arizona* bow showing blast crater (highlighted) and weakened upper deck area from frame 10 to 78, or about 270 ft. of hull (Drawing by NPS-SRC).
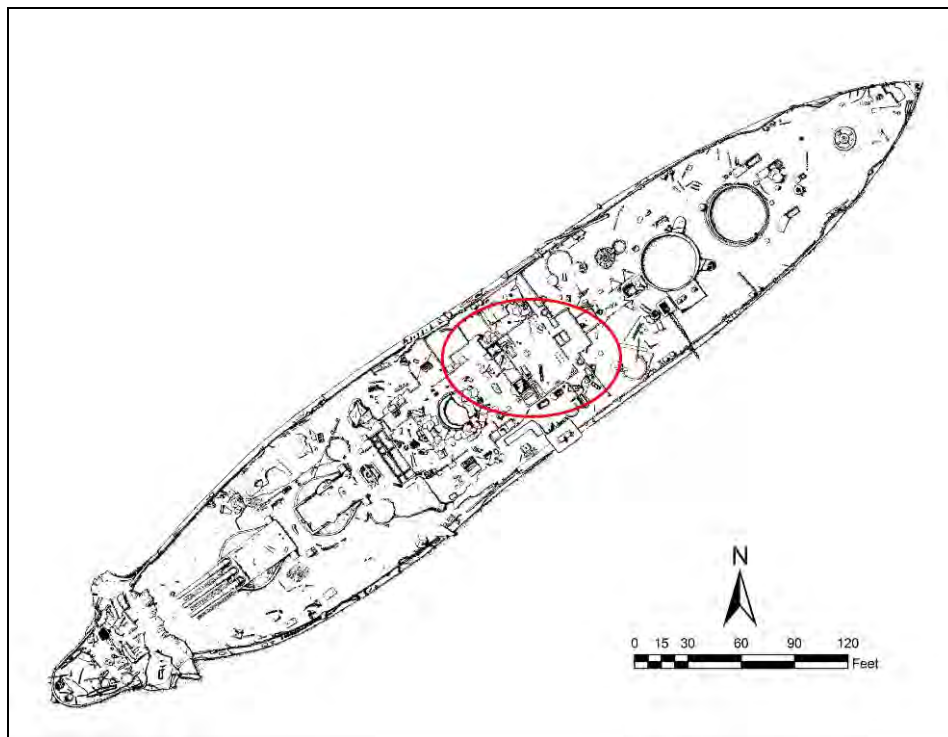
Figure 9.11. Plan view of USS *Arizona* with upper deck galley-area highlighted (Drawing by NPS-SRC).
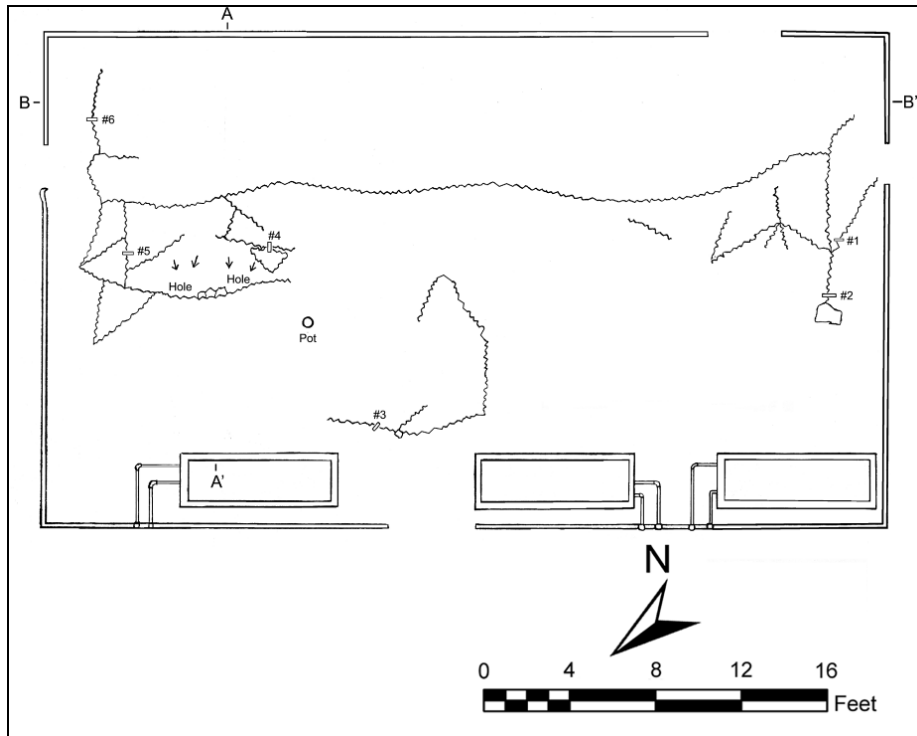
Figure 9.12. Plan view of *Arizona* galley area showing cracks and collapsed areas. *Arizona***'s bow is to the bottom of the drawing, port side to the right. Crack monitors are identified by numbers (Drawing by NPS-SRC).**

Figure 9.13. Crack monitor in *Arizona* galley-area (NPS Photo by Brett Seymour).

note observable changes over time. Interior investigation took place from 2001–2005 in all accessible areas for measuring and monitoring interior environmental factors and corrosion parameters. During this process, overall internal structural condition was observed and noted, and no observable changes to internal spaces were noted during this period. Areas investigated were identified using blueprints and, like all data and imagery, incorporated into the USS *Arizona* (USAR) GIS Project (Figures 9.14–9.16). All areas accessible to the 9 in. x 9 in. x 14 in. ROV were explored, which means that for additional areas to be accessed by either ROV or divers, structural alteration of the interior must occur.

OIL MONITORING

A considerable amount of analytical attention has been directed toward the oil in and around USS *Arizona*. Oil samples have been collected and analyzed, primarily with a gas chromatograph connected to mass spectrometer in selected ion monitoring mode (SIM) and with a flame ionization detector and HP-5 column (see Chapter 8). Primary oil samples are from the hull's interior, from open water release as an oil drop slowly floats to the surface, and from the
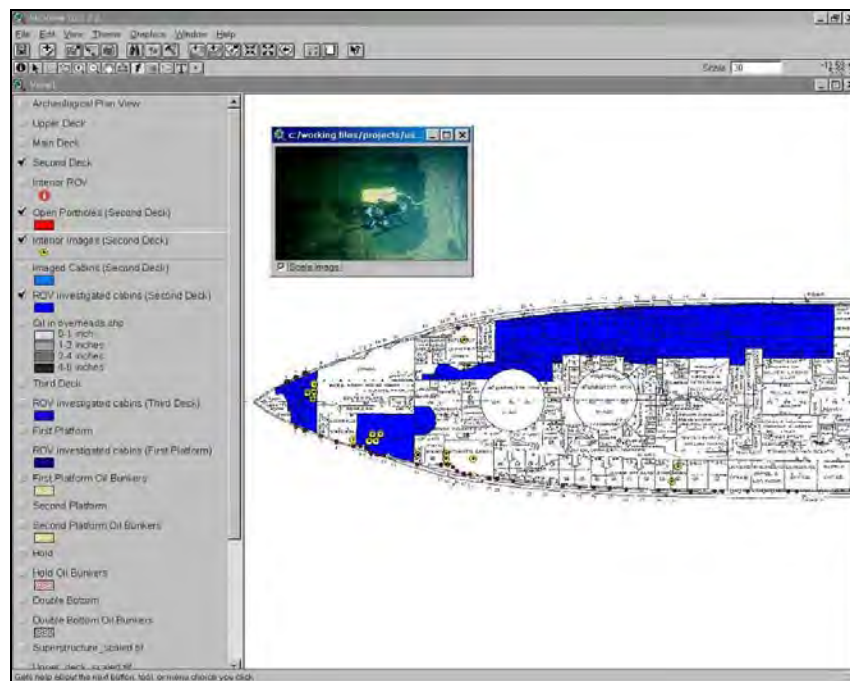
Figure 9.14. Second deck areas investigated with the VideoRay ROV (Image from USAR GIS Project).
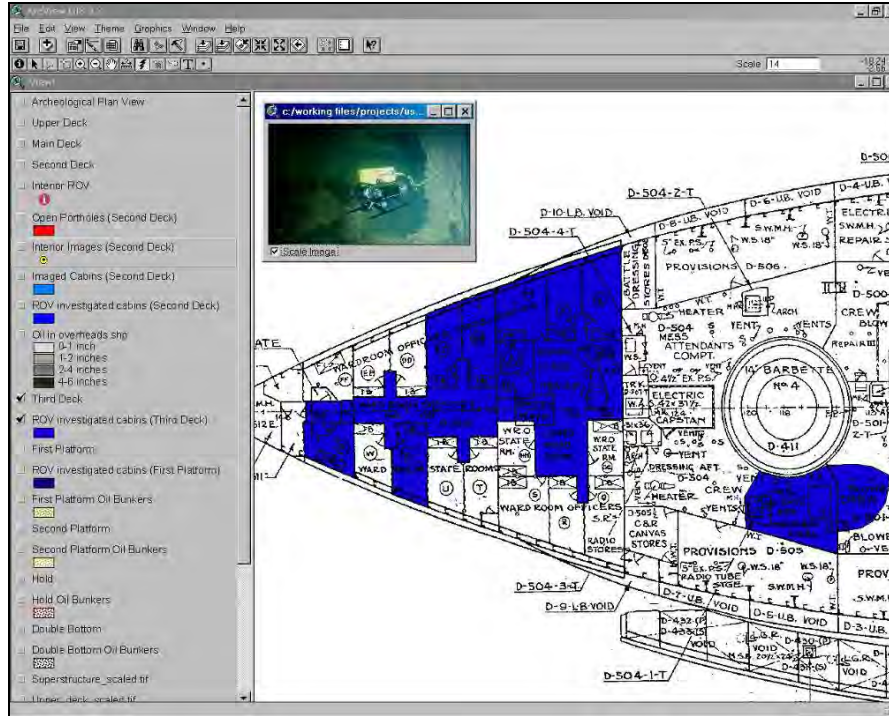
Figure 9.15. Third Deck areas investigated with the VideoRay ROV (Image from USAR GIS Project).
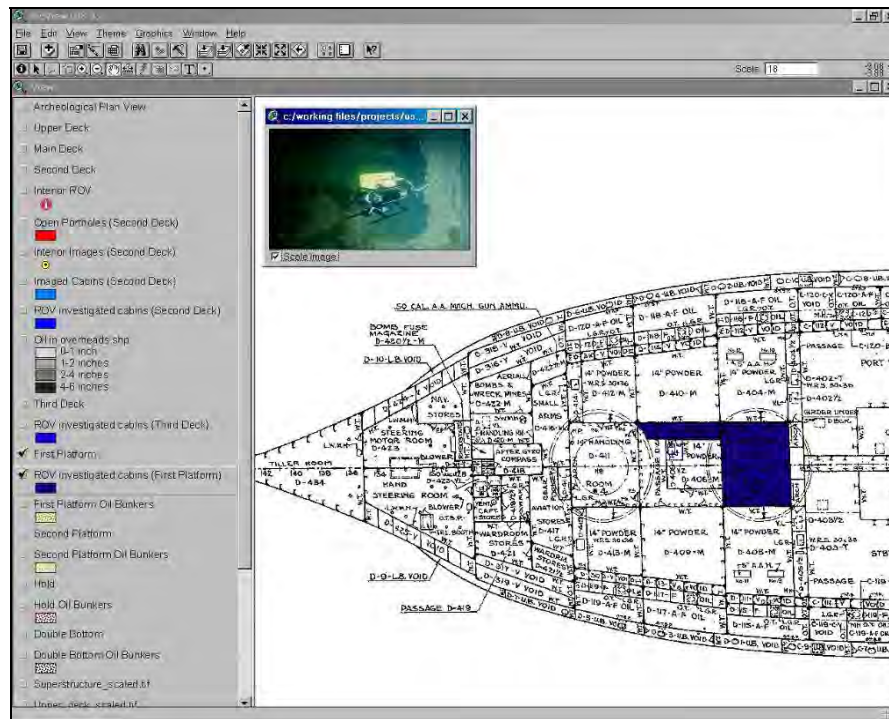
Figure 9.16. First platform areas investigated with the VideoRay ROV (Image from USAR GIS Project).

sediments on and near the ship. Laboratory analysis and experimentation indicate most samples had reduced *n*-alkanes present, which is the result of microbiological degradation and occurs after approximately 30 days of exposure to sea water or sediment-borne microbes. These results allow each oil leak location to be designated "degraded" or "undegraded." Undegraded oil indicates that the oil has been in contact with open sea water (an environment that exists in second and main deck spaces with openings to the outside) for fewer than 30 days. This undegraded oil potentially indicates an interior structural failure of primary oil containment spaces. Only a single source, a hatch on the starboard side of barbette no. 4 at frame 119, produces undegraded oil (see Chapter 8).

INTERNAL OIL MONITORING

Internal oil observations and samples were collected with the VideoRay ROV (Figure 9.17), although most internal oil samples were collected from cabin overheads by reaching through an open second deck port hole on *Arizona*'s starboard side with a PVC pipe. No oil was observed in the port overhead spaces, likely due to the ship's 2–3° port list, which funnels the buoyant oil to the higher, starboard side. Oil has collected in most observable, starboard-side second deck cabin overheads, and the depth of oil in each cabin overhead was measured to give an idea of where internal oil releases are concentrated. A PVC pipe was pushed vertically up to the cabin overhead to obtain a depth (thickness) measurement of the oil layer, and samples were collected when the pipe was extracted (Figure 9.18). The results of oil depth measurements in overhead compartments on the second deck (Figure 9.19) indicate that oil concentrations increase moving forward from the stern, with the highest concentrations between frames 88–98. This is consistent with increased oil release observations in the upper deck, midships area (forward of frame 92). However, it also reinforces the observation that oil release in the midships and galley area is primarily "degraded" oil coming from secondary oil concentrations in second and main deck cabin overheads, not "undegraded" oil coming from primary oil containment spaces. The main deck (aft of frame 92) above oil-containing cabin overheads is apparently sound; there is no oil leakage above these second deck spaces. The closest oil leaks to this area are two open hatches on the main deck that continually release oil drops (see Figure 9.19). The oil coming from the aft-most hatch is different than the oil in cabin overheads, in that

Figure 9.17. VideoRay ROV rigged for interior oil collection (NPS Photo by Brett Seymour).

Figure 9.18. Internal oil measurement and oil sample collected by reaching PVC pipe in porthole and pushing vertically to the overhead. Overhead oil depth is indicated by oil on pipe (NPS Photo by Brett Seymour).
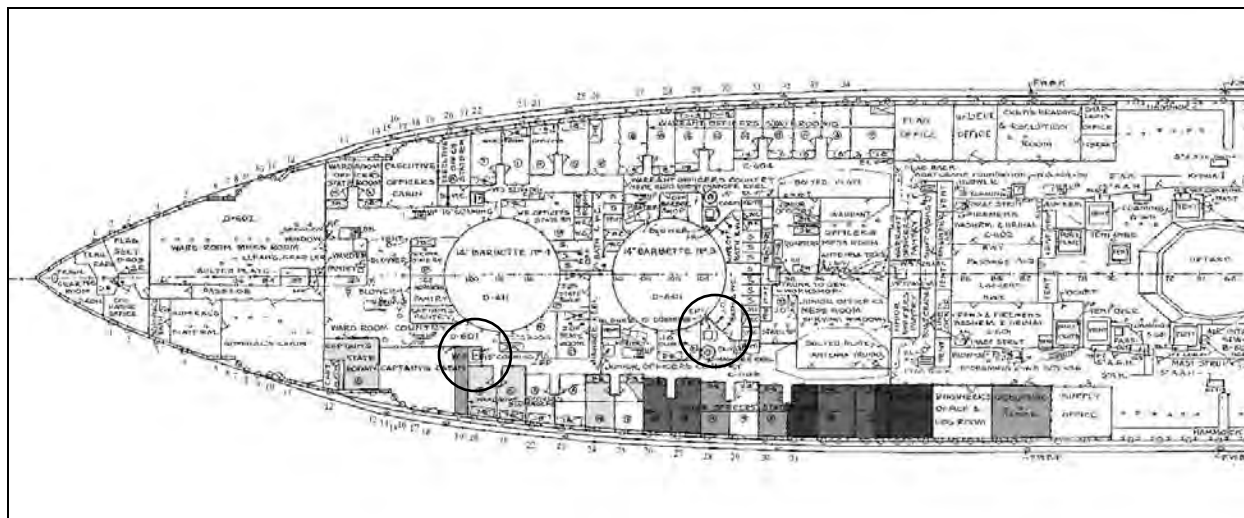
Figure 9.19. Illustration of thickness of overhead oil on *Arizona*'s starboard second deck (stern to the left). Relative darkness represents thickness of oil in each cabin overhead, and hatches releasing oil are circled (Graphic by NPS-SRC).

it is the only location producing undegraded oil. In addition, ROV observations have indicated the source of undegraded oil from the aft-most main deck hatch is below the third deck. All the other released oil tested has reduced *n*-alkanes (and other constituents), matching oil from the cabin overheads, which indicates microbial degradation has occurred through the oil's exposure to seawater (and microbial communities) of more than 30 days (see Chapter 8 and below). Most likely, oil leaking from the forward-most main deck hatch, and all other oil release points, is coming from reservoirs pooled beneath the main and upper decks where it is degraded for some time before being released.

Oil samples will continue to be collected as part of the *Arizona* monitoring program. Differences in oil sample constituents reflect differences in the environment the oil has been subjected to in containment and time of exposure to seawater. Additional and more detailed analysis of various oil leak locations can potentially inform about changes that are occurring within the vessel. At this point, undegraded oil is believed to indicate oil freshly released from primary containment spaces within the ship. An increase in release, either steady or episodic, of undegraded oil implies structural changes may have taken place in oil bunkers.

EXTERNAL OIL RELEASE MONITORING

Since 1998, the SRC and USS *Arizona* Memorial (USAR) have monitored oil release rates from *Arizona*'s hull. Oil release observed during the 1980s *Arizona* documentation project originated from a hatch on the starboard side of barbette no. 3, at frame 103, and later from a hatch on the starboard side of barbette no. 4, near frame 119 (see Figure 9.19).

Open water column samples for analysis are collected by simply catching a drop of oil as it rises to the surface (Figure 9.20). For measuring release rates in the current USS *Arizona* Preservation Project, we used a custom-designed, purpose-built catchment tent that funnels oil droplets into hole in the top fitted for a 32-oz. collection jar (Figure 9.21 and 9.22). The first tent was constructed in 1998 by USIA Corporation (St. Helens, Oregon), followed by a revised version in 2002. The tent is set up above an oil release point and left in place for a specific time period, after which the volume of oil collected is measured, and an average 24-hour release rate calculated. Systematic oil release monitoring began in 1998, focused on the two starboard hatches that had been identified in the 1980s, and continued in 2003, 2004, and 2006, with each including more oil release locations.

Figure 9.20. USS *Arizona* open water oil sampling (NPS Photo by Brett Seymour).

Figure 9.21. Oil catchment tent deployed on *Arizona* (NPS Photo by Brett Seymour).

Figure 9.22. Oil catchment tent deployment on *Arizona* (NPS Photo by Brett Seymour).

During fieldwork from 1998 to the present, gradually increasing quantities of oil have been qualitatively reported from the area forward of the Memorial; however, comprehensive measurement of oil release forward of the Memorial in the upper deck galley was not completed until June 2006. At this point, it is unclear if there has been cumulative increase in the oil being released from the hull. The 2006 oil release monitoring was the first cumulative oil leak collection conducted that collected oil from every observable oil release location on the hull. The 2006 release rates comprise the baseline for comparing all future oil release measurements. Prior to 2006, only selected oil release points were measured; there was no attempt to measure the cumulative quantity from all observable release points.

In June 2006, the catchment tent was set up over eight separate locations on *Arizona*'s deck that actively leak oil. At some locations the tent was left in place for a full 24-hr. period, while others were collected for 3 or 4 hr. and a 24-hr. equivalent release volume calculated. A cumulative total of 9.5 qt. (9.0 l) was measured from the eight leak locations (Figure 9.23). Locations measured in June 2006 represent those leaking more or less continuously and did not include locations that may have sporadic or periodic leaking.
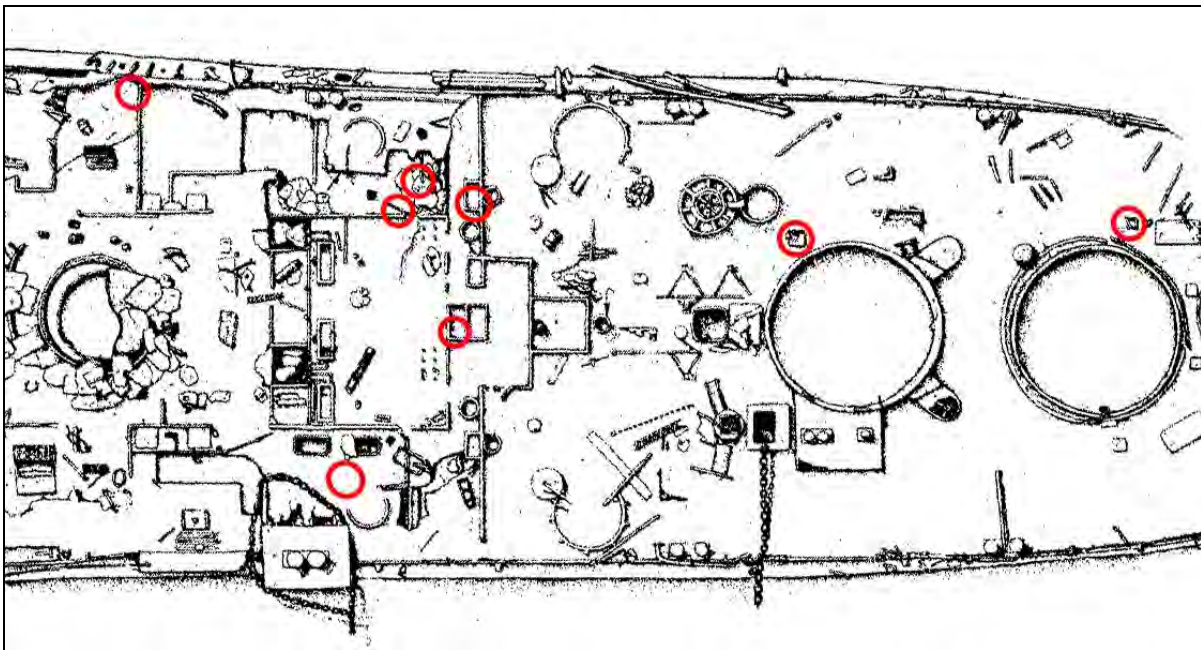
Figure 9.23. Oil release points measured on *Arizona*'s hull, June 2006 (bow is to left) (Graphic by NPS-SRC).

Measured 24-hr release rates have gradually increased each year in direct proportion to the number of locations monitored: in 1998, 1.0 qt. (0.95 l) was measured from one location; in 2003, 2.1 qt. (2.0 l) were measured from two locations; in 2004, 2.3 qt. (2.2 l) were measured from two locations; in 2006, 9.5 qt. (9.0 l) were measured from eight locations (Tables 9.2 and 9.3). June 2006 oil release measurements are the most comprehensive completed to date—increase in oil release over previous years is in part explained by more release locations being systematically measured than previously. Only future monitoring of release points can establish whether there is a cumulative increase or not.

There is no indication of increase in of oil volume released from the primary oil containment spaces in the ship's lower decks. The increase in oil observed appears to be most likely from redistribution of secondary oil contained in overhead spaces on the main and upper decks caused by gradual collapse of upper decks forward of the Memorial, which have the highest corrosion rates and were also affected by the 1941 explosion (see Chapter 5). Primary oil containment spaces (oil bunkers), located on *Arizona*'s lower decks, are well below the harbor bottom and likely have lower corrosion rates than any measured on the outside of the hull. Measured corrosion rates below the harbor bottom are the lowest rates observed on the hull, about 25% of the 4.5 mils per year (mpy) predicted from the laboratory derived corrosion rates of mild steel in seawater (see Chapter 5). This is because corrosion is primarily driven by the presence of dissolved oxygen, and the environment below the mud of the harbor bottom, as well as water in the interior spaces is anaerobic. Periodic measurements of internal water quality, however, should be part of the ongoing monitoring process.

Undegraded oil release measured from the aft-most main deck hatch on the starboard side of barbette no. 4 in June 2006 is lower than in previous years. These data suggest that oil release directly from primary oil containment spaces may have decreased over the last several years,

Year	Number of Locations Measured	Average Total Amount Measured Per 24 Hours (quarts)	Average Total Amount Measured Per 24 Hours (liters)
1998	1	1	0.95
2003	2	2.1	2
2004	2	2.3	2.2
2006	8	9.5	9

Table 9.2. Number of oil locations measured and quantities recovered, by year.

Year	Location	Date	Amount	Time	Total per 24 hr. (qt.)	Total per 24 hr. (l)
1998	Oil hatch starboard of No.3 barbette	8/29/98	800 ml	22 hrs. 39 min.	0.9	0.85
1998	Oil hatch starboard of No.3 barbette	8/31/98	700 ml	27 hrs. 35 min.	0.64	0.61
1998	Oil hatch starboard of No.3 barbette	9/06/98	175 ml	3 hrs.	1.5	1.4
2003	Oil hatch starboard of No.4 barbette	11/18/03	42.5 oz.	24 hrs.	1.33	1.25
2003	Oil hatch starboard of No.4 barbette	11/19/03	42.5 oz.	24 hrs.	1.33	1.25
2003	Oil hatch starboard of No.3 barbette	11/20/03	16-24 oz.	24 hrs.	0.5-0.75	0.47-0.7
2004	Oil hatch starboard of No.4 barbette	11/09/04	14 oz.	6 hrs.	1.75	1.66
2004	Oil hatch starboard of No.3 barbette	11/11/04	16 oz.	24 hrs.	0.5	0.47
2006	Oil hatch starboard of No.4 barbette	06/20/06	5 oz.	4 hrs.	0.94	0.89
2006	Oil hatch starboard of No.4 barbette	06/21/06	5.2 oz.	4 hrs.	0.97	0.92
2006	Oil hatch starboard of No.3 barbette	06/23/06	10 oz.	24 hrs.	0.31	0.3
2006	Starboard of galley, on deck	06/24/06	5 oz.	24 hrs.	0.16	0.15
2006	Starboard of galley starboard bulkhead, forward of doorway	06/26/06	<1 oz.	48 hrs.	<0.016	<0.015
2006	Starboard gunwale, frame 68	06/28/06	8 oz.	24 hrs.	0.25	0.24
2006	Port, forward corner of vegetable locker	06/28/06	9.4 oz.	4 hrs.	1.8	1.7
2006	Port side of galley, on deck	06/29/06	5 oz.	3 hrs.	1	0.95
2006	Starboard side of galley, at transverse bulkhead between upper deck and main deck.	06/29/06	20 oz.	3 hrs.	5	4.7

Table. 9.3. Oil release quantities by year.

supporting the supposition that increased oil release is from secondary oil containment in cabin overheads below the main and upper deck spaces forward of the Memorial, in the area of the observed deck collapse.

Oil release rates can vary considerably with differing wind, tide and harbor conditions. More oil is clearly released during choppy harbor conditions and when tour boat and other ship's wakes pass near *Arizona*'s hull, which further supports the oil source as shallow overhead spaces rather than from primary oil containment spaces. Wake pressure waves can dislodge oil residing in overhead spaces. Large vessel wakes within Pearl Harbor are significant; divers working on the hull are occasionally displaced as large vessels pass. This impact to the hull is somewhat

exacerbated because ships tend to pass close by the USS *Arizona* Memorial in tribute. The June 2006 measurements not only included many more source locations (all that could be located), it is likely that these measurements represent near maximum release rates. The June 2006 oil release measurements were conducted during RIMPAC naval exercises, which is a period when the number of reported ship moves in Pearl Harbor is generally 10 times the normal number. Consequently, June 2006 oil release measurements represent conditions under which maximum release from wake disturbance is expected.

Periodic monitoring of all oil release locations on *Arizona* should be continued and USAR personnel on the Memorial should continue daily recording of oil release observations. To quantify effects of differing weather and harbor conditions on oil release rates, more frequent in-water monitoring under diverse conditions should be considered in the future to produce data that can be correlated with episodic release increases and lead to a prediction as to when wave driven episodic releases may occur. The most comprehensive oil release monitoring can be accomplished by capturing surface oil downstream from *Arizona*'s hull. An oil capturing and monitoring system should be investigated collaboratively with the U.S. Navy and U.S. Coast Guard. This would likely involve a boom erected between *Arizona*'s bow and *Missouri*, with regular oil removal and measurement by Navy or Coast Guard oil response personnel. Ideally, a remote sensing device measuring surface oil could be deployed and alarmed to warn of significant oil increase that requires mobilization of the Pearl Harbor Oil Response capability.

OIL RELEASE IN CREW'S GALLEY AREA

As discussed previously, the upper deck, midships galley-area (frames 80–88), just forward of the Memorial, is presently the principal oil release area on *Arizona*'s hull. This area is heavily damaged from the forward magazine blast that sank the vessel, representing the stern reach of the blast crater (see Figure 9.10 and Chapter 3). The decks are sagging, and there has been limited collapse observed, which is why this area was chosen for deploying the crack monitors (see Figures 9.11 and 9.12). During 1941 salvage investigations, divers noted that there was only access forward to frames 76 and 78. Forward of this location, the main, second, third, first platform, second platform and hold decks collapsed on top of one another to the level of the top of the 13-in. armor belt, as the blast undercut deck support structures. Turret nos. 1 and 2

both collapsed downward more than 20 ft. (Figure 9.24). The lower decks area beneath the galley area were certainly damaged as evidenced by both the forward multiple deck collapse, but also by the original film of *Arizona*'s explosion, which shows the magazine explosion clearly vented upward through the stack area, which is just forward of the galley area (Lott 1978:40). This indicates the blast most certainly affected adjacent spaces aft, including the galley.

The oil escaping from the hull in the galley area comes through the sediments, which appear to be fully saturated with oil in several locations. Oil release has increased in this area based on comparisons with the 1980s fieldwork. Additional oil leaking from lower decks floats to the area beneath these sediments, and dislodges trapped oil that rises to the surface (Figure 9.25). It is a reasonable question to ask "where does the oil leaking through the galley area sediments likely originate?" A partial answer is revealed by an examination of the ship's blueprints on this area, specifically focusing on ship's plans in the area between frames 70–90. The crew's galley was on the upper deck. Directly beneath this area, below the third deck were engine, boiler, distribution and pump spaces (Figures 9.26–9.32). Oil bunkers are on the first platform and below. There is no record of damage to these spaces, only the main and third decks are mentioned as being accessed by divers during the salvage work, but it is very likely there is damage to the engine and boiler spaces in this area. Oil could be coming from associated piping, machinery, cracked or damaged bunkers, and trapped in overhead spaces. Episodic releases may be caused by further collapse of lower decks, much like that observed on the upper deck area. More likely, the oil in the galley area is resulting from original battle damage, and weakened decks collapsing and releasing trapped oil that rises up from engine, boiler and pump spaces, than from deteriorating oil bunkers. The rising oil is directed by collapsed decks to cracked areas surrounding the upper deck galley that contain sediment, where the oil saturates the sediment and is released.
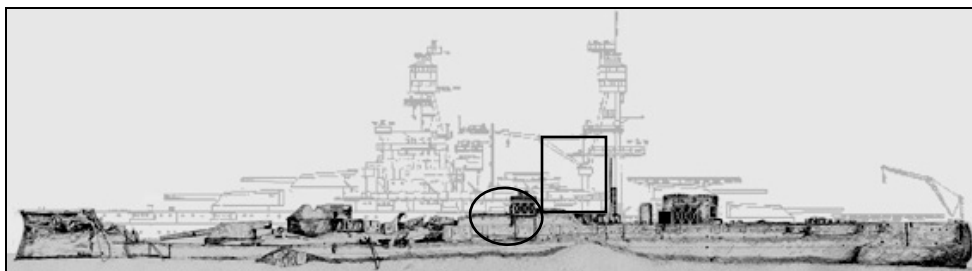
Figure 9.24. USS *Arizona* wreck overlay on intact vessel plans. Oval indicates galley area oil release area and rectangle is Memorial location (Graphic by NPS-SRC).

415

Figure 9.25. Sediments in crew's galley area forward of Memorial. Dark areas are oil saturated sediments. White oval circles a drop of released oil moving toward the surface (NPS Photo by Brett Seymour).
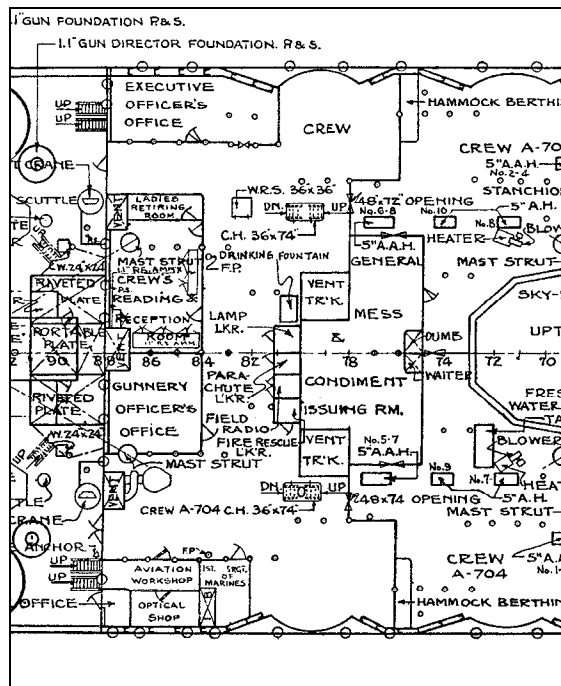
Figure 9.26 *Arizona* main deck blueprint, frames 70-90. Stack is on right, towards the bow. Reportedly, divers were able to reach frame 76 on this deck, which is the condiment issuing room just aft of the stack (USS *Arizona* Memorial Archives).
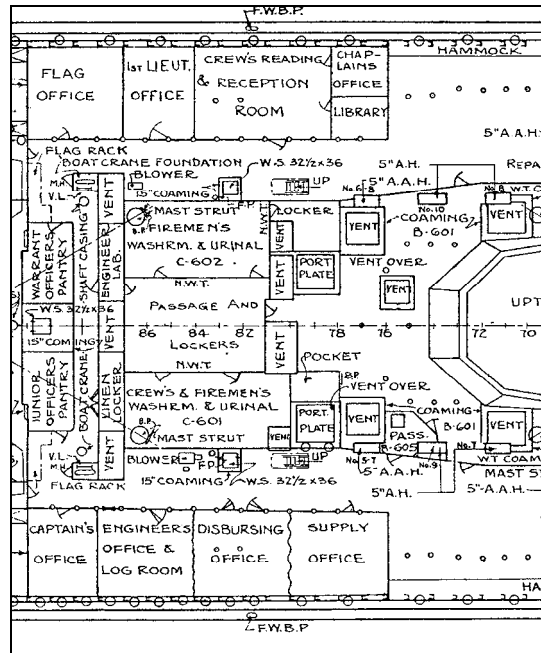
Figure 9.27. Second deck, frames 70-90 (USS *Arizona* Memorial Archives).
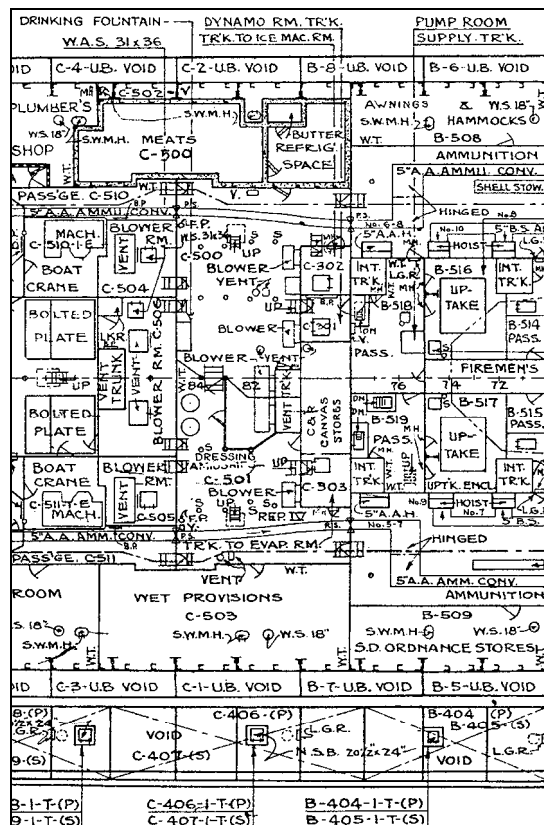
Figure 9.28. Third and splinter deck, frames 70-90. Divers were able to reach frame 78, likely through the centerline fireman's passage. Frame 78 is a watertight bulkhead (USS *Arizona* Memorial Archives).
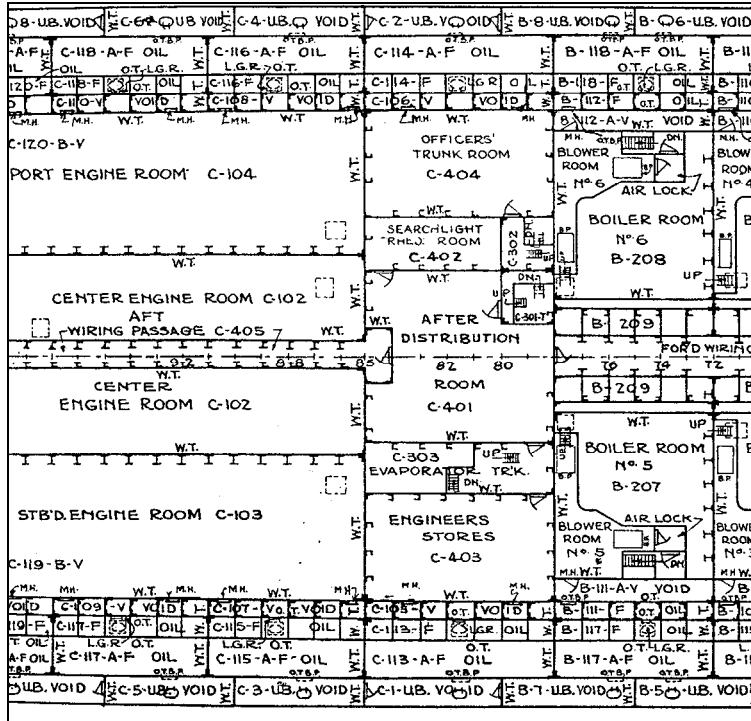
Figure 9.29. First platform, frames 70-98. This area is between the three engine rooms and boiler spaces, and contains the after distribution room. It is the highest level in the ship that contains oil bunkers (USS *Arizona* Memorial Archives).
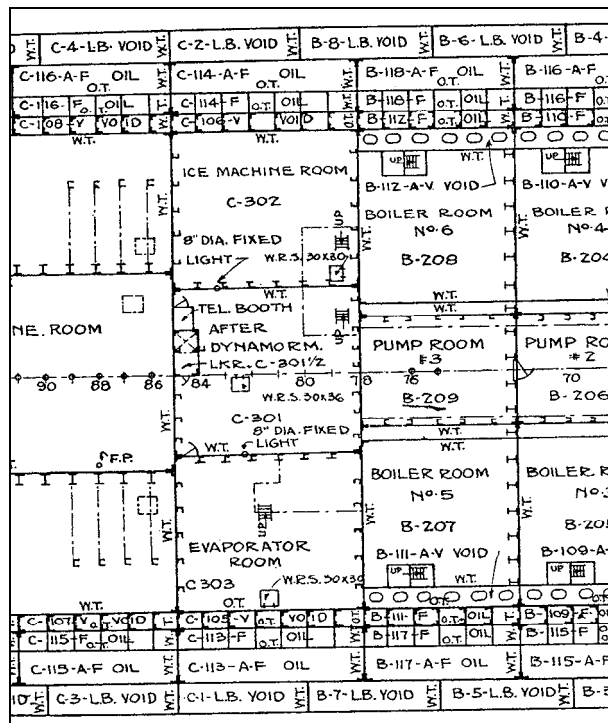
Figure 9.30. Second platform, frames 70-90, contains engine and boiler spaces as well as pump rooms (USS *Arizona* Memorial Archives).
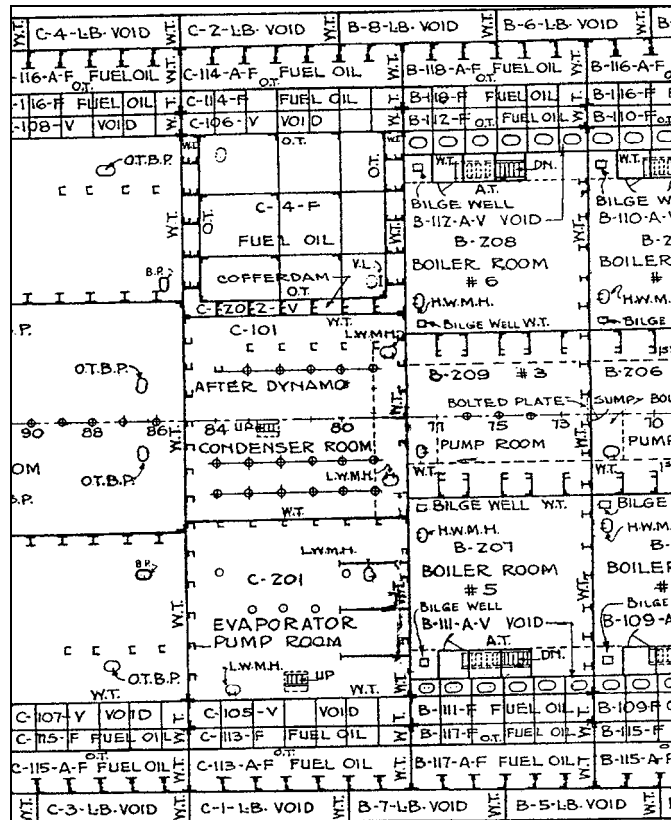
Figure 9.31. Hold, frames 70-90, including engine, boiler spaces, and pump rooms (USS *Arizona* Memorial Archives).
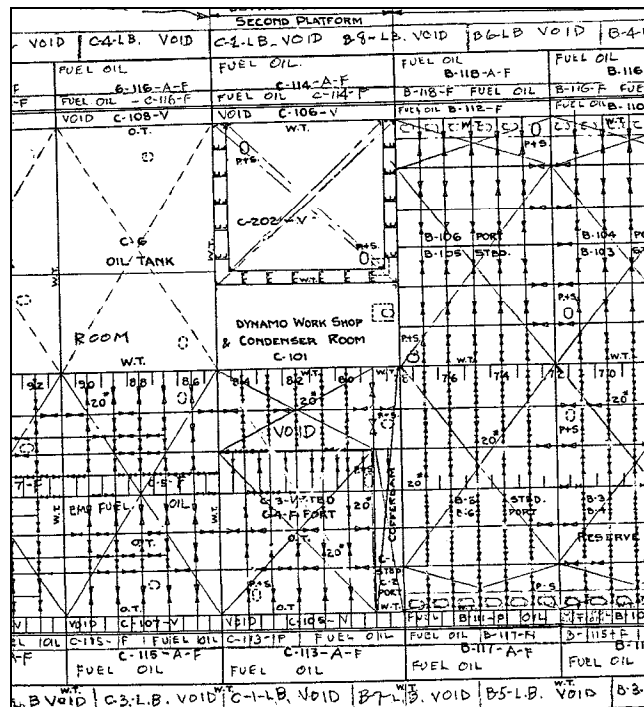
Figure 9.32. Double bottom, frames 70-90. It is unlikely that this area suffered significant damage from the magazine blast (USS *Arizona* Memorial Archives).

419

ARTIFACT MONITORING PROGRAM

Growing concern by USS *Arizona* management prompted by evidence of increased unauthorized diving led to the development of an artifact monitoring program. SRC archeologists conducted an intensive survey of the accessible open deck areas, primarily main and upper decks for visible artifacts. Artifacts were mapped in place through a combination of baseline trilateration, trilateration from mapped features, and a combination of GPS and total station survey. Each artifact received a unique numbered tag with its inventory number on one side and "US Government Property – Do Not Remove," on the other (Figure 9.33). A spreadsheet with the artifact number, general location, description, dates relocated, UTM coordinates and survey data, and photograph and video imagery identifier fields, was created. More than 450 artifacts have been inventoried and are being monitored. The artifact monitoring program is ongoing, and it will become increasingly important as development of Ford Island progresses.

Figure 9.33. USS *Arizona* artifact with monitoring tag affixed (NPS photo by Brett Seymour).

QUALITATIVE ENVIRONMENTAL MONITORING

Submerged Resources Center personnel have been conducting research on USS *Arizona* since 1983. During the course of this research, scientists and archeologists working on *Arizona* have noted a general improvement in overall environmental conditions. This improvement manifests in increased visibility and increased coral growth, and fauna presence and diversity on the hull (Figure 9.34). In 1986, researchers conducted a biological inventory of growth attached to the hull and deck. There were about 25 common taxa of organisms living on the hull and about 25 species of fish observed. Most of the encrusting organisms were filter feeding organisms such as vermetid mollusks, oysters, bryozoans, tube worms, sponges, tunicates and algae. Resurveys were conducted in 1987 and 1988, and monitoring station photographs were taken and analyzed (Henderson 1989). The monitoring program could not be sustained and was discontinued afterwards. In addition, lack of funding prevented a repeat inventory for quantitative inventory comparison as a part of the current research project, which is needed. However, presence of seahorses (identified by USS *Arizona* Memorial personnel as *Hippocampus kuda*, or yellow seahorse, Figure 9.35), first observed in 2005, indicates improving water quality in Pearl Harbor. Qualitative comparisons can also be made through photographic evidence taken of features during the 1980s documentation project and more recent photographs of the same objects (Figures 9.36–9.39). This 20-year observation period of biological indicators on USS *Arizona* show that both the environment in and around *Arizona* is relatively benign, and the general conditions of Pearl Harbor have markedly improved in the last two decades.

Continued biological observations and documentation will be part of a future monitoring program. A full biological inventory of *Arizona*'s hull and proximity is needed, and comparisons with the 1986 inventory and implications should be made. Biological inventories should be conducted periodically, ideally at 3–5-year intervals. In addition, a complete ecotoxicological study is needed of the sediments on and near *Arizona*, and down current along the Ford Island beach zone. Biomarker analysis has provided a signature of *Arizona*'s oil (see Chapter 8). This analysis has also identified constituents, such as butylated hydroxytoluene (BHT), which is not a component of Bunker C fuel, but is found in jet fuel, from a sediment sample just 10 ft. from *Arizona*'s hull. A full analysis of the degradation of *Arizona*'s oil and a quantification of its environmental impact, particularly in the context of Pearl Harbor where there are other point

Figure 9.34. Live coral on *Arizona*'s deck (2006), which requires good water quality to grow. There was no hard coral observed in 1986 (NPS Photo by Brett Seymour).
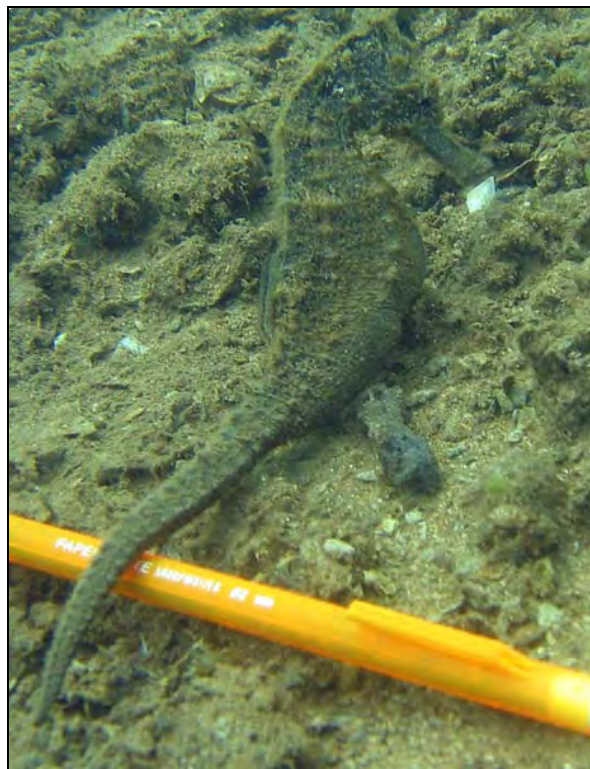
Figure 9. 35. Sea horse (*Hippocampus kuda*) on *Arizona*'s deck, first observed in 2005 (NPS photo by Jennifer Burbank).

Figure 9.36. Gas cylinder *Arizona*'s deck in 1983 (NPS photo by Larry E. Murphy).

Figure 9.37. Gas cylinder *Arizona*'s deck in 2005, with hard coral (NPS photo by Brett Seymour).

Figure 9.38. Inverted ventilator, on *Arizona*'s aft deck in 1983 (NPS photo by Larry E. Murphy).
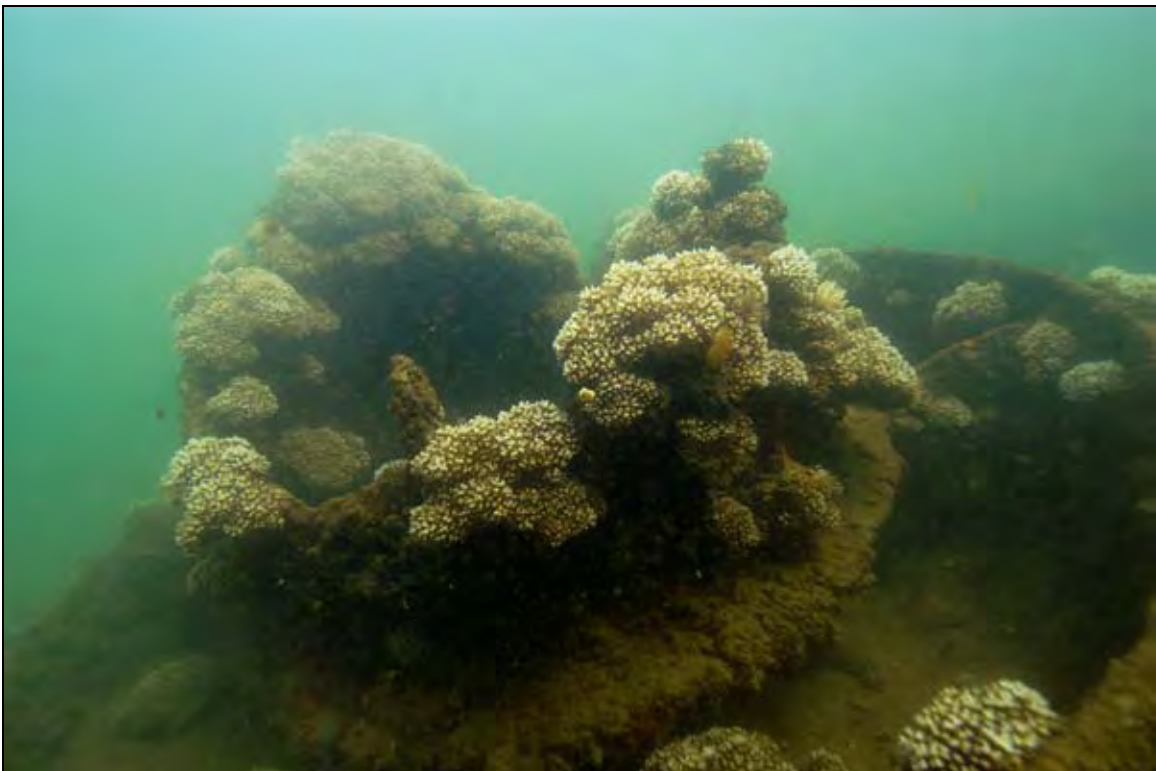
Figure 9.39. Inverted ventilator, on *Arizona*'s aft deck in 2005 (NPS photo by Brett Seymour).

sources of petroleum, is needed to inform management decisions that address the actual environmental impact of the *Arizona* oil release. It is easy in today's climate of growing concern about the environment to intuitively attribute severe environmental impact from the quite visible *Arizona* oil slick (actually only several microns thick) that could prompt ill considered and inappropriate intervention to remove the oil. As should be clear from data presented in this report and incorporated into the predictive FEM in Chapter 6, *Arizona*'s hull does not appear to be in any danger of imminent collapse, and consequently there is no urgency to remove the oil to preserve the environment or prevent "environmental catastrophe." There is certainly sufficient time to collect additional data and refine the predictive model while actively monitoring the environment to determine precisely the impact of the oil leaking from the ship. What is needed is scientific data that describes and quantifies the actual environmental impact of Bunker C fuel oil from *Arizona* and develops a predictive model of environmental impact for various levels of release. Insufficient funding has prevented this important environmental analysis from being accomplished to date. We consider these data critical in future management consideration of the balance between natural environment-impact and the historic and cultural importance of USS *Arizona* and its long-term preservation.

USS *ARIZONA* GEOGRAPHIC INFORMATION SYSTEM (GIS)

GIS technology provides a solution for maintaining a spatially related, cumulative record of information on USS *Arizona* that allows analysis and manipulation to produce additional data sets and relationships not otherwise available. One of the first steps in developing this database was the location, collation, and examination of nearly 8,000 scanned *Arizona* blueprints and technical drawings, which are stored on 75 DVDs. More than 250 original ships plans and blueprints were selected from the blueprint set for incorporation into both the FEM and the GIS. These digital plans were provided to the National Institute of Standards and Technology (NIST) and the NPS-RIMD, who contracted with Northrop Grumman Mission System (Lakewood, CO, a division of defense contractor Northrop Grumman, Los Angeles, CA) to develop a GIS appropriate for long-term management of *Arizona* data that incorporated current and historical data. Currently, the GIS is stored on RIMD servers and available to scientists and researchers.

Upon completion of the USS *Arizona* Preservation Project GIS, it will be made accessible to the general public. The software used for this project is ESRI's (Redlands, CA) ArcIMS software.

The first step in developing the GIS was to vectorize the raster format scanned blueprints and create a geodatabase of USS *Arizona* that includes all information for each cabin and space available on the plans—each object, space or cabin is a digitally separate entity with all attributes linked to it through the geodatabase (Figure 9.40–9.42).

For the GIS to progress all spatial data had to be georectified. This georectification was begun by collecting more than 35 survey grade kinematic points on the ship's hull. These points served as rectification points for the *Arizona* maps created in the 1980s, blueprints and other spatially related data, and as datum points for detailed mapping areas for the artifact inventory and monitoring program. Points were selected on the ship that were easily recognized and collated with the digitized *Arizona* drawings. A combination of underwater tripod and stadia rod survey was used (see above). The "superpoints" discussed earlier were also incorporated into this georectification project as additional rectification points.

Figure 9.40. Georectified blueprints of USS *Arizona* (Image from USAR GIS Project).
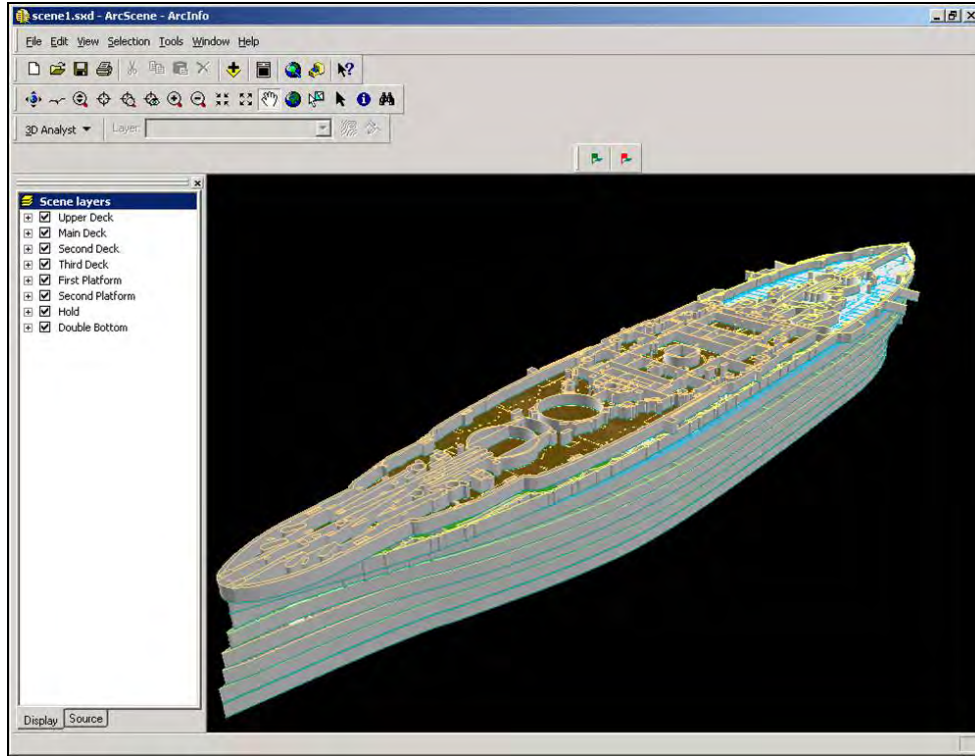
Figure 9.41. *Arizona* **deck layers, georectified, vectorized and set for queries (Image from USAR GIS Project).**
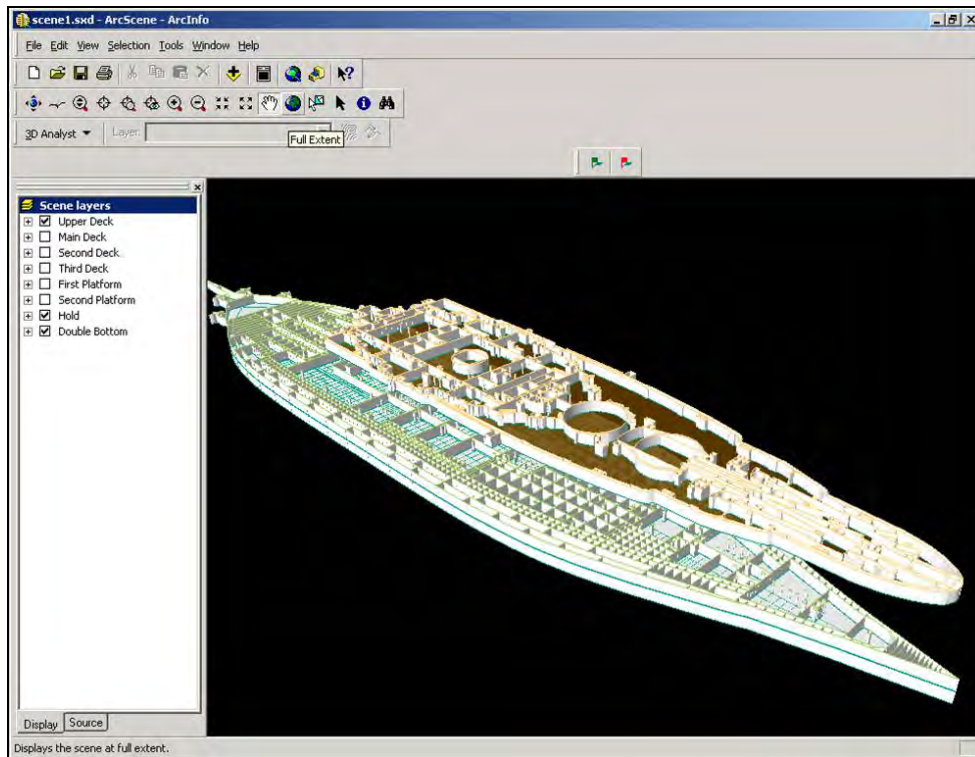
Figure 9.42. *Arizona* **interior deck spaces, each of which can be queried for associated data (Image from USAR GIS Project).**

Observations made by researchers, for instance, portable items found on the decks or bulkhead conditions observed in ship compartments by the ROV, have been recorded in the GIS. Eventually, more than 2,000 engineering drawings of individual rooms and features will be vectorized and added to the geodatabase along with more than 3,000 historical and current photographs, images and documents. All will be searchable either by name or location.

Using these base maps and geodatabase, scanned ship's plans can be "linked" to their appropriate object or location on the ship. Next, a webpage and ArcIMS website was developed that incorporated annotated vector polygon layers of the USS *Arizona* that logically track associations to a database of digital reference imagery. The web map is currently a prototype, and plans are made for its revision and updating of new scientific data and historical and current photographs and video.

The web site currently provides functionality to view all eight layers of USS *Arizona*, query for specific features in each layer, identify features in each layer (name and description fields are most useful), and includes standard interactive map tools such as pan and zoom. Each layer is rendered with 30% transparency so that deck features below the current deck may be seen "through" the top most deck that is displayed. The decks are accurately ordered in the table of contents from top to bottom and georectified. All standard web map functions are included in this HTML map service.

The prototype website has two custom functions that allow scanned engineering drawings to be viewed through the web interface. These tools are located on the left frame under the title "Access Images" and are named: *by Feature* and *by Query*. The first tool enables the user to select a feature on a deck of the ship and query the geodatabase for images and data associated to that feature (Figure 9.43). If multiple images are related to one feature (ammunition passage or gun turret for example), a list of images is returned with their description for selection. The user selects one of the images and it opens a new browser window to view the image. The prototype utilizes Lizard Tech's loss-less image compression format for image storage and viewing. A Lizard Tech browser plug-in is required for viewing the images in a standard web browser and can be downloaded as necessary.

The second custom tool (*Access Images by Query*) queries the database directly to produce a unique list of image themes (Figure 9.44). The user chooses a theme and is returned a list of all the images and their descriptions that fall under that theme. As the user selects an
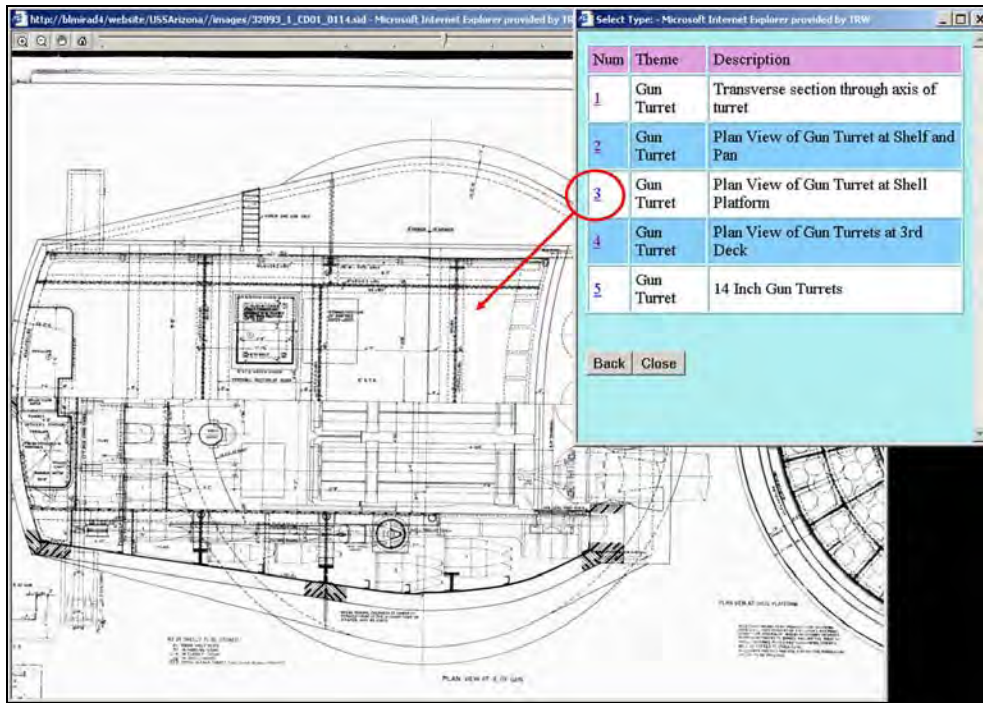
Figure 9.43. Selection by feature from blueprints. Each space is a separate entity and has associated features to access geodatabase. Clicking on a space brings up all additional data (Image from USAR GIS Project).
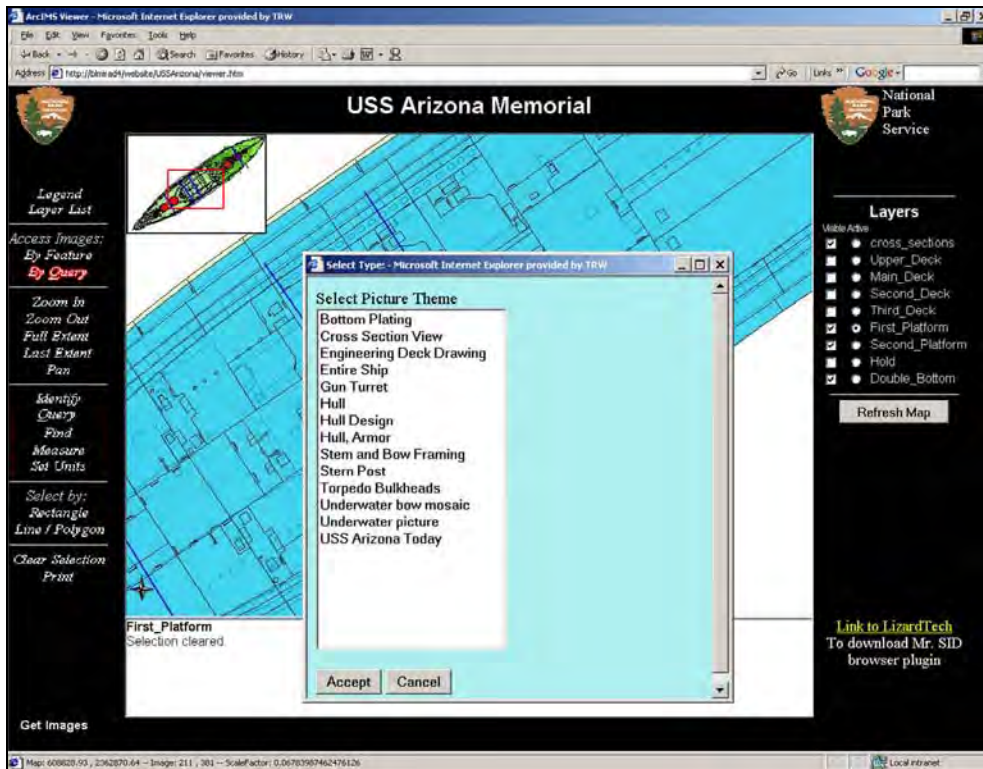
Figure 9.44. Example of accessing images and geodatabase by query (Image from USAR GIS Project).

image, a new browser window is opened to display the image. Each database image must have metadata, whose generation can be time consuming. Metadata enables the document management process to work. Each image is described and given a subject or "theme", much like a keyword, that links to specific features in the eight levels of the geodatabase by a unique feature-id (key field).

The final step in the process is to refine the project and database, eventually incorporating all scanned plans from *Arizona*, and porting the project to an NPS network, which would allow mobile and remote access to the plans and related data in the geodatabase by various researchers and, ultimately, the public.

REFERENCES

Henderson, S.
    1989 Biofouling and Corrosion Study. In *Submerged Cultural Resources Study: USS Arizona Memorial and Pearl Harbor National Historic Landmark*, edited by D. J. Lenihan, pp. 117-156. Submerged Resources Center Professional Papers No. 9. National Park Service, Santa Fe.

Lenihan, D. J. Editor
    1989 *Submerged Cultural Resources Study: USS* Arizona *Memorial and Pearl Harbor National Historic Landmark*. Submerged Resources Center Professional Papers No. 9. National Park Service, Santa Fe.

Lott, A.S. Editor
    1978 *USS* Arizona *Ship's Data: A Photographic History*. Fleet Reserve Association, Honolulu.

McCarthy, M.
    2000 *Iron and Steamship Archaeology: Success and Failure on the S.S. Xantho.* The Plenum Series in Underwater Archaeology, New York.

Murphy, L.E. and T.G. Smith
    1995 Submerged in the Past: Mapping the Beguiling Waters of Florida's Biscayne and Dry Tortugas National Parks. *Geoinfo Systems* 5(10):26-33.

    1996 Global Positioning System (GPS). In Encyclopedia of Underwater Archaeology, edited by James P. Delgado, pp. 171 -172. British Museum Press, London.

Paine R.W.
    October 7, 1943 Memo from Commandant Navy Yard , Pearl Harbor to Chief, Bureau of Ships. Subject: U.S.S. *Arizona* (BB-39) War Damage Report. On file, USS *Arizona* Memorial Archives, Honolulu.

Shope S.M., L.E. Murphy and T. G. Smith
    1995 Found at Sea: Charting Florida's Sunken Treasures *GPS World* 6(5):22-34.

CHAPTER 10

A Geotechnical Investigation of the Stress History and Settlement Potential of Sediment Supporting USS *Arizona*

Robert E. Kayen, Brad Carkin, and Homa J. Lee

INTRODUCTION

In November 2003, the National Park Service contracted a private drilling company, Ernest K. Hirata & Associates, Inc., to sample sediment at three borehole sites surrounding the USS *Arizona* Memorial. During a one week drilling effort, from November 13–20, 52 m of sediment were sampled.

The three boreholes are located as follows: B1A is located midship between the USS *Arizona* and Ford Island (E608813, N2362945) in 8.5 m of water at the time of drilling; B2 is located directly northeast of the vessel (E608943, N23662957) in 11.9 m of water at the time of drilling; B3 is located directly southwest of the vessel (E608749, N23662811) in 11.3 m of water at the time of drilling (Figure 10.1). The boreholes B1A, B2, and B3 have sub-bottom drill depths of 15.2, 21,3, and 15.2 m. USS *Arizona* is currently resting on the floor of Pearl Harbor, submerged and tilting away from Ford Island. Immediately following the attack, on December 7, 1941, portions of the deck and railing were sub-aerially exposed, along with the superstructure and guns removed during salvage operations (Figure 10.2). The superstructure and guns were removed in 1942. Photos taken in the winter and spring of 1942 clearly show much of the vessel

Figure 10.1. Boreholes B1a, B2 and B3 located around the hull of USS *Arizona*, west of Ford Island.
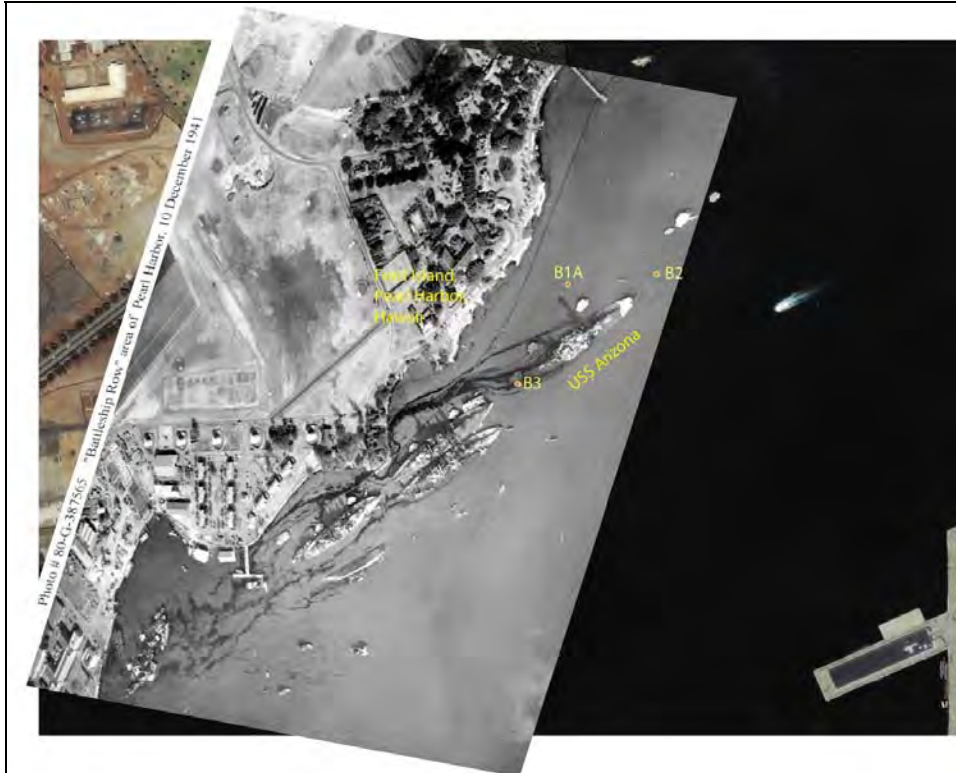
Figure 10.2. An overlay of DOD photo 80-G-387565, taken December 10, 1941, on Figure 10.1, showing the location of the vessel and boreholes. Most of the vessel was still sub-aerially exposed after the attack.

deck at, or above, water level (Figures 10.3–10.5). Today, 63 years later, the deck of the vessel is submerged in up to approximately 2 m of water.

This chapter investigates the settlement and tilt of the vessel through a geotechnical analysis of sediment drilled around the stern, shoreward mid-ship, and bow of the vessel. We characterize the state of stress within the sediment, the relation between that stress state and the effective overburden load placed on the sediment due to the existing sediment load, and the added stress of the submerged USS *Arizona*.

CORING OPERATIONS

Field sampling operations, taken from a small drill barge, were focused on collecting soil samples with several coring devices. In general, the drillers sampled sediment with either 100 mm Shelby tubes or 75 mm steel pipe (Figure 10.6). The Shelby tubes are enameled, non-reactive, sample tubes designed for acquiring sediment with saline pore water. The recovered samples are encased in whole-round steel liner tube and capped by the drillers, and then were transported to an onshore laboratory near the drill site.

The lithology of the samples and drill cuttings are presented in the appendix. The uppermost unit in all three boreholes is a silty sand/sandy silt (SM/ML) with shell fragments (upper yellow unit Figures 10.7, 10.8, and 10.9). Beneath this is a silty sand unit (gray) that thickens toward the north stern area. Borehole B1A is shoreward of the vessel and the silty clay there is interbedded with a coralline rubble and sand. Likewise, the silty sand near the stern is interbedded with silt and sandy silt that coarsens down core. What is most noteworthy regarding the cross-sections in Figures 10.7, 10.8, and 10.9, is the heterogeneity of the sediment beneath the vessel. A relatively stiff profile of silty sands and sandy silts is found near the bow section at B3, whereas, soft deformable fine-grained deposits thicken toward the stern (B2) with a corresponding thinning of stiffer silty sand and sandy silt deposits. Midship on the starboard, shoreward, side, a coraline rubble may provide some stiffening element to the sediment deposit that is not present at the stern, bow, or port side. A seaward thickening wedge of silty-sand is present in the bow (B3) area, whereas, a seaward thickening wedge of finer grained clay is found near the stern.

**Figure 10.3. Gunnery deck and deck railings visible above the harbor water in 1942
(USS Arizona Memorial Photo Archive).**

Figure 10.4. A photograph of USS *Arizona*'s damaged exposed deck (USS Arizona Memorial Photo Archive).

Figure 10.5. Salvage crews in 1942 were able to work on the deck above water and cut entry-ways into the vessel for recovery operations (USS Arizona Memorial Photo Archive).

Figure 10.6. A small anchored barge was used to advance the borehole. The deck and railings of USS *Arizona* are completely submerged in 2003, with the vessel tilting several degrees to the southeast (USGS Photo).
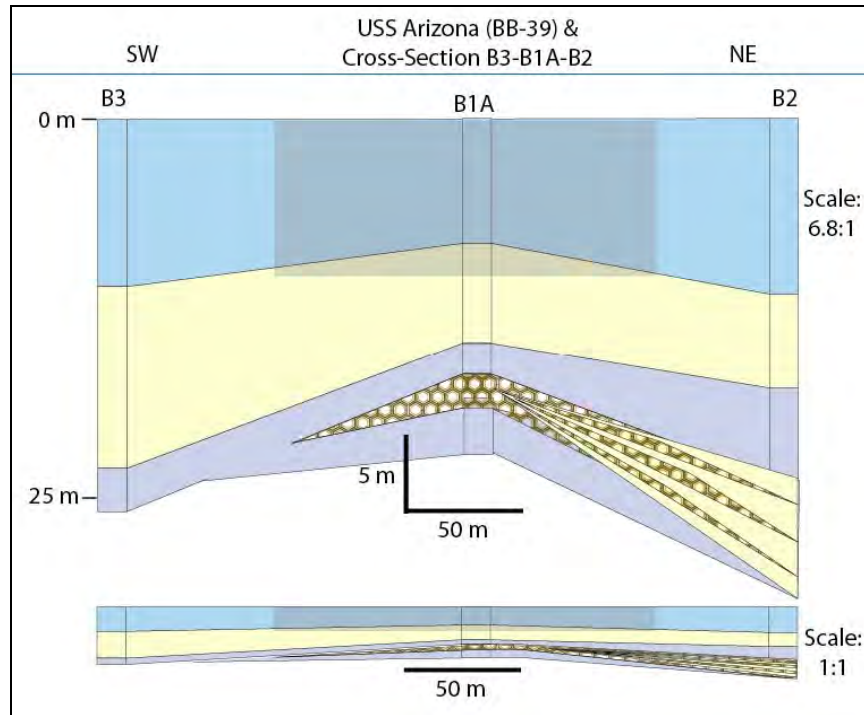
Figure 10.7. Cross-section from bow area (B3) to stern area (B2) through the shoreward midship boring (B1A). The upper blue unit is the water column. The seafloor is a silty sand and sandy silt underlain by a silty clay. The B1A clay unit is interbedded with a coralline rubble. B2 is a silty clay that transitions into a clayey silt with interbedded sandy silt. The gray shaded area is USS *Arizona*.
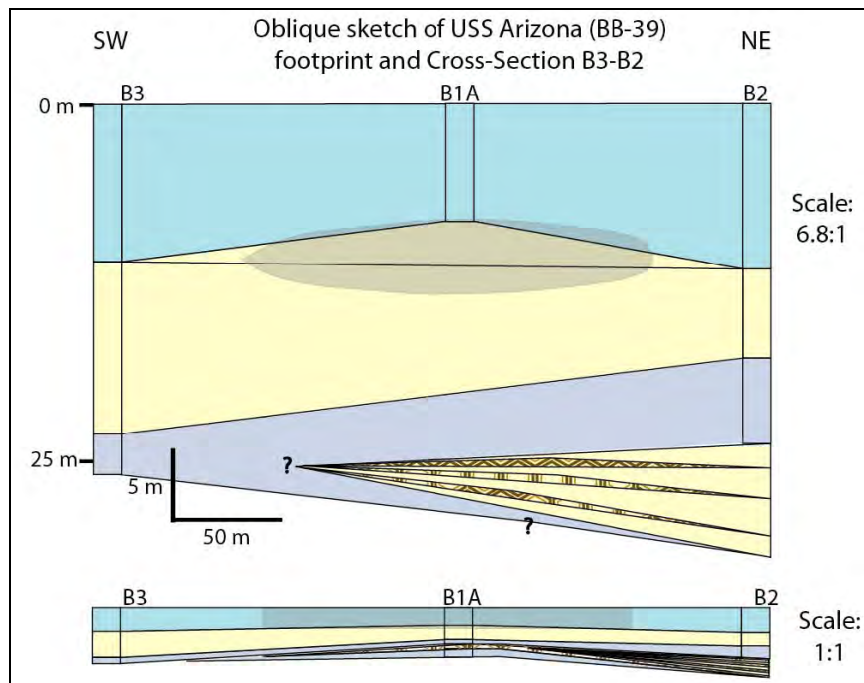
Figure 10.8. A proposed model of the lithology directly beneath *Arizona* between B3 and B2. The silty clay unit thickens toward the northeast (stern). Coraline rubble may be beneath the vessel midship, offshore B1A.
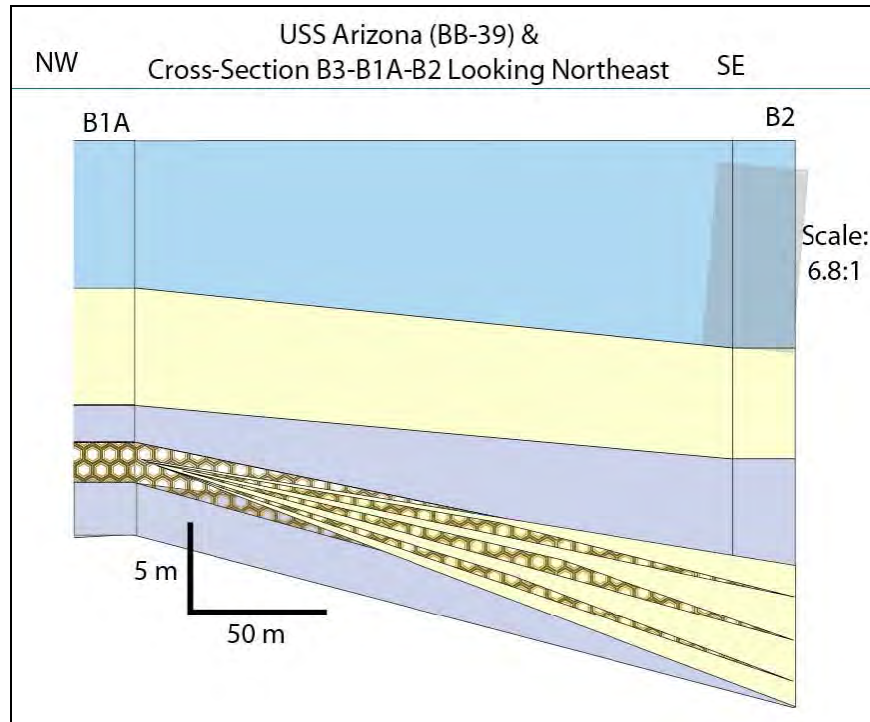
Figure 10.9. A proposed model of the downslope lithology between B1A and *Arizona* based on the B2 borehole to the northeast. The silty clay unit and the clay silt-to-sandy silt thickens toward the southeast (port side). Coralline rubble may be beneath the starboard side of the vessel midship, offshore B1A.

USGS MULTI-SENSOR CORE LOGGER

At the lab in Building 42, on Ford Island, samples in Shelby tubes were logged for their geotechnical properties on the USGS multi-sensor whole core sediment-logging device, built in Great Britain by Geoteck, Ltd. Sealed cylindrical sediment cores were placed horizontally upon a transport sled and moved by a computer-controlled stepper motor through a frame supporting three sensors (Figure 10.10). In a sequence, the logging device measures core diameter and attenuation of gamma rays from a ^{137}Cs source to compute soil wet bulk density. Measurements of density were typically taken at 1cm increments, often within the first hour after the cores are sampled. The transport sled is capable of carrying individual core sections up to 1.5 m in length. Because the core liner is steel, we are able to only characterize the bulk density of the sediment, but not the magnetic susceptibility of p-wave velocity.

The USGS developed an Apple HyperTalk™ driven software program called HYPERSCAN to automate the logger system and support a number of user and system tailored scanning options (Kayen and Phi, 1997). The program includes a suite of subroutines for system

Figure 10.10. USGS core sediment logger set up in Navy Building 42 during the drilling operations. An enameled steel Shelby tube is being scanned (USGS Photo).

calibration and permits the sensors to be activated or disabled. For example, at Pearl Harbor the cores retained sediment within metal core liner (e.g. Shelby tube samples) that not allow for measurement of magnetic properties: in this case we disabled the magnetic susceptibility sensor to increase the efficiency of the system. Computer automation also allows the technician to maintain some physical distance from the Cesium (^{137}Cs) gamma-ray source. During automated scanning, an un-split sediment core is driven down a track system in user-prescribed increments and the Macintosh computer interrogates sensors. As data enter the computer, the bulk density, and p-wave velocity and magnetic susceptibility if they were logged, are calculated, logged into a matrix data file, and presented in real-time on a 3-plot graphics display window.

Wet Bulk Density

Bulk density is the ratio of the total soil weight, to the soil volume. The configuration of our device allows for a core to pass between a scintillation counter and a vessel emitting a

one-cm columnated beam of gamma rays from a radioisotope ^{137}Cs source. Sediment bulk

density (ρ_b) is calculated from the gamma ray attenuation characteristics of the cores according

to Lambert's law. For a user-defined time period, the number of gamma decays emitted from

the Cesium-vessel, passing through the core and received at the scintillation detector is counted.

To address the health and safety concerns of technicians and satisfy the requirements of our

radiation use permits and NRC license, we use lead shielding to reduce the amount of gamma

ray emission away from the scintillation counter sensor to nearly background levels. The

number of scintillation's transmitted from the source to the scintillation counter through air, is

referred to as the unattenuated gamma count, Io. For the case where a homogeneous material of

some thickness, d, lies between the Cesium source and sensor, the attenuated gamma ray count,

I, can be related to the unattenuated number of gamma decays, Io, the material thickness, d, the

soil bulk density, ρb, and the soil Compton scattering coefficient, μs, by Lambert's Law (CRC

1969):

$$I = Io \exp \{-\mu_s \rho_b d\} \qquad [1]$$

The bulk density of the soil can be determined as follows:

$$\rho_b = 1/\mu_s d \ln (Io/I) \qquad [2]$$

For recovered whole sediment cores encased in liners, we must account for the influence of the

core liner to get an accurate estimation of the soil density. The liner correction accounts for

liner attenuation of the gamma-ray beam through absorption and scattering, effects controlled

by 1) the liner Compton scattering coefficient, μl; 2) liner wall thickness, l; and 3) liner wall

density, ρ_l. For sediment contained within a core liner of outer diameter, D, and double-wall

thickness, 2l, equation [2] can be rewritten as:

$$I = Io \exp\{-\mu s \rho_b(D-2l)\} \bullet \exp\{-\mu_l \rho_l 2l\} \qquad [3]$$

Equation 3 relates the attenuated gamma-ray count to the partial scattering influences of the

liner and soil, and can be used to assess the density of material contained within a variety of liner-types, both plastic and metal. To determine the bulk density of soil, equation [3] must first undergo transformation to base-e logarithm.

$$\rho_b = \ln(Io/I) - \mu_l \rho_l 2l / 1 / \mu_s \quad (D\text{-}21) \qquad [4]$$

CALIBRATIONS

Density measurements of soil contained within intact core-liner are calibrated to the known standards of water (ρ_w=1.00 g/cc) and aluminum (ρ_{al}=2.70 g/cc). These two standards serve as end-members that fully-bound the limits of soil density found at Pearl Harbor. The added advantage of using these materials is that their respective Compton scattering coefficients, μ_w and μ_{al}, are similar to those of soil pore water and soil alumina-silicate particles, although we determine these parameters empirically. To account for the influence of the liner, a water-aluminum standard is prepared by inserting a solid-cylinder of 6250 or 1100F aluminum into an unsplit section of core liner identical to the liner used for soil sampling. The length of milled aluminum fills one-half the total length of the "calibration standard"-core liner and distilled water fills the remaining portion. Caliper measurements of the liner diameter and wall thickness are made to determine the travel path-length through the liner and interior space.

During the density calibration, the numbers of scintillation's-per-second are logged for transmission of gamma rays through air to give a measure of Io. Similar measurements are made for the "calibration standard" to determine the scintillation count for water-filled liner, I_w, and aluminum-filled liner, I_{al}. We determine the attenuation ratios for water and aluminum (Io/I_w and Io/I_{al}) and solve for the remaining unknowns, $\mu l \rho_l$ and μs, by setting up two simultaneous equations and eliminating one of the variables. For each soil-core, we scan the whole-round sections using the same Compton scattering parameters that correct the calibration-standards water and aluminum to their known values of density.

Calibration standards are run repeatedly during testing programs. Typically, to calibrate the sediment-core profiles for density, measurements are made from our calibration-standard after every core is logged on our device. The empirical Compton scattering coefficient for soil that is determined by this method tends to be approximately 40% lower than the published value

for water, and at present the reason for this is unknown. The circular cross-section of soil cores, as compared with an idealized tabular cross-section may be the cause of the lower µs, and future experiments are planned to assess the influence of core liner geometry on the scattering of gamma-rays.

After system calibration is complete, soil cores are run through the logger system and calibration corrected densities and velocities are presented, along with magnetic susceptibility, on a real-time graphics display. Typical run-time for driving a 150 cm core through the sensor array is approximately 35 minutes.

SYSTEM QUALITY ASSURANCE AND QUALITY CONTROL

Several approaches are taken to assess the quality of our non-invasive measurements of bulk density and sound speed velocity through a core liner. After extensive use of our system at sea and in our shore-based laboratory, several hundred calibration log files containing 30 or more data points were separated into individual files for water-filled and aluminum-filled core liner. These material dependent sub-sets of the calibration files were then used to calculate the mean and standard deviation for the measured density and velocity and compared with the known values for water and aluminum presented in parenthesis (Table 10.1).

The mean value of the calculated and measured density of distilled water was within 0.4% of the known value and the mean value for aluminum was exactly the known value. It was found that the standard deviation for density measurements is on the order of 0.6-1.0% of the measured value.

Density Statistics	Distilled Water	Aluminum
Mean Density (g/cc) (Known ρb)	1.004 (1.00)	2.700 (2.70)
Density Std. Dev. (g/cc)	0.010	0.016

Table 10.1. Data quality for gamma-ray bulk density (Known values are shown in parentheses).

RESULTS FROM THE USGS MULTI-SENSOR CORE LOGGER

Whole round core samples were scanned using the logger device within 24 hours of their initial sampling. Sediment recovery varied widely depending upon lithology type. Almost no recovery occurred in the uppermost silty sand, sandy silt, gravel, and coralline rubble deposits of the three borings. Beneath the coarse upper unit are silty-clay and sandy-silt deposits that had recovery of 68-100% of the length of the sample tube. The wet bulk density profiles are intermittent sections through the sediment column with gaps of unknown density properties in-between, although the lithologies of these gaps are recorded. The tops of the tubes are only partly filled, such that the computed density falls off due to the large water filled void. This void is eliminated in our stress calculations, but presented here in Figure 10.11.

Consistent with the lithologies noted in the Hirata & Associates report (see Appendix), a higher density deposit, typical of coarse grained sediments is found toward the bow of the vessel (B3); a low density deposit, typical of finer grained sediment is found near the stern of the vessel (B2). At B1A, mid-ship and shoreward of the hull, a coarse higher density deposit fines downward through the sampled section. The density profile for B2 was used to compute the natural seafloor effective overburden stress above consolidation test samples.
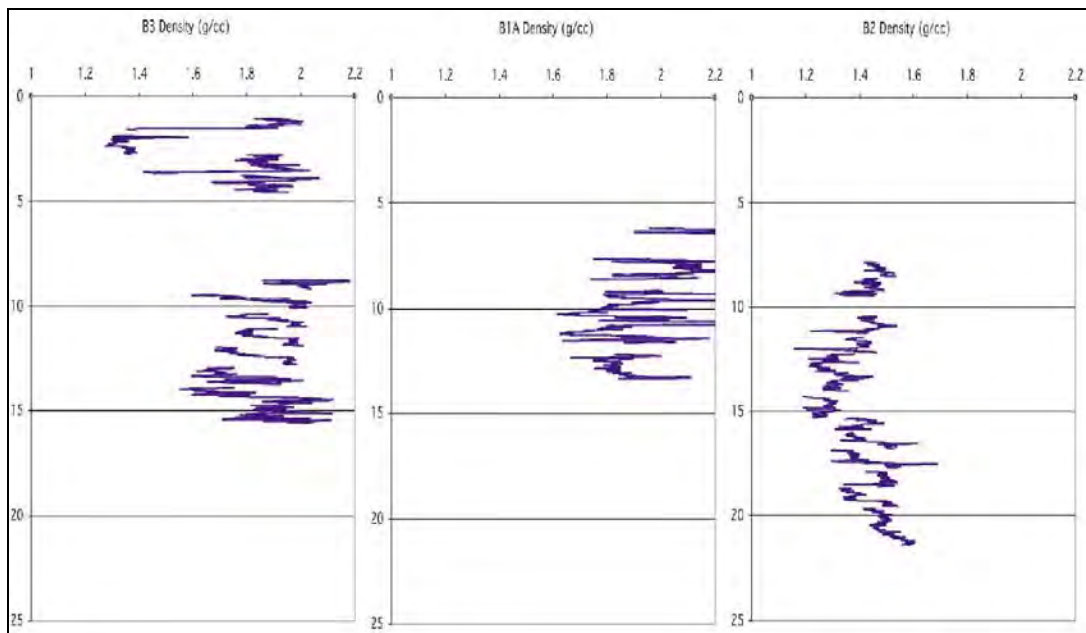
Figure 10.11. Wet bulk density of samples taken at borings B1A, B2, and B3.

CONSOLIDATION TESTING FOR STRESS HISTORY

A suite of 12 consolidation tests were performed on sediment samples from borehole B2, the thickest accumulation of fine grained sediment among the three boreholes (Table 10.2). Consolidation tests are performed to determine the settlement characteristics and the maximum past pressure felt by the sediment (σ'_{vm}). Twelve consolidation tests were performed within a triaxial cell using either a constant rate of strain-loading technique developed by Wissa and others (1971) or the traditional incremental loading method of Casagrande (1936). In preparation for this procedure, a thin wafer of sediment was confined within a cylindrical ring and placed at the base of a fluid filled cell. After the cell was filled with de-aired water the sediment was uniaxially loaded either at a constant rate of compressive strain or incrementally loaded with static weight. During this procedure pore water pressure, axial deformation, and axial load were continually monitored and automatically computer-logged at predetermined intervals.

From the consolidation data the void ratio (e) (volume of the voids/volume of the solids) was plotted versus the log of the vertical effective stress. With such a plot, a curve similar to that in Figure 10.10 is usually produced. The right side of the curve defines a straight line called the "virgin compression line." The slope of this line is the compression index (Cc). The compression index indicates the amount of void ratio change for a tenfold increase in vertical stress beyond σ'_{vm}. Extrapolating the virgin curve to higher void ratios and employing the

Core	Depth ft.	Interval cm	Icon #	σ'_{vm} (ksc)	C_c	e_o	σ'_{vo} (ksc)	OCR	σ'_e (ksc)	Quality	Sample lith type
B2	27.5-30	65.8-68.3	Icon 205			3.23	0.45466071			Unusable	soft clay , swirled disturbed mix
B2	32.5-35	86.3-88.8	Icon 202	0.64	0.97	2.5	0.530125574	1.207261132	0.109874426	Poor	soft, darkgreenish-blackish gray clay, homogeneous
B2	42.5-45	87.5-90	Icon 208			3.11	0.681055301			Poor/Unusable	soft, sticky, dark greenish gray clay
B2	45-47.5	88.3-85.8	Icon 206	0.52	2.3	4.69	0.718787732	0.723440282	-0.198787732	Poor	uniform, soft gray clay
B2	47.5-50	82.3-84.8	Icon 203	0.82		2.31	0.756520164	1.083910302	0.063479836	Good	gray silty clay
B2	47.5-50	87.3-89.8	Icon 204	0.86	2.5	4.34	0.756520164	1.136783976	0.103479836	Fair	soft, gray silty clay, homogeneous; wood fragment?
B2	52.5-55	06.3-08.0	Icon 207	0.93	1.89	3.18	0.031905020	1.117808577	0.098014972	Very Good	soft, greenish gray clay
B2	55-57.5	87.3-89.8	Icon 200	0.86	1.19	2.49	0.86971746	0.988826878	-0.00971746	Very Good	soft, uniform, olive gray clay; minor thin shell fragments
B2	57.5-60	86.2-88.8	Icon 199	0.9	1.2	1.49	0.907449891	0.9917903	-0.007449891	Fair	olive gray sticky clay
B2	65-67.5	86.3-88.8	Icon 201			2.44	1.020647187			Poor/Unusable	soft, dark gray, sticky clay; minor thin-walled shell fragments
B2	67.5-70	81.8-84.3	Icon 197	0.82	0.71	1.98	1.058379618	0.774769266	-0.238379618	Fair	grayish black sticky clay
B2	67.5-70	85-88	Icon 196	0.55	0.71	2.18	1.058379618	0.519662312	-0.508379618	Poor	soft, dark greenish gray, sticky clay
B3	40-42.5	84.6-87.3	Icon 198			1.43				Poor/Unusable	stiff, mottled, yellowish-greenish gray clay

Table 10.2. Consolidation test results from fine-grained samples. Listed are the borehole (core); sub-bottom depth (ft); depth in the Shelby tube (cm); test number; maximum past pressure; compression index; initial void ratio; estimated effective overburden pressure (ksc); OCR; excess effective stress; test quality; and sediment characteristics.

Casagrande (1936) graphical construction, the maximum past stress can be calculated. A measure of the consolidation state is the overconsolidation ratio, the ratio of the maximum past pressure felt by the sample (σ'_{vm}) by the *in situ* effective (buoyant) overburden stress (σ'_c). The individual test plots for each consolidation test are presented in the Appendix with calculations of initial void ratio and the coefficient of compression.

An OCR of 1.0 indicates normally consolidated sediment, meaning that the sediment is in equilibrium with the current thickness of overburden of sediment. For OCR of less than 1.0, the sediment has not yet fully consolidated to the *in situ* overburden stress, whereas for OCR greater than 1.0 indicates that the sediment has experienced pressures in excess of current overburden loads. Overconsolidation of near-surface sediment is caused by, among other factors, electro-chemical bonds, overburden erosion, cementation, and current reworking. Often, overconsolidation is a near surface phenomenon and is lost at depth. Another measure of consolidation state is the effective excess pressure, σ'_e, that is $\sigma'_{vm} - \sigma'_{vo}$. This parameter is useful for estimating the amount of stress equivalent of material removed above a sediment deposit.

The results of the consolidation test suite strongly indicate that the sediment surrounding USS *Arizona* is normally consolidated. Overall, the samples lack excess effective stress; that is, they are in equilibrium with the overburden sediment. Thus any application of new stress will drive the sediment into the virgin compression regime, initiating new settlements of the loaded sediment.

STATIC SEDIMENT STRESS EXERTED BY THE SINKING OF USS *ARIZONA*

USS *Arizona* was commissioned in 1916 at the Brooklyn Navy Yard, New York. The full weight displacement of the vessel, assumed here to be the vessel weight in December 1941, was approximately 37,600 tons. The total and buoyant density of steel is 7.85 and 6.82 g/cc, respectively, thus the submerged weight of the vessel beneath the waterline is approximately 33,000 tons (30.5M kg). The Length and beam, at the waterline, of the vessel are 185 m and 29.6 m, respectively, and we estimate the area of the flat bottom to be 4,300 m^2. Thus the effective stress of the vessel acting uniformly on the seafloor directly beneath the centerline of the vessel is approximately 30.5M kg/43M cm^2, or 0.70 kg/ cm^2. This stress level is equivalent to approximately 9 m of deposited sandy sediment with a bulk density of 1.8 g/cc.

SETTLEMENT ANALYSIS

A preliminary analysis of the vertical settlement of sediment beneath the vessel assumes that the hull is a rigid mat that is uniformly loading the ground beneath the centerline of the vessel. The initial void ratio (volume of the solid particles/volume of the void space) of the soil deposit can be estimated from the core sediment logger profiles assuming a grain specific gravity for the solid particles, and from the initial state and consolidation characteristics of the consolidation test samples. Table 10.3 lists the initial void ratio estimates for each of the Shelby Tube soil samples tested, and the individual test results are presented in the Appendix. Based on the observation of normal consolidation (OCR ~ 1.0) in all the test samples, the void ratio and full consolidation under an additional load of 0.70 kg/ cm^2 is computed as follows:

$$e = eo - C_c LOG \{P/P_o\} \tag{5}$$

where P is the effective overburden stress of the overlying soil (P_o) plus the added stress of the vessel pressure on the seafloor (assumed to be 0.7 kg/ cm^2). The fine-grained portion of the sediment column, susceptible to the majority of the settlement was subdivided into individual layers represented by the Shelby tube sample taken within it. These layers have variable thicknesses $H_{inc.}$ depending on the sampling depths. We compute the individual layer settlement as:

$$\Delta H_{inc.} = H_{inc.} * (eo - e)/(eo + 1) \tag{6}$$

And the total settlement ΔH beneath the vessel as the sum of the incremental settlements, or

$$\Delta H_. = \Sigma \Delta H_{inc.} \tag{7}$$

The addition of the USS *Arizona* pressing on the seafloor exerts 0.7 kg/cm2 on top of the prior stress level of the sediment effective overburden (Table 10.3). We estimate that near the borehole area B2, these loads resulted in ~1.6 m (5 ft.) of settlement of the foundation sediment beneath the vessel. This slow process of consolidation followed the abrupt initial impact of the vessel on the seafloor. These settlements, unlike the initial loading of the seafloor on December 7 that likely resulted in some bearing failure of the near surface sediment, would

Core	Depth ft.	σ'_{vm} (ksc)	C_c	e_o	σ'_{vo} (ksc)	e	H_{inc} (m)	Δh (m)	$\Delta h/H$
B2	27.5-30			3.23	0.455	2.650	2.846	0.391	0.137
B2	32.5-35	0.64	0.97	2.5	0.530	2.145	0.762	0.077	0.101
B2	42.5-45			3.11	0.681	2.670	3.049	0.327	0.107
B2	45-47.5	0.52	2.3	4.69	0.719	4.011	0.762	0.091	0.119
B2	47.5-50	0.82		2.31	0.757	1.902	0.762	0.094	0.123
B2	47.5-50	0.86	2.5	4.34	0.757	3.629			
B2	52.5-55	0.93	1.89	3.18	0.832	2.679	1.524	0.183	0.120
B2	55-57.5	0.86	1.19	2.49	0.870	2.185	0.762	0.067	0.087
B2	57.5-60	0.9	1.2	1.49	0.907	1.192	0.762	0.091	0.120
B2	65-67.5			2.44	1.021	2.115	2.287	0.216	0.095
B2	67.5-70	0.82	0.71	1.98	1.058	1.823	0.762	0.040	0.053
B2	67.5-70	0.55	0.71	2.18	1.058	2.023			
					Total Settlement		TOTAL H (m)	1.576	

Table 10.3. Settlement analysis of sediment beneath the hull of USS *Arizona*. A load of 0.7 kg/ cm^2 was used in addition to the effective overburden pressure to represent the new application of loads of the USS Arizona and overburden sediment on the seafloor directly beneath the centerline of the vessel. At the edges of the hull, and away from the vessel, the load exerted by the hull diminishes as a function of depth and lateral distance.

need years or even decades to complete before equilibrium was reached between the new loads. Thus, portions of the vessel subaerially exposed in the 1942 salvage operations are now submerged beneath approximately1-2 m of water. The tilt of the vessel, seaward is likely due to the seaward thickening wedge of fine-grained sediment. In a future analysis we will estimate the amount of total predicted tilting that can be expected at the memorial site. The heterogeneity of the soil deposits beneath the vessel indicates that the stern overlies a large wedge of soft-fine-grained sediment capable of large settlements, whereas the bow is founded on stiffer deposits of sandy silt and silty sand, with less clay near the surface. It is likely that this sediment variability has resulted in the stern settling to a greater extent than the bow.

CONCLUSIONS

The study presented here, addresses the potential for normal settlement processes to affect the orientation and elevation of USS *Arizona*, with respect to the seafloor and the waterline. Three boreholes around the vessel indicate that the vessel rests upon highly variable sediment. The settlement potential of the vessel is greater toward the stern, and toward the port side (bay side). A coralline rubble layer observed at boring B1A midship on the shoreward side

may act to prevent settlement of the vessel there and may amplify tilting toward the bay. The presence of the stiffer rubble zone may also enhance differential settlement beneath the vessel that can result in hull stresses that deform the underbody of the vessel. In the area of maximum settlement potential, we compute a estimated settlement at full consolidation of approximately 1.6 m. Future measurement of the stiffness properties of the sediment, and monitoring of the settlement of the vessel is recommended. A 2-dimensional settlement analysis is needed to estimate the final degree of seaward tilting that is expected to occur.

REFERENCES

Casagrande, Arthur
1936 The Determination of the Pre-Consolidation Load and Its Practical Significance. In *Soil Mechanics and Foundation Engineering* Vol. III, pp. 60-64. Cambridge, Ma.

Kayen, R. and Phi, T.N.
1997 A Robotics and Data Acquisition Program for Manipulation of the U.S. Geological Survey's Ocean Sediment Core Logger. *SciTech Journal* 7 (5):24-29.

Kayen, R., Edwards, B. D., Lee, H. J.
1999 Nondestructive Laboratory Measurement of Geotechnical and Geoacoustic Properties through Intact Core-liner *Nondestructive and Automated Testing for Soil and Rock Properties, ASTM Special Technical Publication-1350,* W. A. Marr and C.E. Fairhurst *eds*., *American Society for Testing and Materials*, p. 83-94.

Wissa, A. E., Christian, J. T., Davis, E. H., and Heiberg, Sigurd
1971 Consolidation at Constant Rate of Strain. *Journal of the Soil Mechanics and Foundations Division, ASCE,* 97 (SM10):1393-1413.

CHAPTER 11

Conclusions and Recommendations

Matthew A. Russell and Larry E. Murphy

The interdisciplinary research approach to characterizing and understanding USS *Arizona* deterioration and integration into a predictive model reported here was designed to produce cumulative data whose synthesis will inform management actions regarding long-term stewardship of this National Historic Landmark vessel. Beyond informing management decisions about *Arizona*, we believe this research approach has produced results that contribute to the disciplines involved, and are directly applicable to the thousands of steel legacy vessels submerged worldwide. Although lack of complete funding resulted in gaps in our knowledge about critical aspects of *Arizona*'s deterioration, we have learned a great deal that will allow National Park Service (NPS) and U.S. Navy managers to make correct decisions about immediate needs within a stewardship framework. In addition, because the *Arizona* research is not complete and is ongoing, the work reported here is an important step toward refining questions that guide future research directed toward a full understanding of *Arizona*'s deterioration.

In this concluding chapter, we briefly reiterate the goals and objectives of the USS *Arizona* Preservation Project. We then summarize conclusions from each of the research domains that contributed to the overall research project, and synthesize the data to provide some answers to our basic research questions. Finally, we present specific recommendations for future

research, which, along with continuing the monitoring program, requires sufficient dedicated funding to ensure completion.

This chapter's conclusions represent what we have learned so far about USS *Arizona*'s deterioration. Because *Arizona* research is not complete, and data derived from the monitoring program have not been generated and incorporated, these conclusions will be refined and may change as data-gaps are filled and new information is added. Data presented here represents the most informed view of the ship based on observations, investigations and experimentation by experts in numerous fields, but it is necessarily incomplete because not all research domains could be completed.

GOALS AND OBJECTIVES

The USS *Arizona* Preservation Project's primary focus was to acquire requisite data for understanding and characterizing the complex corrosion and deterioration processes affecting *Arizona*'s hull, both internally and externally, and to model and predict the nature and rate of structural changes resulting from corrosion. In simple terms, our basic question, which was articulated by the first two superintendents, Gary Cummins and Bill Dickinson, has been "what is happening to *Arizona*'s hull, and how quickly is it happening?" Hull deterioration rates have direct implications for potential release of oil still contained within the ship. Understanding the complex hull corrosion processes, structural changes and oil release patterns studied during this research project offers the most effective method of mitigating the potential oil-release hazard and achieving the balance between site stewardship and environmental impact.

PRINCIPAL RESEARCH DOMAIN CONCLUSIONS

Each of the specific research domains addressed during this project either directly or indirectly relates to our principal goals and objectives. Here, we briefly discuss each research domain and highlight how they are related, beginning with broadest research domain and working through the contributing studies.

The finite element model (FEM) created by the National Institute of Standards and Technology (NIST) is the cumulative product incorporating field and experimental data that

most directly addresses questions regarding how quickly *Arizona* is deteriorating (Chapter 6). This model incorporates all the data gathered and synthesizes it into a computer-based mathematical projection depicting actual structural deterioration in calendar years, which are derived from corrosion rates. For now, funding has only allowed development of an 80-ft. section, frames 70–90, from the midships of the 608-ft. battleship.

To accurately predict deterioration rates of *Arizona*'s structural elements, we needed to know steel corrosion rates in all locations of *Arizona*'s hull. Determining these corrosion rates was the primary goal of a corrosion study coordinated by University of Nebraska-Lincoln and the NPS (along with contributions by many other organizations) (Chapter 5). The corrosion study included a metallurgical and metallographic analysis to characterize *Arizona*'s steel to allow a more accurate corrosion characterization. It included direct measurements of corrosion rate by sampling *Arizona*'s hull steel, and it also involved a detailed concretion study to determine a minimum-impact way to predict corrosion rates in locations where direct measurement could not be accomplished. In addition to accurately constructing the baseline FEM using original construction data, corrosion rates determined by this corrosion study were the most important elements in the FEM for accurately predicting structural deterioration sequence and rates.

An important element in determining the nature and rate of steel corrosion is characterization of the environment in which steel corrosion is taking place. Basic chemical properties of seawater and data about water movement are critical for accurate corrosion characterization. In addition, because seawater properties directly influence corrosion, correlating measured seawater properties with known corrosion rates on *Arizona*'s directly accessible exterior was an important goal. It allows us to infer corrosion rates inside the hull, where we cannot directly measure corrosion rates either through hull sample collection or concretion analysis, but where we can collect environmental data using an ROV-mounted water quality instrument. Long-term environmental monitoring coordinated by the U.S. Geological Survey (USGS) and the NPS was therefore a key project component (Chapter 4). Although these measurements are ongoing, interior measurements are limited to accessible spaces. However, the interior has very little to no dissolved oxygen present. These data will be incorporated into the next iteration of the FEM to refine interior corrosion rates.

Also contributing to the overall corrosion study is an analysis of microbially induced corrosion undertaken by Harvard University (Chapter 7). The presence and effect of microorganisms on corrosion rates is especially relevant in the anaerobic environment deep within *Arizona*'s hull. Combined with oil within bunker spaces, microbes may have created a unique corrosion environment. Because these areas are impractical to sample, laboratory experimentation will be necessary to determine microbial impact to corrosion in the interior and in the oil bunker spaces.

In addition to the corrosion study, an analysis of hull stability was also necessary for completing an accurate FEM. The FEM would be compromised if *Arizona* were sitting in an unstable geological matrix, or was continuing to shift or sink within the supporting sediments of the Pearl Harbor bottom. In addition, high-resolution GPS hull monitoring would not be valid. To address these concerns, the USGS conducted a detailed geotechnical analysis of sediments surrounding *Arizona* to ascertain their stability and state of compression and determine if *Arizona* were potentially experiencing external movement from sediment shifts (Chapter 10). At the same time, the NPS conducted on-going GPS and other monitoring of the hull to measure both external and internal hull movement (Chapter 9), for which sediment compression provides the basic control.

Finally, the Medical University of South Carolina's (MUSC) chemical characterization of oil being released from *Arizona*'s hull was important for a number of reasons (Chapter 8). First, data were used in a supporting role, indirectly allowing us to make limited inferences about the condition of oil bunkers deep within *Arizona*'s hull that also allows an important monitoring variable. Second, MUSC's oil analysis was a key research domain because it allowed us to trace the environmental impact of the continually seeping oil presently being released into Pearl Harbor from *Arizona*. On-going monitoring of oil release rates by the NPS contribute to this analysis and give us another line of evidence for assessing the overall condition of the battleship's hull (Chapter 9). Continuing periodic analysis of oil samples are important to track potential internal hull structure changes.

In the following sections, we summarize conclusions from each research domain and from supporting studies through the final product, to demonstrate how data from each research domain contributes to the next, building towards answers to our most basic questions.

ENVIRONMENTAL PARAMETERS

Principal Questions: What is the nature of the interior and exterior environment of *Arizona*? How is *Arizona*'s environment changing? How does it affect *Arizona*'s deterioration?

Exterior Environment

Continuous current and wave data, along with water-column properties, were collected on and near *Arizona* from November 2002 to April 2005. Oceanographic measurement indicate that tides are a mixed, semi-diurnal type with a minimum, mean and maximum tidal range of 0.4 m, 0.6 m and 0.9 m, respectively. Generally, waves are not an important factor in the vicinity of USS *Arizona*'s hull. Those observed were, while long period (~20 s), very small (order of cm's) and likely due to open-ocean long-period swell. Vessels passing close to the study site are likely responsible for the high-amplitude, low-period motions that were observed. Water flow along the 10-m isobath is dominated by semi-diurnal and diurnal tidal motions, which are modulated to some degree by what appears to be wind forcing during the mid- to late afternoon. Water flow at the surface is down-wind to the southwest. Water flow throughout most of the water column is primarily parallel to *Arizona*'s hull at 0.01-0.02 m/sec and net flow is to the northeast. Flow closer to the seafloor, however, is weaker and more variable in direction. Flow speeds are faster off the port side than the starboard side of *Arizona*'s, and thus the water replenishment times on the port side of the hull are shorter than off the starboard side.

Water column studies showed temperatures were generally slightly higher (mean = 26.03 °C) and less variable (standard deviation = 1.17 °C) along the 10-m isobath than along the 3-m isobath (mean = 24.55 °C, standard deviation = 2.08 °C). A thermocline was often present in the harbor's waters, with the shallower (3 m) and deeper (10 m) water temperatures often differing by more than 2 °C. Water temperatures along the 10-m isobath were generally cooler and less variable off the port side of the hull than off the starboard side, possibly due to faster replenishment times and greater mixing of the water column. Salinity ranged from 16.78 PSU and 42.56 PSU, with a mean ± one standard deviation of 34.33 ± 4.25 PSU. Salinity appears to positively correlate with water temperature and suggests that Pearl Harbor's waters are influenced by freshwater runoff or groundwater effluence in the winter months. pH ranged

between 7.60 and 9.10, with a mean ± one standard deviation of 8.04 ± 0.15 and dissolved

oxygen 0% and 288.5%, with a mean ± one standard deviation of 69.5 ± 58.8%. Both pH and

dissolved oxygen tended to correlate with the daily insolation cycle, increasing during the

morning into the early afternoon followed by decreasing through the night to minimum levels

just before sunrise. Oxygen-reduction potential ranged between 150.0 mV and 397.2 mV, with a

mean ± one standard deviation of 289.2 ± 50.6 mV. Oxygen-reduction potential had an *inverse*

with pH and the percentage of dissolved oxygen during the summer months and a *positive*

relationship with pH and the percentage of dissolved oxygen during the winter months when

temperature and salinity were more variable. During the vertical profiling, near-surface

temperatures were on average roughly 1.03 °C warmer than the near-bed temperatures, near-

surface temperatures were roughly 0.85 PSU less saline on average than the near-bed salinities

and near-surface dissolved oxygen levels were on average roughly 43.9% higher than the near-

bed dissolved oxygen levels.

Combined, these observations support the conclusion that on *Arizona*'s exterior,

corrosion rates are higher in shallow water near the surface, and they decline in deeper water

near the harbor bottom. In addition, this analysis supports the observation that corrosion rates

are slightly higher on the port side of *Arizona*'s hull than the starboard side.

Interior Environment

On *Arizona*'s interior, in general, most parameters were very similar inside the ship as

outside. Temperature, salinity, and pH were all within a normal range of variability. Dissolved

oxygen and oxygen-reduction potential, on the other hand, varied significantly from baseline

measurements outside the hull. The most significant observation is that dissolved oxygen

decreased to near-zero within interior spaces that do not receive active seawater exchange. Most

significantly, on the third deck, which has no direct access to exterior seawater except through a

single vertical hatch, dissolved oxygen averaged only 4.1% saturated. With the exception of a

small portion of the first platform accessible through barbette no. 3, there is no access to any

interior spaces below the third deck. However, based on data from the third deck and within the

torpedo blisters, which indicate that dissolved oxygen can reach 0.0% saturated in spaces that do

not have seawater exchange, it is probable that *Arizona*'s interior spaces below the third deck

have extremely low levels of dissolved oxygen, and may even be at 0.0% saturated. Because all of *Arizona*'s original oil storage spaces are below the third deck, and the majority of *Arizona*'s remaining oil is likely still stored in those spaces, it is probable they are undergoing very low corrosion rates. These measurements are supported by dissolved oxygen measurements of interior water during removal of hull coupons. There was no detectable oxygen at all in the interior water.

MICROBIOLOGY

Principal Questions: What microbially induced corrosion (MIC) is taking place in *Arizona*'s interior and exterior areas, and what is the impact on structural deterioration? Can laboratory experimentation model microbially induced corrosion on the oil/bunker interface?

The purpose of microbiological research on *Arizona* was to investigate the role of microorganisms in steel hull corrosion. Specific goals included isolating and identifying microorganisms from the Pearl Harbor, especially within the concretion covering *Arizona*'s steel hull; determining the organisms within the community responsible for corrosion of steel; and investigating environmental parameters that may influence the rate of corrosion by microorganisms.

Harvard University researchers examined the potential role of microorganisms from Pearl Harbor in steel corrosion through laboratory experimentation. Preliminary indications suggest a trend toward pitting corrosion caused by microbes in the biofilm. The bacterial community in concretions on *Arizona*'s hull is dominated by organisms from three groups: Firmicutes, Flavobacteria, and Proteobacteria. Further investigations of concretion microorganisms are needed to determine if the results obtained here are applicable to concretions on other submerged heritage sites and to determine the effect of the microorganisms on corrosion of the underlying metal.

Ultimately, this research is a work in progress. Because key elements of this project remained unfunded during the USS *Arizona* Preservation Project, few conclusions can be made regarding the role of microorganisms in *Arizona*'s corrosion rate. Future work to be done on this project includes further study of the potential of microorganisms to cause corrosion of ASTM A-

36 steel, determining the effects of environmental factors such as temperature, nutrient levels and redox on MIC, and examining microbial corrosion rates on other types of steel that may be found in USS *Arizona*.

CORROSION ANALYSIS

Principal Questions: What is the nature and rate of corrosion taking place on *Arizona*? How does concretion formation affect corrosion rate? Is there a difference in corrosion rate among the original construction steel, the refit materials, and structure affected by the blast and fires?

Metallurgical and Metallographic Analysis

Metallurgical and metallographic analysis indicates steel used to fabricate USS *Arizona* battleship during original construction, 1913–1915, and reconstruction, 1929–1931, were consistent with the best steel available during each time period. The structural steel used in original construction was of surprisingly good quality for a basic open hearth steel technology that was only about 25 years old at the time the first materials were ordered for delivery to the New York Navy Shipyard for *Arizona*'s construction. The somewhat lower quality of the early steel in terms of chemistry and microstructure had no measurable consequences on the damage that occurred on December 7, 1941 or on the results of the present investigation into the deterioration of the *Arizona*'s hull. Typical analysis and comparison with present-day ASTM A-36 steel show minor differences in chemistry between the USS *Arizona*-era steel and present-day ASTM A-36 steel, however they are not considered significant with regard to corrosion response.

Heavy banding in steels from both periods could adversely affect the corrosion resistance under anaerobic conditions that prevail during a corrosion cycle developed under hard concretion layers that began to form when the ship sank. Banding would have no effect on corrosion rate under aerobic conditions that may occur on local areas on the exterior hull.

Exterior Corrosion Analysis

Concretion Analysis

Results of concretion analysis confirm that concretion acts as a sink for iron corroded from the adjacent steel hull, accounting at one location for about 60% of the iron lost from the hull. In other words, as the steel corrodes, iron molecules migrate from the hull into the concretion covering the ship. Based on x-ray diffraction (XRD) data, iron appears primarily as iron carbonate with lesser amounts of magnetite. These observations are confirmed from *in situ* corrosion potential and pH measurements by superimposing the data on a calculated potential/pH Pourbaix diagram. The data correspond to fields stable with respect to iron carbonate and magnetite.

Concretion XRD reveals the compounds $FeCO_3$, $CaCO_3$ and Fe_3O_4. A mean iron content of 53% is calculated from environmental scanning electron microscopy (ESEM) data while x-ray fluorescence (XRF) reveals 43% on a different sample. Direct chemical analysis of the same sample used for XRD reveals comparable iron content. Superposition of E_{corr}/pH data on the water-iron-CO_2 system confirms the presence of siderite and magnetite from the steel hull through the concretion cross-section to sea water. Results indicate that concretion characteristics vary as a function of water depth. Studies continue to correlate these properties with corrosion rate.

Corrosion Rate

For assessing corrosion rate of *Arizona*'s hull, direct measurement of hull thickness and comparison to original thickness is the most accurate methodology, but obviously it is not minimum-impact nor is it impractical for quick and cost-effective assessment. An alternative methodology developed on USS *Arizona* by University of Nebraska-Lincoln researchers, Concretion Equivalent Corrosion Rate (CECR), is beginning to prove itself in this and other applications as a minimum-impact approach for assessing corrosion rate.

Sufficient data at exterior hull locations are now available to determine corrosion rates from the water surface to the harbor bottom, port and starboard. While hull coupon sampling

was only undertaken at frame 75, previous E_{corr} transect surveys indicate that these data are typical of corrosion rates anywhere along the hull in contact with sea water above the harbor bottom. Data suggest that the corrosion rate is slightly higher on the port side above about 20 ft. water depth—deeper than that, the rates converge to equivalent values. On the exterior hull, the corrosion rate follows an empirical equation derived from the best fit for combined data, port and starboard, which is valid to just above the harbor bottom and which can be used to predict corrosion rates across the hull:

$$i_{corr} =\ \ 2.956 –\ \ 0.050\ WD)$$

where

i_{corr} is the corrosion rate in mils per year (mpy)

WD is water depth in ft.

Corrosion rate decreases with water depth, as is consistent with a decreasing dissolved oxygen concentration to the harbor bottom. Oxygen concentration inside the torpedo blister decreases into the harbor bottom, suggesting the same behavior occurs beneath the harbor bottom. Based on metal coupon analysis at frame 75, the corrosion rate on the USS *Arizona*'s exterior hull is approximately 3.0 mpy near the surface and decreases by nearly one third to about 1.0 mpy just below the harbor bottom. By comparison, corrosion rates for unconcreted steel in open seawater at the surface are in the 4–8 mpy range. Lower than predicted corrosion rates are directly related to metal-concretion interaction, and subsequent decreased oxygen availability. At the harbor bottom and below, where most of the fuel oil is bunkered, steel-hull coupon samples show that the corrosion rate remains constant or increases somewhat, consistent with potential increased bacterial activity in this region. How far this region extends into the harbor bottom is unknown, although current evidence suggests that corrosion rates below the harbor bottom and in interior compartments of *Arizona* remain low when compared to exterior rates.

As a heuristic device, based on these data, time interval from August 2002 until the plate thickness is reduced to one–half its original thickness can be determined. One–half original thickness was arbitrarily taken as a thickness below which structural integrity is severely compromised, although the FEM provides a more precise value. At 5 ft. depth, port, 27% of 20

lb. plate remains whereas at 5 ft. starboard, 40% of 20 lb. plate remains; these plates have been subjected to corrosion from both sides. Both sides have exceeded the one-half thickness criteria, which are the highest corrosion rates recorded. This area and depth is subject to the heaviest water movement and highest dissolved oxygen; and because the samples were from plate that had corrosion occurring on both sides. At 19½ ft., port, 77% of 37½ lb. plate remains whereas at 15 ft., starboard, 90% of 37½ lb. plate remains. These data translate to time to one–half thickness of 130 years, port, and nearly twice that time, starboard. At 26 ft., port, 87% of 20 lb. plate remains whereas at 22 ft., starboard, 81% of 20 lb. plate remains. These data translate to time to one–half thickness of 160 years, port, and about 90 years, starboard. Below the harbor bottom at 34 ft., port, 90% of 25 lb. plate remains whereas at 32½ ft. starboard, 87% of 30 lb. plate remains. These data translate to time to one–half thickness of 220 years port, and 170 years starboard. These projections are based on exterior shell plate measurements and do not represent what is expected for interior spaces under anaerobic conditions. Further metallographic analysis, especially of the hull coupons, is necessary as well as E_{corr} measurements the hull deeper below the mud line to verify projection of these corrosion rates to the full buried hull.

Interior Corrosion Analysis

Based on a variety of data and analytic methods, a comprehensive understanding of corrosion processes occurring on the hull above the harbor bottom has been accomplished. With this information as background, corrosion analysis at and below the harbor bottom and in interior compartments can be inferred, however, research should continue to further refine calculated corrosion rates on inaccessible hull components. Based on environmental data collected in *Arizona*'s interior spaces, which indicate low to no detectable dissolved oxygen levels, information to date suggests corrosion levels will be at or below the 1.0 mpy rate we recorded just below the harbor bottom. In fact, if the lower spaces within the hull are entirely anaerobic, which is likely, the corrosion rate could be lower than any measured so far.

GEOLOGICAL ANALYSES

Principal Question: How stable are the sediments upon which *Arizona* rests?

The study presented here addresses the potential for normal settlement processes to affect the orientation and elevation of USS *Arizona*, with respect to the seafloor and the waterline. Three boreholes around the vessel indicate that the vessel rests upon highly variable sediment. The settlement potential of the vessel is greater toward the stern, and toward the port side (bay side). A coralline rubble layer observed at the boring midship on the shoreward side may act to prevent settlement of the vessel there and may amplify tilting toward the bay and be responsible for the slight, 2–3° port list. The presence of the stiffer rubble zone may also enhance differential settlement beneath the vessel that can result in hull stresses that potentially deform the underbody of the vessel. For maximum settlement potential, there is an estimated settlement at full consolidation of approximately 1.6 m. Future measurement of the stiffness properties of the sediment and monitoring of the settlement of the vessel is recommended. A two-dimensional settlement analysis is needed to estimate the final degree of seaward tilting that is expected to occur.

<div align="center">STRUCTURAL STABILITY DETERMINATION</div>

Principal Questions: How stable is *Arizona*'s hull? How can we measure structural changes?

<u>External Stability</u>

GPS Monitoring

Horizontal and vertical differences recorded from by high-resolution GPS measurements from 2003–2006 have consistently been below the 5-cm circle of error, well below the 10-cm level we determined necessary to indicate significant movement. From these data we conclude that no measurable movement occurred during that 2½ year period.

Internal Stability

Internal structural monitoring of USS *Arizona* has been a qualitative process primarily using the VideoRay ROV to visually examine interior areas and note observable changes over time. Interior investigation took place from 2001–2005 in all accessible areas for measuring and monitoring interior environmental factors and corrosion parameters. During this process, overall internal structural condition were observed and noted, and no observable changes to internal spaces were noted during this period.

FINITE ELEMENT ANALYSIS

Principal Question: How can the cumulative results of *Arizona* research be used for modeling and predicting long-term changes in the hull, and how and when will those changes occur? Can a predictive model be developed that will allow incorporation of new data and information? How do we validate such a model?

Results of the USS *Arizona* FEA seem to indicate that, after nearly 67 years on the bottom of Pearl Harbor, the wreck is approximately one-fifth to one-fourth of the way to an eventual collapse due to corrosion. A surprising aspect of the results is that collapse is predicted to initiate in the side and bottom of the hull before any significant collapse events in the exposed regions of the upper decks. In addition, an important observation from this analysis is that, while the exposed decks above the harbor bottom become extensively deteriorated, the core cylinder of the wreck, consisting of the volume bounded by the third deck, the inner bottom and the side oil tanks, is still relatively intact even after 95% of steel thickness has corroded. This means that many of the oil containing spaces within the ship may retain integrity until the year 2250 or beyond. This may be a conservative estimation based on the corrosion-rate data incorporated into the model.

We believe this hull section selected for analysis, frame 70–90, to be representative of the rest of the ship, and its investigation and analysis provide a conservative estimate of corrosion rates for the initial FEM for two reasons. Project principals desired a conservative, faster, corrosion rate for the FEM, which should present more the worst case scenario rather than the

most optimistic projection. The analytical hull section's location adjacent to blast-damaged hull areas provides two factors that make the FEM conservative. The forward portion of the hull section was subjected to heat and blast damage during the explosion and sinking of the vessel, and it may be subject to somewhat increased corrosion rates. The second aspect, and more important, is that hull corrosion appears to be mostly oxygen driven. By projecting corrosion rates measured from the analytical hull section's exterior, which has been subjected to normally oxygenated sea water, to the interior, which we know to be nearly to fully anaerobic, we produce a conservative FEM.

The NIST FEM can be increased in accuracy as better data are collected and key variables are added and refined. A variety of refinements are recommended for the model, which are outlined below. To date, however, the model closely matches observations by researchers on site; we, of course, cannot project its accuracy into the future without inclusion of refined variables and verification through long-term monitoring data. During site mapping and other research activities in the 1980s, NPS personnel noted little upper deck damage in the area of *Arizona*'s galley beyond that attributable to initial damage from the Pearl Harbor attack and subsequent salvage activities. No oil release from upper deck breaches was observed. These observations mesh well with the model predicting that at 10% corrosion thickness loss (approximately 1980), the deck beams in the upper deck would jump significantly in stress, while the second, first and main decks remain in a near unstressed state. No collapsing is predicted, and none was observed during research from 1982–1986. In addition, the upper deck area was undercut by the explosions of the forward magazines; consequently, its support structure has been compromised. This is the only area where deck sagging and collapsed has been observed.

As the vessel reaches 20% corrosion thickness loss (estimated at 2020), the model predicts that upper deck areas begin to show sagging of the beams and deck plates as they continue to thin. This corresponds well with recent (2006) observations of limited upper deck collapse in the galley area, and increased release of secondary oil in the area as more breaches begin to open. To date, therefore, the model seems to be predicting actual behavior reasonably well. It will important to monitor this as we move into the future as one way to validate FEM accuracy.

OIL ANALYSES

Principal Questions: What is the nature of *Arizona*'s oil? How and at what rate does it degrade? What is its impact on the immediate environment of the ship? Is there a signature that distinguishes *Arizona* oil from other Pearl Harbor point sources? How do we measure oil leak volume?

The objectives of the oil study included characterizing oil leaking from USS *Arizona*, characterizing petroleum hydrocarbons in the sediments surrounding the ship and determining if oil leaking from the ship was degradable by microorganisms enriched from surrounding sediments. Oil characterized from *Arizona* suggests that oil leaking from different ship locations are exposed to different environments, based on the extent of *n*-alkane weathering for oil leaking from the stern starboard hatches compared to oil leaking near barbette no. 4. Biomarkers in oil leaking from the ship were also identified in sediments collected near and on atop the hull. Several biomarkers were of special interest because they are not found in Bunker C and were detected on the ship and in surrounding sediments, for example, butylated hydroxytoluene, which is a component of jet fuel. It is likely that oil leaking from *Arizona* is present in surrounding sediments, but it is also likely that hydrocarbons, including biomarkers, from other sources are present in the sediments as well. Aerobic enrichment cultures initiated from *Arizona* sediments were capable of degrading different components of Bunker C in 30–40 days. Certain components remained in oil extracted from enrichment cultures and did not decrease in concentration. These enrichments were capable of degrading certain biomarkers. Other biomarkers were also present in sediments, although in varying concentrations.

The oil studies have contributed to our fundamental understanding of the oil that is leaking from *Arizona*, and the potential of microorganisms indigenous to Pearl Harbor sediments in degrading this oil. In addition, the study was the first comprehensive hydrocarbon fingerprint of Pearl Harbor sediments adjacent to and surrounding the ship, and can be used as a baseline for future studies. A full environmental assessment of the area around *Arizona* and down current along the Ford Island shoreline, is needed to accurately determine the leaking oil's environmental impact.

Oil Release Monitoring

Measured release rates have gradually increased each year in direct proportion to the number of locations monitored: in 1998, 1.0 quart (0.95 liters) was measured from one location; in 2003, 2.1 quarts (2.0 liters) were measured from two locations; in 2004, 2.3 quarts (2.2 liters) were measured from two locations; in 2006, 9.5 quarts (9.0 liters) were measured from eight locations. June 2006 oil release measurements are the most comprehensive completed to date— increase in oil release over previous years is in part explained by more release locations being successfully measured than previously.

Although observed rates of oil coming to the surface has gradually increased over the past several years, there is no indication of increase in amount of oil released from the primary oil containment spaces in the ship's lower decks. The increase in oil volume observed is likely from redistribution of secondary oil contained in overhead spaces on the main and upper decks caused by gradual collapse of upper decks forward of the Memorial, which have the highest corrosion rates and were also affected by the 1941 explosion and subsequent salvage activities.

Primary oil containment spaces, located on *Arizona*'s lower decks, are well below the harbor bottom and probably have corrosion rates lower than any measured on the hull so far. Observed deformation of the upper deck in the galley area, whose support structure is weakened and with the highest corrosion rates, does not reflect the condition of primary oil containment spaces in the lower hull.

Undegraded oil release from the hatch on the starboard side of barbette no. 4 measured in June 2006 is lower than in previous years. These latest data suggest that oil release directly from primary oil containment spaces has decreased over the last several years, supporting the supposition that increased oil release is from secondary oil containment in upper and main deck overhead spaces forward of the Memorial.

Oil release rates vary considerably with differing wind, tide and harbor conditions. More oil is released during choppy harbor conditions and when tour boat and other ship's wakes pass over *Arizona*'s hull, which further supports the oil source as shallow overhead spaces rather than from primary oil containment spaces.

RECOMMENDATIONS

PROPOSED FUTURE STUDIES

There are a number of additional studies recommend as the USS *Arizona* Preservation Project continues that are planned to fill data gaps in the research presented in this report. Several of these studies are critical for developing a complete picture of *Arizona* deterioration.

Finite Element Modeling

There are several recommendations regarding the FEM that are necessary for increasing the accuracy of the results presented here. First, this model should be extended to the entire length of the ship. This would increase the calculation time needed dramatically, but key insights into the behavior of structural elements in the present study can be used to cut down the computation time. For example, once it is determined how a section of deck plating and supporting deck beam deform as the members thin, and it is found to be consistent across the model, this region can be replaced with a single element that has hybrid parameters calculated from the model. Thus, instead of performing calculations on thousands of connected elements, one could be used.

Second, a significant unknown in this study is the damage to the internal load-bearing structures in the lower decks. It is almost certain that the region forward of the main stacks suffered significant damage, but since submersibles and divers cannot reach these regions for direct observations, we must speculate and make best and worst case scenario assumptions for our analyses. These assumptions could be fine-tuned with input from experts in blast damage in the naval community, perhaps at the Naval Surface Warfare Center in Carderock, MD. Initial contacts with researchers at that facility indicated interest but inability to assist due to lack of funding. A comprehensive analysis of blast damage to the ship based on multiple lines of data, and modeled by a FEM similar to that for *Arizona*'s deterioration, would increase the accuracy of this and future models.

Third, *Arizona*'s remains are listing slightly to port, and this causes the self-load to be directed slightly off of vertical onto the load bearing structures. Elastic-plastic collapse of

columns and stanchions will be significantly affected by deviations from vertical, and the effect of the list will be for some structures to collapse sooner than predicted in this model. The effect of the list and how it is changing over time is a factor that should be added to refine the model, based on analysis by USGS.

Fourth, in the present study, the differences in corrosion rates from different regions of the ship were only modeled as differences between whole decks above and below the mud line. A further refinement to the model that would allow for more accurate spatial location of potential developing weak points would be to map detailed, measured differences in corrosion rate onto the structure. Collecting detailed corrosion rate data from multiple locations around the hull, and mapping variations, is recommended.

Finally, because Pearl Harbor is an active naval base, with ship traffic constantly entering and exiting, wakes from passing ships could potentially deliver a significant impact to the hull. The present model deals with slow, steady-state decay of the structure, attempting to predict the timeframe of collapse. It is more likely that a significant failure will be precipitated by a more sudden event such as a wave or a large storm. Using new modules developed to study the effect of landslide-induced waves within reservoirs upon dams, a study could be conducted looking at the magnitude of stress spikes in the wreck with the passing of ships or during large storms.

Microbiological Analysis

One of the most important studies that remains on hold due to lack of funding is an analysis of the role of microbially induced corrosion on *Arizona*'s deterioration, as well as the effect of microbes combined with Bunker C fuel oil within the battleship's fuel bunkers on corrosion rates of lower-deck, oil-containing spaces. Early results from this research are reported in Chapter 7, but the experiments have been on hold for several years. This research is critical because the FEM and analysis of long-term structural deterioration is based on measured corrosion rates from *Arizona*'s exterior, with interior rates estimated using data gathered to date, along with several reasonable assumptions. These assumptions do not factor in the role of microbes in corrosion, and therefore their effect is not calculated into the final FEM developed by NIST. Complete characterization of microbially induced corrosion both on *Arizona*'s exterior

and interior spaces is critical for validating experimental results of the FEM reported in this document.

Exterior Corrosion Analysis

While corrosion rate from hull coupon samples is determined to just below the harbor bottom, there is a continuing question about corrosion below it. Right at the harbor bottom, there appears to be some increase in corrosion due to accelerated bacterial activity there, while the corrosion rates a meter below the mud show the lowest corrosion rates found. What is not established yet is the extent of corrosion between this region and the hull bottom. The data are conflicting, but the concern is that this region is deficient in oxygen compared to the region above it in the water and could lead to a large scale oxygen cell causing accelerated corrosion in the lower part of hull. This can be addressed by implementing corrosion potential monitoring. A permanent high chloride reference electrode could be placed in tubing driven well below the harbor bottom toward the hull bottom to a depth of around 15 ft., and monitored remotely via the internet. A decrease in corrosion potential with depth, consistent with trends reported in sea water, would establish that there is no large scale oxygen cell activity and eliminates this as a variable of concern. Because the unit can access four locations, it would be possible to install at least one electrode at this location. The advantage of monitoring for a one year period is that disturbance of the mud in the vicinity of the hull may bias initial readings and extended time in place would assure that *in situ* readings were reliable.

The same instrumentation could be used to monitor over time the effect of season, wind, temperature and other environment variables on corrosion potential at selected hull sites above the harbor bottom. The data we have obtained are extensive above the harbor bottom but each field operation has occurred from June to December and no data has been obtained during the remaining part of the year. Part of the reason for varying corrosion potential data at the same site over several field operations may be related to seasonal effects. Due to dilution in the drill hole before probes are inserted, pH and corrosion potential readings may be biased and may have yielded data that may not represent true values. To determine if this is a problem and to determine how much of an error was created, it is proposed that pH and corrosion potential

probes be permanently embedded in the concretion with the tip of the probes at the interface, sealed with epoxy and monitored for a one year period.

A corrosion rate sensor (Barnacle cell) that sits on top of a sponge placed directly on the concretion, coupled to a linear polarization resistance (LPR) probe, could give instantaneous corrosion rates. Grounding above the water line on barbette no. 3 would assure adequate contact on the hull while calibration would be accomplished at frame 75, since the corrosion rate is already well-known there. The barnacle cell, once calibrated could then be moved to any site desired on the hull for corrosion rate measurement without having to remove the concretion. Such a device could also be used to correlate with concretion equivalent corrosion rate (CECR) data already obtained between frames 70–90. This would allow rapid and improved ability to collect the detailed corrosion rate data necessary to refine the FEM.

Interior Corrosion Analysis

While some information has been obtained on corrosion rate in interior spaces, the data are indirect and not conclusive. It is believed that more could be done with the barnacle cell (LPR) to determine whether or not some arrangement could be made to mount this cell on an ROV in such a way that corrosion rate readings could be taken directly from a bulkhead.

Cathodic Protection

Cathodic protection is a technique for protecting a structure from appreciable corrosion by incorporating a metal into the corrosion circuit that has a greater tendency to corrode than the structure. Alternately, the equivalent effect can be achieved by inducing a direct current into the structure using a rectification circuit design. The prevention or limitation of corrosion of the external fabric using cathodic protection would reduce fresh sea water entry into regions where corrosion could begin to develop on both sides of hull plate as has already noted from analysis of hull coupon samples. Once the outer fabric is penetrated, cathodic protection would be less effective as a protective measure because current cannot be as effectively "thrown" onto the interior side of outer fabric or onto interior load bearing structures. Cathodic protection could potentially be designed to protect the outer hull or torpedo blister into the mud to the keel. Based

470

on data from USS *Bowfin*, current demand would be about 3 ma/ft^2 or roughly ⅓ the demand for bare steel.

It is recommended to continue to develop background information regarding the advantages and limitations of cathodic protection as a timely means of arresting what appears to be a gradual top/down deterioration as fresh sea water enters the structure at lower depths. It should be noted that continuous monitoring of rectifier system effectiveness could be automated, and simple to interpret as in the case of the USS *Bowfin*.

OVERALL CONCLUSIONS

USS *Arizona*'s complete structural deterioration, and eventual release of oil within its hull, is by all indications **NOT** imminent. This study has allowed us to quantify, and therefore better understand, the complex corrosion and degradation processes taking place on *Arizona*'s hull. Data combined from many different research studies have been brought together to give us the most complete picture to date on *Arizona*'s status. These are the key points from the study:

- The FEM, which incorporates a detailed analysis of corrosion nature and rate, indicates that the hull is deteriorating slowly. Since sinking in 1941, the battleship has only progressed one-fifth to one-quarter to the way towards total loss of steel due to seawater corrosion. The model predicts that oil-containing spaces on *Arizona*'s lower decks may remain intact for 200+ years from the present. As predicted, *Arizona*'s upper deck areas, closest to the water surface and with the highest corrosion rates on site, are experiencing increased deterioration. It is important to remember, however, that these areas are not integral to *Arizona*'s structural integrity, and do not include primary oil-containing spaces. All oil-containing spaces are deep below the present harbor bottom, within the structural core of the ship that is presently experiencing the lowest corrosion rates on site, and which are predicted to have not yet suffered significant corrosion.

- Environmental impact of the oil currently being released from *Arizona*'s hull is low. Although the amount of oil released daily from the vessel may have increased slightly over the years, this is likely due to increased release of secondary oil trapped in higher

deck overheads because of increased deterioration of the upper deck. This is likely not indicative of an increase in oil release from primary oil containing spaces.

MANAGEMENT RECOMMENDATIONS

1)   At this time there is no scientific justification to alter current management policies of *in situ* preservation. There are critical variables that need to be refined for inclusion into the FEM.

2)   For the present, status quo should be maintained regarding any intervention in *Arizona*'s hull.

3)   Continued research on both *Arizona* and any environmental impact should be supported and stable, sustainable funding should be developed.

4)   Institute the monitoring program consistent with monitoring variables discussed in this report and make it part of the park's core operations. This requires maintenance and expansion of the park dive team. Unauthorized diving should be eliminated. Submerged remote sensing intrusion devices should be investigated and deployed.

5)   Oil containment and diversion alternatives should be investigated. Remote sensing oil quantity detection devices should be explored.

6)   Public education regarding the status of *Arizona*'s deterioration and the NPS's site stewardship should be expanded. Consideration should be given to continuing development of the USS *Arizona* GIS Project and supporting its access on the Internet along with development of video clips and podcasts directed toward answering the most frequently asked questions.

REFERENCES

Aeckersberg, F., F. A. Rainey, and F. Widdel
    1998 Growth, Natural Relationships, Cellular Fatty Acids and Metabolic Adaption of Sulfate-Reducing Bacteria that Utilize Long Chain Alkanes Under Anoxic Conditions. *Archives Microbiology*. 170: 361-369.

Alberdi, M., and L. Lopes
    2000 Biomarker 18α(H)-oleanane: Ageochemical Tool to Assess Venezuelan Petroleum Systems. *Journal of South American Earth Sciences* 13:751-759.

Altschul S.F., T.L. Madden, A.A. Schäffer, J. Zhang, Z. Zhang, W. Miller, and
        D.J. Lipman
    1997 Gapped BLAST and PSI-BLAST: a New Generation of Protein Database Search Programs, *Nucleic Acids Research* 25:3389-3402.

Anwar, H., J.L. Strap, and J.W. Costerton
    1992 Establishment of Aging Biofilms: Possible Mechanism of Bacterial Resistance to Antimicrobial Therapy. *Antimicrobial Agents and Chemotherapy* 36:1347-1351.

Anderson, R. T., and D. R. Lovely
    2000 Hexadecane Decay by Methanogenesis. *Nature* 404:722.

American Society for Metals
    1975 *Metals Handbook, Failure Analysis and Prevention*. 8th ed 10.

Ashwood, T. L., and C. R. Olsen
    1988 Pearl Harbor Bombing Attack: A Contamination Legacy Revealed in the Sedimentary Record. *Marine Pollution Bulletin* 19:68-71.

Atlas, R. M.
    1981 Microbial Degradation of Petroleum Hydrocarbons: An Environmental Perspective. *Microbiological Reviews* 45:180-209.

    1984 *Petroleum Microbiology*. 1st ed. Macmillan, New York.

Baars, B. J.
    2002 The Wreckage of the Oil Tanker *Erika* : Human Health Risk Assessment of Beach Cleaning, Sunbathing and Swimming. *Toxicology Letters* 128:55-68.

Barron, M. G., T. Podrabsky, S. Ogle, and R. W. Ricker
    1999 Are Aromatic Hydrocarbons the Primary Determinant of Petroleum Toxicity to Aquatic Organisms? *Aquatic Toxicology* 46:253-268.

Bartholomew, C.A. Capt.
>1990 *Mud, Muscle, and Miracles: Marine Salvage in the United States Navy*. Department of the Navy, Washington, D.C.

Beam, H. W., and J. J. Perry
>1974 Microbial Degradation and Assimilation of *n*-Alkyl-Substituted Cycloparaffins. *Journal of Bacteriology* 118:394-399.

Beckles, D. M., C. H. Ward, and J. B. Hughes
>1998 Effect of Mixtures of Polycyclic Aromatic Hydrocarbons and Sediments on Flouranthene Biodegradation Patterns. *Environmental Toxicology and Chemistry* 17:1246-1251.

Bernard L., H. Schäfer, F. Joux, C. Courties, G. Muyzer, and P. Lebaron
>2000 Genetic Diversity of Total, Active and Culturable Marine Bacteria in Coastal Sea Water, *Aquatic Microbial Ecology* 23:1-11.

Bixian, M., F. Jiamo, Z. Gan, L. Zheng, M. Yushun, S. Guoying, and W. Xingmin
>2001 Polycyclic Aromatic Hydrocarbons in Sediments from Pearl River and Estuary, China: Sapatial and Temporal Distribution and Sources. *Applied Geochemistry* 16:1429-1445.

Blumer, M. and J. Sass
>1972 Oil Pollution: Persistence and Degradation of Spilled Fuel Oil. *Science* 176:1120-1122.

Boll, M., G. Fuchs, and J. Heider
>2002 Anaerobic Oxidation of Aromatic Compounds and Hydrocarbons. *Current Opinion in Chemical Biology* 6:604-611.

Bost, F. D., R. Frontera-Suau, T. J. McDonald, K. E. Peters, and P. J. Morris
>2001 Aerobic Biodegradation of Hopanes and Norhopanes in Venezuelan Crude Oils. *Organic Geochemistry* 32:105-114.

Bram J.B., H.M. Page, and J.E. Dugan
>2005 Spatial and Temporal Variability in Early Successional Patterns of an Invertebrate Assemblage at an offshore oil Platform, *Journal of Experimental Marine Biology and Ecology* 317:223-237.

Candries M.
>12 December 2000 Paint Systems for the Marine Industry, *Notes to Complement the External Seminar on Antifoulings*, Department of Marine Technology, University of Newcastle-upon-Tyne, http://www.geocities.com/maxim_candries

Casagrande, Arthur
    1936 The Determination of the Pre-Consolidation Load and Its Practical Significance. In *Soil Mechanics and Foundation Engineering* Vol. III, pp. 60-64. Cambridge, Ma.

Cerniglia, C. E.
    1992 Biodegradation of Polycyclic Aromatic Hydrocarbons. *Biodegradation* 3:351-368.

Chang, Y. J., J. R. Stephen, A. P. Richter, A. D. Venosa, J. Bruggemann, S. J Macnaughton, G. A. Kowlachuk, J. R. Haines, E. Kline, and D. C. White
    2000 Phylogenetic Analysis of Aerobic Freshwater and Marine Enrichment Cultures Efficient in Hydrocarbon Degradation: Effect of Profiling Method. *Journal of Microbial Methods* 40:19-31.

Chosson, P., C. Lanau, J. Connan, and D. Dessort
    1991 Biodegradation of Refractory Hydrogen Biomarkers from Petroleum Under Laboratory Conditions. *Nature* 351(6328):640-642.

Christensen, B.E. and W.G Characklis
    1990 Physical and Chemical Properties of Biofilms, In *Biofilms*, edited by W.G. Characklis and K.C. Marshall, John Wiley and Sons Inc., New York.

Commander Battle Force, US Pacific Fleet
    January 29, 1942 Memorandum for File: Damages Sustained by the Ships of the Battle Force, Pacific Fleet as a result of the Japanese Air Raid on December 7, 1941. Wallin Papers, Box 2, 50 Salvage Reports, Naval History Center, Washington, D.C.

Commander Base Force to Commander in Chief, Pacific Fleet
    December 28, 1941. Damaged Ships – Preliminary Estimates of Problems of Salvage. 7pp. Wallin Papers, Box 1, 50 Salvage Reports, Naval History Center, Washington, D.C.

Cook, E.
    1937 *Open Hearth Steel Making*. ASM International, Cleveland.

Costerton, J.W., Z. Lewandowski, D.E. Caldwell, D.R. Korber, and H.M. Lappin-Scott.
    1995. Microbial Biofilms. *Annual Review of Microbiology* 49:711-745.

Cummins, G. and B. Dickinson
    1989 The Management Experience. In *Submerged Cultural Resources Study: USS Arizona Memorial and Pearl Harbor National Historic Landmark*, edited by D. J. Lenihan, pp. 157-168. Submerged Resources Center Professional Papers No. 9. National Park Service, Santa Fe.

Davison, H.D.
    1941 Statement of Ensign H. D. Davison, US Navy, USS *Arizona*. Wallin Papers, Box 2, 50 Salvage Reports, Naval History Center, Washington, D.C.

DeAngelis, R.
>   2002 X-Ray Diffraction and Environ mental Scanning Electron Microscope Investigation of Concretion from the USS Arizona. Manuscript on File, National Park Service, Santa Fe.

Dean-Ross, D., J. Moody, and C. E.Cerniglia
>   2002 Utilization of Mixtures of Polycyclic Aromatic Hydrocarbons by Bacteria Isolated from Contaminated Sediment. *FEMS Microbiology Ecology* 41:1-7.

de Beer, D., P. Stoodley, F. Roe, and Z. Lewandowski
>   1994. Effects of Biofilm Structures on Oxygen Distribution and Mass Transport. *Biotechnology and Bioengineering* 43:1131-1138.

Delgado, J. P.
>   1989 Memorials, Myths and Symbols. In *Submerged Cultural Resources Study: USS Arizona Memorial and Pearl Harbor National Historic Landmark*, edited by D. J. Lenihan, pp. 169-183. Submerged Resources Center Professional Papers No. 9. National Park Service, Santa Fe.

>   1992 Recovering the Past of USS Arizona: Symbolism, Myth, and Reality. *Historical Archaeology* 26(4):69-80.

Elshahed, M. S., L. M. Gieg, M. J. Mcinerney, and J. M. Suflita
>   2001. Signature Metabolites Attesting to the *in situ* Attenuation of Alkylbenzenes in Anaerobic Environments. *Environmental Science and Technology* 35:682-689.

Environmental Protection Agency [EPA].
>   1984 *List of the Sixteen PAHs with Highest Carcinogenic Effect*. IEA Coal Research, London.

Felkins, K., J. Leighly, H.P and A. Jankovic
>   1998 The Royal Mail Ship Titanic: Did a Metallurgical Failure Cause a Night to Remember? *Journal of Metals* 50(1):12-18.

Ferris, M. J., G. Muyzer, and D. M. Ward
>   1996 Denaturing Gradient Gel Electrophoresis Profiles of 16S rRNA-Defined Populations Inhabiting a Hot Spring Microbial Mat Community. *Applied and Environmental Microbiology* 62:340-346.

Flannigan, G. S. Ensign
>   1941 Statement of G.S. Flannigan, Ensign, D-V (a), USS *Arizona*. Wallin Papers, Box 2, 50 Salvage Reports, Naval History Center, Washington, D.C.

Floodgate, G. D.
>   1984. The Fate of Petrolum in Marine Ecosystems. In *Petroleum Microbiology* (R. M. Atlas, Ed.), pp. 61-98. McMillan Publishing Co., New York, NY.

Fontana, M. G.
    1986 *Corrosion Engineering*. 3rd ed. McGraw-Hill, New York.

Ford, T.E. and R. Mitchell
    1991. The Ecology of Microbial Corrosion. In *Advances in Microbial Ecology,* Vol.
    11, edited by K.C. Marshall, Plenum Press, New York

Fries, E. and W. Puttman
    2002 Analysis of the Antioxidant Butylated Hydroxytoluene (BHT) in Water by Means
    of Solid Phase Extraction Combined with GC-MS. *Water Research* 36:2319-2327.

Frontera-Suau, R., F. D. Bost, T. J. McDonald, and P. J. Morris
    2002 Aerobic Biodegradation of Hopanes and Other Biomarkers by Crude Oil-Degrading
    Enrichment Cultures. *Environmental Science and Technology* 36:4585-4592.

Fuqua, S.G. CDR
    December 15, 1941. USS *Arizona* BB-39, Pearl Harbor Attack: Report of Salvage
    Operations Following Preliminary Dives to Inspect Hull Damage and to Determine what
    Sections of the Vessel Could be Entered. Memo From Commanding Officer, USS
    Arizona to Commander Battleships, Battle Force. Wallin Papers, Box 2, 50 Salvage
    Reports, Naval History Center, Washington, D.C.

    1941 Statement, USN of the attack on the USS Arizona, 7 December 1941. Wallin
    Papers, Box 2, 50 Salvage Reports, Naval History Center, Washington, D.C.

Furlong, W.R.
    March 15, 1942 Salvage operations on USS *Arizona*, USS *Oklahoma*, and USS *Utah* –
    Decision as to Extent of. Wallin Papers, Box 1,50 Salvage Reports, Naval History
    Center, Washington, D.C.

    July 24, 1942 Memo from Commandant, Navy Yard, Pearl Harbor to the Vice Chief of
    Naval Operations. On file, USS *Arizona* Memorial Archives, Honolulu.

Garrett, R. M., I. J. Pickering, C. E. Haith, and R. C. Prince
    1998 Photooxidation of Crude Oils. *Environmental Science and Technology* 32:3719-
    3723.

Geiselman, E.H.
    December 17 1941 From Commanding Officer, USS Arizona to Commander
    Battleships, Battle Force. Material Damages Sustained in Attack on December 7, 1941. 3
    pp. Wallin Papers, Box 2, 50 Salvage Reports, Naval History Center, Washington, D.C.

Giovannoni S.J., T.B. Britschgi, C.L. Moyer, and K.G. Field
    1990 Genetic Diversity in Sargasso Sea Bacterioplankton, *Nature* 345:60-63

Gould, R. A.
  2000 *Archaeology and the Social History of Ships*. Cambridge University Press, Cambridge.

Gregory, D.
  1999 Monitoring the Effect of Sacrificial Anodes on the Large Iron Artifacts on the Duart Point Wreck, 1997. *International Journal of Nautical Archaeology* 28(2):164-173.

  1995 Experiments into the Deterioration Characteristics of Materials on the Duart Point Wreck Site: An Interim Report. *The International Journal of Nautical Archaeology* 24:61-65.

Gu, J.-D., T.E. Ford, and R. Mitchell
  2000 Microbial Corrosion of Metals. In *Uhlig's Corrosion Handbook, Second Edition,* edited by R. Winston Revie, John Wiley and Sons Inc., NY.

Haines, J. R., and M. Alexander
  1974 Microbial Degradation of High Molecular Weight Alkanes. *Applied Microbiology* 28:1084-1085.

Haynes, H.E. Lt. CDR
  November 14, 1943 Memo from Diving Supervisor to Salvage Superintendent re; Diving Operations in Connection with the Salvage of the USS *Arizona*. On file, USS *Arizona* Memorial Archives, Honolulu.

Henderson, S.
  1989 Biofouling and Corrosion Study. In *Submerged Cultural Resources Study: USS Arizona Memorial and Pearl Harbor National Historic Landmark*, edited by D. J. Lenihan, pp. 117-156. Submerged Resources Center Professional Papers No. 9. National Park Service, Santa Fe.

Hir, M. L., and C. Hily
  2002 First Observations in a High Rocky-Shore Community After the *Erika* Oil Spill (December 1999, Brittany France). *Marine Pollution Bulletin* 44:1243-1252.

Ho, K., Patton, J. S., Latimer., R. J. Pruell, M., Pelletier, R. McKinney, and S. Jayaraman 1999 The Chemistry and Toxicity of Sediment Affected by Oil from the *North Cape* Spilled into Rhode Island Sound. *Marine Pollution Bulletin* 38:314-323.

Homann, A. J. Cmdr.
  January 28, 1942 (a) Material Damage Sustained in Attack on December 7. 1941. Memo from USS *Arizona* Commanding Officer to the Chief, Bureau of Ships. Wallin Papers, Box 2, 50 Salvage Reports, Naval History Center, Washington, D.C.

1942 (b) Information on Damage Control, ref. Pacific Fleet Conf. Lrt. No2Cl-42 of January 6, 1942. Memo from USS Arizona Commanding Officer to Chief, Naval Operations. Wallin Papers, Box 2, 50 Salvage Reports, Naval History Center, Washington, D.C.

Hughes, J. B.
1999. Cytological-Cytogentic Analyses of Winter Flounder Embryos Collected from the Benthos at the Barge *North Cape* Oil Spill. *Marine Pollution Bulletin* 38:30-35.

Hughes J.B., J.J. Hellman, T.H. Ricketts, and J.M. Bohannan
2001 Counting the Uncountable: Statistical Approaches to Estimating Microbial Diversity, Applied Environmental Microbiology 67:4399-4406.

Hunt, J. M.
1995 *Petroleum Geochemistry and Geology*. 2nd ed. W.H. Freeman and Company, New York.

Husler, J. and C. Dodson
2003 *X-Ray Fluorescence Analysis of Concretion*. Unpublished Manuscript on File at National Park Service, Santa Fe.

Inui, H., K. Itoh, M. Matsuo, and J. Miyamoto
1979 Studies on Degradation of 2,6-di-*tert*-butyl-4-methylphenol (BHT) in the Environment. Part-II: Biodegradability of BHT with Activated Sludge. *Chemosphere* 6:383-91.

Irwin, R. J., M. VanMouwerik, L. Stevens, M. D. Seese, and W. Basham
1997 National Park Service, Water Resources Division Environmental Contaminants Encyclopedia, Fuel Oil No. 6 Entry.

Jackson CR, KG Harrison, and S.L. Dugas
2005 Enumeration and Characterization of Culturable Arsenate Resistant Bacteria in a Large Estuary, *Systematic Applied Microbiology* 28:727-734.

Jannasch H.W., and C.O. Wirsen
1981 Morphological Survey of Microbial Mats Near Deep Sea Thermal Vents, Applied Environmental Microbiology 41:528-538.

Jeffery, B.
2004 World War II Underwater Cultural Heritage Sites in Truk Lagoon: Considering a Case for World Heritage Listing. *International Journal of Nautical Archaeology* 33(1):106-121.

Johnson, D. L., J. D. Makinson, R. DeAngelis, B. M. Wilson and W. N. Weins
>   2003   *Metallurgical and Corrosion Study of Battleship USS Arizona, USS Arizona Memorial, Pearl Harbor*. Unpublished Manuscript on File at National Park Service, Santa Fe.

Johnson, D.L., W.N. Weins, J.D. Makison, and D.A. Martinez
>   1999 Metallographic Studies of the USS *Arizona*. Proceedings of the International Metallographic Society.

Johnson, D. L., W. N. Weins and J. D. Makinson
>   2000   Metallographic Studies of the U.S.S. Arizona. In *Microstructural Science Vol. 27: Understanding Processing, Structure, Property, and Behavior Correlations*, edited by W. N. Weins, pp. 85-91. ASM International, New York.

Johnson, D. L., B. M. Wilson, J. D. Carr, M. A. Russell, L. E. Murphy and D. L. Conlin
>   2006a Corrosion of Steel Shipwrecks in the Marine Environment: USS Arizona - Part 1. *Materials Performance* 45(10):40-44.

>   2006b Corrosion of Steel Shipwrecks in the Marine Environment: USS Arizona - Part 2. *Materials Performance* 45(11):54-57.

Jones, D. A.
>   1996   *Principles and Prevention of Corrosion*. 2nd ed. Prentice Hall, New York.

Juhasz, A. L. and R. Naidu
>   2000 Bioremediation of High Molecular Weight Polycyclic Aromatic Hydrocarbons: A Review of the Microbial Degradation of benzo[*a*]pyrene. *International Biodeterioration and Biodegradation* 45:57-88.

Jungclaus, G. A., V. Lopez-Avila and R. A. Hites
>   1978 Organic Compounds in Industrial Waste Water: A Case Study of Their Environmental Impact. *Environmental Science and Technology* 12:88-96.

Kanaly, R. A. and S. Harayama
>   2000 Biodegradation of High-Molecular-Weight Polycyclic Aromatic Hydrocarbons by Bacteria. *Journal of Bacteriology* 182:2059-2067.

Kayen, R. and Phi, T.N.
>   1997 A Robotics and Data Acquisition Program for Manipulation of the U.S. Geological Survey's Ocean Sediment Core Logger. *SciTech Journal* 7 (5):24-29.

Kayen, R., Edwards, B. D., Lee, H. J.
>   1999 Nondestructive Laboratory Measurement of Geotechnical and Geoacoustic Properties through Intact Core-liner *Nondestructive and Automated Testing for Soil and Rock Properties, ASTM Special Technical Publication-1350,* W. A. Marr and C.E. Fairhurst *eds*., *American Society for Testing and Materials*, p. 83-94.

Kelly, M.
    1996 Enshrining History: The Visitor Experience at Pearl Harbor's USS Arizona
    Memorial. *Museum Anthropology* 20(3):45-57.

Kerr, R. A.
    2001 Life--Potential, Slow, or Long Dead. *Science* 294(5548):1820-1821.

Korb, L. J.
    1987 *Metals Handbook: Volume 13, Corrosion*. 9th ed. American Society for Metals.

Kvenvolden, K. A., F.D. Hostettler, J. B. Rapp, and P. R. Carlson
    1993 Hydrocarbons in Oil Residues on beaches of Islands of Prince William Sound,
    Alaska. *Marine Pollution Bulletin* 26:24-29.

Kvenvolden, K. A., F. D. Hostettler, P. R. Carlson, J. B. Rapp, C. N. Threlkeld. and A. Warden
    1995 Ubiquitous Tar Balls with a California-Source Signature on the Shorelines of Prince
    William Sound, Alaska. *Environmental Science and Technology* 29:2684-2694.

Kvenvolden, K .A., F. D. Hostettler, R. W. Rosenbauer, T. D. Lorensen, W. T. Castle and S.
    Sugarman
    2002 Hydrocarbons in Recent Sediment of the Monterey Bay National Marine Sanctuary.
    Marine Geology 181:101-113.

Lane D.J.
    1991 16S/23S rRNA Sequencing, In *Nucleic Acid Techniques in Bacterial Systematics*,
    edited by E. Stackebrandt, and M. Goodfellow, pp. 115-175, John Wiley and Sons, New
    York

Lenihan, D. J.
    1989a Introduction. In *Submerged Cultural Resources Study: USS Arizona Memorial
    and Pearl Harbor National Historic Landmark*, edited by D. J. Lenihan, pp. 1-12.
    Submerged Resources Center Professional Papers No. 9. National Park Service, Santa Fe.

    1989b *Submerged Cultural Resources Study: USS Arizona Memorial and Pearl Harbor
    National Historic Landmark*. Submerged Resources Center Professional Papers No. 9.
    National Park Service, Santa Fe.

    1990 *USS Arizona Memorial and Pearl Harbor National Historic Landmark*. 2 ed. Vol.
    No. 23. Submerged cultural resources study. Santa Fe, NM: Southwest Cultural
    Resources Center Professional Papers

Lenihan, D. J. and L. E. Murphy
    1989 Archeological Record. In *Submerged Cultural Resources Study: USS Arizona
    Memorial and Pearl Harbor National Historic Landmark*, edited by D. J. Lenihan.
    Submerged Resources Center Professional Reports No. 9. National Park Service, Santa
    Fe.

Linley E.A.S., R.C. Newell, and M.I. Lucas
>1983 Quantitative Relationships Between Phytoplankton, Bacteria, and Heterotrophic Microflagellates in Shelf Waters, *Marine Ecology Progress Series* 12:77-89.

Linenthal, E. T.
>1991 *Sacred Ground: Americans and Their Battlefields*. University of Illinois Press, Chicago.

Little, B. J., R. I. Ray and R. K. Pope
>2000 Relationship Between Corrosion and the Biological Sulfur Cycle: A Review. *Corrosion* 56(4):433-443.

Lott, A.S. General Editor
>1978 *USS* Arizona *Ship's Data: A Photographic History*. Fleet Reserve Association, Honolulu.

Luckenbach Trustee Council
>2006 *S.S. Jacob Luckenbach and Associated Mystery Oil Spills Final Damage Assessment and Restoration Plan/Environmental Assessment.* Prepared by California Department of Fish and Game, National Oceanic and Atmospheric Administration, United States Fish and Wildlife Service, National Park Service.

Lunel, T., A. Crosbie, L. Davies, and R. P. J. Swannell
>2000 The Potential for Dispersing Bunker C (IFO-380) Fuel Oils: Initial Results. Prepared by: National Environmental Technology Centre, Culham, Abingdon Oxfordshire, United Kingdom. 12 pp.

MacLeod, I. D
>1982 The Electrochemistry and Conservation of Iron in Sea Water. *International Journal of Nautical Archaeology and Underwater Exploration* 2(4):267-275.

>1987 Conservation of Corroded Iron Artifacts – New Methods for On-Site Preservation and Cryogenic Deconcreting. *International Journal of Nautical Archaeology and Underwater Exploration* 16(1):49-56.

>1989 Electrochemistry and Conservation of Iron in Sea Water. *Chemistry in Australia* 56(7):227-229.

>1995 *In Situ* Corrosion Studies on the Duart Point Wreck, 1994. *International Journal of Nautical Archaeology* 24(1):53-59.

>2002 In Situ Corrosion Measurements and Management of Shipwreck Sites. In *International Handbook of Underwater Archeology*, edited by C. V. Ruppe and J. F. Barstad, pp. 697-714. Kluwer Academic/Plenum Publishers., New York.

Mackenzie, A. S.

    1984 Applications of Biological Markers in Petroleum Geochemistry. In *Advances in Petroleum Geochemistry* (J. Brooks, and D. Weite, Eds.), Vol. 1, pp. 115-213. Academic Press, London.

Madsen, D.

    2003 *Resurrection: Salvaging the Battle Fleet at Pearl Harbor.* Naval Institute Press, Annapolis.

Maki J.S., D. Rittschof, A.R. Schmidt, A.G. Snyder, and R. Mitchell

    1989 Factors Controlling Attachment of Bryozoan Larvae: A Comparison of Bacterial Films and Unfilmed Surfaces, *Biology Bulletin* 177:295-302.

Makinson J.D., D.L. Johnson, M.A. Russell, D.L. Conlin, and L.E. Murphy

    2002 *In situ* Corrosion Studies on the Battleship USS *Arizona*, *Materials Performance* 41:56-60.

Marshall K.C., R. Stout, and R. Mitchell

    1971 Mechanism of the Initial Events in the Sorption of Marine Bacteria to Surfaces. *Journal of General Microbiology* 68:337-348.

McDonald, T. J. and M. C. Kennicutt

    1992 Fractionation of Crude Oils by HPLC and Quantitative Determination of Aliphatic and Aromatice Biological Markers by GC-MS with Selected Ion Monitoring. *LC-GC* 10:935-938.

McEldowney, S. and M. Fletcher

    1987 Adhesion of Bacteria from Mixed Cell Suspensions to Solid Surfaces. *Archives of Microbiology* 148:57-62.

McNamara C.J., T.D. Perry, K. Bearce, G. Hernandez-Duque, and R. Mitchell

    2006 Epilithic and Endolithic Bacterial Communities in Limestone from a Mayan Archaeological Site, *Microbial Ecology* 51:51-64.

Makinson, J. D., D. L. Johnson, M. A. Russell, D. L. Conlin and L. E. Murphy

    2002 *In situ* Corrosion Studies on the Battleship USS Arizona. *Materials Performance* 41(10):56-60.

Mardikian, P.

    2004 Conservation and Management Strategies Applied to Post-Recovery Analysis of the American Civil War Submarine H. L. Hunley (1864). *International Journal of Nautical Archaeology* 33(1):137-148.

McCarthy, M.
    1988 S.S. Xantho: The Pre-Disturbance, Assessment, Excavation and Management of an Iron Steam Shipwreck off the Coast of Western Australia. *International Journal of Nautical Archaeology and Underwater Exploration* 17(4):339-347.

    2000 *Iron and Steamship Archaeology: Success and Failure on the S.S. Xantho.* The Plenum Series in Underwater Archaeology, New York.

McClung, M. L. Lt.
    n.d. Survey of Damage on U.S.S. *Arizona*. Reference; Verbal Orders to Conduct a Survey of the Hull of U. S. S. *Arizona*. Correspondence from the Assistant Salvage Engineer to The Salvage Engineer. Wallin Papers, Box 2, 50 Salvage Reports, Naval History Center, Washington, D.C.

Miller J. D.
    1941 Bombing of USS *Arizona*, Report of Ensign Jim D. Miller. Wallin Papers, Box 2, 50 Salvage Reports, Naval History Center, Washington, D.C.

Mills H.J., C. Hodges, K. Wilson, I.R. MacDonald, and P.A. Sobecky
    2003 Microbial Diversity in Sediments Associated with Surface-Breaching Gas Hydrate Mounds in the Gulf of Mexico, *FEMS Microbiology and Ecology* 46:39-52.

Mills, M. A., T. J. McDonald, J. S. Bonner, M. A. Simon, and R. L. Autenrieth
    1999 Method for Quantifying the Fate of Petroleum in the Environment. *Chemosphere* 39:2563-2582.

Michael, J. and M. O. Hayes
    1999 Weathering Patterns of Oil Residues Eight Years After the *Exxon Valdez* Oil Spill. *Marine Pollution Bulletin* 38:855-863.

Mikami, N., H. Gomi, and J. Miyamoto
    1979 Studies on Degradation of 2,6-di-*tert*-butyl-4-methylphenol (BHT) in the Environment. Part-I: Degradation of ^{14}C-BHT in soil. *Chemosphere* 5:305-310.

Minas, W. and W. Gunkel
    1995 Oil Pollution in the North Sea- A Microbiological Point of View. *Helgolander Meeresunters* 49:14-158.

Moldowan, J. M., J. Dahl, M. A. Mcaffrey, W. J. Smith and J. C. Fetzer
    1995 Application of Biological Marker Technology to Bioremediation of Refinery By-products. *Energy and Fuels* 9:155-162.

Moss J.A., A. Nocker, J.E. Lepo, and R.A. Snyder
    2006 Stability and Change in Estuarine Biofilm Bacterial Community Diversity, *Applied Environmental Microbiology* 72:5679-5688.

Mulkins-Phillips, G. J., and J. E. Stewart
1974 Effect of Environmental Parameters on Bacterial Degradation of Bunker C Oil, Crude Oils, and Hydrocarbons. *Applied Microbiology* 28:915-922.

Munoz, D., M. Guiliano, P. Doumenq, F. Jacquot, P. Scherrer, and G. Mille
1997 Long Term Evolution of Petroleum Biomarkers in Mangrove Soil (Guadeloupe). *Marine Pollution Bulletin* 34:868-874.

Murphy, L.E. and T.G. Smith
1995 Submerged in the Past: Mapping the Beguiling Waters of Florida's Biscayne and Dry Tortugas National Parks. *Geoinfo Systems* 5(10):26-33.

1996 Global Positioning System (GPS). In Encyclopedia of Underwater Archaeology, edited by James P. Delgado, pp. 171 -172. British Museum Press, London.

National Climate Data Center, National Oceanographic and Atmospheric Administration
2005 NCDC Hourly Surface Climate Data for Hawaii, Online Dataset, http://www.ncdc.noaa.gov/oa/climate/climatedata.html#hourly

National Oceanic and Atmospheric Administration [NOAA]
1994 NOAA/ Hazardous Materials Response and Assessment Division Fact sheet: No. 6 fuel oil (Bunker C) spills.

National Research Council [NRC]
2003. Oil in the sea III: Inputs, Fates, and Effects.

Navy Department, Bureau of Construction and Repair
1913 *Detail Specifications for Building Battleship No. 39 for the United States Navy*. Government Printing Office, Washington D.C. On file, USS *Arizona* Memorial Archives, Honolulu.

Neilson, A. J.
1994 *Organic Chemicals in the Aquatic Environment: Distribution, Persistence, and Toxicity*. CRC Press, Boca Raton, FL.

New-York-Navy-Yard
1913 Correspondence. National Archives and Records Administration, North East Region, New York.

Nishigima, F. N., R. R. Weber, and M. C. Bicego
2001 Aliphatic and Aromatic Hydrocarbons in Sediments of Santos and Cananeia, SP, Brazil. *Marine Pollution Bulletin* 42:1064-1072.

Norman, R. S., R. Frontera-Suau, and P. J. Morris
2002 Variability in *Psuedomonas aeruginosa* lipopolysaccharide Expression During Crude Oil Degradation. *Applied and Environmental Microbiology* 10:5096-5103.

North, N. A.
1976 Formation of Coral Concretions on Marine Iron. *International Journal of Nautical Archaeology and Underwater Exploration* 5(3):253-258.

North, N. A. and I. D. MacLeod
1987 Corrosion of Metals. In *Conservation of Marine Archaeological Objects*, edited by C. Pearson, pp. 68-98. Butterworth & Co., London.

North N.A.
1976 Formation of Coral Concretions on Marine Iron, *International Journal of Nautical Archaeology and Underwater Exploration* 5:253-258.

Paine R.W.
October 7, 1943 Memo from Commandant Navy Yard , Pearl Harbor to Chief, Bureau of Ships. Subject: U.S.S. *Arizona* (BB-39) War Damage Report. On file, USS *Arizona* Memorial Archives, Honolulu.

Parker W.W.
1941 Statement of William W. Parker, SEA1c, USN. Wallin Papers, Box 2, 50 Salvage Reports, Naval History Center, Washington, D.C.

Pearl Harbor Natural Resource Trustees.
1999 Restoration Plan and Environmental Assessment for the May 14, 1996 Chevron Pipeline Oil Spill into Waiau Stream and Pearl Harbor, Oahu, Hawaii. Prepared by: U.S. Department of Defense, U.S. Department of the Interior, National Oceanic and Atmospheric Administration, and State of Hawaii. 122 pp.

Perry IV T.D., V. Klepac-Ceraj, X.V. Zhang, C.J. McNamara, M.F. Polz, S.T Martin., N. Berke, and R. Mitchell
2005 Binding of Harvested Bacterial Exopolymers to the Surface of Calcite, *Environmental Science and Technology* 39:8770-8775.

Perry, J. J.
1977 Microbial Metabolism of Cyclic Hydrocarbons and Related Compounds. *CRC Critical Reviews in Microbiology* 5:387-412.

1984 Microbial metabolism of cyclic alkanes. *In* "Petroleum Microbiology" (R. M. Atlas, Ed.), pp. 61-98. McMillan Publishing Co., New York, NY.

Peters, K. E., and J. M. Moldowan
1993 *The Biomarker Guide: Interpreting Molecular Fossils in Petroleum.* Prentice-Hall Inc., Englewood Cliffs, NJ.

Pirnik, M. P.
1977 Microbial Oxidation of Methyl Branched Alkanes. *Critical Reviews in Microbiology* 5:413-422.

Pollard, J. T., M. Whittaker, and G. C. Risden
    1999 The Fate of Heavy Oil Wastes in Soil Microcosms I: A Performance Assessment of
    Biotransformation Indices. *The Science of the Total Environment* 226:1-22.

Porter K.G., and Y.S. Feig
    1980 The Use of DAPI for Identifying and Counting Aquatic Microflora, *Limnology and
    Oceanography* 25:943-948.

Postgate, J. R.
    1979 *The Sulphate-Reducing Bacteria*. Cambridge University Press, Cambridge, Great
    Britain.

Pourbaix, M.
    1974 *Atlas of Electrical Chemical Equilibria in Aqueous Solutions*. National Association
    of Corrosion Engineers, Houston.

Prabagaran S.R., R. Manorama, D. Delille, and S. Shivaji
    2007 Predominance of Roseobacter, Sulfitobacter, Glaciecola, and Psychrobacter in
    Seawater Collected off Ushuaia, Argentina, Sub-Antarctica, *FEMS Microbiology and
    Ecology* 59:342-355.

Prince, R. C., D. L. Elmendorf, J. R. Lute, C. S. Hsu, C. E. Halth, J. D. Senius, G. J. Dechert, G.
    S. Douglas, and E. L. Butler
    1994 17α(H),21β(H)-Hopane as a Conserved Internal Marker for Estimating the
    Biodegradation of Crude Oil. *Environmental Science and Technology* 28:142-145.

Prince, R. C., R. T. Stibrany, J. Hardestine, G. S. Douglas, and E. H. Owens
    2002 Aqueous Vapor Extraction: A Previously Unrecognized Weathering Process
    Affecting Oil Spills in Vigorously Aerated Water. *Environmental Science and
    Technology* 36:2822-2825.

Rabus, R., H. Wilkes, A. Behrends, A. Armstroff, T. Fischer, A. J. Pierik, and F. Widdel 2001
    Anaerobic Initial Reaction of *n*-alkanes in a Denitrifying Bacterium: Evidence for (1-
    methylpentyl) Succinate as Initial Product and for Involvement of an Organic Radical in
    n-hexane Metabolism. *Journal of Bacteriology* 183:1707-1715.

Raymer, Commander E. C.
    1996 *Descent into Darkness Pearl Harbor, 1941: A Navy Diver's Memoir*. Presidio
    Press, Novato.

Reed, W. E.
    1977 Molecular Compositions of Weathered Petroleum and Comparison with its Possible
    Source. *Geochimica et Cosmochimica Acta* 41:237-247.

Richmond, S. A., J. E. Lindstrom, and J. F. Braddock
    2001 Effects of Chitin on Microbial Emulsification, Mineralization Potential, and
    Toxicity of Bunker C Fuel Oil. *Marine Pollution Bulletin* 42:773-779.

Rittman, B.E., M. Pettis, H.W. Reeves, and D.A. Stahl
    1999 How Biofilm Clusters Affect Substrate Flux and Ecological Selection. *Water
    Science and Technology* 39:99-105.

Rodgers, B. A., W. M. Coble and H. K. Van Tilburg
    1998 The Lost Flying Boat of Kaneohe Bay: Archaeology of the First US Casualties of
    Pearl Harbor. *Historical Archaeology* 32(4):8-18.

Russell, M. A., D. L. Conlin, L. E. Murphy, D. L. Johnson, B. M. Wilson and J. D. Carr
    2006 A Minimum-Impact Method for Measuring Corrosion Rate of Steel-Hulled
    Shipwrecks in Seawater. *International Journal of Nautical Archaeology* 35(2):310-318.

Russell, M. A. and L. E. Murphy
    1997 Minimum Impact Archaeology. In *Encyclopaedia of Underwater and Maritime
    Archaeology*, edited by J. P. Delgado, pp. 278-279. British Museum Press, London

    2003 *"Long-Term Management Strategies for the USS Arizona: A Submerged Cultural
    Resource in Pearl Harbor, Hawaii." Legacy Resources Management Fund Project No.
    02-170: 2002 Annual Report*. Submerged Resources Center Technical Report No. 14.
    National Park Service, Santa Fe.

    2004 *"Long-Term Management Strategies for the USS Arizona: A Submerged Cultural
    Resource in Pearl Harbor, Hawaii." Legacy Resources Management Fund Project No.
    03-170: 2003 Annual Report*. Submerged Resources Center Technical Report No. 15.
    National Park Service, Santa Fe.

Russell, M. A., L. E. Murphy, D. L. Johnson, T. J. Foecke, P. J. Morris and R. Mitchell
    2004 Science for Stewardship: Multidisciplinary Research on USS Arizona. *Marine
    Technology Society Journal* 38(3):54-63.

Salanitro, J. P., P. B Dorn, M. H. Huesemann, K. O. Moore, I. A. Rhodes, L. M. R. Jackson, T.
    E. Vipond, M. M. Western, and H. L. Wisniewski
    1997 Crude Oil Hydrocarbon Bioremediation and Soil Ecotoxicity Assessment.
    Environmental Science and Technology 31:1769-1776.

Salvage Diary, Pearl Harbor
    1943 1 March – 1942 through 15 November, 1943. Industrial Department War Diary
    Collection, Naval Historical Center, Washington D.C.

Schaeffer, T. L., S. G. Cantwell, J. L. Brown, D. S. Watt, and R. R. Fall
    1979 Microbial Growth on Hydrocarbons: Terminal Branching Inhibits Biodegradation.
    Applied and Environmental Microbiology 38:742-746.

Samanta, S. K., O. V. Singh, and R. K. Jain
    2002 Polycyclic Aromatic Hydrocarbons: Environmental Pollution and Bioremediation. *Trends in Biotechnology* 20:243-248.

Saveur, A.
    1935 *The Metallography and Heat Treatment of Iron and Steel*. McGraw-Hill, New York.

Schumacher, M. (editor)
    1979 *Sea Water Corrosion Handbook*. Noyes Data Corporation, Park Ridge, NJ.

Shikuma N.J., and M.G. Hadfield
    2005 Temporal Variation of an Initial Marine Biofilm Community and its Effects on Larval Settlement and Metamorphosis of the Tubeworm *Hydroides elegans*, *Biofilms* 2:231-238.

Sierfert W. K. and J. K. Moldowan
    1979 The Effect of Biodegradation on Steranes and Terpanes in Crude Oil. *Geochimica et Cosmochimica Acta* 43:111-126.

Simberloff D.
    1978 Use of Rarefaction and Related Methods in Ecology, In *Biological Data in Water Pollution Assessment: Quantitative and Statistical Analysis*, edited by K.L. Dickson, J. Cairns Jr., and R.J. Livingston, ASTM STP 652, American Society for Testing and Materials.

Shope S.M., L.E. Murphy and T. G. Smith
    1995 Found at Sea: Charting Florida's Sunken Treasures *GPS World* 6(5):22-34.

So, C. M., and L. Y.Young
    1999 Isolation and Characterization of a Sulfate-Reducing Bacterium that Anaerobically Degrades Alkanes. *Applied and Environmental Microbiology* 65:2969-2976.

Spormann, A. M., and F. Widdel
    2000 Metabolism of Alkylbenzenes, Alkanes, and Other Hydrocarbons in Anaerobic Bacteria. *Biodegradation* 11:85-105.

Stillwell, Paul
    1991 *Battleship* Arizona: *An Illustrated History*. Naval Institute Press, Annapolis.

Stirling, L. A., R. J. Watkinson, and I. J. Higgins
    1977 Microbial Metabolism of Alicyclic Hydrocarbons: Isolation and Properties of a Cyclohexane Degrading Bacterium. *Journal of General Microbiology* 99:119-125.

Storlazzi, C. D., M. A. Russell, M. D. Owens, M. E. Field and L. E. Murphy
>   2004 *Dynamics of the Physical Environment at the USS Arizona Memorial: 2002-2004*.
>   U.S. Geological Survey Open-File Report 2004-1353,
>   http://pubs.usgs.gov/of/2004/1353/.

Storlazzi, C. D., M. A. Russell, M. K. Presto and J. E. Burbank
>   2005 *Flow Patterns and Current Structure at the USS Arizona Memorial: April, 2005*.
>   U.S. Geological Survey Open-File Report 2005-1334,
>   http://pubs.usgs.gov/sir/2005/1334/.

Strand, J. A., V. I. Cullinan, E. A. Crecelium, T. J. Fortman, R. J. Citterman, and M. L.
>   Fleischmann
>   1992 Fate of Bunker C Fuel Oil in Washington Coastal Habitats Following the December
>   1988 *NESTUCCA* Oil Spill. *Northwest Science* 66:1-14.

Summary of Damage Reported to the Planning Section
>   December 7, 1941 Wallin Papers, Naval Historical Center, Washington, D.C. Wallin
>   Papers, Box 1,50 Salvage Reports, Naval History Center, Washington, D.C.

Swofford D.L.
>   2003 *PAUP*. Phylogenetic Analysis Using Parsimony (*and Other Methods),* Ver. 4,
>   Sinauer Associates, Sunderland, Massachusetts.

Thompson F.L., T. Iida, and J. Swings
>   2004 Biodiversity of Vibrios, *Microbiology And Molecular Biology Reviews* 68:403-431.

Thompson J.D., T.J. Gibson, F. Plewniak, F. Jeanmougin, and D.G. Higgins
>   1997 The ClustalX Windows Interface: Flexible Strategies for Multiple Sequence
>   Alignment Aided by Quality Analysis Tools, *Nucleic Acids Research* 24:4876-4882.

Trudgill, P. W.
>   1978 Microbial Degradation of Alicyclic Hydrocarbons. *In Developments in
>   Biodegradation of Hydrocarbons* (J. R. Watkinson, Ed.), pp. 47-84. Marcel Dekker, Inc.,
>   New York.

Uhlig, H. H. and R. W. Revie
>   1985 *Corrosion and Corrosion Control*. 3rd ed. John Wiley & Sons, New York.

U.S. Navy
>   1998 Fact Sheet No. 2: Pearl Harbor Sediment Remedial Investigation/Feasibility Study.

>   2003 Overview of Survey/Salvage Operation: USS Mississinewa,
>   www.supsalv.org/00c2_posseA0_59.asp?destPage=00c2.

United States Pacific Fleet Battle Force
>   n.d. USS *California*, Flagship, Memorandum No.7. Wallin Papers, Box 1, 50 Salvage
>   Reports, Naval History Center, Washington, D.C.

van Loosdrecht, M.C.M., J. Lyklema, W. Norde, and A.J.B. Zehnder
      1990 Influence of Interfaces on Microbial Activity. *Microbiological Reviews* 54:75-87.

Vandermeulen, J. H., and J. G. Singh
      1994 *Arrow* Oil Spill, 1970-90: Persistence of 20-yr Weathered Bunker C Fuel Oil.
      Canadian Journal of Fisheries Aquatic Science 51:845-855.

Vesilind, P. J.
      2001 Oil and Honor at Pearl Harbor. *National Geographic Magazine* 199(6):84-99.

Volkman, J. K., D.G. Holdsworth, G. P. Neill and H. J. Bavor, Jr.
      1992 Identitfication of Natural, Anthropogenic and Petroleum Hydrocarbons in Aquatic
      Sediments. *The Science of the Total Environment* 112:203-219.

von Graevenitz A., J Bowman., C. Del Notaro, and M. Ritzler
      2000 Human infection with *Halomonas venusta* Following Fish Bite, *Journal of Clinical
      Microbiology* 38:3123-3124.

Walker, J. D., L. Petrakis, and R. R. Colwell
      1976 Comparison of the Biodegradability of Crude and Fuel Oils. *Canadian Journal of
      Microbiology* 22:598-602.

Wallin, H.N. Cmdr.
      December 7, 1941 Memorandum Covering Apparent Damage to Vessels in Pearl As of
      1345 This Date. US Pacific Fleet, USS Pennsylvania, flagship. Wallin Papers, Box 1, 50
      Salvage Reports, Naval History Center, Washington, D.C.

      January 25, 1942 Progress of Salvage Work in Pearl Harbor. Wallin Papers, Box 1, 50
      Salvage Reports, Naval History Center, Washington, D.C.

      February 8, 1942 Present Situation with Respect to Salvage of Vessels in Pearl Harbor.
      3pp. Wallin Papers, Box 1,50 Salvage Reports, Naval History Center, Washington, D.C.

      1946 Rejuvenation of Pearl Harbor. Typescript sent to Admiral Nimitz and Navy
      Director of Public Information. Wallin Papers, Box 1,50 Salvage Reports, Naval History
      Center, Washington, D.C.

      1968 *Pearl Harbor: Why, How, Fleet Salvage and Final Appraisal.* Naval History
      Division, Washington, D.C.

Wang, Z., M. Fingas, S. Blenkinsopp, G. Sergy, M. Landriault, L. Sigouin, J. Foght, K. Semple,
      and D. W. S. Westlake
      1998a Comparison of Oil Compositional Changes Due to Biodegradation and Physical
      Weathering in Different Oils. *Journal of Chromatography* 809:89-107.

Wang, Z., M. Fingas, S. Blenkinsopp, G. Sergy, M. Landriault, L. Sigouin, and P. Lambert

> 1998b. Study of the 25-year-old *Nipisi* Oil Spill: Persistence of Oil Residues and Comparisons Between Surface and Subsurface Sediments. *Environmental Science and Technology* 32:2222-2232.

Wang, Z., M. Fingas, E. H. Owens, L. Sigouin, and C. E. Brown
> 2001 Long-Term Fate and Persistence of Spilled *Metula* Oil in a Marine Salt Marsh Environment: Degradation of Petroleum Biomarkers. *Journal of Chromatography* 926:275-290.

Wang, Z., M. Fingas, and S. P. Page
> 1999 Oil Spill Identification. *Journal of Chromatography A*. 843:369-411.

Wang, Z., M. Fingas, and G. Sergy
> 1994 Study of 22-Year Old *Arrow* Oil Samples Using Biomarker Compounds by GC/MS. *Environmental Science and Technology* 28:1733-1746.

Wang, Z., M. Fingas, and G. Sergy
> 1995 Chemical Characterization of Crude Oil Residues from an Arctic Beach by GC/MS and GC/FID. *Environmental Science and Technology* 29:2622-2631.

Wang, Z., M. Fingas, and L. Sigouin
> 2001 Characterization and Identification of a "Mystery" Oil Spill from Quebec (1999). *Journal of Chromatography A* 909:155-169.

Weeks O.B.
> 1981 The Genus Flavobacterium, *In The Prokaryotes: a Handbook on Habitats, Isolation, and Identification of Bacteria*, edited by M.P. Starr, H. Stolp, H.G. Trüper, A. Balows, pp. 1365-1370, H.G. Schlegel, Springer-Verlag, New York.

Wheeler, A. J.
> 2002 Environmental Controls on Shipwreck Preservation: the Irish Context. *Journal of Archaeological Science* 29:1149-1159.

Whittaker, M., and J. T. Pollard
> 1997 A Performance Assessment of Source Correlation and Weathering Indices for Petroleum Hydrocarbons in the Environment. *Environmental Toxicology and Chemistry* 16:1149-1158.

Whitfield, C.
> 1988 Bacterial Extracellular Polysaccharides. *Canadian Journal of Microbiology* 34:415-420.

Widdel, F., and R. Rabus
>   2001 Anaerobic Biodegradation of Saturated and Aromatic Hydrocarbons. *Current Opinion in Biotechnology* 12:259-276.

Wilson, B. M., D. L. Johnson, H. Van Tilburg, M. A. Russell, L. E. Murphy, J. D. Carr, R. J. DeAngelis and D. L. Conlin
>   2007 Corrosion Studies on the USS Arizona with Application to a Japanese Midget Submarine. *Journal of Metals* 59(10):14-18.

Wissa, A. E., Christian, J. T., Davis, E. H., and Heiberg, Sigurd
>   1971 Consolidation at Constant Rate of Strain. *Journal of the Soil Mechanics and Foundations Division, ASCE,* 97 (SM10):1393-1413.

Witt, G.
>   1995 Polycyclic Aromatic Hydrocarbons in Water and Sediment of the Baltic Sea. *Marine Pollution Bulletin* 31:237-248.

Yiming, X., W. N. Weins and A. Dhir
>   1992 A Metallographic Investigation of Banding Diffusion of Phosphorous in Steels. In *Microstructural Science* 20. ASM International, New York.

Zakaria, M. P., T. Okuda, and H. Takada
>   2001 Polycyclic Aromatic Hydrocarbons (PAHs) and Hopanes in Stranded Tar-balls on the Coasts of Peninsular Malaysia: Applications of Biomarkers for Identifying Sources of Oil Pollution. *Marine Pollution Bulletin* 42:1327-1366.

Zvyaginstev A.Y.
>   1990 Fouling and Corrosion Damage to Supporting Pillars of Oil Platforms in the South China Sea, *Soviet Journal of Marine Biology* 15:392-397.

Zvyaginstav A.Y., and V.V. Ivin
>   1995 Study of Biofouling of the Submerged Structural Surfaces of Offshore Oil and Gas Production Platforms, *Marine Technology Society Journal* 29:59-62.

APPENDIX A

SonTek Triton Information

Instrument:	SonTek Triton; s/n: R57
Transmitting Frequency:	10 Mhz
Depth of Transducer:	10 m
Blanking Distance:	0.18 m
Height of Sampling Volume:	0.80 m
Operating Mode:	High-resolution, broad bandwidth
Beam Angle:	15 deg
Sound Speed Calculation:	Set salinity, updating temperature via sensor

Current Sampling

Sampling Frequency:	1 Hz
Time Ping:	00:00:00.30
Pings per Ensemble:	60
Time Between Ensembles:	00:10:00.00

Waves Sampling

Sampling Frequency:	2 Hz
Time per Ping:	00:00:00.30
Pings per Ensemble:	1024
Time Between Ensembles:	02:00:00.00
Total Files:	7
Data Processing:	The data were averaged over 1 hour (6 ensembles) and all of the data where the beam correlation dropped below 70% were removed for visualization and analysis.

APPENDIX B

YSI 6600 Sonde Information

Instruments:	YSI 6600 Sonde; s/n: 02g0147
Initial Height of Measurement above Bed:	0.25 m
Sampling Frequency:	2 Hz
Samples per Ensemble:	60
Time Between Ensemble:	00:10:00.00
Total Files:	5
Data Processing:	The data were averaged over 1 hour (6 ensembles) and all of the data where the beam correlation dropped below 70% were removed for visualization and analysis.

APPENDIX C

Geotechnical Soil Testing

DRILLING SERVICES FOR NATIONAL PARK SERVICE USS ARIZONA PROJECT

for

ENGINEERING SOLUTIONS, INC.

ERNEST K. HIRATA & ASSOCIATES, INC.
W.O. 03-3832
December 17, 2003

ERNEST K.
HIRATA & ASSOCIATES, INC.

99-1433 Koaha Place
Aiea, Hawaii 96701
Ph: 808-486-0787 Fax: 808-486-0870
Email: eha@hawaii.rr.com

December 17, 2003
W.O. 03-3832

Mr. Richard Frey
Engineering Solutions, Inc.
98-1268 Kaahumanu Street, Suite C-7
Pearl City, Hawaii 96782

Dear Mr. Frey:

Re: **Drilling Services for National Park Service**
USS Arizona Project

This letter summarizes the work performed for the project. Drilling services were conducted in general conformance with the scope of work presented in our proposal dated September 16, 2003. Our work scope for this study included the following:

- Coordinate entry and obtain approval from Naval authorities for the proposed borings.

- Mobilize men and equipment to construct a floating barge and mount drilling equipment.

- Drill and sample 3 exploratory borings at selected locations to depths ranging from 15.2 to 21.3 meters, measured from harbor bottom. Four borings were originally proposed, but one was eliminated by the National Park Service during the time of our fieldwork. The general location of the project site is shown on the enclosed Location Map, Plate 1.1. The approximate boring locations are shown on the USS Arizona Core Location Plan, Plate 1.2, prepared by the National Park Service.

- Provide a field engineer to log all borings and handle soil samples. The boring logs are presented on Plates 3.1 through 3.7. The Boring Log Legend is presented on Plate 2.1, and the Unified Soil Classification System is presented on Plate 2.2.

- Demobilize men and equipment from the project site.

- Preparation of this letter and the attached boring logs.

Drilling Services

Three borings were drilled to depths ranging from 15.2 to 21.3 meters below the harbor bottom. The borings were drilled using portable drilling equipment mounted on a temporary barge. In general, 100 mm O.D. steel casing was driven down to selected sampling depths and cleaned out with a rock-bit. Samples were recovered using thin-walled shelby tubes driven with a 63.5 kg hammer dropped from a height of approximately 760 mm inches. Continuous sampling was performed from the harbor bottom down to the

maximum depths drilled in all borings. Some Shelby tubes were damaged by the granular material present in the soil layers. Therefore, Shelby tubes were placed in 1.5 meter long by 75 mm O.D. schedule 40 steel pipe during sampling to protect the thin-walled tubes. The steel pipe was used from harbor bottom down to the maximum depth drilled in boring B1A and to a depth of about 7.6 meters in boring B2. The blow counts presented on the boring logs are those required to drive the Shelby tube or 75 mm steel pipe sleeved Shelby tubes 300 mm, unless noted otherwise. Zero blow counts are indicated in areas where the weight of the extension rods were enough to drive the sampler through the soil. Therefore, no hammer energy was required.

During drilling operations, the soils were continuously logged by our field engineer and classified by visual examination in accordance with the Unified Soil Classification System. The boring logs indicate the depths at which the soils or their characteristics change, although the change could actually be gradual. Only the ends of the Shelby tubes were visible to our field engineer. Therefore, if the change occurred within the 0.76 meter sample tube, the depth was interpreted based on field observations. Classifications and sampling intervals are shown on the boring logs.

We appreciate this opportunity to be of service. Should you have any questions concerning this letter, please feel free to call on us.

Respectfully submitted,

ERNEST K. HIRATA & ASSOCIATES, INC.

Ernest K. Hirata, President

EKH:EHS:ph

Attachments:
Location Map	Plate 1.1
USS Arizona Geological Core Locations	Plate 1.2
Boring Log Legend	Plate 2.1
Unified Soil Classification System	Plate 2.2
Boring Logs	Plates 3.1 through 3.7

PROJECT SITE

EAST LOCH

PEARL HARBOR

AIEA BAY

9670

FORD ISLAND

SOUTHEAST LOCH

PEARL HARBOR NAVAL RESERVATION
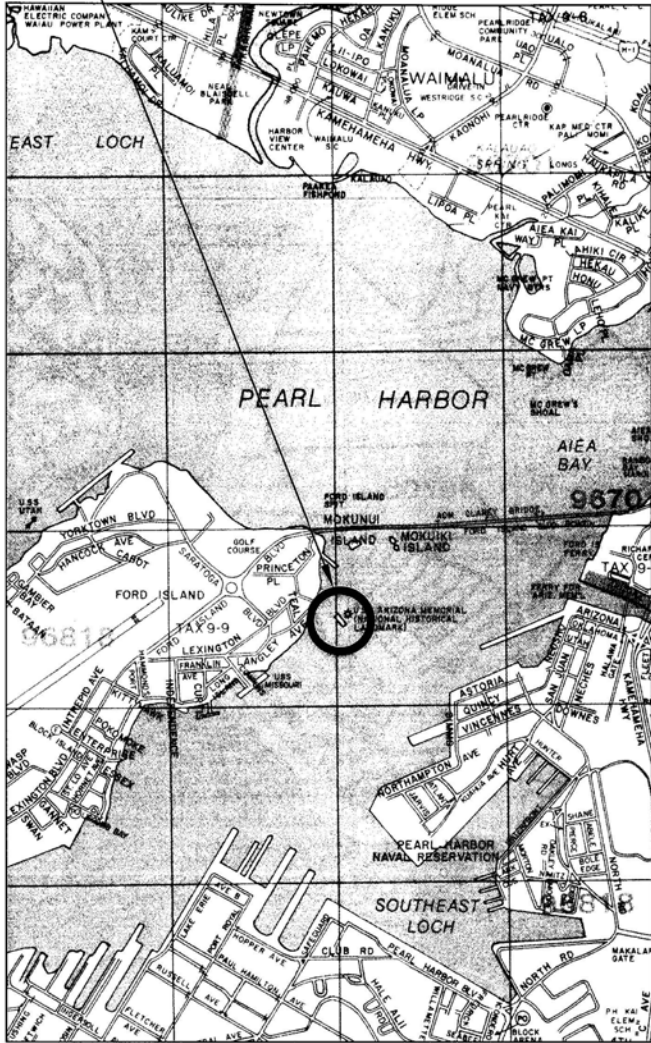
Reference: Bryan's Sectional Maps, 2003 Edition
(Copyright J.R. Clere, used with permission)

Scale: 1:24,000

W.O. 03-3832	USS Arizona Project — Drilling Services
Ernest K. Hirata & Associates, Inc.	LOCATION MAP
	Plate 1.1

Submerged Resources Center
New Mexico

National Park Service
U.S. Department of the Interior

USS Arizona Geological Core Locations
November 2003

Core Location B2
E608943, N2362957

Core Location B1A
E608813, N2362945

Core Location B3
E608749, N2362811
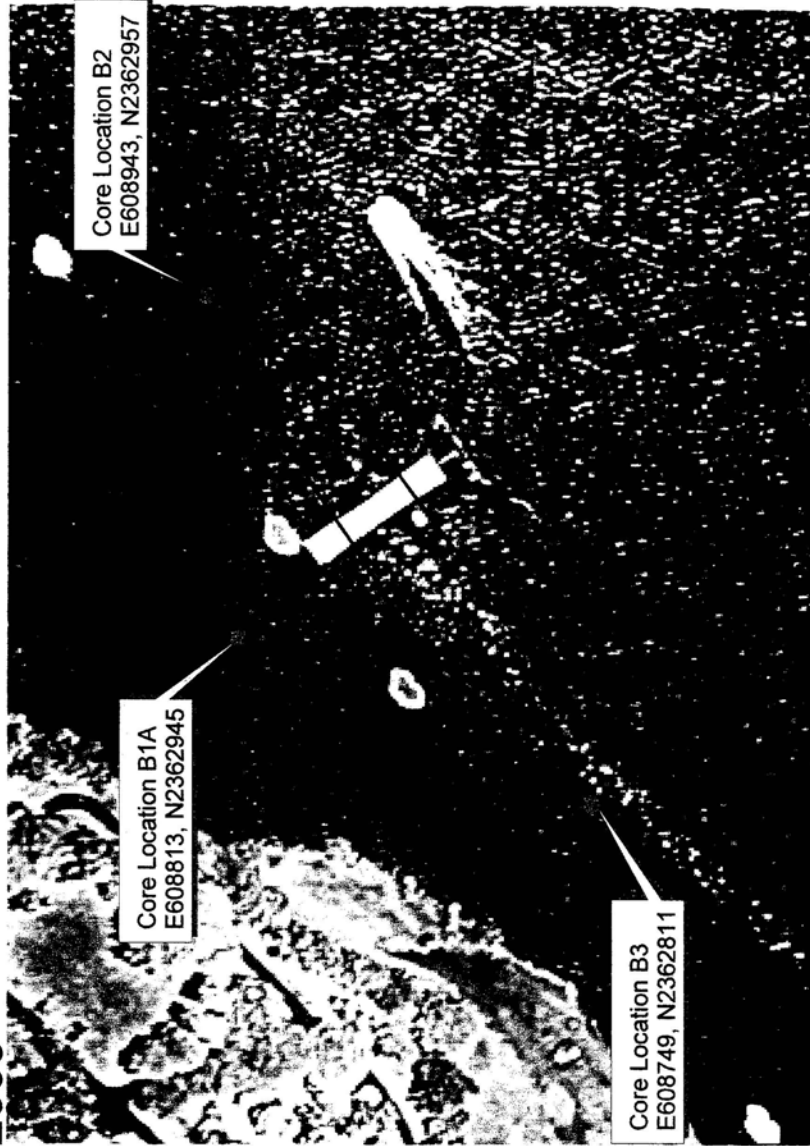
All Coordinates UTM Zone 4, NAD83

Produced by NPS Submerged Resources Center

12/03

N

20 0 20 40 Meters

MAJOR DIVISIONS			GROUP SYMBOLS		TYPICAL NAMES
COARSE GRAINED SOILS (More than 50% of the material is LARGER than No. 200 sieve size.)	GRAVELS (More than 50% of coarse fraction is LARGER than the No. 4 sieve size.)	CLEAN GRAVELS (Little or no fines.)		GW	Well graded gravels, gravel—sand mixtures, little or no fines.
				GP	Poorly graded gravels or gravel—sand mixtures, little or no fines.
		GRAVELS WITH FINES (Appreciable amt. of fines.)		GM	Silty gravels, gravel—sand—silt mixtures.
				GC	Clayey gravels, gravel—sand—clay mixtures.
	SANDS (More than 50% of coarse fraction is SMALLER than the No. 4 sieve size.)	CLEAN SANDS (Little or no fines.)		SW	Well graded sands, gravelly sands, little or no fines.
				SP	Poorly graded sands or gravelly sands, little or no fines.
		SANDS WITH FINES (Appreciable amt. of fines.)		SM	Silty sands, sand—silt mixtures.
				SC	Clayey sands, sand—clay mixtures.
FINE GRAINED SOILS (More than 50% of the material is SMALLER than No. 200 sieve size.)	SILTS AND CLAYS (Liquid limit LESS than 50.)			ML	Inorganic silts and very fine sands, rock flour, silty or clayey fine sands or clayey silts with slight plasticity.
				CL	Inorganic clays of low to medium plasticity, gravelly clays, sandy clays, silty clays, lean clays.
				OL	Organic silts and organic silty clays of low plasticity.
	SILTS AND CLAYS (Liquid limit GREATER than 50.)			MH	Inorganic silts, micaceous or diatomaceous fine sandy or silty soils, elastic silts.
				CH	Inorganic clays of high plasticity, fat clays.
				OH	Organic clays of medium to high plasticity, organic silts.
HIGHLY ORGANIC SOILS				PT	Peat and other highly organic soils.

	FRESH TO MODERATELY WEATHERED BASALT
	VOLCANIC TUFF / HIGHLY TO COMPLETELY WEATHERED BASALT
	CORAL

LAB/FIELD TEST ABBREVIATIONS

TV = Torvane   LL = Liquid Limit
DS = Direct Shear   PI = Plasticity Index
CT = Consolidation   UC = Unconfined
Test   Compression Test

SAMPLE DEFINITION		
2" O.D. Standard Split Spoon Sampler	Shelby Tube	RQD Rock Quality Designation
3" O.D. Split Tube Sampler	NX / 4" Coring	Water Level

W.O. 03-3832	USS Arizona Project — Drilling Services
Ernest K. Hirata & Associates, Inc.	BORING LOG LEGEND
	Plate 2.1

PLASTICITY CHART

Liquid Limit

Plasticity Index

- CH
- A-Line
- CL
- MH & OH
- ML – CL
- ML & OL
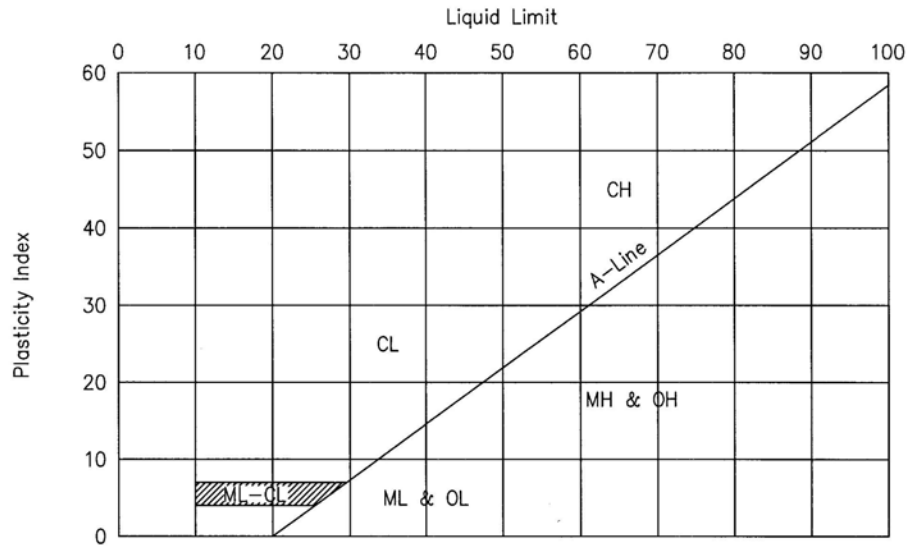
GRADATION CHART

COMPONENT DEFINITIONS BY GRADATION	
COMPONENT	SIZE RANGE
Boulders	Above 12 in.
Cobbles	3 in. to 12 in.

Gravel
  Coarse gravel
  Fine gravel
	3 in. to No. 4 (4.76 mm)
	3 in. to 3/4 in.
	3/4 in. to No. 4 (4.76 mm)

Sand
  Coarse sand
  Medium sand
  Fine sand
	No. 4 (4.76 mm) to No. 200 (0.074 mm)
	No. 4 (4.76 mm) to No. 10 (2.0 mm)
	No. 10 (2.0 mm) to No. 40 (0.42 mm)
	No. 40 (0.42 mm) to No. 200 (0.074 mm)

Silt and clay	Smaller than No. 200 (0.074 mm)

W.O. 03–3832	USS Arizona Project – Drilling Services
Ernest K. Hirata & Associates, Inc.	**UNIFIED SOIL CLASSIFICATION SYSTEM** Plate 2.2

506

ERNEST K. HIRATA & ASSOCIATES, INC.
Geotechnical Engineering

BORING LOG

W.O. 03-3832

BORING NO.	B1A	DRIVING WT.	63.5 kg	START DATE	11/13/03
SURFACE ELEV.	N/A	DROP	760 mm	END DATE	11/14/03

DEPTH	GRAPH	SAMPLE	BLOWS PER 0.3 m	SAMPLE NO.	RECOVERY (%)	DESCRIPTION
0			7			Silty SAND/Sandy SILT (SM/ML) – Gray to brownish gray, soft to firm, with shell fragments.
			5			
			5	1	0	
1			7			
			16			Increase in sand content from 1.2 to 2 meters.
			22			
2			18			
			4	2	5	
			0			
3			0			Increase in sand content from 3 to 3.5 meters.
			52			
			23			
			6	3	0	
4			2			
			0			
			32			
5			51			
			8	4	0	
			4			
6			4			Grade with coralline gravel from 6 meters.
			59			
			47			
7			33	5	30	Silty CLAY (CL–CH) – Grayish brown, medium stiff to stiff, with coralline gravel and sand.
			44			
			42			
			26			
8			35			
			37	6	40	
			51			
9			68			CORAL RUBBLESTONE – Tan, medium dense to dense.
			44			
			23			
10			31	7	100	Plate 3.1

507

ERNEST K. HIRATA & ASSOCIATES, INC.
Geotechnical Engineering

BORING LOG

W.O. __03-3832__

BORING NO. __B1A (Continued)__	DRIVING WT. __63.5 kg__	START DATE __11/13/03__
SURFACE ELEV. __N/A__	DROP __760 mm__	END DATE __11/14/03__

DEPTH	GRAPH	SAMPLE	BLOWS PER 0.3 m	SAMPLE NO.	RECOVERY (%)	DESCRIPTION
0						
			44			
			55			
			101			
11			29			
			38	8	77	Silty CLAY (CL–CH) – Grayish brown, medium stiff to stiff, with coralline gravel and sand.
			59			
12			76			
			20			
			41			
13			83	9	68	
			86			
			104			
			14			
14			26			
			54	10	83	
			76			
15			124			
						End boring at 15.2 meters.
16						Depth to mudline measured at 8.5 meters below water at 11:24 am on 11/13/03.
17						
18						
19						
20						Plate 3.2

508

ERNEST K. HIRATA & ASSOCIATES, INC.
Geotechnical Engineering

BORING LOG

W.O. __03-3832__

BORING NO.	B2	DRIVING WT.	63.5 kg	START DATE	11/18/03
SURFACE ELEV.	N/A	DROP	760 mm	END DATE	11/20/03

DEPTH 0	GRAPH	SAMPLE	BLOWS PER 0.3 m	SAMPLE NO.	RECOVERY (%)	DESCRIPTION
0			0			Silty SAND/Sandy SILT (SM/ML) – Gray to brownish gray, soft to firm, with shell fragments.
			0			
			0	1	0	
1			0			
			0			
			0			
			0			
2			0			
			0	2	5	
			0			
3			0			
			0			
			0			
			0	3	0	
4			0			
			0			
			0			
5			4			Grade with coralline gravel from 6 meters.
			6	4	0	
			7			
			2			
6			6			
			35			Silty CLAY (CL–CH) – Grayish brown, medium stiff to stiff, with coralline gravel and sand.
7			47	5	0	
			95			
			118			
			58			
8			121	6	100	
			87/150mm			
			35			
			65	7	90	
9			44/150mm			
			41			
			97	8	90	
			73/150mm			
10			39			Plate 3.3

509

ERNEST K. HIRATA & ASSOCIATES, INC.
Geotechnical Engineering

BORING LOG

W.O. __03-3832__

BORING NO.	B2 (Continued)	DRIVING WT.	63.5 kg	START DATE	11/18/03
SURFACE ELEV.	N/A	DROP	760 mm	END DATE	11/20/03

DEPTH	GRAPH	SAMPLE	BLOWS PER 0.3 m	SAMPLE NO.	RECOVERY (%)	DESCRIPTION
0						
			47	9	100	
			31/150mm			
			20			
-11-			32	10	80	
			26/150mm			
			22			
-12-			43	11	93	
			29/150mm			
			102			
			160	12	100	Silty SAND/Sandy SILT (SM/ML) – Tan, loose to dense, with coralline gravel and sand, and shell fragments.
-13-			96/150mm			
			46			
			70	13	100	
			16/150mm			
			81			
-14-			110	14	93	
			14/150mm			
			39			
-15-			126	15	60	
			84/150mm			
			44			
			17	16	70	
-16-			16/150mm			
			11			
			17	17	100	
			15/150mm			
			14			
-17-			18	18	63	
			9/150mm			
			20			
-18-			43	19	77	
			29/150mm			
			11			
			17	20	67	
-19-			15/150mm			
			27			
			11	21	93	
			9/150mm			
-20-			0			

Plate 3.4

510

ERNEST K. HIRATA & ASSOCIATES, INC.
Geotechnical Engineering

BORING LOG

W.O. 03-3832

| BORING NO. | B2 (Continued) | DRIVING WT. | 63.5 kg | START DATE | 11/18/03 |
| SURFACE ELEV. | N/A | DROP | 760 mm | END DATE | 11/20/03 |

DEPTH	GRAPH	SAMPLE	BLOWS PER 0.3 m	SAMPLE NO.	RECOVERY (%)	DESCRIPTION
0			0 0/150mm	22	10	
21			0 0/150mm	23	80	
22						End boring at 21.3 meters. Depth to mudline measured at 11.9 meters below water at 8:38 am on 11/18/03.
23						
24						
25						
26						
27						
28						
29						
30						Plate 3.5

511

ERNEST K. HIRATA & ASSOCIATES, INC.
Geotechnical Engineering

BORING LOG

BORING NO.	B3	DRIVING WT.	63.5 kg	START DATE	11/15/03
SURFACE ELEV.	N/A	DROP	760 mm	END DATE	11/15/03

DEPTH 0	GRAPH	SAMPLE	BLOWS PER 0.3 m	SAMPLE NO.	RECOVERY (%)	DESCRIPTION
0			0 0 0/150mm	1	0	Silty SAND/Sandy SILT (SM/ML) — Gray to brownish gray, soft to firm, with shell fragments.
1			0 0 0/150mm	2	0	
2			0 0 0/150mm	3	0	
3			0 0 0/150mm	4	0	
4			0 0 0/150mm	5	0	
5			0 0 0/150mm	6	0	
6			0 0 0/150mm	7	0	
7			0 0 0/150mm	8	100	
8			0 0 0/150mm	9	0	
9			0 2 0/150mm	10	0	
10			0 1 0/150mm	11	0	
			0 4 2/150mm 2	12	77	
			4 2/150mm 4	13	0	

Plate 3.6

512

ERNEST K. HIRATA & ASSOCIATES, INC.

Geotechnical Engineering

BORING LOG

BORING NO. B3 (Continued)   DRIVING WT. 63.5 kg   START DATE 11/15/03
SURFACE ELEV. N/A   DROP 760 mm   END DATE 11/15/03

DEPTH	GRAPH	SAMPLE	BLOWS PER 0.3 m	SAMPLE NO.	RECOVERY (%)	DESCRIPTION
0						
			4 0/150mm	14	0	
11			0 4 2/150mm	15	100	
12			0 0 0/150mm	16	0	
			0 0 0/150mm	17	100	Silty CLAY (CL-CH) — Grayish brown, soft to firm.
13			0 0 0/150mm	18	100	
14			0 0 0/150mm	19	100	
15			0 0 0/150mm	20	100	
16						End boring at 15.2 meters.
						Depth to mudline measured at 11.3 meters below water at 11:25 am on 11/15/03.
17						
18						
19						
20						Plate 3.7

513